# HIGH-ENERGY ASTROPHYSICS

## *American and Soviet Perspectives*



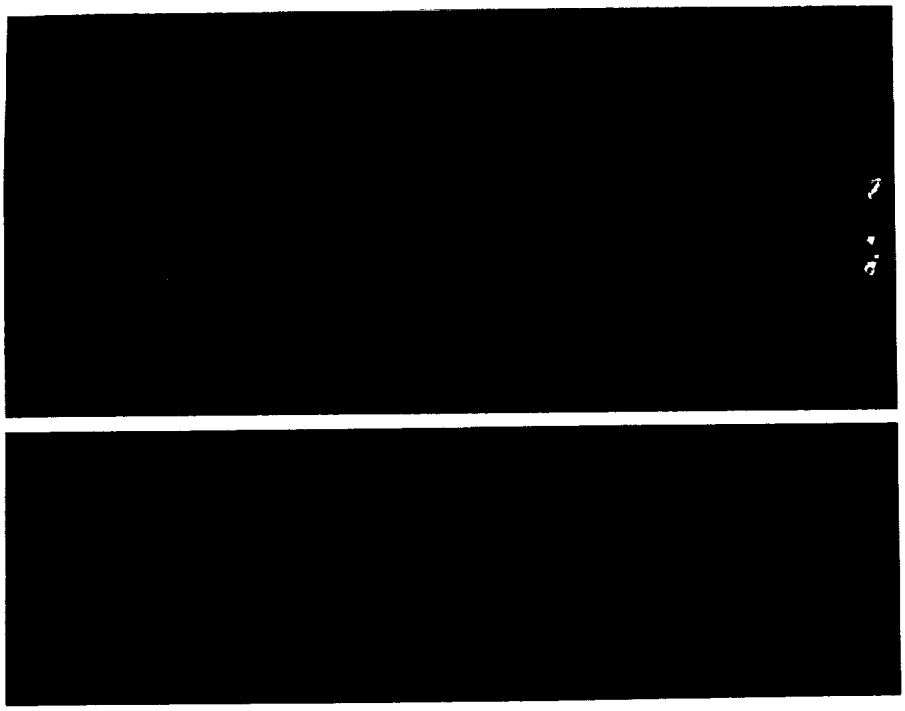

Proceedings from the U.S.-USSR Workshop
on
High-Energy Astrophysics

# High-Energy Astrophysics
## American and Soviet Perspectives

Edited by

Walter H.G. Lewin
George W. Clark
Rashid A. Sunyaev

with

Kathleen Kearney Trivers
David M. Abramson

Proceedings from the U.S.-USSR Workshop
on
High-Energy Astrophysics
June 18 - July 1, 1989

Academy of Sciences of the Union of Soviet Socialist Republics
National Academy of Sciences of the United States of America

National Academy Press
Washington, D.C. 1991

NOTICE: The project that is the subject of this report was approved by the officers of the National Academy of Sciences and the Academy of Sciences of the USSR on January 12, 1988. The members of the committee responsible for the report were chosen for their special competencies and with regard for appropriate balance.

This report has been reviewed by a group other than the authors according to procedures approved by a Report Review Committee consisting of members of the National Academy of Sciences, the National Academy of Engineering, and the Institute of Medicine.

The National Academy of Sciences is a private, nonprofit, self-perpetuating society of distinguished scholars engaged in scientific and engineering research, dedicated to the furtherance of science and technology and to their use for the general welfare. Upon the authority of the charter granted to it by Congress in 1863, the Academy has a mandate that requires it to advise the federal government on scientific and technical matters. Dr. Frank Press is president of the National Academy of Sciences.

The National Academy of Engineering was established in 1964, under the charter of the National Academy of Sciences, as a parallel organization of outstanding engineers. It is autonomous in its administration and in the selection of its members, sharing with the National Academy of Sciences the responsibility for advising the federal government. The National Academy of Engineering also sponsors engineering programs aimed at meeting national needs, encourages education and research, and recognizes the superior achievements of engineers. Dr. Robert M. White is president of the National Academy of Engineering.

The Institute of Medicine was established in 1970 by the National Academy of Sciences to secure the services of eminent members of appropriate professions in the examination of policy matters pertaining to the health of the public. The Institute acts under the responsibility given to the National Academy of Sciences by its congressional charter to be an adviser to the federal government and, upon its own initiative, to identify issues of medical care, research, and education. Dr. Stuart Bondurant is acting president of the Institute of Medicine.

The National Research Council was organized by the National Academy of Sciences in 1916 to associate the broad community of science and technology with the Academy's purposes of furthering knowledge and advising the federal government. Functioning in accordance with general policies determined by the Academy, the Council has become the principal operating agency of both the National Academy of Sciences and the National Academy of Engineering in providing services to the government, the public, and the scientific and engineering communities. The Council is administered jointly by both Academies and the Institute of Medicine. Dr. Frank Press and Dr. Robert M. White are chairman and vice chairman, respectively, of the National Research Council.

Library of Congress Catalog Card No. 90-62813
International Standard Book No. 0-309-04334-4

Copies of this report are available from:

Soviet and East European Affairs
National Research Council
2101 Constitution Ave., N.W.
Washington, D.C. 20418

Additional copies are for sale from:

National Academy Press
2101 Constitution Ave., N.W.
Washington, D.C. 20418

S217

Printed in the United States of America

# Foreword

This book contains the proceedings of the American-Soviet high-energy astrophysics workshop, which was held at the Institute for Space Research in Moscow and the Abastumani Laboratory and Observatory in the republic of Georgia from June 18 to July 1, 1989. This workshop evolved from a similar, very successful workshop held in Protvino in the summer of 1977. Both workshops were attended by only a small number of people from each country (12 Americans were invited in 1977 and 20 in 1989).

The Protvino meeting was of particular importance as it "broke the ice." Since that time, there have been many contacts and exchanges between scientists from the USSR and the United States. U.S. instruments are now scheduled to fly on Soviet space missions.

During the past decade, the field of astrophysics progressed at an impressive rate. This was reflected by the topics discussed at the workshop: the inflationary universe; the large-scale structure of the universe; the diffuse X-ray background; gravitational lenses, quasars and AGNs; infrared galaxies (results from IRAS); supernova 1987A; millisecond radio pulsars; quasi-periodic oscillations in the X-ray flux of low-mass X-ray binaries; and gamma-ray bursts.

The meeting was generously supported by the Academy of Sciences of the USSR, the Academy of Sciences of the Georgian republic, the National Academy of Sciences, and the U.S. National Aeronautics and Space Administration.

This collection of papers reflects some of the active areas of research pursued by scientists of the USSR and the United States. It also contributes to the friendship between the scientists from both countries.

The Editors

# Contents

# Instabilities in SN1987A and Other Supernovae

DAVID ARNETT,* BRUCE FRYXELL,* AND EWALD MÜLLER†


## ABSTRACT

While giving a remarkably good description of many aspects of SN1987A, calculations assuming spherical symmetry have a number of flaws. Many of these problems naturally disappear in the development of a two-dimensional calculation, as nonspherical instabilities grow. This nonspherical bahavior, made evident in SN1987A, has implications for other types of supernovae.


## INTRODUCTION

For the first two weeks, one-dimensional hydrodynamical models of 1987A provide an excellent description of luminosity, effective temperature, and velocity (see the review of Arnett *et al.* 1989, denoted "ABKW"). Lucy (1987) has shown that the predicted spectra of SN1987A begin to deviate after two weeks from those observed, suggesting an inadequacy in the models. Figure 1, from Arnett (1988), indicates the two phenomena that might show what is wrong. The ordinate is expansion velocity, which is closely proportional to the radius. The top panel shows the abundance of hydrogen, helium, $^{56}$Ni and $^{56}$Co; other nuclei are suppressed for clarity. The bottom panel shows temperature. Near the center (at low velocity)

*Department of Physics and Steward Observatory, University of Arizona, Tucson, AZ 85721, USA

†Max Planck Institut für Astrophysik, Garching-bei-München, West Germany

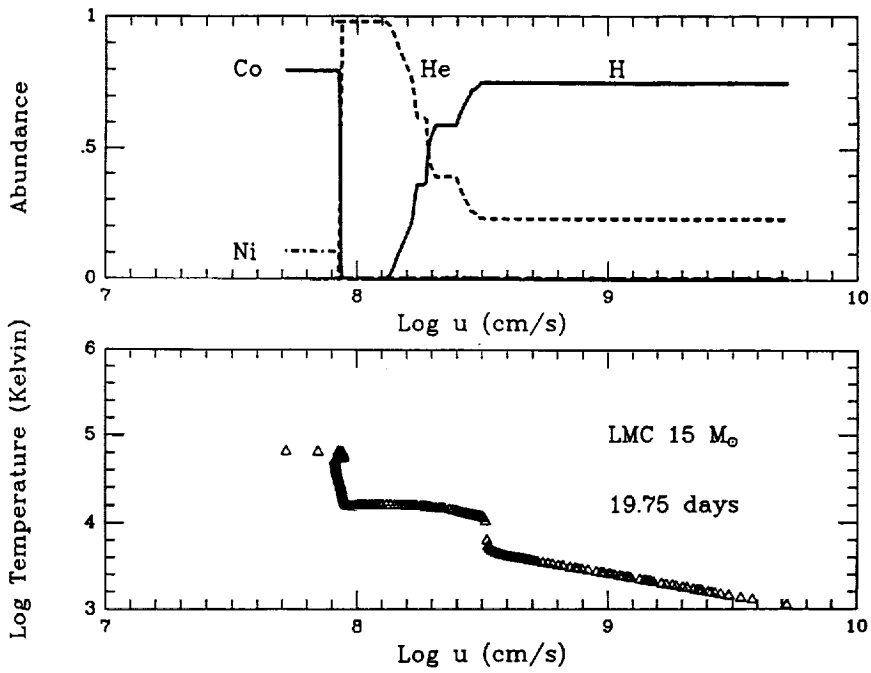


FIGURE 1 Temperature and composition versus velocity at 19.7 days (after Arnett 1988). This shows the status of a one-dimensional numerical model of SN1987A at a time when its predictions for detailed spectral behavior deviate from observations (Lucy 1987). The two dominant phenomena are the development of a hot "Ni bubble" near the center (low velocity) and the penetration of the photosphere to the edge of the helium core. Both are evident as "steps" in temperature. Other abundances are suppressed for clarity.

is the hot "Ni bubble," which is almost certainly Rayleigh-Taylor unstable. Further out, at the edge of the He core, is the photosphere, which appears as a "step" in temperature.

## THE NICKEL BUBBLE

Consider the evolution of an opaque $^{56}$Ni sphere. The decay of $^{56}$Ni (mean life of 8.8 days) releases about 2 MeV, which corresponds to $Q \simeq 4 \times 10^{16}$ erg/s. If this is converted to heat, and by expansion into bulk motion, the mean velocity is $v \simeq \sqrt{2Q} = 2{,}800$ km/s. Compare this to the lower velocities of Ni and Co, shown in Figure 1.

Now suppose this opaque $^{56}$Ni sphere must "snowplow" into a surrounding shell of mass. For an initial velocity at the edge of the Ni of $v_0 \simeq 1{,}000$ km/s (see Figure 1) and homologous expansion (v proportional to r), we have

$$m = m_{Ni}(v/v_0)3$$

and

$$1/2m_{Ni}v_o^2 + m_{Ni}Q = 1/2mv^2$$

so

$$v = [2\{1/2v_o^2 + Q\}v_o^3]1/5 \simeq 1,500km/s.$$

This is the case of perfect spherical symmetry.

Infrared spectral lines show significant amounts of Ni and Co moving at velocities in excess of 2,000 km/s (Witteborn *et al.* 1989). To approach the first case above rather than the second, we need (1) $^{56}$Ni energy to be deposited in the Ni itself (this is true, because gamma attenuation lengths are short for times t $\lesssim$ $\tau_{Ni}$ over which the $^{56}$Ni decay occurs), and (2) holes in the mass distribution of overlying matter for t $\lesssim$ $\tau_{Ni}$. Something similar is needed for the early rise and flat shape of the gamma ray and X-ray luminosities.

The holes can be made by the expansion of the Ni and Co, be pre-existing, or a combination of the two.

## THE LIGHT CURVE

Figure 2 shows the UVOIR and gamma ray light curve for the first 700 days of SN1987A. The good agreement of the theoretical model (solid line: Arnett and Fu 1989) and the SAAO observations (the CTIO and ESO data are similar) has several important implications. First, the amount of $^{56}$Ni needed is small, 0.075±0.01 $M_\odot$ or one-tenth that needed to reproduce a SNIA light curve. This is due to a steep density gradient (so that little mass has the correct conditions for $^{56}$Ni synthesis). This in turn is due to core convergence, which is a direct consequence of $\nu_e\bar{\nu}_e$ cooling after helium burning.

Second, the nearly exponential decay of the bolometric luminosity, from about 120 days on, limits the energy input from the neutron star (pulsar?) to $L_{psr} \lesssim 10^{39}$ erg/s, which is $10^{-2}$ of that suggested prior to 1987.

Third, the good agreement of the analytic model and observations, from 20 days to maximum, implies SN1987A is considerably less spherically symmetric than the one-dimensional numerical models (Arnett 1988, and especially see Figure 1 of Arnett and Fu 1989). The numerical models show dips and peaks not present in the observational data; disagreement ranges up to a factor of two either way. The analytic model does better

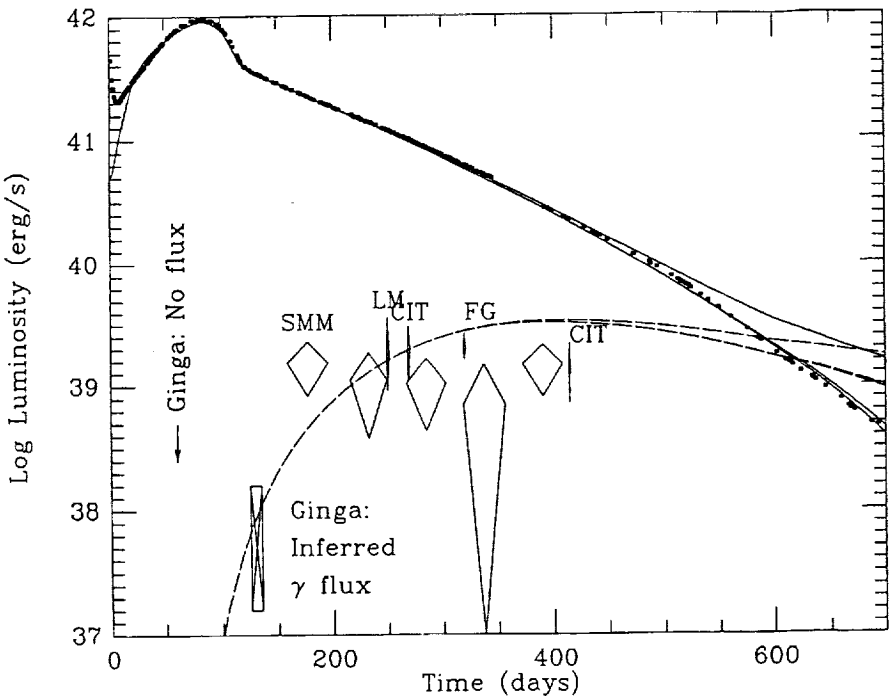


FIGURE 2 Theoretical and observed UVOIR and gamma ray luminosity from SN1987A versus time. The solid squares are combined ultraviolet, optical, and infrared data (UVOIR) from SAAO (Menzies *et al.* 1987; Catchpole *et al.* 1988; and Whitelock *et al.* 1988). The luminosity of escaping gamma rays as measured by Solar Maximum Mission (SMM), Locheed-Marshall (LM), Caltech (CIT), and FloridaGoddard (FG) are shown as rhomboids: detailed references may be found in Arnett *et al.* (1989). Three cases are shown (see Arnett and Fu 1989) having pulsar luminosity (in gamma rays alone) of 2 x $10^{39}$ and $10^{38}$ erg/s, and zero. The higher solid lines correspond to the higher pulsar luminosities; the opposite is true for gamma luminosities, which are shown as dashed lines. The luminosity in X-rays is taken to be equal to that of gamma rays, in rough agreement with numerical results (Burrows, private communication). At 700 days, the UVOIR curves begin to deviate from the data.

because it uses an average opacity rather than the radially varying opacity of the numerical models. Apparently the recombination wave does not move inward through the abundance layers in complete synchronization.

## NONSPHERICAL MODELS

Chevalier (1976) has adapted the stability analysis of Chandrasekhar (1961) to show that the similarity solutions of Sedov develop a Rayleigh-Taylor instability. This work requires the presupernova structure to be approximated by a power law in density ($\rho \propto r^{-\omega}$). A realistic presupernova

model has a more complex structure, so that direct numerical computation is required.

Nagasawa *et al.* (1988, "NNM") have claimed to find violent Rayleigh-Taylor instabilities in n = 3 and 1.5 polytropes for all explosion energies. Subsequent calculations with better resolution (Müller *et al.* 1989; Benz and Thielemann 1989) suggest that this claim is incorrect; the NNM result may be due to asphericity in their initial "point" explosion due to poor resolution.

The question of instabilities in polytropes is only of academic interest; the results of a well-zoned calculation that began from a realistic pre-supernova structure is shown in Figure 3 (after Arnett *et al.* 1989). This two-dimensional calculation used 380 x 380 zones and the Prometheus code (Fryxell *et al.* 1989), which grew from the PPM of Colella and Woodward (1984). The density contours begin to show the characteristic "mushroom" shape of the Rayleigh-Taylor instability at $10^4$ seconds after the explosion. This is well before $^{56}$Ni decay ($\tau_{Ni}$ = 8.8 d). Hydrogen penetrates into velocities as low as 1,000 km/s and heavy elements (Ni and Co) out to velocities as high as 2,400 km/s. Density variations ("clumping") of order $|\delta\rho/\rho| \sim 1$ occur along many lines of sight from the center. Because this directly modifies the attenuation length, which itself appears in an exponential function, the X-ray and gamma ray light curves are strongly affected, making them earlier and flatter, as needed.

The development of the instability is a dynamic process. Whether a perturbation grows into the nonlinear regime depends upon its initial amplitude and the number of e-folding times available. For the shock instability to dominate, it must go nonlinear in a time $t \lesssim \tau_{Ni}$. For this to happen, the initial (nonspherical) perturbation must be of order of a few percent or more, according to the numerical experiments. Figure 3 shows the results of a 10% perturbation.

Such a value may be reasonable. Unlike most collapse calculations, those of Arnett (1977) showed extensive shell flashing prior to core bounce. These calculations bridged the gap between hydrostatic and hydrodynamic evolution more consistently than has been usual. General relativistic dynamics was used in both cases. Exactly the same reaction rates were used. The equation of state was exactly the same, with no glitches in nuclear statistical equilibrium, Fermi-Dirac functions, or Coulomb corrections. This gave a slower collapse initially, during which the silicon and eventually the oxygen shell flashed (see Arnett 1977). It is unlikely this will occur simultaneously around the spherical surface, so that "seed" perturbations should be formed. Crude estimates gave us the 1% and 10% values with which we experimented, but better estimates will require numerical calculations of precollapse through explosion in more than one dimension.

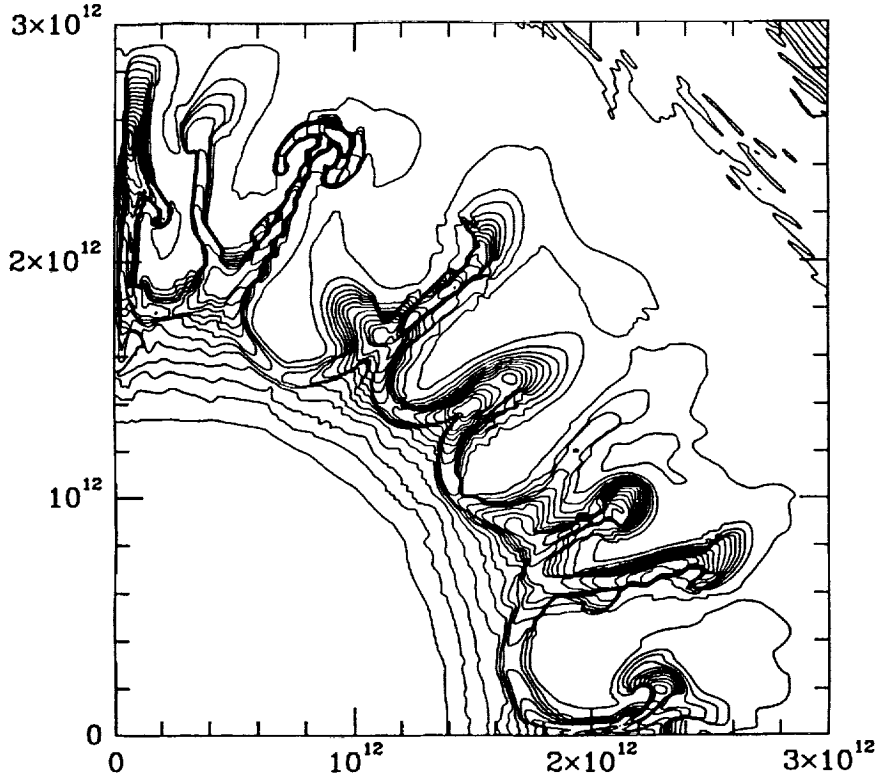


FIGURE 3 Density contours (5 percent spacing) at 9,814 seconds after explosion. There is rotational symmetry about the vertical axis; the equatorial plane lies along the horizontal axis. A 15 $M_\odot$ B3 supergiant presupernova structure with a radius of $3 \times 10^{12}$ cm and a fairly realistic explosion (fitting the early light curve of 1987A) were used. At this time the shock has already propagated off the grid. The "mushroom head" shapes, which are characteristic of a Rayleigh-Taylor instability (followed by Kelvin-Helmholtz) are evident. These represent penetration of heavier elements into the He mass, and some H has already been penetrated by the ascending "mushrooms." Subsequent decay of $^{56}$Ni is expected to have further significant effects. The clumping shown (a factor of two in density already) will modify thermal opacities (removing "wiggles" in the one-dimensional numerical light curves, and favoring higher values of the ejected mass parameter). It will profoundly modify the X-ray and gamma ray escape (making both "earlier"). Even without the added effect of heating from $^{56}$Ni decay, it is sufficient to modify the expected spectral line shapes and polarization.

The question is not whether nonspherical instabilities arise, but the relative importance of at least two mechanisms.

## SNIB AND DIFFUSION MASSES

The width of a radioactive diffusion peak depends on the dimensionless parameter

$$y^2 = \mathcal{H}M/(2\beta c v_{sc}\tau^2),$$

where $\tau$ is the decay time, $v_{sc}$ the scale velocity, $\mathcal{H}$ the opacity, M the mass, c the velocity of light, and $\beta$ is a constant (see Arnett 1982). We can get y and $v_{sc}$ from observations. Then if $\tau$ and $\mathcal{H}$ are known, M can be inferred: we call this the "diffusion mass." The constant $\beta$ comes from integration over the structure of the ejecta. For an inhomogeneous medium such as we have, the effective value of these parameters must change. With "holes" such as in Figure 3, radiation diffuses out more readily, giving a "diffusion mass" that is smaller than the actual mass.

Ensman and Woosley (1988) have attempted to use light curves of Type IB supernovae to constrain the ejected mass to be between 4 and 7 $M_\odot$, originally 15-25 $M_\odot$ on the main sequence. This is a "diffusion mass" and, based on the results shown in Figure 3, should be more lenient by a factor of two. This would move their limit up to 35 or 40 $M_\odot$ on the main sequence. This effect is in addition to that of clumping on gamma ray escape, which they speculate may improve agreement with observation. Quantitative estimates require knowledge of the actual three-dimensional structure.

Finally, note that the instabilities discussed here occur inside the hydrogen envelope, and therefore have a smaller effect on the diffusion mass of supernovae which have a lot of hydrogen: SNII's and SN1987A.

## REFERENCES

Arnett, W.D. 1977. Ap. J. 218: 815.
Arnett, W.D. 1982. Ap. J. 253: 785.
Arnett, W.D. 1988. In: Supernova 1987A in the Large Magellanic Cloud. University Press, Cambridge p. 301.
Arnett, W.D., J.N. Bahcall, R.P. Kirshner, and S.E. Woosley. 1989. Ann. Rev. Astron. Astrophys (in press, denoted ABKW)
Arnett, W.D., B.A. Fryxell, and E. Müller. 1989. Ap. J. (June 15).
Arnett, W.D., and A. Fu. 1989. Ap. J. (in press).
Benz, W., and F.K. Thielemann. 1989. (in press).
Catchpole, R.M., *et al.* 1988. M.N.R.A.S. 229: 15P.
Chandrasekhar, S. 1961. Hydrodynamic and Hydromagnetic Stability. Clarendon Press, Oxford.
Chevalier, R. 1976. Ap. J. 207: 872.
Colella, P., and P.R. Woodward. 1984. J. Comp. Phys. 54: 174.

Ensman, L.M., and S.E. Woosley. 1988. Ap. J. 333: 754.
Fryxell, B.A., E. Müller, and W.D. Arnett. 1989. In: Woodward, P.R. (ed.). Numerical Methods in Astrophysics. Academic Press, New York.
Lucy, L.B. 1987. Astron. Astophys. 182: L31.
Menzies, J.W., *et al.* 1988. M.N.R.A.S. 227: 39P.
Müller, E., W. Hillebrandt, M. Orio, P. Höflich, R. Mönchmeyer, B. Fryxell. 1989. Astron. and Astrophys (in press).
Nagasawa, M., T. Nakamura, and S. Miyama. 1989. Publ. Astron. Soc. Japan (in press).
Whitelock, P.A., *et al.* 1988. M.N.R.A.S. 234: 5P.
Whitteborn, F.C. *et al.* 1989. Ap. J. Lett. 338: L9.
Woosley, S.E. 1989. Ann. Rev. Astron. Astophys (in press, denoted ABKW).

# On the Evolution of Pulsars

V.S. BESKIN, A.V. GUREVICH, YA.N. ISTOMIN
Lebedev Physical Institute

Recently Lyne and Manchester (1988) presented data on the angle $\chi$ between the axis of rotation and the magnetic dipole axis, determined from polarization observations. Such a complete catalogue makes it possible to carry out a detailed comparison of our theoretical results with the observed distribution of radio pulsars over the angle $\chi$.

Before making such a comparison, we recall the main features of our theory (for more details see Beskin *et al.* 1986). The results of such calculations of the generation of particles and of directed pulsar radio emission flux suggest that the properties of pulsars depend substantially on the parameter

$$Q = 2\left(\frac{P}{1s}\right)^{11/10}\left(\frac{\dot{P}}{10^{-15}}\right)^{-4/10} \qquad (1)$$

So, pulsars with $Q \ll 1$ generate particles practically on the entire surface of the polar cap whereas pulsars with $Q > 1$ may generate only within a thin ring, and the generation itself may be of nonstationary, irregular character. In other words, pulsars with $Q > 1$ are located near the death line on the diagram $P\dot{P}$. Indeed, all pulsars exhibiting nulling, subpulse drifts, and mode switching have $Q > 1$, whereas pulsars with $Q < 1$ are characterized by stable radio emission.

The theory of neutron star evolution associated with current losses is different for pulsars with $Q < 1$ and $Q > 1$. It is developed more thoroughly for pulsars with $Q < 1$. It is just for this reason that in all our preceding papers we distinguished between pulsars with $Q < 1$ and those with $Q > 1$ and compared theory with experiment separately for them. The same should be done in the analysis of pulsar distribution over the slope $\chi$.

Let us first see how the distribution of observed pulsars with Q < 1 over $\chi$ will look. To this end we shall make use of the distribution function of pulsars $N_{Q<1}$ (P, $\chi$, $B_{12}$) over the period P (in seconds), over the magnetic field $B_{12} = B/10^{12}$ Gauss and over the slope $\chi$ of the axes (Beskin *et al.* 1986).

$$N_{Q<1} \simeq N P^{\overline{\nu}+1} B_{12}^{\overline{\gamma}-10/7}(1+B_{12})^{-1-\overline{\gamma}-\overline{\beta}} F(\chi)\theta[cos^{0.5}\chi - B_{12}^{-8/7}P^{15/7}] \quad (2)$$

Here N is the total number of observed radio pulsars, $\overline{\nu} = -.1$, $\overline{\gamma} = 3$, $\overline{\beta} = 0.75$, $F(\chi) = \frac{1-cos\chi}{sin\chi}\cos^{-0.5}\chi$ and the $\theta$-function just separates pulsars with Q < 1. As shown by Beskin *et al.* (1986), the distribution function (2) is in agreement with the observed distribution of pulsars (with Q < 1!) over period P and magnetic field $B_{12}$.

Integrating now the distribution function $N_Q < 1$ over the magnetic field B, we can find distribution function $N_Q < 1$ (P, $\chi$) by which one can estimate, for example, the mean value of the angle $\chi$ as a function of period P:

$$\overline{\chi}(p) = \frac{\int N_{Q<1}(P,\chi)\chi d\chi}{\int N_{Q<1}(P,\chi)d\chi} \quad (3)$$

The results are presented in Figure 1. We see that the mean slope $\overline{\chi}$(P) is in perfect agreement with results, *decreases* as P increases, in spite of the fact that for each pulsar the angle $\chi$ increases with time due to the current losses. The reason for this is that pulsars having Q < 1 and large periods P cannot have angles $\chi$ close to 90°. The region Q < 1 on the diagram P – sin $\chi$ is shown in Figure 2. One can see that the generation of particles and radio emission by pulsars with a large enough period P is only possible when $\chi$ are small. Thus, the observed decrease of the mean angle $\overline{\chi}$ with increasing P cannot be regarded as an argument in favor of the decrease of $\chi$ with time. This is rather an indication of the fact that the observed radio emission is indeed associated with particle generation near the star surface.

Similarly, going over in (2) to the variables $B_{12}$, $\chi$ and to dynamical age $\tau_D = P/2\dot{P}$, we obtain

$$N_{Q<1}(\tau_{15}, B_{12}, \chi) \simeq N\tau_{15}^{\overline{\nu}+1} B_{12}^{\overline{\gamma}-10/7(\overline{\nu}+1)}(1+B_{12})^{-1-\overline{\gamma}-\overline{\beta}}(cos\chi)^{1.5(\overline{\nu}+2)}$$
$$F(\chi)\theta[1 - \tau_{15}^{15/7} B_{12}^{92/49} cos\chi] \quad (4)$$

where $\tau_{15} = \tau_D/15$ million years. The analysis of (4) shows that the distribution function $N_{Q<1}$ ($\tau_{15}$, $\chi$) = $\int N_{Q<1}$ ($\tau_{15}$,$B_{12}$, $\chi$)$dB_{12}$, for pulsars

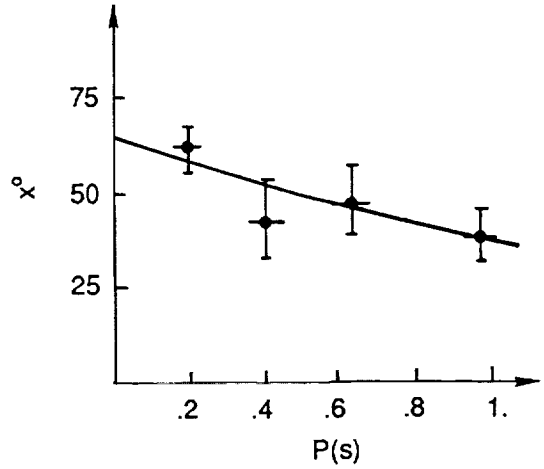


FIGURE 1 The mean value of the slope angle $\chi$ as a function of period P for pulsars with $Q < 1$. The curve corresponds to formula (3), the points correspond to the observations reported by Lyne and Manchester (1988).

with $\tau_D < 15$ million years (i.e., practically for all pulsars with $Q < 1$) must depend weakly on the $\tau_D$ value, and the distribution over $\chi$ must be approximately equiprobable. Indeed, if we consider only pulsars with $Q < 1$, then, as shown in Figure 3, their distribution over $\chi$ for $\tau_D < 2$ million years and $\tau_D > 2$ million years practically coincide, the mean value of $\chi$ even somewhat increasing with time.

$$\begin{aligned} \overline{\chi}(\tau_D < 2\text{mln.yr}) &= 43° \pm 24° \\ \overline{\chi}(\tau_D > 2\text{mln.yr}) &= 48° \pm 29° \end{aligned} \tag{5}$$

But this increase cannot be regarded as statistically significant. Hence, here too, we see close agreement between our theory and experiment.

Let us now consider pulsars with $Q > 1$. The distribution function of such pulsars over the magnetic field B and the angle $\chi$, according to Beskin *et al.* (1986), has the form

$$N_{Q>1}(B_{12}, \chi) = N_{Q<1}[P(\chi, B_{12}), \chi, B_{12}]\dot{P}\tau \tag{6}$$

where $\dot{P} = 10^{-15} B_{12}{}^{10/7} \cos^{1.5}\chi$ is the rotation deceleration velocity in the mechanism of current losses, $\tau = 3 \frac{P}{\sin\chi} B_{12}{}^{-10/7}$ million years is the characteristic life-time of radio pulsars at the stage $Q < 1$, and the relation $P = P(\chi, B_{12})$ corresponds to the condition $Q = 1$ which describes transition of pulsars from the region $Q < 1$ to the region $Q > 1$ as in formula (4). As a result, for the distribution function over the angle $\chi$ for pulsars with $Q > 1$, we obtain

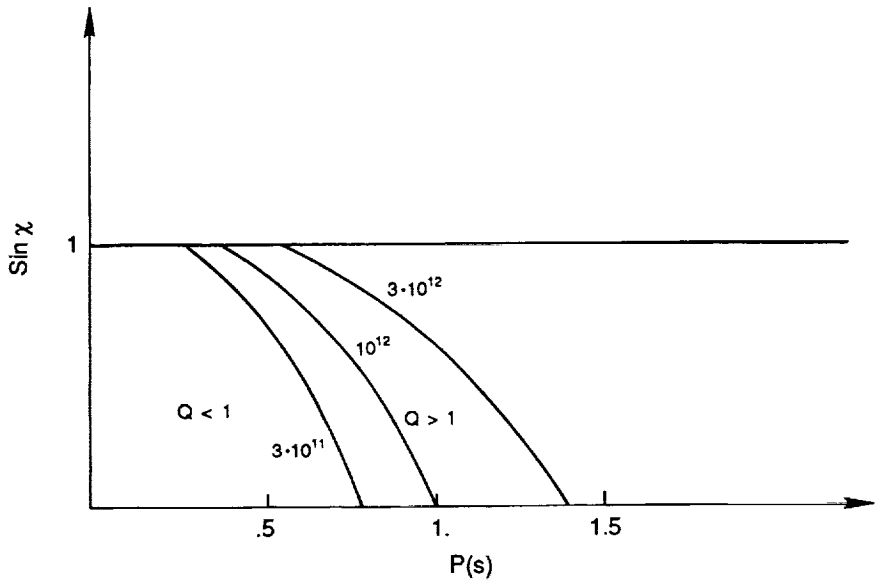


FIGURE 2 The region Q < 1 on the diagram P - sin $\chi$. The boundary is shown for three characteristic magnetic fields $3 \cdot 10^{11}$ Gauss, $10^{12}$ Gauss, $3 \cdot 10^{12}$ Gauss.

$$N_{Q>1}(\chi) = \frac{1 - cos\chi}{sin^2\chi} cos^{1.5}\chi \tag{7}$$

As shown in Figure 4, here we also see agreement between our theory and the experimental results reported by Lyne and Manchester (1988).

Concluding, we would like to emphasize that an unquestionable conclusion of the modern theory is that for rotating pulsar magnetosphere filled with plasma, the law of vacuum deceleration

$$\frac{dW}{dt} = \frac{1}{6} \frac{B_o^2 \Omega^4 R^6}{c^3} sin^2\chi \tag{8}$$

is not obeyed. The presence of plasma in pulsar magnetosphere follows from the very fact of the existence of observed powerful coherent radio emission of pulsars, and the rotation deceleration is determined by the ponderomotive action of current leading to an increase with time of the slope of axes for each individual pulsar. We can see that the conclusions of this theory are in satisfactory agreement with observations.

Thus, the observational data presented by Lyne and Manchester are

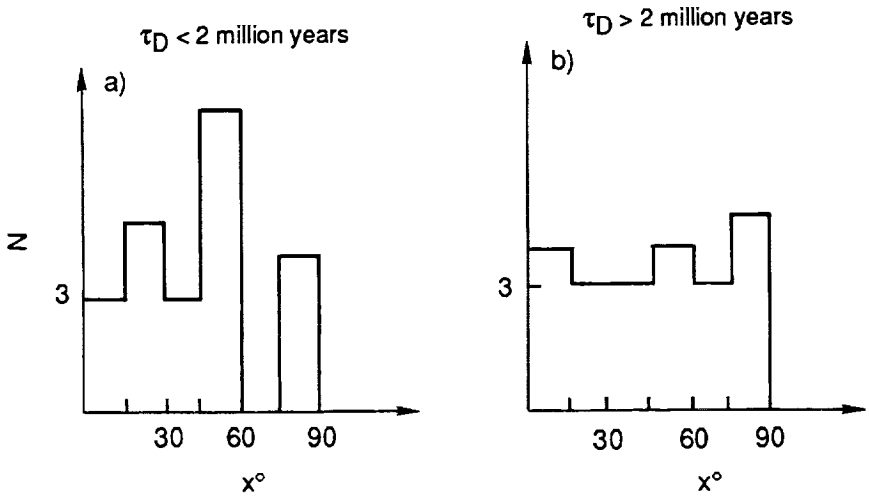


FIGURE 3 Distribution of pulsars with Q < 1 over the slope angle $\chi$ for a) $\tau_D < 2$ million years; b) $\tau_D > 2$ million years.

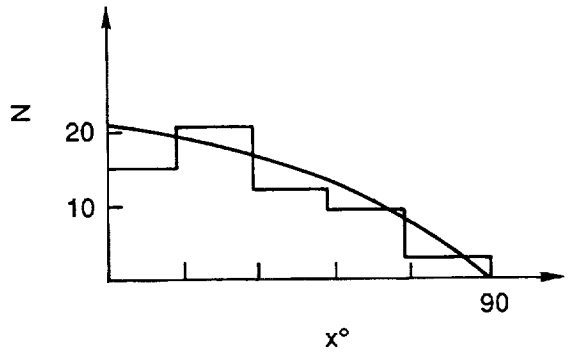


FIGURE 4 Distribution of pulsars with Q > 1 over the slope angle $\chi$. The curve corresponds to formula (7).

in good agreement with our theory of neutron star evolution. New observations which would promote direct estimation of the value $d\chi/dt$ for individual radio pulsars would be, of course, of great interest.

## REFERENCES

Beskin, V.S., A.V. Gurevich, and Ya.N. Istomin. 1986. Sov. Phys. Usp. 29:946.
Lyne, A.G., and R.N. Manchester. 1988. MNRAS. 234:477.

# The Spin Down of the Radio Pulsars. Braking Index

V.S. BESKIN, A.V. GUREVICH, AND YA.N. ISTOMIN
Lebedev Physical Institute

At present, the value of the retardation dP/dt is well known for most radio pulsars. It is negative for all cases except one and is of the order of $10^{-15}$. That single case is when the pulsar, which is located in the star globular system, can have a considerable acceleration leading to the opposite sign of $\dot{P} = dP/dt$ due to the Doppler effect (Wolszczan *et al.* 1989). Careful measurements of the period P also allow one to determine the variation of this retardation with the course of time—$\ddot{P} = d^2P/dt^2$. The results of these measurements are usually represented in the form of the dimensionless retardation index $n = \ddot{\Omega}\,\Omega/\dot{\Omega}^2 = 2 - \ddot{P}P/\dot{P}^2$ ($\Omega$ is the angular velocity). The data for 21 pulsars are given in the table. The parameter n is strongly undetermined both in value and sign in all cases except for four pulsars. Changes of the rotation period P and the inclination angle $\chi$, the angle between the axes of rotation and the magnetic moment are caused by two processes: the regular retardation and nutation due to deviation from the strict spherical shape of the neutron star.

$$\dot{\Omega} = A\Omega^{\alpha} \cdot g(\chi, \Omega); \tag{1}$$

$$\dot{\chi} = \frac{\dot{\Omega}}{\Omega} f(\chi) + \delta\chi\Omega_n \cos\Omega_n t,$$

where $\alpha$ and A are constants and $\Omega_k$ and $\delta\chi$ are the frequency and amplitude of the nutations. The functions $g(\chi,\Omega)$ and $f(\chi)$ depend on the retardation mechanism. In particular, for the magnetodipole losses

$$g(\chi) = sin^2\chi, f(\chi) = ctg\chi, \alpha = 3.$$

Here we consider mainly losses, which are caused by the currents flowing in the magnetosphere of the neutron star and being closed on the

TABLE

| PSR | P | $\dot{P} \cdot 10^{15}$ | $n = 2 - P\ddot{P}/\dot{P}^2$ |
|---|---|---|---|
| 0329 + 54 | 0.714 | 2.05 | $(4.81 \pm 0.18)\ 10^3$ |
| 0531 + 21 | 0.033 | $4.22\ 10^2$ | $2.515 \pm 0.005$ |
| 0540 + 23 | 0.246 | $1.54\ 10^1$ | $(2.5 \pm 0.05)\ 10^1$ |
| 0540 − 69 | 0.050 | $4.79\ 10^2$ | $3.6 \pm 0.8$ |
| 0611 + 22 | 0.335 | $5.96\ 10^1$ | $3.5\ 10^2$ |
| 0823 + 26 | 0.531 | 1.72 | $-1\ 10^4$ |
| 0833 − 45 | 0.089 | $1.25\ 10^2$ | $(4.2 + 1.3)\ 10^1$ |
| 0950 + 08 | 0.253 | $2.29\ 10^{-1}$ | $(-5.2 \pm 0.4)\ 10^4$ |
| 1508 + 55 | 0.740 | 5.03 | $3.25\ 10^3$ |
| 1509 − 58 | 0.150 | $1.490\ 10^3$ | $2.83 \pm 0.03$ |
| 1541 + 09 | 0.748 | $4.3\ 10^{-1}$ | $(-2.5 \pm 0.2)\ 10^5$ |
| 1604 − 00 | 0.422 | $3.06\ 10^{-1}$ | $(1.8 \pm 0.4)\ 10^4$ |
| 1859 + 03 | 0.655 | 7.49 | $(5.5 \pm 0.05)\ 10^3$ |
| 1900 + 01 | 0.729 | 4.03 | $(5.0 \pm 1.2)\ 10^3$ |
| 1907 + 00 | 1.017 | 5.51 | $(-8.7 \pm 0.7)\ 10^3$ |
| 1907 + 02 | 0.495 | 2.76 | $(-9.5 \pm 3.1)\ 10^2$ |
| 1907 + 10 | 0.284 | 2.64 | $(-5.5 \pm 0.2)\ 10^3$ |
| 1915 + 13 | 0.195 | 7.20 | $(-4.2 \pm 0.3)\ 10^1$ |
| 1929 + 10 | 0.226 | 1.16 | $(-2.8 \pm 0.1)\ 10^3$ |
| 2002 + 31 | 2.111 | $7.46\ 10^1$ | $(1.2 \pm 0.05)\ 10^2$ |
| 2020 + 28 | 0.343 | 1.89 | $(1.2 \pm 0.1)\ 10^3$ |

star surface. Such losses are critical for the neutron stars magnetosphere which is full of dense plasma (the density is higher than that of Goldreich-Julian). Since the radioemission is generated in the dense plasma of the polar magnetosphere (Beskin *et al.* 1988), then practically all radio pulsars are retarded by the current mechanism. Two cases can be separated here, when the inclination angle $\chi$ is not too close to 90° and $\chi > \pi/2 - (2\pi R/cP)^{1/2}$, where R is the radius of the neutron star. In the first case (Beskin *et al.* 1983; Beskin *et al.* 1984),

$$\alpha = 1.93, g(\chi) = \cos^{2d}\chi, f(\chi) = -tg\chi, d = 0.75. \quad (3)$$

For $\chi \simeq 90°$ the retardation dynamics are defined by the asymmetrical current $i_A$ which flows out of one half of the polar cap and flows into another

$$\alpha = 4, g(\Omega) = i_A(\Omega), f(\chi) = 0. \quad (4)$$

Using expressions (1) we can easily obtain the formula for the braking index

$$n = \alpha + \frac{\Omega}{g}\frac{\partial g}{\partial \Omega} + f(\chi)\frac{\partial g}{\partial \chi}/g + \delta\chi\Omega_n \frac{\Omega}{g\dot{\Omega}}\cos\Omega_n t, \tag{5}$$

This consists of two portions: the first has the constant sign and is defined by the regular part of star braking; and the second which is changeable over time and caused by the nutations. Values of n presented in the table do not, in most cases, correspond to the regular values, which should be of the order of several units. This means that the last member of the expression (5) is domineering. The exception includes four pulsars 0531 + 21 (Crab), 0540-69, 0833-45 (Vela), and 1509-58, which agree with the picture of the regular braking

$$n = \alpha + \frac{\Omega}{g}\frac{\partial g}{\partial \Omega} + f(\chi)\frac{\partial g}{\partial \chi}/g. \tag{6}$$

For the current losses $\chi \neq 90°$ and $\chi = 90°$ the formula (6) corresponds as follows

$$n = 1.93 + 2dtg^2\chi; \chi < \frac{\pi}{2} - (2\pi R/cP)^{1/2}, \tag{7}$$
$$\partial = 4 + \frac{\Omega}{i_A}\frac{ni_A}{n\Omega}; \chi > \frac{\pi}{2} - (2\pi R/cP)^{1/2}$$

The dependence of the assymetrical current on the rotation frequency has the power form (Beskin *et al.* 1983), so that for current losses at $\chi = 90°$

$$n \simeq 2.6, \chi \simeq 90°.$$

The characteristic dependence of the braking index n on the angle $\chi$ (7) is shown in the figure. The observed values of n for four pulsars included in the table are also shown here. Values of $\chi$ are taken from the observations of X-ray radiation for pulsars 0540-69 and 1509-58; and for the two other pulsars 0531 + 21 and 0833-45 from the tangential condition for the line of observation of the polar cap edge.

We can see that the theory of current losses correctly reflects the character of the dependence of the braking index n on the angle $\chi$. It should be noted that a slight discrepancy between the theory and observations can be explained by the usage of a simple approximation in which the longitudinal current is considered as constant in the whole area of open magnetic field lines. More accurate estimations, when the effect of the electrical current flowing near the internal surface of the hollow cone was taken into consideration, were made by Beskin *et al.* (1986). The result was a decrease of the value n. The angle $\chi = 52° \pm 2°$ was also determined from the observed value of $n = 2.83 \pm 0.03$ (Manchester *et al.* 1985) for

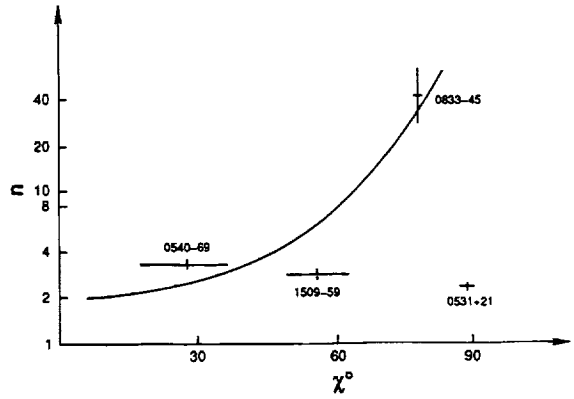


FIGURE 1 The braking index n versus angle $\chi$. The curve corresponds to formulae (7) for the current spin down mechanism. The measurements are presented for the four pulsars with regular braking.

the pulsar 1509-58. This result agrees with the value of angle $\chi$, which was defined from the modulation of the observed pulsar X-ray radiation (Seward and Harnden 1982).

For the remaining pulsars in the table the characteristic values are of the order of $\pm$ ($10^2$ – $10^4$). Then from the expression (5) it follows that

$$P_n/\delta\chi < 10^{-2}P/\dot{P}.$$

For characteristic values P $\simeq 10^{-15}$, P $\simeq$ 1 sec we have

$$P_n/\delta\chi < 10^{13} sec.$$

Note that this value of $P_n$ corresponds to the star asymmetry which is caused by the magnetic field (Goldreich 1970). Actually, in this case

$$\Omega_n = \Omega \frac{B^2 R}{8\pi G M_\rho} \cos\chi, \tag{8}$$

where B is the magnitude of magnetic field, M is the neutron star mass, $\rho$ is the density. Putting characteristic parameters into (8) we get

$$P_n = 3 \cdot 10^{12} P B_{12}^{-2} R_6^{-4} (M/M_\odot)^2 \cos^{-1}\chi. \tag{9}$$

Here $B_{12} = B \cdot 10^{-12}$ G$^{-1}$, $R_6 = R \cdot 10^{-6}$ cm$^{-1}$. Thus, we can see that uncertainty of values n for most pulsars can be caused by slow nutations ($P_n < 10^{12}$ sec, $\delta\chi = \pi/2 - \chi$) due to the magnetic field.

For the quickly decelerated pulsars

$$\dot{P} > \delta\chi \frac{P}{P_n} > 10^{-1}\delta\chi \cos\chi \tag{10}$$

the nutations can become negligible and the braking index n is determined by the regular star braking processes (6). The inequality (10) takes place for four indicated pulsars, when either $\dot{P} \gg 10^{-15}$ or $\chi \simeq 90°$ (or these both).

It should be especially noted that for the pulsar 0531 + 21 (Crab) it was possible to measure the third derivative $\Omega$. It gave us the braking parameter of the second order

$$n^{(2)} = \frac{\ddot{\Omega}\Omega^2}{(\dot{\Omega})^3}$$

It was equal to $n^{(2)} = 10 \pm 1$ (correspondingly, $\ddot{\Omega} = -6 \cdot 10^{-31}$ sec$^{-4}$) (Blandford and Romani 1988; Lyne *et al.* 1988). The determination of $n^{(2)}$ also gives us the possibility to clarify the character of the neutron stars evolution. Indeed, neglecting nutations (as in the case of Crab) from expression (1) we get

$$n^{(2)} = n(2n-1) + f(\chi)\frac{\partial n}{\partial \chi}. \tag{11}$$

Since the pulsar 0531+21 is an interpulse one ($\chi \simeq 90°$), then $f(\chi) = 0$, and we have

$$n^{(2)} = n(2n-1). \tag{12}$$

Expression (12) agrees with the measurement results because n = 2.509. This proves the current mechanism of losses which we proposed (Beskin *et al.* 1983; Beskin *et al.* 1984). At $\chi \simeq 90°$ current losses only lead to expression (12). In this case $\dot{\chi} = 0$, i.e. $\chi = 90°$, and this is the stationary value which the angle $\chi$ between axes approaches due to the evolution of the neutron star rotation.

## REFERENCES

Beskin, V.S., A.V. Gurevich, and Ya.N. Istomin. 1983. Soviet Phys. JETP 58:235.
Beskin, V.S., A.V. Gurevich, and Ya.N. Istomin. 1984. Astrophys. Space Sci. 102:301.
Beskin, V.S., A.V. Gurevich, and Ya.N. Istomin. 1986. Page 361. Proceedings of the Joint Varenna-Abastumani School.
Beskin, V.S., A.V. Gurevich, and Ya.N. Istomin. 1988. Astrophys. Space Sci. 146:205.
Blandford, R.D., and R.W. Romani. 1988. M.N.R.A.S. 234:37.
Goldreich, P. 1970. Astrophys. J. 190:L11.
Lyne, A.G., R.S. Pritchard, and F.G. Smith. 1988. M.N.R.A.S. 233:667.
Manchester, R., J.M. Durdin, and L.M. Newton. 1985. Nature 313: 374.
Seward, F.D., and F.R. Harnden, Jr. 1982. Astrophys. J. 256: L45.
Wolszczan, A., S.R. Kulkarni, J. Middleditch, D.C. Backer, A.S. Fruchter, and R.J. Dewey. 1989. Nature 337:531.

# Axially Symmetrical Supernova Remnants

G.S. BISNOVATYI-KOGAN,[1] T.A. LOZINSKAYA,[2] AND S.A. SILICH[3]


## ABSTRACT

The origin of cylindrically symmetric Supernova Remnants is discussed. The results of numerical simulations of two most distinguished barrel-like SNR SN1006 and G296.5+10.0 are presented.


## INTRODUCTION

Recent high-resolution and high-sensitive observations of Supernova Remnants (SNR) have shown that radio-emitting regions generally do not have spherical symmetry. Many SNR's have a limb-brightened cylindrical or barrel-like structure. There are three principal observational signs of the barrel-shaped SNR morphology: (a) there is an axis of mirror symmetry; (b) the shell has two regions of low intensity near the top and bottom of the symmetry axis; (c) there is a gradient of the radio brightness along the shell.

Kesteven and Caswell (1987) have suggested that the majority of SNRs are barrel-shaped. A number of X-ray and optical remnants falls into this category as well. Cylindrical symmetry is a distinctive feature of both young and old SNRs.

[1] Institute of Space Research
[2] Shternberg Astronomical Institute
[3] Institute of Space Research; Main Astrophysical Observatory, Ukranian Academy of Sciences

Possible mechanisms for generating such a structure include: (a) anisotropy of supernova explosion; (b) large-scale density gradients in the surrounding medium; (c) anisotropy of wind from the progenitor star; (d) compression of a preexisting regular interstellar magnetic field; and (e) interaction of collimated jets of relativistic particles from a central pulsar with the SNR shell. It is possible that more than one of these mechanisms work simultaneously.

Concentration of the ejected material in the equatorial plane is the natural consequence of magnetorotational mechanism of supernova explosion (Bisnovatyi-Kogan 1970) or the thermonuclear explosion of a rotating presupernova star (Bodenheimer and Woosley 1983). Dense interstellar clouds and rarefied interstellar bubbles may affect the expanding shock fronts as well (Lozinskaya 1986). Mass loss by a progenitor star leads to inhomogeneity of circumstellar medium in two ways. First, mass loss by binary systems or rotating stars is concentrated in the equatorial plane (Soker and Livio 1989). Second, progenitor winds generate anisotropic shells and holes in the inhomogeneous surrounding interstellar medium.

There are some difficulties in the interpretation of the barrel structure of SNRs (Roger *et al.* 1988) as the result of compression of a pre-existing interstellar magnetic field. The energy density of the interstellar magnetic field equals approximately $10^{-12}$ erg cm$^{-3}$. This is many orders of magnitude lower than the energy density within a typical SNR during the adiabatic stage. If the explosion energy equals $10^{51}$ ergs and the radius of the SNR is 20 pc, the mean energy density within the SNR will be approximately $10^{-8}$ erg $\cdot$ cm$^{-3}$. As Manchester (1987) has pointed out, it is very difficult to see how a weak interstellar magnetic field could significantly influence the SNR morphology. It is especially difficult to apply this mechanism to a young SNR (in particular, to SN 1006), which have a radially aligned magnetic field component.

It is also difficult to see how pulsars can influence the morphology of the old SNRs except in some special cases as, for example, CTB 80, which is described by Fesen *et al.* (1988).

In this paper we examine the first three mechanisms and do not take into account magnetic field effects. We present the results of numerical simulations of two most distinguished barrel-shaped SNRs: SN 1006 and G296.6 + 10.0.

## SN 1006 AND G296.5 + 10.0 ARE TWO BEST EXAMPLES OF BARREL-LIKE SNRS

The radiomaps of these two remnants (see Figure 1a,b in Roger *et al.* 1988) demonstrate all features of barrel morphology. Optical observations by Kirshner *et al.* (1987) of SN 1006 have revealed narrow and broad

components of the $H_\alpha$ emission. The ratio of the intensities of these components implies a shock velocity in the range 2800-3900 km/s. Distance estimations for SN 1006 made by different methods give 1.5 – 2.1 kpc. Mean value of 1.8 kpc leads to a radius of 7.8 pc and Z = 450 pc. At this distance from the galactic plane ambient gas is dominated by the diffuse component with a number density $n_0 \leq 0.1$ cm$^{-3}$. This estimation is close to the value 0.05cm$^{-3}$, obtained in the X-ray model of Hamilton *et al.* (1986).

The distance and physical parameters of G296.5+10.0 are not well determined. Recent Σ—D distance estimations with account of Z-correction, yield a value 1.1 – 1.9 kpc. The dominant feature of the radio emission from G296.5 + 10.0 is two ridges perpendicular to the galactic plane. The relation of the large axis to the small axis is approximately 1.5:1. The mean distance of around 1.5 kpc results in a linear radii of about 24 pc and 16 pc and Z ≃ 260 pc. It is suggested that there is a connection of the G296.5+10.0 with a depression in HI distribution at the velocities $V_{LSR}$ = -11 – -17 km/s and with weak SNR G300.1 + 9.4 (Dubner *et al.* 1986). The x-ray's remarkable feature is the compact source near the center of the SNR. That point source has a spectrum harder than that of the SNR, but is characterized by a similar absorbing column density and most probably represents the neutron star remnant of the SN explosion. Strong oxygen lines in the optical spectra of G296.5 + 10.0 (Ruis 1983) could indicate on an SNR belonging to O-rich SNRs, which usually are consider results of explosions of massive stars.

The mean ambient number density near the G296.5 + 10.0 from x-ray data is estimated to be 0.24 – 0.08 cm$^{-3}$. Density of the optically emitting filaments is about 5 cm$^{-3}$.

High galactic latitude and low ambient gas densities are the common features of the described above SNRs. One can expect therefore that their evolution is highly influenced by the initial conditions: possible explosion asymmetry and interaction of progenitors with ambient interstellar medium.

## NUMERICAL SCHEME AND INITIAL CONDITIONS

We have assumed cylindrical symmetry in all calculations and used cylindrical coordinate system R, $\varphi$, . We have used the numerical hydrodynamical code described by Bisnovatyi-Kogan *et al.* (1982, 1989), based on thin layer approximation. The main assumptions of this method are that all ejected and swept-up gas collapses into an infinitely thin shell and that gas pressure is uniform inside the cavity.

As a main parameter we adopt explosion energy $E_{ej}$, the temperature $T_0$ and density distribution $\rho = \rho_0 f(R,Z)$ of undisturbed gas, initial ejecta mass $M_{ej}$ and its ratio to the swept-up interstellar gas mass $M_0$. We also

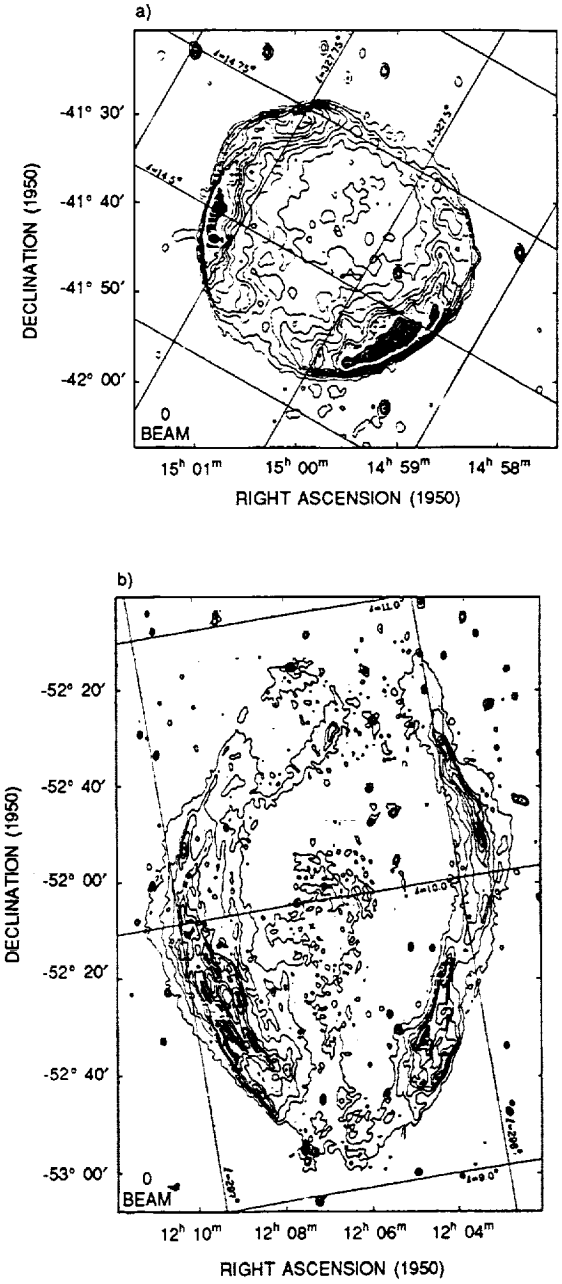


FIGURE 1 The 843 $MH_z$ maps of G327.6 + 14.6(a) and G296.5 + 10.0(b).

define the distribution of surface density $\sigma$ in the shell and the shares of kinetic $E_k$ and thermal energy $E_t$ at the initial time $t_0$. We start from the spherical shell of the radius

$$R_e = \left(\frac{e}{4\pi}\frac{M_{ej}}{\rho_0}\frac{M_0}{M_{ej}}\right)^{1/3} \tag{1}$$

with constant expansion velocity $U_0 = (2E_k/M_{ej})^{1/2}$. Lagrangian coordinates at the onset of calculation are defined by the expressions:

$$R = R_e \sin\lambda,\ Z = R_e \cos\lambda. \tag{2}$$

Anistropy of explosion implies inhomogeneous distribution of the surface density $\sigma_{ej}$ of ejected material along the shell. We assume that at the onset of calculations

$$\sigma_{ej} = \sigma_0(A\sin^2\lambda + B\sin\lambda + C). \tag{3}$$

We adopt normalization A + B = 1 for convenience. Then constant C can be expressed as

$$C = \frac{\sigma_\rho/\sigma_e}{1-\sigma_\rho/\sigma_e}. \tag{4}$$

Integrating initial surface density $\sigma_{ej}(\lambda)$ by $\lambda$, we obtain the expression for initial mass $M_{ej}$. Then constant $\sigma_0$ may be defined as follows:

$$\sigma_0 = \frac{M_{ej}}{4\pi R_e^2\left(\frac{2}{3}A + \frac{\pi}{4}B + C\right)}. \tag{5}$$

Taking into account surface density of the swept-up interstellar gas, we obtain the relation for initial surface density of the shell:

$$\sigma\alpha = \frac{\rho_0 R_e}{3}\left[1 + \frac{M_{ej}/M_0}{\frac{2}{3}A + \frac{\pi}{4}B + C}(Asin^2\lambda + Bsin\lambda + C)\right]. \tag{6}$$

The radio luminosity of the remnants does not arise directly from our hydrodynamical calculations. We assume that radio luminosity is higher as the surface density of the shell is greater. Therefore in this paper we present the results of calculations of the shape and surface density distribution of the shell.

## RESULTS AND DISCUSSION

SN 1006 is a young, almost spherical SNR. It seems to us that it is difficult to interpret its radiobrightness distribution by the influence of the

external factors only. A more convenient interpretation of this observation is that the SN explosion was highly anisotropic with most of the ejecta confined to an equatorial plane. Using our code we investigated the evolution of SNR caused by an asymmetrical SN explosion. The initial surface density of the shell has been taken from formula (3) with $\sigma_p/\sigma_e$ = 0.1 – 0.2, ambient density $n_0$ = 0.05-0.1 $cm^{-3}$, the mass ejecta $M_{ej}$ = 0.5-2.5$M_\odot$, parameter A has been taken in the range 0.8-1.0. The ejected mass has been 250-1000 times greater than the swept-up mass at the onset of the calculations. We have assumed that the shell freely expands with a constant velocity up to the initial moment of calculations. The energy of explosion has been taken as $10^{51}$ ergs. Our calculations show that evolution of SNR caused by asymmetric explosion in homogeneous medium is characterized by elongation of the shock front in Z-direction during the first hundred years. At a later time the material at the shell's poles that has been accelerated by the internal gas pressure begins to decelerate. Expansion velocity of the shell's equatorial region becomes greater than velocities at the poles due to a larger initial mass and momentum. This phase is accompanied by the stretching of the shell in the equatorial plane. Then the shell becomes spherical. Our calculations of the evolution of SNRs caused by anisotropic explosion show many examples of the appearance of apple-like shapes. The reason for the development of such unusual shaping of SNRs is that due to initial surface density distribution of the Lagrangian layers, which, placed between poles and equator (but not at the poles), have a maximum Z-component of momentum. A long time after explosion, the surface density of the shell remains nonuniform with the maximum at the equatorial plane.

The configuration formed by an axisymmetrical explosion on the edge of the gas layer with density enhancement is presented in Figure 2. Initial parameters for this variant have been chosen as follows: ejected mass was equal to 2.0$M_\odot$, total energy of the explosion was $10^{51}$ ergs with 85% in the form of kinetic energy; initial ratio of surface densities was $\sigma_p/\sigma_e$ = 0.1; initial radius was 0.7 pc; parameters A and B from formula (3) were A = 0.97, B = 0.03. Calculations with ejected mass 1.5 – 2.0$M_\odot$ and almost the same parameters give the best coincidence with observed properties of SN 1006. The density of surrounding gas was taken in the form

$$n(z) = n_0 \left[1 + \frac{2}{\pi}\frac{1-\alpha}{1+\alpha} arctan\ \frac{Z}{Z_0}\right]. \qquad (7)$$

The atomic concentration in the point of explosion was taken as $n_0$ = 0.05$cm^{-3}$, the density difference in interstellar media is characterized in (7) by parameters $\alpha = 3$ and $Z_0$ = 1pc. It is clear from Figure 2 that 1000 years after the explosion the surface density distribution remains strongly nonuniform. The maximum of the surface density is shifted relative to the

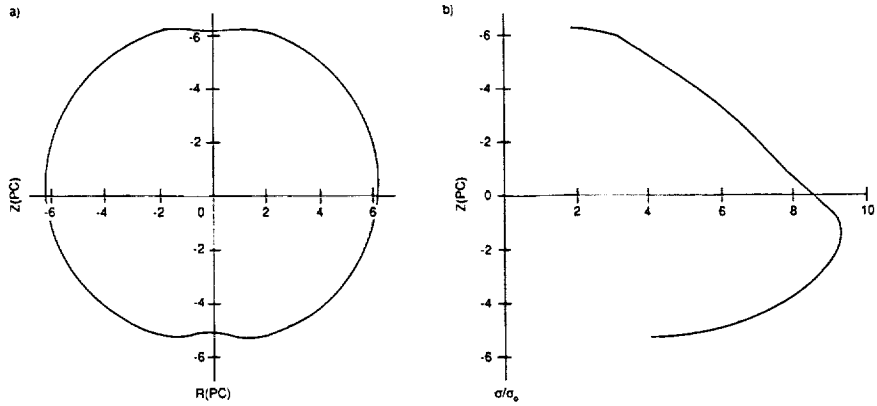


FIGURE 2 Shape (a) and surface density distribution (b) of SNR, caused by an axisymmetrical explosion on the edge of the gas layer. $M_{ej} = 2.0M_{\odot}$, t = 981 yr.

equatorial plane of the explosion Z = 0. The shape of the remnant is close to the spherical one, but apple-like features are present. The radius of the remnant is equal to 6pc and it is situated on the transition phase from free expansion to an adiabatic one. The velocities of the shock waves on the poles are 3900 km/s (up) and 2700 km/s (down) and on the equator that velocity is equal to 5100 km/s. These values agree with the data of Kirshner *et al.* (1986) whose measurements have been made in the north (upper) part of the remnant. When ejected mass is equal to $1.5M_{\odot}$, the radius of the remnant increases up to approximately 7 pc for the same age and initial energies. The radii 6-7 pc determine the distances to the remnant 1.4 – 1.6 kpc.

The radioremnant G296.5 + 10.0 has dimensions much greater than SN 1006 and the gas density in its vicinity is higher. Our calculations have shown that it is impossible to obtain the observed shape and surface density distribution for the explosion in the uniform media using only the asymmetry of the explosion. The observed shape with two extended radioarcs lay rather strong restrictions on the possible gas distribution in the vicinity of the explosion. From several tens of variants for which calculations have been made, the best coincidence with observations has been obtained for the explosion in the tunnel where density falls with increasing Z and the point of the explosion on the axis of symmetry is shifted from the symmetry place. The density distribution in the vicinity of the explosion point (R = 0, $Z = Z_c$) was given by the following formulas

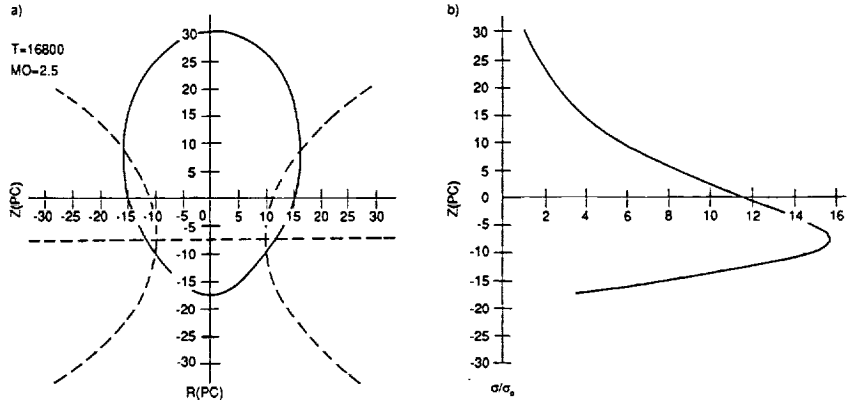


FIGURE 3 Shape (a) and surface density distribution (b) of SNR after the explosion in the gas tunnel for $M_{ej} = 2.5\ M_\odot$ at t = 16800 yr. The center of the coordinate system coincides with the point of explosion. The symmetry plane of the gas distribution is situated 7.5 pc below this point. Dashed lines represent the form and symmetry planes of the gas tunnel.

$$\rho(R,Z) = \rho_0 / \left\{ \left[ \left( \frac{R}{R_0(Z)} - 1 \right)^2 + \beta^2 \right] \left[ \left( \frac{Z}{Z_0} \right)^2 + 1 \right] \right\}, R \le R_0(Z) \tag{8.1}$$

$$\rho(R,Z) = \rho_0 / \left\{ \beta^2 \left[ \left( \frac{Z}{Z_0} \right)^2 + 1 \right] \right\}, R > R_0(Z) \tag{8.2}$$

$$R_0(Z) = R_0[1 + (Z/R_e)^2]. \tag{8.3}$$

The results of our calculations are presented in Figure 3, where the maximum density in the plane of symmetry is $n(R_0, Z = 0) = 1 cm^{-3}$; the density difference in all layers is $n(R_0Z)/n(0, Z) = 3$; and the characterisitic scale of density change along Z axis is $Z_0 = 10$ pc. The radius of the tunnel is equal to $R_0 = 10$ pc in the symmetry plane $Z = 0$ and increases with characteristic scale $R_e = 20$ pc for larger $|Z|$, and the point of the explosion is shifted up from the symmetry plane by $Z_e = 7{,}5$ pc. The initial energy of the explosion is equal to $10^{51}$ ergs with 75% in the form of kinetic energy and the mass ejected in the explosion is equal to $2.5M_\odot$. The age of the remnant in Figure 3 is about 17,000 years, but it is still in the adiabatic stage. The velocities of the shock wave are equal to 1100 km/s on the upper pole, 440 km/s on the lower pole and 250 km/s in the plane of maximum surface density.

The distribution of the gas described by (8.1)-(8.3) may be a result

of partial merging of two old SNR,[1] or the tunnel may be formed by the progenitor's mass loss into the nonuniform gas layer.

## CONCLUSIONS

1. The supernova remnants with axial symmetry may be formed by anisotropic supernova explosions with most of ejecta confined to an equatorial plane as well as a result of the explosions in nonuniform media. The first mechanism determines the asymmetry of a majority of young SNRs, and the second determines the morphology of the older ones.
2. SN 1006 is formed by the anisotropic explosion and corresponds to the stage of transition from free expansion to the adiabatic stage. The distance to the remnant is equal to 1.4-1.6 kpc and corresponds to the lower boundary of observational estimations.
3. The morphology of SNR G296.5+10.0 may be explained if the explosion had occurred in the tunnel with the density falling with increasing Z. The explosion point is situated on the symmetry axis but is shifted up from the symmetry plane.

## REFERENCES

Bisnovatyi-Kogan, G.S. 1970. Astron. Zh. 47:813.
Bisnovatyi-Kogan, G.S., and S.I. Blinnikov. 1982. Astron. Zh. 59:876.
Bisnovatyi-Kogan, G.S., S.I. Blinnikov, and S.A. Silich. 1989. Astrophys. Space Sci. 154:229.
Bodenheimer, P. and S.E. Woosley. 1983. Astrophys. J. 269:281.
Dubner, G.M., F.R. Colomb, and E.B. Giacani. 1986. A. J. 91: 343.
Fesen, R.A., J.M. Shull, and J.M. Saken. 1988. Nature 334:229.
Hamilton, A.J.S., C.L. Sarazin, and A.E. Szymkowiak. 1986. Astrophys. J. 300:698.
Kesteven, M.J., and J.L. Caswell. 1987. Astron. Astrophys. 183:118.
Kirshner, R.P., P.F. Winkler, and R.A. Chevalier. 1987. Astrophys. J. 315:L135.
Lozinskaya, T.A. 1986. Supernovae and Stellar Wind: Interaction with the Galactic Gas. Nauka, Moscow.
Manchester, R.N. 1987. Astron. Astrophys. 171:205.
Roger, R.S., D.K. Milne, M.J. Kesteven, K.J. Wellington, and R.F. Haynes. 1988. Astrophys. J. 332:940.
Ruis, M.T. 1983. Astron. J. 88:1210.
Soker, N., and M. Livio. 1989. Astrophys. J. 339:268.

[1] To one of us (T.A.L.) this possibility seems unrealistic.

# Neutron Starquake Model for Gamma-Ray Bursts

R. D. BLANDFORD
Harvard-Smithsonian Center for Astrophysics
and
California Institute of Technology

## ABSTRACT

A neutron starquake model for gamma-ray bursts is presented and critically analyzed. It is suggested that a slowly accreting neutron star may develop density inversions deep in its crust. These unstable layers, may be subject to elastic Rayleigh-Taylor instability which can liberate sufficient gravitational, and perhaps also nuclear, energy to account for individual bursts. Energy can be transported to the surface by shear waves and slowly transmitted into the magnetosphere as relativistic Alfven waves. Particle acceleration and $\gamma$-ray emission from the outer magnetosphere should ensue. Some observational implications are mentioned.

## INTRODUCTION

This is a report on an interpretation of $\gamma$-ray bursts, a phenomenon studied intensively by space scientists in the United States and the Soviet Union, as neutron starquakes. The work that I shall report on is collaborative with Omer Blaes, Peter Goldreich, Steve Koonin and Piero Madau. The basic model was, of course one of the first suggested (e.g., Pacini and Ruderman 1974; Tsygan 1975; Fabian, Icke *et al.* 1976; Muslimov and Tsygan 1985; Epstein 1988) after the discovery of $\gamma$-ray bursts by Klebesdal *et al.* (1973). Our approach has been to investigate the different components of the starquake model independently. Only an outline of the model, which is still only partially complete, can be presented here; fuller accounts are given in Blaes *et al.* (1989a, 1989b in preparation, 1989c in preparation). In addition, space limitations preclude adequate reference to the extensive

literature on this topic. The articles by Bisnovatyi-Kogan and Chechetkin (1979), Epstein (1988), Lamb (1988), and the book edited by Liang and Petrosian (1986) are good starting points.

## GAMMA RAY BURSTS FROM OLD NEUTRON STARS

As explained in much greater detail by Hurley in these proceedings, $\gamma$-ray bursts are observed about every four days producing emission extending well above 1MeV for roughly 1-10s. On average, the total fluences are $\sim 10^{-6} - 10^{-4}$ erg cm$^{-2}$. Excepting the "soft repeaters," there is a deficit of X-rays relative to $\gamma$-rays; typically, only a few percent of the energy is emitted below 10keV. This imposes a serious constraint on the models. Much circumstantial evidence has been adduced in favor of a local neutron star origin ("rotational" modulation, "cyclotron" lines, "electron-positron annihilation" lines, "association" of GB790305 with a supernova remnant and millisecond temporal structure). None of this is compelling; the interpetation of the first three items can be questioned and the fourth could arise under more exotic conditions than neutron starquakes. The observed isotropy of the sources and the source counts (Schmidt, these proceedings) points to either a local or a cosmological origin.

Using the expected distribution of old pulsars, we find that, in round numbers, the typical burster would have to be a $\sim 10^{10}$ yr old neutron star some $\sim$ 300pc distant producing a $\sim 10^{37}$ erg burst of $\gamma$-rays every 1000yr. The integrated $\gamma$-ray energy radiated over the neutron star lifetime is therefore $\sim 10^{44}$ erg.

## STRUCTURE OF YOUNG NEUTRON STAR CRUSTS

Traditionally, it has been supposed that the structure of the neutron star crust has the composition computed in a classic paper by Baym *et al.* (1971) (or a close variant thereof if we use an improved semi-empirical mass formula for the nuclear binding energies). In this work, it was assumed that the composition of the crust would comprise the lowest energy state at the imposed pressure taking into account the electronic, nuclear and lattice energies and ignoring any thermal contributions. The crust was found to be made of layers of (mostly) magic nuclei, that became increasingly neutron rich with depth. It was therefore implicitly assumed that the nuclei would be able to exchange nucleons freely in order to attain this lowest energy state. Under normal conditions, nucleon exchange amongst high Z nuclei requires thermonuclear reactions at a temperature of $\gtrsim 4 \times 10^9$K (e.g., Bisnovatyi-Kogan and Chechetkin 1979, 1986; Thielemann 1989) when the thermal energy will almost surely result in a mix of nuclei. At lower

temperatures, the nuclear composition is frozen, rather like the helium composition after the epoch of nucleosynthesis in the early universe.

There is a further complication. In the supernova explosion that forms the neutron star, a significant quantity of mass will be ejected with speed just less than the escape velocity and it will subsequently fall back onto the neutron star surface. It may take over a year for the last $\sim 10^{-6}M_{\odot}$ of mass to reach the surface (e.g., Chevalier 1989) and, by this time, the star will have cooled to temperatures well below that at which thermonuclear reactions can occur. The weight of the infalling material can change the pressure in the original crust significantly, and even if the original crust had the composition appropriate to cold catalysed equilibrium, it will, in general, be out of equilibrium at the new pressure. The crustal composition clearly depends subtly on the detailed history of the star.

## SLOW ACCRETION AND CRUSTAL LOADING

Isolated, old, cold neutron stars moving through the interstellar medium accrete interstellar gas at a mean rate $M \sim 10^{10}$g s$^{-1}$ (e.g., Ostriker *et al.* 1970). This can only keep the surface temperature at $\sim 3 \times 10^5$K. The surface area of a neutron star is $A \sim 10^{13}$ cm$^2$ and the surface gravity is $\sim 10^{14}$ cm s$^{-2}$. The original crust can therefore be compressed over a lifetime $t \sim 10^{10}$ yr to a pressure $p \sim Mgt/A \sim 3 \times 10^{28}$ dyne cm$^{-2}$, or equivalently a density $\rho \sim 3 \times 10^{10}$g cm$^{23}$ and an electron chemical potential (essentially the Fermi energy) $\mu e \sim$ 10MeV (e.g., Shapiro and Teukolsky 1983).

As the (predominantly) hydrogen gas is compressed it will eventually be able to undergo cold or pycnonuclear reactions to form helium (e.g., Salpeter and Van Horn 1969; Shapiro and Teukolsky 1983). This helium can undergo a pycnonuclear "triple $\alpha$" reaction to form carbon which in turn may undergo fusion to oxygen, neon and magnesium. The outcome is uncertain, but at some point the Coulomb barrier will inhibit fusion and the nuclei will be compressed by the crustal loading. This behavior is quite different from what happens at higher mass accretion rates where the accreting gas is heated by compression faster than it can be cooled by electron conduction and the hydrogen and helium burns to helium which in turn burns to carbon and iron either steadily or in flashes as in X-ray bursters (e.g., Ayasli and Joss 1982).

When the electron Fermi energy in the compressed lattice becomes sufficiently large, electron capture will occur and the neutron fraction will increase. This may have to occur via an excited state and so there may be some heating associated with this process (e.g., Haensel and Zdunik 1989). However, electron captures can only occur singly as the time scales for double electron capture are excessively long. Now, even-even nuclei

are more tightly bound than odd-odd nuclei and the electron Fermi-energy must be raised to typically $\sim$ 10MeV before an even-even nucleus can capture an electron. However, as soon as a single capture occurs, there will invariably be a second capture to leave the nuclei in an even-even state. For example, at a pressure of $p \sim 7 \times 10^{26}$ dyne cm$^{-2}$ and a density $\rho \sim 1.5 \times 10^{9}$ dyne cm$^{-3}$, $^{56}$Fe will undergo electron capture to form $^{56}$Mn which will rapidly capture a second electron to form $^{56}$Cr, with an overall energy release of 2.1MeV, of which $\sim$ 1.2MeV will be carried off in neutrinos. The remaining $\sim$ 0.9MeV per nucleus is released too slowly to produce significant heating of the interior.

Under these conditions, it is only possible to achieve restricted nuclear equilibrium in the crust. This leads to the possibility of an important instability. Suppose that there is an interface between two layers in which the nuclei have different atomic weights. For example suppose that a layer of $^{56}$Fe rests on $^{62}$Ni. Now suppose that the crust is loaded and compressed essentially isothermally so that only electron capture can occur. When the pressure reaches $p \sim 7 \times 10^{26}$ dyne cm$^{-2}$, the atomic number of the $^{56}$Fe will decrease by two to form $^{56}$Cr, increasing the density discontinuously by 8 per cent. However, the $^{62}$Ni must be compressed to $p \sim 2.1 \times 10^{27}$ dyne cm$^{-2}$ before it can be converted to $^{62}$Fe. There will therefore be a time when $^{56}$Fe is separated from the $^{62}$Ni by a thick layer of $^{56}$Cr. The $^{56}$Cr is 5 per cent denser than the $^{62}$Ni. There is therefore a source of mechanical free energy available if the $^{56}$Cr and $^{62}$Ni layers can be interchanged. The development of few per cent density inversions when layers of the crust are compressed at constant atomic weight is quite general.

## ELASTIC RAYLEIGH-TAYLOR INSTABILITY AND STARQUAKES

When a heavy fluid rests on top of a lighter fluid in a gravitational field, it is Rayleigh-Taylor unstable (e.g. Chandrasekhar 1961). Small perturbations of the interface (with wavelength long enough to overcome the effects of surface tension) will grow through a linear phase in a time $\sim (\rho/\rho)^{-1/2}(gk)^{-1/2}$, where k is the horizontal wavenumber, to the "bubble and spike" non-linear phase. However, a neutron star crust can withstand shear stress and may be stabilized to Rayleigh-Taylor instability (e.g., Landau and Lifshitz 1986). The imposition of the no-slip boundary condition at the interface, as opposed to the free movement allowed in a traditional fluid treatment, inhibits the growth of unstable modes. We have performed a linear analysis of the elastic Rayleigh-Taylor instability and find that for a given, sufficiently large density jump at the interface, there will be a range of unstable horizontal wavenumbers centered on roughly twice the reciprocal of the depth of the interface below the surface. The minimum density jump necessary for a single unstable mode depends upon the ratio of the

shear modulus to the bulk modulus. In a bcc lattice, of iron this ratio is $\sim$ 0.014 (Baym and Pines 1971) and a density jump of about six per cent is necessary for linear instability. Some additional complications change these estimates slightly, but the general conclusion is that, if electron capture-induced density inversions are formed, then they are only marginally stable, and we expect that relatively small perturbations from isostacy, such as will surely be present in a real crust, are sufficient to induce instability. The growth time for the instability is $\sim (p/g^2\delta\rho)^{1/2} \sim 10\mu s$. This is much shorter than any time scale observed in gamma ray bursts.

The gravitational energy released in a local overturn of about a scale height of crust at a density of $\sim 10^9$ - $10^{10}$g cm$^{-2}$ is simply computed from the formula

$$\Delta E = \frac{1}{m_{pg}} \Delta \int \mu dp$$

where $\mu$ is the total chemical potential. This works out to be about 5keV per baryon or $\sim 10^{38}$ erg, adequate to account for a single gamma ray burst provided that the efficiency of conversion to gamma rays is high. It must be emphasized that in this model only a of order a cubic scale height of the crust can overturn in each starquake. In this respect, the starquake model is similar to earthquakes and dissimilar to the highly successful model of X-ray bursts in which it is necessary that a burning front cover most of the stellar surface.

An energy release of $\sim$ 5keV per baryon, is equivalent to a temperature of several billion degrees, well above the melting temperature. This introduces the possibility that the crust will become hot enough to allow thermonuclear reactions to occur and to release additional energy as nuclear rearrangements are catalyzed by free protons, neutrons and alpha particles. Up to $\sim$ 30keV per baryon can be released in this manner. It is not yet clear what conditions are necessary for this to occur.

The proposed model for a starquake releases a lot of energy in the form of heat. However, unlike in an X-ray burst, the heat is released deep below the surface, at a depth $z \gtrsim 300$m and should take a substantial time, typically several hours to reach the surface and to be radiated as soft X-rays.

## SEISMIC WAVES

There is however, a much faster way for the energy released to reach the surface and this is seismically. There are two types of high frequency waves that can propagate through the crust, pressure waves and shear waves. As the shear modulus is roughly one percent of the bulk modulus, the shear speed is about ten per cent of the sound speed. This has the

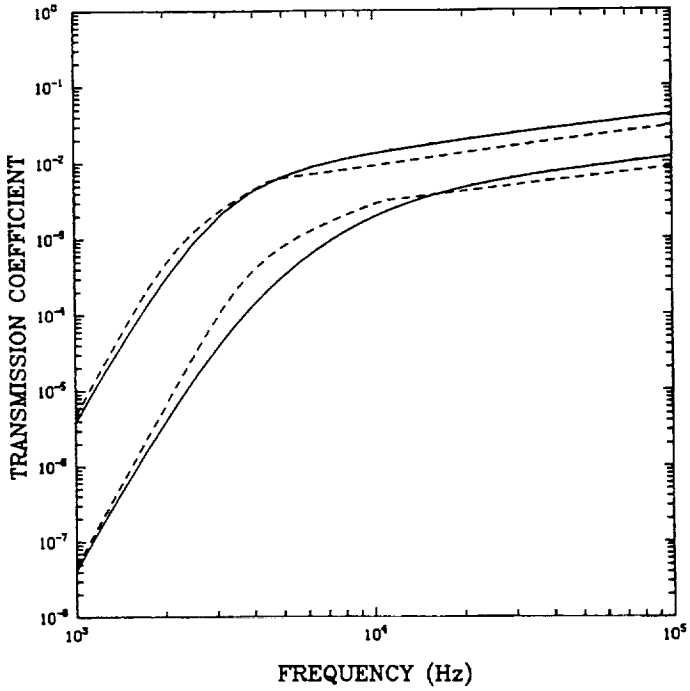


FIGURE 1 Transmission coefficient as a function of frequency for a vertically propagating shear wave. The solid lines refer to numerical calculations, while the dashed lines show WKB solutions. The upper and lower pairs of curves are for $10^{12}$G and $10^{11}$G magnetic field.

consequence that far more power (proportional to the inverse fifth power of the wave speed in the quadrupolar approximation) from a starquake is channeled into shear modes and it is only necessary to consider these.

If we consider shear waves in the WKB approximation, then in the part of the crust supported by the degeneracy pressure of relativistic electrons, a vertically propagating wave's wavelength will decrease $\propto z^{1/2}$, while its horizontal displacement will increase $\propto z^{-7/4}$. However, the amplitude cannot increase indefinitely. When the wavelength becomes comparable with the pressure scale height, $\sim z/4$, the wave will be reflected with high efficiency back towards the stellar core. Refraction in the inner crust will return the wave back towards the surface. It is very difficult to estimate the damping rate (probably dominated by stress-induced motion of dislocations), but if terrestrial measurements are a guide (e.g. Minster 1980), quality factors of several thousand are not out of the question. It should be emphasized that if most of the energy produced in the explosion

is dissipated in heating the crust rather than is carried to the surface seismically then the present model is not viable.

## MAGNETOSPHERIC ALFVEN WAVES

If the neutron star is endowed with a substantial surface magnetic field, then it is possible for there to be an appreciable transmission of energy into the magnetosphere. The magnetosphere will be magnetically-dominated and will support two types of hydromagnetic waves, fast magnetosonic modes, which are similar to vacuum electromagnetic waves, and relativistic Alfven modes (e.g. Melrose 1980) in which field parallel conduction currents compete with displacement current. The phase velocity of an Alfven mode propagating at an angle $\alpha$ to the field is c cos $\alpha$, which can be much less than the speed of the light and can be comparable with the shear speed in the crust for a wave propagating nearly perpendicular to the field. If we treat the surface layers as a plane discontinuity, then standard notions of impedance matching suggest that there will be a significant transmission coefficient. More careful calculations, that take into account the magnetic contributions to the shear stress in the crust, verify this and, for example, give transmission coefficients of a few per cent for 10kHz waves and a $10^{12}$G field. This has the attractive consequence that energy can be stored as waves propagating around the crust for several hundred vertical propagation time scales, typically of order a second, and comparable with the length of the bursts.

Relativistic Alfvén waves in the magnetosphere will also change as they propagate away from the star. In particular, the magnetic amplitude B/B will increase $\propto B^{-1/2}$. They are likely to become non-linear at $\sim$ 5 - 10 stellar radii and may create large parallel electric fields. If this is the location of the $\gamma$-ray emission then only a small fraction of the $\gamma$-rays would be re-radiated from the stellar surface as X-rays as the observations seem to require.

## EMISSION OF GAMMA RAYS

We now turn to the component of the whole problem where there is the greatest prospect for confronting present and future observations, and where I have least to suggest! I have identified a region some 5-10 stellar radii from the surface as the emission site and the location of large, parallel electric fields, capable of accelerating stray electrons and positrons to radiation reaction-limited energies $\lesssim$ 10TeV. The magnetosphere will be relatively starved of charge-carrying particles, but there is the strong possibility of creating fresh electron-positron pairs, primarily through two photon production. These pairs can themselves be re-accelerated and

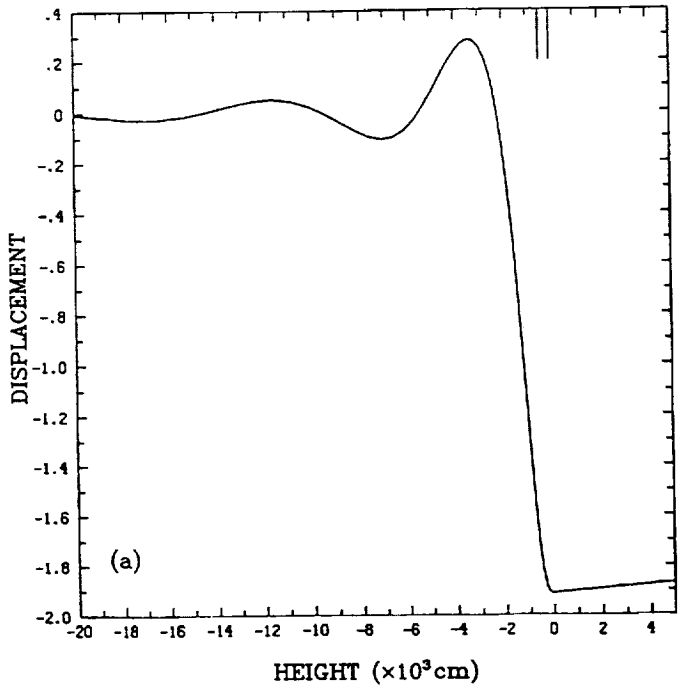


FIGURE 2 The displacement amplitude as a function of height above the surface for a vertically propagating 10kHz shear wave in a $10^{11}$G magnetic field. The evanescent zone is identified by the pair of vertical lines.

produce further generations of particles until the electric fields are locally shorted out. The details are unclear.

Two comments can be made, however. Firstly, it is not just necessary to create electrons and positrons; $\gamma$-ray photons are also necessary (e.g., Zdziarski and Lamb 1988). One way in which they may be multiplied is through the following cycle. An incident soft photon is Compton scattered by a relativistic electron moving along the field in its ground state of gyrational motion and thereby creating a $\gamma$-ray. The electron then recoils into an excited gyrational state, from which it will quickly de-excite by radiating Doppler-shifted cyclotron radiation which can then be scattered and repeat the cycle. Photon yields of $Y \sim m_e c^2/\hbar\omega_G$, where $\omega_G$ is the gyro frequency are possible and so a runaway growth of soft photons only requires there to be a Thomson depth of $\sim Y^{-1}$, typically $\sim 10^{-4}$. Unfortunately, preliminary calculations of the inverse Compton and relativistic electron synchrotron radiation emitted imply a spectrum that is steeper than reported. More realistic modeling should be pursued.

The second point is that it is necessary to account for the "cyclotron" lines in detail. A good start has been made by Loredo *et al.* (1989, preprint) who point out that the relative equivalent widths of the two lines observed in both GB870303 and GB880205 can be accounted for in terms of resonance scattering. However, the atmosphere that is postulated is neither radiatively nor dynamically self-consistent. In addition there is no clear reason why a narrow cyclotron feature should be produced when the field strength will vary by a factor $\sim 2$ over the surface. In the present model, it might be possible to attribute the X-ray continuum to heating of the surface consequent to the starquake and localized to the site of the quake. Again, further study is necessary.

## OBSERVATIONAL IMPLICATIONS

In this report, I have outlined some studies of a particular model for gamma ray bursts involving neutron starquakes. The model, as described, is fairly fragile especially on energetic and demographic grounds. In order to account for the observed frequencies and fluences of observed bursts, it is necessary to tap most of the available nuclear energy from the accreted interstellar gas and to observe most of the "dead" neutron stars within a Galactic scale height every thousand years.

There are alternative possible components to the model which may be substituted. For example, the neutron star cores may contain magnetic fields of far greater strength than are measured on the surface and these may be subject to instability. The discussions of seismic and hydromagnetic waves are not seriously affected by this change. Alternatively, it may be that the radiative conditions on the surface really do allow the "X-ray paucity constraint" to be satisfied and that most of the $\gamma$-ray emission originates here. This would still allow the energy to derive from the sort of deep starquake described above. Another possibility is that a minority of neutron stars accrete at a substantially greater rate than the interstellar rate and yet do not produce X-ray bursts; alternatively some pulsars may be able to store substantial nuclear fuel from their formation and still be able to detonate small pieces of it some $\sim 10^{10}$ yr later.

It is therefore quite hard to test the details of the present model observationally. Nevertheless, it is possible and indeed is far more important to test the most general features of neutron starquake models. In view of the reported anisotropy of bursts, only nearby stars can be involved. They must therefore repeat. Existing constraints cannot yet rule out a neutron star origin (Hartmann 1989 preprint; Paczynski 1989 preprint), but it is anticipated that either frequent repetition or anisotropy should be measurable soon. (If the frequency of bursts reflects current rather than integrated accretion then a much stronger anisotropy is needed.) Should

neither effect become apparent then a cosmological population of exotic objects or a major revision of our ideas on the early stellar evolution of our Galaxy would probably be indicated. The detection of more "cyclotron" and "redshifted electron-positron annihilation" lines would clearly be a boon. The discovery of rotational modulation of the former would be compelling evidence for neutron stars. The discovery of an ultra-violet afterglow from the position of a burst, perhaps using Hubble Space Telescope would also constitute valuable evidence for neutron stars.

This model, in common with several others, does require there to be a strong surface magnetic field, typically $\gtrsim 10^{11}$G. This raises the perplexing question of the evolution of neutron star magnetic fields, a subject which recent observations have made highly confusing. On the one hand, it appears that radio pulsar torques decay in a few million years (e.g., Lyne and Manchester 1988) and become very small in old, millisecond pulsars. In addition models of low mass X-ray binaries generally require them to be weakly magnetised. On the other hand, if old neutron star really do possess fields of strength $\sim 2 \times 10^{12}$G, as the "cyclotron" lines suggest, then we have to understand the reason for these different evolutions. Perhaps a resolution can be found in alignment (e.g. Candy and Blair 1986) or the erasure of low mulitpoles in favor of higher multipoles, (e.g. Flowers and Ruderman 1976). A clearer understanding of radio and X-ray pulsar magnetic fields would have immediate implications for the study of gamma ray bursts.

We eagerly await the launch and successful deployment of HST, GRO, GRANAT and SPEKTRUM-$\gamma$ which should provide answers to some of these pressing questions.

## ACKNOWLEDGEMENTS

In addition to my collaborators listed in the introduction, I am particularly indebted to Friedrich Thielemann for advice on nuclear physics. I thank the Harvard-Smithsonian Center for Astrophysics for hospitality. I also gratefully acknowledge financial support of the Guggenheim Foundation, the Smithsonian Institution and the National Science Foundation (AST86-15325).

## REFERENCES

Ayasli, S., and P.C. Joss. 1982. Astrophys. J. 256: 637.

Baym, G., C.J. Pethick, and P. Sutherland. 1971. Matter at High Densities. Astrophys. J. 170: 299.

Baym, G. and D. Pines. 1971. Ann. Phys. 66: 816.

Bisnovatyi-Kogan, G.S., and V.M. Chechetkin. 1979. Sov. Phys. Uspekhi. 22: 89.

Bisnovatyi-Kogan, G.S., and V.M. Chechetkin. 1986. In: Helfand, D.J. (ed.). Origin and Evolution of Neutron Stars. Proc. IAU Symp. Kluwer, Dordrecht.

Blaes, O.M., R.D. Blandford, P. Goldreich, and P. Madau. 1989. Neutron Starquake Models for Gamma Ray Bursts. Astrophys. J. in press.
Candy, B.N., and D.G. Blair. 1986. Astrophys. J. 307: 535.
Chandrasekhar, S. 1961. Hydrodynamic and Hydromagnetic Stability. Dover.
Chevalier, R. 1989. Neutron Star Accretion in a Supernova. Astrophys. J. in press.
Epstein, R.I. 1988. Phys. Rep. 163: 155.
Fabian, A.C., V. Icke, and J.E. Pringle. 1976. Astrophys. Sp. Sci. 42: 77.
Flowers, E., and M. Ruderman. :-.
Haensel, P., and J.L. Zdunik. 1989. Non-Equilibrium Processes in the Crusts of Accreting Neutron Stars.
Klebesdel, R.W., I.B. Strong, and R.A. Olson. 1973. 182: L85-.
Lamb, D.Q. 1988. Theories of gamma ray burst spectra. In: Gehrels, N., and G. Share (ed.). Nuclear Spectroscopy of astrophysical Sources. American Institute of Physics, New York.
Landau, L.D., and E.M. Lifshitz. 1986. Theory of Elasticity. Pergamon, Oxford.
Liang, E.P., and V. Petrosian, ed. 1986. Gamma Ray Bursts. American Institute of Physics, New York.
Lyne, A.G., and R.N. Manchester. 1988. The Shape of Pulsar Radio Beams. Mon. Not. R. astr. Soc. 234: 477-508.
Melrose, D.B. 1980. Plasma Astrophysics. Gordon and Breach, New York.
Minster, J.B. 1980. Physics of the Earth's interior. In: Dziewonski, A., and E. Boschi (eds.). Proc. Enrico Fermi Summer School in Physics. Academic Press, New York.
Muslimov, A.G., and A.I. Tsygan. 1986. Astrophys. Sp. Sci. 120: 27-.
Ostriker, J., M.J. Rees, and J. Silk. 1970.
Pacini, F., and M. Ruderman. 1974. Nature 251: 399-.
Salpeter, E. ED., and H.M. van Horn. 1969. Astrophys. J. 155: 183-.
Shapiro, S.L., and S.A. Teukolsky. 1983. Black Holes, White Dwarfs and Neutron Stars. The Physics of Comapct Objects. Wiley-Interscience, New York.
Thielemann, F.-K. 1989 (in press). Explosive Nucleosynthesis. In: Lozano, M. (ed.). Nuclear Astrophysics. Springer, Berlin.
Tsygan, A.I. 1975. Astr. Astrophys. 44: 21.
Zdziarski, A., and D.Q. Lamb. 1988. Photon Deficient Compton Scattering by Non-thermal Electrons. Adv. Sp. Res.:-.

# The Shock Breakout in SN1987A Modelled with the Time-Dependent Radiative Transfer

S.I. BLINNIKOV, D.K. NADYOSHIN
Institute for Theoretical and Experimental Physics
O.S. BARTUNOV
Sternberg Astronomical Institute

**ABSTRACT**

The fully implicit high-order scheme has been developed for the time-dependent multi-group radiative transfer coupled with implicit hydrodynamics. The application of this scheme to the SN1987A explosion shows that shortly after the shock breakout a dense shell forms.

Many papers have modeled the early light curve of SN1987A in an approximation of radiation equilibrium diffusion (e.g., Woosley *et al.* 1987; Grasberg *et al.* 1987; Arnett 1987; Shigeyama *et al.* 1987). However, this approximation is never valid in the outermost layers of a supernova. Moreover, at the stage of shock breakout the radiation field changes so quickly, that it is necessary to take into account that the light speed is not infinite (the retardation effect).

We have developed a new gasdynamic code describing the time-dependent radiation transport in the multi-group approximation with variable Eddington factors. The method used is free of the limitation of the equilibrium diffusion.

We assume the Newtonian mechanics and gravitation, taking into account the radiative force in the momentum equation, and the radiative heating in the temperature equation. The temperature of ions is assumed to be equal to that of electrons (cf. Chevalier and Klein 1979, for the opposite case). The time-dependent equations for the radiation energy and the momentum include all therms of order v/c, where v is the matter velocity and c is the light speed (Imshennik and Morozov 1981; Castor

1972; Mihalas and Mihalas 1984). The equations are closed with a space-variable Eddington factor f(r) evaluated from the transfer equation by the Feautrier (1964) method for an instantaneously static atmosphere to which our code calls after the prescribed number of steps. Optionally, the user may take into account the retardation effect more precisely by calculating factors f(r,t) from the time-dependent equation of transfer (Mihalas and Mihalas 1984) at every time step.

The ionization equilibrium is taken into account in the Saha approximation. In the outermost rarefied layers the option for the kinetic (NLTE) treatment of the hydrogen ionization is provided for. The time-dependent radiation transport accounting for all the effects of the order of v/c is combined with the gasdynamics in a common, fully implicit difference scheme, which is based on the high-order predictor-corrector algorithm developed by Gear (1971). We calculate the flux in every energy group from the time-dependent equations as described by Falk and Arnett (1977) and Mihalas and Mihalas (1984). Therefore, we do not encounter the problem of the flux limiting which is the source of some ambiguity in the works using the static expression for the flux (Chevalier and Klein 1979; and for the neutrino transport: Bowers and Wilson 1982; Bruenn 1985; Myra *et al.* 1987).

The implicit gasdynamic part of our code was successfully tested in the problem of strong explosion of the degenerate stellar cores with allowing for the kinetics of the carbon burning. The testing was also done in the investigation of quasistatic and dynamic stages of gravitational collapse with kinetics of beta-processes (Blinnikov and Rudzskiy 1984) and in the purely static problem of white dwarf cooling (Blinnikov 1988).

For SN1987A, we used the model of mass $16M_{\odot}$, radius $47R_{\odot}$, and explosion energy $2\times10^{51}$ ergs. The initial hydrostatic model has been constructed by the special code for initial models (Nadyozhin and Razinkova 1986) and was close to a polytrope of index n = 3.5.

We present now the main results for the simplest case: LTE-ionization; opacity is independent of frequency and depends only on density and temperature; and Compton scattering is treated as pure absorption. The run of the calculated light curve and of the effective temperature, shown in Figures 1 and 2, proves to be very close to the results of Grasberg *et al.* (1987) and Utrobin (1989). In particular, the effective temperature reaches the maximum value of about $5\times10^5$K. (The run on our 1 Mflops computer uses 150 Lagrangian mass zones, 20 geometrically spaced frequency groups and for optical depth $\tau$ greater than 15-30, we switch to the equilibrium diffusion. The results, presented in Figures 1 and 2, are obtained in $\sim$ 1 hour of CPU time. It takes about 20 hours for the next 10,000 steps, when at about the 80th day of the supernova evolution $\tau$ in the center

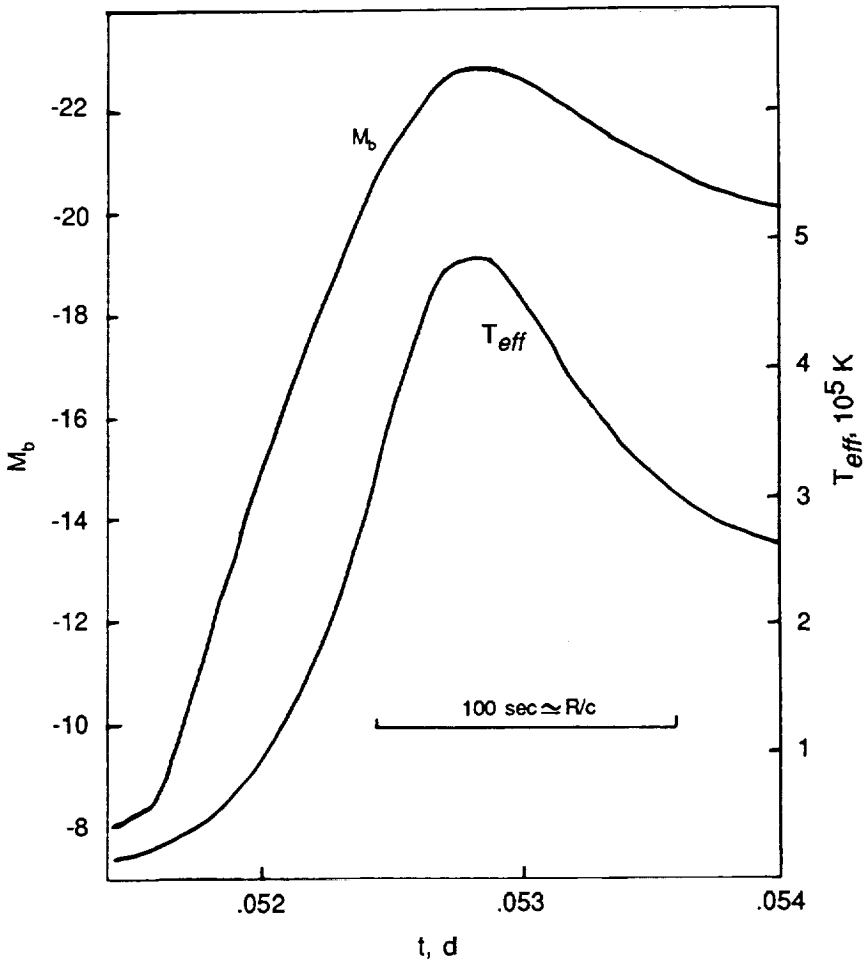


FIGURE 1 The bolometric magnitude $M_b$ and the effective temperature $T_{eff}$, defined as the matter temperature at $\tau = 0.64$, for the epoch of shock breakout.

becomes less than 15, and all of the 150 radial zones are treated with the non-equilibrium radiative transfer.)

Figure 3 displays the evolution of the emergent spectrum. The spectrum is almost black-body, but we wish to point out that it is *not assumed* to be black-body. It is the result of our calculation with the simplified assumption of "grey" opacity and the crude treatment of the Compton effect.

The most important qualitative difference of these new calculations from the results obtained in equilibirum diffusion approximation is the

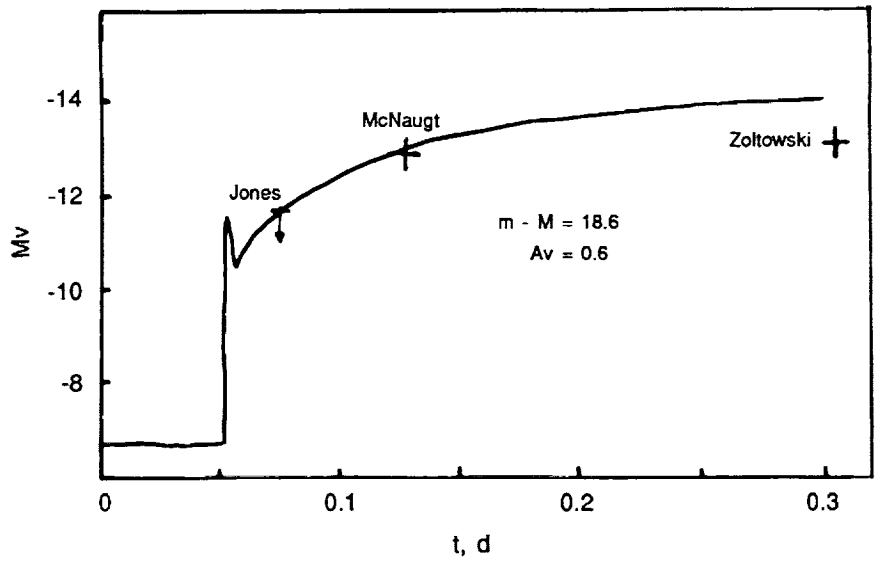


FIGURE 2 The absolute visual magnitude and the earliest observations of SN1987A.

formation of a dense peak (with the density contrast of 30-100 times) in the outermost layers of a compact star (see Figure 4). Such a peak was also discovered by Falk and Arnett (1977), by Chevalier and Klein (1979) and for more extended models by Grasberg and Nadyozhin (1969). Contrary to Chevalier and Klein (1979), the radiative acceleration of matter outside the peak proves in our calculations to be fairly high, and a new high-temperature shock is therefore absent.

In Figure 4 we present the formation of the dense shell in Eulerian coordinates, and Figure 5 shows the structure of the outermost layers of SN1987A in Lagrangian coordinates for the moment when the density peak looks most prominent. The layer containing the density peak has a mass of about $2 \times 10^{-6}$ $M_\odot$ and the optical thickness $\tau \approx 10$. This is in excellent agreement with the analytical estimate of the parameters of the outermost layers, where the shock cumulation described by a self-similar solution has to be cut off (Imshennik and Nadyozhin, 1988, 1989). Thus, this calculation gives an example for a physically correct description of the region where the shock cumulation is saturated.

We may conclude that we have developed a workable method for the time-dependent, multi-group radiative transfer in the continuum. The first application of this method to SN1987A shows that the results of equilibrium diffusion modeling are basically true. One principal feature, not obtained with the equilibrium diffusion, is the formation of a dense shell. The

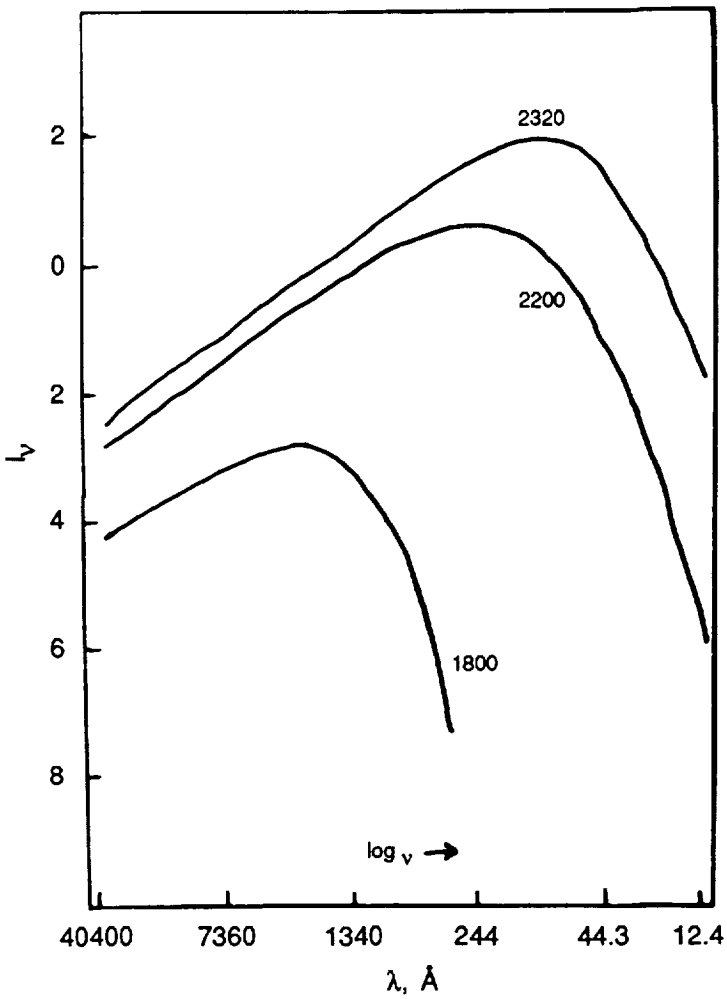


FIGURE 3 The dimensionless spectral intensity, labeled by the number of step. For steps 1800, 2200, and 2320 we have $T_{eff} = 16400, 229000, 480000$ K.

shell is certainly Rayleigh-Taylor and thermally unstable, and it should fragment into small blobs. Further calculations, with other parameters of presupernova models and more accurate treatment of the Compton effect and the influence of lines on the opacity, are expected to show how the shell properties and the emergent spectra can vary.

The described method has good prospects and is being used by us to solve various problems in the dynamics of exploding supernova envelopes and collapsing cores.

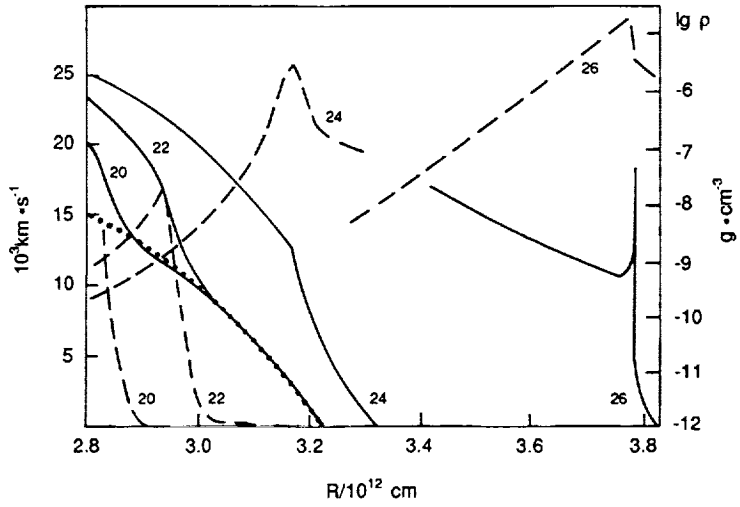


FIGURE 4 Density (solid lines) and velocity (dashed lines) for steps 2000 — 2600 (labeled by 20-26) in Eulerian coordinates.

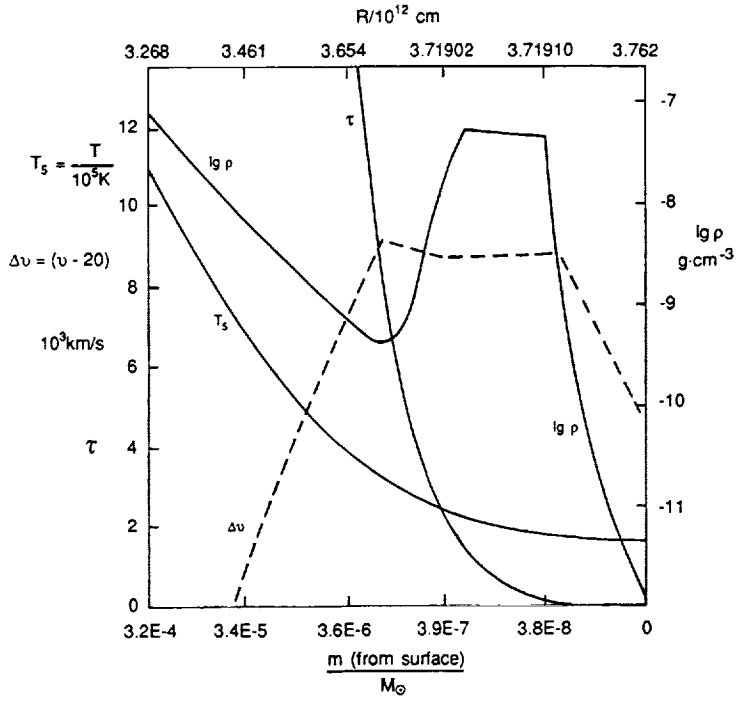


FIGURE 5 Distributions of density $\rho$, temperature T, velocity v, and optical depth $\tau$ near the edge of SN1987A envelope at time t = 4919 s (step 2600).

## REFERENCES

Arnett, W.D. 1987. Ap. J. 319: 136.
Blinnikov, S.I. 1988. Preprint ITEP No. 19.
Blinnikov, S.I., and M.A. Rudzskiy. 1984. Pis'ma Astron. Zh. 10: 363.
Bowers, R.L., and J.R. Wilson. 1982. Ap. J. Suppl. 50: 115.
Bruenn, S.W. 1985. Ap. J. Suppl. 58: 771.
Castor, J.I. 1972. Ap. J. 178: 779.
Chevalier, R.A., and R.I. Klein. 1979. Ap. J. 234: 597.
Falk, S.W., and W.D. Arnett. 1977. Ap. J. Suppl. 33: 515.
Feautrier, P. 1964. C.R. 252: 3189.
Gear, C.W. 1971. Numerical initial value problems in ordinary differential equations. Prentis Hall, Englewood Cliffs.
Grasberg, E.K., and D.K. Nadyozhin. 1969. Astron. Zh. 46: 745.
Grasberg, E.K., V.S. Imshennik, D.K. Nadyozhin, and V.P. Utrobin. 1987. Pis'ma Astron. Zh. 13: 547.
Imshennik, V.S., and Yu.I. Morozov. 1981. Radiation relativistic gasdynamics of high-temperature phenomena. (In Russian.) Atomizdat, Moscow.
Imshennik, V.S., and D.K. Nadyozhin. 1989. Sov. Sci. Rev. Sec. F, 8: Part 1,1.
Imshennik, V.S., and D.K. Nadyozhin. 1988. Pix'ma Astron. Zh. 14: 1059.
Mihalas, D., and B.W. Mihalas. 1984. Foundations of radiation hydrodynamics. Oxford University Press, New York, Oxford.
Myra, E.S., S.A. Bludman, Y. Hoffman, I. Lichtenstadt, N. Sack, and K.A. Van Riper. 1987. Ap. J. 318: 744.
Nadyozhin, D.K., and T.L. Razinkova. 1986. Nauchnye Inform. 61: 29.
Shigeyama, T, K. Nomoto, M. Hashimoto, and D. Sugimoto. 1987. Nature. 328: 320.
Utrobin, V.P. 1989. Pis'ma Astron. Zh. 15: 99.
Woosley, S.E., P.A. Pinto, and L. Ensman. 1988. Ap. J. 324, 466.

# Manifestations of Dynamo Driven Large-Scale Magnetic Field in Accretion Disks of Compact Objects

G.D. CHAGELISHVILI, R.G. CHANISHVILI, J.G. LOMINADZE,
AND Z.A. SOKHADZE
Abastumani Astrophysical Observatory

**ABSTRACT**

Many observations, as well as the possible theoretical explanations of these observations, indicate that the existence of mean (large-scale) magnetic fields in the majority of astrophysical objects is determined by the turbulent dynamo action. The magnetic field generation sources in the turbulent dynamo mechanism are the differential rotation of the medium and the gyrotropic character of the turbulence, existing in this medium (Moffatt 1978; Vainstein *et al.* 1980; Krause and Radler 1980). In the accretion disks of the compact objects the matter is moving due to the Kepler law, i.e. the rotation has a strong differential character. That is why one can suppose that in the convectively active regions of these objects the especially favorable conditions for the large-scale magnetic field generation are realized. In fact, the generation of the large-scale magnetic field in turbulent dynamo theory depends on the value of the so-called dynamo number (Moffatt 1978), determined by the parameters of the medium and turbulence. In the case of the accretion disk, these parameters have such values that when there is a thermal convection, the large-scale magnetic field is generated without any difficulties. The maximum value reached by the magnetic field is determined by nonlinear phenomena, i.e. by suppression of the sources of generation by the magnetic field itself (in the case of the accretion disk it is a suppression of the helical character of turbulence (Chagelishvili *et al.* 1986). The turbulent dynamo nonlinear theory developed by us (Chagelishvili *et al.* 1986, 1988) shows that in the compact objects of accretion disks, the generated large-scale magnetic field (when the generation takes place) has a practically toroidal configuration.

Its energy density can be much higher than turbulent pulsations energy density, and it becomes comparable with the thermal energy density of the medium. On the basis of these constantations the manifestations to which the large-scale magnetic field can lead at the accretion onto black holes and gravimagnetic rotators respectively are presented.

In particular, it is shown below that at the accretion onto the black holes, the dynamical activity of the strong toroidal, large-scale magnetic field as a result of the Parker instability development, in the disk, maximum energy release region, can create such formations (hot, optically thin coronaes) which can explain, for example, the Cyg X-1 spectrum and radiation specifications in the low state of this source.

It is also shown below that at the disk accretion of the magnetized plasma onto an aligned gravimagnetic rotator, the existence of two magnetic fields of different origin in the system leads to the asymmetric accretion of the matter. The accretion mainly takes place selectively onto one of the magnetic poles depending on the co-rotation and Alfven radii ratio.

## BIMODAL ACCRETION ON CYGNUS X-1

Turbulence in accretion disks may be caused by the differential character of matter rotation on Keplerian orbits and/or by the existence of a superadiabatic pressure gradient across the disk (when it does exist). The kinds of turbulence corresponding to these two factors are called shear and convective turbulence, respectively. Both kinds of turbulence can create an anomalous viscosity, transporting angular momentum outwards through the disk and thus causing an accretion. However, there is a basic difference between these kinds of turbulence, which account for the bimodal character of accretion in Cyg X-1. This difference is the following: shear turbulence is mainly two-dimensional and has no gyrotropic character, while convective turbulence is especially three-dimensional and of gyrotropic character. Therefore, convective turbulence in a differentially rotating accretion disk generates helicity and leads to amplification of large-scale magnetic fields (Chagelishvili *et al.* 1986). Thus, unlike shear turbulence, convective turbulence may make an accretion disk magnetically active, but only if there exists a large-scale magnetic seed field which is not too small. On this property of convective turbulence along the bimodal accretion, the model for Cyg X-1 (Chagelishvili *et al.* 1986, 1988) is founded. It predicts, for a "low" state, the formation of hot magnetic arcs: the very inhomogeneities which are able to create MV for this source.

The model assumes (Chagelishvili *et al.* 1986, 1988) a variation of the accretion rate $\dot{M}$ in a certain interval $(\dot{M}_1, \dot{M}_2)$ and the existence of some critical rate $\dot{M}_{cr}$ in it. (Here $\dot{M}_{cr}$ has nothing in common with the critical Eddington accretion rate). Shear turbulence definitely exists in the whole

accretion disk (Chagelishvili *et al.* 1988), but convective turbulence is only inherent to the inner[1] radiation-dominated region of the accretion disk and is always absent in the outer region. Thermal convection is also absent in the middle region if $\dot{M} > \dot{M}_{cr}$, and for $\dot{M} < \dot{M}_{cr}$ the parameters of the region are such that it becomes unstable against thermal convection; that is, the middle region becomes convectively active.

This is the very circumstance that makes the accretion disk magnetically active and switches Cyg X-1 to the "low" state. But how does it actually happen?

Originally a magnetic field is carried to the disk by the matter coming from the optical component of the binary system. A part of this field, being large-scale, may be considered as a seed field for the processes described by the turbulent dynamo equations. In the outer region where helical turbulence is absent (there is no thermal convection), the large-scale magnetic field decreases because of the turbulent diffusion arising from the shear turbulence. If thermal convection in the middle region is still absent ($\dot{M} > \dot{M}_{cr}$), the decrease of the large-scale field transported through by the matter is not able to supply the inner region of the disk with a sufficiently strong large-scale magnetic field. As a result, in spite of the fact that the large-scale magnetic field is generated in the inner, convectively active region of the disk, estimations show (Chagelishvili *et al.* 1986) that it does not have time to increase up to perceptible values, and accretion goes on without a large-scale magnetic field, mainly in accordance with the standard model. Thus, we can say that when $\dot{M} > \dot{M}_{cr}$, Cyg X-1 is in a "high" state.

When $\dot{M} < \dot{M}_{cr}$, thermal convection appears in the middle region of the disk and the generation of a large-scale magnetic field has already begun here long before the matter comes to the inner region. It should be emphasized that the generated large-scale magnetic field is virtually azimuthal (Chagelishvili *et al.* 1986). Under such conditions, the magnetic forces become stronger in the region of the main energy release of the disk and have a real influence on the matter dynamics. Namely they give rise to a Parker instability—rather oblonged parts of some magnetic tubes emerge out of the main volume of the disk, forming arcs of decreased density above it. At the same time the greater part of the magnetic tube matter sinks toward the central plane, forming "clots" situated between the arcs (see Figure 1). The study of Parker instability in the inner region of an accretion disk made by Chagelishvili *et al.* (1988) shows that in the process

[1] It is well known that depending on the nature of opacity (compton scattering $K_{es}$, or free-free transitions $K_{ff}$) and on the ratio of the gas pressure to the radiation pressure $P_g/P_r$), there may be three regions in an accretion disk (Shakura and Sunyaev 1973): an outer region ($K_{es} \ll K_{ff}$; $P_g/P_r \gg 1$), a middle region ($K_{es} \gg K_{ff}$; $P_g/P_r \gg 1$), and an inner region ($K_{es} \gg K_{ff}$; $P_g/P_r \ll 1$).

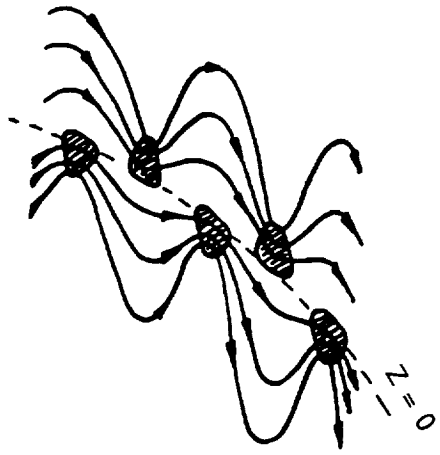


FIGURE 1 Schematic geometry of the disk inner region in the cross section r = const at the Parker instability development. Shaded regions present clusters of concentrated gas. Solid curves with arrows are magnetic lines formed from the initial azimuthal magnetic field.

of instability development, mainly with maximum growth rate perturbations that have no Z → -Z reflection symmetry are amplified (see Figure 1).

The action of Parker instability described above must be considered as a quasiperiodical process. We assume that magnetic flux tubes emerging in the region of the main energy release are heated, forming a hot, optically thin corona. The latter is made up of several magnetic arcs which are connected with the main disk and are sweeping inward in the process of matter accretion. Then the magnetic flux tubes emerge once again and the cycle continues. At any subsequent time, the magnetic flux tube may emerge at a different distance from the black hole.

Thus we propose that a number of these magnetic arcs of decreased density form, due to heating, the hot, optically thin corona so necessary for explaining the power-law spectrum of Cyg X-1 in the "low" state. Such a spectrum is generated in the arcs by comptonization of soft X-ray photons emitted by dense clusters of relatively cold plasma between and under the arcs in the vicinity of the equatorial plane of the disk (see Figure 1). The corona made up of these magnetic arcs will cover only a part of the colder "core" which, in fact, is indirectly confirmed by some observations of Cyg X-1 (Sunyaev and Truemper 1979).

We hold that macroscopic magnetic arcs rapidly rotating in the region of the main energy release are the very "hot spots" necessary to explain millisecond variation phenomena in a "low" state.

# ASYMMETRIC DISK ACCRETION ONTO MAGNETIZED ROTATING COMPACT STARS

The phenomena, occurring at disk accretion onto magnetized rotating compact stars in all their diversity, have been studied since the early 1970s. They have been collected and classified in the books of Shapiro and Teukosky (1983) and Lipunov (1987). The completeness of the research is limited as they considered only the non-magnetized disks, i.e., the cases of the accretion disks without the magnetic field, which can really influence the interaction processes of the accreting gas and compact star's magnetic field. First of all it is relevant to the processes taking place on the Alfven surface. In fact, as the researchers say, under certain conditions (the existence of the convective turbulence of hyrotropic nature in the larger part of the disk) the case where the disk has the large-scale magnetic field generated as a result of the turbulent dynamo action is realized. The field obtained thus is mainly of toroidal configuration (Chagelishvili *et al.* 1986) and is capable of mounting to the meaning where the magnetic pressure of the disk becomes comparable with its thermal pressure (Chagelishvili *et al.* 1986). In other words, it becomes comparable with the compact star magnetic pressure on the Alfven surface. It is easy to understand that this circumstance will radically change the accreting gas penetration ways and means into the star magnetic pole. To be more specific, the strong toroidal magnetic field of a disk will prevent the interchange instability and thus will exclude the scenario of plasma penetration into the magnetosphere developed in papers by Ghosh and Lamb (1979a,b).

The peculiarities of the accretion at a magnetized disk are revealed in the most simple and, consequently, the most easily observed case which we are going to consider: a compact star, whose rotation and magnetic axes coincide (let us direct these axes along z-coordinate). We shall idealize a compact magnetized star as a gravimagnetic rotator with three characteristics: mass, magnetic dipole moment, and rotational moment. Such an object can serve as the model for absolutely different astophysical objects: neutron stars, white dwarfs, magnetic stars and spinars—the supermassive stars. Let us consider that this magnetized thin accretion disk is in the equatorial plane of the star. Moreover, let us suppose the equilibrium rotation of the compact star to be almost achieved (Lipunov 1987): on the Alfven surface the accreting plasma almost corotates with the field lines of the star's magnetic field. This occurs when the Alfven ($R_A$) and corotation ($R_C$) radii are close to each other: $R_A \simeq R_C$. As is known (Lipunov 1987) the similar corelation between these radii is quite widespread and that is why when considering it, one can hope that we encompass the most interesting cases. Besides, it is especially easy to describe the field lines

reconnection process of the rotator and the accretion disk magnetic fields while observing the above-mentioned ratio.

Let us note that the change of the dipole magnetic field direction into the opposite one, in the case of non-magnetized plasma disk accretion in the align rotator, does not influence the accretion physics: the physical processes are symmetrical relatively to the equatorial plane. But in our case the existence of two magnetic fields of different origin, the accretion disk toroidal field ($B_\varphi$) and the rotator dipole field ($B_D$), in the system leads to the occurrence of asymmetry (relative to z-axis) in the direction of the physical phenomena, and this asymmetry is determined by the $B_\varphi$ and $B_D$ mutual orientation. Namely, the manifestation of this asymmetry is such a circumstance when the plasma accretion will take place mainly to one of the rotator magnetic poles and not to both. The accretion will be asymmetrical in the case discussed by us and that, by all means, should adequately describe the observational manifestations of such systems. Concretely, the reason for this asymmetry is the following: the star and the accretion disk magnetic fields are crossed. This fact promotes their reconnection on the Alfven surface and the latter promotes the formation of the "channels" (see Figure 4). The accreting plasma "slips" along the "channels" mainly to one of the two magnetic poles of the rotator.

Let us discuss the reconnection process in detail. The reconnection of the magnetic field lines takes place as a result of the tearing-mode instability development (Furth *et al.* 1963; Lee and Fu 1985; Southwood *et al.* 1986) in similar situations. In our case the dissipative effects are insured by the disk turbulence (Chagelishvili *et al.* 1986) that leads to the Reynolds magnetic numbers $R_m \simeq 10^2 \div 10^3$. The mathematic methods of the tearing mode instability research are quite non-trivial. However, the information necessary for the qualitative description of the field lines behavior during the reconnections on the Alfven surface can be extracted from the papers (Furth *et al.* 1963; Lee and Fu 1985; Southwood *et al.* 1986). In accordance with them the field line dynamics can be schematically presented as follows.

Figure 2 presents the align rotator ($B_D$) and the accretion disk ($B_\phi$) field lines on the Alfven surface separately from each other. The bold lines present the regions, which are magnified in Figure 3 and where the reconnection physics is described. The reconnection of the crossed field lines occurs at the nodal points (Figure 3a) during the characteristic time ($\tau \simeq R_m^{1/2}/\Omega$) where $\Omega$ is the star rotation angular velocity (Furth *et al.* 1963), which is less than the accretion time. The further dynamics of the field lines, resulting in paths formation, is presented in Figures 3(b) and 3(c). Figure 4 shows one of the field tubes, formed as a result of the above processes. The configuration of the given field lines in the equatorial region is such that the matter, included and frozen into it, receives the impulse in the z-direction and "slips" to the upper magnetic pole if the Kepler

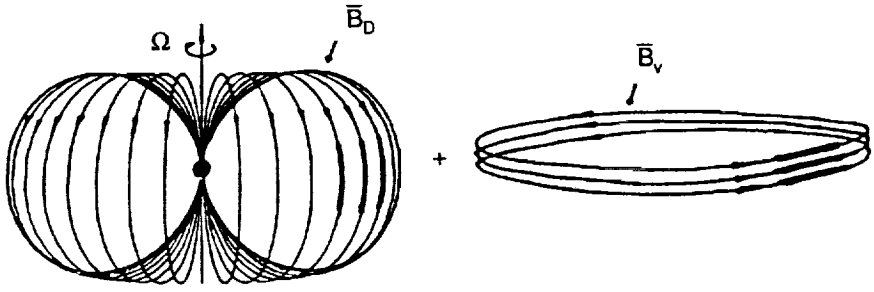


FIGURE 2 The align rotator ($B_D$) and the accretion disk ($B_\phi$) field lines on the Alfven surface separately from each other. The bold lines present the regions, which in Figure 3 are magnified and where the reconnection physics is described.

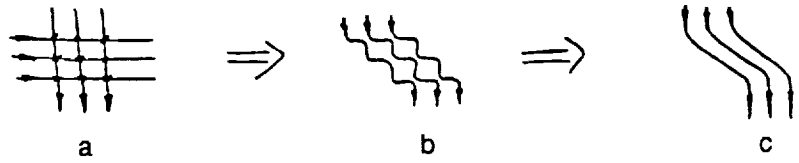


FIGURE 3 The crossed field lines reconnection dynamics.

rotation velocity of the matter in a disk is higher than $\Omega R_A$ on the Alfven radius. In other words, it occurs when $R_C > R_A$ (i.e. when $R_C/R_A - 1 > 0$). Naturally, the "slip" of the matter to the lower magnetic pole will take place at $R_C < R_A$ observance (see Figure 4). We want to reiterate that we discuss the case when $R_A$ and $R_C$ are close to each other, as only in this case the Kepler rotation of the matter does not change the tearing-mode instability development, described in papers by Furth *et al.* (1963); Lee and Fu (1985); and Southwood *et al.* (1986).

This paper has carried out the qualitative analysis of the accretion onto the align gravimagnetic rotator. But it is easy to understand that the main character of the accretion—the asymmetry—will be preserved at the disk accretion of the magnetized plasma ($B\phi \neq 0$) onto the oblique gravimagnetic rotator as well.

Finally we enumerate those observational manifestations to which the above-described accretion can lead due to the asymmetry:

- if such a system is capable of generating jets, then they will be observed only in one direction;
- even the slightest change of the accretion rate can lead to the $R_C/R_A - 1$ sign change. That will lead to the fact that the other pole will become accreting. Taking into account that the Alfven radius may

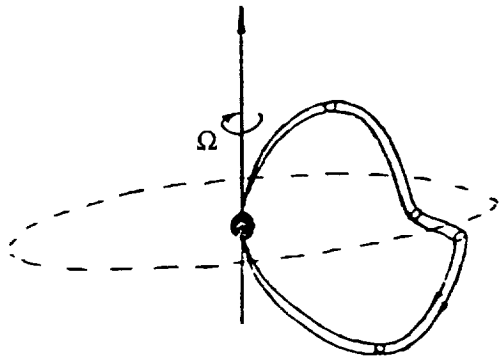


FIGURE 4 One of the field tubes, formed as a result of the connection processes.

be hundreds of times bigger than the radius of the star itself, the above-mentioned will significantly effect the radiation of the given source directed towards the observer. It may become, for example, the explanation of the variability of some transients;

- even a weak quasispheric component always exists in the accreting flow, even at disk accretion on compact objects. That is why in the case considered by us, at least a weak flow of matter is always directed at the non-accreting magnetic pole. Supposing the neutron star to be a compact object, if the pressure of the electromagnetic radiation and the one of the relativistic particles ejected from the polar cap are sufficiently high, then the accreting matter from the above-mentioned quasispheric component is "swept" out of the capture region or out of the light cylinder limits. Then the non-accreting magnetic pole will be an ejector, similar to the single magnetized neutron star.

## REFERENCES

Chagelishvili, G.D., R.G. Chanishvili, and J.G. Lominadze. 1986. Pages 563-568. J.G. Proc. of Joint Varenna-Abastumani Intern. School and Workshop. Sukhumi, USSR (ESA SP-253).

Chagelishvili, G.D., J.G. Lominadze, and Z.A. Sokhadze. 1986. Pages 523-529. Proceed. of Joint Varenna-Abastumani Intern. School and Workshop. Sukhumi, USSR (ESA SP-251).

Chagelishivili, G.D., G.D. Chanishvili, and R.G. Lominadze. 1988. Advanced Space Research. 8(2):216.

Chagelishivili, G.D., G.D. Chanishvili, and J.G. Lominadze. 1988. Ap. Space Sci. 141:361.

Furth, H.P., J. Killen, and M.N. Rosenbluth. 1963. Phys. Fl. 6: 459.

Ghosh, P., and F.K. Lamb. 1979. Ap. J. 232:256.

Ghosh, P., and F.K. Lamb. 1979. Ap. J. 234:296.

Krause, F., and K.H. Radler. 1980. Mean field magnetohydrodynamics and dynamo theory, Pergamon Press.

Lee, L.C., and Z.F. Fu. Geophysical Research Lett. 1985. 12: 105.

Lipunov, V.M. 1987. Astrophysics of neutron stars. Nauka, Moscow.

Moffatt, H.K. 1978. Magnetic field generation in electrically conducting fluids. Cambridge University Press.
Shakura, N.I., and R.A. Sunyaev. 1973. Astr. Ap. 24:337.
Shapiro, S.L., and S.A. Teukolsky. 1983. Black holes, white dwarfs, and neutron stars. John Wiley and Sons, New York.
Southwood, D.J., M.A. Sounders, M.W. Dunlop, W.A.C. Mier-Jedrzejowicz, and R.P. Rijnbeek. 1986. Planet. Space. Sci. 34:1349.
Sunyaev, R.A., and J. Trumper. 1979. Nature. 279:506.

# Turbulization of Shear Flows in Astrophysics

G.D. CHAGELISHVILI, R.G. CHANISHVILI, AND J.G. LOMINADZE
Abastumani Astrophysical Observatory

## INTRODUCTION

According to a most widely spread representation (Shakura and Sunyaev 1973; Pringle 1981; Liang and Nolan 1984), the disk accretion phenomenon is based on the anomalous transport of the accreting matter angular momentum outward due to turbulent viscosity. It is also the turbulence which provides such an accretion law that a bulk of released gravitational energy of the accreting matter in the disk thermalizes, and as a result, is emitted and provides the observed X-ray spectrum for some binary sources. Consequently, the investigation of the turbulence emergence in accretion disks is a problem of paramount importance (of course, to elucidate the possibility of turbulization of other shear flows in astrophysics is also important).

Turbulence can be created in accretion disks by a superdiabatic pressure gradient across a disk (in the regions where such a gradient exists) and by differential rotation of the matter, i.e. by a shear of angular velocity in the Keplerian rotation of the matter, $\Omega \sim r^{-3/2}$ (Shakura *et al.* 1978). The superadiabatic pressure gradient resulting in thermal convection is characteristic of only some parts of the accretion disk (Taylor 1980; Lominadze and Chagelishvili 1984; Chagelishvili *et al.* 1986). Therefore, in the other parts of the disk the presence of the turbulence can be ensured only by the shear instability. The problem of instability in shear flows is treated in quite a number of works (Narayan *et al.* 1987). They give us a global analysis of irrotational (potential) modes in a two-dimensional compressible shear flow, implying that, in the presence of reflecting boundaries, those modes can increase and that the characteristic time of the increase

is several orders as high as the dynamic time in the medium. Due to the slowness of the increase of irrotational modes and to the problematical character of the theory's applicability as presented in Narayan *et al.* (1987) for thin accretion disks, we have tried to develop an alternative theory of turbulization shear flows. It is quite contrary to the above theory. Instead of the global analysis, we make a local one, far from the flow boundaries. Instead of the irrotational perturbations, we examine vortical ones. Lastly, we consider the medium to be incompressible. To gain our aim, the flow in the accretion disk can be modeled by a plane Couette flow, without regard for boundary conditions: it can be modelled by a plane shear flow in infinite incompressible fluid. According to the present scenario, there is a critical perturbation level in the free shear flow. If the level of initial perturbations exceeds the critical one, the flow is turbulized.

We must particularly emphasize that the flow can only be turbulized by non-potential (vortex) perturbations. The fact that the turbulization comes at finite initial perturbations is explained by the non-ordinary nature of the temporal evolution of the vortex perturbations at the linear stage. Such a non-ordinarity for some astrophysical phenomena was found for the first time in the work of Lominadze *et al.* (1988). The distinguishing feature of their analysis, as well as of Goldreich and Linden-Bell (1965), is that the linear equations are integrated in a co-moving coordinate system with moving axes ($X_1OY_1$). That is to say that two local coordinate systems are used to analyze equations (see Figure 1): a Cartesian one (XOY) with the Y-axis pointing the velocity direction and X-axis directed orthogonally, along the shear of the velocity, and another system, with moving axes ($X_1OY_1$). The $Y_1$-axis is parallel to the Y-axis, and the $X_1$-axis moves together with the unperturbed flow. (The relation between (x,y) and ($x_1$,$y_1$) coordinates is given by equation (4)). The idea of the paper is as follows: equations are projected onto the Cartesian coordinate system axes. Then we substitute the variables using equation (4) so as not to change the sense of the projection of the physical quantities. That is, we do not make a physical transition from the XOY frame to the $X_1OY_1$, but a formal substitution of variables that makes the analysis easier. In fact, the linear theory equations (6)-(8) written in the terms of the new variables $x_1$ and $y_1$ are uniform in regard to them (but they are already not uniform in regard to time). So, expanding a perturbance into Fourier modes in regard to $x_1$ and $y_1$, one can follow separately the temporal evolution of every Fourier mode. After returning to the former coordinates, we can see that besides the time variation of every Fourier mode amplitude, there is variation of its wave number along the X-axis in the direction of the velocity shear of the main flow (see equation (19)). There is a pecularity in the temporal evolution of the Fourier modes: the evolution law is not exponential, but power one (see equation (18)). The growth can take place

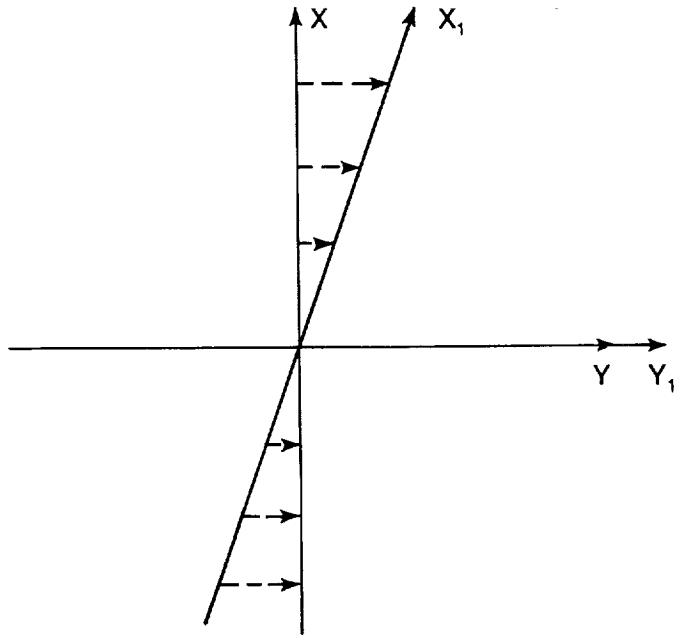


FIGURE 1 The local Cartesian coordinate system XOY and the system with moving axes $X_1OY_1$ are presented. The dashed arrows show the direction of the main flow velocity $\vec{U}_o$ at different distances from the Y-axis. $\vec{U}_o(0,U_{oy},0)$; $U_{oy} = Ax$; $A > 0$. $X_1$-axis moves together with the shear flow.

when $t^* \equiv k_x(t)/k_yA > 0$, and where $k_x(t)$ and $k_y$ are wave numbers of the Fourier modes under consideration along the velocity shear and the main stream velocity, respectively, but in the XOY coordinate system. A is a characteristic parameter of the velocity shear ($U_{oy} = Ax$). When writing the wave number $k_x(t)$ we especially emphasize the time dependence to stress that the spatial scale of Fourier modes varies in time along the X-axis. We must also stress that the Fourier expansion was done in terms of the variables $x_1$ and $y_1$ (see equation (9)), $k_x(t)$ and $k_y$ being the wave numbers of those Fourier modes in the XOY system.

From the condition $k_x(t)/k_yA > 0$ and equation (18) one can see that, according to linear theory, the growth time of every Fourier mode is limited. At first a Fourier mode draws on energy from the main flow and grows; after some time $k_x(t)$ changes its sign, and the growth of the Fourier modes turns into weakening: they "return" the energy back to the main flow.

It follows from the above that the possibility of turbulization of free

shear flows is ambiguous. Indeed, if you start from infinitesimal perturbations, you may assume that because of a limited growth time of Fourier harmonics they will not grow up to non-linearity, that is, up to such values where non-linear effects come into play. So the evolution of the perturbation will be purely linear, and it will disappear "without a trace:" with no turbulization in the media. But if the level of initial perturbations in the media is not too small, then at a certain stage of increase of the Fourier harmonics, non-linear (cascade) processes come into play that can provide turbulization of the flow.

## LINEAR THEORY OF PERTURBATION

Let us consider the linear theory of the temporal evolution of two-dimensional perturbances in a plane, free-shear flow of incompressible fluid. To get the growth effect alone, let us first consider a nonviscous fluid. Allowance for viscosity won't be too difficult, so our result will be generalized for the case of a viscous fluid (see below).

Let us direct the Y-axis of the Cartesian coordinate system along the main flow velocity $\vec{U}_o$ (O,$U_{oy}$, O), and the X-axis along the shear of the flow velocity $U_{oy}$ = Ax (see Figure 1). Considering the problem to be two-dimensional, we write the equations of continuity and motion for the perturbed quantities:

$$\frac{\partial u_x}{\partial x} + \frac{\partial u_y}{\partial_y} = 0, \tag{1}$$

$$\{\frac{\partial}{\partial_t} + Ax\frac{\partial}{\partial y}\}u_x = -\frac{\partial P}{\partial x}, \tag{2}$$

$$\{\frac{\partial}{\partial_t} + Ax\frac{\partial}{\partial y}\}u_y + Au_x = \frac{\partial P}{\partial y}, \tag{3}$$

where $u_x$ and $u_y$ are the components of the perturbance velocity in the Cartesian coordinate system, P is the pressure perturbance normalized by the density of the matter $\rho$.

Now we introduce a coordinate system with moving axes $X_1OY_1$. Its origin and the $Y_1$-axis coincide with the respective characteristics of the XOY system; and the $X_1$-axis moves together with the undisturbed flow (see Figure 1). This is equivalent to the change in variables

$$x_1 = x; \quad y_1 = y - Axt; \quad t_1 = t, \tag{4}$$

or

$$\frac{\partial}{\partial x} = \frac{\partial}{\partial x_1} - At_1 \frac{\partial}{\partial y_1}; \quad \frac{\partial}{\partial y} = \frac{\partial}{\partial y_1}; \quad \frac{\partial}{\partial t} = \frac{\partial}{\partial t_1} - Ax_1 \frac{\partial}{\partial y_1} \tag{5}$$

With the new variables, equations (1)-(3) take on the form

$$\left(\frac{\partial}{\partial x_1} - At_1 \frac{\partial}{\partial y_1}\right) u_x + \frac{\partial U_y}{\partial y_1} = 0, \tag{6}$$

$$\frac{\partial u_x}{\partial t_1} = -\left\{\frac{\partial}{\partial x_1} - At_1 \frac{\partial}{\partial y_1}\right\} P, \tag{7}$$

$$\frac{\partial u_y}{\partial t_1} + Au_x = -\left\{\frac{\partial}{\partial y_1}\right\} P. \tag{8}$$

As it was already noted in the introduction, the substitution of the variables (4) is not a physical transition to the new frame, because in equations (6)-(8), as well as in equations (1)-(3), the quantities $u_x$ and $u_y$ are components of the perturbation velocity in a Cartesian coordinate system. The coefficients of the initial linear equation system (1)-(3) depended on the space coordinate x. After our transformations, this inhomogeneity was changed into a time inhomogeneity. So we can perform a Fourier analysis of equations (6)-(8) in respect to the variables $x_1$ and $y_1$:

$$\begin{Bmatrix} u_x \\ u_y \\ P \end{Bmatrix} = \iint_{-\infty}^{+\infty} dk_{x_1} dk_{y_1} \begin{Bmatrix} \tilde{u}_x(k_{x_1}, k_{y_1}, t) \\ \tilde{u}_y(k_{x_1}, k_{y_1}, t) \\ \tilde{p}(k_{x_1}, k_{y_1}, t) \end{Bmatrix} \exp(ik_{x_1} x_1 + ik_{y_1} y_1) \tag{9}$$

Substituting expansion (9) into equations (6)-(8), we obtain

$$(k_{x_1} - k_{y_1} At_1) u_x + k_{y_1} u_y = 0 \tag{10}$$

$$\frac{\partial u_x}{\partial t_1} = -i(k_{x_1} - k_{y_1} At_1) P, \tag{11}$$

$$\frac{\partial u_y}{\partial t_1} + Au_x = -ik_{y_1} P, \tag{12}$$

Solving equation system (10)-(12), say, for velocity, we get

$$u_x(k_{x_1}, k_{y_1}, t_1) = u_x(k_{x_1}, k_{y_1}, 0) \frac{(k_{x_1}/k_{y_1})^2 + 1}{(k_{x_1}/k_{y_1} - At_1)^2 + 1} \tag{13}$$

$$u_y(k_{x_1}, k_{y_1}, t_1 = u_y(k_{x_1}, k_{y_1}, 0) \frac{[(k_{x_1}/k_{y_1}\}^2 + 1](1 - At_1 k_{y_1}/k_{x_1})}{(k_{x_1}/k_{y_1} - At_1)^2 + 1}, \tag{14}$$

$$u(k_{x_1}, k_{y_1}, t_1) = \{u_x^2 + u_y^2\}^{\frac{1}{2}} =$$

$$u(k_{x_1}, k_{y_1}, 0)\left[\frac{\{k_{x_1}/k_{y_1}\}^2 + 1}{\{k_{x_1}/k_{y_1} - At_1\}^2 + 1}\right]^{\frac{1}{2}}. \tag{15}$$

As one can see from these formulae, only those Fourier harmonics of the initial perturbation grow the wave numbers of which satisfy the inequality

$$\frac{k_{x_1}}{k_{y_1}A} > 0, \tag{16}$$

and the growth takes place in time $t < t^*$, where

$$t^* \equiv k_{x_1}/k_{y_1}A \tag{17}$$

It must be stressed that the solutions obtained here exist when the initial vorticity is non-zero.

Using notation (17), we may write solution (13) in the form

$$u_x(k_{x_1}, k_{y_1}, t_1) = u_x(k_{x_1}, k_{y_1}, 0)\frac{A^2t^{*^2} + 1}{A^2(t^* - t)^2 + 1}. \tag{18}$$

As one can see from this formula, for $t^* \gg 1$ at first (as long as $A(t^* - t) > 1$) the growth of a Fourier harmonic is rather explosive: the growth rate of the perturbations greatly increases in time. However, it is only towards the end (when $A(t^* - t) \approx 1$ that the growth stops abruptly and (when $t > t^*$) a weakening follows (see Figure 2a).

We have performed Fourier analysis of perturbances for the variables $x_1$ and $y_1$ and followed the time evolution of Fourier harmonic amplitudes. What happens to Fourier harmonics in an ordinary space, i.e., in the Cartesian coordinate system (XOY)? Using equations (4) and (9) one can introduce a parameter that determines the characteristic linear dimension of each of the Fourier harmonics along the axis X and Y at every particular instant

$$k_x(t) = k_{x_1} - k_{y_1}At_1, \qquad k_y = k_{y_1}. \tag{19}$$

We can see from these formulae that the space scale along the X-axis of every Fourier harmonics under examination varies in time.

Viscosity plays an important role in many hydrodynamic flows, the more so in turbulization phenomena. For some astrophysical flows, the viscosity was considered in terms of Lominadze *et al.* (1988) in the work of Fridman (1989). Using the results of the latter work, we can easily

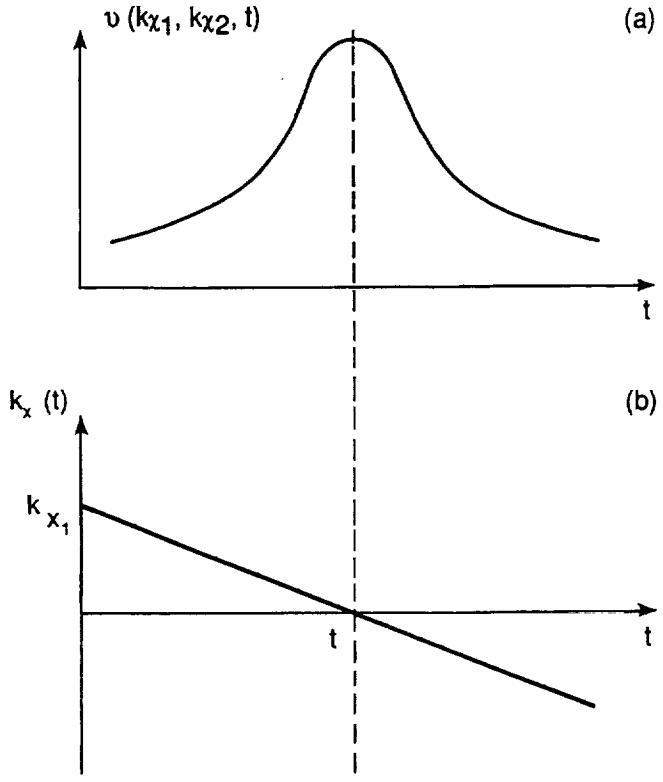


FIGURE 2 (a) Time evolution of the amplitude of a perturbation velocity Fourier harmonic. The graph is plotted in accordance with equation (15). (b) Time dependence of the spatial scale along the X-axis of Fourier harmonics increasing at initial time ($k_x(O)/k_y A > O$). The graph is plotted in accordance with equation (19).

generalize our solutions to a viscous fluid too. For instance, in the case of a viscous fluid equation (13) takes the form

$$u_x(k_{x_1}, k_{y_1}, t_1) = u_x(k_{x_1}, k_{y_1}, 0)\frac{k_{x_1}^2 + k_y^2}{k_x^2(t) + k_y^2} \exp$$
$$\left\{-\nu \int_o^t [k_x^2(t) + k_y^2]\, dt\right\}, \tag{20}$$

where $\nu = \mu/\rho$ is the kynematic viscosity. Naturally, viscosity impedes perturbation growth. For every specific $\nu$ one can find the minimum characteristic dimension of perturbations (maximal $k \equiv \sqrt{k_x^2 + k_y^2}$) at which Fourier harmonics can increase.

## QUALITATIVE SCENARIO OF TURBULIZATION

Let us now describe the processes which can lead, we presume, to turbulization of shear flows. Of course, such a process represents an aggregate of linear and non-linear phenomena. Let us assume that the linear phenomena proceed in accordance to the theory exposed in the previous section. Then any initial perturbation can be presented as a set of Fourier harmonics. For the following discussion it is convenient to introduce a notion of a $\vec{k}$-plane ($k_x O k_y$). Without a loss of generality, we shall also hold that $A > O$. Let us follow linear dynamics of Fourier harmonics. In addition to amplitude variations of Fourier harmonics, their characteristic scales vary in the direction of the velocity shear: along the X-axis (see equation (19)). This variation on the $k_x O k_y$ plane means a drift of Fourier harmonics in the direction shown by the arrows in Figure 3. The Fourier harmonics that satisfy condition $k_x(O)/k_y < O$ ($k_{x1}/k_y < O$), weaken. The Fourier harmonics that satisfy the condition $k_x(O)/k_y > O$ at first draw on energy from the main flow and increase, while $|k_x(t)|$ decreases. Each Fourier harmonics grows till $k_x(t)$ becomes zero (see Figure 2a and 2b). When it becomes zero, $k_x(t)$ reverses sign, as it follows from the linear theory, and the growth changes to weakening: the Fourier harmonic returns the energy back to the main flow. Hence it is clear that if non-linear phenomena do not come to play, any initial perturbations will disappear without leaving a trace.

A turbulence cannot exist without a permanent energy input from the main flow to perturbations. According to equation (16), when $A > O$, this takes place if there are Fourier harmonics with wave numbers corresponding to the first and third quarters of the $k_x O k_y$ plane (see Figure 3) which we shall refer to as a "growth area." But because of the drift of Fourier harmonics from the "growth area," the linear mechanism cannot provide a permanent input of energy from the main flow to the perturbation. Actually, if at the zero time ($t = 0$), in addition to weakening Fourier harmonics, we have a packet of increasing Fourier harmonics (the packet that fills the cross-hatched area in Figure 3), the packet will drift in the $k_x O k_y$ plane (I→II→III), so that in due time ($t = t''$) it will come to be outside the "growth area." Thus, later on the "growth area" will be empty and there will be nothing to draw energy with from the main flow.

What can the non-linear phenomena result in? They take no part in energy exchange with the main flow (Joseph 1976). But they redistribute energy among the Fourier harmonics. So the non-linear phenomena may return a part of the energy of the above packet back to the "growth area," as a result of the decay processes ($\vec{k}' + \vec{k}'' = \vec{k}$, see Figure 3). Then Fourier harmonics which are able to take energy from the main flow reappear and drift in the $k_x O k_y$ plane. It will be easily understood that if there is a

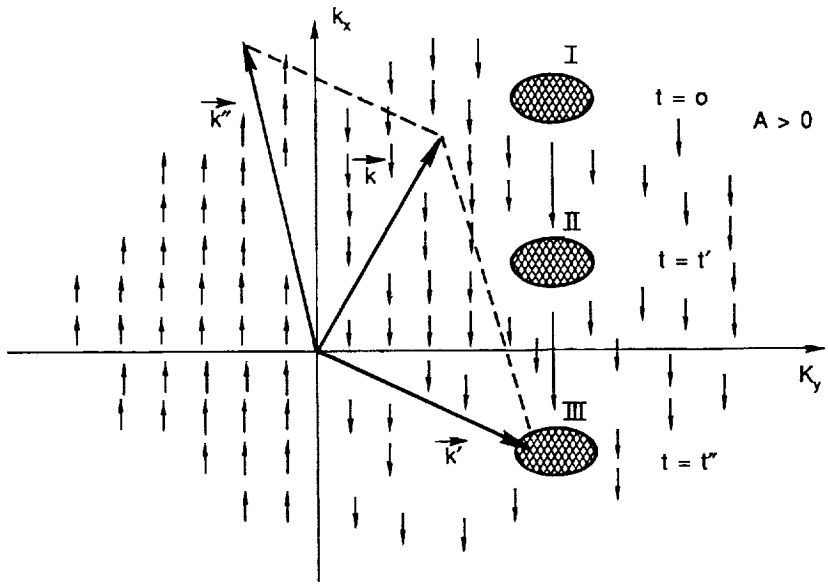


FIGURE 3 The short arrows show the directions of the drift of Fourier harmonics described in the linear theory in the k space (when A > O). A drift of Fourier harmonic packet filling cross-hatched area I in the k space (I→II→III) is shown. After some time (t = t''), the packet comes to be outside of the "growth area" ($k_x(t'')/k_y A < O$). An example of the decay process $\vec{k}' + \vec{k}'' = \vec{k}$ which can return a part of the perturbation energy back to the "growth area" ($k_x(t)/K_y A > O$) is given.

permanent non-linear return of a part of perturbations to the "growth region," the flow will be turbulized.

Thus the comparative analysis of linear and non-linear mechanisms gives us a general idea of the dynamics of Fourier harmonics and energy redistribution among them. What can be observed at small initial perturbations? Because of the linear drift, the Fourier harmonics will be driven out of the "growth area," and because of the smallness of the amplitude, the decay processes will be weak and will not be able to resist the permanent linear theory drift. As a result, the perturbation will be damped without inducing turbulization in the media. The higher the amplitude of initial perturbations, the stronger the effects of non-linearity. Finally, at a certain amplitude (which, of course, must depend on the initial perturbation spectrum and the value of the viscosity coefficient), the decay processes will be able to compensate the linear drift of the Fourier harmonics and ensure a permanent "drawing" of energy from the main flow and lead to the turbulization of the media. So, according to the present scenario, there

is a critical level for initial perturbations in the free shear flow. If the level of initial perturbations exceeds the critical one, the flow gets turbulized.

The local theory of turbulization of a plane Couette flow presented here can be applied not only to accretion disks, but to other shear flows in astrophysics, such as galactic disks, planetary rings, protostellar nebulae and possibly, to some rotating stars as well. We think that beyond astrophysical applications, this theory is a ray of hope for explanations of turbulization of some "earthly" hydrodynamic flows which are steady to infinitesimal perturbations but are turbulized by finite ones. Of course, our theory is qualitative and needs more rigorous mathematical formulation in order to be quite reliable: a theory of weak and strong turbulence is to be developed. We have developed a theory of weak turbulence, but the extent of calculations does not allow us to include it into the present paper. Here we only give the final equation of the theory of weak turbulence:

$$\frac{\partial E_k}{\partial t} - k_y A \frac{\partial E_k}{\partial k_x} - \frac{2k_x k_y A}{k_x^2 + k_y^2} E_k + \nu(k_x^2 + k_y^2) E_k = \frac{1}{A} \int_{-\infty}^{\infty} d\vec{k}' d\vec{k}'' \delta(\vec{k} - \vec{k}' - \vec{k}'').$$

$$\left(\frac{1}{k''^2 - k'^2}\right) \left(\frac{k_x'}{k_y'} - \frac{k_x''}{k_y''}\right)^2 \frac{k'^2 k''^2}{k^2} k_y'^2 k_y''^2 \left\{ \left[\psi(k_x'', k_y'', t) - \psi(k_x', k_y', t)\right] \right.$$

$$\left. \left\{ E_{K'} E_{K''} - 2 \frac{k^2}{k'^2} \frac{k_y'^2}{k_y^2} \left[\psi(k_x'', k_y'', t) - \psi(k_x, k_y, t)\right] E_K E_{K''} \right\} \right. . \qquad (21)$$

Here $E_k$ is the energy density of a Fourier mode of a perturbation with fixed $\vec{k}$, and

$$\psi = \frac{1}{k_y^2} \operatorname{arctg} \left\{ \frac{At}{1 + k_x/k_y(k_x/k_y - At)} \right\}.$$

## REFERENCES


Chagelishvili, G.D., R.G. Chanishvili, and J.G. Lominadze. 1986. Proceedings of the Joint Varenna-Abastumani International School and Workshop. Sukhumi, USSR, (ESA SP-251), p. 563.

Fridman, A.M. 1989. Pis'ma Astron. Zh., in press.

Goldreich, P., and D. Lynden-Bell. 1965. MNRAS 130:125.

Joseph, D.D. 1976. Stability of Fluid Motions. Springer Verlag, New York.

Liang, E.P., and P.L. Nolan. 1984. Space Sci. Rev. 38:353.

Lominadze, J.G., and G.D. Chagelishvili. 1984. Astron. Zh. 61:290.

Lominadze, J.G., G.D. Chagelishvili, and R.G. Chanishvili. 1988. Pis'ma Astron. Zh. 14:856.

Narayan, R., and P. Goldreich. 1987. MNRAS 288:1.

Pringle, J.E. 1981. Ann. Rev. Astron. and Astrophys. 19:137.

Shakura, N.I. and R.A. Sunyaev. 1973. Astron. and Astrophys. 24:337.

Shakura, N.I., R.A. Sunyaev, and S.S. Zilitinkevich.1978. Astron. and Astrophys. 62:179.

# Regular Variability of the Shape of the Primary Minimum of the Orbital Light Curve of SS 433 with the Phase of the Precessional Period

A.M. CHEREPASHCHUK AND S.F. YARLIKOV
Shternberg Astronomical Institute

The regular variations of the shape of the primary minimum of the orbital 13.082-day light curve of SS 433 with the phase of the 162.5-day precessional period have been discovered by analysis of the photometrical databank (1755 photometric V-observations during 1979 to 1988). These variations with the characteristic period of about 26 days appeared near the moment $T_3$ of the maximum separation of the moving emission lines. They are strongly connected with the phase $\psi$ of the precessional 162.5-day period (see Figure 1, where $\Delta\psi = 0^P.02$).

The variations within the period of approximately 26 days (see Figure 2) appeared and disappeared in asymmetry of the primary minimum of orbital light curve and in changing position of the primary minimum for $\Delta\psi_{13} \approx \pm\ 0^P.1$ ($\pm\ 1^d.3$) relatively the medium phase $\varphi_{13} = 0$ of orbital 13.082-day period. In view of the fact of such variations the averaging of observations in the primary minimum for the long interval of phases of the precessional 162.5-day period ($\Delta\psi \geq 0^P.1$) can lead to the false appearance of "plate bottom" on the light curve in the primary minimum.

The regular variability of the shape of the primary minimum of the light curve of SS 433 discovered by us reflects displacement with the 26-day double orbital period of at least two hot bright spots on the surface of precessional accretional disk and their eclipse by a "normal" star. One of these spots can be connected with the ejection of the relativistic collimated jet from the central part of the accretion disk; the second one perhaps is caused by interaction of gas stream coming from a "normal" star with an external border of the precessional accretion disk.

The precession of the accretion disk causes the change of the relative position of hot spots. Consecutive eclipses of the disk and spots by the "normal" star lead to the appearance and disappearance of asymmetry on

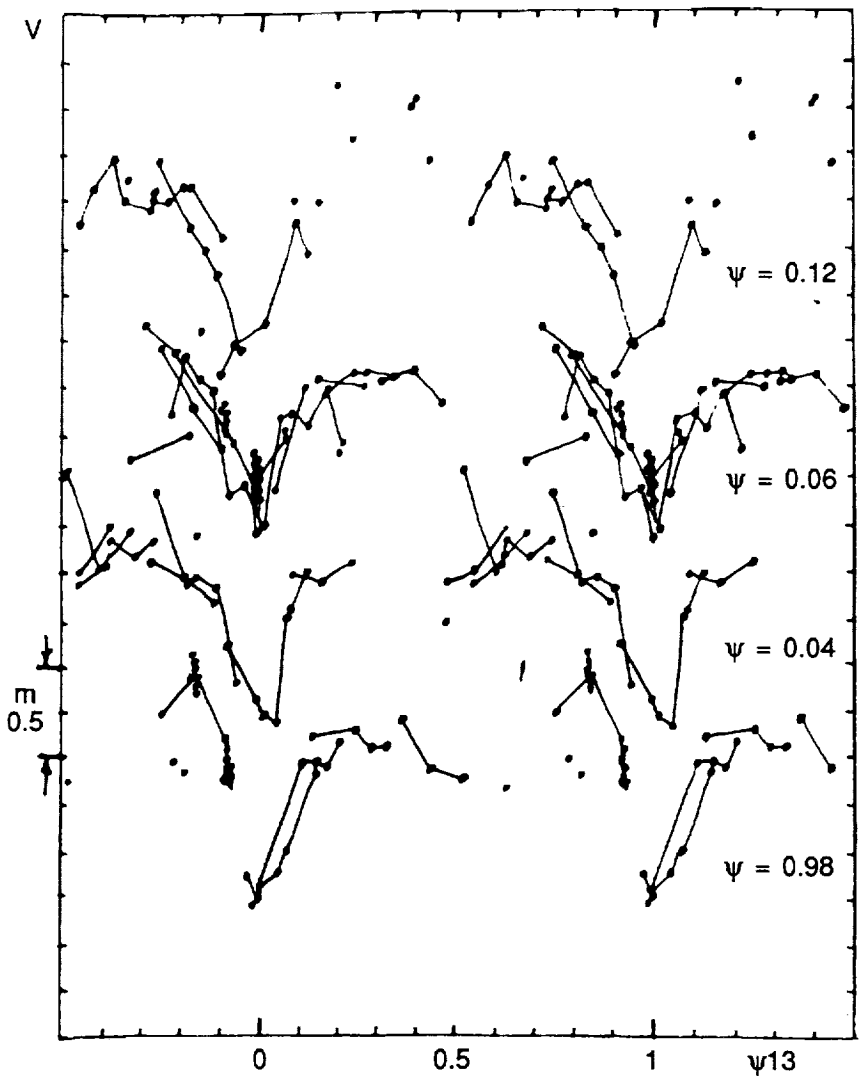


FIGURE 1 Optical orbital light curves of SS433 as a function of the precessional period $\psi$.

the curve of the eclipse and to the characteristic features on it just as it takes place in cataclysmic variable stars.

Quantitative numerical interpretation of the discovered effect will be completed in the future with the help of the light curve synthesis program (Antokhina and Cherepashchuk. 1987. Astron. Zh. 64: 562).

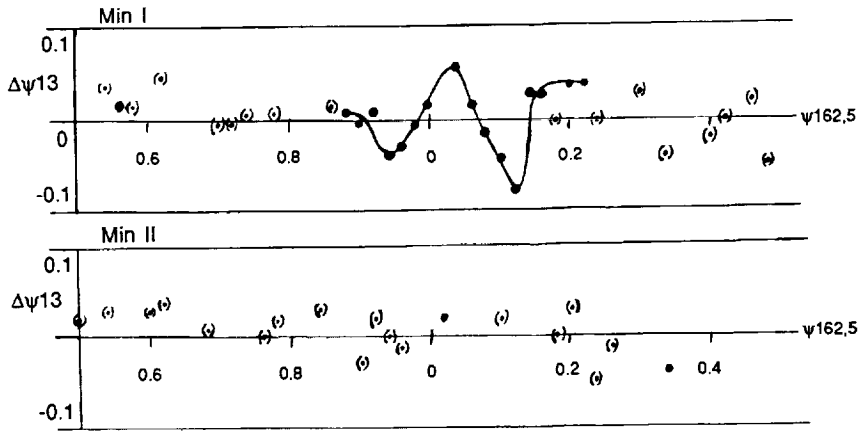


FIGURE 2 Varations of $\Delta\psi 13$ of the position of the primary minimum of optical light curve of SS433 as a function of the phase of the precessional period.

# Chaotic Inflationary Universe and the Anisotropy of the Large-Scale Structure

G.V. CHIBISOV AND YU.V. SHTANOV
P.N. Lebedev Physical Institute

## INTRODUCTION

Inflationary universe models began their history from the seminal paper by Guth (1981), and since then they have won great recognition among physicists. The last years were marked by a considerable progress towards understanding the actual picture of inflation. It was realized that the inflationary universe is in fact chaotic (see Goncharov 1987 for a review), that globally it is strongly inhomogeneous, and that the inflation in the universe as a whole is eternal. In such a picture the region available to modern observations is just a tiny part of the universe, in which inflation finished about $10^{10}$ years ago.

In spite of the great popularity of the chaotic inflationary universe models, it is usually taken for granted that their specific features (such as strong global inhomogeneity of the universe) can hardly lead to any observable consequences. The argument is that all we see is just a tiny part of the universe, a region about $10^{28}$ cm, and the typical scales of considerable inhomogeneities are much greater than this size. In contrast to this opinion we want to show that such observable consequences really can exist. In spite of the tremendous spatial size of the inhomogeneities under consideration they are well inside the actual horizon of the modern observer. Hence their observable manifestation does not contradict causality. The problem is to discover such a manifestation.

The phenomenon we are going to discuss is closely connected with the origin of structure (galaxies, clusters, etc.) in the observable region. As it is now well known (for a review see Brandenberger 1985), primordial density fluctuations relevant to structure formation could originate from vacuum

fluctuations at the inflationary stage during the permanent stretching of fluctuations scales. In most of the works on this topic the vacuum fluctuations evolution was considered on a spatially homogeneous background. At the same time, as already emphasized above, the inflationary universe is not homogeneous even on the classical level. Indeed, permanently produced fluctuations on scales bigger than the Hubble scale (i.e., with wave numbers $k \leq aH$) can be treated as a classical background inhomogeneity of the inflationary universe.

Our main idea then is to consider the vacuum fluctuations evolution on the inhomogeneous background. An essential change is the change of the mode functions which determine the vacuum state. We will see that this leads to a distortion of the resulting primordial fluctuations spectrum as compared with that in a homogeneous background model. The primordial fluctuations spectrum becomes anisotropic. And this in its turn results in the anisotropy of the observable large-scale structure. The phenomenon can be understood in terms of vacuum polarization. The classical background inhomogeneity polarizes the vacuum state, and this results in the distortion of the primordial fluctuations spectrum.

One can see that our phenomenon is very similar to the well-known phenomenon discovered by Sachs and Wolfe (1967). In this phenomenon the anisotropy of the microwave background radiation is due to large-scale metric inhomogeneity. In our phenomenon the large-scale metric inhomogeneity in a similar way influences vacuum fluctuations at the inflationary stage, resulting in the structure anisotropy. The main difference between these effects is that in our case the inhomogeneity on scales much bigger than the size of the observable region are significant. Indeed, vacuum fluctuations spreading with a speed close to the speed of light pass the distance to the true horizon, which at the present time exceeds by many orders of magnitude the size of the observable region.

Using the above-mentioned analogy with the Sachs and Wolfe phenomenon it is not difficult to make simple estimates for the value expected of the large-scale structure anisotropy. On the inflationary stage the small-scale vacuum fluctuations spread almost with the speed of light. Then they pass a Hubble distance in a Hubble time. As it can be shown, metric fluctuations on this distance are of the order

$$\langle h^2 \rangle \sim \dot{\varphi}^2 / M_p^4 \tag{1}$$

where $\varphi$ is the scalar field, the dot denotes its time derivative, and $M_p$ is the Planck mass (we are using the units in which $\hbar = c = 1$). The expression (1) also gives the order of the squared anisotropy produced in a Hubble time. To obtain an estimate for the squared anisotropy produced during the whole evolution we should integrate (1)

$$\langle \xi^2 \rangle \sim \int_{\tau_o}^{\tau_k} \frac{\dot{\varphi}^2}{M_P^4} d\tau \tag{2}$$

where $\xi$ is the effective anisotropy degree and

$$\tau = \ln a \tag{3}$$

is a timelike parameter—the expansion index. The upper integration limit in (2) corresponds to the moment of the Hubble radius crossing (when $k = aH$) and the lower one—to some initial moment. If the scalar field evolution is the so-called slow rolling-down

$$\dot{\varphi} \approx -\frac{1}{3H} \frac{dV(\varphi)}{d\varphi}, \tag{4}$$

then using also the approximate expression valid at the inflationary stage

$$H^2 \approx \frac{8\pi}{3M_P^2} V(\varphi), \tag{5}$$

we obtain from (2)

$$\langle \xi^2 \rangle \sim \frac{V_o - V_k}{3M_P^4}, \tag{6}$$

where $V_o$ is the initial value of the scalar field potential energy, and $V_k$ is the value at the moment of the Hubble radius crossing. Our simple estimate shows that the anistropy can be an appreciable value as typical values of $V_o$ are (Linde 1985)

$$V_o \sim M_p^4, \tag{7}$$

and $V_k \ll V_o$.

## FLUCTUATIONS ON THE INHOMOGENEOUS BACKGROUND

To obtain more exact expressions we must consider the evolution of the mode functions $\delta\varphi_{\vec{k}}$, that describe the scalar field small-scale fluctuations, on the inhomogeneous background metric. We will take into account only the fluctuations of the scalar type. Then we would have for the classical background metric (see Chibisov and Mukhanov 1983; Mukhanov 1985, 1988)

$$ds^2 = a^2(\eta)\left[1 + 2\Phi_c)d\eta^2 - (1 - 2\phi_c)d\vec{\chi}^2\right] \tag{8}$$

where $\phi_c$ is the so-called relativistic potential. It describes the metric fluctuations on scales bigger than the Hubble scale

$$\phi_c = \int_{k \leq aH} \frac{d^3k}{(2\hbar)^3} (\Phi^{(o)}_{\vec{k}} \hat{a}_k + \Phi^{*(o)}_{\vec{k}} \hat{a}^+_{\vec{k}}), \tag{9}$$

where $\Phi^{(o)}_{\vec{k}}$ are unperturbed mode functions, and $\hat{a}_{\vec{k}}$, $\hat{a}^+_{\vec{k}}$ are the usual annihilation-creation operators. In (8) and (9) $\eta$ is the conformal time. For $\Phi^{(o)}_{\vec{k}}$ we can use the approximate expression

$$\Phi^{(o)}_{\vec{k}} \simeq \frac{4\pi\dot{\varphi}}{\sqrt{2}M_P^2} \cdot \frac{1}{k^{3/2}} \exp(-ik\eta + i\vec{k}\vec{x}). \tag{10}$$

We must solve the equation for $\delta\varphi_{\vec{k}}$

$$\bar{\Box}\delta\varphi_{\vec{k}} + m^2(\varphi)\delta\varphi_k = 0, \tag{11}$$

where $\bar{\Box}$ is the d'Alambertian on the background with the metric (8), and $m^2(\varphi) = d^2V(\varphi)/d\varphi^2$. We find the solution for $\delta\varphi_{\vec{k}}$ in the form

$$\delta\varphi_{\vec{k}} = \delta\varphi^{(o)}_{\vec{k}}(1 + \Phi_c - iS_{\vec{k}}). \tag{12}$$

Here $\delta\varphi^{(o)}{}_{\vec{k}}$ is the solution on the homogeneous background, and $S_{\vec{k}}(\eta, \vec{x})$ is a complex valued function linear in $\phi_c$. We develop $S_{\vec{k}}$ in powers of 1/k

$$S_{\vec{k}} = k(S_0 + \frac{1}{k}S_1, + \ldots), \tag{13}$$

and find the solution for $S_0$ and $S_1$:

$$S_o(\eta, \vec{x}) = 2\int_{\eta_o}^{\eta} \Phi_c(\tilde{\eta}, \vec{\chi} - \vec{n}(\eta - \tilde{\eta}))d\tilde{\eta}, \tag{14}$$

$$S_1(\eta, \vec{x}) =^{i} [\Delta - (\vec{n}\nabla)^2] \int_{\eta_o}^{\eta} \phi_c(\tilde{\eta}, \vec{x} - \vec{n}(\eta - \tilde{\eta}))(\eta - \tilde{\eta})d\tilde{\eta}, \tag{15}$$

where $\vec{n} = \vec{k}/k$ is a unit vector in $\vec{k}$-direction. The solution in the shape (12) with (14) and (15) correspond to the choice of the "local" vacuum state for the scalar field.

We trace the evolution of $\delta\varphi_{\vec{k}}$ in the shape (12) with the solutions (14)-(15) up to the moment of the Hubble radius crossing. After this moment the evolution of the fluctuation becomes non-adiabatic. Moreover, the self-gravity of the scalar field becomes important, and we have to include the metric fluctuations into consideration. It is very convenient to work in terms of the gauge-invariant variable $\Phi$, which describes the metric fluctuations. Then in the vicinity of the Hubble radius crossing time we can

link the mode $\delta\varphi_{\vec{k}}$ to the mode $\Phi_{\vec{k}}$. This is easily done by means of the linear perturbation theory equation

$$\left(\Delta + \frac{4\pi a^2\dot{\varphi}^2}{M_P^2}\right)\Phi_{\vec{k}} = \frac{4\pi a^2\dot{\varphi}^2}{M_P^2}\frac{d}{dt}\left(\frac{\delta\varphi_{\vec{k}}}{\dot{\varphi}}\right). \tag{16}$$

Then we have

$$\Phi_{\vec{k}} = \Phi_{\vec{k}}^{(o)}(1 - iC_{\vec{k}}(\eta, \vec{\chi})), \tag{17}$$

where $C_{\vec{k}}$ is a complex valued function, linear $\Phi_c$ and similar to $S_{\vec{k}}$ in (12). Developing $C_{\vec{k}}$ in powers of 1/k similar to (13)

$$C_{\vec{k}} = k(C_0 + \frac{1}{k}C_1 + \ldots), \tag{18}$$

and counting powers of 1/k we obtain from (16)

$$C_0 \equiv S_0, C_1 \equiv S_1 + i(\vec{n}\nabla)S_0 + 3_i\Phi_c. \tag{19}$$

The evolution of $\Phi_{\vec{k}}(\eta, \vec{x})$ after the Hubble radius crossing is determined by the linear perturbation theory (see Mukhanov 1988). After this time the spatial shape of $\Phi_{\vec{k}}$ is "frozen" and only its amplitude changes with time. Thus at the moment of the end of the inflationary stage ($\eta_f$) we have

$$\Phi_{\vec{k}}(\eta_f, \vec{x}) \simeq \Phi_{\vec{k}}^{(o)}(\eta_f, \vec{x})(1 - iC_{\vec{k}}(\eta_k, \vec{x}). \tag{20}$$

Note that $\Phi_{\vec{k}}^{(0)}$ is the unperturbed solution.

## PRIMORDIAL FLUCTUATIONS SPECTRUM

The expression (20) allows us to calculate the primordial fluctuations spectrum. To do this we calculate the correlation function $\langle\Phi(\vec{x})\Phi(\vec{x}')\rangle$, where $\Phi(\vec{x}) \equiv \Phi(\eta_f, \vec{x})$. Developing $C_{\vec{k}}(\vec{x})$ in powers of $\vec{x}$ and then proceeding to the integration over new wave numbers $\vec{k} - \nabla C_0\,|_{\vec{x}=0}$ we will come to the standard shape of the correlation function

$$\langle\Phi(\vec{x})\Phi(\vec{x}')\rangle = \int \frac{d^3k}{(2\pi)^3} \mid \Phi_{\vec{k}}^{(o)} \mid^2 (1 + \nu_{\vec{k}})e^{i\vec{k}\vec{x}}, \tag{21}$$

with

$$\nu_{\vec{k}} = -2\frac{dln(k^3 \mid \Phi_{\vec{k}}^{(o)} \mid^2}{dlnk}. \tag{22}$$

$$* \int_{\eta_o}^{\eta_k} d\eta \cdot (\nabla \vec{n})[\Phi_c(\eta, \vec{x} + \vec{n}(\eta_k - \eta)) - \Phi_c(\eta, \vec{\chi} - \vec{n}(\eta_k - \eta))] \mid \vec{x} = 0$$

It can be shown that the anisotropy which appeared in (21) and which is described by the value $\nu_{\vec{k}}$ is quadrupole at least at 84%, that is

$$V_{\vec{k}} = n_\alpha n_\beta [\Lambda_{\alpha\beta} + \delta_{\alpha\beta} \cdot M], \tag{23}$$

where $\Lambda_{\alpha\beta}$ is a traceless matrix with very weak (logarithmic) dependence on k. A value which will characterize the degree of the anisotropy will be

$$\xi^2 = tr(\Lambda^2). \tag{24}$$

To obtain a characteristic value for the anistropy we must average (24) with respect to the random background inhomogeneities $\Phi_c$. In fact this is averaging over the vacuum state of which the inhomogeneities $\Phi_c$ originated. Using (22) we can obtain an approximate result

$$\langle \xi^2 \rangle \simeq \mu_k^2 \int_{\tau_0}^{\tau_k} \frac{\dot{\varphi}^2}{M_P^4} d\tau, \tag{25}$$

where

$$\mu_k^2 \simeq 10 \left( \frac{d\ ln(k^3 \mid \Phi_{\vec{k}}^{(0)} \mid^2}{d\ ln\ k} \right)^2. \tag{26}$$

The expression (25) differs from the estimate (2) only by a factor. Hence instead of the estimate (6) we will have

$$\langle \xi^2 \rangle \simeq \frac{\mu_k^2}{3} \frac{V_o - V_k}{M_P^4} \tag{27}$$

It can be shown by direct calculations that for the values of k typical for the present clustering

$$\mu_k^2/3 \simeq 10^{-2}. \tag{28}$$

Thus for typical values of $V_o$ given by (7) we obtain

$$\xi \simeq 10^{-1} \tag{29}$$

that is, the anisotropy of the order of 10%.

## CHAOTIC INFLATION

Now let us take into account one of the peculiar features of the chaotic inflationary universe. Namely, that such a universe consists of independent

domains of a physical size $\ell_{ph} = 0(H^{-1})$. They are independent in a sense that physical processes inside any such domains do not depend on the processes inside any other domain (Goncharov *et al.* 1987). From this it follows that the integration in (25) must be taken over a history of the domain of which our observable region has originated. The size of this domain at all times during the inflationary stage must be taken to be of the order of the Hubble size. Then the history of such a domain becomes random. For the random history of the scalar field evolution $\varphi(\tau)$ a Fokker-Planck equation can be obtained (Starobinsky 1986; see also Goncharov *et al.* 1987 for a review)

$$\frac{\partial P(\varphi,\tau)}{\partial \tau} = \frac{\partial}{\partial \varphi}[-AP + \frac{1}{2}(BP)'_{\varphi}], \tag{30}$$

where

$$A = -\frac{1}{3H^2}\frac{dV}{d\varphi}, B = \frac{H^2}{4\pi^2}, \tag{31}$$

$P(\varphi, \tau)$ is a $\tau$-dependent scalar field distribution in the domain considered. Now let us denote the solution to (30) with the initial conditions $P(\varphi,0) = \delta(\varphi-\varphi_0)$ by $Z(\varphi,\varphi_0,\tau)$. Then a formal solution for $Z(\varphi,\varphi_0,\tau)$ can be written in terms of path integral over all trajectories that start at $\varphi_0$ and at $\varphi$:

$$Z(\varphi,\varphi_0\tau) = \int (D\varphi)\exp(-S[\varphi]) \tag{32}$$

where

$$S[\varphi] = \frac{1}{2}\int_0^{\tau}(\frac{d\varphi}{d\sigma} - A)^2 B^{-1} d\sigma \tag{33}$$

is the "action," and

$$(D\varphi) = \prod_{\sigma} B^{\frac{-1}{2}}(\varphi(\sigma))d\varphi(\sigma) \tag{34}$$

is the path integration measure. From the expression (33) it is clear that the most probable path is that which satisfies

$$\frac{d\varphi}{d\sigma} = A, \tag{35}$$

and this is just the slow rolling-down expression (4). Thus we come to a conclusion that our estimate (27) is the *most probable* value of (25).

## ANISOTROPY OF THE LARGE-SCALE STRUCTURE

It is not difficult to show that the anisotropy of the primordial fluctuations spectrum loads the anisotropy of the large-scale structure. The

effect is conserved on scales on which nonlinear processes do not yet play an important role, that is, scales more than 50 Mpc. We can easily calculate the two-point correlation function $\xi(\vec{\chi}) = \langle\delta(\vec{x})\delta(0)\rangle$, where $\delta(\vec{x}) = \delta\rho(\vec{x})/\langle\rho\rangle$. The integrals over $\vec{k}$-space must be taken with some small-scale cutoff (Peebles 1980). This can be done by a simple cut-off function exp (-kl) where $\ell$ is a cut-off scale. Then the isotropic part of the correlation function is found to be

$$\xi_0(x) = \frac{C}{\ell^4 y^4} \frac{3_y^{-2} - 1}{(y^{-2}+1)^3}, \tag{36}$$

and the anisotropic part is

$$\xi(\vec{x}) = -h(x)\Lambda_{\alpha\beta}\frac{x_\alpha x_\beta}{x^2}, \tag{37}$$

where

$$h(\chi) = \frac{C}{\ell^4 y^4} \frac{1}{(y^{-2}+1)^3}, \tag{38}$$

$y = x/\ell$, and C in (36) and (38) is some $\ell$-independent constant.

One can use the correlation function calculated to test experimentally the phenomenon discussed in this paper.

## DISCUSSION

In conclusion, it is easy to show that during the greater part of the inflationary stage the vacuum fluctuations scales of interest are much smaller than the Planck scale. One such scale, an old-fashioned field theory, is likely to be invalid and one is supposed to use, for example, the superstring theory (Green *et al.* 1987). This last however is still in progress, and we don't yet know how to handle it when dealing with such small scales. So we use a field theoretical approach hoping that further investigations based on a more advanced theory will not change our result dramatically. In context of the superstring theory, the phenomenon discussed might be caused by string vacuum polarization due to large-scale inhomogeneity of the inflationary universe.

The problem of small scales disappears to some extent if one takes into account that the fluctuation *scale* is not a gauge invariant variable and thus can be changed by the change of the reference frame. This can be well illustrated in the case of flat space-time: a photon can be of any energy, in particular, of energy exceeding the Planck energy.[1]

[1]The authors are grateful to B.L. Spokoiny and A.A. Starobinsky for this remark.

From the observational point of view our result means a possibility of the large-scale structure anisotropy together with highly isotropic microwave background radiation. Observational discovery of the phenomenon considered might serve as confirmation to the chaotic inflation scenario and, in fact, throw some light upon physics on very small scales, in the context discussed just above.

NOTE ADDED IN PROOF: The extended version of this work is published in the Int. J. Mod. Phys. A52625 (1990).

## ACKNOWLEDGEMENTS

The authors express their gratitude to L.P. Grishchuk, A.V. Gurevich, A.D. Linde, V.F. Mukhanov, B.L. Spokoiny, and A.A. Starobinsky for valuable discussions.

## REFERENCES

Brandenberger, R.H. 1985. Rev. Mod. Phys. 57: 1.
Chibisov, G.V., and V.F. Mukhanov. 1983. Preprint FIAN 154.
Goncharov, A.S., A.D. Linde, and V.F. Mukhanov. 1987. Int. J. Mod. Phys. A2: 561.
Green, M.B., J.H. Schwarz, and E. Witten. 1987. Superstring Theory. Cambridge University Press, Cambridge. Vols 1,2.
Guth, A.H. 1981. Phys. Rev. D23: 347.
Linde, A.D. 1985. Phys. Lett. 162B: 281.
Mukhanov, V.F. 1985. Pis'ma Zh. Eksp. Teor. Fis. 41: 402.
Mukhanov, V.F. 1988. Zh. Eksp. Teor. Fix. 94: 1.
Peebles, P.J.E. 1980. The Large-Scale Structure of the Universe. Princeton University Press, Princeton.
Sachs, R.K., and A.M. Wolfe. 1967. Astrophys. J. 147: 73.
Starobinsky, A.A. 1986. In: de Vega, H.J. and N. Sanchez (eds.). Field Theory, Quantum Gravity and Strings. Springer, Berlin. Lecture notes in Phys. 246: 107.

# The Cyclotron Absorption Line and Eclipse Transition Phenomena of 4U 1538-52

GEORGE W. CLARK
Massachusetts Institute of Technology

**ABSTRACT**

Observations of the eclipsing binary X-ray pulsar 4U 1538-52 by the Japanese satellite Ginga have revealed a cyclotron absorption feature at 20 keV in the X-ray spectrum. The pulse-phase dependence of the intensity and spectrum can be mimicked by a model of X-ray emission from thin accretion-heated slabs at the magnetic poles of a rotating neutron star with its magnetic dipole axis inclined at 45° from the rotation axis. The observations also yielded data on the eclipse transitions which demonstrate that the radial density function at the base of the supersonic wind of the O-type supergiant primary has the form of an exponential like that which characterizes the density run in the similar region of the O-type supergiant primary of Cen X-3. As in the Cen X-3 system, the scale height of the exponential implies a temperature in the base region much greater than that of the supersonic wind.

Recent observations of the eclipsing binary X-ray pulsar 4U 1538-52 with the Ginga satellite have yielded results bearing on two quite different topics. The first is the X-ray spectra and beaming pattern of the pulsar; the second is the density distribution in the winds of the early-type supergiant companions of this and other X-ray pulsars.

Ginga was developed and launched by the Institute of Space and Astronautical Science of Japan. It carries several detectors including a 4,000 $cm^2$ Large Area Counter (LAC) developed by the Leicester University group and specially suited to the measurement of the spectra and variability of compact X-ray sources like binary pulsars. The LAC is sensitive from

1 to 38 keV and records data in 48 pulse-height channels with an energy resolution of 20% at 5.7 keV and a maximum time resolution of 1 msec.

The Japanese group has made time available to U.S. observers in a guest observer program supported on the U.S. side by NASA. In this program an observation of 4U 1538-52 was carried out over a complete 3.7-day orbital cycle in March 1988 in a collaboration between myself and J. Woo of MIT and F. Nagase, K. Makishima and T. Sakao at ISAS.

The X-ray spectra of strongly magnetized plasmas on neutron stars has been the subject of much theoretical work since the pioneering investigations of Sunyaev and coworkers following the discovery of binary X-ray pulsars by Giacconi and colleagues with Uhuru in 1972. In 1975 Basko and Sunyaev suggested that the effects of cyclotron resonance in the Compton scattering cross section might be observed in the form of X-ray emission lines. The subsequent discovery in a balloon experiment by Trümper *et al.* (1977) of the cyclotron feature near 50 keV in the Her X-1 spectrum focused attention on the problem of radiative diffusion in plasma with fields $\geq 10^{12}$ G. One other clear cyclotron line was found in 4U 0115+63 by Wheaton *et al.*, and indications of a line in 4U 1626-67 by Pravdo (1979) and Koyama (1989). Mazets *et al.* (1981) found evidence of cyclotron features in gamma ray burst spectra, though other interpretations have been put forward. And just recently clear evidence of first and second harmonic absorption lines at 20 and 40 keV have been found with Ginga in two gamma-ray bursts.

Our Ginga observation of 4U 1538-52 adds a third definite example of cyclotron absorption line formation in an X-ray binary pulsar under what appear to be specially favorable circumstances for analysis (Clark *et al.* 1989). This object has a 530-second pulse period and an eclipse with a half-angle of about 30°. Considering first the data unaffected by the eclipse, we divided it into ten spectral intervals and plotted the counting rate as a function of pulse phase, as shown in Figure 1. We also divided the data into eight equal intervals of pulse phase and plotted the spectra of each portion, as shown in Figure 2. Four salient properties of the spectra and variability are clearly evident:

1) The pulse profile has symmetrical primary and a secondary peaks of unequal amplitude and separated by 180° in phase.
2) The primary peak has a dimple at low energies.
3) There is an absorption line at 20 keV with a maximum equivalent width in the middle of the secondary peak. Indeed, the line is so strong as to essentially blot out the secondary peak in the spectral interval centered on 20 keV.
4) The pulse fraction increases with energy.

Properties 1), 2), and 4) have been seen in previous observations of

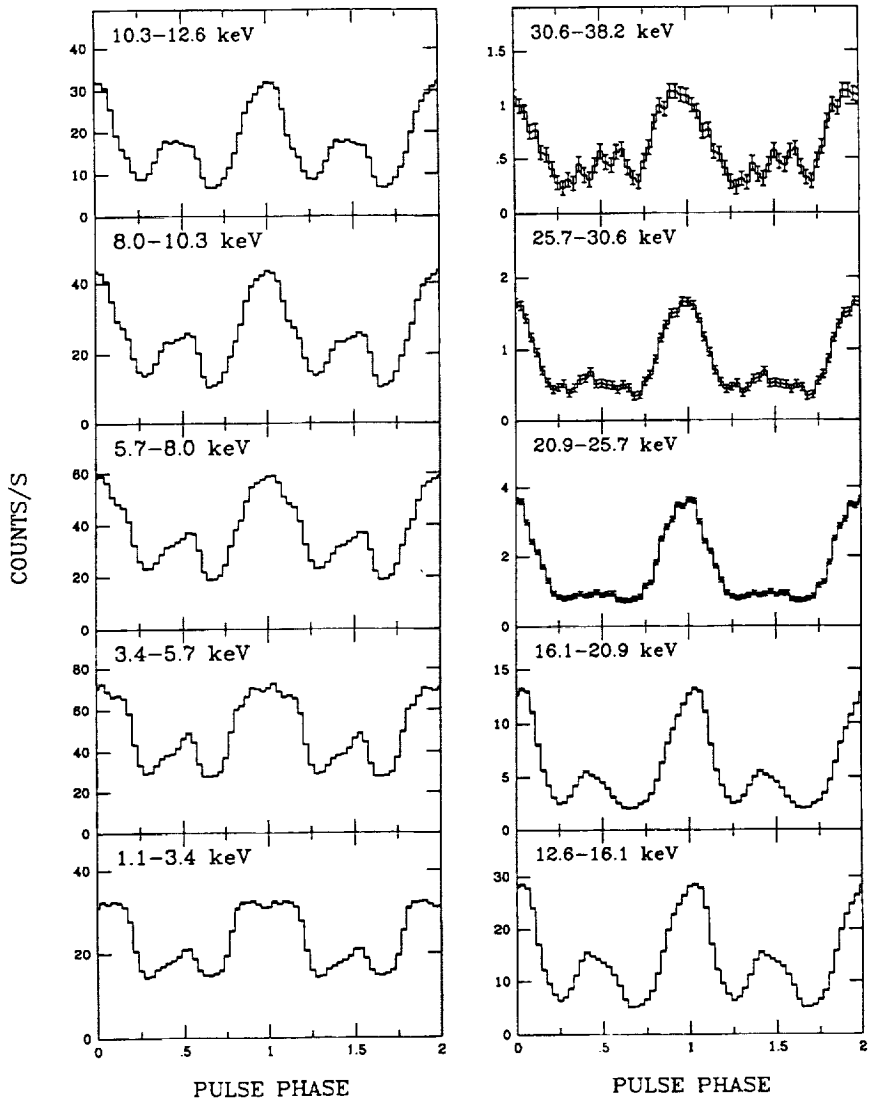


FIGURE 1 X-ray counting rates of 4U 1538-52 plotted against pulse phase (pulse period = 530 s) for ten energy channels.

4U 1538-52. The absorption line at 20 keV is new and opens interesting possibilities for detailed comparisons between the observed phenomena and the results of recent theoretical treatments of the emissions of magnetized slabs and columns of accretion-heated plasmas at the poles of magnetized neutron stars.

C-2

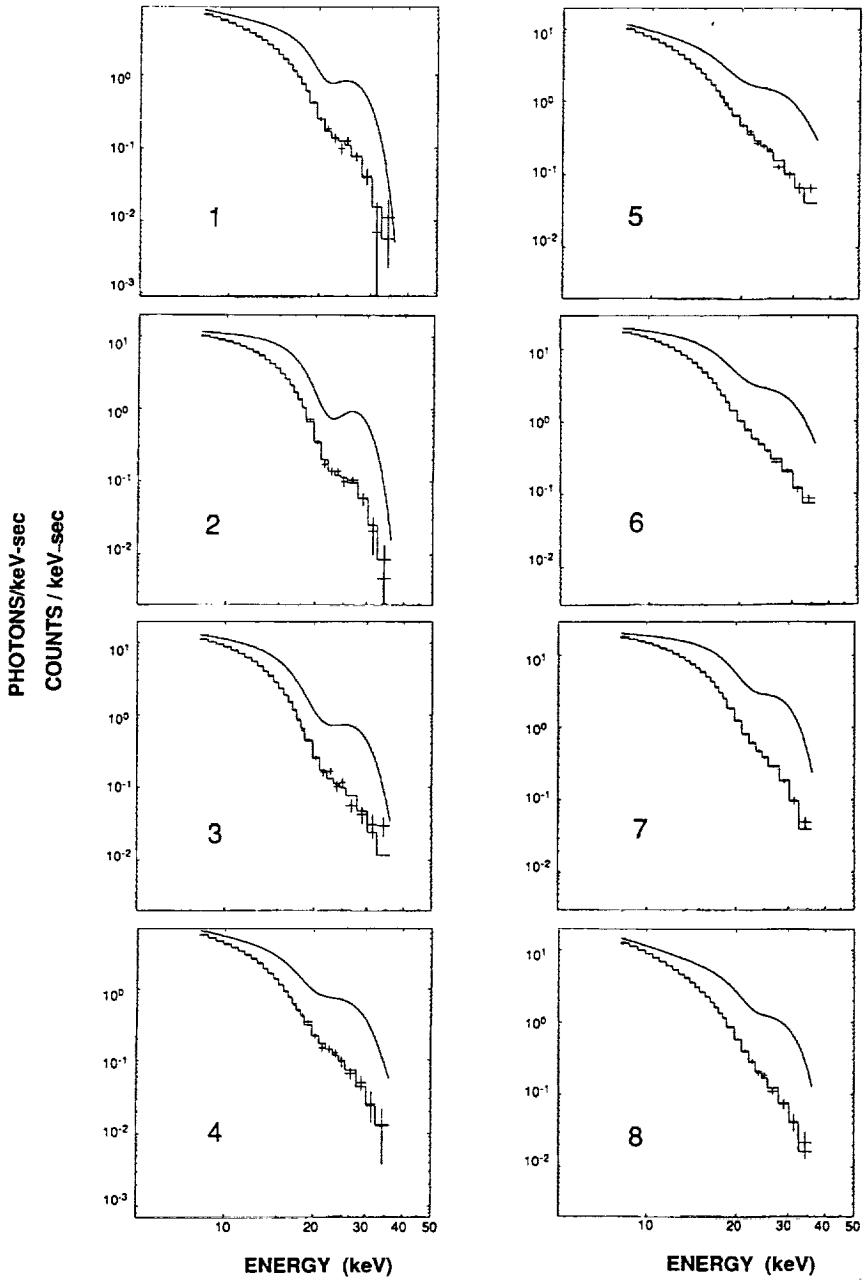


FIGURE 2 Pulse height spectra and inferred incident energy spectra of 4U 1538-52 for eight intervals of pulse phase.

To explore how the new data might be understood I constructed a pulsar model based on the theoretical results of Nagel (1985) and of Mészáros and Nagel (1987) on the radiative diffusion of X-rays in strongly magnetized slabs and columns. The idea was to explore whether the beam patterns and cyclotron absorption lines predicted by the theoretical analyses of slab or column emission geometries can be fitted to the data by an appropriate choice of the angles between the dipole axis and the rotation axis of the pulsar, and the angle between the rotation axis and our line of sight.

The eclipse duration coupled with the orbit analysis places a lower limit of $60^\circ$ on the inclination $\Theta$ of the orbit, and therefore, plausibly, of the rotation axis of the neutron star. Equatorial fan beams emitted by column geometries yield, in general, two peaks of equal amplitude, unlike 4U 1538-52. Moreover, the X-ray luminosity is near the lower limit for stopping free fall of the accreting material and formation of a settling column of emitting plasma. So a slab geometry with pencil-beam emission was assumed, and an interpolating function was fitted to the results of Nagel on the angle and energy dependence of emission from a slab. The angle $\Psi$ between the rotation and dipole axes was bounded by the conditions $(\Theta - \Psi) > 90^\circ$ and $\Theta \neq 90^\circ$ so that emission is observed from the slabs at both magnetic poles, but with different amplitudes. Finally, taking a cue from the theoretical results of Mészáros and Nagel (1985) on the formation of the cyclotron absorption line, the strength of the cyclotron absorption line was assumed to have a maximum in directions that make an angle of $70^\circ$ with the magnetic field. The minimum angles between the "north" and "south" magnetic poles and the line of sight are, respectively, $(\Theta - \Psi)$ and $(180^\circ - \Theta - \Psi)$. Setting $\Theta = 65^\circ$ and $\Psi = 45^\circ$ brings the north pole close enough to the line of sight to produce a dimple in the center of the primary peak at low energies, and maximizes the cyclotron absorption line during the secondary peak when the south pole dwells at the minimum angle of $70^\circ$. Finally, to achieve a pulse fraction less than 100%, but increasing with energy, we arbitrarily add an unpulsed component with a softer spectrum. The results are shown in Figure 3. All of the four prominent characteristics mentioned above are mimicked by this model. This gives encouragement for a more ambitious effort to achieve a precise theoretical accounting of the observations.

The second topic concerns the winds of O and B0 supergiants and what can be learned about their regions of subsonic acceleration from observations of the eclipse transitions of X-ray pulsars in massive binary systems. The companion of 4U 1538-52 is a B0 supergiant with an optical luminosity 400 times the X-ray luminosity. Thus the X-ray heating effects are negligible, though X-ray ionization of the wind may perturb the radiation pressure that drives the wind. The eclipse transitions are generally

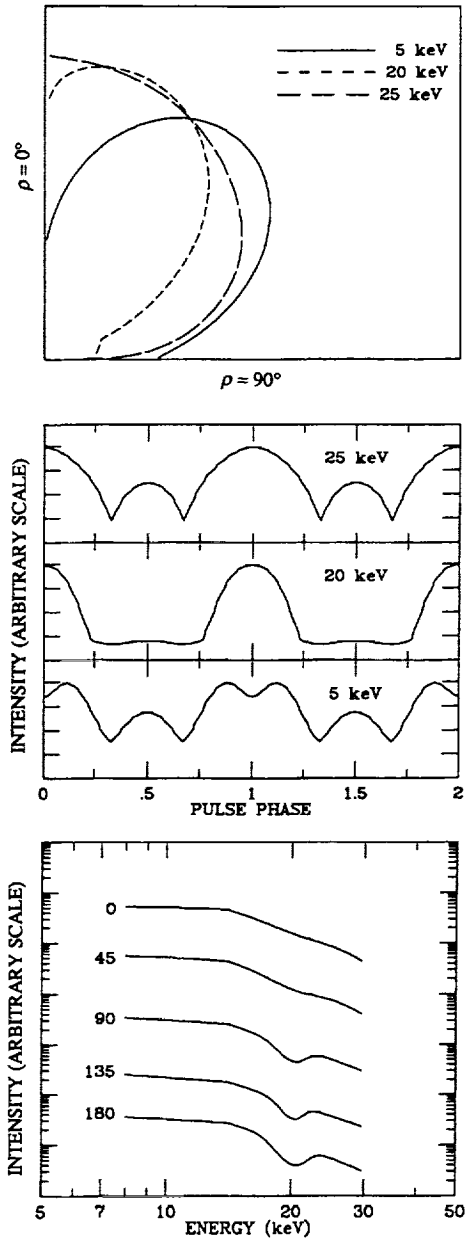


FIGURE 3 Calculations of the pulse light curve (middle panel) and pulse-phase resolved energy spectra (bottom panel) for a model X-ray pulsar with the radiation pattern illustrated in the top panel and the orientations of magnetic dipole axis and spin axis specified in the text.

gradual, though one abrupt transition was apparently observed by Davison *et al.* (1977) with Ariel.

A gradual eclipse immersion or emersion of an eclipsing X-ray binary, of which six are known, is obviously caused by absorption in an extended atmosphere of the primary, which opens a new direct way to a determination of the radial density distribution. The situation can of course be complicated by streams or blobs of matter flying around in the system as in Vela X-1 and sometimes in Cen X-3. But often in the case of Cen X-3, SMC X-1, LMC X-4, Her X-1 and 4U 1538-52 the transitions are fairly clean and uniform, indicating that the measured column densities are fair measures of the radial density functions. The situation can be ideal because the size of the X-ray source, i.e. the neutron star, is negligible compared to the scale size of the atmosphere, and X-ray absorption from 1 to 10 keV is a relatively simple measure of column density along the line of sight. Compare this with the indirect arguments that must be used to interpret spectroscopic, radio and IR data in terms of atmospheric structure.

The first remark about the significance of a gradual eclipse transition was made by Schreier *et al.* (1972) in the paper announcing the discovery of the binary nature of Cen X-3. They characterized the eclipse transition by ascribing a "scale height" of $5 \times 10^{10}$ cm to the atmosphere of the primary implying thereby an exponential form of the density function.

Following the discovery of intense, cool (30,000-50,000 K), supersonic winds in O and B stars by Morton (1967) in rocket UV spectroscopy, theories of the wind acceleration process developed around the idea of radiation pressure arising from scattering of light from the Doppler-shifting UV lines of the metals in the wind. This works well in the supersonic regime, and since the radiation intensity varies as $1/r^2$, the resulting acceleration leads to velocity curves with a characteristic rapid initial rise and then a slow approach to an asymptotic terminal velocity with values in the range of 1000 to 3000 km/s, as observed in the P Cygni profiles of UV absorption lines. There has always been a problem, though, in how the winds get started because the passage from sub to supersonic is blocked by the sound barrier as expressed in the singularity in the hydrodynamic equation governing the flow. Only by carefully tailoring the outward force by judicious combinations of thermal and radiation pressure can one achieve a steady flow from sub to supersonic with the requisite mass flux and cool temperature. Hearn suggested in 1975 that there may be a coronal layer at the base of the wind in which thermal pressure can cause the early acceleration, with sudden cooling and radiation pressure taking over when the velocity is high enough for Doppler shifting to prevent line saturation. Then Castor, Abbott and Klein (1975) showed the way to a theory of a radiation pressure driven cool wind from start to finish, and came up with velocity curves with the same rapid initial change, and then a slow approach to asymptotic terminal

velocity, which turns out to be, in general, about three times the escape velocity from the stellar surface (Abbott 1978).

Near the end of the SAS 3 mission we undertook a detailed study of Cen X-3 eclipses using data from a continuous two-week observation when Cen X-3 was in a high luminosity state (Clark *et al.* 1988). The transitions are well accounted for by an exponential density function with a scale height of $6 \times 10^{10}$ cm, and not by a density function implied by the conventional $1/r^2$ radiation force-driven wind theories. Here, as in the case of 4U 1538-52, the optical/UV luminosity of the companion is much greater than the X-ray luminosity of Cen X-3, so the X-ray heating effects are presumably negligible. Day *et al.* (1988), using data from several continuous observations of eclipse transitions by EXOSAT, drew the same conclusion, i.e. that the density run is exponential. Such a scale height, if interpreted as the characteristic of an isothermal, hydrostatic atmosphere of a 19 solar mass star, corresponds to a temperature of $10^6$ K. Following Hearn's idea that there may be a coronal layer at the base of the wind, heated by some mysterious process, in which the initial acceleration takes place, we constructed an ad hoc model with a $10^6$ K base corona governed by the usual hydrodynamic flow equation with a gravity reduced by half by radiation pressure, and terminating at 1.4 $R^*$ at the high temperature sonic point where we assumed the heating mechanism turns off, the temperature drops to 50,000 K, and radiation driving takes over in the cool but supersonic regime. This hybrid model yields a density curve that can be fit to the data for reasonable mass loss rates. A major problem of the model is that its coronal layer has an enormous soft X-ray luminosity (about 10% of the optical luminosity of KRZ) which must be absorbed by the outer wind. Other ways to get more mass loss out of a cool subsonic flow is to fine tune the effective gravity by allowing for centrifugal force (which may amount to 1/6 to 1/3 of the gravity) and radiation pressure without the benefits of the large Doppler shifts that keep it effective in the supersonic regime. But I am not aware of rigorous treatment of this subsonic regime that yields a density curve that explains the Cen X-3 eclipse transition data.

Now, with the 4,000 $cm^2$ sensitive area of Ginga, we have good data on 4U 1538-52, another massive binary pulsar, providing similar results. The variation with orbital phase of column density deduced by spectral analysis is displayed in Figure 4 along with the results of least squares fittings of three different functions—an exponential, an isothermal hydrostatic function, and a $1/r^2$ force-driven wind. The latter fails again because of its too rapid initial fall in density. The isothermal hydrostatic function fits well, allowing, to be sure, for the fluctuation that cannot be fitted by any reasonably smooth function. Of course, the situation is not hydrostatic, so a transition to a radiation-driven regime must occur, and one can undoubtedly construct another ad hoc hybrid model, combining an initial subsonic acceleration

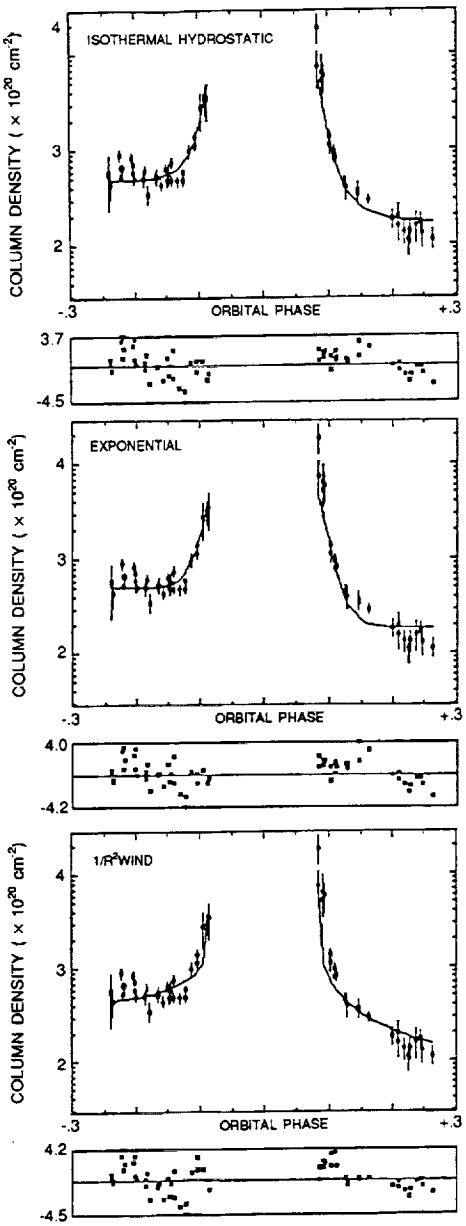


FIGURE 4 Measured column densities (H-atoms/cm$^2$) along the lines of sight to 4U 1538-52 plotted against orbital phase during one eclipse ingress and egress. The solid curves are least-squares fits of column density curves derived from three trial atmospheric density functions of the primary B0 star plus constant terms before and after eclipse. Deviations of the data from the fitted column densities are displayed below each plot. (In each case the line integration is terminated at two orbital radii).

with an exponential density run with a radiation-driven supersonic regime. But what is needed now is theoretical attention to the facts of X-ray eclipse transitions and the direct information they provide about the mysterious subsonic acceleration phase of early star wind generation.

## REFERENCES

Abbott, D.C. 1978. Ap. J. 225: 893.
Basko, M.M., and R.A. Sunyaev. 1975. Astr. Ap. 42: 311.
Castor, J.I., D.C. Abbott, and R.I. Klein. 1975. Ap. J. 195: 157.
Clark, G.W., J.W. Woo, F. Nagase, K. Makishima, and T. Sakao. 1990. Ap. J. 353-274.
Clark, G.W., J.R. Minato, and G. Mi. 1988. Ap. J. 324: 974.
Crampton, D., J.B. Hutchings, and A.P. Cowley. 1978. Ap. J. (Letters) 225: L63.
Day, C. 1988. Thesis, Cambridge University.
Davison, P.J.N., M.G. Watson, and J.P. Pye. 1977. M.N.R.A.S. 181: 73P.
Giacconi, R., H. Gursky, E. Kellogg, E. Schreier, T. Matilsky, D. Koch, and H. Tananbaum. 1971. Ap. J. Suppl. 237(27): 37.
Hearn, A.G. 1975. Astr. Ap. 40: 277.
Koyama, K. *et al.* 1989. Pub. Astr. Soc. Japan, in press.
Mazets, E.P., S.V. Golonetskii, R.L. Aptekar', Y.A. Gur'yan, V.N. Al'inskii. 1981. Nature 290: 378.
Mészáros, P., and W. Nagel. 1985. Ap. J. 298: 147.
Morton, D.C. 1967. Ap. J. 147: 1017.
Nagel, W. 1981. Ap. J. 251: 278.
Pravdo, S.H., N.E. White, E.A. Boldt, S.S. Holt, P.J. Serlemitsos, J.H. Swank, and A.E. Szymkowiak. 1979. Ap. J. 231: 912.
Schreier, E., R. Levinson, H. Gursky, E. Kellogg, H. Tananbaum, and R. Giacconi. 1972. Ap. J. (Letters) 172: L79.
Trümper, J., W. Pietsch, C. Reppin, W. Voges, R. Staubert, and E. Kendziorra. 1978. Ap. J. (Letters) 219: L105.
Wheaton, Wm. A. *et al.* 1979. Nature 282: 240.

# Radio Telescopes as the Detectors of Super-High-Energy Neutrinos

R.D. DAGKESAMANSKY, Lebedev Physics
I.M. ZHELEZNYKH, Institute for Nuclear Research

The registration of super-high-energy neutrinos is a very difficult and also very important problem that requires construction of detectors with large effective target masses. In 1961, Askaryan pointed out the possibility of registering cascades in dense media by the Cherenkov radioemission of an excess of negative charges in the cascades which arose in interaction between high energy particles and the atoms of medium. The total energy (W) emitted is proportional to $E^2$, where E is the primary particle energy (Gusev and Zheleznykh 1983; Markov and Zheleznykh 1986):

$$W \simeq 10^{-10}(E(eV)/10^{14})^2[\text{ergs}]. \quad (1)$$

Most of this energy will be emitted by radio band at frequencies $f \leq f_{max} \simeq 10^9$ Hz, where the cascade's radioemission will be coherent. At $f < f_{max}$ the spectrum of radioemission will be proportional to f:

$$P_f df = (2W/f_{\max}^2) f^{df} \quad (2)$$

The corresponding "telescopes" for cosmic high-energy neutrino detection by radioemission of cascades induced underground, but whose development continues in the atmosphere were proposed in Markov and Zheleznykh (1986); Dedenko *et al.* (1981); Markov and Zheleznykh (1979). The effective target masses of such detectors could be $\sim 10^9$ tons and more. The properties of Cherenkov radioemission of cascades and the properties of ice in the Antarctic Region (very weak radiowave absorption at low temperature) make it possible to propose Radio Antarctic Muon and Neutrino Detection (RAMAND): antennas should be placed on the ice surface of $\sim 10$ km$^2$ to search for radio signals from neutrino (muon)

cascades of energy $10^{14} - 10^{15}$ eV and higher in a volume of $\sim 10^{10}$ m$^3$ (Gusev and Zheleznykh 1983).

To search for astrophysical neutrinos of energies higher than $10^{19}$ eV, observations with radio telescopes were proposed (Zheleznykh 1988). Indeed, by using available high sensitive radio telescopes we can hope to detect the coherent Cherenkov radioemission that has arisen in very distant targets. For example, we can try to observe such radioemission from cascades in the surface layer of the Moon (the surface area is about $10^7$ km$^2$!).

The energy W is emitted as a very short pulse ($\Delta t_p \sim 10^{-8}$ s) because of the short lifetime of the cascade at a relatively dense medium. The emission is concentrated within the "thick hollow cone" with the opening angle $\theta \simeq 50°$ and the solid angle $\Omega \simeq 0.5$ steradians. Therefore, the peak flux density measured by observers inside the "thick hollow cone" will be:

$$S_{peak} = \frac{2fW}{f_{max}^2 \Omega D^2 \Delta t_p} = 3.10^{-23} f g E_{20}^2 [W \cdot m^{-2} Hz^{-1}] \qquad (3)$$

where D is the distance to the Moon, $f_9$ is frequency in GHz and $E_{20}$ is the neutrino energy in $10^{20}$eV.

On the other hand, the sensitivity of radio telescope is

$$\Delta S_{\text{lim}} = 2kT_{\text{sys}} A_{\text{eff}}^{-1} (\Delta f \tau)^{-1/2}, \qquad (4)$$

where $T_{sys}$ is the telescope system noise temperature, $A_{eff}$ is the effective area of the radio telescope, k is Boltzman's constant, $\Delta$f is the frequency bandwidth of the radiometer and $\tau$ is integration time ($\tau \geq 1/\Delta$f).

There is some restriction however. The receiver's frequency bandwidth has to be equal or less than $\Delta f_{disp} = 10^{-19} f^3$ Hz—the largest possible bandwidth defined by the frequency dispersion of signals in the ionosphere. Therefore, the integration time cannot be less than $\tau_{disp} = 1/\Delta f_{disp}$, and so we shall observe usually spreaded pulses. On the other hand, it will be possible to use multichannel receivers with the total (effective) bandwidth $\Delta f_{eff} = n \cdot \Delta f_{disp} \approx 0.3f$. In this case we can write effective sensitivity relative to the pulse-type signal as following:

$$\Delta S_{eff} = 2kT_{sys} (A_{eff} \Delta t_p)^{-1} (\Delta f_{disp} \cdot \Delta f_{eff})^{-1/2} = \qquad (5)$$

$$= 1.5 \cdot 10^{-13} T_{sys} (A_{eff} \cdot \Delta t_p)^{-1} f^{-2} [W \cdot m^{-2} \cdot Hz^{-1}]$$

Figure 1 shows the dependences of $S_{peak}$ and $\Delta S_{eff}$ from frequency f calculated for the three values of neutrino energy and for the three large radio telescopes. It is evident from Figure 1 that the largest radio

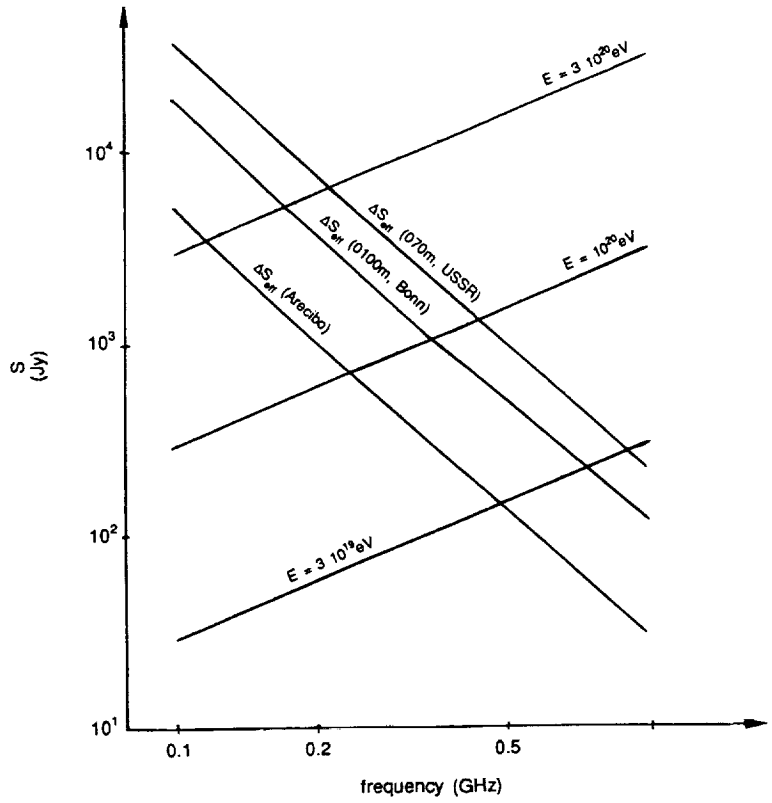


FIGURE 1 Frequency dependencies of expected cascade's peak flux densities ($S_{peak}$) and of effective sensitivities ($\Delta S_{eff}$) of several large radio telescopes.

telescopes give us already today the opportunity for registartion of the cascades induced by neutrinos with the energies $E \geq 10^{20}$ eV.

Now, it will be interesting to estimate the expected rate of such events. Unfortunately, at present there is no good prediction of high-energy neutrinos fluxes. However, many modern models of the universe, for example the models with superconductive cosmic strings or with supermassive particles (monopoles, maximons), predict super-high-energy neutrinos ($E \simeq 10^{20} - 10^{22}$ eV or even $10^{25} - 10^{28}$ eV).

Some speculative estimates of high-energy neutrinos fluxes were made by Hill *et al.* (1987) using the extrapolation of Fly's Eye limit on deeply penetrating particles. From this estimate one can conclude only that an

upper limit to the rate of the events induced by neutrinos in the five-meter Moon surface layer would be about $10^5$ year$^{-1}$ for neutrinos with $E \geq 10^{20}$ eV (here we used for the neutrino-nucleon cross-section $\sigma_{\nu n} \simeq 10^{-31}$ cm$^{-2}$, see for example Butkevich *et al.* (1988)). In most models of the universe with superconductive strings (see also Hill *et al.* 1987) it may be expected from $10^1$ to $10^5$ observable cascades per year for the same neutrino energies.

It should be noted also that the same cascades and pulses of radioemission could be raised (and may be much more often) by interaction of high energy protons with the Moon. However, proton interactions will be observed only near the edge of a lunar disk, whereas neutrino interactions will occur at every part of the disk with approximately the same probability.

There is additional difficulty concerning the registration of such relatively rare sporadic radio pulses in the presence of different kinds of interference. To increase the reliability of detection we can try to use the specific features of signal. The delay of pulses at lower frequencies on account of the ionospheric dispersion is one of such specific features. For example, the delay will be about $0.4\mu$ sec. at 300 MHz and about $4\mu$ sec. at 100 MHz. Therefore, the corresponding digital filter will be very useful for detection of the pulses.

Another way to increase the reliability of detection is the simultaneously use of two or more radio telescopes for Moon monitoring. It should be noted however, that none of the radio telescopes currently has suitable receivers to make these observations. Moreover, the beam width of large radio telescopes at decimeter wavelengths are usually much less than the lunar disk's diameter. Consequently, there is the necessity of construction of a special kind of feed antenna (perhaps a matrix feed antenna) that will permit simultaneous reception of pulses from most parts of the lunar disk. We hope that all these difficulties can be overcome in the near future.

## REFERENCES

Askaryan, G.A. 1961. Zh. Eksp. Teor. Fiz. (Sov. Phys. JETP) 41: 616-618.

Gusev, G.A., and I.M. Zheleznykh. 1983. Pis'ma Zh. Eksp. Teor. Fiz. (JETP Lett.) 38:505-507.

Markov, M.A., and I.M. Zhelznykh. 1986. Nucl. Instr. Meth. Phys. Res. A248:242-251.

Dedenko, L.G., M.A. Markov, and I.M. Zheleznykh. 1981. In: Cense, R., E. Ma, and A. Roberts (eds.). Proc. 1981 International Conference on Neutrino Physics and Astrophysics. Maui, Hawaii. 1:292.

Markov, M.A., and I.M. Zheleznykh. 1979. Page 177. In: Learned, J. (ed.). DUMAN Workshop at Khabarovsk and Lake Baikal. Honolulu.

Zheleznykh, I.M. 1988. Proc. "Neutrino-88" (in press) Boston.

Hill, C.T., D.N. Schramm, T.P. Walker. 1987. Phys. Rev. D. 36: 1007-1016.

Butkevich, A.V., A.B. Kaidarov, P.I. Krastev, A.V. Leonov-Vendrovski, and I.M. Zheleznykh. 1988. Z. Phys. C - Particles and Fields. 39:241-250.

# Optical Observations of Active Galactic Nuclei

ALEXEI V. FILIPPENKO
University of California, Berkeley

## ABSTRACT

I describe the most important observed characteristics of active galactic nuclei, concentrating on their optical spectra. Connections with the "standard model" of such objects are emphasized. Some of the new observational developments that are leading to modifications of the standard model are outlined; these include spatial variations of the ionization parameter in the broad-line region, the possible existence of a very dense component in the broad-line region, and the presence of an intermediate-density zone between the broad-line and narrow-line regions. Evidence for "hidden" Seyfert 1 nuclei and anisotropic ionizing radiation is also reviewed. The search for, and properties of, intrinsically weak Seyfert 1 nuclei are subsequently summarized, with special attention given to the very low-luminosity object in the late-type dwarf galaxy NGC 4395. I conclude with a discussion of the possibility that low-level activity in some galactic nuclei might actually be produced by bursts of star formation and their associated supernovae.

## BASIC OBSERVATIONS AND THE STANDARD MODEL

The optical and ultraviolet (UV) spectra of QSOs and Seyfert 1 nuclei are dominated by strong, broad-permitted emission lines superposed on a featureless continuum (Osterbrock and Mathews 1986, and references therein). These lines typically have full-widths at half maximum (FWHM) of 3,000–6,000 km $s^{-1}$, and full-widths near zero intensity (FWZI) of 10,000–20,000 km $s^{-1}$. In addition, one often sees narrower cores (FWHM $\approx$ 500

km $s^{-1}$) to the permitted lines, as well as forbidden lines of comparable (relatively narrow) width. The forbidden lines include a wide range of ionization states, from [O I] to [Fe VII] or higher. In Seyfert 2 nuclei, the broad permitted lines seem to be absent, although new data indicate that in at least some cases they are actually present at a very low level.

The featureless continuum of classical AGNs has a roughly power-law shape with index $\alpha \approx 1 - 2$ ($f_\nu \propto \nu^{-\alpha}$) at red through near-infrared wavelengths, but it generally becomes flatter ($\alpha \approx 0 - 1$) at higher frequencies (Neugebauer *et al.* 1979). In the UV region, the slope is often quite flat ($\alpha \approx 0$). There appears, in essence, to be a broad excess, or "big blue bump," over an extrapolation of the near-infrared power law. Starlight is an important contaminant in the spectra of low-luminosity Seyfert 1 nuclei (Malkan and Filippenko 1983), but their nonstellar spectra are similar to those of QSOs.

It has long been recognized that the flux of H$\beta$ and other permitted lines is, to first order, directly proportional to the flux density of the optical nonstellar continuum in large samples of AGNs (Yee 1980; Shuder 1981). Thus, the lines are probably produced by gas photoionized by the UV extension of the featureless continuum emerging from the active nucleus. Photoionization calculations have reinforced our belief in this simple picture, since most of the emission-line intensity ratios can be reproduced (Netzer and Ferland 1984). The models depend primarily on the ionization parameter, which is simply the ionizing photon number density divided by the nucleon (or electron) number density at the exposed face of a slab of gas.

The broad permitted lines are formed by gas having $n_e \approx 10^9 - 10^{10}$ $cm^{-3}$. This is deduced from the weakness or absence of broad forbidden [O III] $\lambda\lambda$4959, 5007 emission, and by the presence of broad semi-forbidden (intercombination) C III] $\lambda$1909. Other, similar diagnostics also exist. Photoionization models imply that $T_e \approx 10,000 - 20,000$ K. Comparable temperatures are also found from various intensity ratios among the narrow lines, although the derived densities are much lower ($n_e \approx 10^3 - 10^5$ $cm^{-3}$). With such low temperatures, the thermal widths of emission lines are only 10–20 km $s^{-1}$. Bulk motions of gas are undoubtedly responsible for broadening the lines to the observed widths; other proposed mechanisms (e.g., electron scattering) have serious difficulties (Davidson and Netzer 1979).

The gas emitting the line radiation is distributed in clouds or filaments occupying only a small fraction ($10^{-4} - 10^{-7}$) of the volume they encompass. This is deduced directly from the observed luminosities of the lines and their average distances from the central source, as determined by photoionization models. In low-luminosity AGNs, these clouds often have a covering factor of nearly unity and absorb soft X-rays traveling along our line of sight

(Elvis and Lawrence 1985), but in luminous QSOs the clouds only cover 1%–10% of the sky. Supporting evidence includes the fact that a sharp drop at 912 Å, the hydrogen Lyman limit, is rarely seen in the continua of high-redshift QSOs.

The calculated radial distances for clouds in the broad-line region (BLR) are usually 0.01–1 pc, and in the narrow-line region (NLR) 10–1,000 pc. It is therefore not surprising that the BLR has never been spatially resolved in optical images or spectra, while the NLR is often resolved in nearby AGNs. This is also consistent with the absence of narrow-line variability in most AGNs (Peterson 1988), whereas variability of the broad lines over time scales of weeks, months, or years is common. Photoionization models and observations at X-ray energies (Halpern 1982) show that the column density of neutral hydrogen, $N_H$, is $\sim 10^{23}$ cm$^{-2}$ and $\sim 10^{22}$ cm$^{-2}$ in the BLR and NLR, respectively, almost independent of the intrinsic luminosity of the AGN.

Accretion of matter onto a central, massive black hole has long been thought of as the ultimate source of energy emitted by QSOs and Seyfert 1 nuclei (Zel'dovich and Novikov 1964; Salpeter 1964), largely because of the absence of other viable mechanisms. Although spherical accretion has been considered, it is now generally believed that the gas forms an accretion disk around the black hole. Infalling matter almost certainly has specific angular momentum greater than that of the least stable orbit around a black hole, and accretion disks provide efficient release of energy (up to $0.37\,mc^2$ for a Kerr black hole). Also, the well-collimated jets spewing out of some AGNs suggest the presence of disks (Rees 1984). Direct observational evidence for disks is difficult to find, but many (not all!) researchers believe that the "big blue bump" represents thermal emission from an accretion disk (Shields 1978; Sun and Malkan 1989, and references therein).

## COMPLICATIONS TO THE STANDARD MODEL

Despite its success, the simple picture described above is far from complete; many problems have been pointed out over the past decade. In particular, there remain serious difficulties in reproducing the observed emission-line spectrum of active galaxies (Ferland and Shields 1985; Netzer 1989). Here I briefly discuss several complications that must be addressed in current and future calculations.

### Spatially Variable Ionization Parameter

A single set of clouds, characterized by one value for the ionization parameter, probably cannot be invoked to explain all the intensity ratios of broad emission lines in AGNs (Collin-Souffrin *et al.* 1988). Specifically,

a large ionization parameter is needed to generate highly ionized species such as C IV and O VI, whereas great quantities of X-rays are necessary to penetrate deep into thick clouds to produce the observed Fe II emission. As one possible solution, Netzer (1987) suggests that the ionizing UV radiation is emitted by a thin accretion disk, whereas the X-ray continuum comes from a hot, spherical bulge at the center of the disk. Clouds near the disk axis would have a much higher ionization parameter than those at large angles from the axis. An additional requirement is that the cloud covering factor must increase with increasing angle away from the disk axis. This is reasonable if the clouds have considerable angular momentum. It may also be the case that extra heating sources, other than the normal photoionizing continuum, are necessary for a good fit to the data (e.g., Joly 1987).

### Ultra-High and Intermediate Densities

Another, equally serious problem is that the broad emission lines are observed to vary rapidly in response to changes in the luminosity of the ionizing continuum; see Peterson (1988) for a thorough review. Based on the sizes of the BLR calculated from the ionization parameter (inferred from spectra), time delays of a month to a year were expected in many Seyfert 1 galaxies. The measured delays, on the other hand, can be as short as a week to a month. This means that the BLR is typically a factor of three to ten smaller than had previously been thought. In the simplest models, the gas density must be 10–100 times higher to prevent the calculated values of the ionization parameter to deviate significantly from those deduced with spectra. Such high densities, however, produce other problems. The C III] $\lambda$1909 line, for example, should be collisionally suppressed (relative to permitted lines) at the newly derived densities of $n_e \approx 10^{11} - 10^{12}$ cm$^{-3}$. Thus, it probably arises from gas of lower density ($\sim 10^9$ cm$^{-3}$), yet it often has nearly the same profile as the permitted lines.

There is also evidence for multiple zones in the gas primarily responsible for the forbidden lines in AGNs. Many studies conducted over the past few years have shown that the concept of distinct, well-separated NLRs and BLRs is often an oversimplification. Rather, it appears that there exists an "intermediate zone," in which $n_e \approx 10^6 - 10^8$ cm$^{-3}$ and velocities of clouds are between those in the NLR and BLR. The evidence is the strong correlation, found in many objects, between line width and critical density for collisional de-excitation (Filippenko 1985; Whittle 1985; De Robertis and Osterbrock 1986); see Figure 1. Forbidden lines having $n_e$(crit) $\approx 10^6 - 10^7$ cm$^{-3}$ are quite broad in some objects. Moreover, detailed analysis of the H$\beta$ spectral region in Seyfert 1 galaxies indicates that broad

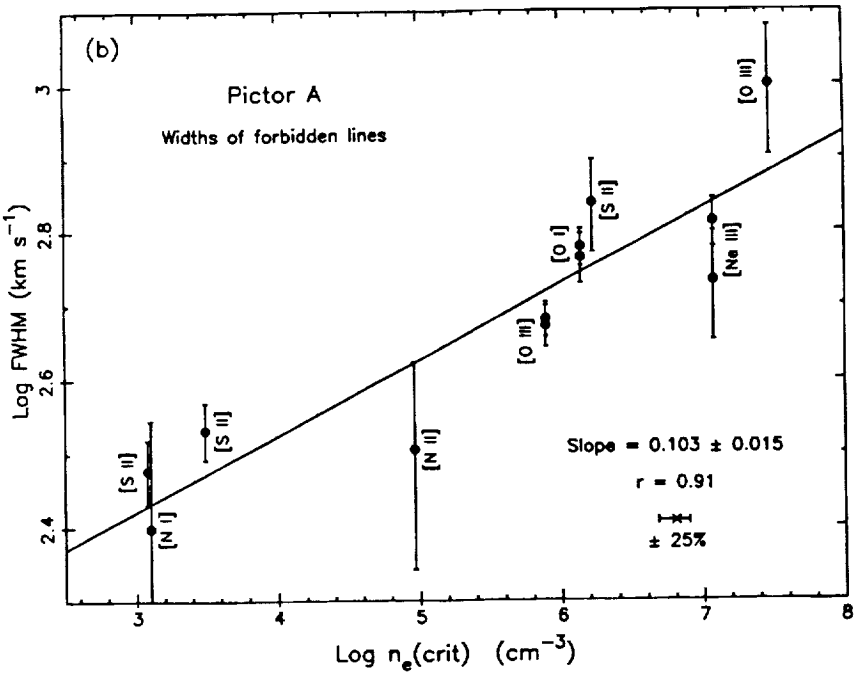


FIGURE 1 The Seyfert 1 galaxy Pictor A shows a strong correlation between the FWHM and the critical density of emission lines (Filippenko 1985). A very high correlation coefficient of 0.91 is found. The data were obtained with the 2.5 m du Pont reflector at Las Campanas Observatory.

[O III] emission may exist at a low intensity level, and is probably produced by clouds having $n_e \approx 10^7 - 10^8$ cm$^{-3}$ (Crenshaw and Peterson 1986, and references therein). The simple two-zone models are clearly inadequate, except for first-order approximations to the emission-line intensity ratios.

### Anisotropic Ionizing Radiation

There is now considerable evidence that in some AGNs, ionizing radiation might be preferentially beamed along certain directions. The radio galaxy PKS 2152–69, for example, exhibits a high-excitation knot of emission at a projected distance of 8 kpc from its nucleus (Tadhunter *et al.* 1987). Without the presence of beamed radiation, it is difficult to reproduce this knot's isolated nature and its very high ionization parameter. The polarized blue continuum detected in this knot is probably caused by scattering of the beamed radiation (di Serego Alighieri *et al.* 1988).

Powerful evidence for a disk-like (rather than spherically symmetric)

geometry is found in the study of NGC 1068 done by Antonucci and Miller (1985). Optical spectra of NGC 1068 show it to be a bright type 2 Seyfert galaxy, with permitted and forbidden lines having similar widths (FWHM $\approx 1100$ km s$^{-1}$). A spectrum of the *polarized* flux alone, however, is virtually indistinguishable from normal (total flux) spectra of type 1 Seyferts and QSOs! Broad permitted lines of hydrogen and Fe II are visible, and there is a very blue, featureless continuum. Furthermore, Miller (1989) has observed broad Balmer lines scattered from an off-nuclear H II region in NGC 1068. The obvious interpretation of these data is that NGC 1068 actually harbors a type 1 Seyfert nucleus that is located inside an optically and geometrically thick torus. Photons from the continuum source and the BLR are scattered into our line of sight, and therefore polarized, by free electrons above and below the disk. The NLR is sufficiently extended that it is not obscured by the disk. It is quite possible that the thick torus feeds into an accretion disk close to the black hole.

Pogge's (1988) discovery of a high-ionization emission-line "cone" in NGC 1068 supports the hypothesis advanced by Antonucci and Miller (1985). Moreover, the luminosity of the ionizing continuum from the nucleus of NGC 1068, deduced from the total flux spectrum and the assumption of spherical symmetry, cannot account for the luminosity of forbidden lines in the NLR. No problem exists, on the other hand, if the NLR clouds have a much more direct view of the compact nucleus. Similar conclusions regarding hidden BLRs (Miller and Goodrich 1990), high-ionization emission-line cones (Pogge 1989), and the energetics of the NLR (Wilson *et al.* 1988) have been made for many other Seyfert 2 galaxies; thus, NGC 1068 is not an isolated example of this phenomenon. In addition, radio observations (Antonucci 1984) show that the optical polarization position angle of Seyfert 2 galaxies is almost always perpendicular to the radio axis, as expected if they contain an opaque torus which we view from the side.

## LOW-LUMINOSITY SEYFERT 1 NUCLEI

### Searching for Broad H$\alpha$ Emission

The nonstellar continuum of QSOs typically has an absolute blue magnitude ($M_B$; $\lambda \approx 4500$ Å) between $-30$ and $-23$ (i.e., $L_B \approx 10^{11} - 10^{14}\, L_\odot$), while that of Markarian Seyfert 1 nuclei lies in the range $-23$ to $-18$ ($L_B \approx 10^9 - 10^{11}\, L_\odot$). The well-known continuity in many observed characteristics of these objects gives strong evidence for the idea that their physical properties are also similar. Observations of low-redshift QSOs suggest that all QSOs occur in galaxies; hence, we certainly expect there to be at least a few local Seyfert 1 nuclei with *very* low luminosity, if

some of these objects result from the fading of old QSOs as their fuel supply steadily dwindles. Continuity in the observed properties of QSOs and Seyfert 1 nuclei further suggests the existence of such objects, but there *might* be a lower limit to the activity. If so, it could be of fundamental importance, like the lower mass limit ($\sim 0.08\,M_\odot$) of main-sequence stars. The nucleus of the nearby, frequently studied spiral galaxy NGC 4051 was for many years the least luminous known Seyfert 1 ($M_B \approx -16$; Véron 1979).

Owing to contamination by starlight, it is quite difficult to detect the nonstellar blue continuum in very low-luminosity Seyfert 1 nuclei. Broad H$\alpha$ emission, on the other hand, is easier to discern. For convenience, we will adopt the relation $M_B \approx -2.5 \log L(\mathrm{H}\alpha) + 84.7$ (where $\log x \equiv \log_{10} x$), as empirically derived by Weedman (1985; $H_0 = 75$ km s$^{-1}$ Mpc$^{-1}$) for the nuclei of Markarian galaxies having broad H$\alpha$ emission with luminosity $L(\mathrm{H}\alpha)$ ergs s$^{-1}$. Low-luminosity Seyfert 1 nuclei, arbitrarily defined to be those with $M_B \gtrsim -18$ mag, have a corresponding broad H$\alpha$ luminosity of $L(\mathrm{H}\alpha) \lesssim 10^{41}$ ergs s$^{-1}$. The standard interpretation for such objects (e.g., Filippenko 1988) is that they have rather small central black holes ($M \lesssim 10^6\,M_\odot$), or that they are accreting material at very sub-Eddington rates.

Many low-luminosity Seyfert 1 nuclei have now been found in nearby galaxies (Stauffer 1982; Keel 1983; Filippenko and Sargent 1985). An excellent example is M81 (Figure 2), whose distance is about 3.3 Mpc; weak, broad H$\alpha$ emission was discovered by Peimbert and Torres-Peimbert (1981) and confirmed by Shuder and Osterbrock (1981). An accurate measurement of the broad H$\alpha$ luminosity, $L(\mathrm{H}\alpha) \approx 1.2 \times 10^{39}$ ergs s$^{-1}$ (Filippenko and Sargent 1988), together with Weedman's (1985) relation given above, yields $M_B \approx -13.0$ mag for the blue nonstellar continuum, which has not yet been detected. The nucleus of this galaxy is also a strong, variable X-ray source, as well as a bright, compact, variable, flat-spectrum radio source. There is almost no doubt that its activity is similar to that in QSOs; it could reasonably be called a "microquasar" (Elvis 1984). Of relevance to the discussion above, its spectrum (Figure 2) shows that forbidden lines associated with high critical density (e.g., [O I] $\lambda\lambda$6300, 6364; $n_e(\mathrm{crit}) = 1.4 \times 10^6$ cm$^{-3}$) are considerably broader than those with low critical density (e.g., [S II] $\lambda\lambda$6716, 6731; $n_e(\mathrm{crit}) \approx 2 \times 10^3$ cm$^{-3}$).

In an attempt to quantify the luminosity function of intrinsically faint Seyfert 1 nuclei, W. L. W. Sargent (Caltech) and I are searching for broad H$\alpha$ emission in optical spectra of the nuclei of the 500 brightest galaxies in the northern sky; see Filippenko and Sargent (1985) for initial results. NGC 4639 is an excellent example of a bright, nearby Shapley-Ames galaxy whose Seyfert 1 characteristics had previously gone unnoticed. The spectrum at blue wavelengths (Figure 3) is comparable to those of

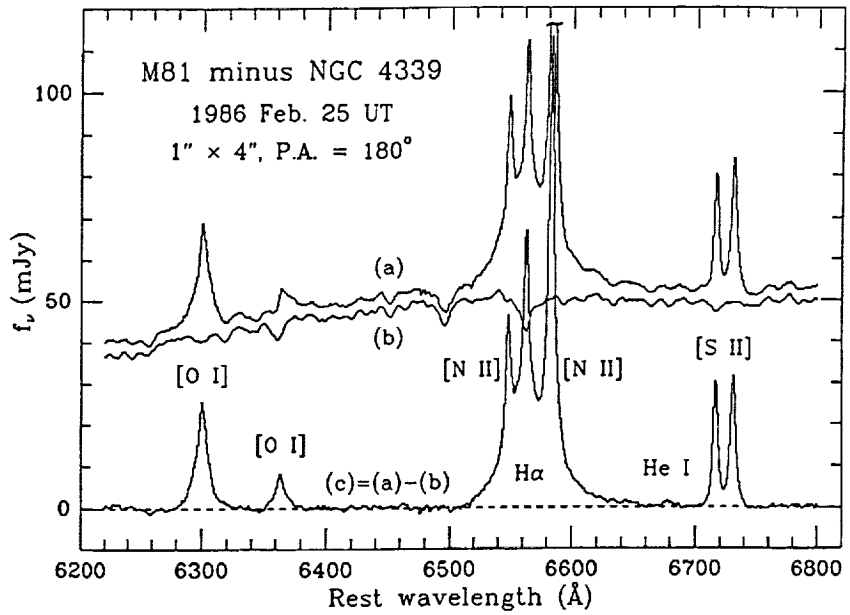


FIGURE 2 Red spectrum of M81 (Filippenko and Sargent 1988), obtained with the 5 m Hale reflector at Palomar Observatory. A spectrum of the absorption-line template galaxy NGC 4339 is subtracted from M81 in (c). M81 has a low-luminosity Seyfert 1 nucleus; broad H$\alpha$ is clearly visible. Note that the widths of the forbidden lines span a wide range.

normal, inactive galaxies devoid of strong emission lines. The red spectrum (Figure 4), by contrast, exhibits prominent, broad H$\alpha$ emission with FWHM $\approx 3,000 - 4,000$ km s$^{-1}$ and FWZI $\approx 8,000 - 9,000$ km s$^{-1}$. A majority of old redshift surveys of galaxies did not include the red spectral region, so it is possible that quite a few objects of this type have been overlooked. Furthermore, in most galaxies the broad H$\alpha$ emission line is very weak, requiring careful deconvolution of the H$\alpha$ + [N II] $\lambda\lambda$6548, 6583 blend for detection and measurement.

## A Seyfert 1 Nucleus in a Dwarf Sd Galaxy

It seems reasonable that most low-luminosity Seyfert 1 nuclei have been found in early-type spiral galaxies, given the distribution of classical Seyferts among different Hubble types. Moreover, early-type spirals with well-developed bulges are thought to have much deeper potential wells than late-type spirals, perhaps promoting the formation of supermassive black holes and the retention of gas. Indeed, with the possible exception

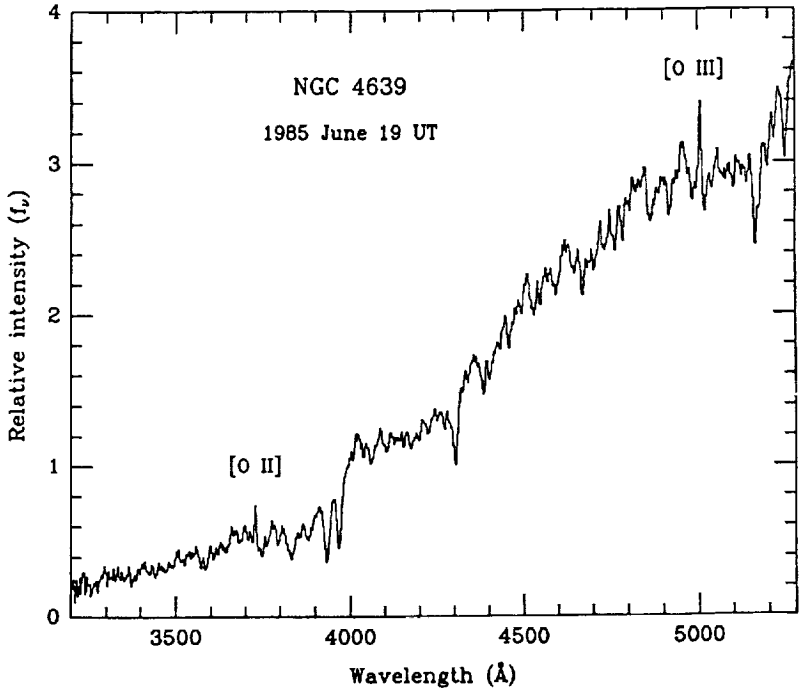


FIGURE 3 Blue spectrum of NGC 4639, obtained with the 3 m Shane reflector at Lick Observatory. The galaxy redshift has been removed. An absence of strong emission lines suggests that this is not a Seyfert galaxy.

of G1200–2038 (Kunth *et al.* 1987), until recently not a single Seyfert 1 nucleus had been found in Sd, irregular, or dwarf galaxies.

We were very surprised, therefore, to discover that NGC 4395, a nearby ($d \approx 2.6$ Mpc) low-luminosity ($M_B \approx -16.4$ mag) Sd galaxy, harbors a very faint Seyfert 1 nucleus (Filippenko and Sargent 1989). A superb photograph of this object is shown in panels 10 and 56 of the Atlas of Galaxies compiled by Sandage and Bedke (1988). The faint star-like nucleus emits a narrow-line spectrum similar to that of a type 2 Seyfert, with emission lines of very high ionization (up to [Ne V] and [Fe X]) superposed on a featureless continuum. Photoionization by a reasonably hard continuum is almost certainly responsible for their relative strengths, but [O I] $\lambda$6300 and [S II] $\lambda\lambda$6716, 6731 are unusually intense with respect to [N II] $\lambda\lambda$6548, 6583, as illustrated in Figure 5. The narrow lines have FWHM $\lesssim 60$ km s$^{-1}$, smaller than in any other known Seyfert nucleus.

Weak, broad components are clearly visible in the permitted-line profiles, but not in the forbidden lines. The FWZI of H$\alpha$ is 6,000–7,000 km

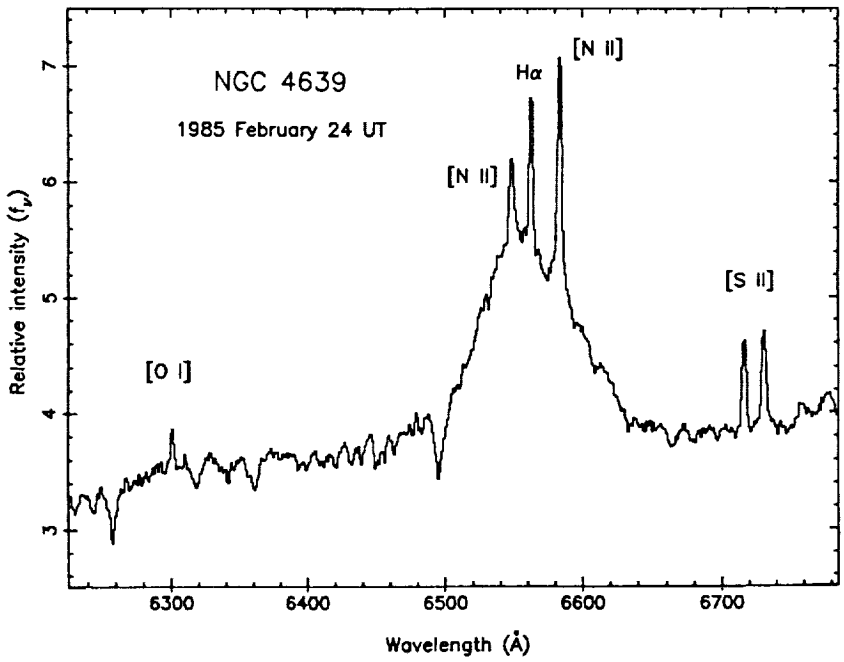


FIGURE 4 Red spectrum of NGC 4639 (Filippenko and Sargent 1986), obtained with the 5 m Hale reflector at Palomar Observatory. The galaxy redshift has been removed. Atmospheric $O_2$ produces the absorption line near 6260 Å. The obvious presence of broad H$\alpha$ emission indicates that the nucleus is a type 1 Seyfert.

$s^{-1}$ in the very high-quality spectrum (Figure 5), although the FWHM is only about 600–700 km $s^{-1}$. The luminosity of the broad H$\alpha$ line is $\sim 1.2 \times 10^{38}$ ergs $s^{-1}$, about one tenth that in M81, and $M_B \approx -9.8$ mag is measured from the spectrum. Hence, NGC 4395 has the intrinsically weakest known Seyfert 1 nucleus, with a blue luminosity no greater than that of the most luminous supergiant stars! If NGC 4395 were much farther away, so that the spectroscopic entrance aperture included a large amount of extranuclear light, its spectrum would have been dominated by emission lines from H II regions and continuum from OB associations, making the Seyfert activity difficult to detect.

At optical wavelengths the featureless continuum of NGC 4395 can be described by a power law with spectral index 1.5, comparable to that of other Seyfert 1 nuclei. Moreover, the equivalent width of the broad H$\alpha$ emission, 270 Å, is also typical of type 1 Seyferts. If we assume that the bolometric luminosity of the nucleus is roughly 1000 times that of the broad H$\beta$ emission, as for other Seyfert 1 nuclei (Weedman 1976), we find that $L_{Bol} \approx 1.5 \times 10^{40}$ ergs $s^{-1}$. This could be emitted by a black hole having

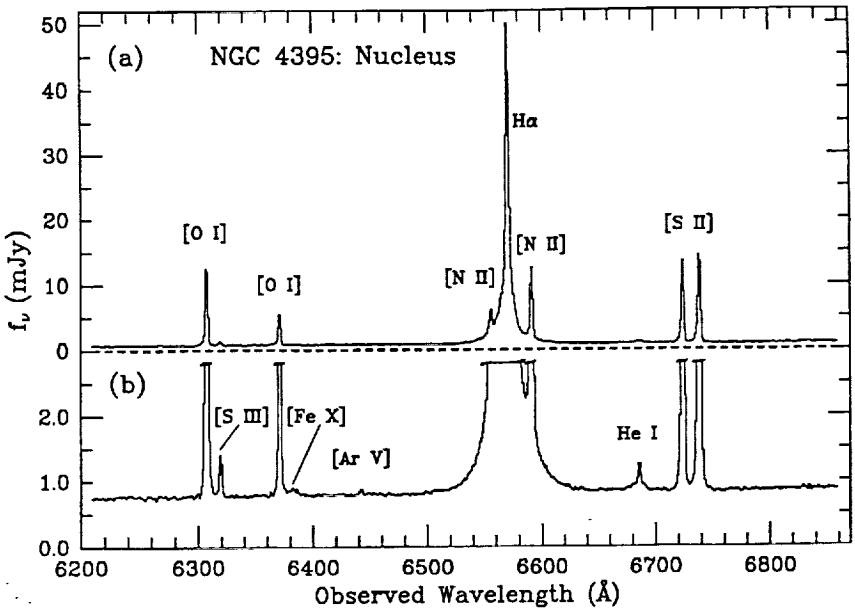


FIGURE 5 Red spectrum of the nucleus of NGC 4395 (Filippenko and Sargent 1989), obtained with the 5 m Hale reflector at Palomar Observatory. The galaxy's heliocentric radial velocity is 320 km $s^{-1}$. The luminosity of the broad H$\alpha$ line is the lowest measured in any Seyfert 1 nucleus.

a mass of only $\sim 100\ M_\odot$ if it were accreting at the Eddington limit! Such a black hole could be produced in only 200 million years if it started out with one solar mass and always accreted at the Eddington limit. Adopting the formalism of Wandel and Yahil (1985), on the other hand, we find that the current dynamical mass is about $10^4\ M_\odot$, if gravity accelerates the emission-line clouds to typical observed speeds of $\sim 500$ km $s^{-1}$. Thus, it is possible that $L \approx 0.01\ L_{Edd}$.

Given its low luminosity, it is interesting to consider whether the nucleus of NGC 4395 is actually a single very massive star ($M \approx 200\ M_\odot$?). Its spectrum, of course, is unlike that of known objects such as main-sequence O-type stars or even Wolf-Rayet stars, but this is nonetheless an interesting idea; we might never have observed such a star, because they form rarely and have very short lives. If the broad emission lines are caused by an outflowing wind, then the mass loss rate can be calculated under the assumption of steady-state conditions. Photoionization models give a distance of $\sim 10^{15}$ cm between the star and the emission-line clouds, and the absence of broad forbidden lines suggests that $n_e \gtrsim 10^9$ $cm^{-3}$. Adopting an outflow velocity of 500 km $s^{-1}$, the equation of continuity

yields $\dot{M} \approx 0.02\ M_\odot\ \mathrm{yr}^{-1}$. At this rate, the 200 $M_\odot$ star would only last about $10^4$ years!

It is very important to obtain additional observations, at all wavelengths, of low-luminosity Seyfert 1 nuclei such as that in NGC 4395. They offer counterexamples to the conventional wisdom that activity is restricted to early-type galaxies with large bulges. If a massive black hole is ultimately responsible for the observed phenomena in the nucleus of NGC 4395, we must explain how it was able to form in this particular object, but not in a majority of other extended, low-mass galaxies. On the other hand, perhaps most dwarf and very late-type galaxies can, in principle, be active, but are usually quiescent because the fueling mechanism does not operate efficiently. Basically, we do not yet know what conditions are necessary for a galaxy to have an active nucleus.

### Warmers: A Different Point of View

The narrow emission lines in classical AGNs, even those without broad emission lines, are almost certainly the result of photoionization of gas by a relatively flat UV and X-ray continuum. The intensities of the lines generally satisfy, very roughly, [O III] $\lambda5007/\mathrm{H}\beta \approx 10$ and [N II] $\lambda6583/\mathrm{H}\alpha \approx 1$, and high-ionization lines such as [Ne V] $\lambda3426$ and He II $\lambda4686$ are present (e.g., Osterbrock 1977; Koski 1978). [O I] $\lambda6300$ is considerably stronger than in H II regions, whose O and B stars produce Strömgren spheres with thin, well-defined boundaries between the zones of neutral and ionized hydrogen.

Most researchers believe that the continuum arises from the vicinity of a massive black hole, and is of nonstellar origin, as described above. There is, however, a very different possibility, at least for AGNs of relatively low luminosity. In a thought-provoking paper, Terlevich and Melnick (1985) showed that ionizing radiation from evolved, very massive ($M \gtrsim 60\ M_\odot$) stars in metal-rich H II regions can produce emission-line intensity ratios typical of Seyfert 2 nuclei. These Wolf-Rayet stars, which they call "Warmers" (extreme WC or WO stars), have effective surface temperatures of $(1-2) \times 10^5$ K; plenty of high-energy ionizing photons are therefore emitted. A key point is that stellar mass loss increases with increasing metal abundance in massive stars, so that very massive stars formed in high-metallicity environments can end their lives as bare He-C-O cores with surface temperatures comparable to those of the hottest known nuclei of planetary nebulae but with considerably higher luminosities.

Calculations show that after 3 million years, the ionizing continuum of a cluster created during a large burst of star formation (initial mass function slope = 3.0; Lequeux 1979) is nearly a power law, $f_\nu \propto \nu^{-1.5}$, with a cutoff at $\sim 20$ Ryd. Thus, the resulting emission-line spectrum from surrounding

clouds of gas having roughly solar composition closely resembles that of Seyfert 2 galaxies. Moreover, the weak featureless continuum observed in some type 2 Seyferts may be the reddened spectrum of the ionizing cluster. As the cluster ages, the spectrum evolves into one characterized by low-ionization emission lines, similar to those seen in Heckman's (1980) LINERs (low-ionization nuclear emission-line regions). Motivated by the success of their earlier work, Terlevich *et al.* (1987) went on to postulate that typical *Seyfert 1 nuclei* may also ultimately be produced by starburst activity. In their scenario, the broad emission lines are produced by supernovae (SNe), and by the interaction of SNe with a dense interstellar medium.

Although there are a number of potential difficulties with this hypothesis, here I speculate that NGC 4395 may represent an example of a Seyfert nucleus powered by a burst of star formation; in this case, the narrow-line spectrum is produced by a cluster of Warmers. Detailed photoionization models must be computed in order to see whether the observed emission-line spectrum can be reproduced under conditions appropriate for the Warmers scenario. It is not clear, for example, whether the low [N II] strength reflects peculiar abundances or unusual excitation.

The observed velocity of the broad-line gas is unlikely to be produced by gravitational effects; a sufficiently compact and massive star cluster would also be very short lived, due to stellar collisions. If, on the other hand, the broad permitted lines are produced by SNe, as suggested by Terlevich *et al.* (1987), only one very old SN is needed to explain their low luminosity. Indeed, if the total broad-line luminosity is $10^{39}$ ergs $s^{-1}$ (a reasonable value, given the observed strengths of H$\alpha$ and H$\beta$), the entire visible energy emitted by a typical SN ($\sim 10^{49}$ ergs) could power the nucleus for 300 years at a constant rate! Adding even a small fraction of the kinetic energy ($10^{51}$ ergs) greatly increases this estimate. Near maximum, a SN is far more luminous than the nucleus of NGC 4395; the SN in NGC 4395 must therefore be very old. Goodrich *et al.* (1989) detected weak, broad H$\alpha$ emission nearly three decades after the discovery of the more distant ($d \approx 8$ Mpc) SN 1961V, so a late-time detection of a SN in NGC 4395 is not unreasonable. Note, however, that Goodrich *et al.* (1989) believe that SN 1961V was actually *not* a SN, but rather an exaggerated $\eta$-Carinae-like outburst. This may be consistent with the single-star hypothesis of NGC 4395 briefly discussed in the preceding section.

It might be argued that the spectral characteristics of Seyfert 1 nuclei cannot possibly be produced by SNe, since the spectra of SNe are not generally thought to resemble those of Seyfert 1 nuclei. Figure 6, however, shows that there are some exceptions; the spectrum of SN 1987F was quite similar to that of 3C 48 at optical wavelengths (Filippenko 1989). There are, of course, some important differences if the spectra are examined carefully. The broad line near 5900 Å, for example, is attributed to Na I

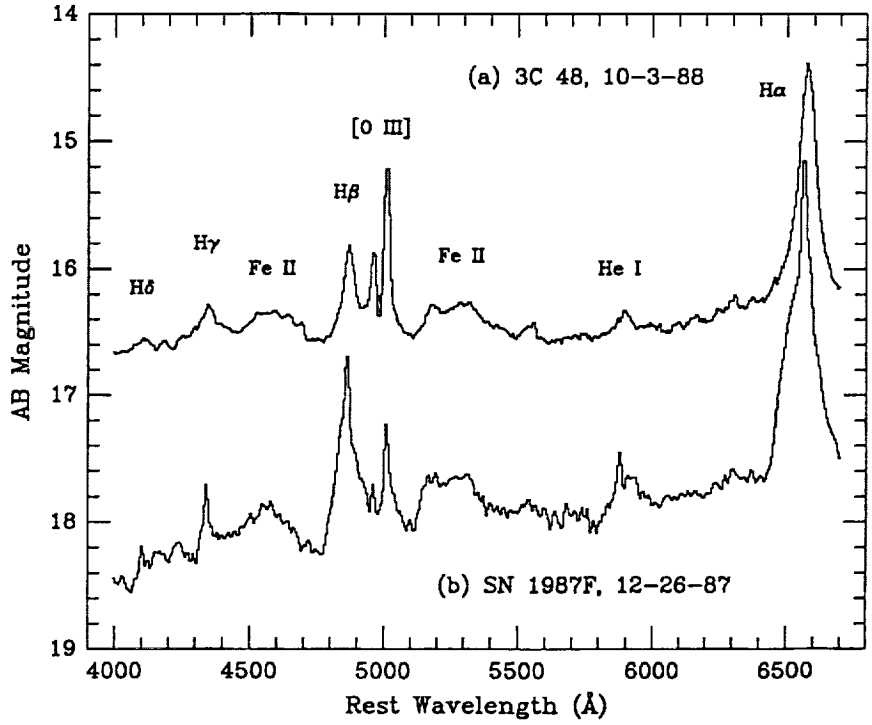


FIGURE 6 Spectra of (a) the quasar 3C 48, and (b) SN 1987F in NGC 4615 roughly 9 months after discovery. The data were obtained with the Shane 3 m reflector at Lick Observatory (Filippenko 1989). AB magnitude = $-2.5 \log f_\nu - 48.6$, where the unites of $f_\nu$ are ergs $s^{-1}$ $cm^{-2}$ $Hz^{-1}$.

D in SN 1987F and to He I in 3C 48. Moreover, the centroid of the broad H$\alpha$ line in SN 1987F and in other, similar SNe is blueshifted relative to the narrow component, whereas the broad H$\alpha$ in Seyfert 1 nuclei tends to be redshifted at least as often as blueshifted. Finally, the continuum of SN 1987F begins to drop rapidly at near-UV wavelengths, whereas that of 3C 48 remains quite strong.

Nevertheless, had SN 1987F occurred in the nucleus of a normal galaxy, a low-resolution spectrum undoubtedly would have led to a Seyfert 1 classification for the galaxy, especially if some Warmers were present to produce high-ionization narrow lines and a blue continuum. If we further *assume* that physical conditions (e.g., a dense interstellar medium, as may have been the case for SN 1987F) in certain galactic nuclei somehow enhance the production of SNe like SN 1987F, then the spectrum could remain Seyfert-like for long periods of time, and exhibit variability as well.

Thus, it is possible that *some* catalogued type 1 Seyfert galaxies, especially those of low luminosity, owe their observed characteristics to objects such as SN 1987F; we simply do not know enough about the evolution of SNe and their remnants in dusty, dense environments.

I do not want to use this spectral resemblance to argue for the above scenario as a *general* explanation for Seyfert 1 galaxies, and certainly not for luminous radio-loud QSOs. However, the spectral similarity of SN 1987F and 3C 48 at optical wavelengths can be used to teach us a great deal about the physical processes in both types of objects. Many more comparisons must be made, over as large a range of wavelengths as possible, in order to obtain a more thorough physical understanding of AGNs. I am certain we will encounter numerous surprises along the way.

## ACKNOWLEDGMENTS

Some of the observations reported here were taken at Palomar Observatory, where I was a Guest Investigator collaborating with W. L. W. Sargent. Data were also obtained at Lick Observatory, which receives partial funding from NSF Core Block grant AST–8614510, and from Las Campanas Observatory, which is owned and operated by the Carnegie Institution of Washington. My research on AGNs and SNe has been supported by the California Space Institute, most recently through grant CS–41–88, and by NSF grants AST–8957063 (Presidential Young Investigator Award) and AST–9003829. I thank the Office of International Affairs of the National Research Council, especially Kathleen Trivers, as well as George Clark, Walter Lewin, and Rashid Sunyaev, for organizing the successful NAS-ASUSSR Workshop on High Energy Astrophysics. I am also very grateful for the warm hospitality of our hosts in Moscow and Soviet Georgia.

## REFERENCES

Antonucci, R.R.J. 1984. Optical spectropolarimetry of radio galaxies. Astrophysical Journal 278: 499-520.

Antonucci, R.R.J., and J.S. Miller. 1985. Spectropolarimetry and the nature of NGC 1068. Astrophysical Journal 297: 621-632.

Collin-Souffrin, S., J.E. Dyson, J.C. McDowell, and J.J. Perry. 1988. The environment of active galactic nuclei–I. A two-component broad emission line model. Monthly Notices of the Royal Astronomical Society 232: 539-550.

Crenshaw, D.M., and B.M. Peterson. 1986. Evidence for a low-density component in the broad-line region of Seyfert 1 galaxies. Publications of the Astronomical Society of the Pacific 98: 185-191.

Davidson, K., and H. Netzer. 1979. The emission lines in quasars and similar objects. Reviews of Modern Physics 51: 715-766.

De Robertis, M.M., and D.E. Osterbrock. 1986. An analysis of the narrow line profiles in Seyfert 2 galaxies. Astrophysical Journal 301: 727-741.

di Serego Alighieri, S., L. Binette, T.J.-L. Courvoisier, R.A.E. Fosbury, and C.N. Tadhunter. 1988. A blue, polarized continuum source near radio galaxy PKS 2152-69. Nature 334: 591-593.

Elvis, M. 1984. "Microquasars" and the X-ray background. Advances in Space Research 3(10-12): 207-209.

Elvis, M., and A. Lawrence. 1985. X-ray spectra of active galaxies and quasars. Pages 289-331. In: Miller, J.S. (ed.). Astrophysics of Active Galaxies and Quasi-Stellar Objects. University Science Books, Mill Valley, CA.

Ferland, G.J., and G.A. Shields. 1985. The theory of emission-line regions in active galactic nuclei. Pages 157-184. In: Miller, J.S. (ed.). Astrophysics of Active Galaxies and Quasi-Stellar Objects. University Science Books, Mill Valley, CA.

Filippenko, A.V. 1985. New evidence for photoionization as the dominant excitation mechanism in LINERs. Astrophysical Journal 289: 475-489.

Filippenko, A.V. 1988. Indirect evidence for massive black holes in nearby galactic nuclei. Pages 104-119. In: Kafatos, M. (ed.). Supermassive Black Holes. Cambridge University Press, Cambridge.

Filippenko, A.V. 1989. The "Seyfert 1" optical spectra of the type II supernovae 1987F and 1988I. Astronomical Journal 97: 726-734.

Filippenko, A.V., and W.L.W. Sargent. 1985. A search for "dwarf" Seyfert 1 nuclei: the initial data and results. Astrophysical Journal Supplement Series 57: 503-522.

Filippenko, A.V., and W.L.W. Sargent. 1986. The properties of "dwarf" Seyfert nuclei in nearby galaxies. Pages 21-45. In: Giuricin, G., F. Mardirossian, M. Mezzetti, and M. Ramella (eds.). Structure and Evolution of Active Galactic Nuclei. Reidel, Dordrecht.

Filippenko, A.V., and W.L.W. Sargent. 1988. A detailed study of the emission lines in the Seyfert 1 nucleus of M81. Astrophysical Journal 324: 134-153.

Filippenko, A.V., and W.L.W. Sargent. 1989. Discovery of an extremely low luminosity Seyfert 1 nucleus in the dwarf galaxy NGC 4395. Astrophysical Journal (Letters) 342: L11-L14.

Goodrich, R.W., G.S. Stringfellow, G.D. Penrod, and A.V. Filippenko. 1989. SN 1961V: an extragalactic eta Carinae analog? Astrophysical Journal 342: 908-916.

Halpern, J.P. 1982. X-ray spectra of active galactic nuclei. Ph.D. Thesis, Harvard University. University Microfilms International, Ann Arbor, MI.

Heckman, T.M. 1980. An optical and radio survey of the nuclei of bright galaxies. Astronomy and Astrophysics 87: 152-164.

Joly, M. 1987. Formation of low ionization lines in active galactic nuclei. Astronomy and Astrophysics 184: 33-42.

Keel, W.C. 1983. Spectroscopic evidence for activity in the nuclei of normal spiral galaxies. Astrophysical Journal 269: 466-486.

Koski, A.T. 1978. Spectrophotometry of Seyfert 2 galaxies and narrow-line radio galaxies. Astrophysical Journal 223: 56-73.

Kunth, D., W.L.W. Sargent, and G.D. Bothun. 1987. A dwarf galaxy with Seyfert characteristics. Astronomical Journal 93: 29-32.

Lequeux, J. 1979. A quantitative study of the upper HR diagram and a new determination of the local initial mass function. Astronomy and Astrophysics 80: 35-41.

Malkan, M.A., and A.V. Filippenko. 1983. The stellar and nonstellar continua of Seyfert galaxies: nonthermal emission in the near-infrared. Astrophysical Journal 275: 477-492.

Miller, J.S. 1989. Observational studies of the structure of active galactic nuclei and QSOs. Pages 273-283. In: Osterbrock, D.E., and J.S. Miller (eds.). IAU Symposium 134: Active Galactic Nuclei. Kluwer, Dordrecht.

Miller, J.S., and R.W. Goodrich. 1990. Spectropolarimetry of high-polarization Seyfert 2 galaxies and unified Seyfert theories. Astrophysical Journal 355:456-467.

Netzer, H. 1987. Quasar discs–II. A composite model for the broad-line region. Monthly Notices of the Royal Astronomical Society 225: 55-72.

Netzer, H. 1989. Structure and nature of AGNs. Pages 69-84. In: Miller, J.S., and D.E. Osterbrock (eds.). IAU Symposium 134: Active Galactic Nuclei. Kluwer, Dordrecht.

Netzer, H., and G.J. Ferland. 1984. Some comments on models of photoionized nebulae. Publications of the Astronomical Society of the Pacific 96: 593-597.

Neugebauer, G., J.B. Oke, E.E. Becklin, and K. Matthews. 1979. Absolute spectral energy distributions of quasi-stellar objects from 0.3 to 10 microns. Astrophysical Journal 230: 79-94.

Osterbrock, D.E. 1977. Spectrophotometry of Seyfert 1 galaxies. Astrophysical Journal 215: 733-745.

Osterbrock, D.E., and W.G. Mathews. 1986. Emission-line regions of active galaxies and QSOs. Annual Reviews of Astronomy and Astrophysics 24: 171-203.

Peimbert, M., and S. Torres-Peimbert. 1981. Physical conditions in the nucleus of M81. Astrophysical Journal 245: 845-856.

Peterson, B.M. 1988. Emission-line variability in Seyfert galaxies. Publications of the Astronomical Society of the Pacific 100: 18-36.

Pogge, R.W. 1988. An extended ionizing radiation cone from the nucleus of the Seyfert 2 galaxy NGC 1068. Astrophysical Journal 328: 519-522.

Pogge, R.W. 1989. The circumnuclear environment of nearby, noninteracting Seyfert galaxies. Astrophysical Journal 345: 730-751.

Rees, M.J. 1984. Black hole models for active galactic nuclei. Annual Reviews of Astronomy and Astrophysics 22: 471-506.

Salpeter, E.E. 1964. Accretion of interstellar matter by massive objects. Astrophysical Journal 140: 796-800.

Sandage, A., and J. Bedke. 1988. Atlas of Galaxies Useful for Measuring the Cosmological Distance Scale. Carnegie Institution of Washington, Washington D.C.

Shields, G.A. 1978. Thermal continuum from accretion disks in quasars. Nature 272: 706-708.

Shuder, J.M. 1981. Emission-line–continuum correlations in active galactic nuclei. Astrophysical Journal 244: 12-18.

Shuder, J.M., and D.E. Osterbrock. 1981. Empirical results from a study of active galactic nuclei. Astrophysical Journal 250: 55-65.

Stauffer, J.R. 1982. A nuclear spectroscopic survey of disk galaxies. II. Galaxies with emission lines not excited by stellar photoionization. Astrophysical Journal 262: 66-80.

Sun, W.-H., and M.A. Malkan. 1989. Fitting improved accretion disk models to the multiwavelength continua of quasars and active galactic nuclei. Astrophysical Journal 346: 68-100.

Tadhunter, C.N., R.A.E. Fosbury, L. Binette, I.J. Danziger, and A. Robinson. 1987. Detached nuclear-like activity in the radio galaxy PKS 2152–69. Nature 325: 504-507.

Terlevich, R., and J. Melnick. 1985. Warmers: the missing link between starburst and Seyfert galaxies. Monthly Notices of the Royal Astronomical Society 213: 841-856.

Terlevich, R., J. Melnick, and M. Moles. 1987. Starburst models for AGNs. Pages 499-519. In: Khachikian, E.Ye., K.J. Fricke, and J. Melnick (eds.). IAU Symposium 121: Observational Evidence of Activity in Galaxies. Reidel, Dordrecht.

Véron, P. 1979. The luminosity function of Seyfert 1 galaxy nuclei and BL Lac objects, and the X-ray background. Astronomy and Astrophysics 78: 46-52.

Wandel, A., and A. Yahil. 1985. Universal mass-luminosity relation for quasars and active galactic nuclei? Astrophysical Journal (Letters) 295: L1-L4.

Weedman, D.W. 1976. Luminosities of Seyfert galaxies and QSOs. Astrophysical Journal 208: 30-36.

Weedman, D.W. 1985. Evolution of active galactic nuclei and quasars. Pages 497-519. In: Miller, J.S. (ed.). Astrophysics of Active Galaxies and Quasi-Stellar Objects. University Science Books, Mill Valley, CA.

Whittle, M. 1985. The narrow line region of active galaxies — III. Profile comparisons. Monthly Notices of the Royal Astronomical Society 216: 817-855.

Wilson, A.S., M.J. Ward, and C.A. Haniff. 1988. High-resolution emission-line imaging of Seyfert galaxies. II. Evidence for anisotropic ionizing radiation. Astrophysical Journal 334: 121-129.

Yee, H.K.C. 1980. Optical continuum and emission-line luminosity of active galactic nuclei and quasars. Astrophysical Journal 241: 894-902.

Zel'dovich, Ya.B., and I.D. Novikov. 1964. Relativistic astrophysics. I. Uspekhi Fizicheskikh Nauk 84: 377-417. (Soviet Physics Uspekhi 7: 763-788.)

# On Two-Dimensional Relativistic Stellar Winds

M.E. GEDALIN, J.G. LOMINADZE, AND E.G. TSIKARISHVILI
Abastumani Astrophysical Observatory

Stellar wind is of great interest, because many of the astrophysical systems, besides stars, possess wind-like structures. For a long time only nonrelativistic winds have been investigated. However, recently (Kennel *et al.* 1983; Kennel and Coroniti 1984; Kennel *et al.* 1984) it was proposed that the relativisitic pulsar wind with the plasma, consisting of electrons and positrons, can be responsible for the observed features of the Crab nebula. The study in Kennel *et al.* (1983) has revealed the inconsistency of the assumption of the wind zero temperature with the observational data. It has been shown that only for high relativisitic temperatures can high Mach numbers be reached, which allows the possibility of a shock formation.

However, the analysis of Kennel *et al.* (1983) is rather incomplete, since it ignores the essentially three-dimensional wind structure and deals with a one-dimensional object. It means in spherical coordinates only $\partial/\partial r = 0$ and $\theta = \pi/2$. In this case, all connections between neighboring field lines are lost and only one is considered. The essentially three-dimensional structure requires a smooth transition from one field line to another, and thus a distortion of the "monopole solution" arises so that the last can be only an approximation at large distances.

An attempt to investigate a two-dimensional wind structure has been made in Okamoto (1978). However, temperature is taken at zero and parameter variations across field lines are not considered.

In the present paper we extend the analysis of Kennel, *et al.* (1983) into the two-dimensional case $\partial/\partial\phi = 0$, $\partial/\partial\theta \neq 0$, $\partial/\partial r \neq 0$. As it was proposed in Okamoto (1978) and Kennel *et al.* (1983) and confirmed in Kennel *et al.* (1988), we use conventional MHD equations for a relativistic plasma with an isotropic relativistic temperature. The state equation is assumed polytropic. One can readily see that plasma is always cold at r

$\rightarrow \infty$, so that one should rather say that the temperature is high at the injection point.

To be mathematically formal we introduce curvilinear orthogonal coordinates ($\xi$, $\eta$, $\subset$) with the metric

$$dl^2 = h_\xi^2 d\xi^2 + h_\eta^2 d_\eta^2 + h_\varphi^2 d_\varphi^2$$

where $\xi$ is the coordinate along the poloidal magnetic field line and $\eta$ numbers field lines. When $\xi \rightarrow \infty \xi \approx \zeta$, $\eta \approx \theta$.

With the new coordinates one can derive the following set of constants of motion along the field line:

$$Bh_\eta h_\varphi = f_1(\eta)$$

$$nuh_\eta h_\varphi = f_2(\eta)$$

$$h_\eta(u_\varphi B - uB_\varphi) = \gamma f_3(\eta)$$

$$f_2\gamma\mu - f_3 h_\varphi B_\varphi/4\pi = f_4(\eta)$$

$$f_2\mu u_\varphi h_\varphi - f_1 h_\varphi B_\varphi/4\pi = f_5(\eta) \qquad (1)$$

The equation for the transverse variations of parameters looks as follows:

$$nh_\xi^2 h_\varphi^2 \frac{\partial \mu}{\partial \eta} = (n\mu u^2 h_\varphi^2/2)\frac{\partial}{\partial \eta} h_\xi^2 - (n\mu u_\varphi^2 h_\varphi^2/2)\frac{\partial}{\partial \eta} h_\varphi^2 =$$

$$(1/8\pi)\frac{\partial}{\partial \eta}(h_\xi h_\varphi f_3/h_\eta)^2 - (h_\varphi^2/8\pi)\frac{\partial}{\partial \eta} b^2 h_\xi^2 - (h_\varphi^2/8\pi)\frac{\partial}{\partial \eta} B_\varphi^2 h_\varphi^2 \qquad (2)$$

It does not give a constant of motion, but a constraint on the preceeding set. Physically the constraint arises because of the distortion of the field lines due to the interaction with the neighboring ones. It is essential and describes the global features of the wind structure, since it cannot be one-dimensional. One could assume that (2) could be ignored when the equatorial plane is considered (cf. Kennel *et al.* 1983). We show below, that even if this is the case, (2) defines a new "global" parameter.

The set (1) can be used in the same manner, as it has been used in 1 to derive the "wind algebraic equation":

$$N^2 = K^2(-B^2 + [S^2(EY - H)^2 - (qY - HS^2)]^2)/S^2Y^2(Y + S^2 - 1)^2) \quad (3)$$

$$Y = KX_\infty(1 + \propto N^{\gamma-1})/N$$

where $Y = M^2$ (where M is the Alfvenic Mach number), $S = \Omega h\varphi$ (where $\Omega$ is angular velocity), and $\Omega$, K, E, H, Q, $X_\infty$, $\propto$ are constants along the field line (cf. [1]).

The analysis is straightforward and the results of Kennel *et al.* (1983) can be easily rederived. The system posesses critical points of three types: slow, intermediate, and fast. The only was to have $M_F > 1$ when $\xi \to \infty$ is to pass through the fast critical point of to have initially $M_F > 1$ at the injection point. We will not discuss the topological features of the solutions of (3). The reader is referred to Kennel *et al.* (1983) where he should ignore all the points where $B \sim r^{-2}$ is assumed.

Here we briefly discuss the most interesting asymptotics $S^2 \to \infty$ (open field lines). One can easily see that there are no solutions with $Y/S^2 \to 0$. It can be also shown that if $Y/S^2 \to \infty$, then $BS^2 \to 0$. However, there must be $B \sim 1/S^2$ on the open field lines. Therefore, the only possibility is $Y/S^2 \to c^2 = \text{const}$.

One can obtain

$\gamma \to Ec^2/(c^2 + 1)$ $\mu_*\gamma_*/m$, $\mu_*$ - initial specific enthalpy,
$SU_\varphi \to (qc^2 - H)/(c^2 + 1) \to U_\varphi \sim 1/S$,
$SB_\varphi \to -E/(c^2 + 1) \to B_\varphi \sim 1/S$,
$U \to U_\varphi = \text{const}$ $(\eta)$.

Since we are mostly interested in the wind structure at large distances, we may assume $\xi \approx r + 0(1)$, $\eta \simeq \theta + 0(1/4r)$. One can approximately solve (3) for this conditions to have

$$B_\varphi h_\varphi \to 1(\theta), 1^2/\gamma^2 = \text{const.} \quad (4)$$

This ratio does not depend on $\theta$. It is easy to obtain the important relation

$$\Omega Z/X_\infty = p, z = c^2 \quad (5)$$

where now p is constant not only on a particular field line, but for the whole two-dimensional structure. It is a "global" parameter.

Thus, one should replace one of the parameters in (1) with the global constant of motion p.

The asymptotic velocity is then determined by p:

$$u_\infty = p\Psi/\Omega, \Psi = BS^2, S^2_{\to}\infty$$

Thus, the asymptotic energy is completely determined by the magnetic flux, angular velocity, and p.

One can see that for a given p only one solution exists for $r \to \infty$. It means that the two solutions of Kennel *et al.* (1983) with $M_F > 1$ and $M_F < 1$, cannot coexist: only one family is consistent with the given p.

As a conclusion we state that the two-dimensional relativistic winds with $M_F > 1$ at $r \to \infty$ can exist, when the plasma is relativistically hot at the injection point. In this case the structure is defined by the set (1) of constants of motion along the field line. Additional constraint arises from the transverse continuity requirement, which gives life to a global parameter, that is constant for the whole structure. The number of asymptotic solutions is reduced to one.

## REFERENCES

Kennel, C.F., and F.V. Coroniti. 1984. Ap. J. 283: 694.
Kennel, C.F., and F.V. Coroniti. 1984. Ap. J. 283: 710.
Kennel, C.F., F.S. Fujimura, and I. Okamoto. 1983. Fluid Dynamics. Geophys. Astrophys. 26: 147.
Kennel, C.F., M.E. Gedalin, and J.G. Lominadze. 1988. Proc. Joint Varenna-Abastumani Int. School and Workshop Plasma Astrophys. p 137.
Okamoto, I. 1978. MNRAS. 185: 69.

# Cluster Research with X-Ray Observations

RICCARDO GIACCONI AND RICHARD BURG
Space Telescope Science Institute

## ABSTRACT

Past X-ray surveys have shown that clusters of galaxies contain hot gas. Observations of this hot gas yield measurements of the fundamental properties of clusters. Results from a recent study of the X-ray luminosity function of local Abell clusters are described. Future surveys are discussed and the potential for studying the evolution of clusters is analyzed.

## INTRODUCTION

The systematic study of clusters began with the surveys of Abell (1958) and Zwicky *et al.* (1968) who each created well-defined catalogues according to specific definitions of the object class. In particular Abell defined clusters as overdensities of galaxies within a fixed physical radius around a center, classifying such objects as a function of their apparent magnitude (distance) and of their overdensity ("richness").

The first X-ray survey of the sky by the UHURU X-ray satellite showed that "rich" nearby clusters were powerful X-ray sources (Gursky *et al.* 1971; Kellogg *et al.* 1972). Subsequent spectroscopic studies detected X-ray emission lines of highly ionized iron and demonstrated that the X-ray emission was produced by thermal radiation of a hot gas with temperatures in the range of 30 to 100 million degrees (Mitchell *et al.* 1976; Serlemitsos *et al.* 1977).

With the launch of the HEAO1 and the *Einstein* Observatories, surveys of significant samples of nearby clusters demonstrated that as a class, clusters of galaxies are bright X-ray sources with luminosities between $10^{42}$

and $10^{45}$ ergs/sec (Johnson *et al.* 1983; Abramopoulos and Ku 1983; and Jones and Forman 1984). The increased sensitivity of the *Einstein* imaging detectors also provided the capability to study clusters at large redshifts ($z \gtrsim 0.5$) (Henry *et al.* 1979).

The general problem one wishes to attack by means of X-ray observations is the study of the formation and dynamic evolution of structures consisting of gravitationally bound galaxies. It has been pointed out by several authors (Kaiser 1986; Shaeffer and Silk 1988) that X-ray observations of such systems may offer important advantages with respect to studies in other wavelength domains, particularly at early epochs of the universe. In Table 1 we list the fundamental properties of clusters that can be measured in X-ray surveys along with a brief description of the measurement. We also include, for comparison, the analogous measurement in the optical.

In order to be efficiently detected in X-rays, such systems can be empirically defined as having the following properties:

1. They must contain sufficient intergalactic gas (typically 1/10 of the cluster mass).
2. The gas must have been heated to X-ray emitting temperatures typically larger than those corresponding to escape velocity from a single galaxy. It should be noted that the efficiency of X-ray emission depends on metallicity.
3. The gas must be centrally concentrated in the cluster, ($L_x \sim \rho^2$), although not more so than the galaxies in nearby observed systems.

Such properties have been shown to exist in Abell-type clusters, as well as in much poorer systems such as cD groups (Kriss *et al.* 1980). Thus the class of X-ray luminous clusters of galaxies which may be retrieved in future sensitive X-ray surveys in a sufficiently soft X-ray band (for example 0.1-2 KeV), will include both optically defined classes of rich clusters (such as Abell or Zwicky) as well as poorer clusters or any gravitationally bound system of galaxies containing high-temperature gas. The *Einstein* Observatory Medium Sensitivity Survey which uses the IPC data (0.35 to 3.5 keV) has in fact detected a number of optically poor X-ray emitting clusters (Gioia *et al.* 1982).

## X-RAY LUMINOSITY FUNCTION

We would like to briefly summarize some of the recent work by Forman, Jones, and ourselves on the X-ray luminosity function of Abell cluster as an introduction to the subject.

The earliest determinations of the X-ray luminosity function for Abell-like clusters of galaxies were based on the UHURU and Ariel surveys.

TABLE 1

| Property | Optical | X-rays |
|---|---|---|
| Detection | $N_{gal}(m_3 - m_3 + 2) \geq n$ | $S > S_{min}$ |
| | in $R_A = 1.7/z$ arcmin | $\theta > \theta_{min}$ |
| | $R_A = 3h_{50}^{-1}$mpc | |
| Luminosity | $L_{opt} = \Sigma L_{gal}$ | $L_x = \Sigma L_{xgal} + \rho^2_{gas} V_{gas} T^{1/2}_{gas}$ |
| Mass | $M_{tot} = \frac{3R_G\sigma_r^2}{G}$ | $M(R) \sim 3(kTR/\mu m_h G)$ |
| | $3\sigma_r^2 = (\nu^2)$ | $M(\leq R) = -\left(\frac{kTr}{G\mu m_n}\right)\left(\frac{d\log\rho}{d\log r} + \frac{d\log T}{d\log r}\right)$ |
| Temperature | $\sigma^2_{gal}$ | $T_{gas}$ |
| Metallicity | $Z_{gal}$ | $Z_{gas}$ |
| Morphology | Morphology with $N_{gal}$ | Morphology gas($\rho^2$) |

Schwartz used a sample of 6 clusters and McHardy a sample of 20 clusters to derive luminosity functions. Extensions of these first attempts included the analysis of HEAO1-A2 data (Piccinotti *et al.* 1982) with samples of 30 clusters. More recent surveys with HEAO1-A2 were based on 128 detected clusters (Johnson *et al.* 1983). Finally, Abramopoulos and Ku (1983) used *Einstein* imaging observations of 74 nearby clusters with $z \leq 0.27$. It should be noted that while the UHURU, Ariel and HEAO1 surveys were X-ray flux limited surveys which, in principle, could have studied the X-ray luminosity of a more general cluster population, they were severely biased by their sensitivity and energy range to the detection of Abell-like rich, high-temperature clusters, although some X-ray emitting groups were observed (Schwarz *et al.* 1980).

These determinations of the X-ray luminosity function of Abell-like clusters were based on relatively small samples and had intrinsic limitations or deficiencies. In particular, previous determinations of the Abell-like cluster X-ray luminosity function did not take into account the incompleteness for richness 0 clusters (Abramopolos and Ku 1983), did not include richness 0 clusters (Kowalski *et al.* 1983), or were not sensitive to low temperatures because of their effective energy band (Piccinotti *et al.* 1982; Kowalski *et al.* 1983). The last limitation could be quite important in attempting to understand the low end of the X-ray luminosity function since there appears to be (at least for $R \geq 1$) a correlation between X-ray luminosity and temperature (Mushotzky 1988).

In our recent work we have investigated the statistical properties of the 226 Abell clusters with $z \lesssim 0.15$ observed by the *Einstein* Observatory (Burg *et al.* 1990, hereafter referred to as BFGJ). This sample is taken from the larger compilation of Einstein cluster observations analyzed by Jones and Forman. We show that this set of clusters form, for the purpose of this work, an unbiased sample of Abell clusters that spans richness classes 0 to 2. We use the Einstein sample to derive an X-ray luminosity function which is free of some of the problems which beset previous analyses. The main advantages of this determination are: the ability to detect low-temperature clusters because of the energy band (0.5 to 4.5 keV) (in common with the Abramopoulos and Ku survey); the larger sample which allows us to adopt stringent criteria to insure completeness and allows us to determine the X-ray luminosity function for different richness classes; and the higher sensitivity which allows us to explore the low-luminosity end of the luminosity function.

The redshift limit of 0.15 was chosen for our sample since within this range the Abell richness classification is distance independent. Furthermore we have established that for redshifts $< 0.15$ there is no correlation between redshift and X-ray luminosity (see Figure 1). Thus this subset of the Abell catalog can indeed be considered a proper sample to derive the shape of

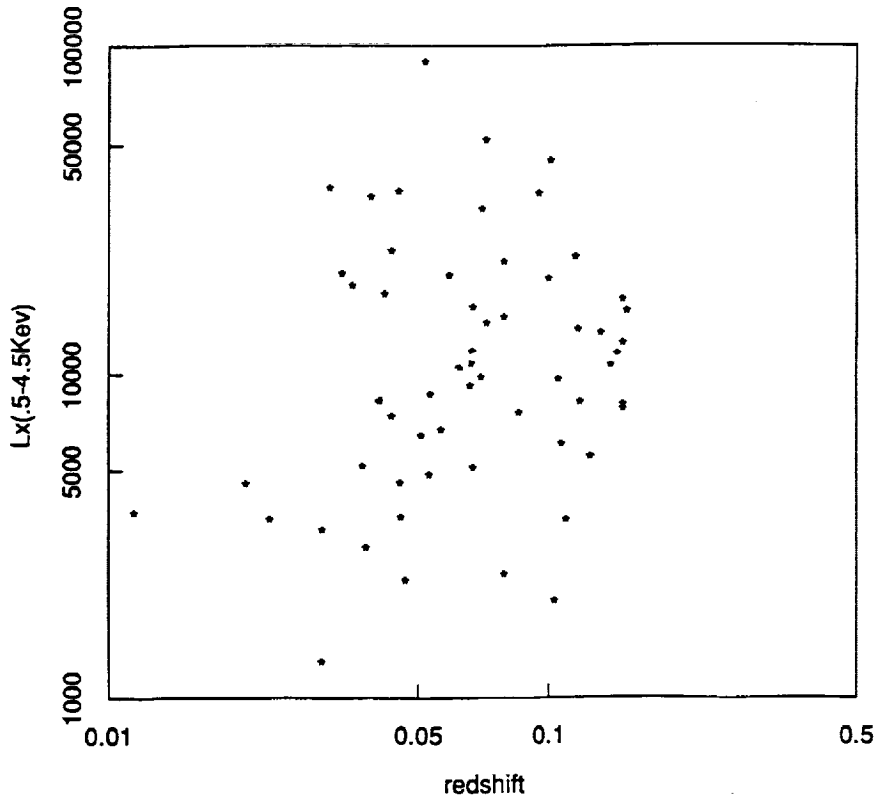


FIGURE 1 Scatter diagram of X-ray luminosity versus redshift for richness 1 clusters.

the X-ray luminosity function by richness class since the entire range of X-ray luminosity can be observed throughout the chosen volume.

The IPC fluxes from the compilation of Jones and Forman (1990) have been obtained by integration over a region of 1 Mpc radius centered on the X-ray determined cluster center. These fluxes are computed in the 0.5-4.5 keV (observed) band, from the observed counting rates, using the hydrogen column density and either the observed or estimated gas temperature. The estimated gas temperature is computed using the observed luminosity temperature relation, which we have rederived for our sample and which is given by $L_x \propto T^{5/2}$ (Mushotzky 1988).

The luminosity at the source is computed utilizing the measured X-ray flux and the measured or estimated redshift. K-corrections have been computed using the Raymond-Smith model, assuming 0.5 solar metallicity, and they are of order 20% over the redshift and temperature range of the sample (Burg and Giacconi 1990). The method used for computing the

luminosity function is dictated by the criteria used in selecting the sample. In this work the underlying sample is defined by optical properties (i.e. the number of galaxies in an Abell radius) and not by X-ray properties. Thus the computed luminosity function is a bi-variate function of both $L_x$ and cluster richness R.

The sample is volume limited in the sense that the Abell sample (with the same redshift cutoff) is volume limited and with the same incompleteness problems. Therefore each cluster contributes $1/V_{Abell}$ to the luminosity function. This is different from the methodology used for an X-ray flux limited survey where each cluster would contribute

$$\frac{1}{V\max(S_{\lim}, L_x)}$$

To calculate the cumulative luminosity function, we use the Kaplan-Meier product limit estimate method (Cox and Oakes 1984; Schmitt 1985; Feigelson and Nelson 1985). This is equivalent to the techniques developed by Avni *et al.* (1980). Specifically, the following probability is calculated:

$$P(L_x > L'_x) = 1 - \prod(1 - \frac{N(L'_x)}{N(L_x \leq L'_x)})$$

This is the unnormalized cumulative luminosity function and is formally the maximum likelihood estimate of the luminosity function. The results are shown in Figure 2a.

Since our X-ray sample is not an independently complete sample, we must rely on the understanding of the completeness characteristics of the Abell sample to derive the normalization. The Abell Catalogue is known to be incomplete for richness class 0. Abell recognized this and did not include the richness class 0 objects in his "statistical" sample. Later work by Bahcall (1979; see also Lucy 1983), based on analysis of the multiplicity function (the number of clusters per unit volume versus richness) has shown that richness 0 clusters are incomplete by a factor of $> 3$. Quantitatively we fit Schechter functions to the data with the results shown in Figure 2b. It must be stressed that the normalization does not affect the shape of the luminosity function.

Some aspects of our results are immediately apparent:

a. The shape of the luminosity function is similar for each richness class, although there is a change in scale.
b. Richer clusters are systematically brighter in X-rays. The value of $L^*_x$, the characteristic luminosity for each richness class is roughly proportional to $(N^*_{gal})^\gamma$, (where $N^*$ is the characteristic number of galaxies per richness class, Lucy 1983), $\gamma = 1.6 \pm 0.4$.

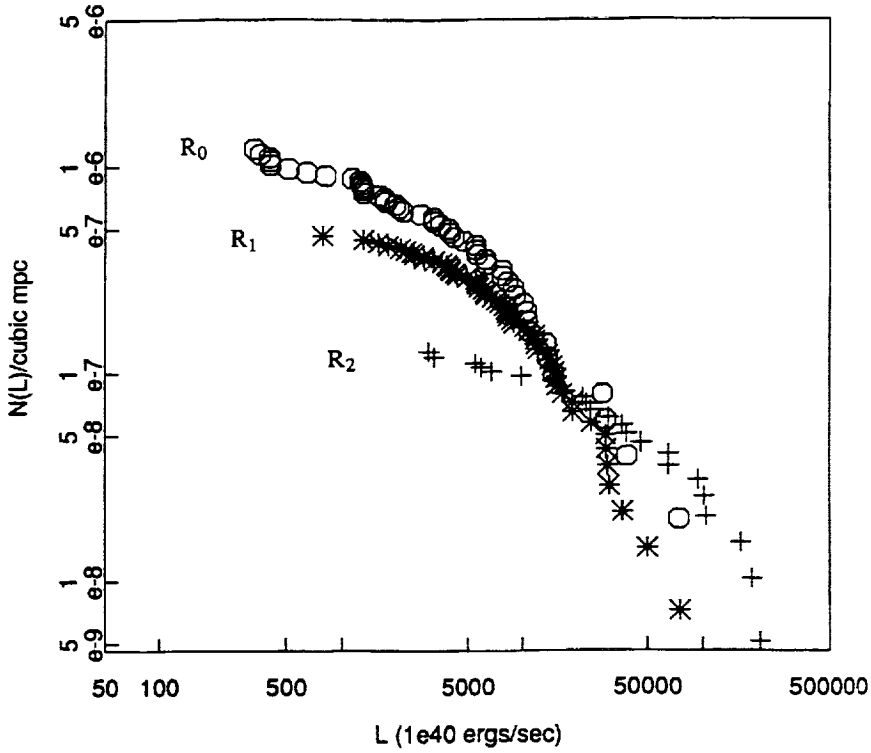


FIGURE 2a Non-parametric luminosity function by richness class.

(See Figure 3). This is to be compared with Abramopoulos and Ku (1983) who derived $L_x \sim N_{gal}^{1.2}$

c. There is within each richness class a wide range of X-ray luminosities. There is an apparent flattening of the slope of the luminosity function for each richness class.

d. Our observed luminosity functions can be described as Schechter functions with approximately the same slope and different $L_x^*$.

A less obvious aspect of our result deserves some note. A priori we would have expected to observe a distribution of X-ray luminosity of clusters bound between two values. A minimum due to the integrated contribution of the individual galaxies (Mushotzky 1988) and a maximum which corresponds to the X-ray emission of clusters whose state of dynamic evolution, central condensation and original conditions lead to the maximum energy dissipation in X-rays at the current epoch.

In Figure 4 we present our combined luminosity function for $R \geq 1$ and $R \geq 0$. We show both cases since for $R \geq 0$ we are dominated by the

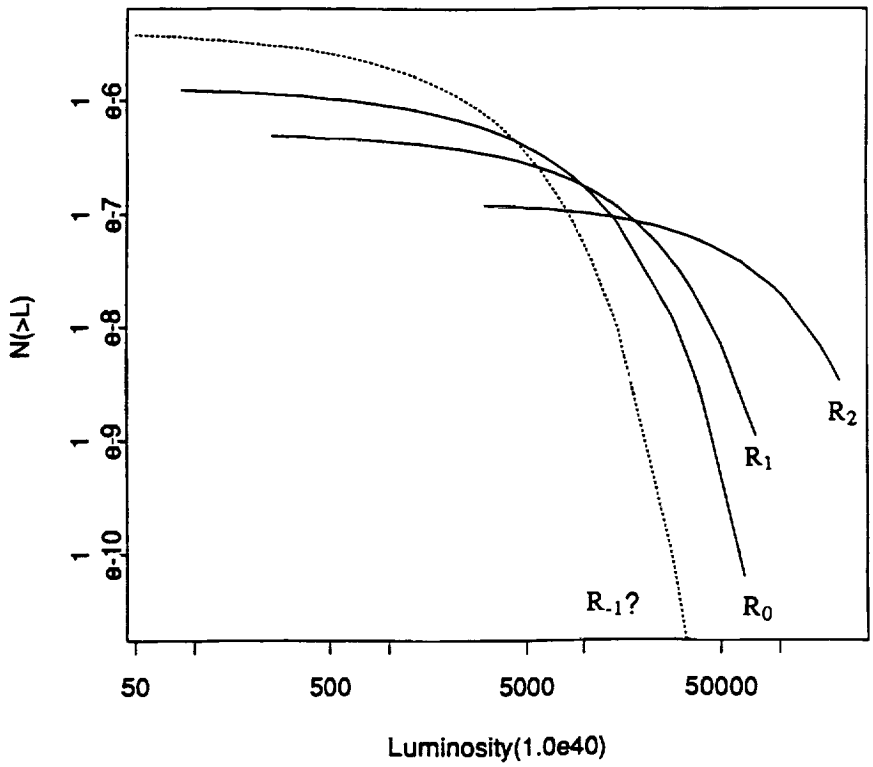


FIGURE 2b Schechter function fits.

normalization uncertainty. On the same plot we include previously reported luminosity functions. We agree at the high-luminosity end with previous results and we are not inconsistent at the low-luminosity end where use of the Bahcall normalization, to take into account R = 0 incompleteness, has the biggest effect. As mentioned above, the X-ray luminosity which we measure must be in all cases the sum of the X-ray luminosity of the individual galaxies plus a component due to intergalactic hot dense gas. For evolved systems we would expect this latter component to dominate. For instance a cluster such as Coma (R = 2) has an X-ray luminosity of $3.7 \times 10^{44}$ ergs $s^{-1}$, while the integrated emission from single galaxies is about $10^{43}$ erg $s^{-1}$. A1367, which was previously studied in some detail (Bechtold *et al.* 1983) could be an example of a cluster where summed galaxy emission is a large fraction of the total cluster luminosity. A1367 is a loose, seemingly unevolved structure, the relatively low temperature of 4 keV. In their work Bechtold *et al.* showed that the summed contribution of the 10 brightest galaxies was $\sim 3 \times 10^{42}$ ergs/sec. This is 5% of the total

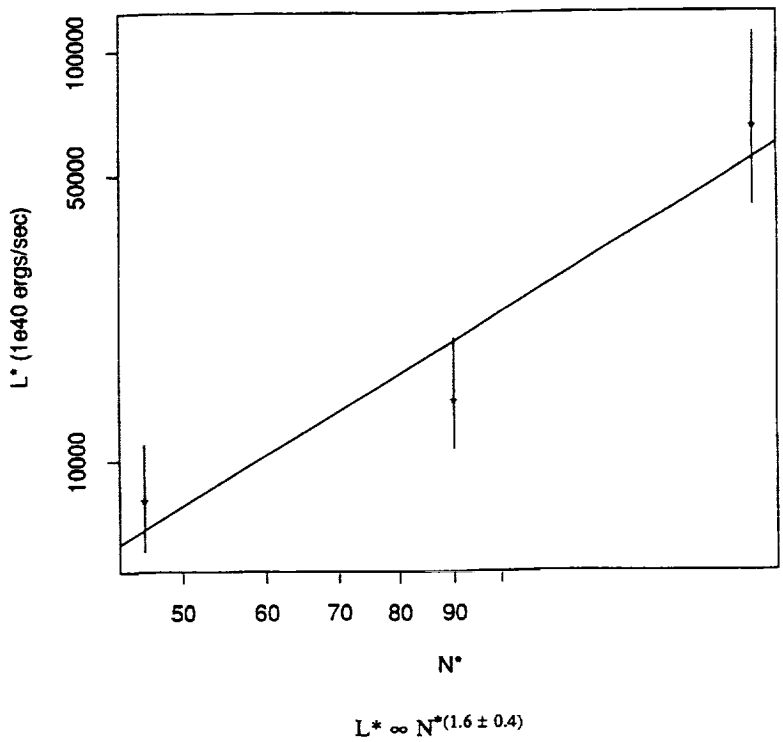


FIGURE 3 Characteristic luminosity versus richness.

luminosity of the cluster. Roughly 80% of the galaxies (brighter than L*) were not detected as individual sources (the high background due to the intracluster medium causes a high-detection threshold) but they may still have contributed significantly to the cluster emission.

We note that in our data the minimum observed X-ray luminosities for R = 0, 1 and 2 clusters are $3 \times 10^{42}$, and $8 \times 10^{42}$ and $3 \times 10^{43}$ erg $sec^{-1}$, respectively. In the three cases the expected summed contribution from individual galaxies (Forman *et al.* 1983) is roughly $4 \times 10^{42}$, $6.4 \times 10^{42}$ and $10^{43}$ erg $sec^{-1}$ respectively. This is evidence that there is a substantial number of clusters in which the X-ray emission from intracluster gas is not dominant.

## INTERPRETATION OF THE LUMINOSITY FUNCTION

Studying the wide range of X-ray luminosity of clusters selected by richness class (presumably therefore of given total mass) we are in a position to emphasize a fundamental property of X-ray emission from clusters.

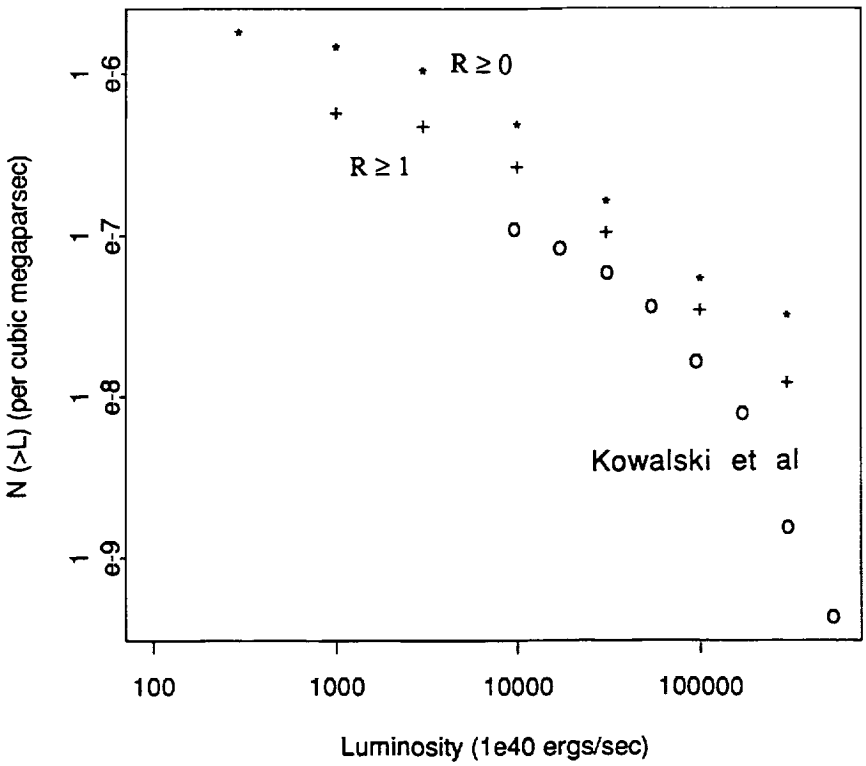


FIGURE 4 Summed non-parametric luminosities for R $\geq$ 0 and R $\geq$ 1. Also included is HEAO1-A1 R $\geq$ 1 luminosity function.

Specifically we can attempt to separate out the factors which determine the X-ray emission and relate them to initial conditions and dynamic evolution of the cluster. Using the thermal bremmstrahlung expression we can write:

$$L_x \sim \rho \text{gas} M \text{ gas} T_{\text{gas}}^{1/2}$$

Using the virial theorem and equipartition we can relate $T_{gas}$ to the virial gas mass, $M_v$, and density, $\rho_v$,

$$kT \sim G\frac{M_v}{R_v} \simeq \frac{GM_v}{\left(\frac{M_v}{4\pi\rho_v}\right)^{1/3}}$$

$$\text{or } T \sim M_v^{2/3}\rho_v^{1/3}$$

$$\text{and } L_x \sim \rho \text{gas} M \text{gas} M_v^{2/6}\rho_v^{1/6}.$$

We can then postulate:

$$\rho\text{gas} = \frac{M_v(0) f_p (1 + \frac{1}{f_p}\xi(t))}{V_v(t)}$$

and

$$M\text{gas} = M_v(0) f_p (1 + \frac{1}{f_p}\xi(t)),$$

then

$$L_x \sim f_p^2 (1 + \frac{1}{f_p}\xi(t))^2 \rho_v^{7/6} M_v(0)^{4/3}.$$

This allows us to separate the various contributions to the X-ray luminosity namely:

- the initial fraction $f_p$ of gas and any injection mechanism of gas after formation;
- a term which includes the effects of cosmology and dynamical evolution;
- the virial mass of the cluster.

We are currently working with A. Cavaliere (Cavaliere *et al.* 1989) on a refinement of this approach, where we directly relate these various quantities to the density fluctuation spectrum, $|\delta|^2 \sim k^n$. This results in an expression for $L_x$ of the form

$$L_x = A\delta^{a+b+c} M^d$$

in which a represents the cosmological term, b the dynamical term, and c the gas injection or stripping mechanisms.
In summary:

- The X-ray emission of a cluster depends not only on its mass but also on the initial conditions, the subsequent dynamical evolution of the system and the mechanism and history of the gas injection.
- Studying the luminosity function at the current epoch is not sufficient to disentangle the various contributions.
- On the other hand, coupling the local luminosity function for each range of masses with luminosity functions for the same mass objects at different redshifts will allow us to study in detail the various processes in the evolution of the gas.

- Future X-ray surveys will allow us to obtain direct information on the initial density fluctuation spectrum.

## FUTURE SURVEYS

We focus our attention in this discussion on only two missions: ROSAT, the precursor survey mission to be launched in 1990 and AXAF, the follow-on mission which will dominate X-ray astronomy for many years after its planned launch in 1996. In Table 2, we summarize the principal characteristics of the two missions from the point of view of the relevant instrumentation. Figure 5 shows the effective area of ROSAT and AXAF as a function of energy.

It is clear that with these capabilities many of the investigations initiated with *Einstein* can be pursued with greater depth and scope. They can be roughly divided in a few general headings. (See Table 3)

A good starting point to understand the impact of the new X-ray missions on the topics of cluster research is the review "The Advanced X-ray Astrophysics Facility", a special volume of Astrophysical Letters and Communications (Vol. bf 26, 1987), and references herein. We would like to discuss here in some detail only one aspect of the program in which we are personally interested. It deals with the study of cluster formation and evolution by means of surveys with ROSAT and AXAF. The two missions differ in a fundamental way. For each cluster the X-ray observations can yield two basic quantities:

1. The X-ray surface brightness distribution at the source as well as its integral.
2. The spectrum (and/or temperature) at each point or (for weaker sources) the spectrum (or temperature) of the integrated source emission. The detection of redshifted line emission from heavy elements may permit direct determination of the redshift and metallicity. 1 and 2 together yield a direct measure of $M_v$ (the virial mass).

As we discussed above, X-ray emission from a cluster will ultimately depend both on the initial conditions at formation and on its state of chemical and dynamic evolution. Thus, at least two observables will be required to characterize each cluster, in order to derive its properties without a very large number of simplifying assumptions. Basically, the ROSAT experiments only yield one quantity (the distribution of $L_x$). Future missions such as ASTRO-D, Jet X and XMM will yield spectra with some angular resolution for the nearest systems but only integral luminosity and integral spectra for the more distant ones. Only with AXAF will one have

TABLE 2

| Telescope | ROSAT | AXAF |
|---|---|---|
| Diameter | 84 cm | 120 cm diameter |
| Number of surfaces | 4 | 6 |
| field of view | 2 degrees | 1 degree |
| geometric area | 1141 $cm^2$ | 1700 $cm^2$ |
| Angular resolution | | |
| Center of field | ~3" | ~.5" |
| 8′ off axis | ~5" | ~3.5" |
| 30′ off axis | ~60" | ~60" |
| Imaging Instruments (field, spectral resolution) | | |
| | HRI~40′, none | HRI~30′, none |
| | PSPC~120′. $\frac{\Delta E}{E}$~.43 at 1 kev | CCD~14′ ΔE~150 eV (.5-8) keV |
| Spectroscopy | | Transmission gratings high energy R~100 at 4.5 keV, R~700 at .4 keV |
| | | low energy R~100 at 1.5 keV, R~750 at .1 keV |
| | | Calorimeter .78 sq. arc min. $\Delta E \leq 12$ eV |

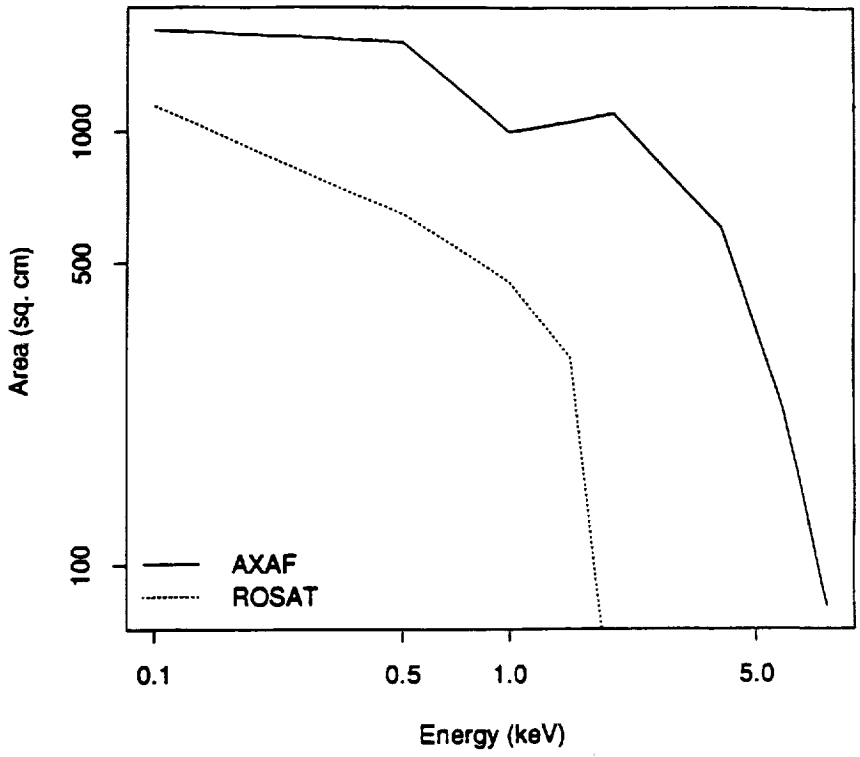


FIGURE 5 Comparison of ROSAT and AXAF.

high-angular resolution coupled with spectral resolution for the most distant detectable clusters ($\sim z \gg 1$).

The ROSAT all-sky survey is an important precursor to AXAF. No cluster for which one plans to do detailed spectral or morphological studies with AXAF can be much fainter than those detected in the ROSAT all-sky survey. The detection capabilities of ROSAT are such that we expect to detect a large sample of clusters. Figures 6 and 7 show the Log N–Log S relation derived by Burg and Giacconi (1990) for $z < 0.5$ and 1.0 respectively. These figures are derived from the luminosity function of Burg *et al.* 1989 for Rge0 Abell clusters at $z < 0.15$. It is important to note that uncertainties in the normalization parameter (of the Schechter functions fitted to the local luminosity functions) result in large uncertainties in Log N - Log S. However, the relative z distribution of clusters by richness class (Figure 8) assuming no evolution is a direct consequence only of the shape of the luminosity function, which is much better established. This means that we expect to detect in the ROSAT surveys a substantial fraction of

TABLE 3

Individual galaxies-interaction with the intracluster medium
- Galaxy halos
- Galaxy stripping (M86)
- Cooling flows (M87)

The intracluster medium
- $\rho$, $\rho$ (r)
- metallicity (spectra from SSS Einstein)

Cluster emission
:Morphology and state of dynamic evolution (double clusters)
:$S(r) = S(0)(1 + r^2/a^2)^{-3\beta+1/2}$ surface brightness density profiles

Correlations
: $L_x$ vs N
: $L_x$ vs $N_o$
: $L_x$ vs $T_{gas}$
: $L_x$ vs % spiral
: $\beta = \mu\, m_p \frac{\sigma_r^2}{\kappa T_{gas}}$

Cluster evolution
evolution of intergalactic medium with $z$
(evolution of a single cluster in time)
evolution of the luminosity function
evolution of metallicity

Cluster formation and cosmology
dark mass
correlation functions
protoclusters
primordial gas
Zeldovich-Sunyaev effect, Krolik-Raymond method: $H_0$, $q_0$

clusters at $0.5 < z < 1.0$. However, the angular resolution of the PSPC, the detector with which the survey will be conducted, is of order $\sim 30''$ and except for nearby clusters ($z \leq 0.2$) it will be difficult from X-ray observations alone to classify the objects as clusters rather than stars or AGNs.

A collaboration between the Max Planck Institute, STScI and ROE is planning a rapid (quasi real-time) classification of X-ray sources in the all sky ROSAT survey by utilizing existing ground based optical sky surveys. The purpose of this program is to permit the follow up of PSPC detections

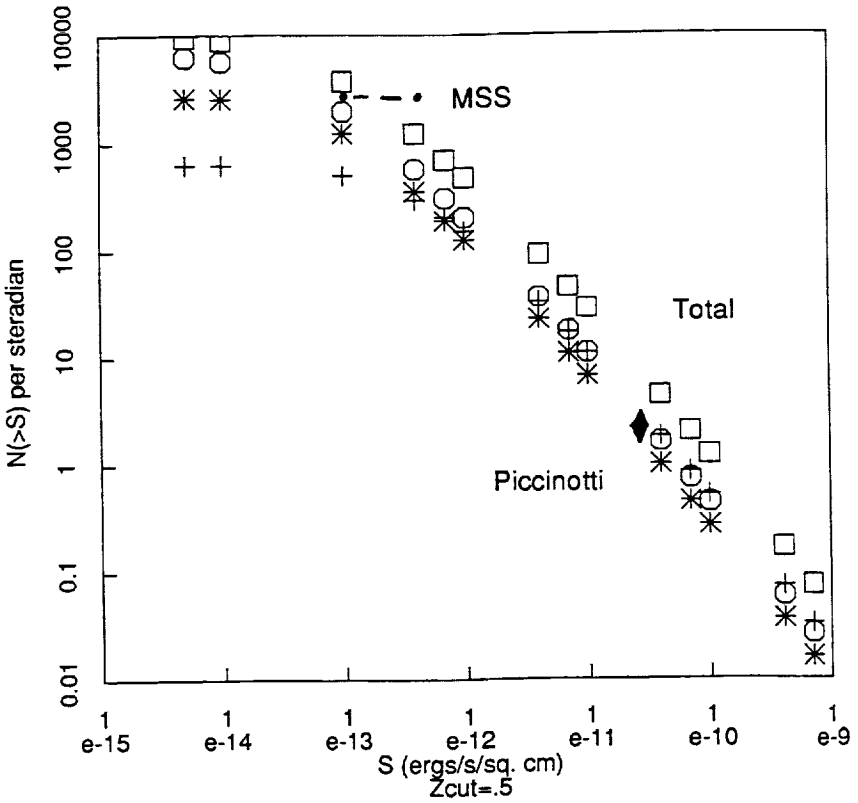


FIGURE 6 Log N-Log S for clusters using BFGJ luminosity functions (Burg *et al.* 1989) with no evolution and cut-off redshift of 0.5.

of particularly interesting clusters with HRI high angular resolution observations capable of resolving the details of the cluster morphology. This classification technique relies on utilizing all available X-ray and optical information and the observational constraints derived from the MSS survey to divide the ROSAT survey sources into appropriate bins. The observational base for discrimination is given by studies such as those of Maccacaro and Gioia on the MSS sources which are shown in Figure 9. In Figure 10 we show a tentative conceptual flow diagram which will be refined and implemented in an automated expert system. We hope by these means to isolate an enriched sample of distant clusters which could then be further studied with later X-ray missions.

What we hope to achieve from the ROSAT all-sky survey is the following:

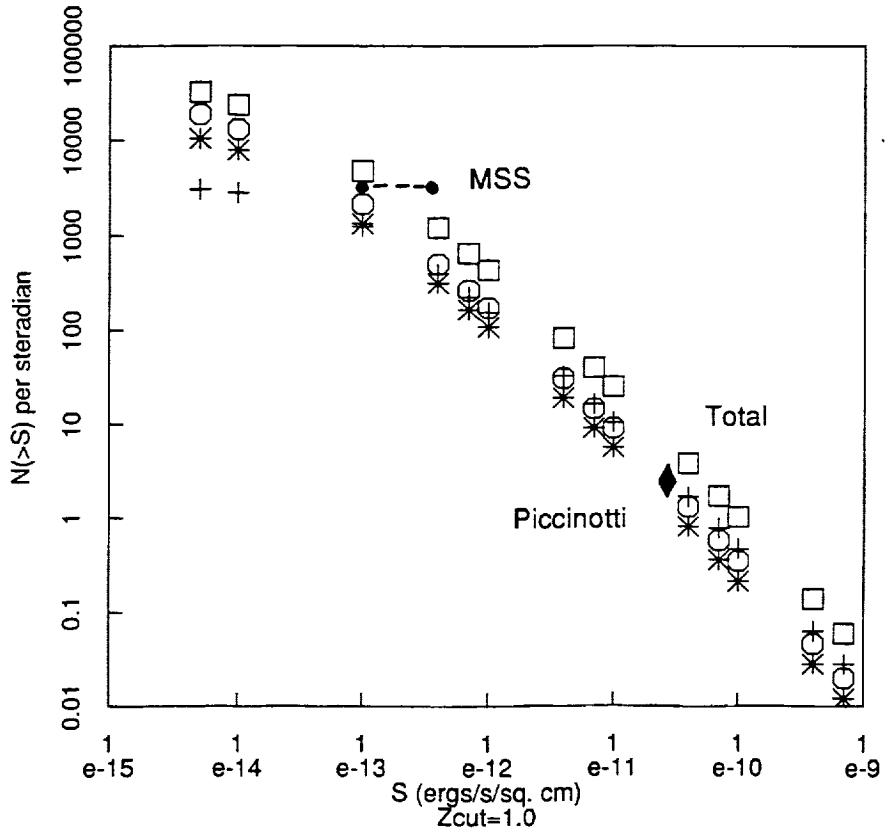


FIGURE 7 Log N-Log S with redshift cut-off of 1.0.

- X-ray flux measurements (or upper limits) for all classes of optically defined clusters (whether Abell, Zwicky or poor groups). We will be able to derive bivariate luminosity functions with methods similar to those used for the *Einstein* sources (Burg *et al.* 1990).
- A flux limited X-ray survey for all types of clusters defined as gravitationally bound systems of galaxies containing intracluster gas with a high degree of metallicity and central condensation. Such surveys are naturally biased toward systems which are both chemically and dynamically evolved.
- Detailed study of morphology and rough temperature determination (for low-temperature systems) for all nearby systems.
- Point to point correlations (with a large sample of X-ray defined clusters) to study large-scale structure.

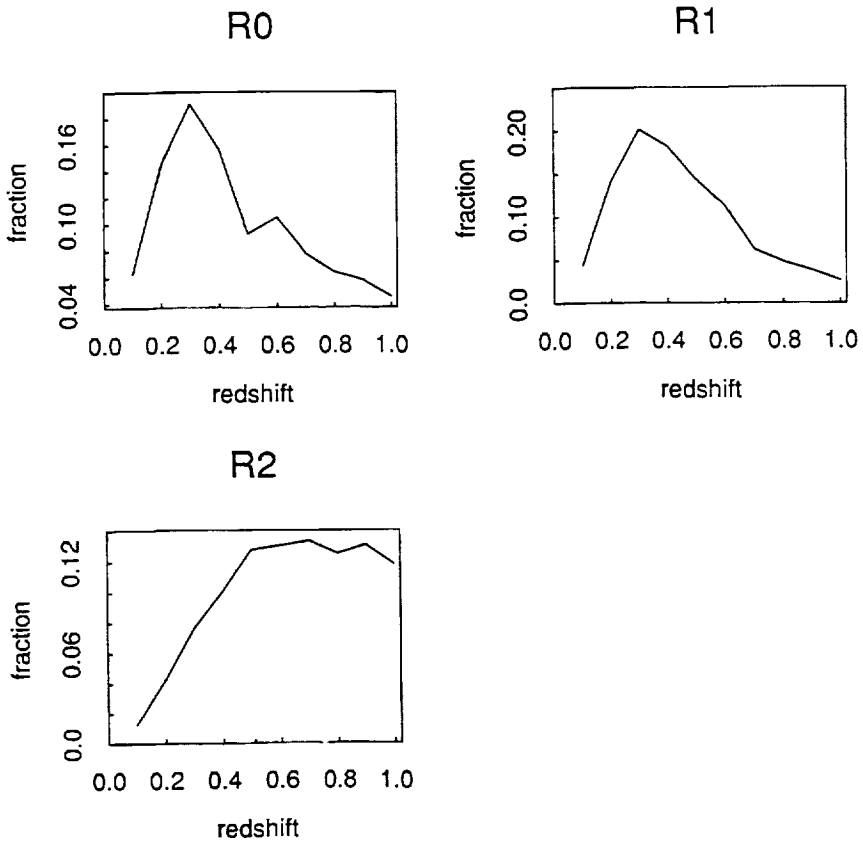


FIGURE 8 Redshift distribution of clusters to $S_{min} = 10^{-13}$ ergs $s^{-1}$ $cm^{-2}$.

- Study of prevalence of cooling flows, galactic halos, (both in clusters and in isolated systems), etc. for nearby systems.
- Confrontation between model-predicted redshift distributions and observed redshift distributions for optically characterized subsamples.

The tremendous advantage of AXAF with respect to ROSAT is given by two specific technical improvements coupled together: the high-quantum efficiency and spectral resolution of the CCD detectors coupled to a high-angular resolution telescope. Within the field of view of the CCD, any cluster, at any z, which is detected, can be resolved as an extended structure.

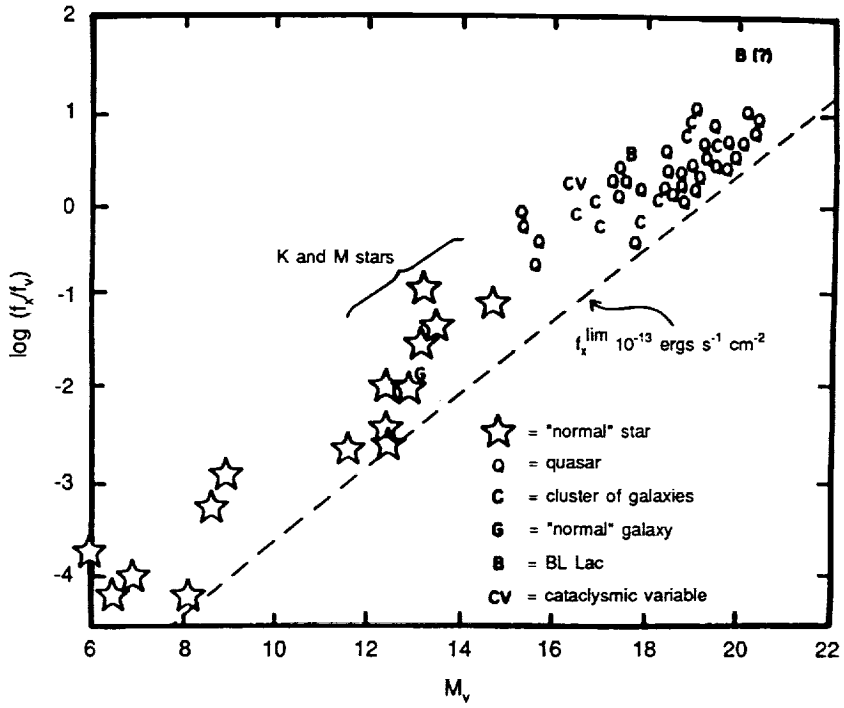


FIGURE 9 Classification of Einstein Medium Sensitivity Survey.

For given models of cluster evolution we can estimate the characteristic core radius of clusters at different z's:

For n = -1 and Friedman cosmology with $q^* = 1/2$ and $H^* = 50$ $kms^{-1}$ $Mpc^{-1}$ the linear dimensions of clusters at z = 1 and 2 would correspond to angular diameters of 15 to 7 arc seconds. This angular extent can easily be measured by AXAF within the field of view of the CCD. AXAF therefore possesses the angular resolution and spectroscopic capability to directly determine the angular extent of a cluster as well as the ability to directly measure its redshift (if the X-ray emitting gas is enriched). Figure 11 shows a simulation carried out by G. Garmire and colleagues of the expected surface brightness profile and spectrum which will be obtained with the AXAF CCD X-ray camera for a rich cluster at different redshifts.

## SUMMARY

- With ROSAT observations we will obtain the only all-sky X-ray flux limited sample of clusters for years to come. We might be able to show the existence of evolutionary effects by extensive

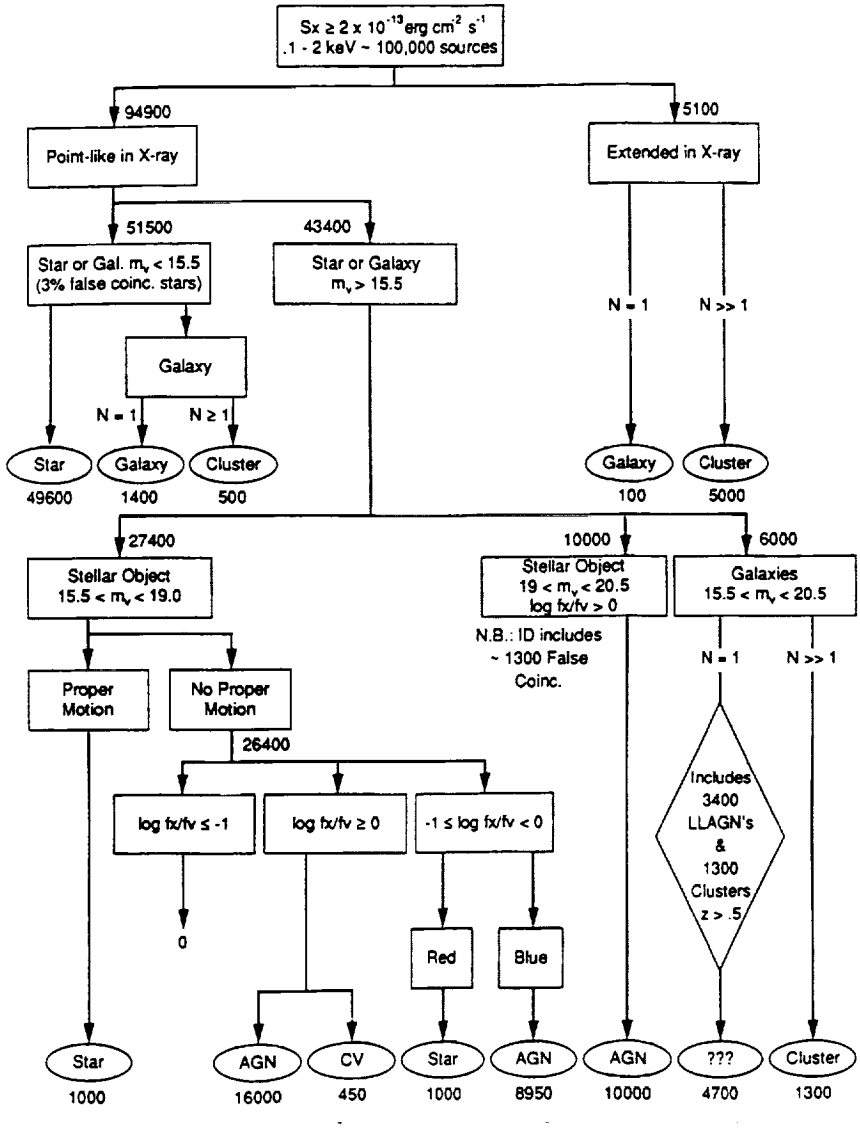


FIGURE 10 Proposed categorization algorithm for ROSAT.

optical follow-up (to measure z) and by studying the z distribution of carefully selected subsamples. However, the causes for the apparent evolutionary effects, if any, will be difficult to determine. In particular, given the lack of X-ray spectroscopy we will be unable to measure the evolution of metallicity and gas of temperature and mass (except with very restrictive assumptions).

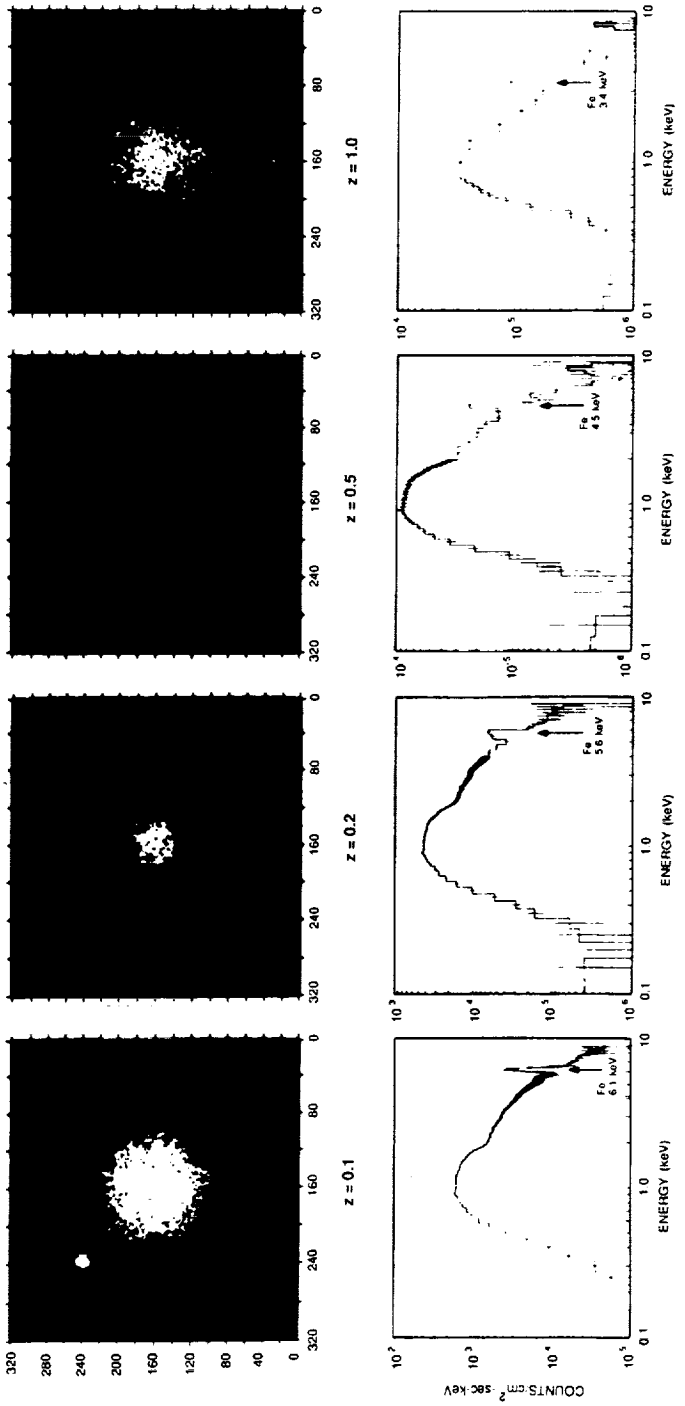


FIGURE 11 AXAF CCD simulation.

- With the advent of ASTRO-D and Jet X, etc., which will combine moderate angular and spectral resolution capabilities with a wide bandwidth, we will be able to directly measure redshift, metallicity and temperature. For low-redshift systems ($z < 0.25$) we will be able to also measure the distribution of surface brightness, temperature and metallicity. This will enable us to determine the state of dynamic and chemical evolution and directly measure the dark mass.
- Similar measurements can be extended by AXAF to very large redshifts, from $z > 0.25$ to z of order of 2.

When this program is completed there will emerge a new understanding of the formation and evolution of these objects, among the most massive gravitationally bound structures in the Universe. Furthermore, we hope this will lead to a more complete picture of the structure of the Universe.

## REFERENCES


Abell, G.O. 1958. Astrophys. J. Suppl. 3: 211.

Abramopoulos, F., and W. Ku. 1983. Astrophys. J. 271: 446. Avni, Y., A. Soltan, H. Tannenbaum, and G. Zamorani. 1980. Ap. J. 238: 800.

Bahcall, N. 1979. Ap. J. 232, 689.

Bechtold, J., W. Forman, R. Giacconi, C. Jones, J. Schwarz, W. Tucker, and L. VanSpeybroeck. 1983. Astrophys. J. 265: 26.

Burg, R., and R. Giacconi. 1990. In preparation.

Burg, R., W. Forman, R. Giacconi, and C. Jones. 1990. In preparation, (BFGJ).

Cavaliere, A., R. Burg, and R. Giacconi. 1989. In preparation.

Cox, D.R., and D. Oakes. 1984. Analysis of Survival Data, Chapman and Hall, Cambridge.

Feigelson, E.D., and P.I. Nelson. 1985. Ap. J. 293: 192.

Forman, W., C. Jones, and W. Tucker. 1983. Astrophys. J. 293, 102.

Gioia, I.M., M.J. Geller, J.P. Huchra, T. Maccacaro, J.E. Steiner, and J. Stocke. 1982. Ap. J. (Letters), 255: L 17.

Gursky, H., E.M. Kellog, S. Murray, C. Leoug, H. Tananbaum, and R. Giacconi. 1971. Ap. J. (Letters) 169: L81.

Henry, J.P., G. Brandvardi, V. Briel, D. Fabricant, E. Feigelson, S. Murray, A. Soltan, and H. Tananbaum. 1979. Ap. J. (Letters) 238: L15.

Johnson, M.W., R.G. Cruddace, M.P. Ulmer, M.P. Kowalski, and K.S. Wood. 1983. Ap. J. 266: 425.

Jones, C., and W. Forman. 1984. Ap. J. 276: 38.

Jones, C., and F. Forman. 1990. In preparation.

Kaiser, N. 1986. M.N.R.A.S. 222: 323.

Kellog, E.M., H. Gursky, H. Tanabaum, R. Giacconi, and K. Pounds. 1972. 174: L65.

Kowalski, M.P., M.P. Ulmer, R.G. Cruddace. 1983. Ap. J. 268, 540.

Kriss, G.A., C.E. Canizares, J.E. McClintock, and E.D. Feigelson, 1980, Ap. J. (Letters) 235: L61.

Lucy, J.R. 1983. M.N.R.A.S. 204: 33.

Mitchell, R.J., J.L. Culhane, P.J. Davison, and J.C. Ives. 1976. M.N.R.A.S. 176: 29.

Mushotzky, R. 1988. Proceedings of the NATO summer school on Hot Astrophysical Plasmas, Palluviccini, R., Editor.

Piccinotti, G., R.F. Mushotzky, E.F. Boldt, S.S. Holt, F.E. Marshall, P.J. Serlenitsos, and R.A. Shafer. 1982. Ap. J. 253: 485.

Schmitt, J.H.M.M. 1985. 293: 198.

Serlemitsos P.J., B.W. Smith, E.A. Boldt, S.S. Holt, and J.A. Swank. 1977. 211: L63.

Shaeffer, R., and J. Silk. 1988. Ap. J. 333: 509.

Shwartz, D.A., M. Davis, R.E. Doxsey, R.E. Griffiths, J. Huchra, M.D. Johnston, R.F. Mushotzky, J. Swank, and J. Tonry. 1980. Ap. J. (Letters) 238: L53.

Stocke, J.T. *et al.* 1983. Ap. J. 273: 458.

Zwicky F., E. Herzog, P. Wild, M. Karpowicz, and C.T. Kowal. 1961-1968. Catalogue of Galaxies and Clusters of Galaxies. Volumes 1-6. Caltech, Pasadena.

# Observations of X-Ray Pulsars from the Kvant Module

M. GILFANOV, R. SUNYAEV, E. CHURAZOV, V. LOZNIKOV, V. EFREMOV, A. KANIOVSKIY, A. KUZNETSOV, N. YAMBURENKO, A. MELIORANSKIY, G.K. SKINNER, O. AL-EMAM, T.G. PATTERSON, A.P. WILLMORE, A.C. BRINKMAN, J. HEISE, J.J.M. IN'T ZAND, R. JAGER, W. PIETSCH, S. DOEBEREINER, J. ENGLHAUSER, C. REPPIN, J. TRUEMPER, W. VOGES, E. KENDZIORRA, M. MAISACK, B. MONY, R. STAUBERT, A.N. PARMAR, AND A. SMITH.*

## INTRODUCTION

The Roentgen international X-ray observatory on the Kvant module of the Mir space station has been operating successfully since the beginning of June 1987. Many X-ray sources were observed in 1987-1989 and among them were several X-ray pulsars. Four telescopes mounted on board the Kvant module cover a wide energy range with good timing resolution: Coded Mask Imaging Spectrometer TTM (2-30 keV; timing resolution 1 s), GSPC (2-100 keV; 1.25 ÷ 2.5 ms); Phoswich type detectors HEXE (20-200 keV; 0.3 ÷ 25ms), and Pulsar X-1 (50-1300 keV; 5-10 s). Timing analysis of the Kvant module data suffers from the presence of only short continuous intervals of source observations (10-25 min), separated by 90 minute gaps (90 min. is the orbital period of the Mir space station around the Earth). On average there are approximately four sessions per day. The presence of 90 min. gaps leads to the appearance of beat frequences $\nu=\nu_o \pm n/90$ min ($n = 1, 2, 3..$). Special analysis was applied to avoid this difficulty.

Presented below are the results of the pulsation period measurements of the X-ray pulsars Her X-1, Cen X-3, SMC X-1, Vela X-1, A0535 + 26 by the instruments on board the Kvant module in 1987-1989 (Table 1 and Figures 1,2,3,5,7,8). The values of the periods are reduced to the solar

* Space Research Institute, Academy of Sciences, Moscow, USSR; Space Research Laboratory, Utrecht, The Netherlands; Department of Space Research, University of Birmingham, Edgbaston, Birmingham; Max Planck für Physik and Astrophysik, Institute für Extraterrestrische Physik; Astronomisches Institute der Universitat Tubingen, Garshing, Germany; Noordwijk, The Netherlands.

TABLE 1 Pulse periods of X-ray pulsars measured with KVANT module in 1987-1989. Errors are 1 $\sigma$ values.

| Source name | Date | JD* | Period,s | Error,s |
|---|---|---|---|---|
| Her X-1 | VIII.1987 | 7021 | 1.2377728 | $2.5 \cdot 10^{-7}$ |
| | VII.1988 | 7368 | 1.237767 | $1.8 \cdot 10^{-6}$ |
| | X.1988 | 7441 | 1.2377643 | $6.0 \cdot 10^{-7}$ |
| SMC X-1 | X.1988 | 7452 | 0.7100972 | $2.2 \cdot 10^{-6}$ |
| | III.1989 | 7591 | 0.7099830 | $3.0 \cdot 10^{-5}$ |
| Cen X-3 | II.1989 | 7563 | 4.822583 | $1.4 \cdot 10^{-5}$ |
| Vela X-1 | XI.1988 | 7490 | 283.1676 | $5.3 \cdot 10^{-3}$ |
| | II.1989 | 7561 | 283.1466 | $3.0 \cdot 10^{-2}$ |
| A0535+26 | IV.1989 | 7600 | 103.267** | $3.1 \cdot 10^{-3}$ |

* Julian date of observation JD - 2440000

** Without reduction to binary system barycenter

system barycenter and to the binary system barycenter (excluding A0535 + 26).

## CRAB NEBULA PULSAR OBSERVATIONS

More than 100 among 2000 sessions performed until now by the Roentgen observatory were shared with the Crab Nebula Observations in order to calibrate all instruments.

The reduction of time series from the Kvant module to UT (Universal Time) was performed using the data of an onboard timer with the accuracy $\approx 5 \cdot 10^{-8} s \cdot s^{-1}$ (Gavrilova *et al.* 1988). Observation of the Crab Nebula pulsar NP0532 allows us to confirm the validity of the reduction procedure.

Usually the data combined over one day (3-4 sessions) were used for timing analysis via the epoch folding method (Leahy *et al.* 1983). The results of pulsation period measurements in September-October 1987 are presented on Figure 1. The values of periods are reduced to the solar system barycenter. The predicted values of the periods arising from radioobservations are shown by a solid curve (the reference is given in Haizinger 1984): $P(t) = P + \dot{P} \cdot (t-t_o) + \ddot{P} \cdot (t-t_o)^2/2$, where P(t) – is the period at the time of observations, $P = 0.033235335646$ s, $\dot{P} = 4.219036 \cdot 10^{-13}$ s/s, $\ddot{P} = -2.81107 \cdot 10^{-24} s/s^2$, $t_o$ = JD 2444128.5 (12.9.79). The deviations

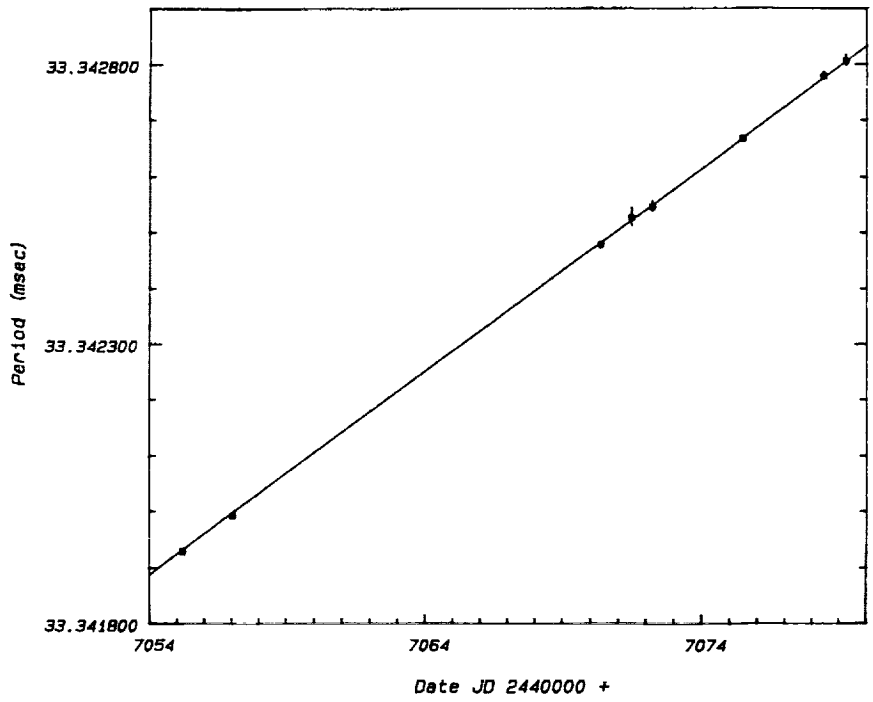


FIGURE 1 Pulsation period of the pulsar in Crab Nebula as measured by GSPC instrument on board the Kvant module in September-October 1987. The errors are $1\sigma$ values. The solid line shows the extrapolation of radio data.

of the measured values from the fit are within statistical errors $\Delta P/P \approx 1 \cdot 10^{-7}$.

These measurements of the NP0532 pulsation period and comparisons with the radiodata confirmed the correctness of all timing analysis procedures, which were applied below for other pulsars.

## HERCULES X-1

Well-known X-ray pulsar Her X-1 was intensively monitored by the instruments on board the Kvant module (Figure 2 and Table 1). The measurements of the HEXE and GSPC instruments have shown (Voges *et al.* 1988; Sunyaev *et al.* 1988) that the pulsar entered the stage of quasistationary acceleration analogous to ones observed in 1972-1978. The orbital parameters are from Deeter *et al.* (1981). Average spin-up rate over the period of Kvant observation was $\dot{P}/P = (-4.9 \pm 1.5) \cdot 10^{-8} \mathrm{yr}^{-1}$.

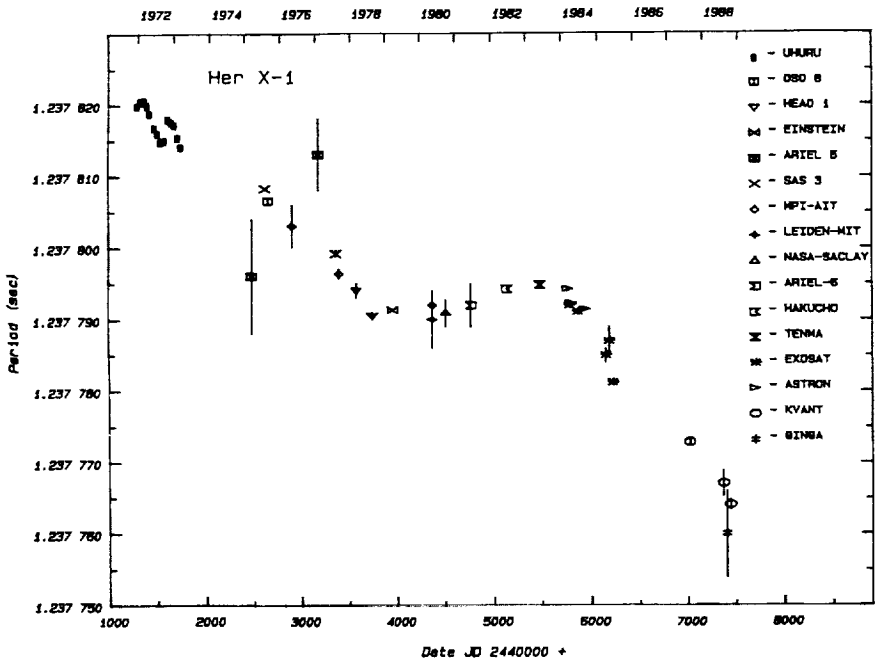


FIGURE 2 Pulsation period history for Her X-1. Errors are $1\sigma$ values. References on the previous experiments are presented in the papers of Sunyaev *et al.* (1988) and Nagase (1989).

## SMC X-1

The results of HEXE observations were used for SMC X-1 period determination. Two successful sets of sessions were performed in 1988-1989, when the source was within the field of view of the telescope (Figure 3 and Table 1). The observations of another telescope on board the module - Coded Mask Imaging Spectrometer TTM - detected an X-ray eclipse of source on January 8, 1989 (the pulsar was beyond the field of view of the HEXE instrument with the smaller field of view). The time of the sessions when there is no significant flux from the source coincides with the predicted time of the eclipse based on the orbital parameters of Gruber (1988). The count rate measured by the TTM instrument during three sets of sessions of SMC X-1 observations (7-11 January 1989) is shown on Figure 4. Upper limits on the source intensity during the eclipse are shown by triangles. Continuous spin-up of this pulsar with the average rate $\dot{P}/P = (-4.2\pm0.2)\cdot10^{-4}\mathrm{yr}^{-1}$ (during Kvant module observations) agrees well with the simplest models of disk-accretion fed pulsars (Pringle and Rees 1972; Ghosh and Lamb 1979).

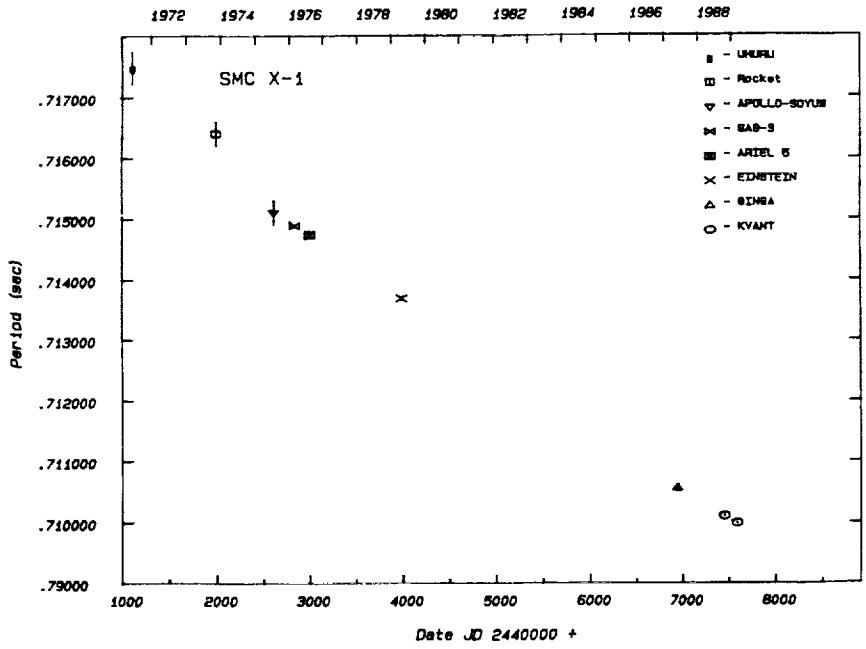


FIGURE 3 Pulsation period history for SMC X-1. References on previous experiments are given in Darbro *et al.* (1981) and Nagase (1989).

## CENTAURUS X-3

Roentgen observatory performed four sets of Cen X-3 observations at the beginning of 1989. On February 5, 1989, the source was in eclipse with the upper limit on its intensity in the 2-30 keV energy band 4 mCrab ($3\sigma$ upper limit). The TTM data were used for timing analysis. The value of the period based on all observations is presented in Figure 5 and in Table 1. Figure 6a shows the pulsation period, measured in single sessions without reduction to the binary system baricenter. The solid line shows the predicted Doppler shift of period due to the neutron star motion in the binary system according to parameters from Nagase *et al.* (1983); Nagase *et al.* (1984); and Kelly *et al.* (1983). Unfortunately this set of observations was too short to allow us to measure the orbital parameters accurately. The best fit orbital parameters are within $1\sigma$ with that in the references above.

## VELA X-1

This X-ray pulsar was observed by TTM, HEXE, and Pulsar X-1 instruments in November-December 1988 and January-February 1989 (Figure

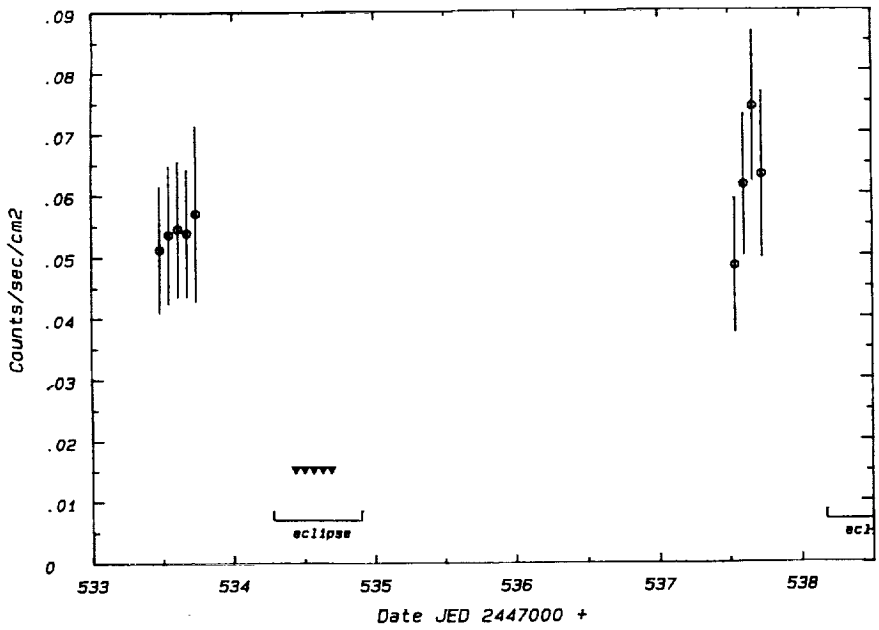


FIGURE 4 The count rate of SMC X-1. Triangles mark upper limits during eclipse.

7 and Table 1). The measured value of the pulsation period is the highest over the whole history of Vela X-1 observations since 1972. Comparison of the periods values measured in single sessions with the predicted Doppler shifts due to orbital motion confirmed the stability of the binary system parameters since the last measurements of Tenma in 1983 (Nagase *et al.* 1984b). Average spin-down rate since Tenma up to Kvant measurements is $\dot{P}/P = 1.4 \cdot 10^{-4} yr^{-1}$. Note that the spinning-up of the pulsar in 1975-1979 was of the same absolute value (Nagase 1984a).

## A0535+26

Observations of this pulsar were performed during the giant outburst of the transient, the beginning of which was detected by the Ginga satellite on March 31, 1989 (Makino 1989). For timing analysis the data of TTM were mainly used. There are both A0535+26 and Crab Nebula in the field of view of TTM (7°.5 × 7°.5). This allows us to express the intensity of the source in Crab units via direct comparison of corresponding count rates: 0.6 Crab in 2-6 keV energy band and 1.5 Crab in 6-10 keV (Sunyaev *et al.* 1989). The high count rate of the sources within the field of view of the telescope leads to the overflow of its telemetry channels approximately two times. Therefore on the whole, energy band (2-30 keV), which is

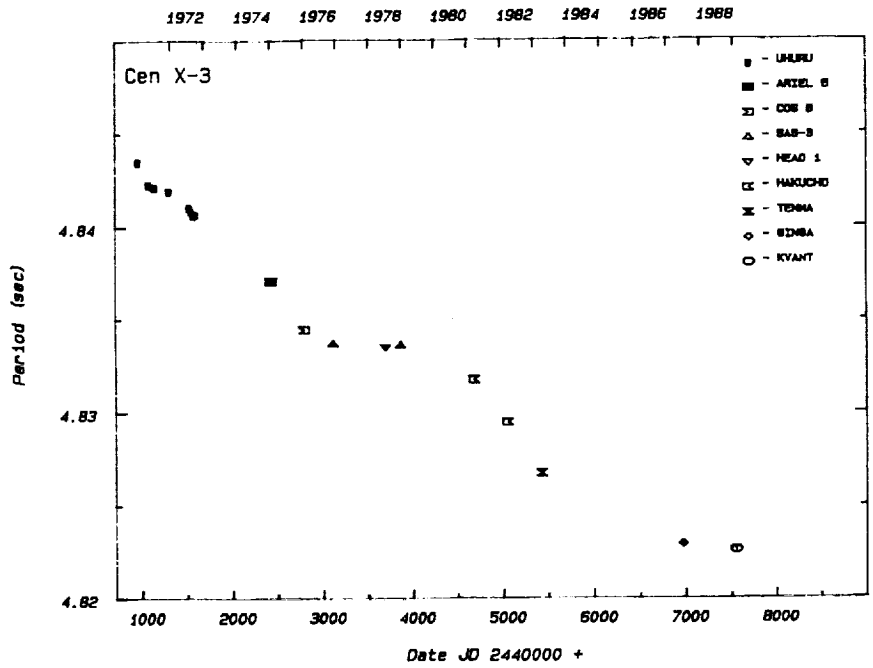


FIGURE 5 Pulsation period history for Cen X-3. References on previous experiments are given in Kelly *et al.* (1983); Murakami *et al.* (1983); Howe *et al.* (1983); Nagase *et al.* (1984b); and Nagase (1989).

transmitted every 8 seconds, was used for the determination of period. The value of the period measured on April 9-10, 1989, and published by Sunyaev *et al.* (1989) is presented in Table 1 and Figure 8. Since the parameters of the binary system are not yet known, the value of the period was just reduced to the binary system barycenter. Further measurements are to show whether the acceleration of this pulsar does exist during the flares when the rate of accretion is large.

The authors are pleased to thank E. Gavrilova for her assistance with reduction of all timing data to UT, V. Blagov, G. Kondrashina, A. Prukoglyad, V. Rodin, the teams headed by the corresponding member of the Academy of Sciences of the USSR Yu. P. Semyonov, and the Space Flight Center team for control of the observatory operations and cosmonauts Yu. Romanenko, A. Alexandrov, A. Laveykin, M. Manarov, V. Titov, A. Volkov, and S. Krikalev for help with the work of the observatory.

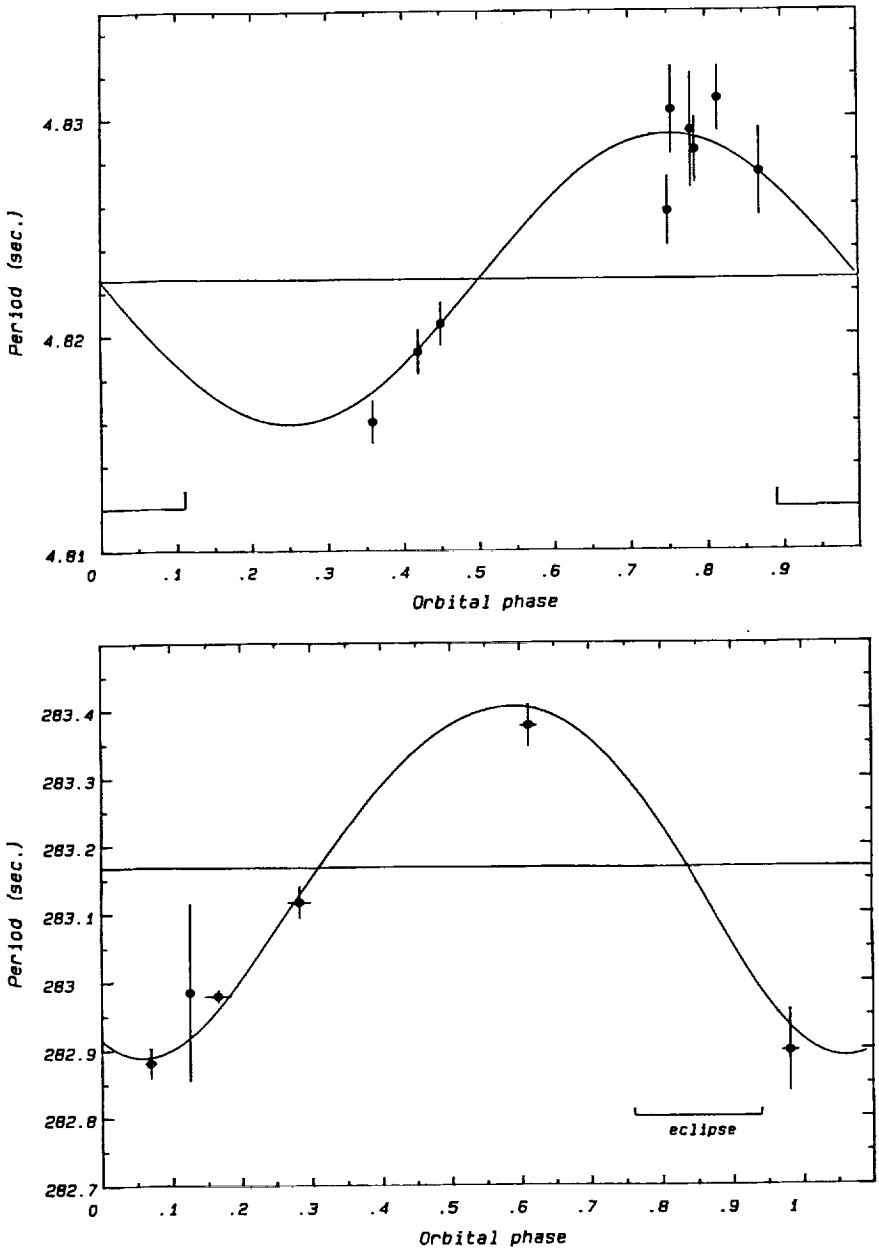


FIGURE 6 Doppler shift of the periods due to orbital motion in binary system for Cen X-3 (a) and Vela X-1 (b). Circles mark the values measured in single sessions (a) and sets (b) of observations. Errors are $1\sigma$ values. Solid curves show the predicted variation of periods.

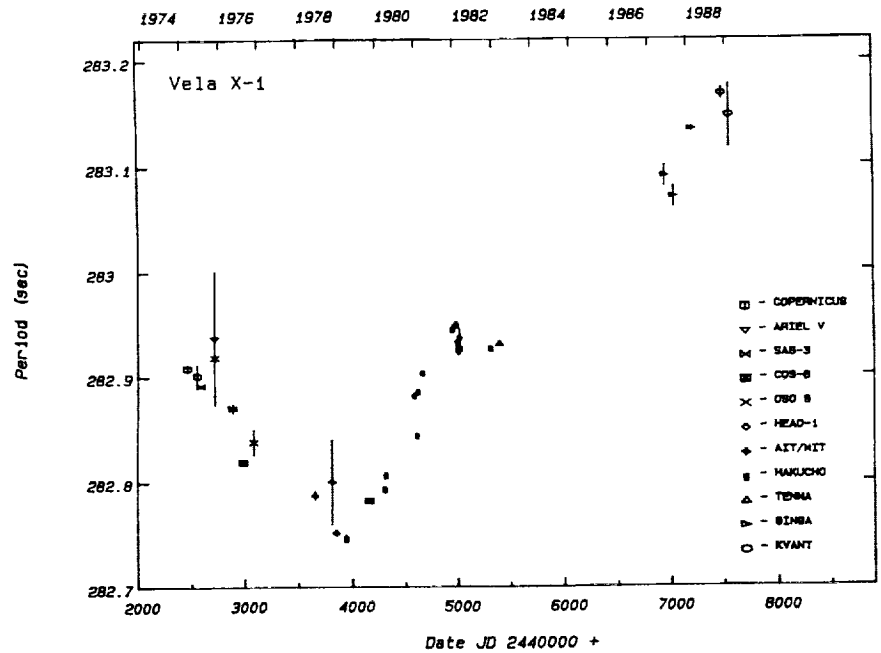


FIGURE 7 Puls-period history for Vela X-1. References on previous experiments are given in Nagase *et al.* (1984a) and Nagase (1989).

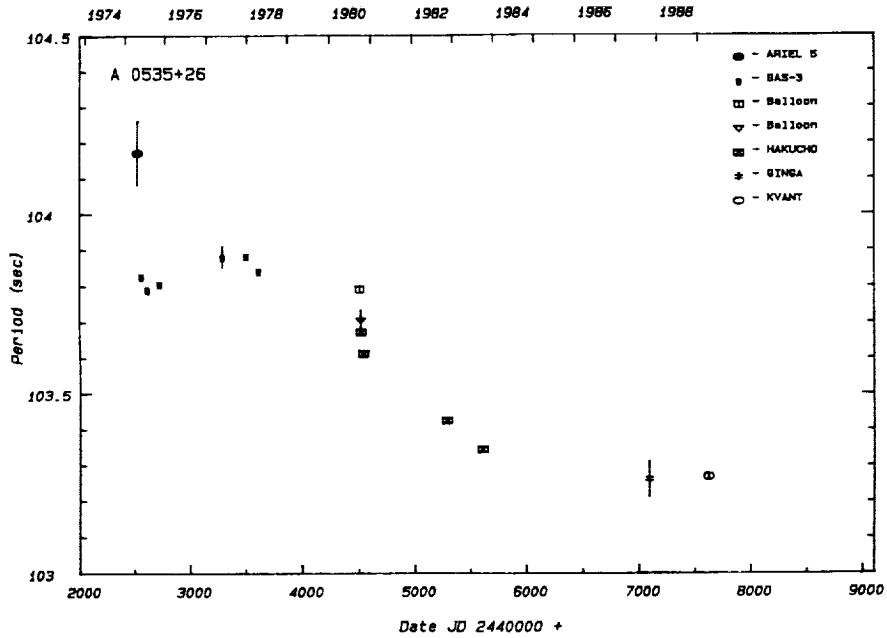


FIGURE 8 Puls-period history for A0535 + 26. References on previous experiments are given in Nagase *et al.* (1982), Nagase *et al.* (1984b) and Nagase (1989). See also Ricker *et al.* 1976.

## REFERENCES

Darbro, W., P. Ghosh, R.F. Elsner, *et al.* 1981. Astrophys. J. 246: 231.
Deeter, J.E., *et al.* 1981. Astrophys. J. 247: 1003.
Gavrilova, E., *et al.* 1988. Preprint IKI Pr-1422.
Gruber, D. 1988. Private communication.
Ghosh, P., and F.K. Lamb. 1979. Astophys. J. 234: 296.
Hasinger, H. 1984. Dissertation.
Howe, S.K., F.A. Primini, M.W. Bautz, *et al.* Astrophys. J. 1983. 272: 678.
Kelley, R.L., S. Rappaport, G. Clark, *et al.* 1983. Astrophys. J. 268: 790.
Leahy, D.A., W. Darbro, R.F. Elsner, *et al.* 1983. Astrophys. J. 266: 160.
Makino, F. 1989. IAU Circ. No. 4768.
Murakami, T., H. Inoue, N. Kawai, *et al.* 1983. Astrophys. J. V. 264: 563.
Nagase, F., S. Hayakawa, H. Kunieda, *et al.* 1982. Astrophys. J. 263: 814.
Nagase, F., S. Hayakawa, H. Kunieda, *et al.* 1984a. Astrophys. J. 280: 259.
Nagase, F., N. Sato, K. Makishimi, *et al.* 1983. ISAS Preprint No. 234.
Nagase, F. 1989. Publ. Astron. Soc. Japan. 41: 1.
Pringle, J.E., and M.J. Rees. 1972. Astron. and Astrophys. 21: 1.
Ricker, G.R., A. Scheepmaker, J.E. Ballintine, J.P. Doty, G.A. Kriss, S.G. Ryckman, and W.H.G. Lewin. 1976. Astrophys. J (Lett) 204, L73.
Sunyaev, R., *et al.* 1988. Soviet Astronomy Letters. 14: 979.
Sunyaev, R.A. 1989. IAU Circ. No. 4769.
Voges, W., W. Pietsch, C. Reppin, *et al.* 1982. Astrophys. J. 263: 803.

# Generation of Ultrahigh-Energy Gamma Rays in Accreting X-Ray Pulsars

YU.N. GNEDIN AND N.R. IKHSANOV
Central Astronomical Observatory

## ABSTRACT

Relativistic protons producing ultrahigh-energy gamma rays as a result of nuclear collisions are expected to generate close to the neutron star surface as a result of accretion. The high efficiency of the accreting matter's gravitational energy conversion into the acceleration energy and high efficiency of the acceleration itself are the main peculiarities of the considered mechanism. It is shown that a distribution of the "loss cone" type accreting protons takes place during accretion onto a neutron star with a strong magnetic field. This distribution effectively generates small-scale Alfvén, proton cyclotron waves, and non-linear waves (magneto-acoustic and Alfvén solitons) due to instabilities. The electric field of the moving solitons may accelerate the protons to energies $> 10^{15}$ eV. The region of acceleration covers the Alfvén surface to distances of 2-3 radii of the neutron star from its surface. New possible sources of ultrahigh-energy gamma-rays are predicted. They may be binary X-ray systems with neutron stars permeated by magnetic fields of $\sim 10^9$ Gauss.

## INTRODUCTION

One of the recent and most interesting astronomical discoveries was the detection of very high-energy ($10^{12}$ to $10^{14}$ eV) and ultrahigh-energy ($10^{14}$ to $10^{16}$ eV) Gamma rays from X-ray binaries. Radiation of ultrahigh-energy quanta of four binary systems (Her X-1, 4U0115+63, Vela X-1, and Cyg X-3) have been observed by at least two independent groups (Lamb and Weekes 1987). The radiation detected pulsates with the star's rotation

period. Table 1 gives the basic characteristics of these sources. As it follows from this table, the main physical property—luminosity in the gamma-ray range: x-ray range ratio—is within

$$L_\gamma / L_x > 10^{-3} \tag{1}$$

and perhaps $\sim 1$.

It is evident that such a traditional model as radiation of relativistic particles generating in the electric and magnetic fields of a fast-rotating neutron star, will not do for this physical situation. The rotation rate of neutron stars in Her X-1 and 4U0115+63 is too small to provide the necessary energy. Thus, relativistic protons and electrons originating very high-energy gamma rays should generate close to the neutron star's surface as a result of accretion.

At present there is no general theoretical conception of the mechanism of relativistic proton generation near the surface of the accreting neutron star, although there are quite a few ideas (see Brecher 1987; Hillas 1987).

The main peculiarities of such a mechanism should be as follows:

1. High efficiency of gravitational energy conversion of accretion matter into the acceleration source energy, since the ratio of the ultrarelativistic particle energy power to the X-ray emission energy power can be rather large:

$$L_p / L_x < 1 \text{ and even } L_p / L_x > 1 \tag{2}$$

(Lamb and Weekes 1987; Hillas 1987).

2. High efficiency of the mechanism of acceleration, since the characteristic time of energy losses due to synchrotron radiation of protons is very short

$$t_{\text{syn}} \cong 4.4 \times 10^{-12} E_{15}^{-1} B_{12}^{-2} \tag{3}$$

where $E_{15}$ is the proton energy given in $10^{15}$ eV and $B_{12}$ is the magnetic field measured in $10_{12}$ Gauss.

3. Another essential difficulty for acceleration is the high density of the accelerated plasma which prevents accumulation of the energy of the accelerating particle because of frequent coulomb collisions. There must be a mechanism in the accreting plasma, which causes a strong inhomogeneity of the plasma such as dense and small plasma drops.

The goal of the present paper is to find such a mechanism of conversion of the accreting plasma gravitational energy in the neutron star's magnetosphere into the relativistic proton energy. This conversion should provide for the necessary energy and high efficiency of acceleration. Such a mechanism is generation of non-linear waves (Alfvén and fast magneto-acoustic

TABLE 1

| Source | Rotational Period of N.S. | | Orbital Period | Precession Period | Cyclotron Line | $L_x$ | L |
|---|---|---|---|---|---|---|---|
| Her X-1 | $1^s,24$ | | $1^d,7$ | 35d | 50 | $10^{35}$-$10^{37}$ | $10^{35}$-$10^{37}$ (some episodes) |
| 4U 0115+63 | $3^s,61$ | | $24^d$ | | | $10^{35}$-$10^{37}$ | $10^{35}$-$10^{37}$ (some episodes) |
| Vela X-1 | $283^s$ | | $8^d,974$ | $93^d,3$ | | $10^{36}$-$10^{37}$ | $10^{36}$ |
| Cyg X-3 | $0^s,01259$ | ? | $4^h,8$ | $19^d,2$ | | $10^{37}$-$10^{38}$ | $10^{35}$-$10^{37}$ |
| | 0,00922 | ? | | | | | |
| Cen X-3 | $4^s$, 84 | | $2^d,087$ | $43^d,0$ | | $10^{35}$-$10^{37}$ | $10^{36}$ |
| LMC X-4 | | | $1^d,4$ | | | $10^{37}$-$10^{38}$ | $10^{35}$ |
| Cir X-1 | | | $16^d,6$ | | | $2\ 10^{38}$ | $3 \times 10^{36}$ |
| 2A 1822-37.1 | | $0^d,23$ | | | | | $F=(1.2\pm0.4)\times10^{-15}cm^{-2}s^{-1}$ |
| 1700-377 | | | $3^d,4$ | | | | |
| SN 1987A | | | | January 14-15, 1988 | | | $2.2\sigma$; $3.3\sigma$ |

The first four binaries have been observed by at least two independent groups. The next three binaries have been observed only once. For the last three sources, only the light evidence of UHE gamma rays is available.

solitons) in the accreting plasma. The accreting plasma automatically becomes essentially inhomogeneous.

## MECHANISM OF THE CONVERSION OF GRAVITATIONAL ENERGY TO ULTRA-RELATIVISTIC PROTON ENERGY

The idea of the proposed mechanism lies in the assertion that a distribution of accreting protons of "the loss cone" type takes place during accretion onto the neutron star with a strong magnetic field (Leroy and Mangeney 1984; Benz and Thejappa 1989). This distribution is characteristic for generation of instabilities and given by

$$F(\vec{P}_\perp, P_\parallel) = C \exp\left[-\frac{(P_\parallel - P_{0\parallel})^2}{2\Delta P_\parallel^2} - \frac{(\vec{P}_\perp - \vec{P}_{\perp 0})^2}{2\Delta P_\perp^2}\right] \Delta P_\perp^2 \gtrsim \Delta P_\parallel^2 \quad (4)$$

where

$$C = \left[\pi^{3/2}\Delta P_\perp^2 \Delta P_\parallel \left\{\exp\left(-\frac{P_{0\perp}}{\Delta P_\perp^2}\right) + \sqrt{\pi}\frac{P_{0\perp}^2}{\Delta P_\perp^2}\left[1 + erf\left(\frac{P_{0\perp}}{\Delta P_\perp}\right)\right]\right\}\right]^{-1} \quad (5)$$

In the case of sperical accretion $\vec{P} = m_p \times \vec{V}_{ff}$, where $m_p$ is the proton mass and $\vec{V}_{ff}$ is the free-fall velocity of the accreting plasma.

What is the physical justification of the above assertion? First of all this distribution (4) can take place at the entrance of the accreting plasma onto the cusp level of the magnetized neutron star due to the conservation of the adiabatic invariant $\Delta P_\perp^2/B$ = Const. Another possible reason for this distribution may be plasma reflection from a strong shock wave formed during the accretion. One can note three possible locations of the shock wave: Alfvén surface where the shock wave is formed as a result of the interaction of the accreting matter with the neutron star's magnetospheric plasma, in the region of the so-called magnetopause. The protons may reflect from the magnetopause forming distribution (4) or a bit different distribution (Leroy and Mangeney 1984). This reflection may take place deep in the magnetosphere closer to the neutron star's surface as a result of the formation of a shock wave or a strong narrowing of the magnetic cusp in the region of the accretion energy release. In the latter case, we have to deal with the reflection from a magnetic mirror (Vlahos 1987).

As to the shock wave, it can be formed due to the radiation pressure if its strength is close to the Eddington limit (Basko and Sunyaev 1976). The cross section of the photon scattering by the electron is resonant at the cyclotron frequency $\omega_{Be}$ in the magnetic field of the neutron star. This

increases the pressure in comparison with the case without the magnetic field (Mitrophanov and Pavlov 1982; Gnedin and Nagel 1984; Zheleznyakov and Litvinchuk 1986).

A distribution of the (4) type is unstable and generates small-scale Alfvén, proton cyclotron and hybrid waves (Meerson and Rogachevskii 1983; Machabeli *et al.* 1987) as well as nonlinear waves: solitons which are magneto-acoustic and Alfvén vortices in plasma (Petviashvili and Pohotelov 1973). Solitons are effectively generated at the moment of the reflection e.g., from the magnetic wall or in the region of the shock wave formation (Alsop and Arons 1988; Arons 1988) of the moving plasma.

The frequency of the excited linear waves is given by $\omega \approx \omega_{Bi} V_A/V$ where $\omega_{Bi}$ is the ion cyclotron frequency, $V_A$ is the Alfvén velocity, and V is the plasma beam velocity equal to $V_{jj}$.

The instability increment is equal to (Zaitsev and Stepanov 1985)

$$\gamma \approx 0.4(8\pi W_p/B^2)W_{jj} \tag{6}$$

where $W_p$ is the energy density of the proton beam causing instability. In our case we may assume this value to be close to the density of the accreting plasma gravitational energy, i.e.,

$$W_p < W_{jj} = 1/2\rho V_{jj}^2 \tag{7}$$

where $\rho$ is the accreting plasma, with density depending on accretion rate $\dot{M}$.

The generated waves become more intensive in direction close to that of the magnetic field lines: $K_1/K_{11} < (\omega/\omega_{Bi})^{1/2}$. On the Alfvén surface $V_A \approx V_{jj}$ and $\omega \approx \omega_{Bi}$, i.e., ion cyclotron waves are effectively generated. Within the magnetosphere: $\omega > \omega_{Bi}$.

A soliton as a magneto-acoustic vortex may be considered as a nonlinear packet of fast magneto-acoustic waves. This packet is an axial-symmetric formation, propagating along the magnetic field $\vec{B}$. Its dimensions in the direction of the propagation $\ell_z$ and in the direction of the radius $\ell_r$ are given by

$$\ell_z \approx \frac{V_A}{\omega_{Bi}A^2}; \ell_r \approx \frac{V_A}{\omega_{Bi}A^3} \tag{8}$$

where A is the dimensionless amplitude of the vortex. Since $A < 1$, as a rule, the vortex is flattened along the magnetic field lines. The magnetic field of the magneto-acoustic vortex is mainly radial, $\Delta B_r = AB$, and its propagates with the velocity, $V_s = V_A (1\text{-}A^2)$.

The Alfvén vortex on the contrary, is elongated along $\vec{B}$, ($\ell_z \gg \ell_r$) and its magnetic field is predominantly azimuthal $\Delta B_\varphi = AB$. It can be

considered as a waveguide along the direction of the $\vec{B}$ radius $\rho = 1/AK_{11}$. There are other types of Alfvén solitons (see Mihailovskiy *et al.* 1976; Ovenden *et al.* 1983).

In order to provide for effective development of the instabilities of the (4)-(6) type one should have: $\gamma t_D > 1$, where $t_D$ is the characteristic dissipation time of the process in question. This dissipation leads to damping of linear and nonlinear waves and, in particular, to breaking of solitons. One of the effective channels of dissipation is coulomb collisions:

$$t_D \approx 1/\nu_e \sim V_{ff}^3/Ne \tag{9}$$

where $\nu_e$ is the effective frequency of collisions of the accreting proton beam with the background plasma. $\gamma t_D \sim 10^4$ for the Alfvén surface, i.e., mechanism (4) operates effectively. This condition $\gamma t_D > 1$ is also satisfied near the neutron star's surface. The mechanism of soliton dissipation is widely discussed in scientific literature, although the problem has not yet been finally solved.

We can put down the final conclusion as follows: the conversion of the accreting flux gravitational energy into the ultrarelativistic particle energy as a result of the development of the "loss cone" type instability (4) takes place at a characteristic distance to the neutron star. This generation radius is:

$$R_s \leq R_{gen} \leq R_A \tag{10}$$

## PROTON ACCELERATION TO ULTRARELATIVISTIC ENERGIES IN THE REGION OF THE "LOSS CONE" TYPE INSTABILITY GENERATION

The electric field of a fast solution can be the most effective mechanism of the proton acceleration to ultrarelativistic energies:

$$\vec{E} = 1/C[\vec{V}_A \Delta \vec{B}]; \Delta B = AB \tag{11}$$

On the Alfvén surface $V_A \approx V_{ff}$; that is, it is equal to the plasma free-fall velocity. Inside the accretion column $V_A \approx C$. Since the magnetic field of the magneto-acoustic soliton is radial $\Delta B_r \neq 0$, and that of the Alfvén soliton is azimuthal $\Delta B_\varphi \neq 0$ relative to the magnetic field lines of the neutron star $\vec{B}$, the electric field acts transverse to the magnetic field $\vec{B}$ lines in accordance with (11). It is the azimuthal $E_\varphi \neq 0$ in the case of the generation of magneto-acoustic solitons and the radial $E_r \neq 0$ in the case of the Alfvén solitons. Therefore, the main source of energy losses of the accelerating protons is synchrotron radiation.

The equation for the accelerating proton energy acquired due to the electric field $\vec{E}$ has the form

$$\frac{dE}{dT} = \epsilon \vec{E} \vec{v} \tag{12}$$

where $\vec{v}$ is the accelerating proton velocity $\nu \approx c$. Solution (12) accounting for (11) gives:

$$E_{15} = 0.2(A/B_{12})^{1/2}, \tag{13}$$

if it is the characteristic time of the proton synchrotron losses.

Coulomb collisions only slightly influence the propagation of protons. Nuclear collisions become important for them. Hence, the presence of a very inhomogeneous distribution of plasma is needed, for instance, in the region of the accretion column, to provide for the escape of ultrarelativistic protons from the acceleration region.

It should be noted that an analysis of observational data on X-ray pulsars lead many authors (Basko and Sunyaev 1976; Bai 1980) to the conclusion that the plasma distribution is inhomogeneous in the Alfvén range and within the accretion column. In X-ray binary systems where the compact object is a magnetized white dwarf (objects of AM Her type or "polars") a noticeable excess of soft X-ray radiation in comparison with the hard X-ray radiation, i.e., $L_{xs}/L_{xh} > 1$ is observed. Lasota *et al.* (1988) interpreted this result in a model of very inhomogeneous accretion, when the accreting matter arrives in either magnetic pole region of the white dwarf as separate blobs elongated along the magnetic field lines.

Note, that the mechanism of soliton generation causes the accretion inhomogeneity, because the plasma density inside a soliton is noticeably greater than outside of the soliton: $\Delta\rho \sim (\Delta B)^2$.

The difficulty of the ultrarelativistic protons escape from the generation region can be overcome, if one assumes that the source of gamma rays is neutrons, not protons. The neutrons are formed in the generation region as a result of nuclear collisions formed in the generation region as a result of nuclear collisions of ultrarelativistic protons with the surrounding plasma.

In conclusion, we would like to emphasize the fact that soliton mechanism explains also the freezing-in of the accreting plasma to the strong magnetic field of the neutron star, since the magnetic field will penetrate quickly to plasma blobs, formed by solitons.

## OBSERVATIONAL CONSEQUENCES OF THE PROPOSED MECHANISM

The luminosity of the X-ray pulsar in a binary is fully determined by the rate of accretion on the neutron star according to the traditional theory

$$L_x = GM_s\dot{M}/R_s. \tag{14}$$

The main parameter of our model is the ratio of the power of ultra-high energy protons to the X-ray luminosity:

$$\frac{L_p}{L_x} = \frac{\Delta W_{gr}(R_{gen}}{\Delta W_{gr}(R_s)} \approx \eta(R_{gen})\frac{R_s}{R_{gen}} \tag{15}$$

The value $\Delta W_{gv}(R_{gen})$ takes into consideration the reflection of the accreting plasma in the region of the interaction (e.g., polar cusp) and can considerably exceed the portion of the gravitational energy released in the X-ray range. Hence, the coefficient $\eta$ can be larger than unit $\eta(R_{gen}) > 1$.

Let us analyse the case when the ultrarelativistic protons are generated on the Alfvén surface: $R_{gen} \approx R_A$. Then from most typical conditions for X-ray pulsars: $\dot{M} = 10^{-8}$ $M_\odot$/year, $B_s = 10^{12}$ the ratio is

$$L_p/L_x \approx R_s/R_A \approx 10^{-2}. \tag{16}$$

This ratio is characteristic for a number of sources from Table 1, if one accepts $\sim$ 10% for efficiency of the generation of gamma rays. As to Cyg X-3, this ratio is close to 1. This means that according to (17) the Alfvén radius $R_A \approx R_S$, which corresponds to the value of the magnetic field on the neutron star's surface $B_S \approx 10^9$ Gauss. This result is well confirmed by the recent observational data, which indicate that the neutron star in the Cyg X-3 system is a millisecond pulsar (Watson 1987; Zyskin *et al.* 1987).

In accordance with (15) and (16) one should expect noticeable fluxes of ultrahigh-gamma-rays from such X-ray binaries, whose compact companions are neutron stars with comparatively weak magnetic fields ($\approx 10^9$ Gauss). Possible candidates of that type can be Cir X-1, SS433, Sco X-1, LSI+61°30′. Recently there was an announcement concerning the discovery of a variable gamma-ray radiation of ultrahigh energy from Cir X-1 and 2A 1822-37,1 (Ciampa and Clay 1989; Ciampa *et al.* 1989).

## REFERENCES

Alsop, D., and J. Arons. 1988. Phys. Fluids. 31:839.
Arons, J. 1988. Page 1. Proceedings of the Joint Varenna-Abastumani Workshop on Plasma Astrophysics. Varenna.
Bai, T. 1980. Astrophys. J. 239:299.
Basko, M.M., and R.A. Sunyaev. 1976. Mon. Nat. R. ast. Soc. 175:395.
Benz, A.O. and G. Thejappa. 1988. Preprint. Institute of Astronomy, ETH, Zurich.
Ciampa, D., and R.W. Clay. 1989. Preprint. Department of Physics and Mathematical Physics, University of Adelaide.
Ciampa, D., R.W. Clay, and P.G. Edwards. 1989. Astrophys. J. In press.
Gnedin, Yu.N., and W. Nagel. 1984. Astron. Astrophys. 138:356.

Hillas, A.M. 1987. Page 71. In: Turver, K.E. (ed.). Very High Energy Gamma Ray Astronomy. D. Reidel Publ. Co.
Lamb, R.C., and T.C. Weekes. 1987. Science 238:1528.
Lasota, J.P., J.M. Hameury, and A.R. King. 1988. Astron. Astrophys. 193:113.
Leroy, M.M., and A. Mangeney. 1984. Ann. Geophys. 2:449.
Machabeli, J.Z., D.M. Sehokija, and A.L. Taktashvili. Sov. Lett. in Astron. J. 13:201.
Meerson, B.I., and N.K. Rogachevskiy. 1983. Sol. Phys. 87:337.
Michailovskiy, A.B., V.I. Petviashvili, and A.M. Fridman. 1976. Sov. Letters in JETP 24:53.
Mitrophanov, I.G., and G.G. Pavlov. 1982. Mon. Not. R. astr. Soc. 200:1033.
Ovenden, C.R., H.A. Shan, and S.J. Schwartz. 1983. J. Geophys. Res. A88:6095.
Petviashvili, V.I., and O.A. Pohotelov. 1973. Sov. JETP 73:498.
Vlahos, L. 1987. Sol. Phys. 111:155.
Watson, A.A. 1987. Page 53. In: Turver, K.E. (ed.). Very High Energy Gamma Ray Astronomy. D. Reidel Publ. Co.
Zaitsev, V.V., and A.V. Stepanov. 1985. Solar Phys. 99:313.
Zheleznyakov, V.V., and A.A. Litvinchuk. 1986. Page 375. ESA SP-251. Noordwikj: ESA Publ. Div.
Zyskin, Yu.L., Yu.I. Neshpor, A.A. Stepanyan, *et al.* 1987. Sov. Astron. Circ. 1508:1.

# Can A Man-Made Universe Be Achieved by Quantum Tunneling Without an Initial Singularity?*

ALAN H. GUTH
Massachusetts Institute of Technology
and
Harvard–Smithsonian Center for Astrophysics

## ABSTRACT

Essentially all modern particle theories suggest the possible existence of a false vacuum state—a metastable state with an energy density that cannot be lowered except by means of a very slow phase transition. Inflationary cosmology, which is briefly reviewed, makes use of such a state to drive the expansion of the big bang, allowing the entire observed universe to evolve from an initial mass of only about 10 kilograms. A sphere of false vacuum in our present universe could inflate into a "child" universe, and general relativity is used to learn where the new universe would go. It is not yet settled, but it seems likely that the known laws of physics permit in principle the possibility of creating a child universe by man-made processes.

## THE COSMIC COOKBOOK

During the past decade, a radically new picture of cosmology has emerged. The novelty of this picture is particularly striking when one considers the question of what it takes to produce a universe. According to the standard big bang picture of a decade ago, the visible universe could be assembled, at $t \approx 1$ sec for example, by mixing approximately $10^{89}$

*Based in part on *"Inflation and False Vacuum Bubbles,"* by A. H. Guth, in **Proceedings of the Storrs Meeting** (1988 Meeting of the Division of Particles and Fields of the American Physical Society, Storrs, Connecticut, August 15 – 18, 1988), eds.: K. Haller, D.B. Caldi, M.M. Islam, R.L. Mallett, P.D. Mannheim, and M.S. Swanson (World Scientific, Singapore, 1989), pp. 139-153.

photons, $10^{89}$ $e^+e^-$ pairs, $10^{89}$ $\nu\bar{\nu}$ pairs, $10^{79}$ protons, $10^{79}$ neutrons, and $10^{79}$ unpaired electrons. The total mass/energy of these ingredients is about $10^{65}$ grams $\approx 10^{32}$ solar masses $\approx 10^{10}\times$ present mass of visible universe. The mass is much larger than the present mass of the visible universe, because most of the energy is lost to gravitational potential energy as the universe expands.

With the advent of grand unified theories (GUTs) and inflationary cosmology, however, a much simpler recipe for a universe can now be formulated. [For a review of inflation, see Linde (1984a and 1987), Brandenberger (1985), Turner (1987), Steinhardt (1986), Blau and Guth (1987), or Abbott and Pi (1986).] To produce a universe at $t \approx 10^{-35}$ sec, the ***only*** necessary ingredient is a region of false vacuum. And the region need not be very large. For a typical GUT energy scale of $\sim 10^{14}$ GeV (which I will use for all the numerical examples in this paper), the minimum diameter is about $10^{-24}$ cm. The total mass/energy of this ingredient is only about 10 kg $\approx 10^{-29}$ solar masses $\approx 10^{-51}\times$ present mass of visible universe. This recipe sounds so easy that one cannot resist asking whether it is possible to produce a universe by man-made processes. Unfortunately we do not yet have a definitive answer to this question, but in this paper I will try to summarize our current understanding.

In considering this question, one difficulty is immediately obvious: the mass density of the required false vacuum is about $10^{75}$ g/cm$^3$. This mass density is certainly far beyond anything that is technologically possible, either now or in the foreseeable future. Nonetheless, for the purposes of this discussion I will whimsically assume that some civilization in the distant future will be capable of manipulating these kinds of mass densities. There are then some very interesting questions of principle that must be addressed in order to decide if the creation of a new universe is possible. While I will discuss these questions in terms of the possibility of man-made creation, I want to emphasize that the same questions will no doubt also have relevance to various natural scenarios that one could imagine.

The outline of this paper will be as follows. The first section will summarize the properties of the false vacuum, and the second section will review the inflationary universe model—readers familiar with inflationary cosmology should either skim these sections or skip them entirely. The third section will discuss the evolution of a false vacuum bubble. In the last section, I will discuss the key question: Do the laws of physics as we know them permit in principle the creation of a new universe by man-made processes?

## PROPERTIES OF THE FALSE VACUUM

A false vacuum is a peculiar state of matter which arises when a

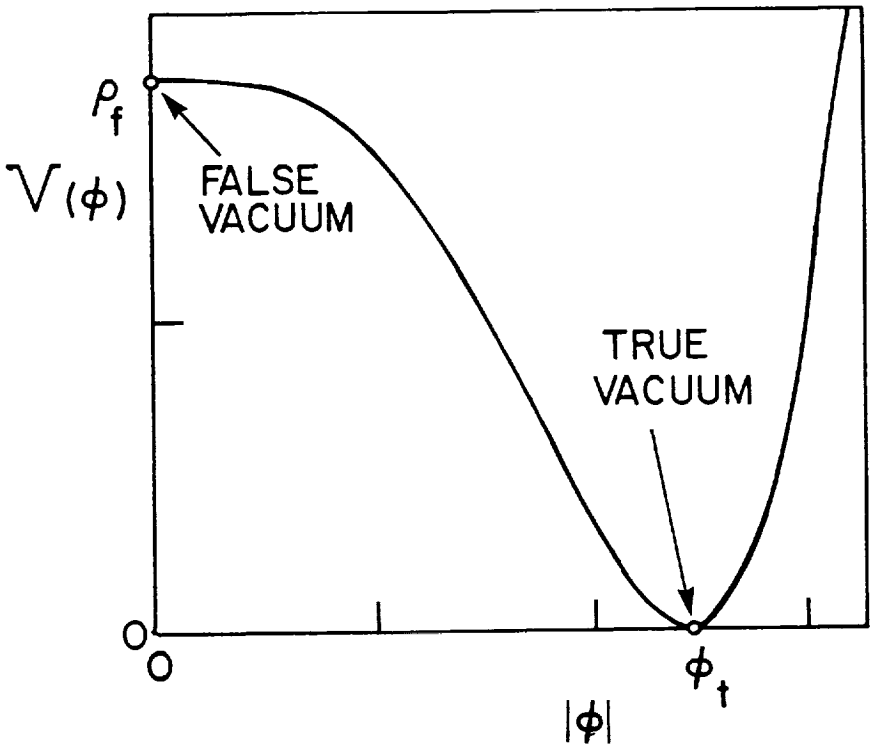


FIGURE 1 Potential energy density for a scalar field $\phi$. The form shown contains a very flat plateau, a shape that is suitable for a new inflationary scenario. The true vacuum is the state of lowest energy for the field, and the false vacuum is the metastable state in which the scalar field has a value at the top of the plateau.

particle theory contains a scalar field $\phi$ with a potential energy density similar to that shown in Figure 1. The state $\phi = \phi_t$ is the state of minimum energy density, and therefore is the true vacuum. If, however, there is a region of space in which $\phi \approx 0$, this region is called a false vacuum. The false vacuum is obviously not stable, since the scalar field will sooner or later roll off the "hill" of this potential energy diagram. The false vacuum can, however, be highly metastable, if the plateau in the potential energy diagram is flat enough. I will assume that I am talking about a false vacuum with a lifetime that is long compared to the other time scales of interest for the early universe.

The mass density of the false vacuum is fixed by the value of the potential energy density for $\phi \approx 0$, which for typical grand unified theory numbers has a value of about

$$\rho_f \approx (10^{14}\ \text{GeV})^4 \approx 10^{74}\ \text{g/cm}^3\ .$$

(I will generally use units with $\hbar = c = 1$, but for clarity I will sometimes write formulas with factors of $c$ included.) The false vacuum has the very unusual property that this mass density is fixed. If a region of false vacuum is enlarged, the mass density does not decrease as it would for a normal material. Instead it is held at this constant value, provided of course that there is not enough time for the scalar field to roll down the hill. This constancy of the mass density implies a peculiar property for the pressure $p$. To see this, consider a chamber filled with false vacuum, as shown in Figure 2. When the chamber is enlarged by the piston moving outward, the volume of the chamber increases by $\Delta V$. Since the energy density is constant at $\rho_f c^2$, this implies that the agent that pulled the piston out must have done work $\Delta W = \rho_f c^2 \Delta V$. Since the pressure outside the piston is just the pressure of the true vacuum, which is zero, we conclude that the pressure inside must be negative. Since the work done in the expansion of a gas is given by $\Delta W = -p\Delta V$, one finds immediately that

$$p = -\rho_f c^2\ .$$

So the pressure of the false vacuum is huge, and negative.

If the early universe went through a false vacuum phase, then the evolution can be determined by putting the energy density and pressure of the false vacuum into Einstein's field equations. For those familiar with cosmology, the effect can be described by saying that the false vacuum acts exactly like a (positive) cosmological constant, except of course that the false vacuum is not permanent—it will eventually decay. To see the consequences more explicitly, note that the gravitational deceleration of the cosmic expansion is, according to general relativity, proportional to

$$\rho + \frac{3p}{c^2}\ .$$

Ordinarily the second term is a small relativistic correction. During the radiation-dominated period of the early universe, however, the second term is equal in magnitude to the first term. For the false vacuum, however, the pressure term is negative, and in fact it overwhelms the positive contribution from the mass density. The net effect is to create a huge gravitational repulsion, causing the universe to go into a period of exponential expansion.

## THE NEW INFLATIONARY UNIVERSE

While the original form of the inflationary universe model (Guth 1981) failed to provide a smooth ending to inflation, this problem was overcome

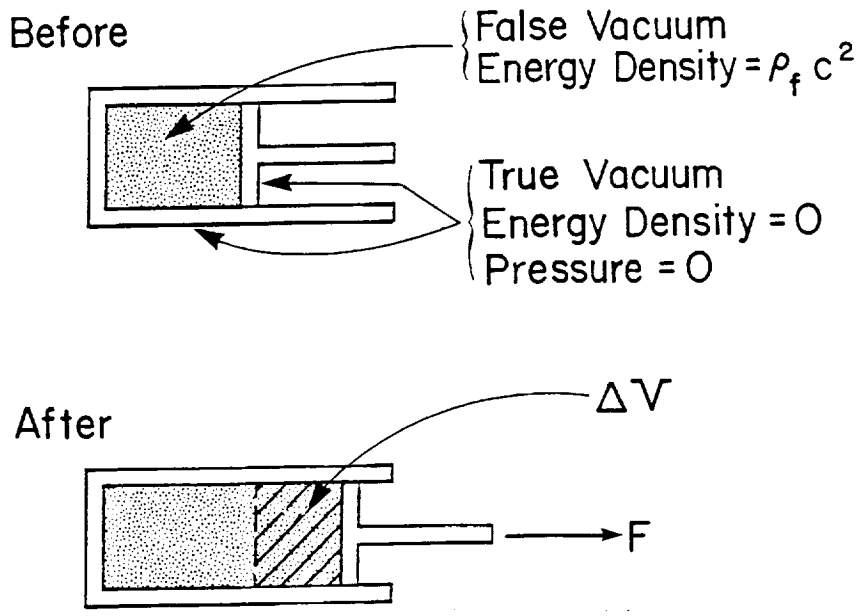


FIGURE 2 A thought experiment to derive the pressure of the false vacuum. The piston chamber is filled with false vacuum, and is surrounded by true vacuum. When the piston is pulled out the energy density remains constant, so the additional energy must be furnished by the force needed to pull the piston against the negative pressure of the false vacuum.

by the introduction of the new inflationary universe scenario (Linde 1982; Albrecht and Steinhardt 1982). The scenario begins with a patch of the universe somehow settling into a false vacuum state. The mechanism by which this happens has no influence on the later evolution, and at least three possibilities have been discussed in the literature:

1) *Supercooling from high temperatures.* This was the earliest suggestion (Guth 1981; Linde 1982; Albrecht and Steinhardt 1982). If we assume that the universe began very hot, as is traditionally assumed in the standard big bang model, then as the universe cooled it presumably went through a number of phase transitions. For many types of scalar field potentials, supercooling into a false vacuum occurs naturally. This scenario has the difficulty, however, that there is no known mechanism to achieve the desired pre-inflationary thermal equilibrium state. For fields as weakly coupled as is needed for inflation (Starobinsky 1982; Guth and Pi 1982; Hawking 1982; Bardeen *et al.* 1983), there is not nearly enough time for thermal equilibrium to be achieved by the normal dynamical processes. It has been shown, however, that true thermal equilibrium is not really necessary: a variety of random

configurations give results that are very similar to those of thermal equilibrium (Albrecht *et al.* 1985).

2) *Tunneling from "nothing"* (Tryon 1973; Vilenkin 1982 and 1985a; Linde 1983a and 1984b; Hartle and Hawking 1983). These ideas are of course very speculative, since they involve a theory of quantum gravity that does not actually exist. The basic idea, however, seems very plausible. If geometry is to described by quantum theory, then the geometry of space can presumably undergo quantum transitions. One can then imagine an initial state of absolute nothingness—the absence of matter, energy, space, or time. The state of absolute nothingness can presumably undergo a quantum transition to a small universe, which then forms the initial state for an inflationary scenario.
3) *Random fluctuations in chaotic cosmology.* Linde (1983b,c) has advocated a chaotic cosmology in which the scalar field $\phi$ begins in a random state in which all possible values of $\phi$ occur. Inflation then takes place in those regions that have appropriate values of $\phi$, and these inflated regions dominate the universe at later times. In these models it is not necessary for the scalar field potential energy function $V(\phi)$ to have a plateau, since inflation can occur as the scalar field rolls downward, starting from a very large value. As in other models, however, it can be shown that the potential must be very flat in order minimize the density perturbations that result from quantum fluctuations (Starobinsky, 1982; Guth and Pi 1982; Hawking 1982; Bardeen *et al.* 1983).

Regardless of which of the above mechanisms is assumed, one expects that the correlation length of the scalar field just before inflation is of the order of the age of the universe at the time. Assuming again a GUT energy scale of about $10^{14}$ GeV, one finds a correlation length of about $10^{-24}$ cm.

The patch then expands exponentially due to the gravitational repulsion of the false vacuum. In order to achieve the goals of inflation, we must assume that this exponential expansion results in an expansion factor $\gtrsim 10^{25}$. For typical grand unified theory numbers, this enormous expansion requires only about $10^{-32}$ sec of inflation. During this inflationary period, the density of any particles that may have been present before inflation is diluted so much that it becomes completely negligible. At the same time, any nonuniformities in the metric of space are smoothed by the enormous expansion. The explanation for this smoothness is identical to the reason why the surface of the earth appears to be flat, even though the earth is actually round—any differentiable curve looks like a straight line if one magnifies it enough and looks at only a small segment. The correlation length for the scalar field is stretched by the expansion factor to become at least about 10 cm. If the duration of inflation is more than the minimal

value, which seems quite likely, then the final correlation length could be many orders of magnitude larger. There appears to be no upper limit to the amount of inflation that may have taken place.

The false vacuum is not stable, so it eventually decays. If the decay occurs by the usual Coleman–Callan (Coleman 1977; Callan and Coleman 1977) process of bubble nucleation, as was assumed in the original version of inflation, then the randomness of the bubble nucleation process would produce gross inhomogeneities in the mass density (Guth and Weinberg 1983; Hawking *et al.* 1982). This problem is avoided in the new inflationary scenario (Linde 1982; Albrecht and Steinhardt 1982) by introducing a scalar field potential with a flat plateau, as was shown in Figure 1. This leads to a "slow-rollover" phase transition, in which quantum fluctuations destabilize the false vacuum, starting the scalar field to roll down the hill of the potential energy diagram. These fluctuations are initially correlated only over a microscopic region, but the additional inflation that takes place during the rolling can stretch such a region to be large enough to easily encompass the observed universe.

When the phase transition takes place, the energy that has been stored in the false vacuum is released in the form of new particles. These new particles rapidly come to thermal equilibrium, resulting in a temperature with $kT \approx 10^{14}$ GeV. At this point the scenario rejoins the standard cosmological model.

The baryons are produced [see, for example, Kolb and Turner 1983 or Yoshimura 1981] by baryon nonconserving processes ***after*** inflation. Any baryons that may have been present before inflation are simply diluted away by the enormous expansion factor. Thus, inflationary cosmology requires an underlying particle theory, such as a grand unified theory, in which baryon number is not conserved.

The inflationary universe model has a number of key successes, the most of important of which are the following:

1) It cures the "magnetic monopole problem." In the context of grand unified theories, cosmologies without inflation generally lead to huge excesses of magnetic monopoles. These monopoles are produced at the grand unified theory phase transition, when the GUT Higgs fields acquire their nonzero values. The rapidity of the phase transition implies that the correlation length of the Higgs fields is very short, and the fields therefore become tangled in a high density of knots—these knots have the physical properties of superheavy ($\sim 10^{16}$ GeV) magnetic monopoles ('t Hooft 1974; Polyakov 1974; for a review, see Goddard and Olive 1978). For typical grand unified theories the expected mass density of these magnetic monopoles would exceed

(Zel'dovich and Khlopov 1978; Preskill 1979) the mass density of everything else by a factor of about $10^{12}$.

2) It explains why the universe is so homogeneous. The most striking evidence for the homogeneity of the universe is seen in the cosmic background radiation, which is known to have a temperature that is uniform in all directions to an accuracy of a few parts in $10^5$. This implies that the temperature of the universe was uniform to this accuracy when the background radiation was released, a few hundred thousand years after the big bang. In standard cosmology, the establishment of thermal equilibrium at such an early time over such a huge volume would require the transfer of information at approximately 100 times the speed of light. In the inflationary model, on the other hand, thermal equilibrium could have been established in an incredibly small region before the onset of inflation. The process of inflation would then take this very small region and magnify it to become large enough to encompass the entire observed universe.
3) It explains why the mass density of the early universe was so close to the critical value. The critical mass density, $\rho_c$, is defined as that mass density which is just barely sufficient to eventually halt the expansion of the universe. Today the crucial ratio $\Omega \equiv \rho/\rho_c$ (where $\rho$ is the mass density of the universe) is known to lie in the range $0.1 \lesssim \Omega \lesssim 2$. Despite the breadth of this range, the value of $\Omega$ at early times is highly constrained, since $\Omega$ diverges from one as the universe evolves. At $t = 1$ sec, for example, $\Omega$ must have been equal to one (Dicke and Peebles 1979) to an accuracy of one part in $10^{15}$. Standard cosmology provides no explanation for this fact—it is simply assumed as part of the initial conditions. In the inflationary model, however, $\Omega$ is driven during the period of inflation very rapidly toward one, regardless of where it begins.
4) It provides a possible origin for the density fluctuations that seed galaxy formation. In standard cosmology an entire spectrum of primordial density fluctuations must be assumed as part of the initial conditions. In the inflationary model, on the other hand, density fluctuations are produced naturally by quantum fluctuations during the inflationary phase transition (Starobinsky 1982; Guth and Pi 1982; Hawking 1982; Bardeen *et al* 1983). These density fluctuations, moreover, have a spectrum that is at least roughly what is desired for galaxy formation. This success of inflation, however, occurs only at a price: for the magnitude of the density fluctuations to turn out correctly, the scalar field that drives inflation must be coupled incredibly weakly. For a simple $\lambda\phi^4$ theory, for example, the value of $\lambda$ must be about $10^{-12}$. This incredibly weak coupling is necessary regardless of whether one is using a chaotic inflationary model, or a standard (new) inflationary

model. It should also be mentioned that particle physics provides an alternative possibility for generating primordial density perturbations: it could be that the perturbations produced by inflation were negligibly small, while the important fluctuations developed later from the random formation of cosmic strings (for a review, see Vilenkin 1985b).

5) It explains the origin of essentially all the matter, energy, and entropy in the universe. While this statement may seem to violate known conservation principles, in fact it does not—provided that baryon number is not conserved. Energy conservation is no problem. The gravitational contribution to the energy of the universe is negative, and in any model with $\Omega \geq 1$, the gravitational energy precisely cancels the energy of matter (Tryon, 1973).

Any physical theory should be testable, and fortunately there are at least a few tests of inflation that are in principle possible. First, inflation predicts that $\Omega$, even today, should be equal to one. More precisely, the prediction is

$$\Omega + \frac{\Lambda}{3H^2} = 1 \pm O(10^{-4}) \ ,$$

where $\Lambda$ is the cosmological constant. The term $\Lambda/3H^2$ can be thought of as the contribution to $\Omega$ from the energy density of the vacuum. The uncertainty of $O(10^{-4})$ allows for quantum fluctuations, and its magnitude is estimated not from first principles, but instead from the fluctuations that are required for galaxy formation. Second, inflation predicts the spectral form of the primordial density fluctuations. In particular it predicts a scale-invariant Gaussian spectrum known as the Harrison-Zel'dovich spectrum (Harrison 1970; Zel'dovich 1972). The scale-invariance can in principle be tested by precise measurements of anisotropies in the cosmic background radiation, and/or by developing a detailed theory of galaxy formation. These tests are of course extremely difficult, but the problems do not appear to be insurmountable.

## EVOLUTION OF A FALSE VACUUM BUBBLE

By a false vacuum bubble, I mean a region of false vacuum surrounded by anything else. I will discuss in detail the simplest case: a spherical region of false vacuum surrounded by true vacuum. In considering the evolution of such a region one is lead immediately to a paradox. If the region of false vacuum is large enough, one expects that it would undergo inflation. An observer in the outside true vacuum region, on the other hand, would see the false vacuum region as a region of negative pressure. The pressure gradient would point inward, and the observer would not expect to see

the region increase in size. The resolution of this paradox hinges on the dramatic distortion of spacetime that is caused by the false vacuum bubble.

Here I will outline the solution to this problem, but a reader interested in the technical details will have to consult the literature (Sato *et al.* 1981 and 1982; Berezin *et al.* 1983, 1985, and 1987; Ipser and Sikivie 1984; Aurilia *et al.* 1984 and 1985; Lake 1979, Lake and Wevrick 1986). The description given here follows the work that I did with Blau and Guendelman (Blau *et al.* 1987).

The first step in solving the problem is to dissect it, dividing the spacetime into three regions. The exterior region is spherically symmetric empty space, for which the unique solution, in general relativity, is the well-known Schwarzschild metric. The interior region consists of spherically symmetric false vacuum, and is required to be regular at $r = 0$. This spacetime also has a unique solution: de Sitter space. At the interface between these two regions is a domain wall—a region in which a scalar field is undergoing a transition between its true and false vacuum values. The solution that I will describe uses a thin-wall approximation, in which the thickness of the wall is assumed to be negligibly small compared to any other distance in the problem. In this approximation it can be shown that the surface energy-density is equal to the surface tension and is independent of time, and we take this surface energy density $\sigma$ as an additional parameter of the problem. The wall can then be described mathematically by a set of junction conditions (Israel 1966) which are obtained by applying Einstein's equations to an energy-momentum tensor restricted to a thin sheet. (These equations are just the gravitational analogue of the well-known statement that the normal component of an electric field has a discontinuity of $4\pi\sigma$ at a sheet of surface charge density $\sigma$.) The evolution is completely determined by using these junction conditions to join the interior and exterior forms of the metric.

The evolution of the bubble wall can be described by the function $r(\tau)$, where $r$ is the radius of the bubble wall (defined as $1/2\pi$ times the circumference), and $\tau$ is the proper time as would be measured by a clock that follows the bubble wall. The junction conditions described above imply an equation of motion for $r(\tau)$ that can be cast into a form identical to that of a nonrelativistic particle moving in a potential $V(r)$, as shown in Figure 3. The energy of the fictitious particle is related to the mass of the physical false vacuum bubble. As can be seen in the potential energy diagram, there are three kinds of solutions. First, there are "bounded" solutions in which the bubble grows from $r = 0$ to a maximum size and then collapses. Second, there are "bounce" solutions. Here the bubble starts at infinite size in the asymptotic past, contracts to a minimum size, and then expands without limit. Finally, there are "monotonic" solutions—bubbles that start at zero size and grow monotonically. The monotonic solutions require a

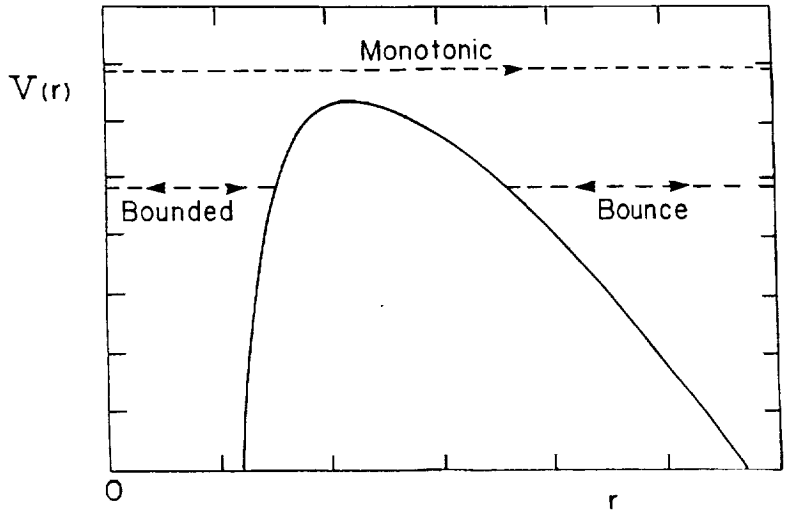


FIGURE 3 In the thin-wall approximation the trajectory of the bubble wall is equivalent to the motion of a nonrelativistic particle in the potential energy curve shown above. The energy of the fictitious particle is related to the mass of the false vacuum bubble; the energy increases with the mass, and approaches the top line of the diagram as $M \rightarrow \infty$.

minimum mass, so that the energy of the fictitious particle is high enough to get over the potential barrier in Figure 3. For small values of the surface energy density ($\sigma \ll \sqrt{\rho_f/G}$), this critical mass is given simply by

$$M_{cr} = \frac{4\pi}{3}\chi^{-3} \ ,$$

where $\chi$ is the rate of the exponential expansion (i.e., scale factor $\propto \exp(\chi t)$), which is related to the false vacuum energy density $\rho_f$ by

$$\chi^2 = \frac{8\pi}{3}G\rho_f \ .$$

For typical GUT parameters, $M_{cr} \approx 10$ kg.

Having described the evolution of the bubble wall, I must still describe how the bubble wall is embedded in spacetime. Here I will describe only the behavior of the monotonic solutions. A spacetime diagram for this situation is shown as Figure 4. The true vacuum region, to the right of the bubble wall, is shown in the standard Kruskal-Szekeres coordinates. The false vacuum region, to the left of the bubble wall, is shown in peculiar coordinates designed solely to allow the two halves of the diagram to fit together in the plane. The diagram is constructed so that lightlike lines lie at 45° to the vertical, but the metric is highly distorted. In particular

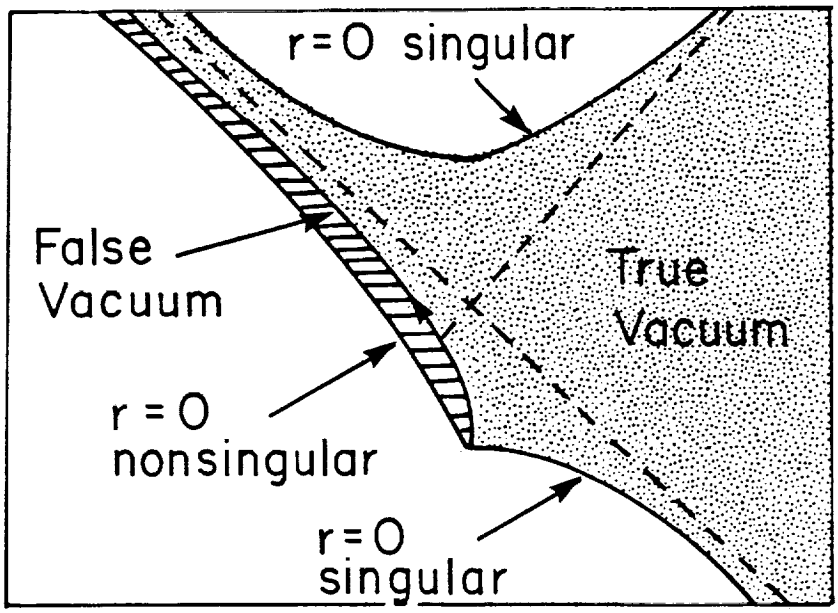


FIGURE 4 A spacetime diagram of a monotonic false vacuum bubble solution. Angular coordinates are suppressed, and the diagram is plotted so that lightlike lines are at 45°. The bubble wall is shown as a heavy line with an arrow on it. The true vacuum region (dotted) is to the right of the bubble wall, and the false vacuum region (horizontal lines) is to the left. The diagram shows initial (lower) and final (upper) $r = 0$ singularities, and also a nonsingular $r = 0$ line (i.e., the center of a spherical coordinate system) that runs along the left edge.

the exponential expansion of the false vacuum region, which occurs as one moves upward and to the left in the diagram, is completely hidden by the distortion of the metric.

The physical meaning of a spacetime diagram of this type can be seen most clearly by examining a sequence of equal-time slices. Figure 5 shows the positions of four slices, labeled (a), (b), (c), and (d), and Figure 6 shows a representation of each slice. For purposes of illustration, Figure 6 shows only two of the three spatial dimensions. Since the spaces of interest are spherically symmetric, this results in no loss of information. The two-dimensional sheet is shown embedded in a fictitious third dimension, so that the curvature can be visualized. Figure 6(a) shows a space which is flat at large distances, but which has a singularity at the origin. In Figure 6(b) a small, expanding region of false vacuum has appeared at the center, replacing the singularity. The false vacuum region is separated from the rest of space by a domain wall. Figure 6(c) shows the false vacuum region beginning to swell. Note, however, that the swelling takes place by the

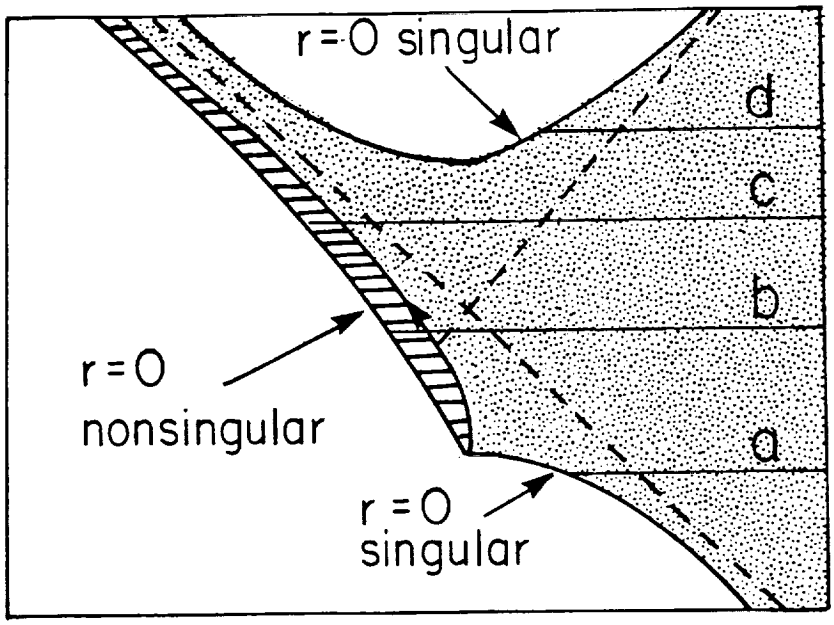


FIGURE 5 Horizontal lines indicating spacelike hypersurfaces to be illustrated in Figure 6.

production of new space; the plane of the original space is unaffected. The false vacuum region continues to inflate, and it soon disconnects completely from the original space, as shown in Figure 6(d). It forms an isolated closed universe which Sato *et al.* (1981 and 1982) have dubbed a "child" universe.

Note, by the way, that Figure 6 shows clearly how the paradox raised at the beginning of this section is resolved. The net force on the bubble wall points from the true vacuum region to the false vacuum region, as expected. Due to the inversion shown in Figures 6(c) and 6(d), however, this force causes the bubble wall to expand, rather than contract.

To summarize, the false vacuum bubble appears from the outside to be a black hole. From the inside, however, it appears to be an inflating region of false vacuum, with new space being created as the region expands. The region completely disconnects from the original spacetime, forming a new, isolated closed universe.

Although the problem that has been solved is very idealized, it nonetheless appears to contain the essential physics of more complicated inhomogeneous spacetimes. The paradox discussed at the beginning of this section will exist whenever an inflating region is surrounded by noninflating regions, and the qualitative behavior of the system seems to be determined by the way in which this paradox is resolved. Thus, one concludes that if inflation

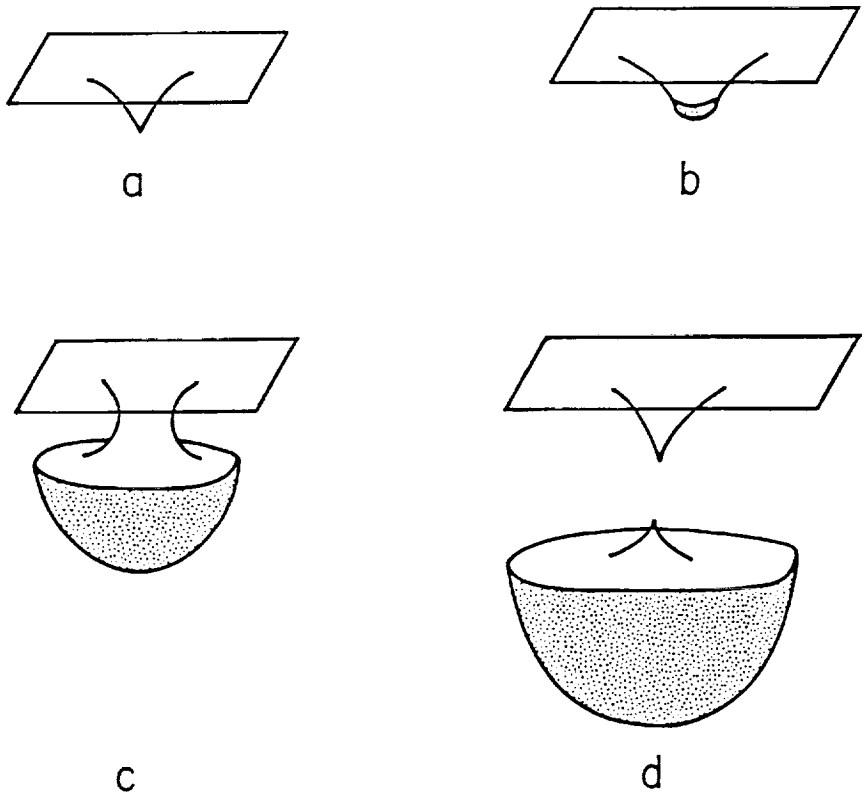


FIGURE 6 The evolution of a monotonic false vacuum bubble solution. Each lettered diagram illustrates a spacelike hypersurface indicated in Figure 5. The diagrams are drawn by suppressing one dimension of the hypersurface and embedding the resulting two-dimensional surface in a fictitious three-dimensional space so that the curvature can be displayed. The false vacuum region is shown as dotted. Note that diagram (d) shows a child universe detaching from the original spacetime.

occurred in an inhomogeneous universe, then many isolated child universes would have been ejected.

Furthermore, even if inflation somehow began in a completely homogeneous way, one still expects the universe to break apart into a host of child universes. The reason stems from the intrinsic nonuniformity, on very large scales, of the decay of the false vacuum (Aryal and Vilenkin, 1987). This process occurs exponentially,[1] like most other decay processes, but for inflation to be successful the parameters must be arranged so that the

[1] I have studied a simplified but exactly soluble model of a slow-rollover phase transition with S.-Y. Pi (Guth and Pi 1985).

exponential decay constant is slow compared to the exponential expansion rate. This implies that the total volume of false vacuum ***increases*** with time. Thus, no matter how long one waits there will still be regions of false vacuum. These regions have no reason to be spherical, but the arguments of the previous paragraph lead one to expect a high likelihood of producing child universes.

## CAN ONE IN PRINCIPLE CREATE AN INFLATIONARY UNIVERSE IN THE LABORATORY?

Figures 4–6 illustrate the creation of a new universe, but there is one undesirable feature. The sequence begins with an initial singularity, shown as the lower $r = 0$ singularity in Figures 4 and 5, and as part (a) of Figure 6. Although an initial singularity is often hypothesized to have been present at the big bang, there do not appear to be any initial singularities available today. So we ask whether it is possible to intervene in some way, to modify the early stages of this picture, so that an inflationary universe could be produced ***without*** an initial singularity. This question can be addressed at either the classical or quantum levels.

At the classical level Farhi and I (Farhi and Guth 1987) have shown that the initial singularity cannot be avoided. Any false vacuum bubble which grows to become a universe necessarily begins from an initial singularity.

The argument rests on an application of the Penrose theorem.[2] The inflationary solutions are very rapidly expanding, and the Penrose theorem implies that such rapid expansion can result only from an initial singularity. (The Penrose theorem is more widely known in a form which is the time-reverse of the present application: if a system is collapsing fast enough, there is no way to avoid the collapse to a singularity.)

The application of the Penrose theorem involves two technical loopholes. First, if the final bubble is not spherically symmetric, then we have not been able to show that the Penrose theorem applies. We believe that this shortcoming, however, is probably the result of our own limitations, and does not provide a way to avoid the theorem. Second, if a material can be found with a pressure that exceeds its energy density, then the Penrose theorem would not apply. In quantum field theories it is possible to construct states that have this property, but it is not clear if a large enough region of this type can be attained.

At the quantum level, on the other hand, the Penrose theorem does not apply, since it is derived from the classical equations of motion. With E. Fahri and J. Guven (Farhi *et al.* 1990), I have studied the question of

[2] We thank R. Wald, W. Israel, J. Bardeen, and W. Unruh for pointing out to us the relevance of this theorem.

whether quantum physics allows the creation of an inflationary universe without an initial singularity. In particular, we have been exploring the following recipe. Suppose a small bubble of false vacuum (with mass less than the critical mass $M_{cr} \approx 10$ kg) is created and caused to expand at a moderate rate. Since the bubble is not expanding rapidly, the Penrose theorem does not preclude its production by classical processes, without an initial singularity. We have not explored in detail the mechanisms by which such a region might be created, but presumably it could be created either by supercooling from high temperatures or perhaps by compressing a gas of fermions that couple to the scalar field. If such a bubble were allowed to evolve classically, it would correspond to one of the bounded solutions, as discussed in the context of Figure 3. It would expand to a maximum size and then the pressure gradient would halt the expansion and cause the bubble to collapse. By quantum processes, however, one might imagine that the bubble could tunnel through the potential energy barrier shown in Figure 3, becoming a bounce solution that would continue to grow until eventually the false vacuum decayed. The late-time behavior of this bounce solution would strongly resemble that shown in Figures 6(c) and 6(d). Although no fully satisfactory theory of quantum gravity exists, we have attempted to *estimate* the tunneling amplitude by using a semiclassical (WKB) approximation.

Specifically, we used the same kind of Euclidean field theory technique that was used by Coleman and De Luccia[3] (1980) to calculate the decay rate of the false vacuum in curved spacetime. That is, we assume that the amplitude to go from one three-geometry to another is well-approximated by $e^{iI_{cl}/\hbar}$ where $I_{cl}$ is the action of the classical solution to the field equations which interpolates between the two three-geometries. If no real-time solution exists then we seek a Euclidean four-geometry that solves the imaginary time field equation and whose boundary is the two three-geometries of interest. The tunneling amplitude is then estimated as $e^{-I_E/\hbar}$, where $I_E$ is the properly subtracted classical action of the Euclidean solution—that is, it is the action of the solution, minus the action of a configuration that remains static at the initial state of the tunneling process for the same Euclidean time as the solution requires for its transit.

We have found, however, that no true Euclidean interpolating manifold exists. There is no difficulty or ambiguity in analytically continuing the bubble wall trajectory into the Euclidean regime, but when this trajectory is plotted on a Euclidean spacetime diagram it is found to cross both the initial and final surfaces of the tunneling problem. These intersection points prevent a conventional manifold interpretation.

[3] See also Section 6 of Guth and Weinberg 1983, which includes a discussion of a spacetime region that was omitted in the original reference.

We admit that we are not sure what the absence of a true interpolating manifold implies about the tunneling problem. Perhaps it indicates that the stationary phase method has failed, perhaps it indicates that one cannot extrapolate the thin-wall approximation into the Euclidean regime, or perhaps it is a suggestion that tunneling is for some reason forbidden.

We find it difficult to believe, however, that the tunneling process is forbidden, since there is no barrier to constructing a well-defined manifold (with either Lorentzian or Euclidean signature) that interpolates between the initial and final states. Such a manifold is not a solution, but it would constitute a path contributing to the functional integral. Furthermore, since any small variation about such a path would also contribute, the measure of these paths appears naively to be nonzero. The amplitude would then be nonzero unless the various paths conspire to cancel each other, as they do for an amplitude that violates a conservation principle associated with a symmetry. In the present case, however, there is no apparent symmetry or conservation law at work. We therefore conjecture that the tunneling process is allowed, and that the semiclassical approximation is valid.

Although no Euclidean interpolating manifold exists, it is nonetheless possible to generalize the notion of a manifold to describe a well-defined Euclidean interpolation. In our paper we defined a object that we called a "pseudomanifold," which we described in two alternative ways. In the simpler description the pseudomanifold closely resembles a true manifold, except that $\sqrt{g}$ is allowed to vanish and to change sign. We assume that the action of the pseudomanifold can be taken as the usual expression for the Euclidean action, except that $\sqrt{g}$ is not positive definite.

We have used our definition of the action to estimate the tunneling amplitude as a function of the various parameters in the problem, and we have found that it behaves very reasonably: the tunneling action decreases monotonically to zero as the bubble mass $M$ approaches the critical mass $M_{cr}$ at which tunneling would not be necessary, and it diverges monotonically as the gravitational constant $G \to 0$. The action is negative definite by the standard sign conventions, but we argue that, regardless of the sign of the action, the tunneling probability is always exponentially suppressed.

In a recent paper, Fischler *et al.* (1990) have calculated an amplitude for this same process, using a Hamiltonian method somewhat different from the method we used. In their formalism they find no inconsistencies, and their answer is identical to ours.

The final result is obtained by a numerical integration, and it is shown graphically in Figure 7. The (subtracted) Euclidean tunneling action $I_E$ depends on $M/M_{cr}$, and also on the dimensionless parameter

$$\gamma \equiv \frac{2}{\sqrt{1 + (\rho_f / 6\pi G\sigma^2)}} \, .$$

C-3

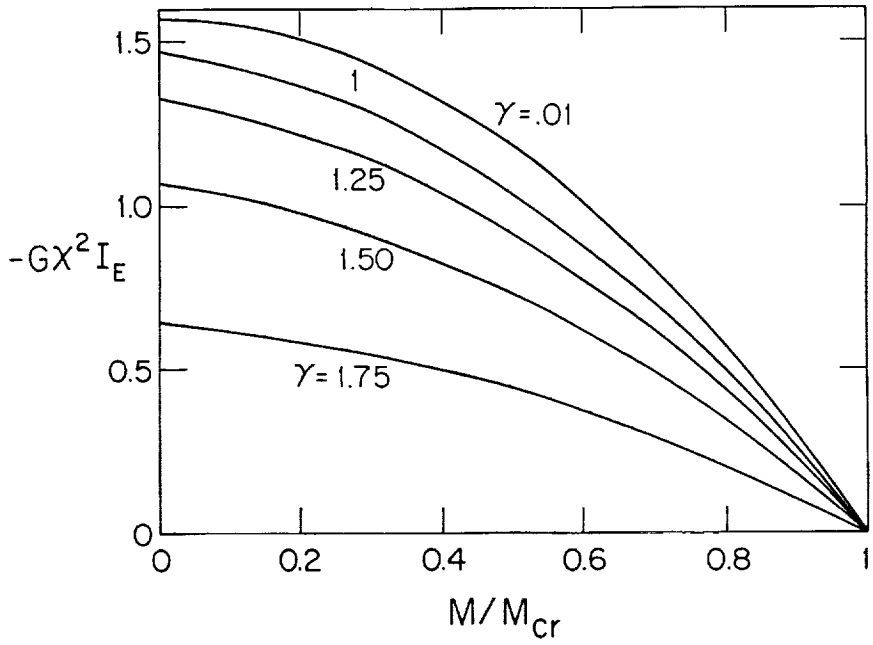


FIGURE 7 Graph of $-G\chi^2 I_E$, where $I_E$ is the Euclidean tunneling action. It is shown as a function of $M/M_{cr}$, for various values of the parameter $\gamma$.

For typical GUT parameters, $\gamma \approx 10^{-4}$.

As a rough estimate, the action $I_E$ is of order $1/(G\chi^2)$, as long as $G\sigma^2$ is smaller than or comparable to $\rho_f$, and $M$ is not too near $M_{cr}$. For typical grand unified theory parameters, this would give an outrageously small tunneling probability, such as $10^{-10^{18}}$. Even with this small probability, however, there might still be a large probability of an event of this sort occurring somewhere in a universe that has undergone a large amount of inflation. Thus, the possibility of a chain reaction by which one universe produces more than one universe is not obviously ruled out by this estimate. On the other hand, if we are talking about creating a universe in a hypothetical laboratory, then a probability this small must be considered equivalent to zero. Thus the production of a universe at the GUT scale seems prohibitively unlikely, but it might be possible at energy scales approaching the Planck scale. In any case, I find it fascinating that the creation of a new universe can even be discussed in scientific terms.

If our semiclassical result is correct, then it seems to raise an important issue in quantum gravity: how does a pseudomanifold arise in a quantum gravity path integral? It might mean that such objects occur in the physical

definition of the path integral, or it might mean that they arise as saddle points which are obtained by the distortion of integration contours in the complex plane.

To summarize: in this paper I have presented several conclusions, some of which are firmer than others. I believe that the following conclusions are well-established:

- A false vacuum bubble can inflate without limit, detaching from the original universe to become an isolated, closed "child" universe. From the "parent" universe, the false vacuum bubble looks like a black hole.
- By the laws of classical physics, a child universe cannot be created without an initial singularity (provided that $|p| \leq \rho c^2$).

In addition, the following conclusions are strongly indicated by present research, but ambiguities remain to be resolved:

- In any model of inflation, whether of the new inflation or chaotic type, isolated child universes are likely to be produced, presumably in infinite numbers.
- A new universe can in principle be created in a hypothetical laboratory, without an initial singularity, by a process of quantum tunneling.

Work in these areas is continuing, and we hope to get a better idea of what exactly is needed in order to create an inflationary universe.

## ACKNOWLEDGMENTS

This work is supported in part by funds provided by the U. S. Department of Energy (D.O.E.) under contract #DE-AC02-76ER03069.

## REFERENCES

Abbott, L. F. and S.-Y. Pi (eds.). 1986. Inflationary Cosmology. World Scientific, Singapore.

Albrecht, A., R. Brandenberger, and R. Matzner. 1985. Numerical Analysis of Inflation. Physical Review D 32: 1280-1289.

Albrecht, A. and P. J. Steinhardt. 1982. Cosmology for Grand Unified Theories with Radiatively Induced Symmetry Breaking. Physical Review Letters 48: 1220-1223.

Aryal, M. and A. Vilenkin. 1987. The Fractal Dimension of Inflationary Universe. Physics Letters 199B: 351-357.

Aurilia, A., G. Denardo, F. Legovini, and E. Spallucci. 1984. An Effective Action Functional for the Inflationary Cosmology. Physics Letters 147B: 258-262.

Aurilia, A., G. Denardo, F. Legovini, and E. Spallucci. 1985. Vacuum Tension Effects on the Evolution of Domain Walls in the Early Universe. Nuclear Physics B252: 523-537.

Bardeen, J. M., P. J. Steinhardt, and M. S. Turner. 1983. Spontaneous Creation of Almost Scale-Free Density Perturbations in an Inflationary Universe. Physical Review D 28: 679-693.

Berezin, V. A., V. A. Kuzmin, and I. I. Tkachev. 1983. Thin Wall Vacuum Domains Evolution. Physics Letters 120B: 91.

Berezin, V. A., V. A. Kuzmin, and I. I. Tkachev. 1985. Dynamics of Inflating Bubbles in the Early Universe. Pages 605-622 In: M. A. Markov, V. A. Berezin, and V. P. Frolov (eds.). Proceedings of 3rd Seminar on Quantum Gravity, 1984. World Scientific, Singapore, 1985.

Berezin, V. A., V. A. Kuzmin, and I. I. Tkachev. 1987. Dynamics of Bubbles in General Relativity. Physical Review D 36: 2919-2944.

Blau, S. K., E. I. Guendelman, and A. H. Guth. 1987. The Dynamics of False Vacuum Bubbles. Physical Review D 35: 1747-1766.

Blau, S. K. and A. H. Guth. 1987. Inflationary Cosmology. Pages 524-603 In: S. W. Hawking and W. Israel (eds.). 300 Years of Gravitation. Cambridge University Press, Cambridge, England.

Brandenberger, R. H. 1985. Quantum Field Theory Methods and Inflationary Universe Models. Reviews of Modern Physics 57: 1-60.

Callan, C. G. and S. Coleman. 1977. The Fate of the False Vacuum. 2. First Quantum Corrections. Physical Review D 16: 1762-1768.

Coleman, S. 1977. The Fate of the False Vacuum. 1. Semiclassical Theory. Physical Review D 15: 2929-2936 [see errata 16: 1248 (1977)].

Coleman, S. and F. De Luccia. 1980. Gravitational Effects On And Of Vacuum Decay. Physical Review D 21: 3305-3315.

Dicke, R. H. and P. J. E. Peebles. 1979. The Big Bang Cosmology—Enigmas and Nostrums. Pages 504-517 In: S. W. Hawking and W. Israel (eds.). General Relativity: An Einstein Centenary Survey. Cambridge University Press, Cambridge, England.

Farhi, E. and A. H. Guth. 1987. An Obstacle to Creating a Universe in the Laboratory. Physics Letters 183B: 149-155.

Farhi, E., A. H. Guth, and J. Guven. 1990. Is It Possible to Create a Universe in the Laboratory by Quantum Tunneling? Nuclear Physics B339: 417-490.

Fischler, W., D. Morgan, and J. Polchinski. 1990. Quantum Nucleation of False Vacuum Bubbles. Physical Review D 41: 2638-2645. See also W. Fischler, D. Morgan, and J. Polchinski, Quantization of False Vacuum Bubbles: A Hamiltonian Treatment of Gravitational Tunneling. University of Texas preprint UTTG-17-90.

Goddard, P. and D. I. Olive. 1978. Magnetic Monopoles in Gauge Field Theories. Reports on Progress in Physics 41: 1357-1437.

Guth, A. H. 1981. The Inflationary Universe: A Possible Solution to the Horizon and Flatness Problems. Physical Review D 23: 347-356.

Guth, A. H. and S.-Y. Pi. 1982. Fluctuations in the New Inflationary Universe. Physical Review Letters 49: 1110-1113.

Guth, A. H. and S.-Y. Pi. 1985. Quantum Mechanics of the Scalar Field in the New Inflationary Universe. Physical Review D 32: 1899-1920.

Guth, A. H. and E. J. Weinberg. 1983. Could the Universe Have Recovered from a Slow First Order Phase Transition? Nuclear Physics B212: 321-364.

Harrison, E. R. 1970. Fluctuations at the Threshold of Classical Cosmology. Physical Review D 1: 2726-2730.

Hartle, J. B. and S. W. Hawking. 1983. Wave Function of the Universe. Physical Review D 28: 2960-2975.

Hawking, S. W. 1982. The Development of Irregularities in a Single Bubble Inflationary Universe. Physics Letters 115B: 295-297.

Hawking, S. W., I. G. Moss, and J. M. Stewart. 1982. Bubble Collisions in the Very Early Universe. Physical Review D 26: 2681-2693.

't Hooft, G. 1974. Magnetic Monopoles in Unified Gauge Theories. Nuclear Physics B79: 276-284.

Ipser, J. and P. Sikivie. 1984. Gravitationally Repulsive Domain Wall. Physical Review D 30: 712-719.

Israel, W. 1966. Singular Hypersurfaces and Thin Shells in General Relativity. Il Nuovo Cimento 44B: 1-14 [see errata in 48B: 463 (1967)].

Kolb, E. W. and M. S. Turner. 1983. Grand Unified Theories and the Origin of the Baryon Asymmetry. Annual Review of Nuclear and Particle Science 33: 645-696.

Lake, K. 1979. Thin Spherical Shells. Physical Review D 19: 2847-2849.

Lake, K. and R. Wevrick. 1986. Evolution of Bubbles in Vacuum. Canadian Journal of Physics 64: 165-173.

Linde, A. D. 1982. A New Inflationary Universe Scenario: A Possible Solution of the Horizon, Flatness, Homogeneity, Isotropy and Primordial Monopole Problems. Physics Letters 108B: 389-393.

Linde, A. D. 1983a. The New Inflationary Universe Scenario. Pages 205-249 In: G. W. Gibbons, S. W. Hawking, and S. T. C. Siklos (eds.). The Very Early Universe: Proceedings of the Nuffield Workshop. Cambridge University Press, Cambridge, England.

Linde, A. D. 1983b. Chaotic Inflating Universe. Pis'ma v Zhurnal Eksperimental'noi i Teoriticheskio Fiziki (Letters to Journal of Experimental and Theoretical Physics) 38: 149-151 [English translation: JETP Letters 38: 176-179 (1983)].

Linde, A. D. 1983c. Chaotic Inflation. Physics Letters 129B: 177-181.

Linde, A. D. 1984a. The Inflationary Universe. Reports on Progress in Physics 47: 925-986.

Linde, A. D. 1984b. Quantum Creation of the Inflationary Universe. Lettere al Nuovo Cimento 39: 401-405.

Linde, A. D. 1984c. Generation of Isothermal Density Perturbations in an Inflationary Universe. Pis'ma v Zhurnal Eksperimental'noi i Teoriticheskio Fiziki (Letters to Journal of Experimental and Theoretical Physics) 40: 496-498. [English translation: JETP Letters 40: 1333-1336 (1984)].

Linde, A. D. 1987. Inflation and Quantum Cosmology. Pages 604-630 In: S. W. Hawking and W. Israel (eds.). 300 Years of Gravitation. Cambridge University Press, Cambridge, England.

Polyakov, A. M. 1974. Particle Spectrum in the Quantum Field Theory. ZhETF Pis'ma v Redaktsiyu 20: 430-433 [English translation: JETP Letters 20: 194-195 (1974)].

Preskill, J. P. 1979. Cosmological Production of Superheavy Magnetic Monopoles. Physical Review Letters 43: 1365-1368.

Sato, K., M. Sasaki, H. Kodama, and K. Maeda. 1981. Creation of Wormholes by First Order Phase Transition of a Vacuum in the Early Universe. Progress of Theoretical Physics 65: 1443-1446.

Sato, K., H. Kodama, M. Sasaki, and K. Maeda. 1982. Multiproduction of Universes by First Order Phase Transition of a Vacuum. Physics Letters 108B: 103-107.

Starobinsky, A. A. 1982. Dynamics of Phase Transition in the New Inflationary Universe Scenario and Generation of Perturbations. Physics Letters 117B: 175-178.

Steinhardt, P. J. 1986. Inflationary Cosmology. Pages 567-617 In: M. J. Bowick and F. Gürsey (eds.). High Energy Physics, 1985, Volume 2, Proceedings of the Yale Theoretical Advanced Study Institute. World Scientific, Singapore.

Tryon, E. P. 1973. Is the Universe a Vacuum Fluctuation? Nature 246: 396-397.

Turner, M. S. 1987. Cosmology and Particle Physics. Pages 513-680 In: P. Ramond and R. Stora (eds.). Architecture of Fundamental Interactions at Short Distances, Part II. North Holland, Amsterdam.

Vilenkin, A. 1982. Creation of Universes From Nothing. Physics Letters 117B: 25-28.

Vilenkin, A. 1985a. Quantum Origin of the Universe. Nuclear Physics B252: 141-151.

Vilenkin, A. 1985b. Cosmic Strings and Domain Walls. Physics Reports 121: 263-315.

Yoshimura, M. 1981. Cosmological Baryon Production and Related Topics. Pages 235-288 In: M. Konuma and T. Maskawa (eds.). Grand Unified Theories and Related Topics: Proceedings of the 4th Kyoto Summer Institute. World Scientific, Singapore.

Zel'dovich, Ya. B. 1972. A Hypothesis, Unifying the Structure and the Entropy of the Universe. Monthly Notices of the Royal Astronomical Society 160: 1P-3P.

Zel'dovich, Ya. B. and M. Y. Khlopov. 1978. On the Concentration of Relic Magnetic Monopoles in the Universe. Physics Letters 79B: 239-241.

# On the Origin of the Diffuse X-ray Background

DAVID J. HELFAND
Columbia University

## ABSTRACT

We report the first measurement of the intensity and spectrum of the diffuse X-ray background in the 0.16–3.5 keV band which is free from contamination by sources with fluxes greater than $\sim 6 \times 10^{-14}$ erg cm$^{-2}$ s$^{-1}$. This result has been made possible by the development of a number of techniques for reducing cosmic ray contamination and instrumental artifacts in the data collected by the *Einstein* Observatory imaging proportional counter. Our analysis of the background data reveals a mean absolute intensity for the emission $I_x(0.16 - 3.5\,\mathrm{keV}) \approx 5.6 \times 10^{-8}$erg cm$^{-2}$s$^{-1}$sr$^{-1}$. The intensity is dependent on galactic longitude even when only high galactic latitude data are used, allowing us to set a lower limit of 20% on the galactic contribution to the mean emission in this band. The spectrum of the total background is consistent with a power law of slope $\sim 0.7$ between 0.16 keV and 3.5 keV with evidence for a steep rise toward lower energies. This intensity is greater than that expected from extrapolation of the HEAO A-2 results at higher energies and the slope is steeper than that which obtains between 3 and 20 keV. A reanalysis of the faint end of the $\log N - \log S$ distribution for X-ray point sources in the 1.0–3.0 keV band reveals an extragalactic source surface density of only 6 to 10 per square degree at the *Einstein* Deep Survey limit of $4 \times 10^{-14}$erg cm$^{-2}$s$^{-1}$ in this band; the integrated contribution of all detected sources above this limit to the observed diffuse intensity is $\sim$ 12%. We also report preliminary evidence for the association of faint radio sources with peaks in the arcminute-scale fluctuations of the diffuse X-ray surface brightness distribution and then

briefly consider some of the implications of these results for the origin of the cosmic X-ray background.

## INTRODUCTION

The detection of an intense, apparently diffuse, isotropic flux of X-rays in the 2–10 keV band was one of the major discoveries of the 1962 rocket flight which gave birth to X-ray astronomy (Giacconi *et al.* 1962). Measurements over the ensuing quarter century by a variety of instruments including those on OSO-3 and OSO-5, numerous rocket flights, and particularly the A-2 experiment on HEAO-1 (Rothschild *et al.* 1983) have established that the X-ray background rises above the radio-to-gamma-ray $\nu^{-0.7}$ power law over the band 0.1–300 keV; its total energy density is $\sim 4 \times 10^{-5}$eV cm$^{-3}$ or 0.02% that of the cosmic microwave background radiation. Between 3 and 100 keV, the spectrum of the radiation can be characterized by an optically thin thermal bremmstrahlung model with $kT \approx 40$ keV (e.g., Marshall *et al.* 1980). The radiation is isotropic on scales $\gtrsim 5°$ to an accuracy of one part in $10^{-3}$, with the exception of a possible dipole anisotropy (Shafer and Fabian 1983) very similar to that seen in the microwave background which represents our motion with respect to the frame in which the microwave photons were emitted at $z \sim 1500$. A definitive review of the observational situation with respect to the X-ray background measurements above 3 keV prior to 1986 is given by Boldt (1987).

Although the diffuse X-ray background was discovered several years before the cosmic microwave radiation, its origin remains a matter of considerable discussion and debate. One of the principle difficulties has been that only the brightest members of source classes which are potential contributors to the background have X-ray intensities and spectra which are measurable with the non-imaging detectors used to record the flux from the background itself. Although operating over the relatively limited bandwidth between 0.16 and 3.5 keV, the imaging proportional counter (IPC) onboard the *Einstein* Observatory had the potential to remove this difficulty by measuring simultaneously the X-ray flux from both the background and the candidate sources of which it may be composed. While the ten years since the launch of the satellite has seen tremendous progress in characterizing the X-ray luminosity functions and spectra of potential point-source contributors such as active galactic nuclei (AGN), measurement of the diffuse emission in this band has remained relatively unaddressed.

We report here the development of a number of techniques necessary for the analysis of diffuse X-ray emission observed by the IPC. Their application to six deep-exposure fields at high galactic latitudes (the Deep Survey) has allowed us to measure the intensity and spectrum of the background in the 0.16–3.5 keV band with an accuracy of $\sim 5\%$. We have

also undertaken a reanalysis of the X-ray point-source population at faint fluxes derived from these same fields and present a new assessment of the contribution of discrete X-ray emitters to the diffuse background.

In the next section, we discuss in some detail the origin of "counts" detected by the IPC and then describe a set of algorithms we have developed to distill from these raw counts a measure of the true diffuse X-ray flux incident on the detector. These techniques include editing the data to remove solar X-rays scattered into the detector by the residual atmosphere, a source excision algorithm which removes the effects of photons scattered far from a source's centroid by imperfections in the telescope mirror surface, a flat-fielding algorithm for removal of spatial irregularities in the counter response, and, most importantly, a determination of the fraction of counts which result from the interaction of cosmic rays with the detector. We present our principal scientific result in the third section: a source-free spectrum of the diffuse X-ray background in the 0.16–3.5 keV band, where "source-free" implies removal of the contribution of all discrete sources for which $f_x > 4 \times 10^{-14}$erg cm$^{-2}$s$^{-1}$. The galactic longitude dependence of the result determines an upper limit to the fraction of the flux in this band which is of cosmic origin. The fourth section presents the application of our new source detection algorithms to the clean IPC data and concludes that there are only 6 to 10 sources per square degree at the Deep Survey threshold. In the final section we include a brief report on our search for radio counterparts to the background fluctuations and then summarize our conclusions regarding the origin of the X-ray background.

## DATA ANALYSIS

### What is an IPC count?

The imaging proportional counter (IPC) at the focus of the *Einstein* Observatory X-ray telescope collected data in the $0.1 - 4.5$ keV X-ray band from $\sim 5000$ $1^\circ \times 1^\circ$ fields scattered over the celestial sphere. The angular resolution of the instrument was $\sim 1'$ and the spectral resolution scaled as $R \sim 0.5(E/1\,\mathrm{keV})^{-1}$; effective exposure times ranged from $\sim 10^2$ to $\sim 10^5$ seconds. Over the course of the Einstein mission, the IPC recorded the position (in $8''$ cells), energy (in 32 pulse-height bins), and time-of-arrival of $\sim 20$ million "events" arising from the deposition of energy in the counter gas. These events result from a number of distinct stimuli:

- from cosmic ray interactions with the detector. Low-energy electrons and gamma rays may be directly detected, while higher energy cosmic rays produce spallation in the walls of the counter as well as neutron activation of the detector and spacecraft, leading to secondary events in the instrument.

- from a low-level leak of the iron fluorescence calibration source
- from detector and/or electronic malfunctions (e.g., breakdown or "sparking" in the counter gas)
- from solar X-rays scattered from the residual atmosphere above the satellite and collected by the mirror
- from cosmic X-ray sources. While the detection of such events was the primary purpose of most of the observations conducted with the IPC, these photons must be excised in a study of the background. In particular, the distribution of source counts outside the nominal instrument point-response function which results from photons which scatter off imperfections in the mirror surface must be treated with care.
- from diffuse X-rays of galactic origin — the hot bubble of gas $\sim$ 100 pc across which surrounds the sun (McCammon *et al.* 1983), the ridge of emission along the galactic plane (Iwan *et al.* 1972; Koyama *et al.* 1986), and the putative halo of hot gas surrounding the Galaxy.
- from the cosmic X-ray background, the principal object of this study.

Additional complications in studying diffuse emission with the IPC include non-uniformities in the spatial response of the instrument, detector gain changes, and the off-axis response of the telescope mirrors which introduces an energy-dependent vignetting for X-rays but does not affect cosmic ray-induced events.

A few of these problems are handled adequately by the standard IPC processing routines. Data from the small number of periods exhibiting anomalous detector behavior are excluded from all further analysis. The calibration source leak is confined to the high-energy pulse-height channels and is said to contribute $< 2\%$ of the counts in channels below number 7 which corresponds, at nominal detector gain, to 1.5 keV. For the higher energy channels, we adopt information from the *Einstein* Software Specification document (Harnden *et al.* 1984), and fold this through our algorithm to find new estimates for the effect of the calibration source on our results (see Wu *et al.* 1990 for details).

### Solar Scattered X-rays

The fraction of the counts detected in an IPC image which are attributable to solar X-rays scattered into the optical path by the residual atmosphere is a function of solar activity and of the geometry of the Earth-Sun-satellite system. In the standard processing software, the latter factor is parametrized by viewing geometry ($VG$) flags where $VG = 1$ ("best") describes data collected with the satellite over the night-time side of the Earth (i.e., the sun is fully occulted by the Earth and the solar scattered flux should be essentially zero), $VG = 2$ and $VG = 3$ are the "better" and

"good" data, respectively, implying increasing contributions of solar scattered flux, and $VG \geq 4$ data are excluded from all standard images. Since these parameters each represent a range of Earth-Sun, Earth-satellite, and Sun-satellite viewing angles, and since the incident level of solar X-ray flux varies significantly with time, the contribution of solar-scattered flux to the IPC count rate in any given field is *not* simply a function of the fraction of $VG = 1$, 2, and 3 data in the image. To quantify this contribution, we have examined data from 54 fields in the IPC survey of the Large Magellanic Cloud conducted by Columbia. Comparing the mean, source subtracted count rates in the inner 30′ of each field for the $VG = 1$ and $VG = 2 + 3$ data taken separately, we find a median solar-scattered component in the $VG = 2 + 3$ data of $\sim 2.6 \times 10^{-4}$ct $s^{-1}$arcmin$^{-2}$, in excess of the mean level of cosmic ray contamination found below; the total range of solar contamination is from $\sim 0$ to $\sim 8 \times 10^{-4}$ct $s^{-1}$arcmin$^{-2}$. The spectrum of the solar scattered radiation is, as expected, extremely soft and, as a result of its steep energy distribution at the lower level cutoff for acceptable events, small gain variations over the face of the detector produce a greater level of spatial fluctuations for solar scattered X-rays than is observed for celestial X-rays or for cosmic ray particles. A quantitative analysis of this effect (Wu *et al.* 1990) has led us to conclude that, when studying sources near the detection threshold, the sytematic errors introduced by including data contaminated with solar-scattered flux are significant; in addition, the presence of a time-variable component of counter illumination is clearly inimical to a precise measurement of the diffuse X-ray background flux. Thus, in all that follows, we have included only $VG = 1$ (satellite-night) data in our analysis.

## Source Excision

By definition, a characterization of the "diffuse" X-ray background must include an analysis of only those photons not attributable to discrete sources. To eliminate point-source photons, it is necessary first to identify the sources and then to subtract the system point response function, appropriately normalized, from the data. In the *Einstein* mirror/detector system, the point response profile is energy dependent both as a result of a blur circle pulse-height dependence of the counter response (lower energy photons are spread over a greater area – Harnden *et al.* 1984) and as a result of scattering by imperfections on the surface of the grazing incidence mirror (higher energy photons scatter to larger distances from the source centroid – Mauche and Gorenstein 1984). We have modeled the instrument response function using the convolution of an azimuthally symmetric Gaussian core plus exponential wings and a constant underlying background (see Wang and Helfand 1990 for details). In the analysis reported here, all bright

sources are subtracted using this technique, while sources fainter than 0.1 IPC ct $s^{-1}$ have been eliminated by simply excluding from consideration regions within a radius proportional to $\ell n$ (intensity) (i.e., within a contour of constant signal to noise ratio). This assures that < 1% of the photons in a field originate in point sources above the detection threshold.

### A Flat-Field Image for the IPC

Data collected with the *Einstein* IPC possess two inherent, instrument-imposed symmetries: the radially symmetric X-ray sensitivity resulting from the (energy-dependent) mirror vignetting function, and the rectangular symmetry of the detector body, the window support ribs, and the crossed grids of position-sensing wires. In order to eliminate non-uniformities in the response of the instrument conforming to the latter symmetry, we have produced the first "flat field" image for the IPC. We summed over four hundred individual pointings after 1) eliminating all fields with potentially significant extended emission (e.g., clusters of galaxies, SNRs, star formation regions, etc.), 2) excising all point sources as described above, and 3) rotating the fields to zero roll angle (referred to hereafter as "machine coordinates"). The data selected were from the standard "broad band" (PHI channels 2–10) and were binned in 64″ × 64″ pixels; the mean pixel contained nearly 1000 counts implying statistical errors at the 3% level.

The two-dimensional, flat-field image with ~ 1′ resolution formed from these data (corrected for vignetting) is shown in Figure 1. Highly significant features are clearly present in the detector response on scales from 0.′5 to 5′. The amplitude of these features is a weak function of pulse-height channel and detector gain, although the overall morphology of the flat-field image is independent of these parameters. Note that here, and in all of the analysis which follows, we delete all data within ±3.′5 of the window support ribs as being unreliable for most purposes. The features are remarkably reproducible, appearing in all subsets of the data we examined: the Large Magellanic Cloud fields, the satellite-night-only Deep Survey fields, 50 fields at the same galactic latitude as the LMC, and the remaining fields included in the final composite image. The fractional intensity of the features appears to be relatively independent of the ratio of X-rays to particles in the summed images: the LMC fields with their extensive diffuse emission shows structure of the same amplitude (measured as a percent of total count rate) as do the Deep Survey fields. To first order, then, it appears that both X-ray and cosmic ray-induced events respond similarly to these detector nonuniformities.

The fluctuations have a peak-to-peak amplitude of .75 to 1.34 of the mean value and an rms deviation of 9%. In order to obtain the particle

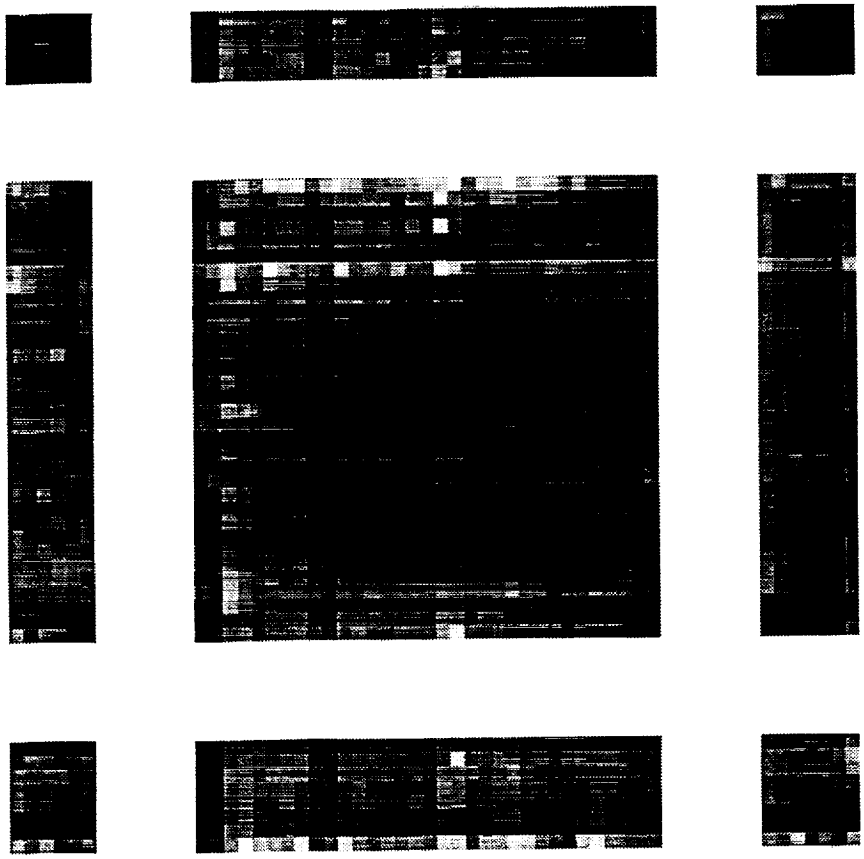

FIGURE 1 A flat-field image for the *Einstein* IPC broad band with $64'' \times 64''$ pixels. Maximum deviations from the mean value are $-0.26$, $+0.34$; the rms deviation is 9%. Each pixel contains $\gtrsim$ 900 photons for a statistical uncertainty of $\sim$3%.

count rates derived below and in utilizing our source detection algorithms, we first apply this flat-field correction to all data by multiplying the flat-field image value in a given pixel by the exposure map used to turn raw count rate maps into fluxed images.

### A Determination of the Cosmic Ray Particle Contamination in the IPC

From the flattened, source-free, night-only images, we proceed via two independent methods to estimate the cosmic ray-induced contamination in the IPC count rate. The first method relies explicitly on the radial symmetry imposed on all detected X-ray photons by the Observatory's

mirror system. The mirror vignetting function was measured in ground calibrations; it is reasonably constant within the energy range 0.16–3.5 keV and our adopted function is shown in Figure 2a superposed on the radial distribution from the summed, night-only LMC data. The best-fit normalization clearly does not describe the data well. This discrepancy is attributable to a second component of the detected counts — namely, cosmic-ray induced events — which do not follow the mirror vignetting function. As a working hypothesis we adopted a flat radial distribution for these so-called "particle" events. Any first-order departures from this assumption have been removed by the flat-fielding algorithm. (Note that the flat field was derived by normalizing each pixel to the adopted vignetting function to remove this lowest order Fourier component of the spatial fluctuations – see Wu *et al.* 1990 for details.) The two-component fit to the radial distribution of LMC data (flat particle, plus vignetted X-ray contributions) is shown in Figure 2b. The result is both a substantial improvement in the fit to the radial surface brightness distribution of the IPC, and a direct measurement of the mean particle component in these fields: $1.39 \pm .03 \times 10^{-4} \mathrm{cts}^{-1}\mathrm{arcmin}^{-2}$. Separate measurements of the particle rate for each of the six Deep Survey pointings yields a value of $1.41 \pm .03 \times 10^{-4} \mathrm{cts}^{-1}\mathrm{arcmin}^{-2}$, consistent with the result based on the LMC fields and with an error in the mean of only 2%.

To test the robustness of this important measurement, we have made a completely independent estimate of the mean IPC particle event rate by taking advantage of the large number of overlapping pointings which comprise the Columbia LMC survey. The essence of the approach is the fact that, for a given sky direction, two separate IPC observations with different field centers will receive the same number of diffuse X-rays, but will record different numbers of events because

1) a different distance from the field center results in a different diminution in X-ray intensity from vignetting, and

2) the two data sets, recorded at different times, will have a different level of particle contamination.

It is possible then, to construct from the original data a highly constrained simultaneous solution for both the true X-ray intensity for each sky position and a particle contamination level for each observation by producing a $\chi^2$ minimization solution for the equation

$$C_{\mathrm{ijk}} = \left[F_{\mathrm{ij}} T_{\mathrm{ijk}} V_{\mathrm{ijk}} + P_{\mathrm{k}} T_{\mathrm{ijk}}\right] S_{\mathrm{mn}}$$

where

- $C_{\mathrm{ijk}}$ represents the counts recorded in the sky pixel i (RA), j (Dec) in the $k^{th}$ field

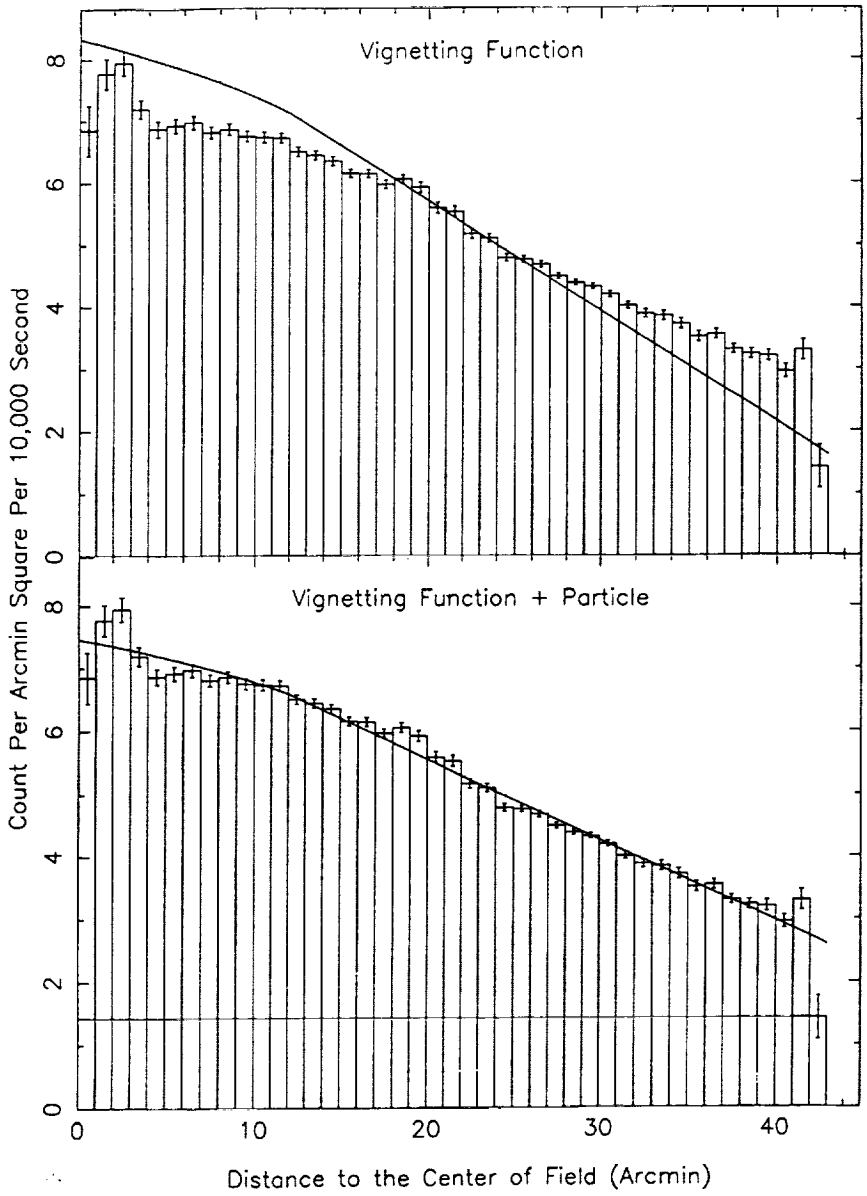


FIGURE 2 (a) The radial distribution of total counts in the summed $VG$=1 LMC data fitted to the nominal *Einstein* mirror vignetting function. (b) The same radial distribution fitted to the vignetting function plus a constant particle rate of $1.4\times10^{-4}$ ct $s^{-1}$ arcmin$^{-2}$.

- $F_{ij}$ represents the diffuse X-ray flux from that sky pixel
- $V_{ijk}$ represents the vignetting function value for that sky pixel in field k
- $P_k$ represents the particle value for field k
- $T_{ijk}$ represents the exposure time at sky position ij in field k (e.g., $T_{ijk} = 0$ under a rib)
- $S_{mn}$ represents the flat-field correction to the exposure time in the detector pixel labelled by mn which corresponds to the current pixel of interest.

The night-only LMC data includes 114 fields with exposure times $> 500$ s. The $\sim 5° \times 5°$ region covered by these fields has been divided into 4293 sky pixels $4'.3 \times 4'.3$ in size (corresponding to $32 \times 32$ 8″ IPC pixels); multiple overlaps (up to 12 fields covering a given sky pixel) result in a total of 20,908 $C_{ijk}$ values. Solving for the 4293 sky fluxes ($F_{ij}$'s) and the 114 particle fluxes ($P_k$'s) yields a mean particle rate of

$$\langle P \rangle = 1.45 \times 10^{-4} \mathrm{cts^{-1} arcmin^{-2}}$$

with a reduced $\chi^2$ value for the fit of 0.99. This independently derived estimate is indistinguishable from the value obtained from the radial distribution of the Deep Survey fields and gives us considerable confidence in our understanding of particle contamination in the IPC. The fit also yields an estimate of the range of particle values in typical, short-exposure IPC fields for which direct fits to the radial distribution are compromised by poor statistics and the absence of an overlapping pointing renders a simultaneous solution (as in our LMC example) impossible. The range of values in the 114 LMC fields runs from $\sim 0$ to $\sim 3 \times 10^{-4} \mathrm{cts^{-1} arcmin^{-2}}$ with an rms dispersion about the mean of $\sim 35\%$. Finally, of incidental interest here, but of considerable scientific importance, the simultaneous fit yields a map of the absolute sky flux in the 0.16 – 3.5 keV band with $\sim 4'$ resolution over the whole LMC; the implications of this result are discussed elsewhere (Wang *et al.* 1990).

In order to measure the spectrum of the X-ray background, it is necessary to extend this analysis to derive the *spectrum* of the particle contamination. Thus, we have repeated the radial profile fitting analysis on the summed Deep Survey fields for each pulse height bin independently. We find particle contamination levels which vary smoothly from 29% in channel 2 (0.15–0.3 keV) to 9% in channel 6 ( 1.1 to 1.4 keV, the minimum particle background channel) to 30% in channel 10 (2.7 to 3.5 keV) although calibration source leakage contributes an additional $\sim 50\%$ of the total counts in this channel. We are in the process of acquiring the entire *Einstein* data base so that we can construct flat fields and particle contamination

spectra as a function of gain with the highest possible statistical precision, but we do not expect the basic results reported here to change significantly.

## THE SPECTRUM OF THE X-RAY BACKGROUND

Having measured or eliminated all extraneous sources of IPC counts and minimized to the extent possible sources of systematic error, we are now in a position to measure the intensity and spectrum of the low-energy diffuse X-ray background. We present the result in Figure 3.

The integrated flux in the 0.16–3.5 keV band as measured by *Einstein* is 35 ph $cm^{-2}s^{-1}sr^{-1}$. This is clearly in excess of the extrapolation of the power law with a slope of $-0.4$ observed in the 3–30 keV band. The amount of the excess is unclear, however, because of a long-standing but little-known discrepancy between the normalization of the 3–10 keV background spectrum. The HEAO-1 A-2 experiment medium energy detectors measure a flux of $8.3E^{-1.4}$ph $cm^{-2}s^{-1}sr^{-1}keV^{-1}$ whereas a series of several rocket flights by the Wisconsin group (Nousek 1978; Fried 1978; Burrows 1982) designed specifically to study the diffuse X-ray background obtained precisely the same slope but a normalization which is 30% higher in the same band. Both used the Crab Nebula as a calibration source and obtained consistent values for its flux, and both claim errors in the normalization of $\lesssim 10\%$. Apart from an error in the calibration of the collimator responses of the two experiments, it is difficult to imagine the cause of this discrepancy. At present, the situation is unresolved, and we have plotted both 3–10 keV spectra in Figure 3. An extrapolation of the HEAO-1 spectrum to the 0.16–3.5 keV band implies an expected intensity of 28.5 ph $cm^{-2}s^{-1}sr^{-1}$, $\sim 25\%$ below the measured value.

The complex shape of the low-energy spectrum of the background is apparent in the figure. There is a steep rise at the lowest energies ( $\lesssim .3$ keV) which is consistent with emission from the $\sim 10^6$K plasma filling the $\sim 100$ pc cavity around the sun (McCammon *et al.* 1983). Between .5 and 3.5 keV, the slope of the spectrum is $\sim 0.7$, significantly steeper than that at higher energies, but similar to that of the spectra of nearby AGN in the 2–10 keV band as measured by HEAO-1 (Mushotsky 1982) and Ginga (Tanaka 1989).

The limited information we have on the spatial distribution of the diffuse background in the *Einstein* band demonstrates that at least part of this emission is galactic in origin. A plot of the diffuse intensity in each of the 35 high galactic latitude ($30° < |b| < 70°$) fields as a function of galactic longitude shows a significant increase between longitudes $300° < \ell < 60°$: the mean intensity for 12 fields between 120° and 240° is $3.1 \pm .2 \times 10^{-4}$ct $s^{-1}$arcmin$^{-2}$ while the value for 10 fields with $330° < \ell < 30°$ is $6.7 \pm .5 \times 10^{-4}$ct $s^{-1}$arcmin$^{-2}$. This substantial excess is clearly a large-scale

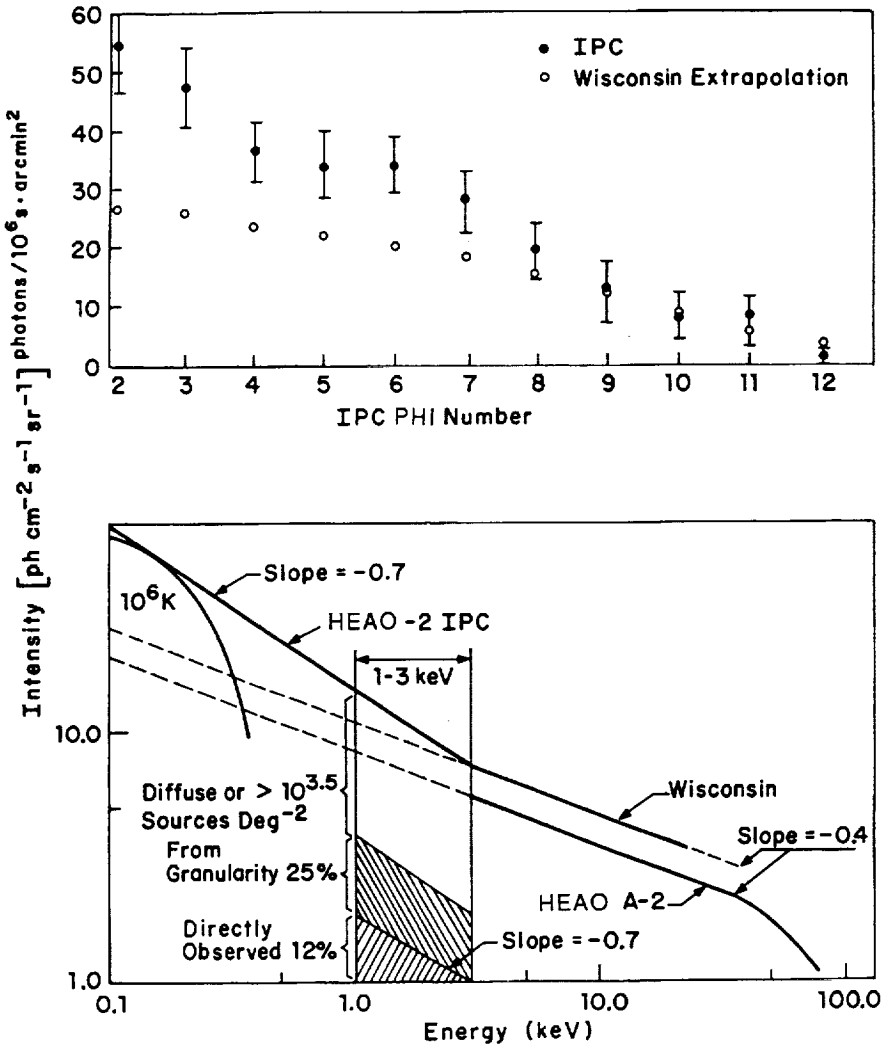


FIGURE 3 (a) The photon spectrum of the X-ray background as measured in the *Einstein* Observatory IPC compared to an extrapolation of the Wisconsin 3–9 keV background spectrum folded through the IPC response. The integrated contribution of discrete sources with 1–3 keV fluxes $\geq 6 \times 10^{-14}$ erg cm$^{-2}$ s$^{-1}$ has been subtracted from the Wisconsin results to provide an appropriate comparison with the source-free *Einstein* data. (b) A schematic representation of the X-ray Background spectrum with various measured and potential contributions indicated.

galactic component since it is not confined to local features such as the North Polar Spur, a region of enhanced soft X-ray and nonthermal radio emission thought to be a piece of an old supernova remnant. Further analysis of the spectrum and the spatial distribution of the excess using the entire database is required before the relative contributions of local emission, a thick galactic ridge (e.g., Iwan *et al.* 1982; Koyama *et al.* 1986; Watson 1989), and a bulge or coronal component can be assessed. In the discussion that follows we use the 1–3 keV background flux derived from high galactic latitude fields in the longitude range $120° < \ell < 240°$ as our best estimator of the cosmic background intensity, although a residual galactic contribution cannot be excluded; the adopted value in this band is $2.5 \times 10^{-8}$erg cm$^{-2}$s$^{-1}$sr$^{-1}$.

## THE POINT SOURCE CONTRIBUTION

A number of extragalactic source classes contribute to the integrated surface brightness of the X-ray sky; the most important known sources are galaxy clusters, Seyferts, BL Lac objects, and quasars. Considerable effort has been expended in attempting to derive a total discrete source contribution by extrapolating from the relatively small number of known examples in each class. These determinations are limited by selection effects in the X-ray data, uncertainties in the optical luminosity functions and X-ray-to-optical luminosity ratios, poorly-known broad-band X-ray spectra, and the imponderables of source luminosity and density evolution. It is beyond the scope of the present work to review these calculations. Rather, we will adopt a strictly empirical approach in which we apply an optimized source detection algorithm to the edited, flat-fielded data of the six Deep Survey fields to define the faint end of the $\log N - \log S$ distribution of discrete X-ray sources.

We have developed a method of identifying sources in *Einstein* IPC data which relies on a statistical interpretation of flux enhancements but then uses morphological fitting techniques for the determination of source locations and fluxes. The specific parameters of our algorithm were determined by running the program with a wide variety of parameters on several sets of real and artificial data. The final parameters were then chosen so that the program detected real sources with maximum efficiency and spurious sources in an evenly distributed manner. This second goal is fairly difficult to achieve with IPC data because calculating a reasonably accurate background for a potential source requires collecting photon events from an area of $\sim 100$ arcmin$^2$ and the IPC detector has significant structure, from ribs and mirror vignetting, on these scales.

Before searching a data set for sources we constructed two maps: one, a record of the number of events per pixel (usually 32 or 64 arcseconds on

a side), and a second recording the adjusted exposure time determined by taking the total integration time for the observation and applying corrections for the effect of mirror vignetting and counter flat-fielding as discussed above. We then inspected every pixel in the field to determine the probability that a source lies within it. To measure the statistical significance of flux enhancements $F$, we construct a local background model by computing weighted (by adjusted exposure time) average flux over a background annulus. This annulus is centered on the point which is being analyzed and excludes areas which are either adjacent to the pixel of interest, under the IPC ribs, or near another source (this latter facet obviously requires multiple iterations; see below). The expected background counts $B$ for the central source region is, then, the computed flux times the adjusted exposure time for the candidate central source. The expected statistical width of the background $\Delta B$ is also computed by taking the counting statistics of the background annulus and weighting the result by the ratio of adjusted exposure times. A signal to noise measure is calculated as

$$S/N = (F - B)/(F - \Delta B^2)^{\frac{1}{2}}. \tag{1}$$

We determined the optimum values for the algorithm parameters — the inner and outer radii of the annulus and the outer radius of the central candidate region — by analyzing real and Monte Carlo generated fields with a variety of values and parameters. Increasing the size of the background annulus has the desirable effect of reducing the statistical error in the background model and the potentially undesirable effect of enabling diffuse sources of emission (which cannot be readily eliminated from the data) to degrade the accuracy of the background calculation.

A somewhat more difficult problem arises when the statistics of faint point source detections is considered in detail. Because increasing the size of the candidate region adds an amount of noise which scales linearly with the area while adding a signal contribution which drops exponentially, the optimum size of the candidate region is considerably less than the size which includes almost all of the true source flux. Consider a case in which the candidate region is increased in area by a factor of 2. Equation (1) would then read

$$S/N = \frac{(F(1+\alpha) - B(1+\alpha))^2}{F(1+\alpha) + B(1-\alpha) + 4\Delta^2 B^2} \tag{2}$$

where $\alpha$ is the percentage increase in flux gained by going to the larger area. The optimum value for the flux in the candidate region was determined by applying the algorithm to Deep Survey and Monte Carlo-generated fields and was found to be 70% of the total power. As a result of this strategy, our candidate region is immediately surrounded by a region containing a

flux level enhanced by the excluded photons from the source. This region must, in turn, be excluded from consideration in calculating either the source flux or background. Clearly, this method is not a reliable way to measure the flux or position of a source. We use it merely to establish a source's existence. Each source falling above a specified significance level is later analyzed in detail using more realistic models for the point response function. Thus, our procedure cannot be completed in less than three iterations. First we identify the relatively bright sources in a field. Then using this source list as a basis for excluding regions from background annuli, we search the field again, this time finding the faintest sources. Finally, we look at the data a third time to calculate fluxes and positions of each identified source.

The results of our application of this procedure to the six *Einstein* Deep Survey fields are described in detail in Hamilton *et al.* (1990). We detected a total of 29 sources at a significance level of $> 3\sigma$. The faintest detected sources have an X-ray flux in the 1–3 keV band of $4 \times 10^{-14}$erg cm$^{-2}$s$^{-1}$ if a power law spectrum with a slope of 0.7 is adopted and the absorbing column density is assumed to be negligible (i.e., $N_{\rm H} < 10^{20.5}$ cm$^{-2}$).

Preliminary analysis of three of these fields have appeared in the literature (Giacconi *et al.* 1979; Griffiths *et al.* 1983) and considerable work aimed at optical identification of the candidate X-ray sources has been undertaken. From this partially complete optical program we find that 6 of the sources we detect in the three fields common to this earlier work are foreground galactic stars. In fact, all 11 of the optically identified sources listed in the earlier analysis are found in our survey, whereas only 6 of the 38 other source candidates found earlier are now detected. The other three Deep Survey fields show a similar surface density of sources. These results agree well with recent work by Primini *et al.* (private communication), and lead to a $\log N - \log S$ amplitude of 6 (counting only the sources with extragalactic optical IDs) to 10 (including all unidentified sources as extragalacitc) sources deg$^{-2}$ at a Deep Survey threshold of $4 \times 10^{-14}$ erg cm$^{-2}$ s$^{-1}$ (1–3 keV). Adopting a $\log N - \log S$ slope of $-1.5$, consistent with the results of the data from the Medium Sensitivity Survey (Gioia *et al.* 1984), and integrating the contribution of all extragalactic sources *detected in the Einstein band*, we find that they comprise $\sim$ 12% of the diffuse X-ray background flux *detected in this same band by this same instrument.*

## THE ORIGIN OF THE X-RAY BACKGROUND

The flux theshhold for detectable sources in the Deep Survey is set by the photon counting statistics of the images and our adopted significance criterion. Clearly, however, sources fainter than this theshold contribute to

the flux observed in each field, and the characteristics of the $\log N - \log S$ below the significance cutoff can be studied by analyzing the arcminute-scale fluctuations in the images. Two years ago, we published such an analysis (Hamilton and Helfand 1987), concluding that the $\log N - \log S$ of discrete X-ray emitters must extend below the Deep Survey limit by at least a factor of 3 to explain the graininess of the images, but that the entire background was too smooth to be explained completely by such a population. The upper limit to the contribution of discrete sources was set at $\sim 50\%$, with the remainder of the emission requiring a source surface density of greater than several thousand per square degree. These fractional contributions were based on an assumed background level derived from an extension of the high energy $\nu^{-0.4}$ power law. As indicated in Figure 3b, the percentages of the *observed* background in the 1–3 keV band are now 12% from resolved discrete sources, $\sim 25\%$ from a fainter extension with the same $\log N - \log S$ slope of the observed population, and $\sim 65\%$ from either truly diffuse emission or a very numerous population of objects.

Given the evidence cited above that a population of objects other than AGN is required to explain the background, we have undertaken a search for such objects utilizing the VLA in conjunction with our X-ray fluctuation analysis. The results are presented in detail in Helfand and Hamilton (1990). Briefly, we obtained a deep (24 hours) integration of the Draco Deep Survey field utilizing the C configuration of the VLA at 20 cm. A total of $\sim 100$ discrete radio sources was detected down to a limiting flux density of $\sim 150\mu$Jy. We then compared the positions of these sources (accurate to $\sim 1''$) with the positions of the brightest $\sim 5\%$ of the $\sim 300$ independent pixels making up the X-ray image. The expected rate of chance associations was 4, while the observed number of radio/X-ray coincidences was 9. One of the matches was with an optically identified X-ray source, whereas the remainder represent coincidences between 2.0–3.0$\sigma$ positive fluctuations in the X-ray background and 0.2–2 mJy radio point sources. We are currently pursuing optical, infrared, and radio followup observations of these faint radio sources in an attempt to establish the nature of this potential new contributor to the X-ray background.

The quest for an understanding of the origin of the X-ray background remains frustrated by the simple fact that the bulk of the energy density which we must explain is contained in photons above 4 keV, while the best data on the spatial distribution of the background and the characteristics of the sources which contribute to it are measured below this energy. Nonetheless, the constraints on the intensity, spectrum, and fluctuation statistics derived from the *Einstein* data as well as the telescope's faint threshold for discrete source detection have added considerably to our knowledge of this cosmic radiation. For example, we require a very strong evolution in the X-ray-to-optical luminosity ratio for quasars if they are to

contribute more than $\sim$ 30% of the background at energies below 4 keV; furthermore, the spectra of quasars in this band (Wilkes and Elvis 1987) are often steeper than the integrated spectrum of the background, setting an additional constraint on their contribution. Shaeffer and Silk (1988) have shown that, by invoking rather extreme evolutionary assumptions, a major (even dominant) contribution to the 1–3 keV background can arise from hot gas in clusters and groups of galaxies, although such sources would not add significant flux at higher energies. Models for galaxy formation which invoke superconducting cosmic strings have recently been used to make a prediction about the structure of the 1–3 keV background (Ostriker and Thompson 1987); to wit, that as such strings "explode" they create superbubbles in the intergalactic medium at $z \sim 10 - 30$ which should lead to correlated structure in the background on scales of $\sim 3 - 100$ arcminutes. Unfortunately, it appears that the *Einstein* data are not quite sufficient to provide a quantitative test of this prediction. Primordial galaxies themselves are a potential background contributor and the high-source surface density our fluctuation analysis requires plus the tantalyzing evidence for associated faint radio sources makes this an attractive option to pursue. The most obvious explanation for a diffuse background — a hot diffuse medium — has not been excluded, although it suffers from severe problems on energetic grounds (Field and Perronod 1977) and may also have difficulties matching the observed broad-band spectrum once the known discrete contributors are removed (Giacconi and Zamorani 1987).

It is clear that what is needed is data which can reach fainter flux levels and can measure the properties of contributing source populations with greater precision and over a broader bandwidth. The ROSAT Observatory, to be launched next year, will allow us to push the $\log N - \log S$ curve to somewhat lower flux levels, albeit only in the band below 2 keV. Major progress should be forthcoming a few years hence when the higher energy imaging missions Astro-D and, particularly, Spectrum-RG, are launched. The extremely high throughput and broad spectral coverage of the Sodart telescopes on Spectrum-RG will provide qualitatively new data on the spectrum and spatial structure of the background itself as well as on the characteristics of sources which contribute to it down to fluxes an order of magnitude below the *Einstein* Deep Survey limit. Perhaps then, three decades after its discovery, we will finally understand fully the origin of the X-ray background and will be able to exploit this understanding for the constraints it will set on the evolution of the Universe and its contents.

## ACKNOWLEDGMENTS

The author acknowledges the major contributions to this work of his collaborators T.T. Hamilton, X.-Y. Wu and Q. Wang, as well as the support

of the National Aeronautics and Space Administration under grant NAG8-497, the U.S. National Academy of Sciences for making attendance at this workshop possible, and the Academy of Sciences of the U.S.S.R. for their warm and gracious hospitality during the meeting. This is contribution number 397 of the Columbia Astrophysics Laboratory.

## REFERENCES

Boldt, E. 1987. Physics Reports 146: 216.
Burrows, D. 1982. Ph.D. Dissertation. University of Wisconsin.
Field, G., and S. Perronod. 1977. Ap. J 215: 717.
Fried, P.M. 1978. Ph.D. Dissertation. University of Wisconsin.
Giacconi, R., *et al.* 1979. Ap. J. (Letters) 234: L1.
Giaconni, R., and G. Zamorani. 1987. Ap. J. 313: 20.
Gioia, I.M., T. Maccacaro, R. Schild, J.T. Stocke, J.W. Liebert, I.J. Danziger, D. Kunth, and J. Lub. 1984. Ap. J. 283: 495.
Griffiths, R.E., *et al.* 1983. Ap. J. 269: 375.
Harnden, F.R., D.G. Fabricant, D.A. Harris, and J. Schwartz. 1984. SAO Report 393.
Hamilton, T.T., and D.J. Helfand. 1990. Ap. J. (Letters) Submitted.
Hamilton, T.T., and D.J. Helfand. 1987. Ap. J. 318: 93.
Hamilton, T.T., D.J. Helfand, and X.-Y. Wu. 1990. In preparation.
Iwan, D., F.E. Marshall, E.A. Boldt, R.F. Mushotzky, R.A. Shafer, and A. Stottlemyer. 1982. Ap. J. 260: 111.
Koyama, K., K. Makishima, Y. Tanaka, and H. Tsunemi. 1986. PASJ 38: 121.
Marshall, F.E., E.A. Boldt, S.S. Holt, R.B. Miller,
R.F. Mushotzky, L.A. Rose, R.E. Rothschild, and P.J. Serlemitsos. 1980. Ap. J. 235: 4 L1.
Mauche, C.W., and P. Gorenstein. 1986. Ap. J. 302: 371.
McCammon, D., D.N. Burrows, W.T. Sanders, and W.L. Kraushaar. 1983. Ap. J. 269: 107.
Mushotzky, R. 1985. Ap. J. 256: 92.
Nousek, J. 1978. Ph.D. Dissertation. University of Wisconsin.
Ostriker, J.P., and C. Thompson. 1987. Ap. J. (Letters) 323: L97.
Shaeffer, R. and J. Silk. 1988. Ap. J. 333: 509.
Tanaka, Y. 1989. In Proceedings of $23^{rd}$ ESLAB Symposium in press.
Wang, Q., and D.J. Helfand. 1990. Ap. J. Submitted.
Wang, Q., T.T. Hamilton, D.J. Helfand, and X.-Y. Wu. 1990. Ap. J. Submitted.
Watson, M. 1989. Windows on Galaxies. Erice Summer School in press.
Wilkes, B., and M. Elvis. 1987. Ap. J. 323: 243.
Wu, X.-Y., T.T. Hamilton, D.J. Helfand, and Q. Wang. 1990. Ap. J. Submitted.

# Gravitational Lenses: The Current Sample, Recent Results, and Continuing Searches

JACQUELINE N. HEWITT
Massachusetts Institute of Technology

Gravitational lensing is one of the topics in astrophysics that was quite extensively discussed over many decades in the theoretical literature before it was actually observed. We are now at the tenth anniversary of the discovery of the first gravitational lens in 1979, and it is interesting to note how the field has developed over the past decade. After an initial slow rate of discovery of gravitational lens systems (about one per year), the last few years have seen an explosion in the number of reported cases. The variety in the types of systems has also increased markedly. Attention was drawn to the first few cases because quasars at the same redshift, with similar optical spectra, were observed with angular separations of only a few arc seconds. Recent verified and proposed gravitational lenses include the giant luminous arcs, their accompanying more common small blue "arclets," the radio rings, a field of twin galaxies, statistical lensing, and microlensing.

In the last decade, most observational effort has been devoted to searching for new candidate lens systems and carefully measuring their properties, both to test whether they are indeed lensed and to provide constrains for modeling. Theoretical efforts have been extensive, and have included modeling of the known lens systems and more general theoretical calculations aimed at understanding gravitational potentials with some simplifying properties. The case of an elliptically symmetric potential is the most complicated potential that can be said to be thoroughly understood. Blandford and Kochanek (1987) and Kochanek and Blandford (1987) have examined the solutions for such a potential in considerable detail, and have simulated the statistical properties of an ensemble of elliptical lenses. As pointed by Narayan and Grossman (1989), the different solutions for the elliptical lens provide a useful framework for categorizing the known gravitational lens systems. If a source falls on the optical axis of the lens,

four bright images surrounding the center of the lens are formed. If the quadrupole moment of the lens is sufficiently small, or the extent of the source is sufficiently large, the four images merge to form a ring surrounding the center of the lens. For an extended source that is moved off the axis of the lens, the ring breaks up into arcs; if the quadrupole moment of the lens is large, one long arc dominates. A smaller source moved off the axis breaks up into four small images, and two of the images merge (giving three images) and disappear (leaving one image) as the source moves farther from the optical axis. Therefore, a convenient classification of the lenses is into rings, arcs, multiples, and doubles, where the progression is from sources close (compared to their extent) to the optical axis to far from the optical axis. Table 1 lists the known candidate systems. I have attempted to include all candidate systems that have appeared in the refereed literature, including some for which the evidence for lensing is not very strong. The field is changing rapidly, and it is somewhat a matter of judgment which systems are candidates, so my list may differ slightly from other published lists. I have been generous in attributing lensing characteristics, and some rather speculative systems are included in this list. In addition to the individual lens systems described above, two other signatures of gravitational lensing have recently been discovered, statistical lensing (Webster *et al.* 1988) and microlensing (Irwin *et al.* 1989).

The energy and ingenuity of observers and theorists are beginning to be brought together in this new astrophysics laboratory, and some of the long discussed promise of gravitational lensing is being realized. We are beginning to gather clues about the distribution and nature of dark matter, both inside and outside galaxies, and there are real prospects for measuring the values of cosmological parameters and learning about the structure of quasars. Available space limits me to a discussion of only a few topics.

## MICROLENSING: MEASURING THE MASS FUNCTION OF A GALAXY AND THE SIZE OF A QUASAR?

Microlensing has been discussed extensively in the literature, and was predicted to occur when a small lens (for example, a star) passes through the line of sight from the observer to the source and causes an apparent brightening of the source. The gravitational lens 2237+0305 is the system most likely to show microlensing effects: the quasar images surround the central region of the lensing galaxies where the surface density of stars is high; the low redshift of the galaxy causes the characteristic angular lensing region of each microlens to be large; and the low redshift of the lens causes the apparent relative velocities of the observer, microlens, and source to be large (Kayser and Refsdal 1989). Microlensing in principle can do a lot of astrophysics by allowing us to measure the number density

TABLE 1 Proposed and verified gravitational lens systems, grouped according to morphology. For B1900+14, 2345+007, 1635+267, 1146+111, 0023+171, and 0249-186 it is generally accepted that the existing evidence is sufficient to conclusively demonstrate that they are gravitational lenses.

| | Image Separation[1] | Flux Ratio[1] | Type of Lens | Discovery Reference |
|---|---|---|---|---|
| **RINGS** | | | | |
| MG1131+0456 | 2.1″ | ~ 1 | ? | Hewitt *et al.* 1988 |
| MG1654+1346 | 2.1″ | ~ 1 | Galaxy | Langston *et al.* 1989 |
| **ARCS** | | | | |
| Abell 370 | ~ 50″[2] | — | Cluster | Soucail *et al.* 1987 |
| Cl 2244-02 | 22″[2] | — | Cluster | Lynds and Petrosian 1989 |
| Abell 963 | 30″ | — | Cluster | Lavery and Henry 1988 |
| Cl 0500-24 | 52″[2] | — | Cluster | Giraud 1988 |
| Abell 2218 | Arclets | — | Cluster | Pello-Descayre *et al.* 1988 |
| **MULTIPLES** | | | | |
| 1115+080 | 0.5″ | ~ 1 | Galaxy | Weymann *et al.* 1980 |
| 2016+112 | 3.4″ | ~ 1 | 2 galaxies | Lawrence *et al.* 1984 |
| 2237+0305 | 1.8″ | 1 | Galaxy | Huchra *et al.* 1985 |
| B1900+14 | ? | ~ 1.5 | ? | Paczynski 1986 |
| 3C324 | 3″ | 1.7 | Galaxy | Le Fèvre *et al.* 1987 |
| H1413+117 | 0.8″ | 1.1 | Galaxy? | Magain *et al.* 1988 |
| **DOUBLES** | | | | |
| 0957+561 | 6.1″ | 1.3 | Galaxy, cluster | Walsh *et al.* 1979 |
| 2345+007 | 7.3″ | ~ 4 | ? | Weedman *et al.* 1982 |
| 1635+267 | 3.8″ | 4.4 | Galaxy?? | Djorgovski and Spinrad 1984 |
| 1146+111 | 157″ | ~ 1 | ? | Turner *et al.* 1986 |
| 0023+171 | 4.8″ | 3 | Galaxy | Hewitt *et al.* 1987 |
| UM673 | 2.2″ | 7.6 | Galaxy | Surdej *et al.* 1987 |
| 0249-186 | 2.0 – 2.6″ | 1.0-1.1 | Cosmic string??? | Cowie and Hu 1987 |
| UM425 | 6.5″ | 70 | Galaxy? | Meylan and Djorgovski 1989 |

[1] When there are more than two images, the image separation and flux ratio of the brightest pair are tabulated.

[2] Twice the radius of curvature of the dominant arc.

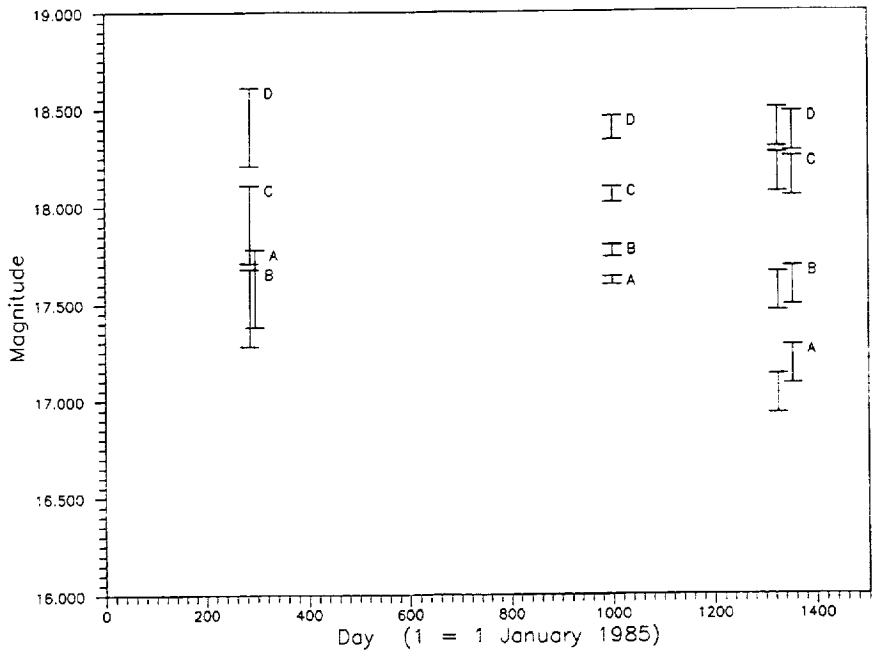


FIGURE 1 Light curves of the quasar images of 2237+0305, constructed from the data of Schneider *et al.* (1988; day 286), Yee (1988; day 998), and Irwin *et al* (1989; days 1325 and 1354). Component A for day 286 has been offset 10 days to the right for clarity. The error bars represent the estimated errors in the absolute flux scales.

of compact objects inside galaxies, and to measure the size of the emitting region of quasars. For the geometry of the 2237+0305 system, the expected characteristic timescale for microlensing is

$$\Delta t = 8\sqrt{\frac{M}{M_\odot}}\frac{6000 \text{ km/sec}}{V} \text{ years}$$

where $V$ is the apparent transverse velocity. An apparent transverse velocity as large as 6000 km/sec is expected for relative source, lens, and observer velocities of several hundred km/sec; therefore, we may expect to find variations in the brightness of the images of 2237+0305 on times scales of months to years. "High amplification events" occur when a compact source crosses a caustic in the source plane. From the rise time of these events, the size of the source can be measured. The overall time scale of the variations gives the mass of the lensing objects.

Figure 1 shows a plot of a light curve of 2237+0305 constructed from the data of Irwin *et al.* (1989), Schneider *et al.* (1988), and Yee (1988),

including their estimated errors. A direct comparison of these data must be viewed with caution since the measurements were carried out with different instruments; furthermore, the measurements of the first two dates are of the Thuan and Gunn $r$ magnitudes, and those of the last two dates are of the Mould $R$ magnitudes. In any case, the evidence for microlensing in 2237+0305 is in the change in the magnitude of component A relative to the other quasar components. For example, the last two measurements show a change in the magnitude difference between components A and B, relative to the second measurement, of 0.38 and 0.26, well above the estimated error in the relative magnitudes (0.02 for the second measurement, and 0.05 for the last two measurements). Since the time delay between the images is expected to be of order a day, the variation is probably due to microlensing rather than intrinsic variations in the quasar. The light curve is not well enough sampled to determine the mass of the microlens, nor whether we have witnessed a "high amplification event" in which the quasar passes behind a lens caustic. However, reasonable assumptions give a range in the estimated microlens mass of $0.0001 M_{\odot} \leq M \leq 0.1 M_{\odot}$, but larger masses are of course consistent with the data (Irwin *et al.* 1989). Models predict a large lensing optical depth, so continued, frequent monitoring of the quasar images of 2237+0305 is important.

## DO COSMIC STRINGS EXIST?

If cosmic strings exist, they may be observable through their lensing effects. Lensed images caused by cosmic loops that have radii smaller than the image separation are likely to be difficult to distinguish from lensed images caused by centrally condensed mass distributions such as galaxies and clusters. Lensed images caused by strings with radii of curvature much larger than the image separation may be easier to distinguish because of the following properties unique to straight string lenses: (1) the images are not magnified; (2) the parity of the images is the same; (3) if there is a sufficient surface density of background sources, many pairs of images will stretch along the string; and (4) if the string is moving relativistically, there is a small systematic velocity shift between the images on either side of the string (see Hogan 1987 and references therein). Cowie and Hu (1987) discovered an unusual field of "twin galaxies" in which there are four pairs of galaxies with angular separations between 2.0″ and 2.6″, magnitude differences of 0.15 or less, and velocity differences (for the three pairs in which they have been measured) consistent with zero. More recent optical work (Hu and Cowie, private communication) shows that one pair has significantly different colors, but has also discovered four more pairs with similar magnitudes and colors. Comparison with control fields shows that the number of pairs is much larger than would be expected by chance.

In collaboration with R. Perley and E. Turner, I have acquired a $\lambda 20$ cm VLA image of the field. A contour plot of the radio emission (henceforth referred to as 0249-184) is shown in Figure 2, superimposed on an optical image (kindly provided by E. Hu) for comparison. One may use the radio data to address the question of lensing by a cosmic string in two ways. First, is the emission peculiar in some way that would be explained by lensing? The answer to this question is no. The coincidence of the 0249-184 and the optical galaxy implies the two are physically associated. The radio emission has Fanaroff and Riley Type I (FRI, Fanaroff and Riley 1974) morphology which is common among radio galaxies. The radio power implied by the redshift of the optical galaxy falls within the range commonly seen in FRI sources (Shaver *et al.* 1982), though it is brighter than that usually seen in optically selected elliptical galaxies (Hummel *et al.* 1983). If a string fell in front of the jet, one would expect to see a distortion of the type sketched in Figure 3; none is seen. Second, do the properties of 0249-184 *exclude* the possibility that there is a cosmic string in the field? Our judgment in this case is that the answer is probably, but not definitely. At galaxy A2, the radio emission is at the position of optical emission that is "known" to be doubly imaged. The lack of corresponding doubling of the radio emission is evidence against the lensing interpretation. However, given the uncertainty in the registration of the optical and radio images (about 0.6″) and their finite resolution, it is possible that the radio emission falls just outside the doubly-imaged region. In summary, the case for lensing has been weakened by the radio data and by the discovery of color differences in one galaxy pair; however, the evidence may not rule it out, and the field has peculiar properties that would be well explained by string lensing. In any case, gravitational lensing brings a phenomenon predicted by theories of the early universe under observational scrutinity.

## MASS-TO-LIGHT RATIO MEASUREMENTS IN GALAXIES

Gravitational lensing is one of the few phenomena in astrophysics in which the system under study is not necessarily luminous, and is therefore well suited to studying dark matter. Gravitational lensing has been used to provide an independent measure of the mass-to-light ratio in two systems in which the mass distribution is reasonably well constrained by surrounding images and in which the redshifts of both the source and the lens are known. The first system is 2237+0305, already discussed in the context of microlensing above. The foreground galaxy has a small redshift ($z$ = .0394), and its surface brightness can be used directly in lens models. Four images of the background quasar, surrounding the central region (radius $< 0.5$ kpc) of the galaxy, constrain models of the mass distribution in that region. Schneider *et al.* (1988) calculated models based on the observed

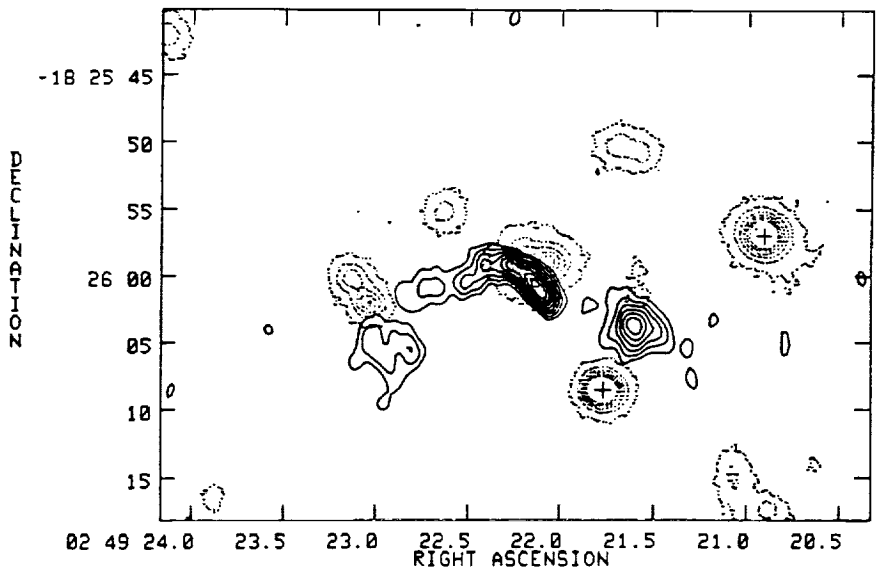


FIGURE 2 Contour plot of a $\lambda 20$ cm radio map (solid contours) of 0249-184 superimposed on an optical $I$ band image (dotted contours) of the field. The radio contours are 20%, 30%, 40%, 50%, 60%, 70%, 80%, and 90% of the peak brightness of 370 $\mu$Jy/beam; the resolution is approximately $2''$. No attempt has been made to calibrate the optical image; the contours are linear in the CCD data numbers.

light distribution, in a $12'' \times 12''$ region centered on the bulge of the galaxy, and a constant mass-to-light ratio. The best model has a blue mass-to-light ratio of $9.4h$ ($H_o = 100h$ km/sec/Mpc) with 20% variations causing significant differences between the data and the model. MG1654+1345 is the second Einstein ring to be discovered, and consists of the ring image of the radio lobe of a $z = 1.74$ quasar lensed by a $z = 0.254$ galaxy (Langston *et al.* 1989). The strength of the lens in this case can be estimated from the angular radius of the observed ring, and the enclosed mass calculated from the measured redshifts, assuming $q_o = 1/2$, is $9.5 \pm 1.9 \times 10^{10} \frac{1}{h} M_\odot$. From the measured brightness of the galaxy, the blue mass-to-light ratio with the central 5 kpc of the galaxy is $19 \pm 4h$. The above values of the mass-to-light ratio are completely independent of measurements made using dynamical techniques.

In addition to using gravitational lens systems as astrophysics laboratories, work continues on searches for new systems. I know of six deliberate searches at radio and optical wavelengths for which results have been published. Gravitational lensing is a relatively rare event; therefore, all these searches require some sort of filter to select objects which we believe are

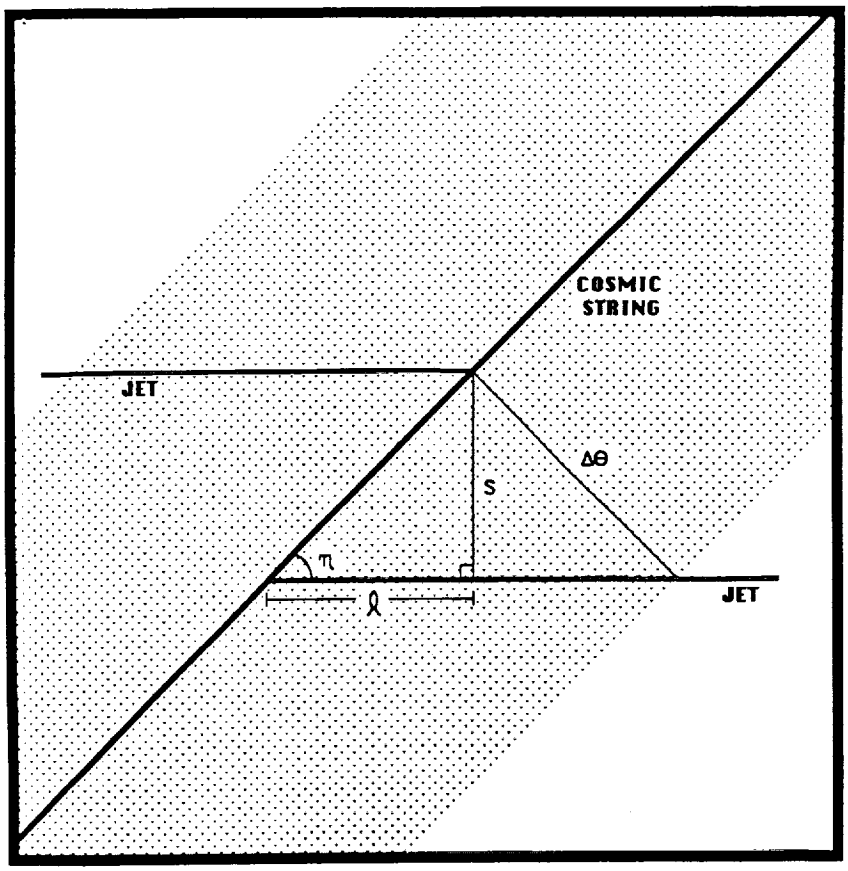


FIGURE 3 Schematic diagram of lensing of a linear structure, such as a radio jet, by a cosmic string. The angle between the string and the jet is $\eta$, and the part of the sky that is imaged twice is represented by the shaded region. A point source in the shaded region has two images with angular separation $\Delta\theta$. The cosmic string causes an apparent break in the jet with separation $s$ and overlap $l$.

more likely to be lensed. More than half the searches use the morphology of the object as the criterion in selecting lens candidates. The others use the fact that gravitationally lensed images, because of their magnification, will appear brighter than they otherwise would. This property indicates that objects of high absolute luminosity (calculated from the redshift and the apparent luminosity, not corrected for the magnification of any lens) are good lens candidates. Once the lens candidates have been selected, further tests must be carried out to test whether images are lensed. Possible tests include: (1) Do the images have the same spectra (and the same

redshift)? (2) Do the images have the same polarization properties? (3) If there is any structure in the images, is it consistent with gravitational lensing? (4) Do the images have the same light curve, offset by the time delay between the images? (5) If there are other distant objects behind the lens, are they also imaged? (6) Are there more than two images of the source? (7) Is there a lens visible? (8) Is the source redshift larger than the lens redshift? It is a question of judgment at what point one decides that a system is a gravitational lens, and opinion on this issue varies somewhat. In many cases, optical spectra showing emission lines at the same wavelengths with approximately the same relative intensities have been the primary evidence for gravitational lensing. Most of the searches rely on optical spectroscopy as a means of verification. However, there is at least one clear counterexample. In the double quasar 1145-071, the two components have very similar optical spectra, but one is a radio source and the other is not (Djorgovski *et al.* 1987). The following is a brief summary of the gravitational lens searches.

(1) **VLA Survey** This search makes use of a large program of VLA snapshots (Hewitt *et al.* 1989; Lawrence *et al.* 1986) of radio sources from the MIT-Green Bank (MG) single-dish survey (Bennett *et al.* 1986). The observations are at 5 GHz, giving a resolution of approximately 0.4″. Sources are selected as lens candidates on the basis of their radio morphology. The goal of the project is the detection of multiply-imaged quasars, since these are likely to be verifiable with optical and very long baseline (VLB) radio observations. Therefore, sources with more than one unresolved component are given the highest priority. Four gravitational lens systems have resulted from the survey: 2016+112, MG1131+0456, MG1654+1346, and MG0414+0534 (Hewitt *et al.* 1989). Two are Einstein ring images of radio lobes; the other two are multiple images of compact stellar objects. A fifth source, 0023+171, shows two stellar objects with similar spectra, but the radio morphology is not easily explained through gravitational lensing, and its interpretation remains uncertain (Hewitt *et al.* 1987). Four of these objects have been detected on VLBI baselines.

(2) **High Luminosity Quasars I** Surdej *et al.* (1988) selected 111 quasars from the Véron et Véron (1985) catalog by the following criteria: $m_v \leq 18.5$, $M_v \leq -29.0$, and declination $\leq 20°$. These quasars were imaged with the 2.2m ESO/MPI telescope and a CCD camera, often under conditions of good seeing. Twenty-five candidates appear "interesting" in that they display multiple structure or are near a faint galaxy, and the lens systems UM673 and H1413+117 have been discovered. The evidence for lensing is good in both cases; in addition to the spectroscopic evidence, the lensing galaxy of UM673 has been detected, and H1413+117 shows four lensed images.

**(3) High Luminosity Quasars II** Djorgovski and Meylan (1989) have selected high luminosity quasars with large redshifts from the Hewitt and Burbidge (1987) catalog and are carrying out CCD observations. So far one probable gravitational lens has been discovered: UM425 with four components, of which two show very similar spectra (Meylan and Djorgovski 1989). Spectra of the other two components have not yet been measured.
**(4) Pairs of Quasars I** Webster and collaborators are using the Automated Plate Measuring machine in Cambridge to scan direct and objective prism plates (Webster *et al.* 1988). Quasar candidates are selected on the basis of their spectra, and the morphology of the quasar candidates is known from the scanning of the direct plates. Note that quasar candidates are *not* limited to just stellar objects; multiply-imaged quasars and quasar-galaxy associations are included in the sample. This survey has resulted in the detection of statistical lensing described above, and one multiply imaged quasar (Hewett *et al.*, preprint).
**(5) Pairs of Quasars II** Weedman and Djorgovski (1988) examined seven grens plates for close pairs with similar spectra. Eight candidate lensed pairs of images, with separations ranging from 4″ to 9.5″ were found through visual inspection. CCD images and spectra for eight of the pairs were obtained, and it was found that none is lensed. From the area of the sky surveyed and quasar counts, Weedman and Djorgovski estimate that 200 to 300 quasars were examined, and from the quality of their plates estimate the limits on the frequency of lensing. They find their results are consistent with the theoretical results of Turner *et al.* (1984), but are perhaps surprising if the known wide separation lens candidates really are gravitational lenses.
**(6) Pairs of Blue Objects** Reboul *et al.* (1987) have selected pairs of blue objects from several catalogs. The 62 candidate lens systems consist of 46 pairs of blue objects separated by less then 9″, and 16 pairs in which one of the objects is blue. Fifteen of the systems have been investigated spectroscopially, but none is lensed.

In addition to the lens searches described above, there are a number that are in preliminary stages. There are at least three other searches in grens and objective prism plates (see Webster and Hewett 1989 and references therein). Gorenstein, Elby, Rogers, and myself are examining archived Mark III VLBI data for lensed compact radio sources. The existing data can be reprocessed to extend the search in interferometric delay and rate so that regions in the sky of typically several arc seconds on a side are examined. The advantage of this technique over the VLA survey technique is that a major component of confusion, classical double radio sources, are resolved out. Hogan (1987) has proposed a search for lensing by cosmic strings in CCD data collected for other purposes. The expected signature

of multiple pairs of galaxies stretching along the string is well suited to an automatic search. Burke, Turner, and Gott have observed a sample of high luminosity quasars at the VLA looking for radio structure that might be a product of gravitational lensing. Tyson, Fort, Mellier, Turner, and collaborators are surveying clusters of galaxies for evidence of luminous arcs.

In summary, the searches for gravitational lenses are proving to be successful, and more lenses continue to be discovered serendipitously. Many searches are under way, and new instruments that will routinely increasely the resolution of astronomical imaging (such as the Hubble Space Telescope and the Very Long Baseline Array), and automated data analysis techniques may greatly increase their yield. A wide variety of types of lenses are being discovered, many particularly well suited to a specific application, and we are beginning to see results of astrophysical interest.

## ACKNOWLEDGMENT

This work was supported by grant AST86-18257 from the National Science Foundation.

## REFERENCES

Bennett, C. L., Lawrence, C. R., Burke, B. F., Hewitt, J. N., and Mahoney, J. H. 1986; Ap. J. Supp; 61; 1.
Blandford, R. D., and Kochanek, C. S. 1987; Ap. J.; 321; 658.
Cowie, L. L., and Hu, E. M. 1987; Ap. J.; 318; L33.
Djorgovski, S., and Meylan, G. 1989, in Gravitational Lenses, Lecture Notes in Physics, Vol. 330 (eds. J. M. Moran, J. N. Hewitt, and K.-Y. Lo), Berlin: Springer-Verlag. Djorgovski, S., Perley, R., Meylan, G., and McCarthy, P. 1987; Ap. J. Lett.; 321; L17.
Djorgovski, S., and Spinrad, H. 1984; Ap. J. Lett.; 282; L1.
Fanaroff, B. L., and Riley, J. M. 1974; M.N.R.A.S.; 167; 31p.
Giraud, E. 1988; Ap. J. Lett.; 334; L69.
Hewitt, J. N., Burke, B. F., Turner, E. L., Schneider, D. P., Lawrence, C. R., Langston, G. I., and Brody, J. P. 1989, in Gravitational Lenses, Lecture Notes in Physics, Vol. 330 (eds. J. M. Moran, J. N. Hewitt, and K.-Y. Lo), Berlin: Springer-Verlag.
Hewitt, A., and Burbidge, G. 1987; Ap. J. Supp.; 63; 1.
Hewitt, J. N., Turner, E. L., Lawrence, C. R., Schneider, D. P., Gunn, J. E., Bennett, C. L., Burke, B. F., Mahoney, J. H., Langston, G. I., Schmidt, M., Oke, J. B., and Hoessel, J. G. 1987; Ap. J.; 321; 706.
Hewitt, J. N., Turner, E. L., Schneider, D. P., Burke, B. F., Langston, G. I., and Lawrence, C. R. 1988; Nature; 333; 537.
Hogan, C. J., 1987, in 13th Texas Symposium on Relativistic Astrophysics (ed. M. P. Ulmer), Singapore: World Scientific Publishing Company.
Huchra, J., Gorenstein, M., Kent, S., Shapiro, I., Smith, G., Horrine, E., and Perley, R. 1985; A. J.; 90; 691.
Hummel, E., Kotanyi, C. G., and Ekers, R. D. 1983; Astron. Astroph.; 127; 205.
Irwin, M. J., Webster, R. L., Hewett, P. C., Corrigan, R. T., and Jedrzejewski, R. I. 1989, A. J., in press.
Kayser, R., and Refsdal, S. 1989; Nature; 338; 745.
Kochanek, C. S., and Blandford, R. D. 1987; Ap. J.; 321; 676.

Narayan, R., and Grossman S. 1989, in Gravitational Lenses, Lecture Notes in Physics, Vol. 330 (eds. J. M. Moran, J. N. Hewitt, and K.-Y. Lo), Berlin: Springer-Verlag.
Langston, G. I., Schneider, D. P., Conner, S., Carilli, C. L., Lehár, J., Burke, B. F., Turner, E. L., Gunn, J. E., Hewitt, J. N., and Schmidt, M. 1989; A. J.; 97; 1283.
Lavery, R. J., and Henry, J. P. 1988; Ap. J. Lett.; 329; L21.
Lawrence, C. R., Bennett, C. L., Hewitt, J. N., Langston, G. I., Klotz, S. E., and Burke, B. F. 1986; Ap. J. Supp.; 61; 105.
Lawrence, C. R., Schneider, D. P., Schmidt, M., Bennett, C. L., Hewitt, J. N., Burke, B. F., Turner, E. L., and Gunn, J. E. 1984; Science; 223; 46.
Le Fèvre, O., Hammer, F., Nottale, L., and Mathez, G. 1987; Nature; 326; 268.
Lynds, R., and Petrosian, V., 1989; Ap. J.; 336; 1.
Magain, P., Surdej, J., Swings, J.-P., Borgeest, U., Kayser, R., Kühr, H., Refsdal, S., and Remy, M. 1988; Nature; 334; 325.
Meylan, G., and Djorgovski, S. 1989; Ap. J. Lett.; 338; L1.
Paczynski, B. 1986; Ap. J.; 308; L43.
Pello-Descayre, R., Soucail, G., Sanahuja, B., Mathez, G. and Ojero, E. 1988; Astron. Astroph.; 190; L11.
Reboul, H., Vanderriest, C., Fringant, A. M., and Cayrel, R. 1987; Astron. Astroph.; 177; 337.
Schneider, D. P., Turner, E. L., Gunn, J. E., Hewitt, J. N., Schmidt, M., and Lawrence, C. R. 1988; A. J.; 95; 1619.
Shaver, P. A., Danziger, I. J., Ekers, R. D., Fosbury, R. A. E., Goss, W. M., Malin, D., Moorwood, A. F. M., and Wall, J. V. 1982, in Extragalactic Radio Sources (ed. D. S. Heeschen and C. M. Wade), Dordrecht: D. Reidel Publishing Company.
Soucail, G., Fort, B., Mellier, Y., Picat, J. P. 1987; Astron. Astroph.; 172; L14.
Surdej, J., Swings, J.-P., Magain, P., Borgeest, U., Kayser, R., Refsdal, S., Courvoisier, T. J.-L., Kellermann, K. I., and Kühr, H. 1988 in Proceedings of a Workshop on Optical Surveys for Quasars (eds. P. S. Osmer, A. C. Porter, R. F. Green, and C. B. Foltz), San Francisco: Astronomical Society of the Pacific.
Surdej, J., Magain, P., Swings, J.-P., Borgeest, U., Courvoisier, T. J.-L., Kayser, R., Kellermann, K. I., Kühr, H., and Refsdal, S. 1987; Nature; 329; 695.
Turner, E. L., Ostriker, J. P., and Gott, J. R., III. 1984; Ap. J.; 284; 1.
Turner, E. L., Schneider, D. P., Burke, B. F., Hewitt, J. N., Langston, G. I., Gunn, J. E., Lawrence, C. R., and Schmidt, M. 1986; Nature; 321; 142.
Véron-Cetty, M.-P., and Véron, P. 1985, ESO Sci. Rep. No. 4.
Walsh, D., Carswell, R. F., and Weymann, R. J. 1979; Nature; 279; 381.
Webster, R. L., and Hewett, P. C. 1989, in Gravitational Lenses, Lecture Notes in Physics, Vol 330 (eds. J. M. Moran, J. N. Hewitt, and K.-Y. Lo), Berlin: Springer-Verlag.
Webster, R. L., Hewett, P. C., Harding, M. E., and Wegner, G. A. 1988; Nature; 336; 358.
Webster, R. L., Hewett, P. C., and Irwin, M. J. 1988; A. J.; 95; 19.
Weedman, D. W., and Djorgovski, S. 1988, in Proceedings of a Workshop on Optical Surveys for Quasars (eds. P. S. Osmer, A. C. Porter, R. F. Green, and C. B. Folts), San Francisco: Astronomical Society of the Pacific.
Weedman, D. W., Weymann, R. J., Green, R. F., and Heckmann, T. M. 1982; Ap. J. Lett.; 255; L5.
Weymann, R. J., Latham, D., Angel, J. R. P., Green, R. F., Liebert, J. W., Turnshek, D. A., Turnshek, D. E., and Tyson, J. A. 1980; Nature; 285; 641.
Yee, H. K. C. 1988; A. J.; 95; 1331.

# Cosmic Gamma-Ray Bursts

K. HURLEY
University of California, Berkeley
and
Centre d'Etude Spatiale des Rayonnements, Toulouse, France

## ABSTRACT

A review of the cosmic gamma-ray burst phenomenon is presented. Both the light curves and the energy spectra of these short transient events display a great diversity. However, rapid rise times and periodicities sometimes observed in the light curves suggest a compact object origin. Similarly, absorption and emission features in the energy spectra argue strongly in favor of this interpretation. Counterparts to gamma-bursters in other energy ranges, such as optical and soft X-ray, have still not been identified, however, leading to a large uncertainty in the distances to bursters. Although gamma-ray burst sources have not yet been observed to repeat, numerous bursts from three objects which may be related to the gamma-bursters, called Soft Gamma Repeaters, have been recorded; there is weak evidence that they may be relatively distant on a galactic scale. Future missions, particluarly those emphasizing high energy, time, and/or spatial resolution, as well as a multiwavelength approach, are likely to advance our understanding of this enigmatic phenomenon.

## INTRODUCTION

Cosmic gamma-ray bursts (GRBs) are brief transient events with durations in the 10's of milliseconds to minutes range. The emission in this short interval consists of photons with energies from several keV to 10's of MeV and above, and generally most of the power is in gamma rays of energies around an MeV, making GRB energy spectra among the hardest of all astrophysical objects. The spatial distribution of GRBs is apparently

isotropic and, with only 3 known exceptions, each GRB source has been observed to burst only once. A lower limit to the time between bursts from a single source may be estimated from the data to be at least several years. Despite numerous deep searches for burster counterparts at many wavelengths, no unambiguous candidate for a quiescent counterpart has yet been identified; as a result, the distances to bursters are completely unknown.

It now seems indisputable that some fraction, perhaps 20% at least, of the GRB sources are neutron stars, most likely in our galaxy. This conclusion follows from the observation of line features in GRB energy spectra. While hard evidence for a galactic origin is still lacking for the majority of the bursts observed, it seems likely that advances in instrumentation in the near future will provide unambiguous data to resolve this uncertainty.

Some 500 GRBs have been detected since the announcement of their discovery (Klebesadel *et al.* 1973). Since 1978, most have been observed with dedicated instruments aboard the spacecraft of many nations: U.S. experiments on the Pioneer Venus Orbiter and International-Sun-Earth-Explorer 3; Soviet and Franco-Soviet detectors on the earth-orbiting Prognoz 6,7, and 9 missions, and on the interplanetary Venera 11, 12, 13 and 14, and Phobos 1 and 2 probes; and U.S. experiments on the German Helios-2 mission. Currently operating experiments include those aboard Pioneer Venus Orbiter, the Mir station, and U.S.-Japanese investigations aboard the Ginga satellite.

This paper will review only the essential aspects of the GRB phenomenon, with emphasis on the more recent results. An in-depth treatment of the subject, including both experiment and theory, has appeared recently (Liang and Petrosian 1986), as well as a more detailed review article (Hurley 1989). In what follows, GRBs will be introduced by their time histories, which provide some evidence for a compact object origin. The energy spectra of bursts are then presented, and they will be seen to demonstrate practically unambiguously that the origin of some GRBs involves neutron stars. Counterpart searches will be reviewed briefly, and the statistical properties of bursters will then be treated. One section is devoted to a review of the three known repeating bursters (the Soft Gamma Repeaters). In the concluding section, some models will be mentioned, and future prospects assessed.

## TIME HISTORIES

A gamma-ray burst may last from about 30 ms to 1000 s. Three examples are shown in Figures 1a-c. When the time histories are relatively simple (e.g., Figure 1a), e-folding rise and decay times may be calculated (Barat *et al.* 1984a); they range from 10 to 1000 ms, with some tendency to

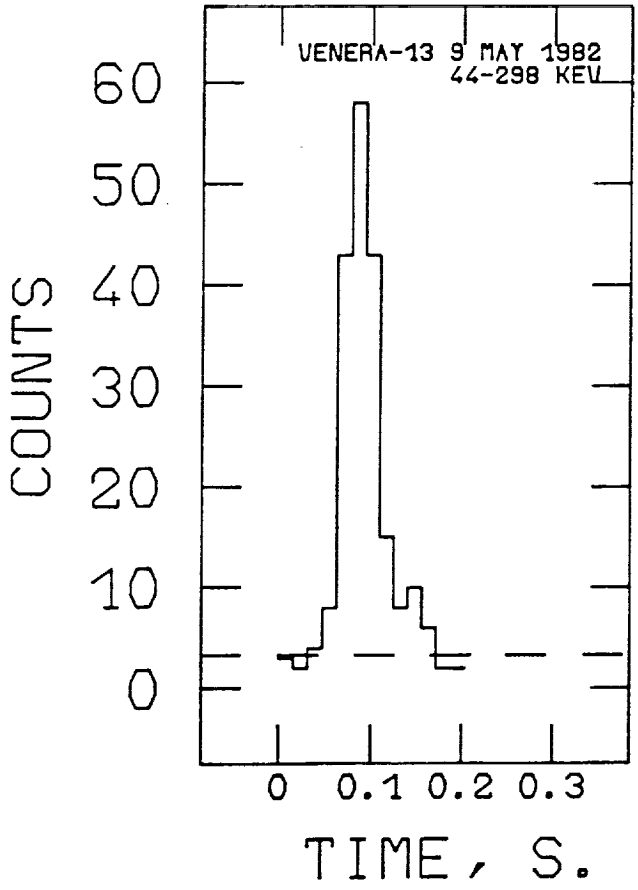


FIGURES 1a-c Time histories of three gamma bursts observed by Franco-Soviet experiments aboard the interplanetary Venera 13 and 14 spacecraft. Raw counts in 16, 32 and 500 ms intervals, in an energy band several hundred keV wide, are plotted as a function of time. Dashed lines indicate background levels.

cluster about 500 and 100 ms, respectively. The longer events (e.g., Figures 1b, 1c) tend to be more complex, displaying many peaks which appear in a chaotic fashion: there is generally little resemblance between peaks, no apparent relation between their amplitudes, and no clearly defined periodicities. It is possible that the short, apparently simple events have a complex underlying structure which only becomes apparent when they are observed with better statistics (Laros *et al.* 1985).

The wide diversity of time history shapes and durations is perhaps a clue to an equally wide diversity of mechanisms which are responsible for them, or even to a number of source types. It is also possible that we have

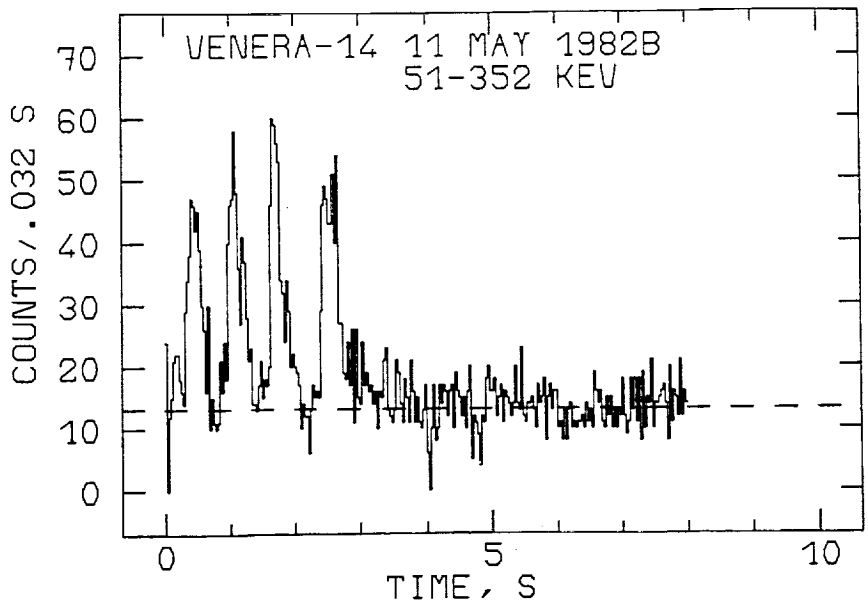


Figure 1b

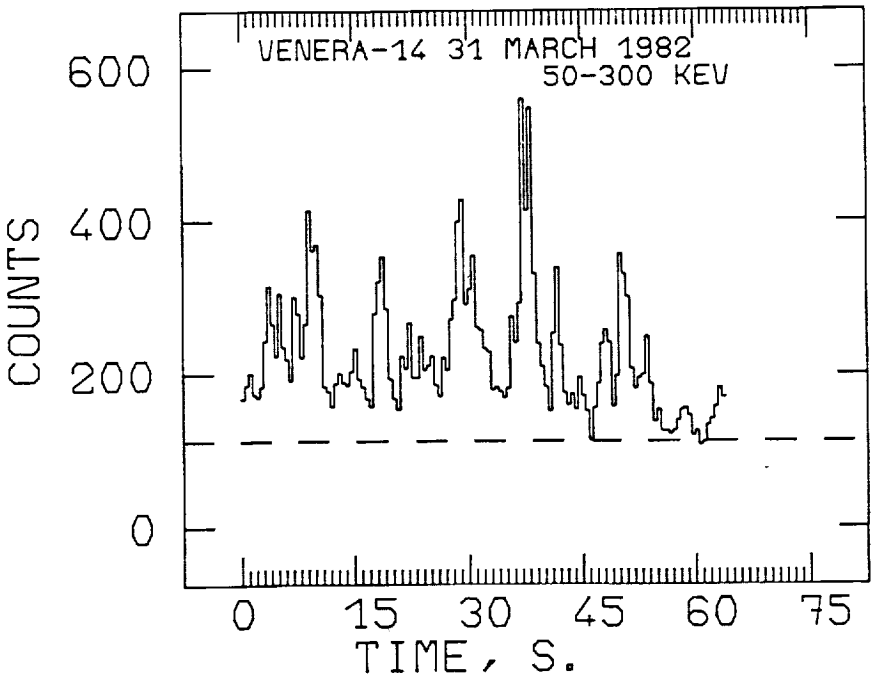


Figure 1c

not exhausted the burster morphologies with current instruments, since it can be shown that present experiments discriminate strongly against short bursts (Kuznetsov *et al.* 1987). As there is no obvious reason why such bursts should not exist, the durations may span an even greater range.

In discussing bursts, one exceptional event must be mentioned: that of March 5, 1979. As far as the time history is concerned, it was noteworthy (Cline *et al.* 1980) first, because of its rise time, $< 0.2$ ms, the shortest observed to date and second, because of a clearly resolved 8 s periodicity which lasted for several minutes. These characteristics are indicative of a compact object origin: the rise time may be related to the source size, $<$ 60 km, by causality arguments, and is also consistent with dynamical time scales near the surface of a neutron star (Lamb *et al.* 1973). The periodicity implies a minimum density of about $5 \times 10^6$ gm/cm$^3$ to withstand centrifugal breakup, and is in the period range of X-ray pulsars, which are known to involve neutron stars. In addition, the rise times of other bursts, in the 500 ms range, are consistent with the free-fall times from the magnetopause of a neutron star to its surface (Lamb *et al.* 1973), suggesting that some GRBs may be powered by accretion, like some steady X-ray sources. Thus there is circumstantial evidence in the time histories that GRBs may originate on or near neutron stars.

## ENERGY SPECTRA

GRB energy spectra tend to be almost as diverse in some respects as the time histories. However, a composite spectrum illustrating their most important features is shown in Figure 2. The continuum has been observed from X-rays of several keV (Laros *et al.* 1984) to gamma rays of 100 MeV (Share *et al.* 1986). Superimposed upon this continuum, two types of line features are sometimes detected (Mazets *et al.* 1981; Teegarden and Cline 1980). The first is an absorption line in the 20-70 keV range, with line-to-continuum ratios reaching 0.8 and line widths of about 20%. The second is an emission feature in the 350-500 keV range, with line-to-continuum ratios up to 0.3 and line widths around 30%. The former are observed in 15-20% of all GRB energy spectra, and the latter in about 10-20%. In all, lines have been observed in the spectra of some 100 bursts.

Until very recently, all observations of the absorption features were of *single* lines. Although it was generally felt that these were due to cyclotron scattering or absorption in a strong magnetic field, other interpretations were possible. New evidence from Ginga satellite data, however, have strengthened this conclusion considerably (Murakami *et al.* 1988; Fenimore *et al.* 1988): *double* absorption lines, at 20 and 40 keV, have been observed in the spectra of two bursts. The line energies provide very convincing evidence that the features are indeed the first and second harmonics in a

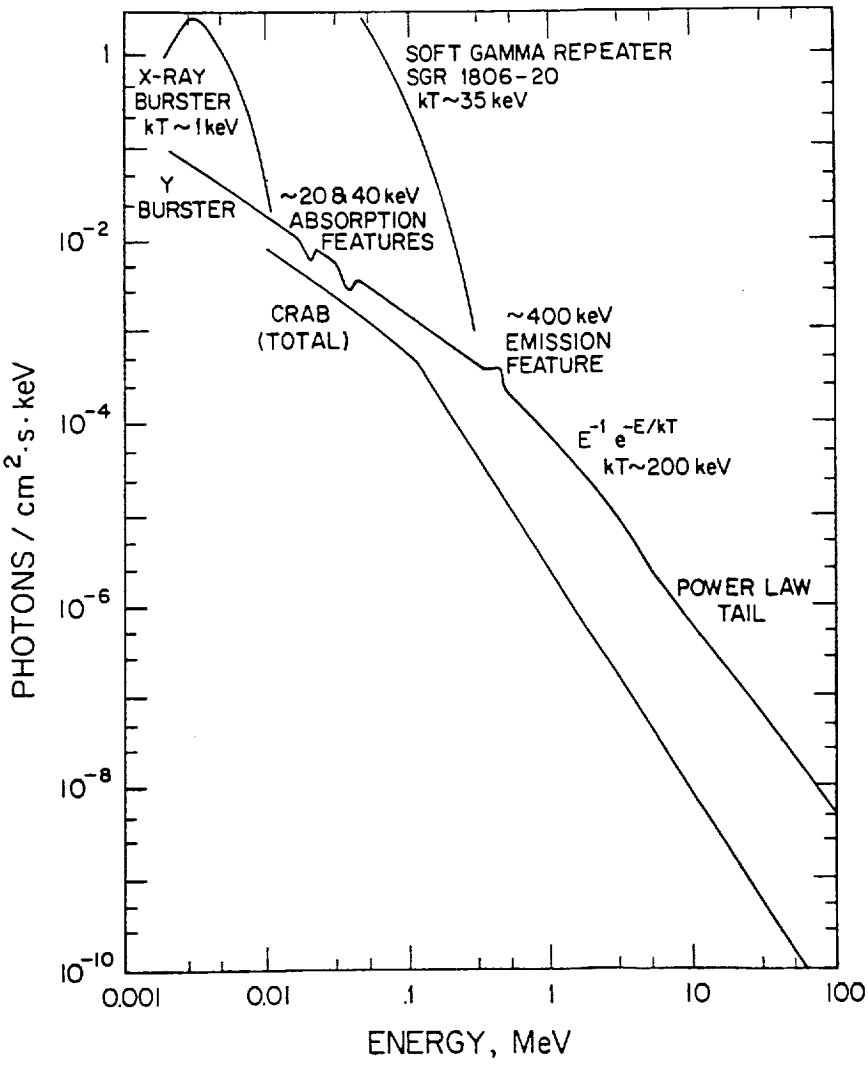


FIGURE 2 Typical photon number spectra of some astrophysical objects. The GRB spectrum is a composite, illustrating some of the important features which have been found in numerous observations.

B field whose strength is about $2 \times 10^{12}$ gauss. In fact, a detailed analysis (Wang *et al.* 1989) shows that one can derive not only the field strength, but also the angle of view with respect to the field, the temperature of the emitting region, the ratio of the line intensities, and numerous other parameters from careful modeling of these observations.

The emission features are attributed to 511 keV electron-positron annihilation radiation, gravitationally redshifted by about 20% to around 400 keV, implying that the radiation originates near the surface of a 1 solar mass, 10 km radius object. The source of the positrons is presumably in photon-photon or photon-B field interactions. This interpretation raises the interesting question of how the lines can remain relatively narrow in the presence of a hot continuum. In the case of the cyclotron features, the answer appears to be that the absorbing medium is optically thin to the continuum but, due to the magnetic field, thick to photons at resonant energies (Wang *et al.* 1989). There is, however, no accepted explanation in the case of the emission lines.

Figure 3 summarizes what is known about GRB emission at other energies during the bursting phase. The ordinate is energy flux, or differential of power by log energy, and the normalization is such that the integral gamma ray energy flux above 30 keV is arbitrarily set to 1, so that the ratio of the gamma ray luminosity to that in any other range may be read off the ordinate directly. Practically all points at energies other than X- and gamma rays are upper limits. The exceptions are first, optical transient sources detected in and near 6 GRB regions, but not in conjunction with a burst (Schaefer 1981; Barat *et al.* 1984b; Cline *et al.* 1984; Pedersen *et al.* 1984; Hudec *et al.* 1988; Moskalenko *et al.* 1989); for the purposes of this graph, it has been assumed that each was associated with an undetected GRB. A second exception is a radio burst detected in near-coincidence with a GRB whose location is somewhat uncertain (Mandolesi *et al.* 1977; Ciapi *et al.* 1979).

Where GRB emission is detectable, from about 2 keV to 100 MeV, the energy flux spectrum has a very unusual shape. First, it is X-ray deficient (X-ray to gamma ray luminosity ratios of about 0.02), and second, the power output peaks in the MeV range (which justifies the name gamma ray burst). These characteristics have some important consequences for source models (Epstein 1986). Simply to cite one, it means that if gamma radiation is generated near the surface of a neutron star (which is what is suggested by the observations of gravitationally redshifted emission lines), a large fraction of the gamma rays may be directed towards the surface, where they will Compton scatter and reemerge as X-rays, violating the observed X-ray deficiency. Beaming the gamma rays away from the surface, or generating them far from the neutron star can solve this problem.

## QUIESCENT COUNTERPART SEARCHES

With only a few possible exceptions (e.g., the March 5, 1979, event [Cline *et al.* 1982], discussed below with the Soft Gamma Repeaters), deep searches at numerous energies for quiescent burster counterparts have been

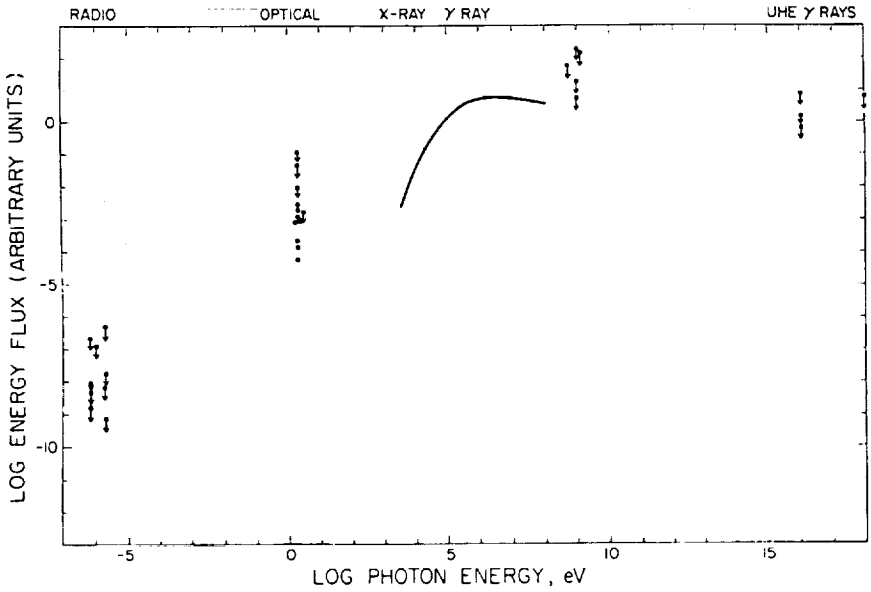


FIGURE 3 The energy flux spectrum of gamma-bursters. Although some of the radio upper limits (Baird *et al.* 1975; Mandolesi *et al.* 1977; Ciapi *et al.* 1979; Cortiglioni *et al.* 1981; Inzani *et al.* 1982) were originally published for GRBs whose locations were unknown, subsequent analysis has retained only points above the horizon of the stations used, with one possible exception (Mandolesi *et al.* 1977; Ciapi *et al.* 1979). Optical (Schaefer 1981; Barat *et al.* 1984b; Cline *et al.* 1984; Pedersen *et al.*1984; Hudec *et al.* 1988; Moskalenko *et al.* 1989; Grindlay *et al.* 1974; Hudec *et al.* 1987), VHE gamma-ray (O'Brien and Porter 1976; Bhat *et al.* 1981), and UHE gamma-ray (Clay *et al.* 1982) upper limits are also shown.

fruitless. Quiescent emission searches have been carried out in the radio range using the VLA (Schaefer *et al.* 1988); in the infrared using IRAS and ground-based telescopes (Schaefer *et al.* 1987); in the optical (e.g. Schaefer *et al.* 1987; Motch *et al.* 1985) to $m_B = 25$; in soft X-rays using the Einstein (Pizzichini *et al.* 1986) and EXOSAT (Boer *et al.* 1988) observatories; in the hard X-ray range with HEAO A-4 (Hueter 1987); and in the gamma ray range with COS-B (Sumner *et al.* 1987). The lack of positive identification with any known objects makes it practically impossible to establish the distances to gamma-bursters, even if one accepts the galactic neutron star hypothesis.

Space Telescope time has been granted for gamma-ray burst optical counterpart studies. This will eventually allow U magnitudes of about 27 to be reached, and it is quite likely that we will begin to understand better the nature of the objects which are detected optically in GRB error boxes.

## STATISTICAL PROPERTIES OF GAMMA-BURSTERS

While there are numerous subjects which could be treated under this heading, only three will be singled out here. They are:

1. the recurrence time between bursts from a single source, which tells us something about the neutron star population involved;
2. the spatial distribution (e.g. in galactic coordinates, or in multipole moment expansions, or the angular correlation function), which informs us about the geometrical source distribution; and
3. the number-intensity relation (e.g., log N-log S, or $V/V_{max}$), which gives us information on the geometrical distribution of sources about us and how it is sampled.

These three properties are not unrelated, but for simplicity they will be decoupled from one another for the following discussion.

With the exception of three Soft Gamma Repeaters (discussed below), no GRB source has yet been observed to repeat. The best lower limit to the recurrence time between bursts from a single source is about 10 years (Atteia *et al.* 1987; Schaefer and Cline 1985). Yet it is clear that GRB sources must repeat on some time scale from the following argument. Suppose that a fraction f of the bursters are due to galactic neutron stars. The total number of such objects is about $10^8$. We detect about 0.5 - 1 GRB/day, and there are probably many more which we do not detect due to sensitivity considerations, imperfect sky coverage, etc. Thus if each source burst only once, there would only be enough to last $5 \times 10^5/f$ years. Taking the age of the galaxy to be $10^{10}$ years, this means that if $f > 5 \times 10^{-5}$, recurrence must occur on some time scale. In fact, a value $f = 0.2$ is suggested by the line observations, implying a maximum recurrence time of $2.5 \times 10^6$ years. Even if the number of neutron stars in the galaxy is a factor of 10 greater, burster recurrence is necessary.

Since the lack of GRB counterparts leaves the distance scale undetermined, much effort has been focused on understanding the spatial distribution of bursters, in the hope that, for example, an underlying galactic distribution might become evident at some level. It is possible to quantify the isotropy or anisotropy in a coordinate system-independent fashion, by first expanding the source distribution in spherical harmonics, and then calculating moments of the distribution (Hartmann and Epstein 1989). The dipole and quadrupole moments have values about equal to those expected for an isotropic distribution, indicating no point or plane concentrations. The distance to which sources are sampled may be estimated calculating the angular correlation function introduced by Peebles (1973). The application of this method to GRB source catalogs has shown that if the sources are extragalactic, they are sampled out to a distance of at least 140 Mpc, while if they are distributed in the disk of our galaxy with a scale height

H, they are sampled out to a distance of at most H/2 (Hartmann and Blumenthal 1989). Thus these studies allow one to set limits on the observed distribution, although they do not settle the question of the distance scale.

Yet another approach to the distance scale is that of source counts, or the log N-log S relation (e.g. Ryle 1968). Here the data simply indicate, once more, that we are in the presence of an apparently isotropic distribution, but give no information on the distance scale. Such information is likely to leave its signature on the log N-log S curve at low S, where the weak and presumably distant sources are counted. Although instrumental effects distort this portion of the curve, the same data may be used in a different formulation to test the hypothesis that GRB sources are drawn from a uniform space distribution. This is the $V/V_{max}$ test, first used to test the distribution of quasars (Schmidt 1968), and recently revised for GRB sources (Schmidt *et al.* 1988). While the $V/V_{max}$ test eliminates the detector-induced biases of the log N-log S test, it does introduce other biases (e.g. the Malmquist bias) which may become important when large data sets are employed (Hartmann *et al.* 1989). To date, however, the test has only been carried out on small data sets, where it confirms, once more, that the GRB source distribution is uniform.

## THE SOFT GAMMA REPEATERS

While the vast majority of the gamma-bursters have not been observed to repeat, three unusual repeating sources are known (Atteia *et al.* 1987b; Laros *et al.* 1987; Mazets *et al.* 1982; Golenetskii *et al.* 1987). They are unusual not simply because they repeat, but also because their energy spectra are soft (kT~25 keV), hence the name "Soft Gamma Repeaters", or SGR. In addition, all have relatively short time histories. Although three events obviously do not constitute a distribution, each source has what might be termed a "distance indicator" associated with it. The March 5, 1979, event has a location consistent with the N49 supernova remnant in the LMC (Cline *et al.* 1982) (distance 55 kpc). SGR 1806-20 may be located in the bulge, near the galactic center (Atteia *et al.* 1987b) (distance 8.5 kpc). And B1900+14 is apparently near the galactic plane, suggesting that its distance may be several kpc. Thus a trend may be emerging for these sources to be relatively distant (Cline *et al.* 1987). This, of course, may only be confirmed by observations of many new repeating sources. However, a suggestion as to why distant sources might be soft has been proposed (Kazanas 1988): the distant sources are inherently the most luminous, and thus convert their gamma-radiation to an optically thick electron-positron pair plasma which thermalizes and softens the emerging spectrum.

## DISCUSSION AND CONCLUSIONS

What are the distances to the gamma-bursters? Table 1 summarizes the energetics for a relatively intense source ($10^{-4}$ erg/cm$^2$ at earth); the intrinsic energy is then $10^{34}R_{pc}{}^2$ erg (isotropic emission assumed). The last column in the Table gives an example of a known steady X- or gamma ray source at the distance indicated, along with its X- or gamma ray luminosity, simply to show that energetics may become more of a problem at large distances.

What causes gamma-bursts? In the framework of the galactic neutron star hypothesis, it may be thermonuclear explosions (Woosley and Wallace 1982), accretion of cometary matter (Tremaine and Zytkow 1986), star-quakes (Schklovskii and Mitrofanov 1985), or accretion disk instabilities (Epstein 1985), simply to name a few ideas.

If all GRBs are indeed due to galactic neutron stars, they will yield a considerable amount of information on a number of topics of current interest: the behavior of matter, including its radiation mechanisms, under extreme conditions of gravitational and magnetic fields and temperatures, the evolutionary path followed by the neutron star which leads to the burster phase, and the retention of a strong magnetic field as it evolves are just a few examples.

Future missions will deploy new, sensitive, high resolution and multi-wavelength experiments to resolve the issues surrounding GRB origin. "High resolution" means not just in energy (to better resolve the emission and absorption features) but also in time (because the features are time variable, and because very short GRBs may be going undetected) and in space (to assist in the deep searches for counterparts which will take place using advanced instrumentation such as HST, ROSAT, and AXAF). Three examples of future experiments which address these needs will be discussed briefly.

The Burst and Transient Source Experiment (Fishman 1988) aboard the Gamma Ray Observatory, to be launched in 1991, will survey the sky to a sensitivity level about an order of magnitude better than current detectors and provide coarse source localizations. If GRB sources are distributed in the galactic disk, it is possible that the localization data from this experiment for weak sources will reveal this. In addition, the instrument has a fast timing capability for intense events, and an array of scintillators for moderate energy resolution studies of energy spectra.

The Transient Gamma Ray Spectrometer on the WIND spacecraft may be launched at the end of 1992 (Teegarden 1986). It will utilize a large, passively cooled Germanium detector to study the energy spectra of bursts from 10 keV to 10 MeV with an energy resolution of several keV. This will be essentially the first dedicated, high resolution GRB experiment to fly in

over a decade, and it is expected to return a wealth of information on the low-energy absorption lines, the high-energy emission lines, and possibly also higher energy nuclear line contributions (as yet undetected). If, as seems plausible, the spectra of a large fraction of bursts contain line features which are presently going undetected by low resolution experiments, this instrument should identify them.

The High Energy Transient Experiment (Ricker *et al.* 1988) (HETE) represents a multi-wavelength approach to the study of gamma-bursters, and one which focuses on obtaining the maximum amount of information possible during the GRB and relaying it to the ground in near-real time. It is currently scheduled for a 1994 launch. HETE will employ a complement of wide field UV CCD cameras, X-ray and gamma-ray monitors to localize GRB sources to an accuracy of several arc seconds aboard the satellite. Using a novel "message-forwarding" capability, the experiment will transmit information to simple ground receiving stations around the globe, to permit rapid searches for counterparts with short-lived emission at, e.g., optical and radio wavelengths. It is anticipated that such an experiment will revolutionize GRB studies and resolve many outstanding problems, by providing the long-sought burster identifications.

## REFERENCES


Atteia, J.-L., C. Barat, K. Hurley, M. Niel, G. Vedrenne, W. Evans, E. Fenimore, R. Klebesadel, J. Laros, T. Cline, U. Desai, B. Teegarden, I. Estulin, V. Zenchenko, A. Kuznetsov, and V. Kurt. 1987. Ap. J. Supp. 64: 305-382.

Atteia, J.-L., M. Boer, K. Hurley, M. Niel, G. Vedrenne, E. Fenimore, R. Klebesadel, J. Laros, A. Kuznetsov, R. Sunyaev, O. Terekhov, C. Kouveliotou, T. Cline, B. Dennis, U. Desai, and L. Orwig. 1987. Ap. J. Lett. 320: L105-L110.

Baird, G., T. Delaney, B. Lawless, D. Griffiths, J. Shakeshaft, R. Drever, W. Meikle, J. Jelley, W. Charman, and R. Spencer. 1975. Ap. J. Lett. 196: L11-L13.

Barat, C., R. Hayles, K. Hurley, M. Niel, G. Vedrenne, I. Estulin, and V. Zenchenko. 1984a. Ap. J. 285: 791-800.

Barat, C., K. Hurley, M. Niel, G. Vedrenne, T. Cline, U. Desai, B. Schaefer, B. Teegarden, W. Evans, E. Fenimore, R. Klebesadel, J. Laros, I. Estulin, V. Zenchenko, A. Kuznetsov, V. Kurt, S. Ilovaisky, and C. Motch. 1984b. Ap. J. Lett. 286: L6 - L9.

Bhat, P., N. Gopalakrishnan, S. Gupta, P. Ramana Murthy, B. Sreekantan, and S. Tonwar. 1981. Phil Trans. R. Soc. Lond. A 301: 659-660.

Boer, M., J.-L. Atteia, M. Gottardi, K. Hurley, M. Niel, C. Barat, G. Pizzichini, K. Mason, G. Branduardi-Raymont, F. Cordova, J. Laros, W. Evans, E. Fenimore, R. Klebesadel, M. Sims, and C. Martin. 1988. Astron. Astrophys. 202: 117-123.

Ciapi, A., P. Inzani, G. Sironi, S. Cortiglioni, N. Mandolesi, and G. Morigi. 1979. Proc. 16th ICRC OG5-1: 209-214.

Clay, R., P. Gerhardy, and A. Gregory. 1982. Astrophys. Space Sci. 83: 279-286.

Cline, T., U. Desai, B. Teegarden, C. Barat, K. Hurley, M. Niel, G. Vedrenne, W. Evans, R. Klebesadel, J. Laros, I. Estulin, A. Kuznetsov, V. Zenchenko, V. Kurt, and B. Schaefer. 1984. Ap. J. Lett. 286: L15-L18.

Cline, T., U. Desai, G. Pizzichini, B. Teegarden, W. Evans, R. Klebesadel, J. Laros, K. Hurley, M. Niel, G. Vedrenne, I. Estulin, A. Kuznetsov, V. Zenchenko, D. Hovestadt, and G. Gloeckler. 1980. Ap. J. Lett. 237: L1-L5.

Cline, T., U. Desai, B. Teegarden, W. Evans, R. Klebesadel, J. Laros, C. Barat, K. Hurley, M. Niel, G. Vedrenne, I. Estulin, V. Kurt, G. Mersov, V. Zenchenko, M. Weisskopf, and J. Grindlay. 1982. Ap. J. Lett. 255: L45-L48.

Cline, T., C. Kouveliotou, and J. Norris. 1987. Proc. XX ICRC OG1.1-12, Vol. 9: 121-125.

Cortiglioni, S., N. Mandolesi, G. Morigi, A. Ciapi, P. Inzani, and G. Sironi. 1981. Astrophys. Space Sci. 75: 153-161.

Epstein, R. 1985. Ap. J. 291: 822-833.

Epstein, R. 1986. In: Winkler, K., and D. Mihalas (eds.). Radiation Hydrodynamics in Stars and Compact Objects. 305-310. Springer-Verlag, New York.

Fenimore, E., J. Conner, R. Epstein, R. Klebesadel, J. Laros, A. Yoshida, M. Fujii, K. Hayashida, M. Itoh, T. Murakami, J. Nishimura, T. Yamagami, I. Kondo, and N. Kawai. 1988. Ap. J. Lett. 335: L71-L74.

Fishman, G. 1988. In: Gehrels, N., and G. Share (eds.). Nuclear Spectroscopy of Astrophysical Sources. 378-388. AIP Press, New York.

Golenetskii, S., R. Aptekar, Yu. Guryan, V. Ilinskii, and E. Mazets. 1987. Sov. Astron. Lett. 13(3): 166-168.

Grindlay, J., E. Wright, and R. McCrosky. 1974. Ap. J. Lett. 192: L113-L114.

Hartmann, D., and G. Blumenthal. 1989. Ap. J. 342: 521-526.

Hartmann, D. and R. Epstein. 1989. Ap. J. 346: 960-966.

Hartmann, D., J. Gonzalez, and K. Hurley. 1989. Ap. J. Submitted.

Hudec, R., J. Borovicka, S. Danis, V. Franc, R. Peresty, and B. Valnicek. 1988. Adv. Space Res. 8(2): 665-668.

Hudec, R., J. Borovicka, W. Wenzel, J.-L. Atteia, C. Barat, K. Hurley, M. Niel, G. Vedrenne, W. Evans, E. Fenimore, R. Klebesadel, J. Laros, T. Cline, U. Desai, B. Teegarden, I. Estulin, V. Zenchenko, A. Kuznetsov, and V. Kurt. 1987. Astron. Astrophys. 175: 71-80.

Hueter, G. 1987. HEAO-1 Observations of Gamma-Ray Bursts, PhD. Thesis, University of California, San Diego, Department of Physics.

Hurley, K. 1989. Cosmic Gamma Ray Bursts. Pages 337-370. In: Shapiro, M., and J. Wefel (eds.). Cosmic Gamma-Rays and Cosmic Neutrinos. Reidel Pub. Co, Boston, MA. p. 337-370.

Inzani, P., G. Sironi, N. Mandolesi, and G. Morigi. 1982. In: Lingenfelter, R., H. Hudson, and D. Worrall (eds.). Gamma Ray Transients and Related Astrophysical Phenomena. 79-84. AIP Press, New York.

Kazanas, D. 1988. Nature 331: 320-321.

Klebesadel, R., I. Strong, and R. Olson. 1973. Ap. J. Lett. 182: L85-L88.

Kuznetsov, A., R. Sunyaev, O. Terekhov, J.-L. Atteia, M. Boer, K. Hurley, and M. Niel. 1987. Sov. Astron. Lett. 13(6): 419-423.

Lamb, D., F. Lamb, and D. Pines. 1973. Nature Phys. Sci. 246: 52-54.

Laros, J., W. Evans, E. Fenimore, R. Klebesadel, S. Shulman, and G. Fritz. 1984. Ap. J. 286: 681-690.

Laros, J., E. Fenimore, M. Fikani, R. Klebesadel, M. van der Klis, and M. Gottwald. 1985. Nature 318: 448-449.

Laros, J., E. Fenimore, R. Klebesadel, J.-L. Atteia, M. Boer, K. Hurley, M. Niel, G. Vedrenne, C. Kouveliotou, T. Cline, B. Dennis, U. Desai, L. Orwig, A. Kuznetsov, R. Sunyaev, and O. Terekhov. 1987. Ap. J. Lett. 320: L111-L115.

Liang, E. and V. Petrosian, (eds.). 1986. Gamma-Ray Bursts. AIP Press, New York.

Mandolesi, N., G. Morigi, P. Inzani, G. Sironi, F. DelliSanti, F. Delpino, M. Petessi, and A. Abrami. 1977. Nature 266: 427-429.

Mazets, E., S. Golenetskii, R. Aptekar, Yu. Guryan, and V. Ilinskii. 1981. Nature 290: 378-382.

Mazets, E., S. Golenetskii, Yu. Guryan, and V. Ilyinskii. 1982. Astrophys. Space Sci. 84: 173-189.

Moskalenko, E., G. Popravko, E. Kramer, I. Shestaka, A. Karnashov, V. Nazarenko, L. Skoblikova, V. Lemeshchenko, S. Nazarenko, and Ju. Gorbanev. 1989. Astron. Astrophys. 223: 141-146.

Motch, C., H. Pedersen, S. Ilovaisky, C. Chevalier, K. Hurley, and G. Pizzichini. 1985. Astron. Astrophys. 145: 201-205.
Murakami, T., M. Fujii, K. Hayashida, M. Itoh, J. Nishimura, T. Yamagami, J. Conner, W. Evans, E. Fenimore, R. Klebesadel, A. Yoshida, I. Kondo, and N. Kawai. 1988. Nature 335: 234-235.
O'Brien, S., and N. Porter. 1976. Astrophys. Space Sci. 42: 73-76.
Pedersen, H., J. Danziger, K. Hurley, G. Pizzichini, C. Motch, S. Ilovaisky, N. Gradmann, W. Brinkmann, G. Kanbach, E. Rieger, C. Reppin, W. Trumper, and N. Lund. 1984. Nature 312: 46-48.
Peebles, P. 1973. Ap. J. 185: 413-440.
Pizzichini, G., M. Gottardi, J.-L. Atteia, C. Barat, K. Hurley, M. Niel, G. Vedrenne, J. Laros, W. Evans, E. Fenimore, R. Klebesadel, T. Cline, U. Desai, V. Kurt, A. Kuznetsov, and V. Zenchenko. 1986. Ap. J. 301: 641 - 649.
Ricker, G., J. Doty, S. Rappaport, K. Hurley, E. Fenimore, D.Roussel-Dupre, M. Niel, G. Vedrenne, D. Lamb, and S. Woosley. 1988. In: Gehrels, N., and G. Share (eds.). Nuclear Spectroscopy of Astrophysical Sources. 407-416. AIP Press, New York.
Ryle, M. 1968. Ann. Rev. Astron. Astrophys. 6: 249-266.
Schaefer, B. 1981. Nature 294: 722-724.
Schaefer, B., and T. Cline. 1985. Ap. J. 289: 490-495.
Schaefer, B., T. Cline, J.-L. Atteia, C. Barat, U. Desai, I. Estulin, W. Evans, E. Fenimore, K. Hurley, R. Klebesadel, A. Kuznetsov, J. Laros, M. Niel, and B. Teegarden. 1989. Ap. J. 340: 455-457.
Schaefer, B., T. Cline, U. Desai, B. Teegarden, J.-L. Atteia, C. Barat, K. Hurley, M. Niel, W. Evans, E. Fenimore, R. Klebesadel, J. Laros, I. Estulin, and A. Kuznetsov. 1987. Ap. J. 313: 226-230.
Schaefer, B., P. Seitzer, and H. Bradt. 1983. Ap. J. 270: L49-L52.
Schklovskii, I., and I. Mitrofanov. 1985. M.N.R.A.S. 212: 545-551.
Schmidt, M. 1968. Ap. J. 151: 393-408.
Schmidt, M., J. Higdon, and G. Hueter. 1988. Ap. J. Lett. 329: L85-L87.
Share, G., S. Matz, D. Messina, P. Nolan, E. Chupp, D. Forrest, and J. Cooper. 1986. Adv. Space Res. 6(4): 15-18.
Sumner, T., D. Clements, O. Williams, and G. Rochester. 1987. Astron. Astrophys. Supp. 71: 557-560.
Teegarden, B. 1986. Adv. Space Res. 6(4): 93-96.
Teegarden, B., and T. Cline. 1980. Ap. J. Lett. 236: L67-L70.
Tremaine, S., and A. Zytkow. 1986. Ap. J. 301: 155-163.
Wang, J., D. Lamb, T. Loredo, I. Wasserman, E. Salpeter, E. Fenimore, J. Conner, R. Epstein, R. Klebesadel, J. Laros, A. Yoshida, M. Fujii, K. Hayashida, M. Itoh, T. Murakami, J. Nishimura, T. Yamagami, I. Kondo, and N. Kawai. Phys. Rev. Lett. 63(15): 1550-1553.
Woosley, S., and R. Wallace. 1982. Ap. J. 258: 716-732.

# Georgian Space Research Program

G.P. KAKHIDZE
Abastumani Astrophysical Observatory

## ABSTRACT

This paper presents considerations of telescopes and spectrometers planned to be designed and made by the Abastumani Astrophysical Observatory of the Georgian SSR Academy of Sciences. The purpose of this topic is to clarify actual scientific problems which are to be solved by using telescopes. The experiments will begin in 1995.

## INTRODUCTION

Telescopes and spectrometers are designed for mounting on the orbital scientific station of the Mir type with the following characteristics (Orbital Station Mir 1988): inclination 51.6°; flight altitude 300-400 km; orbit period 90 min. The total mass determined by the Georgian Academy of Sciences is 10,000 kg; telemetric information 1.m bit/s; energy consumption 700 W.

Telescopes and spectrometers can be mounted in a hermetic compartment in the station and on an independent platform enabling one to carry out astrophysical observations not related to any problems of the station. The independent platform provides pointing and stabilization not worse than 1 min. The mass of scientific equipment is $\approx$ 10,000 kg with dimensions $5 \times 5 \times 3$ m$^3$.

After consideration and determination of the actual problems to be solved, the telescopes and spectrometers will be improved according to scientific engineering offers.

Project Marina-3, consisting of a complex of scientific equipment, has been proposed for consideration.

Project Marina-3, consisting of a complex of scientific equipment, has been proposed for consideration.

1. An omnidirectional telescope Marina-1M consisting of seven moduli. The telescope modulus is shown in Figure 1. The telescope is designed for finding and localizing transient X-ray and gamma ray sources for measurements of energy and temporal spectra and for determination coordinates in the energy range from 2 keV to 10 MeV with the energy flux $10^{-8} - 10^{-4}$ erg/cm$^2$s. Time resolution of X-ray and gamma ray bursts is 0.1 msec.

To measure energy spectra, proportional counters are used for detecting X-rays in the energy range 2-30 keV with the sensitive surface $1.2 \times 10^3$ cm$^2$, combined scintillation detectors NaI/CsI with the diameter of 200 mm are for detection of gamma radiation in the range 15 keV - 10 MeV, and their sensitive surface is $1.2 \times 10^3$ cm$^2$.

Bursts $1.5 \cdot 10^{-6}$ erg/cm$^2$ s are registered by a scintillation detector with the diameter 60 mm and with a semiconductor detector of mercury diodide with a sensitive surface of 1 cm$^2$.

The coordinates of X-ray and gamma bursts are determined by a single coordinate chamber with a coded aperture (Horstman *et al.*; Bradt *et al.* 1988) with the field of view $6 \times 60°$, permitting observation of an image of the celestial sphere with a transient X-ray source. The expected accuracy of coordinate determination is of the order of 10 arc sec for the energy flux $10^{-8}$erg/cm$^2$ s at the energy 20 keV.

The telescope is mounted on a platform outside of the scientific station, without orientation. Coordinates of transient sources obtained by the telescope are corrected by a stellar sensor.

## TELESCOPE-SPECTROMETER TAMARA (FIGURE 2)

Scientific problems to be solved with a telescope-spectrometer are: determination of coordinates of X-ray sources with the angular resolution 2s and measurements of energy and temporal spectra in the energy range 2-30 keV with the time resolution 0.1 m sec, that can be obtained by separate measurements of coordinates and energy and temporal spectra.

To measure coordinates it is necessary to use a telescope with a mask (Orbital Station Mir) in order to obtain an image of a region of the celestial sphere in the energy range 2-30 keV with the energy resolution of the order of 20%, field of view $8 \times 8°$ with the angular resolution 2 sec and the effective area 600 cm$^2$ and time resolution required for image construction 1 s.

Measurements of energy and temporal spectra in the energy range 2-50 keV are carried out with proportional counters (Bradt *et al.* 1988) with

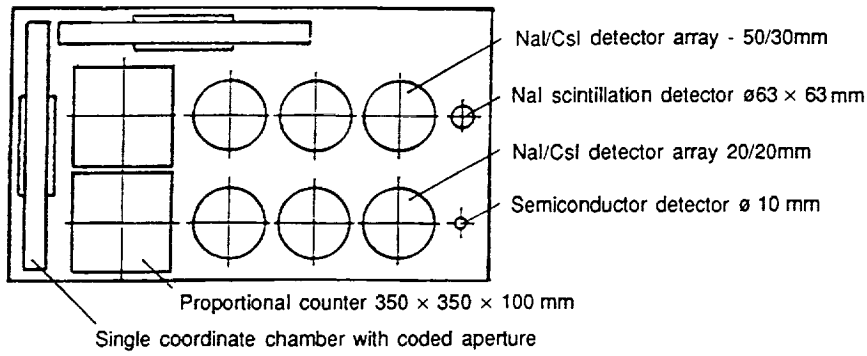


**Position of the detectors on a modulus**

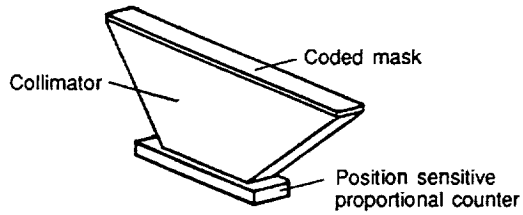


**Single coordinate chamber with a coded aperture**

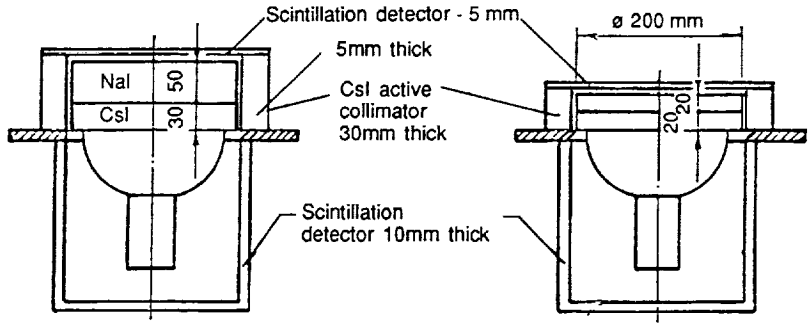


**NaI/CsI detector**

FIGURE 1 Omidirectional Telescope Marina-1M. (a) Position of the omnidirectional telescope on a platform. (b) Single coordinate chamber with a coded aperature. (c,d) NaI/CsI detector.

the angular resolution 2 × 2° and the sensitive area $10^5$ cm$^2$ enabling the study of millisecond pulsars.

It was suggested that the NASA department of High-Energy Astrophysics consider a possibility of construction of spectrometers with the sensitive area $10^6$ cm$^2$ (Teletype 1989).

A telescope-spectrometer is mounted on an independent platform with orientation.

## TELESCOPE-SPECTROMETER NINO (FIGURE 3)

Scientific problems to be solved with a telescope-spectrometer are: determination of coordinates of X-ray sources with the angular resolution 6s and measurements of energy and temporal spectra in the energy range 15-200 keV, with temporal resolution 0.1 msec, it can be reached by separate measurements of coordinates and energy spectra. It is suggested to use a telescope with a mask to measure coordinates (Rivier *et al.* 1982; Proposal 1982; Carter *et al.* 1982). It allows construction of an image of the celestial sphere in the energy range 20 to 200 keV with the field of view 8 × 8° with angular resolution 6s, and the effective area $10^4$ cm$^2$. A gamma chamber is used in the telescope. The gamma chamber, unlike that of Anger (1958), is constructed on NaI/CsI combined detectors that decrease the registered background in the image plane. The modulus construction of the telescope allows construction of telescopes with the sensitive area $10^4$ cm$^2$ and to use more effective methods (Ricker 1976) for the image reconstruction than a two-dimensional image construction. A stellar sensor operates coaxially with the telescope, which allows correction of the image at its construction. The image is constructed in 1s. Measurements of energy and temporal spectra in the energy range 15 to 200 keV and the time resolution 0.1 msec is carried out using the combined NaI/CsI detectors with an active and passive collimator, with the angular resolution 2 × 2°, and with the sensitive surface 2 × $10^4$ cm$^2$. Telescope-spectrometers are mounted on an independent platform providing orientation not less than 1 min.

Construction of the celestial sphere image by telescopes in the energy range of gamma-quanta 0.2 - 0.66 MeV is difficult, since there is a Compton effect in the NaI crystal leading to image defocusing. Combined detectors BGO/CsI give a possibility of increasing image brightness. The annihilation line 511 keV will be registered with the efficiency of 50%. A position sensitive detector BGO/CsI can be used in telescope Nino.

This offer is based on the findings of the Abastumani Astrophysical Observatory with the realization of proportional counters in ISZ Proton-1, 2, 3, 4, and of combined scintillation detectors in ISZ Cosmos -856, 914, 1106 and in OS Mir.

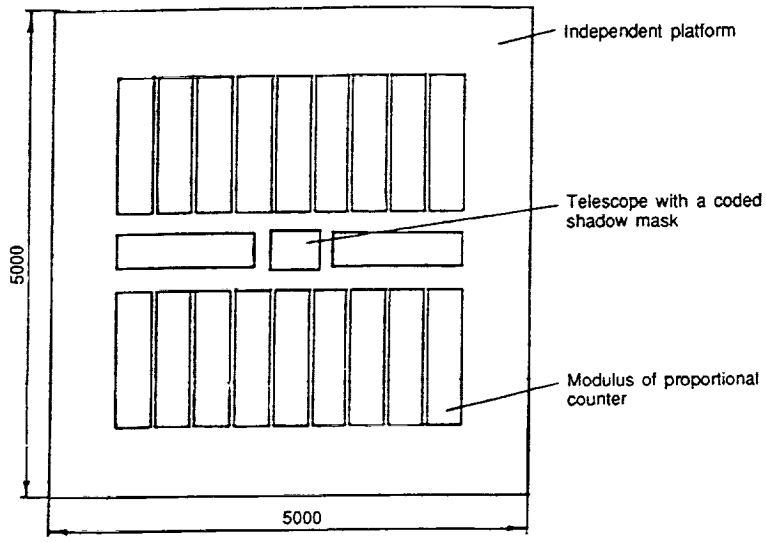


Position of the telescope-spectrometer on the independent platform

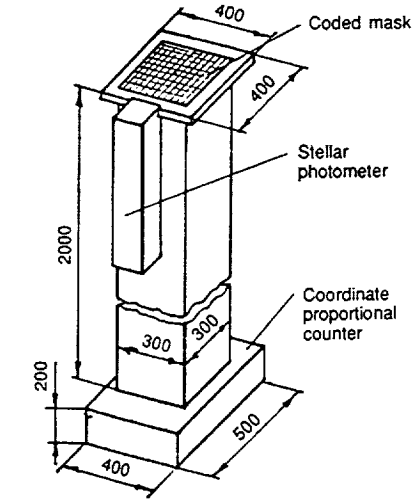


Telescope with a coded shadow mask

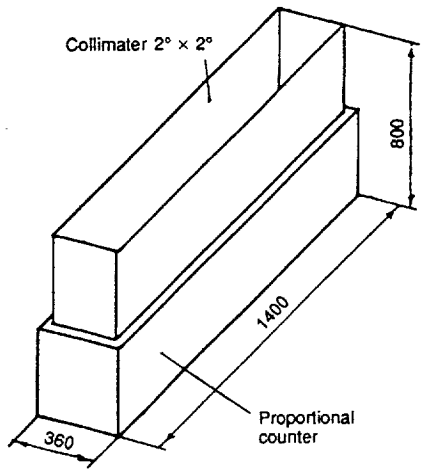


Modulus of proportional counter F = 0.5m$^2$

FIGURE 2 Telescope-Spectrometer Tamara. (a) Position of the telescope-spectrometer on the independent platform, (b) Telescope with a coded shadow mask, (c) Modulus of proportional counter F = 0.5 m$^2$.

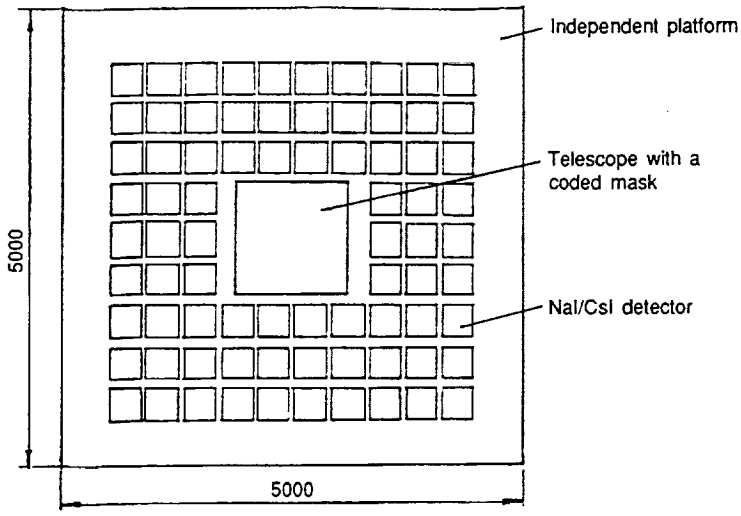


**Position of the telescope-spectrometer on the independent platform**

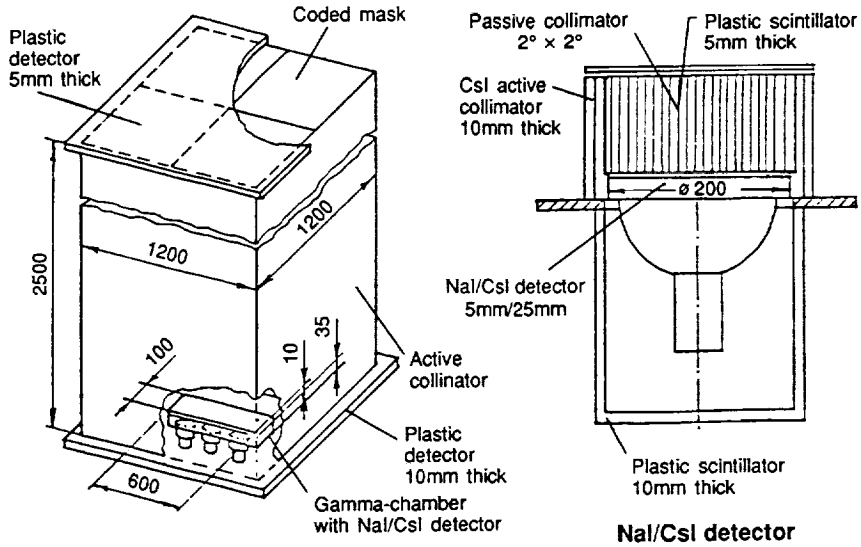


**Telescope with a coded mask** **NaI/CsI detector**

FIGURE 3 Telescope-Spectrometer Nino. (a) Position of the telescope-spectrometer on the independent platform, (b) Telescope with a coded mask, (c) NaI/CsI detector.

## REFERENCES

Anger, N.O. 1958. Rev. Sci. Instr. 29: 27.

An X-ray telescope with coded shadow mask TTM-Netherlands. Technical description of the modulus "Quant" at the orbital Station "MIR."

Bradt, H.V., J.H. Swank, and R.E. Rothschild. 1988. The X-ray timing explorer. Page 7,11. Preprint No. MIT-CSR-HEA-88-14.

Carter, J., P. Charalambous, A.I. Dean, and J. Stephen. 1982. A Gamma-Ray Telescope for the 1980's Journal of British Interplanetary Society. 35: 296 (The Zebra Telescope).

Horstman, H., E. Horstman Moretti, F. Fuligni, G. DiCocco, W. Dusi, F. Forntera, E. Morelli, and A. Spizzichino. Performance of gamma ray camera for astrophysics. Laboratoria TE.S.R.E./C.N.R., via De'Castagnoli 1, 40126 Bologna, Italy. Page 539.

Orbital Station MIR. 1988. Reference book for the user.

Proposal to the Science and Engineering Council for a British-led Space Project in Gamma-Ray Astronomy. November 1982.

Ricker, G.R. 1976. A diffraction-limited X-ray shadow camera. Submitted for Publication in the Astrophysics Journal (Letters).

Rivier, G., J. Paul, P. Manprue. 1982. Sigma: project of space observatory with high angular resolution to study gamma-ray sources. 33rd Congress of the International Astronautical Federation, Paris, France.

Teletype information to NASA Department of High Energy Astrophysics. 1989.

# On the Nature of Pulsar Radiation

A.Z. Kazbegi, G.Z. Machabeli, and G.I. Melikidze
Abastumani Astrophysical Observatory

## INTRODUCTION

A key question in the interpretation of the emission of pulsars is that of the excitation and propagation of waves in a magnetospheric plasma. The magnetosphere of a pulsar has an extremely complex structure and there are many difficulties in the development of its self-consistent model, the bases of which were considered in Goldreich and Julian (1969); Sturrock (1971); and Ruderman and Sutherland (1975). At present there exist some sufficiently well-grounded models not exactly agreeing with each other (e.g. Ruderman and Sutherland 1975; Cheng and Ruderman 1980; Arons and Sharlemann 1979; and Arons 1981). However, the creation of a dense, relativistic, electron-positron plasma in the polar regions of rotating neutron star magnetospheres is the point of similarity among these models. The pulsar radiation should be generated in such a plasma.

A spinning magnetized neutron star generates the electric field which extracts electrons from the star surface and accelerates them forming low density ($n_b = 7 \cdot 10^{-2} \cdot B_0 P^{-1}$, where P is the pulsar period and $B_0$ the magnetic field at the star surface) and the energetic (the Lorentz-factor of particles is $\gamma_b = 3 \cdot 10^6 \div 10^7$ for typical pulsars) primary beam. In a weakly curved magnetic field, electrons generate $\gamma$-quanta which produce in turn electron-positron pairs. Further energetic radiation will be produced, and this will go on to produce more pairs and so on until the plasma becomes dense and screens the electric field (Goldreich and Julian 1969; Sturrock 1971). As a result, sufficiently dense ($n_p \simeq 10^{16} - 10^{17}$ cm$^{-3}$) electron-positron plasma with an averaged Lorentz-factor $\gamma_p = 3$ - 10 is formed. The investigation of the kinetics of this avalanche process shows

that the plasma flowing along the open magnetic force lines possesses the aysmmetrical distribution function with a tail stretched out in the direction of the positive momenta (from the pulsar to the observer, e.g., Arons 1981). Due to the strong magnetic field, the transversal components (with respect to the magnetic field $\vec{B}_0$) of the particles momenta $p_\perp$ decay, and the distribution function tends to be one-dimensional.

Most probably the magnetic field near the pulsar has a complicated structure differing greatly from a dipole. Though at a sufficiently large distances from the stellar surface up to the light cylinder, the magnetic field can be considered as dipolar: $B = B_0(R_0/R)^3$ if $R_0 \ll R < c/\Omega$, where $R_0 = 10^6$ cm is a neutron star radius, $\Omega$ is the pulsar angular velocity. The dependence of the plasma density from the distance is the same $n = n_0(R_0/R)^3$, where index "0" denotes the values taken at the star surface.

In our opinion the maser emission mechanisms (Ginzburg and Zheleznyakov 1975) are the only valid and well-grounded among the others (e.g. antenna mechanisms; for more details see Lominadze *et al.* 1986).

To consider the curvature of the magnetic field lines exactly the cylindric coordinates x, r, $\varphi$ will be used below. The x-axis is directed transversely to the plane where the curved field lines lie, r- is the radial and $\varphi$- the azimuthal coordinates. The latter describes the curvature of the field line (torsion is neglected and $\partial R_B/\partial r = 0$, $R_B$ - is the curvature radius of the field line). In such geometry one has the following integrals of motion: $\gamma$, $p_x - \omega_{B\alpha} \cdot r/c$, $p_\varphi \cdot r$. Here $p_i = v_i \cdot \gamma/c$ and $v_i$ are the particle momentum and velocity, $\omega_{B\alpha} = e_\alpha \cdot B/m \cdot c$. The particle distribution function should depend on the integrals of motion. Using the method of integration along the particle trajectory one obtains the components of the dielectrical permeability tensor:

$$\epsilon_{xx} = 1 - \frac{1}{2}\sum_\alpha \frac{\omega_{p\alpha}^2}{\omega^2}\int \frac{dp_\varphi}{\gamma}\left((\omega - k_\varphi v_\varphi - 2k_\varphi u_\alpha^2/c)\left(\frac{1}{\Omega_\alpha^+} + \frac{1}{\Omega_\alpha^-}\right) f_\alpha + 2\omega \frac{u_\alpha^2}{c^2}\frac{\gamma}{\Omega_\alpha^0}\frac{\partial f_\alpha}{\partial_\varphi}\right);$$

$$\epsilon_{rr} = 1 - \frac{1}{2}\sum_\alpha \frac{\omega_{p\alpha}^2}{\omega^2}\int \frac{dp_\varphi}{\gamma}\left\{(\omega - k_\varphi v_\varphi - k_x u_\alpha)\left(\frac{1}{\Omega_\alpha^+} + \frac{1}{\Omega_\alpha^-}\right) f_\alpha\right\};$$

$$\epsilon_{\varphi\varphi} = 1 + \sum_\alpha \frac{\omega_{p\alpha}^2}{\omega^2}\int dp_\varphi \frac{v_\varphi^2}{c^2\Omega_\alpha^0}\frac{\partial f_\alpha}{\partial \gamma};$$

$$\epsilon_{xr} = +\frac{i}{2}\sum_\alpha \frac{\omega_{p\alpha}^2}{\omega^2}\int \frac{dp_\varphi}{\gamma}\left\{(\omega - k_\varphi v_\varphi - k_x u_\alpha)\left(\frac{1}{\Omega_\alpha^+} - \frac{1}{\Omega_\alpha^-}\right) f_\alpha\right\};$$

$$\epsilon_{rx} = -\frac{i}{2}\sum_{\alpha}\frac{\omega_{p\alpha}^2}{\omega^2}\int\frac{dp_\varphi}{\gamma}\left\{(\omega - k_\varphi v_\varphi - 2k_\varphi u_\alpha^2/c)\left(\frac{1}{\Omega_\alpha^+} - \frac{1}{\Omega_\alpha^-}\right)f_\alpha\right\};$$

$$\epsilon_{x\varphi} = -\frac{1}{2}\sum_{\alpha}\frac{\omega_{p\alpha}^2}{\omega^2}\int\frac{dp_\varphi}{\gamma}\frac{v_\varphi}{c}\left(\left[k_x c\left(\frac{1}{\Omega_\alpha^+} + \frac{1}{\Omega_\alpha^-}\right) - ik_r c\left(\left(\frac{1}{\Omega_\alpha^+} - \frac{1}{\Omega_\alpha^-}\right)\right]f_\alpha\right.\right.$$
$$\left.\left. + 2\omega\frac{u_\alpha^2}{c^2}\frac{\gamma}{\Omega_\alpha^0}\frac{\partial f_\alpha}{\partial_\gamma}\right);$$

$$\epsilon_{\varphi x} = -\frac{1}{2}\sum_{\alpha}\frac{\omega_{p\alpha}^2}{\omega^2}\int\frac{dp_\varphi}{\gamma}\frac{v_\varphi}{c}\left(\left[(k_x c - 2k_\varphi u_\alpha)\left(\frac{1}{\Omega_\alpha^+} + \frac{1}{\Omega_\alpha^-}\right)\right.\right.$$
$$\left.\left. + ik_r c\left(\frac{1}{\Omega_\alpha^+} - \frac{1}{\Omega_\alpha^-}\right)\right]f_\alpha + 2\omega\frac{u_\alpha^2}{c^2}\frac{\gamma}{\Omega_\alpha^0}\frac{\partial f_\alpha}{\partial_\gamma};\right.$$

$$\epsilon_{r\varphi} = -\frac{1}{2}\sum_{\alpha}\frac{\omega_{p\alpha}^2}{\omega^2 c}\int\frac{dp_\varphi}{\gamma}v_\varphi\left\{\left[k_r c\left(\frac{1}{\Omega_\alpha^+} + \frac{1}{\Omega_\alpha^-}\right) - i(k_x c - 2k_\varphi u_\alpha)\right.\right.$$
$$\left.\left.\left(\frac{1}{-\Omega_\alpha^-} - \frac{1}{\Omega_\alpha^+}\right)\right]f_\alpha\right\};$$

$$\epsilon_{\varphi r} = -\frac{1}{2}\sum_{\alpha}\frac{\omega_{p\alpha}^2}{\omega^2 c}\int\frac{dp_\varphi}{\gamma}v_\varphi\left\{\left[k_r c\left(\frac{1}{\Omega_\alpha^+} + \frac{1}{\Omega_\alpha^-}\right) + i(k_x c - 2k_\varphi u_\alpha)\right.\right.$$
$$\left.\left.\left(\frac{1}{-\Omega_\alpha^-} - \frac{1}{\Omega_\alpha^+}\right)\right]f_\alpha\right\} \qquad (1)$$

$\Omega_\alpha^\pm = \omega - k_\varphi v_\varphi - k_x u_\alpha \pm \omega_{B_\alpha}\gamma^{-1}$; $\Omega^0{}_\alpha = \omega - k_\varphi v_\varphi - k_x u_\alpha$; $\omega_{p\alpha}^2 = \frac{4\pi e^2}{m}n_{p\alpha}$; $f_\alpha = \int dp_\perp p F_\alpha$; F is the particle distribution function; $p_\perp = \sqrt{p_r^2 + (p_x - u\gamma/c)^2}$; the sum over $\alpha$ is taken over the particle species and the integration from—$\infty$to $+\infty$; $v_\varphi$—is the particle velocity along the field line, $p_\varphi = v_\varphi \cdot \gamma/c$, $u\alpha = \frac{v_\varphi P_\varphi}{\sqrt{w_{B\alpha}R_B}}$ C is the particle drift velocity caused by the weak inhomogeneity of the magnetic field and directed along the x-axis for positrons (hereafter for the values without the subscript $\alpha$ the sign of the charge is assumed to be positive). For the particles of the bulk of plasma, the drift velocity u tends to be zero. Hence, if one assumes $u_\alpha = 0$, then equation (1) reduces to the standard form which we designate as $\epsilon_{ij}^p$.

In the electron-positron plasma described by $\epsilon_{ij}^p$, there exists two types of waves: the purely transversal electromagnetic t-wave with an electric vector $\vec{E}^t$ directed transversely to the plane where the magnetic force line lies, and the potential-nonpotential lt-wave with the electric field $\vec{E}^{lt}$ in the plane of $\vec{k}$ and $\vec{B}_0$. The spectra of the waves are as follows:

$$w^t = kc\left(1 - \frac{1}{4}\frac{\omega_p^2}{\omega_B^2}\frac{1}{\gamma_p^3}\right) \equiv kc(1-\delta) \tag{2}$$

$$\omega^{lt} = k_\varphi C\left(1 - \frac{k_\perp^2 c^2}{16\omega_p^2\gamma_p}\right) \tag{3}$$

note that formulae (2) and (3) are obtained for $\omega < \omega_B\gamma_p$, and expression (3) describes only the low-frequency branch of the lt-waves. The phase velocity of the high-frequency branch exceeds the speed of light and cannot interact with particles. The pulsar emission mechanisms provide information on wave excitation and propagation in the magnetosphere plasma along with their emergence in vacuum. The electromagnetic waves leave the magnetosphere without transformation.

## THE PULSE RADIATION MECHANISMS

Sagdeev and Shafranov (1960) were the first to point out the existence of the cyclotron instability in plasma with the anisotropic temperature. Let us investigate the possibility of t-wave generation on the cyclotron resonance:

$$\omega - k_\varphi c - k_x u_\alpha \pm \frac{\omega_{B\alpha}}{\gamma} = 0 \tag{4}$$

Substituting formula (2) and the expressions $k = k\varphi(1 + k_\perp{}^2/2k_\varphi{}^2)$ and $v_\varphi = c(1 - 1/2\gamma^2 - u^2/2c^2)$ in formula (4) one obtains:

$$\frac{k_r^2}{2k_\varphi^2} + \frac{1}{2\gamma_{res}^2} + \frac{1}{2}\left(\frac{k_x}{k_\varphi} - \frac{u_\alpha}{c}\right)^2 - \delta = \mp\frac{\omega_B}{k_\varphi c\gamma_{res}} \tag{5}$$

As it was shown by Machabeli and Usov (1979) the t-waves are being excited in the pulsar magnetosphere only at the anomalous Doppler-effect (upper sign of the equation (5)). The lower sign of equation (5) corresponds to wave damping. In the plasma rest frame these conditions are fulfilled for the velocities satisfying the condition (Lominadze *et al.* 1986):

$$\frac{v}{C} = \frac{\omega_o k_\varphi v_\varphi \pm |\omega_B| \sqrt{\omega_B^2 + k_\varphi^2 v_\varphi^2 - \omega_o^2}}{\omega_B^2 + k_\varphi^2 v_\varphi^2} \tag{6}$$

It is obvious that for the whole range of frequencies $\omega_0 = kc < \omega_B\gamma_p$ damping (lower sign in formula (6)) can occur only on particles having negative velocities, and for the distribution function given on Figure 1, at $\omega_0 \ll \omega_B\gamma_p$ it is absent. In the case when the resonance condition $\omega_0 - k_\varphi v_\varphi - k_x u - \omega_B/\gamma = 0$ is nevertheless fulfilled, waves are strongly

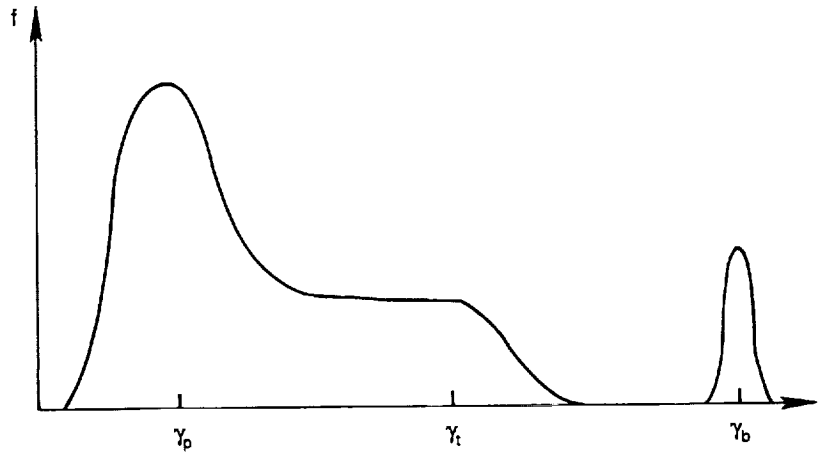


FIGURE 1 The particle distribution function in the pulsar magnetosphere.

damped and cannot reach an observer. Hence, for energetic particles only the resonance at the anomalous Doppler-effect (upper sign of equation (5)) can be satisfied. Assuming that the electron and positron distribution functions are about the same, and considering the perturbations propagating nearly along the magnetic field in the $k_\perp v_\perp/\omega_B \ll 1$ approximation one obtains the following dispersion relation for t-waves:

$$\frac{k^2c^2}{\omega^2} = \epsilon_{xx} \tag{7}$$

For the development of the cyclotron instability it is necessary to satisfy the following conditions (Machabeli and Usov 1979):

1. The distance R between the star and the instability development region should be less than the pulsar light cylinder radius:

$$R = R_o \left(\frac{\gamma_p}{\gamma_b}\right)^{\frac{1}{3}} \left(\frac{\omega_{Bo}}{\omega_{po}}\right)^{\frac{2}{3}} \leq \frac{c}{\Omega} \tag{8}$$

2. The characteristic time $\tau_c$ of the instability development should be less than the time of the plasma escape from the light cylinder $\tau_e$.

Using the definition of the $n_b$ (Goldreich and Julian 1969) and that $n_p \simeq n_b\gamma_b/\gamma_p$ the condition (8) can be rewritten in the following way:

$$\gamma_p \leq 5 \cdot 10^{-3}\gamma_b^{\frac{2}{3}} \left(\frac{B_o}{10^{12}G}\right)^{-\frac{1}{3}} \left(\frac{P}{1s}\right)^{\frac{2}{3}} \tag{9}$$

In the case of the "typical" pulsar ($B_0 \simeq 10^{12}$G, P $\simeq$ 1s) for the beam particles we have the following limitation on the average Lorentz-factor of the particles of the bulk of plasma $\gamma_p \leq 50$; as for the particles of the tail the limitation is $\gamma_p \leq 10$.

The value of $\gamma_p$ and consequently the satisfaction of the condition (8) (or its equivalent (9)) depends on the configuration of the external magnetic field of the pulsar. As it was shown earlier (Lominadze *et al.* 1983) in the dipole magnetic field the cyclotron instability can develop only in the magnetospheres of the rapidly rotating pulsars (like PSR 0531+21 and PSR 0833-45). Besides the energy flow carried away by the particles from the pulsar should be of the same order as the energy released when the rotation of the pulsar slows down. The difficulty for the pulsars with a dipole magnetic field to satisfy the condition (9) is due to a very large value of $\gamma_p \geq 10^2 \div 10^3$ (Cheng and Ruderman 1980). On the other hand it seems more probable that the magnetic field of a neutron star near the stellar surface differs greatly from the dipole one, and the curvature of the field lines $R_B$ is on the order of $R_0$ (Ruderman and Sutherland 1975). Observational data on pulsars (Davies *et al.* 1984) and accreting neutron stars in the binary systems, such as Her-X1 (Pines 1980) testify to the above assumption. In the magnetic field with $R_B \sim R_0$ one obtains $\gamma_p < 10$. Consequently in the magnetic field of this configuration the region of the cyclotron instability development may be inside the light cylinder both for the beam of the primary particles and for the high-energy tail of the plasma particles.

The resonance condition (5)(the upper sign) is satisfied only if

$$\delta \gg \frac{1}{2\gamma_{res}^2} \tag{10}$$

The latter is fulfilled at $k_\perp \to 0$. Thus the waves are being excited in very narrow angles. The growth rate of cyclotron instability is

$$\Gamma = \pi \frac{\omega_{pres}^2}{\omega_o \gamma_T} \text{ if } \frac{1}{2}\frac{u^2}{c^2} \ll \delta \tag{11}$$

and

$$\Gamma = \pi \frac{\omega_{pres}^2 u^2}{2\omega_o \gamma_T c^2} \cdot \frac{1}{\delta} \tag{12}$$

at that the resonant frequency is defined as

$$\omega_o \approx \frac{\omega_B}{\delta \gamma_{res}} \tag{13}$$

($\gamma_T$ and $\gamma_{res}$ are the thermal spread and the average Lorentz-factor of the resonant particles respectively). As for the damping of t-waves, it occurs

on the particles of the bulk of plasma and the corresponding decrement is given by:

$$\Gamma' = -\pi \frac{\omega_p^2}{2\omega_o \omega_B} \frac{1}{\gamma_p^2} \tag{14}$$

the frequency of damped waves is $\omega_0 \approx 2\gamma_p \omega_B$. However, as it was already mentioned above, the damping for the distribution function given on Figure 1 and at $\omega_0 \ll \gamma_p \omega_B$ is absent.

Note that the expressions (11) and (12) are valid only if the resonance width is more than the growth rate (the so-called condition of kinetic approximation). This leads to the following limitation on

$$\Gamma \ll \omega_B \frac{\gamma_T}{\gamma_{res}^2} \tag{15}$$

From the expressions (11), (12), and (15) it follows that for the particles of the tail, the excitation of t-waves is possible at the distances $R \simeq 10^8$ cm from the center of the pulsar. As for the particles of the primary beam the distance R is: $R \simeq 10^9$ cm.

The interaction of the excited t-waves with the beam particles brings about the quasilinear diffusion of particles in the momentum space. As a result the beam particles acquire non-zero pitch-angles $\psi(\mathrm{tg}\psi = p_\perp/p_\varphi)$. Besides the particles in the inhomogeneous magnetic field B(R) drift with the velocity $u_x$. As it is shown by Machabeli and Usov (1979) in the central parts of the magnetosphere the value of $\psi \propto R_B{}^2$ and so it may exceed $u_x$. In this case the resonance condition $\omega_0 - k\varphi v\varphi - k_x u_x = 0$ due to the fact that $v\varphi/c = 1 - 1/2\gamma_{res}{}^2 - \psi^2/2 - u_x{}^2/2c^2$ will take the following form:

$$\left(\frac{k_\perp}{k_\varphi}\right)^2 + \psi^2 \simeq 2\delta \tag{16}$$

This type of Cherenkov resonance can be easily fulfilled. Let us consider the possibility of the t-wave excitation by the beam particles at a Cherenkov resonance (Kazbegi *et al.* 1987). Solving the imaginary part of the dispersion relation we obtain the growth rate of t-waves:

$$\frac{\Gamma}{\omega_o} = \frac{\pi}{2}\frac{\omega_b^2}{\omega_o^2}\left(\frac{k_\perp p_{\perp o} c}{2\omega_B}\right)^2 p_{\perp o}^2 \frac{\gamma b}{1 + p_{\perp o}^2}\left(\frac{\partial f_\varphi}{\partial p_\varphi}\right)_{p_\varphi = p_\varphi^{res}} \tag{17}$$

Or using the relativistic Maxwell distribution function of the beam we obtain:

$$\frac{\Gamma}{\omega_o} = \frac{\pi}{8}\left(\frac{\omega_b}{\omega_B}\right)^2 \frac{k_{\perp o}^2}{k^2} \gamma_B \left(\frac{\gamma_{\perp o}}{\gamma_T}\right)^2 \sim 10^{-5} \div 10^{-6} \tag{18}$$

The condition of the kinetic approximation yields to

$$\frac{\Gamma}{\omega_o} < \psi^2 \frac{\gamma_T}{\gamma_b} \sim 10^{-4} \div 10^{-5} \tag{19}$$

The comparison of the formulae (16) through (19) gives an estimate $\Gamma/w_0 \sim \delta^{4/3}$, which shows the possibility of the instability development on the distance $R \simeq 5 \cdot 10^8 \div 10^9$ cm.

The substitution of the lt-waves spectrum (3) in the Cherenkov resonance condition yields to

$$\psi^2 = \left(\frac{k_\perp}{k_\varphi}\right)^2 \frac{\omega_o^2}{8\omega_p^2 \gamma p} \tag{20}$$

And the growth rate of the lt-waves, when $\partial f_\varphi / \partial p_\varphi > 0$ is given by

$$\frac{\Gamma}{\omega_o} = \pi \left(\frac{\omega_b}{\omega_o}\right)^2 \gamma_b^3 \left(\frac{k_x}{k_\varphi}\right)^2 \frac{1}{\gamma_T^2 \gamma_{\perp o}^2} \tag{21}$$

The kinetic approximation condition is the same, i.e. (19). Note that when $k_\perp \to 0$ lt- and t-waves turn into one purely electromagnetic branch describing the perturbations with an arbitrary polarization.

According to its definition the drift velocity $u_x$ of the beam, with the motion of particles from a pulsar to the light cylinder increases ($u_x \propto (R/R_0)^a$, where $a \simeq 2$ depending on the dependence of $R_B$ from R). In the region where $u_x > \psi$ the Cherenkov resonance condition looks like

$$\delta - \frac{k_r^2}{k_\varphi^2} - \frac{1}{2}\left(\frac{u_x}{c} - \frac{k_x}{k_\varphi}\right)^2 = 0 \tag{22}$$

for the t-waves and

$$\frac{u_x^2}{c^2} = \frac{k_\perp^2}{k_\varphi^2} \frac{\omega_o^2}{8\omega_p^2 \gamma_p} + 2\frac{k_x}{k_\varphi}\frac{u_x}{c} \tag{23}$$

for the lt-waves. Making use of form. (1) one obtains the growth rate of the t- and lt-waves that equal each other in this case:

$$\frac{\Gamma}{\omega_o} \simeq \pi \frac{\omega_b^2}{\omega_o^2} \frac{\gamma_b}{\gamma_T^2} \left(\frac{k_r}{k_\perp}\right)^2 \tag{24}$$

The condition of the kinetic instability for both types of waves is given by:

$$\frac{\Gamma}{\omega_o} < \left(\frac{u_x}{c}\right)^2 \frac{\gamma_T}{\gamma_b} \tag{25}$$

It is clear that for the considered parameters of the typical pulsar the drift motion causes the t- and lt-wave excitation at the distances $R \simeq 10^9$ cm and in the radio frequency range $\omega_0 \simeq 10^8 \div 10^{10}$ Hz.

Therefore, the wave excitation in the plasma of the pulsar magnetosphere is possible. The first possibility originates when the cyclotron instability develops at the anomalous Doppler-effect resonance between the t-waves and both the particles of the beam and the high-energetic particles of the tail of the distribution function. The excited waves propagate along the magnetic force lines with $k_\perp \to 0$ producing the "core"-type emission. Note that this mechanism is most stable among the others and can be applied to the young pulsars. The development of the cyclotron instability is accompanied by the quasilinear diffusion of waves with the energetic particles. As a result, the beam particles obtain non-zero pitch angles ($p_\perp \neq 0$). At the same time and the same distance ($R \simeq 10^9$ cm for the typical pulsars) the particle drift motion caused by the magnetic field inhomogeneity becomes substantial. In this case the Cherenkov resonance can be satisfied in different parts of the magnetosphere: in the central part taking into account that $\psi > u_x/c$, and at the edges where $\psi < u_x/c$. In both cases t- and lt-waves are being excited. These mechanisms are valid mainly for pulsars with $P \geq 0.1$ s producing the "cone"-type radioemission.

## APPLICATION TO THE CENTRAL OBJECT IN SN1987A REMNANT

The detection of neutrinos from supernova 1987A suggests the formation of a neutron star in its interior. While the star left over from the supernova explosion is now obscured by the ejecta material, a pulsar can be detected within the next few years. The period of a new-born pulsar can be even $1 \div 2$ ms (Friedman *et al.* 1986; Ostriker 1987). But such values of periods require very high luminosities of a pulsar $L \simeq 10^{40} \div 10^{41}$ e/s. By this moment one can put an upper limit on the possible luminosity $L \leq 10^{38}$ e/s. Hence the period increases too. The recently discovered radioemission from SN (Chini *et al.* 1988) suggests the following parameters of a pulsar: $P = 43$ ms and $L = 10^{38}$ e/s (Salvati *et al.* 1989). At the same time it is supposed that pulsars are born having sufficiently long periods $P \sim 0.1$s and even more (Narayan 1987). Let us assume that the new-born pulsar in SN1987A has the period of the order of $P \sim 0.05 \div 0.1$s. Our task is now to predict the range of frequencies in which the pulsar having these periods will emit.

One should know the plasma parameters to apply the results of the preceding chapter to PSR in SN1987A. Assume the magnetic field at the star surface $B_0 \simeq 10^{12}$G. Then the Goldreich-Julian density is $n_b \approx 7 \cdot 10^{11} \div 2 \cdot 10^{12}$ cm. The "tale" consists of the particles of the second generation

(Arons 1981; Tademaru 1973). The estimate of "tale" particles Lorentz-factor is $\gamma_t \sim 10^5 \div 10^6$ (Lominadze *et al.* 1983). Substituting the obtained parameters in the formulae (11), (13), and (15), one finds that the instability develops in the vicinity of the light cylinder at the distances - $R \approx 2 \cdot 10^8$ cm for P = 0.05s and $R \approx 5 \cdot 10^8$ cm for P = 0.1s. At these distances as it follows from eq.(14) the following frequencies are being excited $\nu_{cycl}$(P = 0.05s)$\approx 10^{14} \div 10^{15}$ Hz and $\nu_{cycl}$(P = 0.1s) $\approx 2 \cdot 10^{11} \div 10^{13}$ Hz).

The development of the cyclotron instability is accompanied by the quasilinear diffusion of the particles in the momentum space both along and across the magnetic field. The particles obtain non-zero pitch-angles of the order of $\psi \approx 10^{-2} \div 10^{-3}$ (Machabeli and Usov 1979). In this case the inequality $\psi < 1/\gamma_t$ is fulfilled for the "tale" particles and the synchrotron emission peaks at the frequencies:

$$\nu_{syn}^{max} = \frac{\omega_b}{\pi} \psi \gamma_t^2 \simeq 5 \cdot 10^{21} (P = 0.05s) \div 10^{19} (P = 0.1s)$$

contributing to X-ray radiation of SN1987A that is thought to be mainly from the decay of radioactive $Co^{56}$ (Dotani *et al.* 1987; Sunyaev 1987).

Thus if the pulsar in SN1987A is formed having the considered parameters it should produce the energetic radiation having much in common with Crab, Vela-pulsars and PSR 0540-69, and PSR 1509-58. The range of emitted frequencies generated at cyclotron instability decrease with the pulsar slow-down and if $P \geq 0.1 \div 0.2$s the frequency range will lower to radio frequencies and soft X-rays or UV (for radiation produced by synchrotron mechanism), as it is in PSR 1509-58. And conversely, if the period of the new-born pulsar is in the millisecond range (Kristian *et al.* 1989) the corresponding frequencies are $\nu_{cycl} \simeq 10^{17}$ Hz and $\nu_{syn} \simeq 10^{24} \div 10^{25}$ Hz (Kazbegi *et al.* 1988).

At the same time the luminosity of the pulsar in SN1987A should not resemble that of Crab, Vela, or PSR 0540-69, being of the order of $L_{opt} \simeq 10^{30} \div 10^{32}$ e/s and $L_x \simeq 10^{35} \div 10^{36}$ e/s.

Despite the optically thick shell the pulsar emission should emerge from the interior of SN1987A. In our opinion (Kazbegi and Machabeli 1990) the detected radioemission from the shell with the wavelength $\lambda \approx$ 1.3 mm (Chini 1988) is a result of hydrogen atom recombination emission at the transition from the 32 to 31 level. The photoexcitation exceeds the pulsar rotation period. In the time $10^9 \div 5 \cdot 10^9$s after the explosion the shell should become transparent enough to detect pulsed radioemission.

Thus we predict the range of frequencies in which the new-born pulsar in SN1987A with P = 0.05 ÷ 0.1s should originate. Applications to the other periods can be easily done.

Eventually some conclusions can be drawn. The offered theory of pulsar radiation is based on the investigation of all plasma instabilities able

to develop in the electron-positron plasma of pulsar magnetospheres. As it was shown here and previously (Kazbegi *et al.* 1989a) the only plasma instabilities are: the cyclotron developing at the anomalous Doppler-effect resonance; and Cherenkov with the consideration of the particle transversal momenta caused by the quasilinear diffusion in one case and by the drift motion in the other one. These mechanisms can produce the well-known pulse profiles (see e.g. Rankin 1983): "core" (caused by the cyclotron mechanism) and "cone" (by the other two). On the basis of this model virtually all observational features listed in the papers by Rankin (1986) and Taylor and Stinebring (1988) can be explained: mode changing, pulse nulling and the presence of the orthogonal modes (Kazbegi *et al.* 1989b); the existence and behavior of the circular polarization (Kazbegi *et al.* 1990a); and subpulse drift (Kazbegi *et al.* 1990b). The analysis of the emission mechanisms' dependence on the pulsar rotation period P and its application to the expected pulsar in the interior of the SN1987A shows that it should be a source of a high-frequency radiation.

## REFERENCES


Arons, J. 1981. Proc. Varenna Summer School and Workshop on Plasma Astrophysics, ESA 273.

Arons, J., and E.T. Scharlemann. 1979. Astrophys. J. 231:854.

Cheng, A.F., and M.A. Ruderman. 1980. Astrophys. J. 235: 576.

Chini, R. 1988. LAU Circ. 4652.

Davies, J.G., A.G. Lyne, F.G. Smith, V.A. Izvekova, A.D. Kuzmin, Yu. P. Shitov. 1984. Mon. Not. R. astr. Soc. 211: 57.

Dotani, T. *et al.* 1987. Nature. 330: 230.

Friedman, J.L., J.R. Ipser, and L. Parker. 1986. Astrophys. J. 304: 115.

Ginzburg, V.L. and V.V. Zheleznyakov. 1975. Ann. Rev. Astron. Astrophys. 13: 511.

Goldreich, P. and W. Julian. 1969. Astrophy. J. 157: 869.

Kazbegi, A.Z., G.Z. Machabeli, and G.I. Melikidze. 1987. Austral. J. Phys. 40: 755.

Kazbegi, A.Z., G.Z. Machabeli, G.I. Melikidze. 1988. Physics of Neutron Stars. Structure and Evolution. Leningrad. 94.

Kazbegi, A.Z., G.Z. Machabeli, G.I. Melikidze, and V.V. Usov. 1989a. Proc. Joint Varenna-Abastumani International School and Workshop on Plasma Astrophysics, ESA SP-285. 1: 271.

Kazbegi, A.Z., G.Z. Machabeli, and G.i. Melikidze. 1989b. Proc. Joint Varenna-Abastumani International School and Workshop on Plasma Astrophysics, ESA SP-285. 1: 277.

Kazbegi, A.Z., and G.Z. Machabeli. 1990. Submitted to Nature.

Kazbegi, A.Z., G.Z. Machabeli, and G.I. Melikidze. 1990a. Submitted to Mon. Not. R. astr. Soc.

Kazbegi, A.Z., G.Z. Machabeli, and G.I. Melikidze. 1990b. In preparation.

Kristian, J.A. *et al.* 1989. Nature. 338: 234.

Lominadze, J.G., G.Z. Machabeli, G.I. Melikidze, and A.D. Pataraya. 1986. Sov. J. Plasma Phys. 12: 712.

Machabeli, G.Z., V.V. Usov. 1979. Sov. Astron. Lett. 5: 445.

Narayan, R. 1987. Astrophys. J. 319: 162.

Ostriker, J.P. 1987. Nature. 327: 287.

Pines, D. 1980. Usp. Fiz. Nauk. 131: 479.

Rankin, J.M. 1983. Astrophys. J. 274: 333.

Rankin, J.M. 1986. Astrophys. J. 301: 901.

Ruderman, M.A., and P.G. Sutherland. 1975. Astrophy. J. 196: 51.
Sagdeev, R.Z., and P.G. Shafronov. 1960. ZETF. 39: 181.
Salvati, M., F. Pacini, E. Oliva, and R. Bandiera. 1989. Astron. Astrophys. 208: L5.
Sturrock, P.A. 1971. Astrophys. J. 164: 529.
Sunyaev, R.A., *et al.* 1987. Nature. 330: 227.
Tademaru, E. 1973. Astrophys. J. 183: 625.
Taylor, J.H., and D.R. Stinebring. 1988. Ann. Rev. Astr. Astrophys. 24: 285.

# Observing SN 1987A with the International Ultraviolet Explorer

ROBERT P. KIRSHNER
Harvard-Smithsonian Center for Astrophysics

## INTRODUCTION

The International Ultraviolet Explorer (IUE) satellite has played a leading role in elucidating the nature of SN 1987A, providing a unique ultraviolet perspective on the brightest supernova since 1604. One fundamental property of the IUE project proved essential: it is a satellite whose program can be rapidly changed to take advantage of scientific opportunities. On both sides of the Atlantic, there was a target-of-opportunity proposal in place, so that an orderly, though very exciting, series of observations was carried out starting within 4 hours of the first report, on February 24, 1987, as recounted by de Vorken (1988) and by Kirshner (1988).

IUE observations of SN 1987A began promptly after the discovery and have been frequent through 1988 and 1989, using the FES for photometry, low dispersion spectra for the supernova spectrum as described in the next section, high dispersion observations for the interstellar medium when the supernova was bright (see below), and for circumstellar gas surrounding the supernova as the initial event faded (see below). The UV data have been especially useful in determining which star exploded, assessing the ionizing pulse produced as the shock hit the surface of the star, and in constraining the stellar evolution that preceded the explosion through observations of a circumstellar shell. These discoveries are placed in a broader context by the review of Arnett *et al.* (1989) and earlier reports on the ultraviolet data are summarized by Kirshner (1988). The ultraviolet spectrum of the supernova itself is produced by the superposition of many lines of Fe, Co, and other elements in the stellar photosphere, and it has remained opaque

long after the infrared and optical have changed to emission-line spectra. High-dispersion IUE observations provide a detailed look at the ionization structure of the line-of-sight to the supernova, both in our Galaxy and in the LMC. Future observations will include a UV observation of the light echo, monitoring the decay of the circumstellar emission, and perhaps a glimpse into the enriched material that was formerly the interior of Sanduleak -69 202.

Supernova 1987A in the Large Magellanic Cloud has moved the subject of supernovae from plausible argument to observational demonstration in a number of areas and the IUE observations have helped in essential ways. While the supernova was the first visible to the unaided eye since Kepler's 1604 supernova, retinal observations have not proved the most novel. Instead, the advances in technology, including geosynchronous satellites, have provided the data for real insight. The Large Magellanic Cloud is ideally placed for observation: circumpolar for the outstanding observatories of the Southern hemisphere, it is also near the ecliptic pole, facilitating observations with the IUE at almost any time of the year. The observations gathered over the entire spectrum from radio to gamma rays and the direct detection of neutrinos from SN 1987A have helped sketch the most complete picture of the life and death of a massive star.

A combination of stellar evolution theory and astronomical observation supports the picture that one class of supernova explosions (Type II) results from massive stars, which release $10^{53}$ ergs of neutrinos as their iron cores collapse to become neutron stars (Woosley and Weaver 1986). In a remarkable leap of scientific intuition, the essence of this picture was sketched by Baade and Zwicky (1933), shortly after the discovery of the neutron. Testing this picture for SN 1987A required neutrino detectors, which caught enough of the neutrinos to make a convincing case that we understand the binding energy of a neutron star, as well as the temperature and duration of the neutrino emission (Bahcall 1989). The neutrino observations provide a fiducial point: the moment of core collapse at 1987 February 23.316. One interesting sidelight (see section Future Observations of SN 1987A) is that UV observations of a light echo may provide a way to observe the flux emitted from the surface of the star in the hours between the arrival of the shock and the discovery of the supernova by Ian Shelton on February 24.23 (Madore and Kunkel 1987). A key part of this picture was the identification of the star which exploded. As described in the section "Circumstellar Matters," IUE provided essential data to identify directly the massive progenitor. This is the first time that a pre-supernova star has been observed, and the star is Sanduleak -69 202, a B3 I star of about 20 solar masses. Many of the unique features of SN 1987A as observed in the ultraviolet trace their origin to the explosion of a blue supergiant, rather than the red supergiants favored for most extragalactic

SN II's. IUE observations of a nitrogen-rich circumstellar shell help trace the stellar evolution of SK -69 202 into the recent past, as described in the section on the Ultraviolet Echo.

Supernovae are essential players in the chemical enrichment of the universe. When the star destroys itself, the accumulated products of stellar energy generation such as helium, nitrogen, carbon, oxygen, calcium and silicon are dispersed into the interstellar gas along with the elements synthesized in the explosion, such as the radioactive isotopes of the iron peak. The chemistry of the stellar interior can now be probed by infrared observations (Rank *et al.* 1988), and the gamma ray detections (Matz *et al.* 1988) provide strong proof that radioactive $^{56}$Ni is produced in the explosion. The indirect effects of the energy release are seen in the light curve, measured with the Fine Error Sensor on IUE, as presented in in the first section, but the direct measurement of the interior composition through ultraviolet lines will occur only after the opaque atmosphere turns transparent. Clues to a possible neutron star remnant may also be embedded in the light curve for SN 1987A, but the resolution of these tantalizing questions lies in the future.

## OBSERVATIONS

The first IUE spectra of SN1987A were taken from Goddard on the afternoon of Tuesday, February 24, about 4 hours after the report from the Central Bureau for Astronomical Telegrams. The first frame of 15 seconds duration was heavily overexposed, and good low dispersion spectra were eventually obtained with 1.5 second exposures. The initial spectra were unlike the other IUE spectra of supernovae (Blair and Panagia 1987, Benvenuti *et al.* 1982), and changed very rapidly in the first few days of observation. Interestingly, by February 26 the UV spectrum of SN 1987A resembled the spectrum of a Type I supernova (SN I) as seen in the ultraviolet, while the combined optical and UV spectrum showed that the supernova had distinct hydrogen Balmer lines: the identifying criterion for SN II. The solution to this paradox is straightforward: in SN I, as shown by Branch and Venkatakrishna (1986) and in the atmosphere of the blue supergiant SK -69 202, as shown by Lucy (1987) the strong blended lines of Fe II and Co II dominate the opacity in the ultraviolet region of interest. In SN II, like SN 1979C, the analysis of Fransson *et al.* (1984) shows that the slow, dense wind of a red supergiant plays a key role in determining the UV spectrum.

The conspicuous P-Cygni lines in the UV and optical indicated an initial expansion velocity near 30,000 km/sec in the first hours of observation and a temperature near 14,000 K. Model atmospheres for SN 1987A have been calculated by Eastman and Kirshner (1989) which provide a good

understanding of the effects of scattering and spherical geometry in the expanding atmosphere. These models allow the distance to the LMC to be determined by the Expanding Photosphere Method (Kirshner and Kwan 1974): the result of 50 ± 6 kpc is in good accord with the distances found from Cepheids and from RR Lyrae stars (Walker 1987; Walker and Mack 1988), and raises the prospect of using SN II as an important tool in establishing the extragalactic distance scale.

The apparent velocity declined rapidly as the fastest-moving layers turned transparent, and the temperature declined rapidly as the supernova atmosphere expanded and cooled adiabatically. The effect on the ultraviolet flux was profound: both the cooling and the onset of powerful line blanketing combined to reduce the UV flux in the SWP range by a factor of 1,000 in the first three days. The level flux at later times is due to the presence of the two B stars near SK -69 202 which are in the IUE aperture.

The plummeting UV seen on Feb 24 is presumably the cooling tail of a much hotter photosphere which must have been present on Feb 23, when the shock from the stellar interior first reached the surface of Sk -69 202 about 2 hours after core collapse. Theoretical calculations show that the temperature might have reached the range of 2-5 $\times$ $10^6$ K for a brief time on Feb 23. This ultraviolet flash is the source of photoionization of the circumstellar matter, as described in the section on circumstellar matters, where ionization up to N V is observed. Another way to detect the ultraviolet flash emitted before the supernova was discovered is through its UV echo from interstellar dust, as described in the section on the Ultraviolet Echo. Empirical evidence that the surface of the Sanduleak star was very hot comes from the photograph of the LMC taken by McNaught (1987) on February 23.443, which showed that SN 1987A was already at about mag 6. The product of velocity and age requires a temperature of order 100,000 K to produce the observed flux. To press the UV observations back to the earliest possible moment, we have begun to examine the badly over-exposed images taken in the first attempts to get IUE spectra of SN 1987A. In the depths of the absorption lines, and in the regions of the spectrum where IUE has the least sensitivity, some reliable measurements may be recovered which will help trace the arrival of the shock at the surface of the Sanduleak star.

Following the dramatic changes of the first days, the IUE spectrum of SN 1987A has remained remarkably constant. There are changes in the UV flux through this period, but the spectrum, set by the atomic physics of photospheric iron and cobalt shows only subtle variations. Although the optical spectrum is now dominated by strong emission lines which arise from material that was originally far below the photosphere of the star, the UV photosphere has remained opaque. Although there have been predictions of a "UV Renaissance" when the ultraviolet finally turns

transparent (McCray *et al.* 1987), Figure 1 indicates that we must first endure the ultraviolet Dark Ages of 1989. To obtain Figure 1, the LWP spectra have been integrated over broad wavelength intervals. Ultraviolet observations of the material from the stellar interior should eventually prove very helpful in determining the mass of carbon, magnesium, and silicon produced by SN 1987A, but that time has not yet arrived. These elements are important in comparing the observed composition for SN 1987A with the theoretical results for massive star evolution, and they are difficult to observe at optical wavelengths.

Measurements from the Fine Error Sensor have proved surprisingly accurate and useful in monitoring the flux from SN 1987A. Even though the FES was never intended as an accurate photometer, we have found that careful attention to calibration by a standard star during the same observing session produces a marked decrease in the random errors of FES measurements. While the carefully integrated bolometric measures of the Cerro Tololo workers (Suntzeff *et al.* 1988) and of the South African group (Whitelock 1988) are the primary data for comparing the radiative output of SN 1987A with models, the FES data are instructive, illustrating every major feature of the bolometric light curve, as shown in Figure 2. The familiar features of the rise to maximum in late May 1987, the long exponential tail from age 110 days to 300 days, and the subsequent drop below the extrapolated output of $^{56}$Co are all illustrated in the FES light curve. The most recent data show that the steepening decline in the FES light curve has abated. One possible interpretation is that a constant source at a luminosity of $5 \times 10^{37}$ erg/sec is now contributing to the SN 1987A light curve. Whether this is related to the putative pulsar (Kristian *et al.* 1989) or possible accretion onto the neutron star (Chevalier 1989) remains to be seen. The FES measurements will continue, unaffected by weather or seeing and never vulnerable to the errors that accrue at large hour angles! Ultimately, contamination from the neighboring stars will become a serious problem, and only the superb images of HST will permit a light curve for SN 1987A into the 1990's.

The UV light curves of Figure 1 show a distinctly different behavior. While they share the rise to maximum seen in the FES data, they did not experience the long exponential decline. Evidently, the small fraction of the energy coming out in the UV rose during that period, presumably as a result of decreasing line blanketing. The future of the UV light curve is hard to predict, but it may show a dramatic change when the spectrum changes to emission lines.

## THE INTERSTELLAR MEDIUM TOWARDS SN 1987A

Although SN 1987A reached its maximum bolometric luminosity in

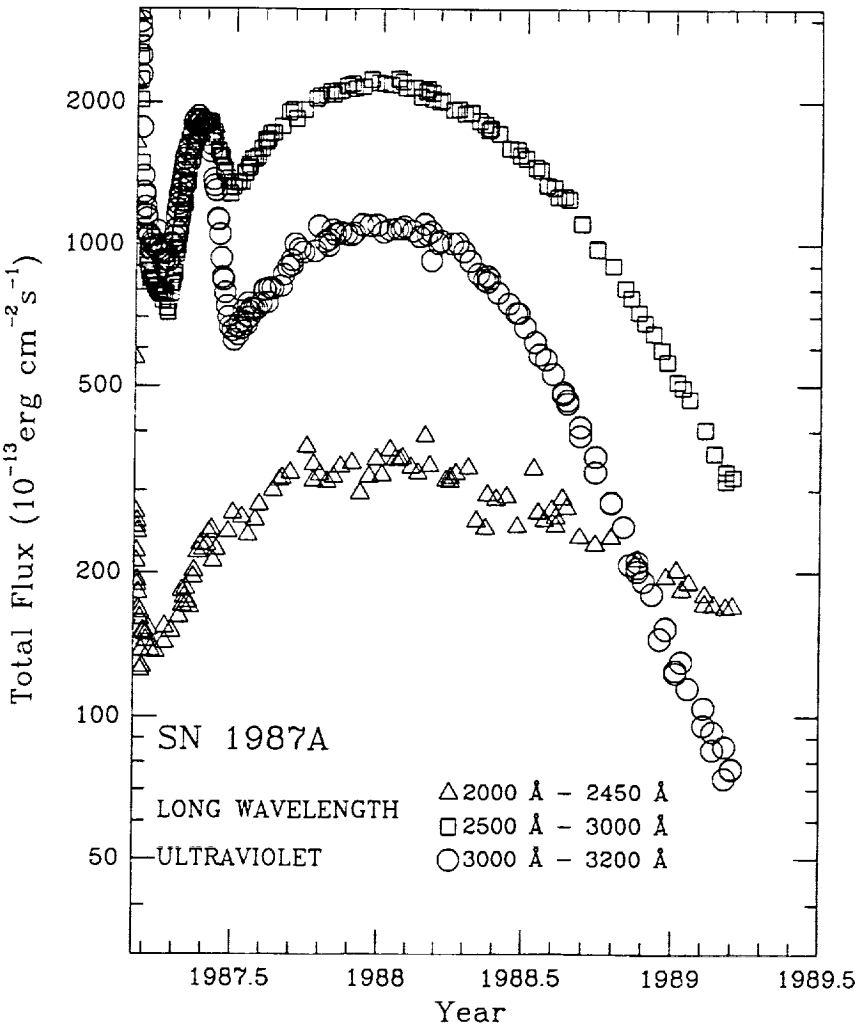


FIGURE 1 The long wavelength light curve of SN 1987A as observed with IUE.

late May 1987, the rapid decline in the UV flux made the fruitful time for high resolutions observations very brief. During February 24 and 25, IUE high resolution spectra were obtained which provided the best signal-to-noise for study of the interstellar gas from Earth to the Sanduleak star. The brightness of the supernova as a background source allowed much shorter exposures than previous studies of the ISM toward the LMC were compelled to use, and the resulting particle background in the data was much lower. Because the time span for obtaining these exquisite data was

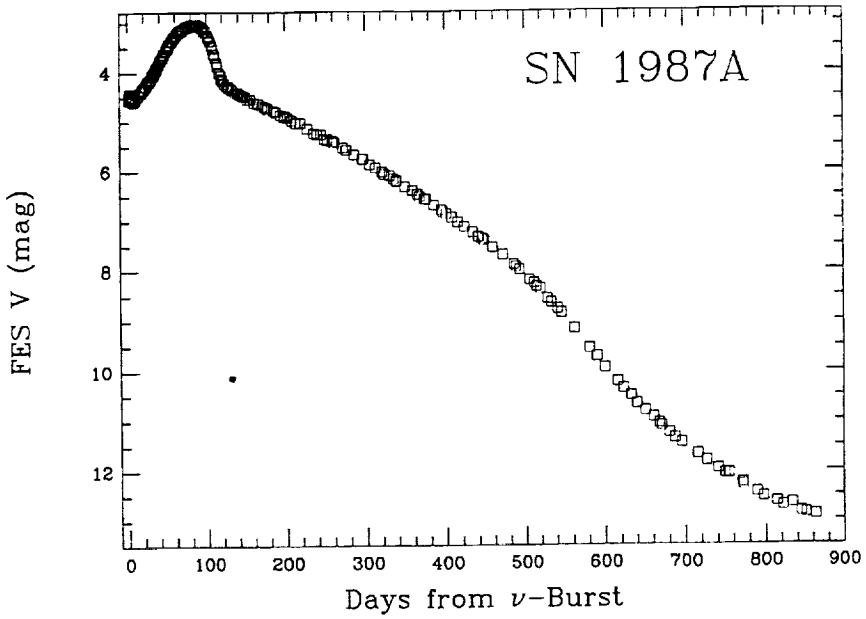


FIGURE 2 An optical light curve for SN 1987A as observed with the Fine Error Sensor on IUE.

short, there was little opportunity to study the time-dependent effects of the ionizing flash from SN 1987A, but the very high quality of the data that were obtained not only allowed them to confirm kinematic results obtained at higher resolution from the ground but to extend them by providing the chemical composition of the intervening absorbers.

Several velocity components were detected in a wide range of ionization stages ranging from neutral gas to triply ionized carbon (de Boer *et al.* 1987, Dupree *et al.* 1987, Blades *et al.* 1988a,b, Savage *et al.* 1989). The observed UV absorption components to SN 1987A have a velocity distribution which is similar to that observed on the lines of sight to other stars in the LMC (e.g., Savage and de Boer 1979; Savage 1986) and which agrees with the main optical absorption systems found by Andreani *et al.* (1987) in the spectrum of SN 1987A.

The absorption features over the velocity range from 0 to +300 km/sec arise in the disk and halo of our Galaxy and in the LMC. While it is not controversial to assign the absorptions with $v > 200$ km/sec to gas in the LMC and those with $v < 70$ km/sec to our Galaxy, intermediate velocities require more discussion. An abundance analysis of the intermediate velocity components at 129 and 171 km/sec by Blades *et al.* (1988a) shows that they are not intergalactic clouds, but belong to the LMC. These clouds may

have their origins in gas that is stripped by tidal interactions or may arise from wind-driven shells or supernova remnants in the LMC.

The absence of N V absorption in the spectrum of SN 1987A has been used by Fransson *et al.* (1987) to constrain the luminosity of the UV flash. From the observed upper limit to N V absorption, they derived an upper limit to the N V column density of $3 \times 10^{14}$ cm$^{-2}$ and inferred a limit to the number of ionizing photons $S < 1.6 \times 10^{57}/n^2$ (where n is the ambient density) for a temperature $T_{eff} = 5 \times 10^5$ K. Comparison with models for the shock arriving at the surface of a star (Klein and Chevalier 1978) shows that a red supergiant would produce too much ionization, but a blue supergiant, such as SK -69 202 would be a good match to the observational constraint.

## CIRCUMSTELLAR MATTERS

Blue supergiants like SK -69 202 often have low density, high velocity stellar winds, but IUE observations of SN 1987A show that this star had a dense circumstellar shell that resulted from an interesting stellar history. The weak radio emission from SN 1987A (Turtle *et al.* 1987) was interpreted (Chevalier and Fransson 1987) as arising from a shock in the low density blue supergiant wind of SK -69 202. After 1987 May 24, the short wavelength IUE spectra began to show evidence for narrow emission lines, as shown in Figure 3. Here the flux from the two neighboring stars as observed in March 1987 has been subtracted from the subsequent spectra.

The observed lines include He II, C III, N III, N IV, N V and O III, and they increased in strength with time. The observed velocities are low, and the velocity widths of the lines are unresolved at the low dispersion, implying velocities less than 1,000 km/sec. All of these clues point toward a circumstellar origin for the emission lines. First, the fact that we can see the emission, while the supernova photosphere is opaque to the UV implies that the source of the emission is outside the expanding star. Second, the low velocities do not correspond to the debris, where the characteristic velocities are a few thousand km/sec. The great strength of the nitrogen lines is consistent with the CNO-enriched composition of material that results from a massive star's mass loss (Chevalier 1987; Fransson *et al.* 1989) and constrains the history of SK -69 202.

The excitation of this circumstellar shell results from the UV flash that took place when the shock traversing the Sanduleak star hit the surface. This initial pulse of energy would have been very hot ($T > 10^5$ K) and brief (<1 hour). Since the supernova was not discovered on the day of the neutrino burst, but the day after, the declining UV seen on 24 February was just the tail of this violent UV flash.

The observed UV flux from the circumstellar shell increased with time

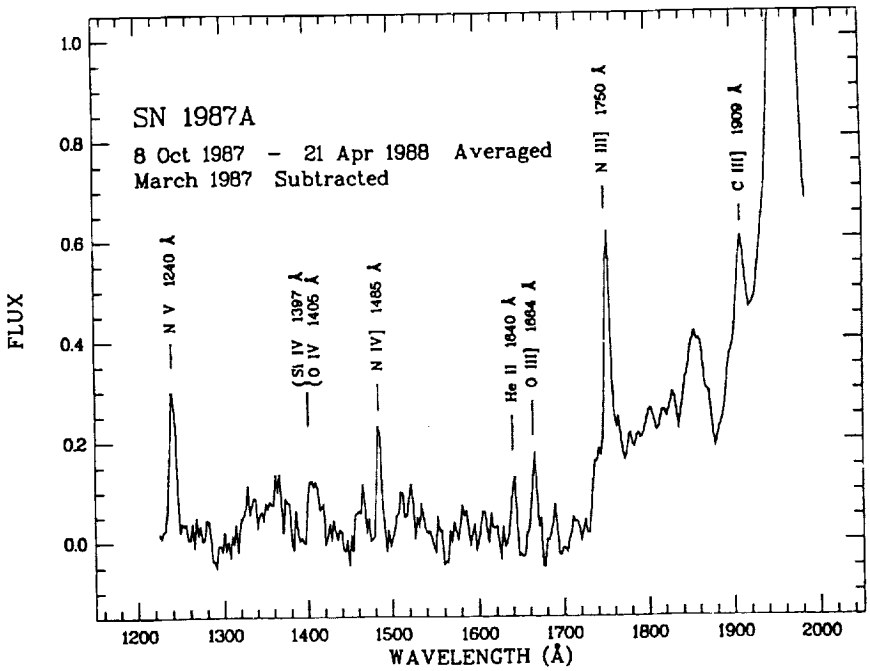


FIGURE 3 Averaged spectrum of the narrow emission lines from the circumstellar shell of SN 1987A. The spectrum of stars 2 and 3, as observed in March 1987 is subtracted from the subsequent spectra.

until 400 days after the explosion, then began a symmetric decline, at least in some lines. A plausible geometrical picture for the fluorescent material is a shell at a distance of 200 light days from the supernova site. Light travel times are important in determining the observed flux, and this dimension of order $5 \times 10^{17}$ cm is indicated by the duration of the increase. The spatial extent of this shell would be about one arc second, not measurable with IUE, but well within the reach of HST.

Because the flux increased, high dispersion IUE measurements of the circumstellar lines were possible. They remain unresolved at 30 km/sec resolution. The observed line ratios are consistent with a density of order $10^4$ in the emitting gas, and ground based observations of narrow [O III] help determine the temperature at about 45,000 K (Wampler and Richichi 1988). With the physical conditions reasonably well determined, the chemical abundances result from a nebular analysis. Fransson *et al.* find $N/C = 7.8 \pm 4$ and $N/O = 1.6 \pm 0.8$. These are respectively factors of 37 and 12 higher than the solar values, implying that the gas has undergone substantial CNO processing. To reveal CNO-processed material at the

surface, the progenitor of SN 1987A is likely to have lost much of its hydrogen envelope before the explosion. This, and the existence of the shell, are consistent with models where a red supergiant evolves to the blue supergiant stage before exploding.

High nitrogen abundance was also found in the circumstellar matter of an earlier SN II with IUE (Fransson *et al.* 1984). There, the explosion took place while the star was a red supergiant: here, the circumstellar matter was evidently ejected from the star as a red supergiant, but the star evolved to the blue before exploding. Thus the IUE observations help establish the history of SK -69 202 for the 20,000 years before it exploded.

Matching the path in the H-R diagram and the chemical composition of the circumstellar matter has proved a challenging task for theorists, who were already struggling with the question of why the star exploded as a blue supergiant. The evolution from blue (on the main sequence) to red (as a mass-losing red supergiant) back to the blue (to explode as a B3 Ia star) has been examined, for example, by Saio *et al.* (1988). Key ingredients seem to be the lower heavy element abundance in the LMC, thorough mixing of hydrogen-burning products, and substantial mass loss as a red supergiant.

One prediction based on the presence of a circumstellar shell is that the rapidly expanding debris, moving at 1/10 c, will strike the shell, at 1/2 light year, in the next several years. So for the end of the century, we may expect a recrudescence of SN 1987A, with a hot shock interaction producing copious X-rays and perhaps renewed nonthermal radio emission.

## THE ULTRAVIOLET ECHO?

The discovery of two echo rings in the optical (Crotts 1988; Rosa 1988; Heathcote *et al.* 1988; and a third echo ring reported by Bond *et al.* 1989) attributed to dust scattering of light from the supernova by matter in the LMC, has provided the opportunity for an interesting IUE investigation. In the optical, the rings reflect light from the optical maximum observed in May 1987. This is demonstrated by spectra of the rings taken in 1988, in which the light from the rings has the spectrum of the supernova in May, 1987. The expected UV ring would be the result of the UV maximum, the brief flash of UV emitted in the first hours of the event. This means that, if detected, the UV echo could provide direct information on the supernova spectrum at the time of shock breakout: the observations would show the properties of the supernova before discovery!

From an inspection of the optical images of the echo rings and a comparison with pre-SN images, the brightest patch of the inner ring was selected for the IUE observation (Gilmozzi 1988), since a simple calculation following Chevalier and Emmering (1988) shows that the UV echo should be just a few arcsec external to the optical ring. The ring was observed

on 1 May, 1988, with the long axis of the IUE aperture perpendicular to the ring, to obtain spatial information on the distribution of UV light. A second, longer exposure on May 25 confirms the presence of a weak UV signal. Although the feature near 1550 Å may be spurious, the rise around 1250Å is real.

No background star contamination is expected, since the slit location includes no stars brighter than 18 mag. The coincidence of the emission and the calculated position for the echo are consistent with the flux observed arising from a UV echo. However, there is still the possibility that the emission is due to diffuse matter scattering the light from nearby hot stars. The key test is to observe the same location in 1989: if the flux is still present, it is not due to the echo ring, which will have expanded to a larger diameter.

If the detected signal is the UV echo, the spatial extent of the emission (about 5 arc minutes) is a good measure of the thickness of the scattering cloud, since the UV emission is the echo of a very brief event (Chevalier and Emmering 1988). The derived cloud thickness is about 40 pc, which agrees well with the upper limit of 50 pc derived from the optical observations.

The flux from the UV echo, if confirmed, will also be instructive. If it is of the same order as the optical echo, this implies that the energy emitted in the UV represents about 10% of the total energy radiated by the supernova. Since the optical maximum lasted at least 100 times as long as the UV peak (two months compared to less than a day), and the scattering efficiency in the UV is about 10 times better (Chevalier and Emmering 1988), then equal observed fluxes would imply that the integrated UV luminosity was about 10% of the bolometric luminosity radiated near the SN peak. If this observation is confirmed, it will provide a useful constraint on theoretical models of the outburst.

While the case is not yet proven, the IUE results provide the tantalizing possibility of detecting a signal which was emitted two days before the IUE first pointed at SN 1987A, and which may prove useful in understanding the physics of supernova explosions.

## FUTURE OBSERVATIONS OF SN 1987A

IUE observations of SN 1987A in 1989 and beyond will depend on the behavior of the supernova, but will surely include a diligent monitoring of the UV spectrum, with the hope that the opaque atmosphere will begin to turn transparent and reveal the internal composition of the now-vanished Sanduleak -69 202. The changes in ionization of the circumstellar shell should provide a time-lapse view of the recombination of that gas, and an improved understanding of the physical setting for the emission. A

carefully planned observation of the UV echo position should provide the decisive test for that possible observation.

Continued ultraviolet investigation of the supernova should continue with HST. Its powerful UV spectrometers will allow the interstellar medium near SN 1987A to be studied by looking in absorption at the nearby stars 2 and 3. The UV flux from the supernova itself will be safely resolved from those neighbors so it can be followed down to much fainter levels both in spectroscopic and photometric observations. The circumstellar shell that IUE detects spectroscopically should be a good target for HST imaging. While IUE observations of the debris from the supernova hitting the circumstellar shell would be interesting, it is reasonable to hope that when this event occurs in 1999 we will have another instrument to use! Finally, HST should be an effective tool for studying the expanding debris itself, and perhaps the pulsar within SN 1987A. Even though we can anticipate these desirable observations, the most intriguing possibilities may be the observations that we have not yet conceived. The ability to change the observing program, sometimes on short notice, in response to events in the LMC rather than constraints imposed from Earth, is an essential part of studying an evolving object.

The fact the target-of-opportunity proposals were in place, and that interested observers were ready to carry out a planned program of observation is only half the story of the UV observations of SN 1987A. The target-of-opportunity proposals focused on the aspects of supernovae which had been important in previous investigations: the explosion physics and the chemical analysis of the debris. But astronomy is an observational science and the observed objects have rarely read the proposals. In the case of SN 1987A, the contributions of IUE turned out to be especially important in areas that were not anticipated, using the satellite in ways which were not customary. For example, the identification of the progenitor by using the astrometry and the imaging properties of IUE was a useful contribution that required novel use of IUE. Employing the FES as an accurate photometer was not anticipated, but new calibration methods make those measurements quite helpful. No one predicted that IUE short-wavelength observations of narrow emission lines from a fluorescent circumstellar shell would be a major constraint on the late stages of stellar evolution for the LMC supernova, but a careful background subtraction technique has made this a reality. While the jury is still out on the UV echo, there is a chance that the IUE observations may provide a glimpse of the supernova explosion's flux before it was discovered.

The key ingredient in the success of the IUE observations of SN 1987A has been the ability to modify the observing program in response to the behavior of the supernova. On the first day, this meant a rapid change in schedule and real-time adjustment of exposure times. Later, it

implied changing the balance of long and short wavelength exposures, and combining shifts for very long exposures. For the echo observations, it required precise choice of dates of observation. In every case, the IUE Observatory has had the flexibility to accommodate these requirements, and a deeper understanding of this unique event has been the result.

## REFERENCES


Andreani, P., R. Ferlet, and A. Vidal-Majar. 1987. Nature 326: 770.

Arnett, W.D., J.N. Bahcall, R.P. Kirshner, and S.E. Woosley. 1989. Ann. Rev. Astron. Astrophys. 27.

Baade, W., and F. Zwicky. 1933. Phys. Rev 45: 138.

Bahcall, J.N. 1989. Neutrino Astrophysics. Cambridge University Press, Cambridge.

Benvenuti, P., *et al.* 1982. ESA SP-1046.

Blades, J.C., J.M. Wheatley, N. Panagia, M. Grewing, M. Pettini, and W. Wamsteker. 1988a. Ap. J (Lett.) 332: L75.

Blades, J.C., J.M. Wheatley, N. Panagia, M. Grewing, M. Pettini, and W. Wamsteker. 1988b. Ap. J. 334: 308.

Blair, W.P., and N. Panagia. 1987. In: Kondo, Y. (ed.). Exploring the Universe with IUE. Reidel.

Branch, D., and K.L. Venkatakrishna. 1986. Ap. J. (Letters) 306: L21.

Cassatella, A., J. Barbero, and P. Benvenuti. 1985. Astron. Astrophys. 144: 335.

Cassatella, A., C. Fransson, J. van Santvoort, C. Gry, A. Talavera, W. Wamsteker, and N. Panagia. 1987. Astron. Astrophys. 177: L29.

Chevalier, R. 1987. Nature 328: 44.

Chevalier, R.A. 1989. Bull. Am. Astron. Soc.

Chevalier, R.A., and C. Fransson. 1987. Nature 328: 44.

Crotts, A. 1988. IAU Circular no. 4561.

de Boer, K., M. Grewing, T. Richtler, W. Wamsteker, C. Gry, and N. Panagia. 1987. Astron. Astrophys. 177: L37.

de Vorken, D. 1988. Air and Space Smithsonian.

Dupree, A.K., R.P. Kirshner, G.E. Nassiopoulos, J.C. Raymond, and G. Sonneborn. 1987. Astrophys. J. 320: 597.

Fransson, C. *et al.* 1984. Astron. Astrophys. 132: 1.

Fransson, C., M. Grewing, A. Cassatella, N. Panagia, and W. Wamsteker. 1987. Astron. Astrophys. 177: L33.

Fransson, C., A. Cassatella, R. Gilmozzi, R.P. Kirshner, N. Panagia, G. Sonneborn, and W. Wamsteker. 1989. Astrophys. J. 336: 429.

Gilmozzi, R. 1988. In: Couch, W. (ed.). Elizabeth and Frederick White Research Conference on "Supernova 1987A." Proc. Astron. Soc. Australia. In press.

Gilmozzi, R., A. Cassatella, J. Clavel, C. Fransson, R. Gonzalez, C. Gry, N. Panagia, A. Talavera, and W. Wamsteker. 1987. Nature 328: 318.

Gry, C., A. Cassatella, W. Wamsteker, L. Sanz, N. Panagia. 1987. IAU Circular No. 4327.

Heathcote, S., N. Suntzeff, N. Caldwell, J. Huchra, and R. Olwin. 1988. IAU Circular No. 4567.

Kirshner, R.P. 1988. National Geographic Magazine 173: 618.

Kirshner, R.P. 1988. In: A Decade of UV Astronomy with the IUE Satellite. ESA SP-281.

Kirshner, R.P., and J. Kwan. 1974. Ap. J. 193: 27.

Klein, R.I., and R.A. Chevalier. 1978. Ap. J. (Lett.) 223: L109.

Kristian, J., *et al.* 1989. Nature.

Lucy, L.B. 1987. Astron. Astrophys. 182: L31.

Madore, B., and W. Kunkel. 1987. IAU Circular No. 4316.

Matz, S.M., *et al.* 1988. Nature 331: 416.

McCray, R., J.M. Shull, and P. Sutherland. 1987. Ap. J. (Letters) 317: L73.

McNaught, R.H. 1987. IAU Circular No. 4316.
Panagia, N., R. Gilmozzi, J. Clavel, M. Barylak, R. Gonzalez Riestra, C. Lloyd, L. Sanz Fernandez de Cordoba, and W. Wamsteker. 1987. Astron. Astrophys. 177: L25.
Rank, D.M. *et al.* 1988. Nature 331: 505.
Rosa, M. 1988. IAU Circular No. 4564.
Saio, H., M. Kato, and K. Nomoto. 1988. Ap. J. (Lett.).
Sanduleak, N. 1969. CTIO Publications no. 89.
Savage, B. 1986. Proc. Joint NASA/ESA/SERC Conf., ESA SP-263, page 259.
Savage, B., and K.S. de Boer. 1979. Astrophys. J. (Lett.) 230: L77.
Savage, B., E.B. Jenkins, C.L. Joseph, K.S. de Boer. 1988. Wisconsin Astrophysics preprint No. 295.
Sonneborn, G., B. Altner, and R.P. Kirshner. 1987. Ap. J. (Lett) 323: L35.
Sonneborn, G., and R.P. Kirshner. 1987. IAU Circular No. 4333.
Suntzeff, N.B., M. Hamuy, G. Martin, A. Gomez, R. Gonzales. 1988. A. J. 96: 1864.
Turtle, A.J., *et al.* 1987. Nature 327: 38.
Walborn, N., B.M. Lasker, V.G. Laidler, and Y.-H. Chu. 1987. Ap. J. (Lett.) 320: L41.
Wampler, E.J., and A. Richichi, A. 1989. Astron. Astrophys.
Walker, A.R. 1987. M.N.R.A.S. 225: 627.
Walker, A.R., and P. Mack. 1988. M.N.R.A.S.
West, R.M., A. Lauberts, H.E. Jorgensen, and H.-E. Shuster. 1987. Astron. Astrophys. 177: L1.
Whitelock, P.A., R.M. Catchpole, J.W. Menzies, M.W. Feast, H. Winkler, *et al.* 1988. M.N.R.A.S. 234: 5P.
Woosley, S.E., and T.A. Weaver. 1986. Ann. Rev. Astron. Astrophys. 24: 205.
Woosley, S.E., P.A. Pinto, P.G. Martin, and T.A. Weaver. 1987. Ap. J. 318: 664.

# Quasi-Periodic Oscillations in Low-Mass X-ray Binaries

W.H.G. LEWIN*, J. VAN PARADIJS†, AND M. VAN DER KLIS†

Variability on short time scales in the X-ray flux (Lewin *et al.* 1968) is a very general property of binary X-ray sources. Until recently, most efforts in studying such variability were spent on two types of intensity variations, periodic X-ray pulsations and X-ray bursts. Due to the lack of a direct and transparent interpretation, relatively little attention was paid to noise in X-ray intensity variations. An outstanding exception has been the study of the very fast variability of the black-hole candidate Cyg X-1 and sources long thought to be of a similar nature such as Cir X-1 and GX 339-4 (for a comprehensive review of the studies of noise in X-ray intensity variations of binary X-ray sources up to 1980, we refer to Bradt *et al.* 1982).

Consequently the bright persistent X-ray sources in the central regions of the Galaxy (the galactic bulge sources) which showed neither pulsations nor bursts were somewhat neglected. Not until after the discovery (Van der Klis *et al.* 1985) of intensity-dependent quasi-periodic oscillations (QPO) and associated red noise from these luminous low-mass X-ray binaries (see Figure 1) were systematic studies of the shape of these power-spectral components made. In this note we give a brief account of the main developments since this discovery which have led to a new picture of the properties of LMXB. Since this is not intended to be a review paper, we will not give extensive references here but instead refer the reader to the

*Center for Space Research and Department of Physics, Massachusetts Institute of Technology 37-627, Cambridge, MA 02139, USA

† Astronomical Institute "Anton Pannekoek", University of Amsterdam, Roetersstraat 15, 1018 WB Amsterdam, The Netherlands and Center for High-Energy Astrophysics, NIKHEF-H, Amsterdam, The Netherlands

comprehensive reviews of Lewin et al. (1988), Lamb (1988, 1990), Van der Klis (1989), and a recent article by Hasinger and Van der Klis (1989).

Slow QPO (frequencies in the range one to tens of milli-Hertz) had been reported prior to 1985 from several sources. It is likely that these QPO have a different origin from those which are the subject of this note.

Short trains of fast oscillations during a number of type I X-ray bursts (i.e., runaway thermonuclear events) had been reported (for a review see Lewin and Joss 1983). The association of these oscillations with X-ray bursts makes it difficult to compare them with the QPO seen in the persistent flux of galactic bulge X-ray sources.

Tawara *et al.* (1982) discovered quasi-periodic ($\sim$ 2 Hz) oscillations in 2 out of 64 long type II X-ray bursts from the Rapid Burster. The frequency of these oscillations differed between the bursts and drifted within each burst, so Tawara *et al.* concluded that they could not be a direct manifestation of the rotation of the neutron star. There were at least two reasons why this discovery of QPO in the Rapid Burster received much less attention than the QPO discovery in GX 5-1 a few years later. (i) The Rapid Burster was (and still is) a very peculiar source (Lewin and Joss 1983), and the 2-Hz QPO were seen as "just another" strange phenomenon. (ii) The frequency of the QPO in GX 5-1 depended strongly on the source intensity; there were no obvious connections between the QPO in the Rapid Burster and other characteristics of this source.

Alpar and Shaham (1985) proposed that the intensity-dependent QPO discovered in GX 5-1 (Van der Klis *et al.* 1985) are caused by some interaction between the magnetic field of the rapidly rotating neutron star and the inner accretion disk (bounded by the magnetosphere) in which matter orbits the neutron star in approximately Keplerian orbits. The QPO frequency is then the difference ("beat frequency") between the Keplerian frequency at the inner disk edge and the neutron star spin frequency. Modulation of the accretion rate through magnetic gating was proposed as a feasible mechanism for causing the X-ray intensity variations, and it was shown that the red-noise component was a natural consequence of accretion-modulation mechanism (Lamb *et al.* 1985). From the observed intensity dependence of the QPO frequency, Alpar and Shaham derived a neutron star rotation period of 10 ms and a magnetic dipole field strength of a few $10^9$ G. These parameters agree very well with the spin-up scenario for the binary msec radio pulsars. In this scenario the msec radio pulsars are the descendants of low-mass X-ray binaries (see, e.g., Van den Heuvel 1986 for a review of the evolution of X-ray binaries). For this reason the "beat frequency" model of Alpar and Shaham was greeted with enthusiasm. However, if 10 ms were the correct rotation period, it was somewhat puzzling why this period did not show up as coherent pulsations in the

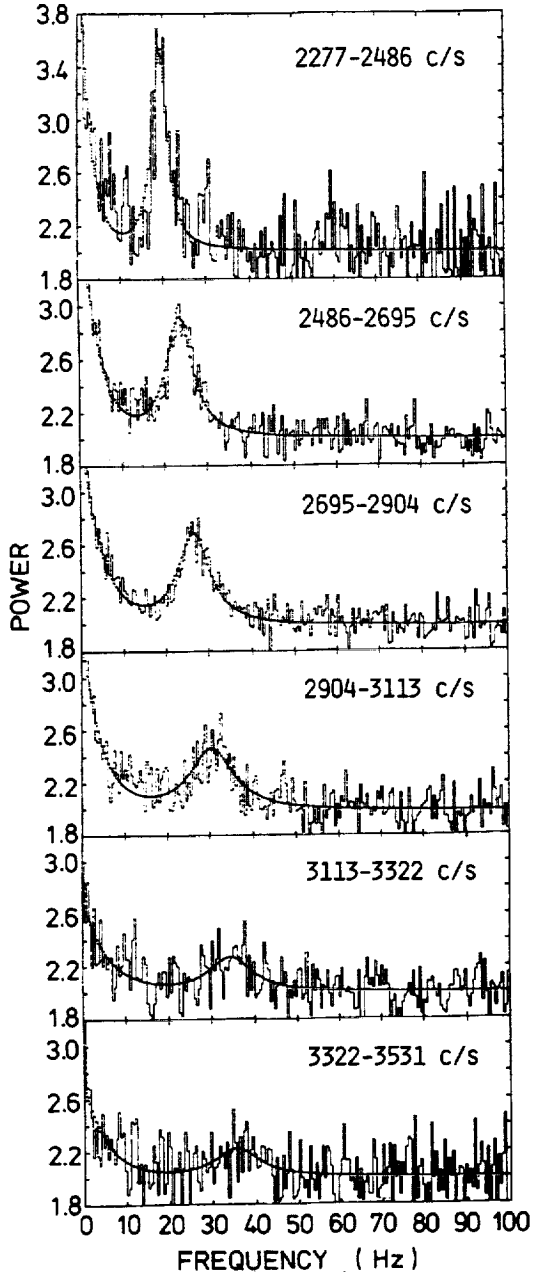


FIGURE 1 Display of average power spectra from GX 5-1 in six different source intensity intervals (indicated in the panels). The lines drawn through the data indicate fits described by a function which is the sum of a constant (Poisson noise), a line with a Lorentzian profile (the QPO peak), and an exponentially rising red noise component. This figure is from Van der Klis *et al.* 1985.

power spectrum since the existence of a magnetosphere implies that in the vicinity of the neuron star the magnetic field influences the accretion flow.

QPO discovered subsequently in Sco X-1 (Middleditch and Priedhorsky 1986; Van der Klis *et al.* 1986) had quite different properties. Their frequency was sometimes low (near 6 Hz) and approximately constant or even slightly anti-correlated with X-ray intensity, while at other times, it was high (10-20 Hz) and either positively correlated or varying erratically as a function of source intensity depending on the intensity of the source. Red noise was weak compared to the QPO. Both results seemed to pose a problem for the beat-frequency model.

The "beat-frequency" model was clearly unable to account for the complicated picture presented by the observations; alternative models were proposed and ways were worked out to broaden the range of phenomena that could be explained within the beat-frequency model.

An underlying organization in the phenomena revealed itself when correlations were found between the spectral properties of the sources and their QPO characteristics. Three of the newly discovered QPO sources were known to exhibit two different X-ray spectral states, distinguishable as "branches" in an X-ray hardness versus intensity diagram. In GX 5-1 the 20-40 Hz QPO were only and always observed when the source was found in the so-called "horizontal-branch" of this diagram (Van der Klis *et al.* 1987, see Figure 2). Its red noise was shown to consist of two components; one of these is the low-frequency noise associated with the QPO and only present in the horizontal-branch state; the other ("very low frequency noise") is a power-law component that is seen in all spectral states, and dominates the power spectrum below $\sim$ 0.1 Hz. A similar pattern was observed in Cyg X-2 (Hasinger 1987a). In Sco X-1 a strong correlation was also found between QPO and the spectral state; two-branched spectral behavior occurred with strongly intensity-dependent high-frequency QPO in one spectral branch and weakly intensity-dependent $\sim$ 6 Hz QPO in the other. However, both the morphology of the branches and the way in which the QPO frequency varied among them were quite different from that in GX 5-1 and Cyg X-2.

A key contribution came from Hasinger (1988) who observed that the normal branch of Cyg X-2, known to be connected at its upper end to the horizontal branch, showed a sharp bend near its lower end suggesting a transition to yet another branch. Hasinger, therefore, proposed that there are three branches: the horizontal branch, the normal branch, and the flaring branch which form a Z-shaped pattern in the X-ray hardness vs. intensity diagram and each of which has its characteristic power spectral behavior. In GX 5-1 and Cyg X-2 it was the upper part of the Z that had so far been observed; in Sco X-1 it was the lower part. Subsequent observations have beautifully confirmed Hasinger's proposal, and the class of "Z sources" is now well established (see Figure 3).

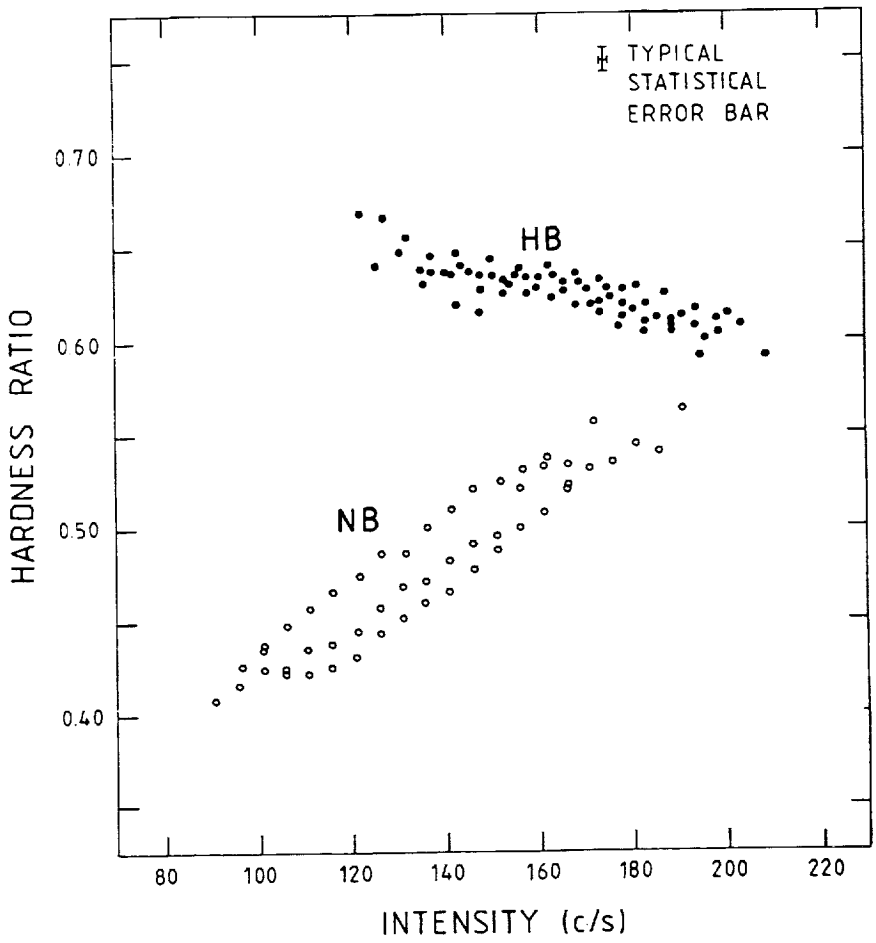


FIGURE 2 Spectral hardness (ratio of the 6-10 keV and 3-6 keV count rate) versus intensity (3-10 keV) diagram for some EXOSAT data on GX 5-1. The solid dots in the "horizontal branch" (HB) represent data when strong 20-40 Hz QPO were observed; the power spectra represented by open circles on the "normal branch" (NB) showed no significant high-frequency QPO. This figure is from Van der Klis *et al.* (1987).

With this clarification, attempts to explain all observed QPO behavior within the framework of the beat frequency model were abandoned, and the model was proposed to be valid only for the horizontal-branch high-frequency QPO (and associated LFN). Models for the 6 Hz normal-branch QPO have been proposed in terms of radiation-dominated accretion flows near the Eddington limit (Lamb 1988, 1990; Hasinger 1987a).

Millisecond time lags were discovered in the intensity-dependent hori-

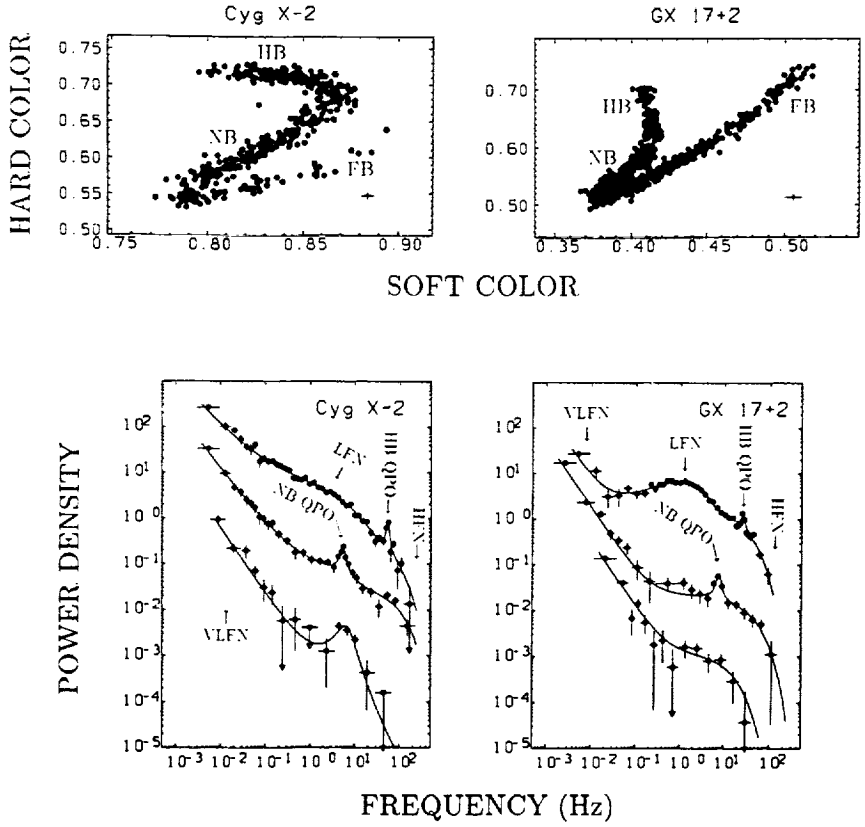


FIGURE 3 Display of the X-ray color-color diagrams and power spectra for the Z sources Cyg X-2 and GX 17 + 2 illustrating the correlation between the QPO behavior and the location of the source on the Z-shaped track. This figure has been adapted from Van der Klis (1989).

zontal-branch QPO between X-ray spectral bands (Hasinger 1987b). This suggested that X-rays originating from the near vicinity of the neutron star were Compton scattered in a surrounding hot plasma before they could escape. This Comptonization model had been proposed before to account for the absence of coherent millisecond X-ray pulsations through smearing and was consistent with some interpretations of the shape of the X-ray spectrum. The problem of accounting for the effect of scattering on QPO and beamed pulsar radiation stimulated a substantial theoretical effort. The idea that the magnetosphere in these systems is very small (a few neutron star radii, rather than hundreds as in X-ray pulsars) stimulated a reassessment of magnetospheric theories. It was pointed out that magnetospheric

formation might be qualitatively different in these systems from that in massive X-ray binaries since the boundaries of such small magnetospheres are located in the radiation-pressure dominated part of the disk (White and Stella 1988).

Further observations showed that not all low-mass X-ray binaries conformed to the above Z scheme. Some of them should have shown QPO, but they did not while others exhibited QPO with properties that did not fit into the Z scheme. Hasinger and Van der Klis (1989) distinguished, in addition to the Z sources, a second class of low-mass X-ray sources that shows a different pattern of correlated X-ray spectral and power-spectral behavior; many of these sources are X-ray bursters. In their X-ray color-color diagrams one can distinguish a "banana" shaped spectral branch and isolated "islands". Both spectral branches have a characteristic associated type of power spectrum (see Figure 4). These so-called "atoll sources" are, on average, less luminous than the Z sources, and they do not exhibit the QPO found in the latter. Most of the persistently accreting low-mass binary X-ray sources can be classified as either a Z source or an atoll source; however, some (mostly transient) sources can not (e.g. the Rapid Burster, and Cir X-1).

Besides the fast-variability characteristics, other properties of low-mass X-ray binaries are correlated to their X-ray spectral states as well. It was recently discovered that the radio intensities of the Z sources GX 17 + 2, Cyg X-2, and Sco X-1 (Penninx *et al.* 1988; Hjellming *et al.* 1989, 1990) are strongly correlated with the location of these sources on the Z shaped track in the X-ray color-color diagram (see Figure 5). When these sources are in the flaring-branch state their radio brightness is relatively low, it increases when the source moves up the normal branch, becoming relatively high on the horizontal branch. Since the radio emission is probably caused by relativistic electrons (synchrotron radiation), this correlation suggests that perhaps the required non-thermal processes and particle acceleration are connected with the boundary layer between the inner disk and the magnetosphere of the neutron star.

A second, very recent, development is the discovery that for atoll sources there is a strong correlation between the spectral state of the source (i.e. "island" vs. "banana" state) and the properties of X-ray bursts (Van der Klis *et al.* 1990). In particular, during the island state the duration of the bursts is much longer than during the banana state. This may be indicative of a difference in the hydrogen content of the layers in which the thermonuclear flash occurs that gives rise to the burst. Although it is likely that the accretion rate is the governing parameter for the properties of both the X-ray bursts and the persistent X-ray spectrum, the nature of the connection between the flashing layer and the (superficial) regions where the persistent (accretion) luminosity is emitted is presently unclear.

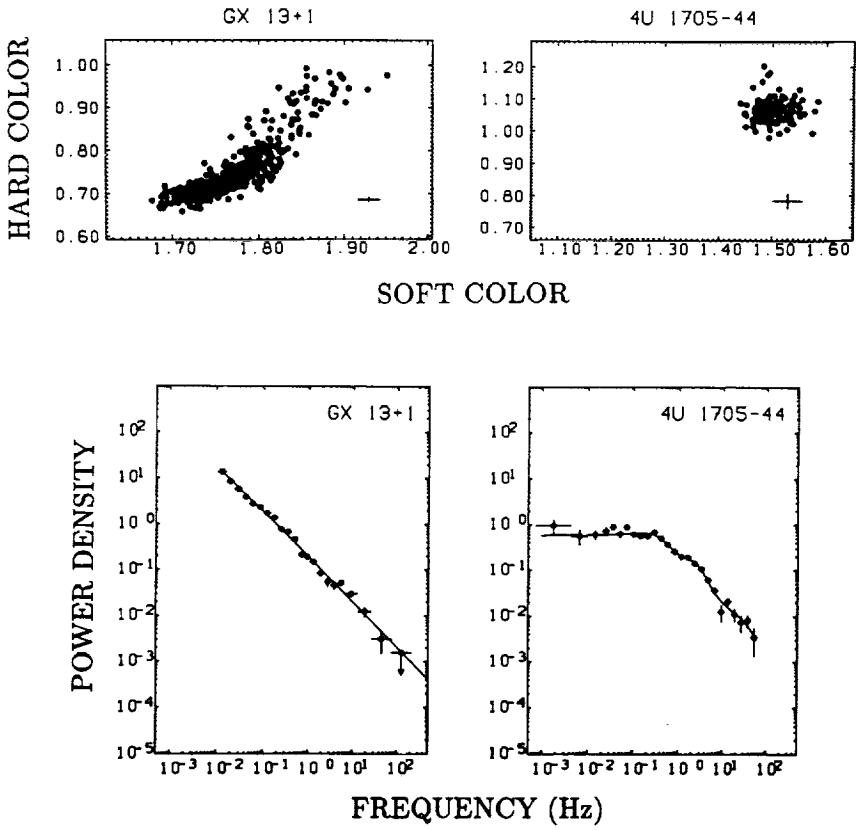


FIGURE 4 Display of the X-ray color-color diagrams and power spectra of the atoll sources GX 13 + 1 and 4U 1705-44 illustrating the correlation between power spectrum and the source spectral state ("island" versus "banana" state). This figure has been adapted from Van der Klis (1989).

In general, the rms variations of the QPO is only a few percent, and therefore most studies discussed so far have been based not on X-ray intensity curves but on power spectra of the intensity variations. An exception is the Rapid Burster. QPO rms variation up to ~ 30% have been observed from this source which made it possible with Ginga to observe trains of individual oscillations (Dotani *et al.* 1990). These observations showed that the finite width of the QPO peak in the power spectrum is caused by frequency modulation of the signal. Since the Rapid Burster is a very peculiar source, it is unclear whether the underlying mechanism holds for other sources as well.

Finally, studies of the power spectra of some high-mass X-ray binaries

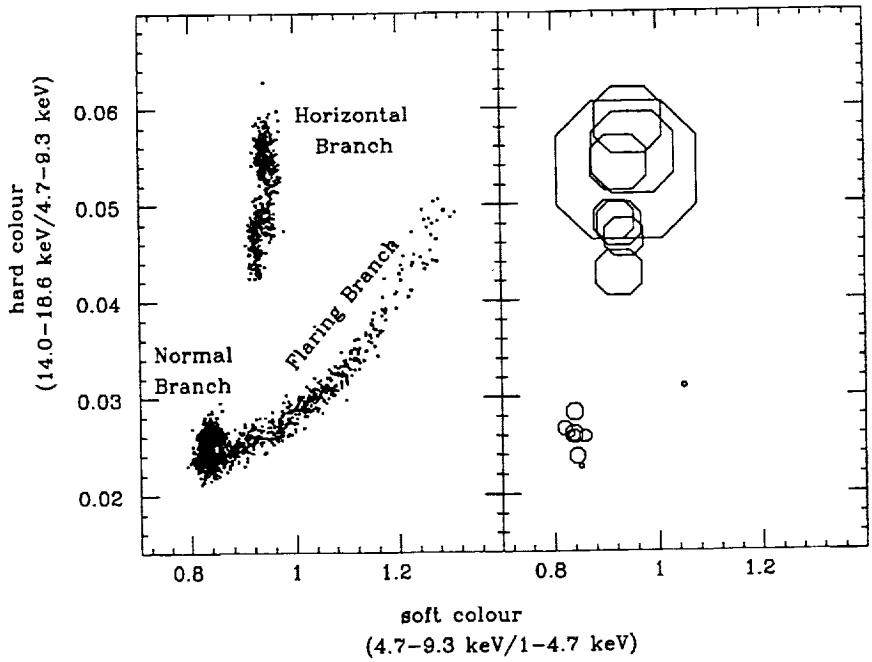


FIGURE 5 Display of the correlation between the radio intensity and X-ray spectral properties of the Z source GX 17 + 2. In the left-hand panel the three branches are indicated in the X-ray color-color diagram. In the right-hand panel the size of the octagon is a measure of the radio intensity; its location indicates the spectral state of the source.

(most of them pulsars) have shown that these power spectra also contain QPO and broad noise components, somewhat similar to those found in low-mass X-ray binaries (Ebisawa *et al.* 1989; Belloni and Hasinger 1989). In the case of the pulsating high-mass transient source EXO 2030 + 375 (Angelini *et al.* 1989) the variation of the QPO frequency with X-ray luminosity combined with the known spin frequency of the neutron star was consistent with the beat frequency relation. However, recent results obtained by Norris *et al.* (1989) and by Mitsuda *et al.* (1989) may pose problems for the beat frequency model.

In closing, the recent division of the low-mass X-ray binaries in Z sources and atoll sources has clarified matters a great deal. It seems that the beat frequency model is at present a promising (though not generally accepted) model for the horizontal-branch QPO in Z sources. The normal-branch and the flaring-branch QPO in Z sources probably have a common origin which is different from the origin of the horizontal-branch QPO.

C-4

## REFERENCES


Alpar, M.A., and J. Shaham. 1985. Nature 316: 239.

Angelini, L., L. Stella, and A.N. Parmar. 1989. Astroph. J. In press.

Belloni, T., and G. Hasinger. 1989. Astron. Astroph. In press.

Bradt, H.V., R.L. Kelley, and L.D. Petro. 1982. In: Sanford, P.W., *et al.* (eds.). Galactice X-ray Sources. Wiley. 89.

Dotani, T., K. Mitsuda, H. Inoue, Y. Tanaka, N. Kawai, Y. Tawara, K. Makishima, J. Van Paradijs, W. Penninx, M. Van der Klis, J. Tan, and W.H.G. Lewin. 1990. Astroph. J. 350: 395.

Ebisawa, K., K. Mitsuda, and H. Inoue. 1989. Publ. Astron. Soc. Japan 41: 519.

Hasinger, G. 1987a. Astron. Astroph. 186: 153.

Hasinger, G. 1987b. In: White, N., and J.-H. Huang (eds.). The Origin and Evolution of Neutron Stars. IAU Symp. 125: 333.

Hasinger, G. 1988. Adv. Space Res. Vol. 8, No. 2: 377.

Hasinger, G., and M. Van der Klis. 1989. Astron. Astroph. In press.

Hjellming, R.M., X.H. Han, F.A. Cordova, and G. Hasinger. 1989. Astron. Astroph. In press.

Hjellming, R.M., R.T. Stewart, G. L. White, R. Strom, W.H.G. Lewin, P. Hertz, K. Wood, K. Mitsuda, W. Penninx, and J. Van Paradijs. 1990. Astrophs. J. In press.

Lamb, F.K. 1988. Adv. Space Res. Vol. 8, No. 2: 421.

Lamb, F.K. 1990. Astroph. J. In press.

Lamb, F.K., N. Shibazaki, M.A. Alpar, and J. Shaham. 1985. Nature 317: 681.

Lewin, W.H.G., G.W. Clark, and W.B. Smith. 1968. Astroph. J. 152: L55.

Lewin, W.H.G., and P.C. Joss. 1983. In: Lewin, W.H.G., and E.P.J. van den Heuvel (eds.). Accretion-driven Stellar X-ray Sources. Cambridge University Press. 41.

Lewin, W.H.G., J. Van Paradijs, and M. Van der Klis. 1988. Space Sci. Rev. 46: 273.

Middleditch, J., and W.C. Priedhorsky. 1986. Astroph. J. 306: 230.

Mitsuda, K., *et al.* 1989. Proceedings of the Bologna conference, and paper submitted to Publ. Astron. Soc. Japan.

Norris, J., P. Hertz, K. Wood, B. Vaughan, M. Michelson, K. Mitsuda, and T. Dotani. 1989. Proceedings of the Bologna Conference, and Astrophys. J. Submitted.

Penninx, W., W.H.G. Lewin, A.A. Zijlstra, K. Mitsuda, J. Van Paradijs, and M. Van der Klis. 1988. Nature 336: 146.

Tawara, Y., S. Hayakawa, *et al.* 1982. Nature 299: 38.

Van den Heuvel, E.P.J. 1986. In: Trümper, J., W.H.G. Lewin, W. Brinkman (eds.). The Evolution of Galactic X-ray Binaries. Reidel Publ. Cy. 107.

Van der Klis, M. 1989. Ann. Rev. Astron. Astroph. 27: 517.

Van der Klis, M., F. Jansen, J. Van Paradijs, W.H.G. Lewin, E.P.J. Van den Heuvel, J. Trümper, and M. Sztajno. 1985. Nature 316: 225.

Van der Klis, M., F. Jansen, J. Van Paradijs, W.H.G. Lewin, M. Sztajno, and J. Trümper. 1987. Astroph. J. 319: L13.

Van der Klis, M., E. Damen, W. Penninx, J. van Paradijs, and W.H.G. Lewin. 1990. Astroph. J. (Lett) 360: L19.

White, N.E., and L. Stella. 1988. Monthly Not. Roy. astron. Soc. 231: 325.

# The Evolution of the Gravitational Radiation from Stellar Components of Galaxies

V.M. LIPUNOV, E.YU. OSMINKIN, M.E. PROKHOROV
Sternberg Astronomical Institute

## ABSTRACT

This paper discusses the evolution of gravitational waves spectra produced by binary stars, supernova explosions and coalescences of binary compact stars in outer galaxies. These spectra are integrated over a simple model of the universe to give an estimate of the stokhastic gravitational waves background due to astrophysical sources.

## INTRODUCTION

Different kinds of gravitational waves (GW) exist in nature. The major types of GW are the cosmological GW and GW from astrophysical sources—such as binary stars and supernova explosions (SNE) (Thorne 1987).

The evolution of the ensemble of the binary systems in an arbitrary galaxy has been investigated by the method of statistical simulation. We have taken into account the following evolutionary processes: the mass transfer in close binaries, the evolution inside a common envelope, possible binary disruption due to the SNE, and creation of the compact objects and their evolution (see Lipunov 1987). The method and scenario are considered in detail in Kornilov and Lipunov (1982) for massive stars and in Lipunov and Postnov (1987b, c) for low and moderately massive binaries.

In this paper we will consider two different kinds of GW. The first type is the continuous gravitational radiation produced by binaries. A binary is assumed to emit the GW as two point-like masses on the circular orbit strictly at twice the orbital frequency. In this case the GW spectrum

from a galaxy is composed of thin "lines." The projected nonresonant GW detectors with a band $\Delta\nu \approx \nu$, will detect such a signal as continuous. Below, we shall calculate the amplitude of the signal on such a detector.

The second sort of GW sources can be connected with catastrophic processes occuring during the stellar evolution. First of all, these are the SNE and the coalescence of binary compact objects (white dwarves, neutron stars, or black holes). These GW are believed to be powerful and short in the duration pulse. Due to existing uncertainties in the calculation of this GW, we will use an estimation given by Shapiro and Teukolsky (1983).

Stochastic GW background from the binaries in our galaxy has been calculated by Lipunov and Postnov (1987a). The simple estimations show that the stochastic GW background from all of the external galaxies should be lower than from our own. However, there is a possibility of distinguishing both types of signals by using the fact of their different distributions over the sky. This can be done by a GW detector with a narrow diagram (Lipunov *et al.* 1987).

In our study we deal with the extragalactic GW sources, taking into account their evolutionary effects.

## THE METHOD OF CALCULATION OF GW EVOLUTION

To investigate the evolution of GW with time from galaxies having the different star formation laws, the following procedure has been used. At first the evolution of a quantity G(t, $\tau$) is calculated (for example, the GW flux or the rate of SNE) for an ensemble of binaries with $\delta$ (t - $\tau$ ) star formation rate. We assumed the parameters of the scenario do not change with time, and so, the Green function is

$$G(t,\tau) = G(t-\tau).$$

For a galaxy with an arbitrary star formation rate $\phi$ (t) the corresponding value G(t) can be presented by the convolution

$$G(t) = \int_{-\infty}^{+\infty} \phi(\tau) G(t-\tau) d\tau$$

The Green function for a continuous spectrum of GW from binaries was constructed by the following. The time interval from 0 to 15 billion years was equally spaced to $\Delta t = 10^9$ yrs bins. The frequency range ($10^{-8} \div 10^{-3}$ Hz) was divided by bins with $\Delta\nu = \nu_{i+1} - \nu_i$, so that $\ell g(\nu_{i+1}/\nu_i) = 0.25$. For each time interval $\Delta t_j$ and frequency bin $\Delta\nu_i$ the average GW flux has been calculated

$$F_{GW}(\nu_i, t_j) = \frac{1}{\Delta t_j} \int_{t_j}^{t_j+\Delta t_j} F_{GW}(\nu_i) dt \,|_{\nu_i \le \nu \le \nu_i + \Delta\nu_i}$$

where $F_{GW}(\nu_i)$ is the total gravitational flux from all binaries.

All results are presented in terms of dimensionless metric strain amplitude (Lipunov, Postnov 1987a)

$$h_\nu = \sqrt{\langle h_\nu^2 \rangle \Delta\nu} = \sqrt{\frac{4G}{\pi c^3} \langle F_{GW} \rangle \nu \frac{1}{\nu^2} \Delta\nu}$$

The number of events from the sources of GW pulses has been calculated inside each time bin $\Delta t$. Time interval was taken to be $\Delta t = 10^6$, $10^7$, $10^8$, $10^9$ years.

## RESULTS

The spectral evolution of gravitational radiation from a galaxy with $\delta$-like star formation rate is plotted in Figure 1. The results are for a galaxy, containing $3 \cdot 10^{11}$ stars, with a half of their total number entering the binaries. A distance to the galaxy is assumed to be 1 Mpc. The simulations have been carried out with the following parameters of the scenario.

- the masses of initially more massive stars in binary are supposed to be distributed according to Salpeeter's law

$$dN \propto M^{-2.35} dM, \qquad 0.1 M_\odot \leq M_1 \leq 120 M_\odot.$$

- the mass ratios $q \equiv M_2/M_1$ and semimajor axes a are distributed as

$$dN \propto dq, \qquad 0 \leq q \leq 1$$

and

$$dN \propto da/a, \qquad 1 R_\odot \leq a \leq 10^7 R_\odot.$$

A full description of the evolutionary scenario parameters can be found in Kornilov and Lipunov (1982) and in Lipunov and Postnov (1987b,c, 1988).

Note that the GW spectrum changes significantly during the first two billion years. The magnitude h in the frequency range $10^{-6}$ - $10^{-3}$ Hz decreases approximately by a factor of 30 ($\ell gh \approx -19.7$) at $t = 10^9$ yr and $\ell gh \approx -21.5$ at $10^{10}$ yr). This drop can be explained both by the binaries' disruption due to the SNE and by a diminishing mass in binary stars in mass through the stellar wind and common envelope processes.

To obtain the GW spectrum dependence upon time for an arbitrary star formation function, the function in Figure 1. must be integrated with star formation function $\phi(t)$. The star formation rate is supposed to be

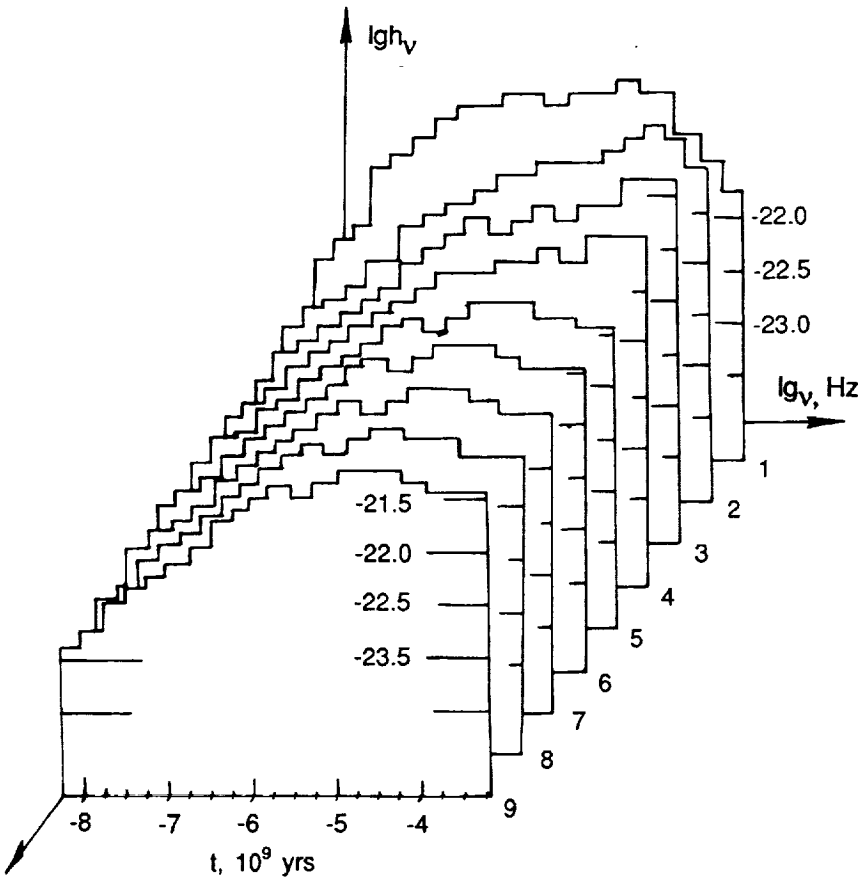


FIGURE 1 The evolution of GW spectrum from a galaxy with $\delta$-like star formation rate. A metric strain amplitude $h_\nu$ has been calculated at distance 1 Mpc. The galaxy contains $3 \cdot 10^{11}$ stars.

$$\phi(t) = \begin{cases} const, & 0 \le t \le 10^9 yrs \\ 0, & t > 10^9 yrs \end{cases}$$

for elliptical, and

$$\phi(t) = \text{const}$$

for spirals.

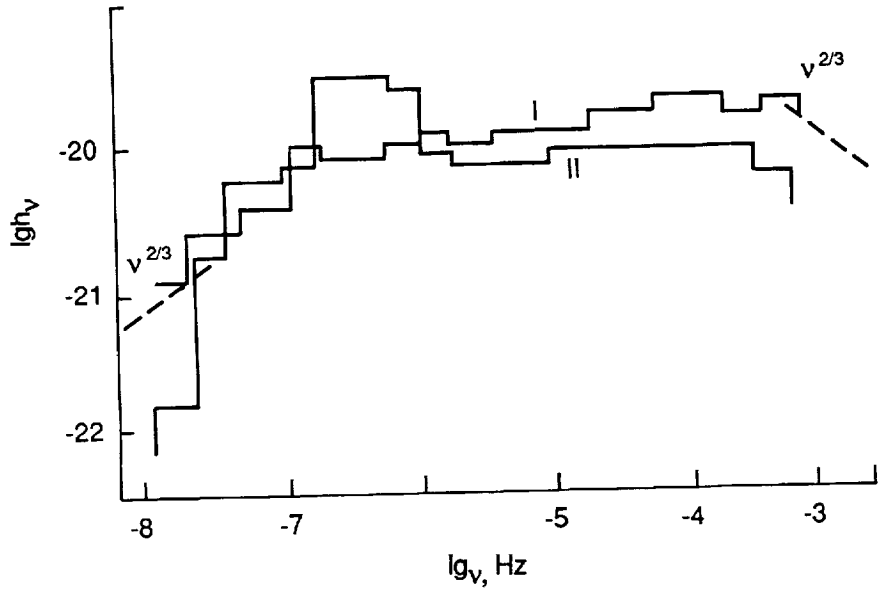


FIGURE 2 The GW background from binaries in outer spirals (I) and ellipticals (II).

The GW spectrum emitted by ellipticals (II) and spirals (I) from the modeling universe are plotted in Figure 2. The galaxies are assumed to be distributed homogeneously within $0 < z < 3$. The contributions of ellipticals and spirals are 30% and 70% respectively. The density of the visible matter is assumed to be $\beta = 1/30$ of the average density of the universe. The Hubble constant is taken to be $H = 75$ km/sec/Mpc, $\Omega \equiv \rho/\rho_{cr} = 1$, and zero pressure equation of state. In these calculations we have taken into account the redshift of gravitational radiation and a curvature of the universe (Zel'dovich and Novikov 1970).

The influence of massive black holes (BH) on the spectrum shape has been considered separately. We assumed that such objects result from massive SN progenitors with masses $M > 35\ M_\odot$. The collapse into such black holes occurs without significant mass loss. The spectra of GW from a galaxy having the same parameters as above in age of $7 \cdot 10^9$ years with (I) and without (II) massive BH are presented in Figure 3. From this figure it follows that in the second case there is a considerable increase of gravitational radiation at frequencies below $10^{-5.5}$ Hz. This can be due to the massive binary black holes. Its evolution is fully determined by orbital decay caused by GW radiation on the time scale

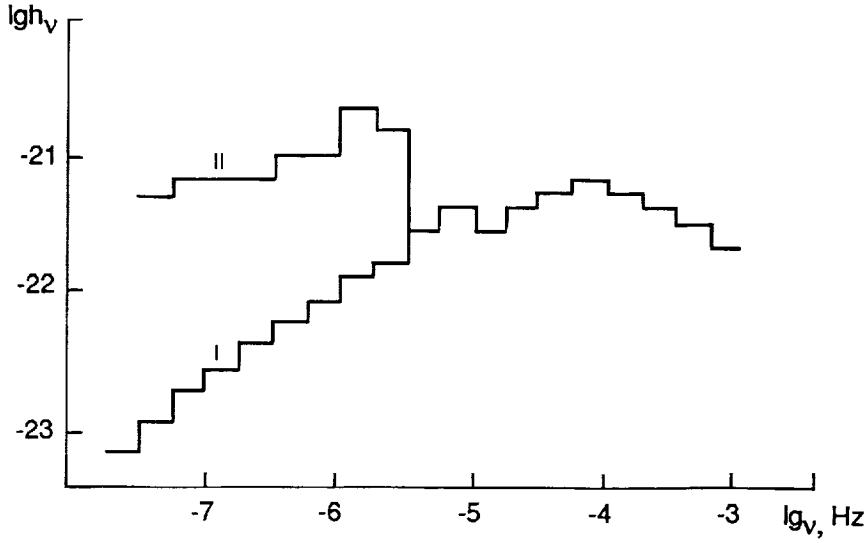


FIGURE 3 The spectra of GW from galaxy in age of $7 \cdot 10^9$ years with (I) and without (II) massive BH.

$$t_{GW} = (1.5 \cdot 10^8 yrs) \frac{(a/r_\odot)^4}{\frac{M_1 M_2}{M_\odot^2} \frac{(M_1+M_2)}{M_\odot}}$$

which exceeds a Hubble time for pairs with $a > 70R_\odot$. The shape of this spectral feature strongly depends on the assumptions about the massive BH formation and can sufficiently differ from this rough model. However, the existence of such a spectral feature could in principle be used as an indicator for massive BH presence.

In Figure 4, the event rate for GW pulses versus time is presented for a galaxy with the parameters described above and with a $\delta$-like star formation function. The type II SN results from the collapse of massive stars ($M > 10M_\odot$) at final stages of its evolution.

So the SNII explosions in such a galaxy occur only during the first $\sim$ 40 million years. In the time range 1 - 10 million years, this rate can be approximated by the formula:

$$f_{SNII}(t) = 50 \frac{N}{10^{11}} \{\frac{t}{10^6 yr}\}^{-0.46}$$

Another kind of event we considered is the coalescences of WDs, which occur within the interval of $10^7$ - $1.5 \cdot 10^{10}$ years. This event rate weakly depends on time and varies from 1 to 0.01 $yr^{-1}$.

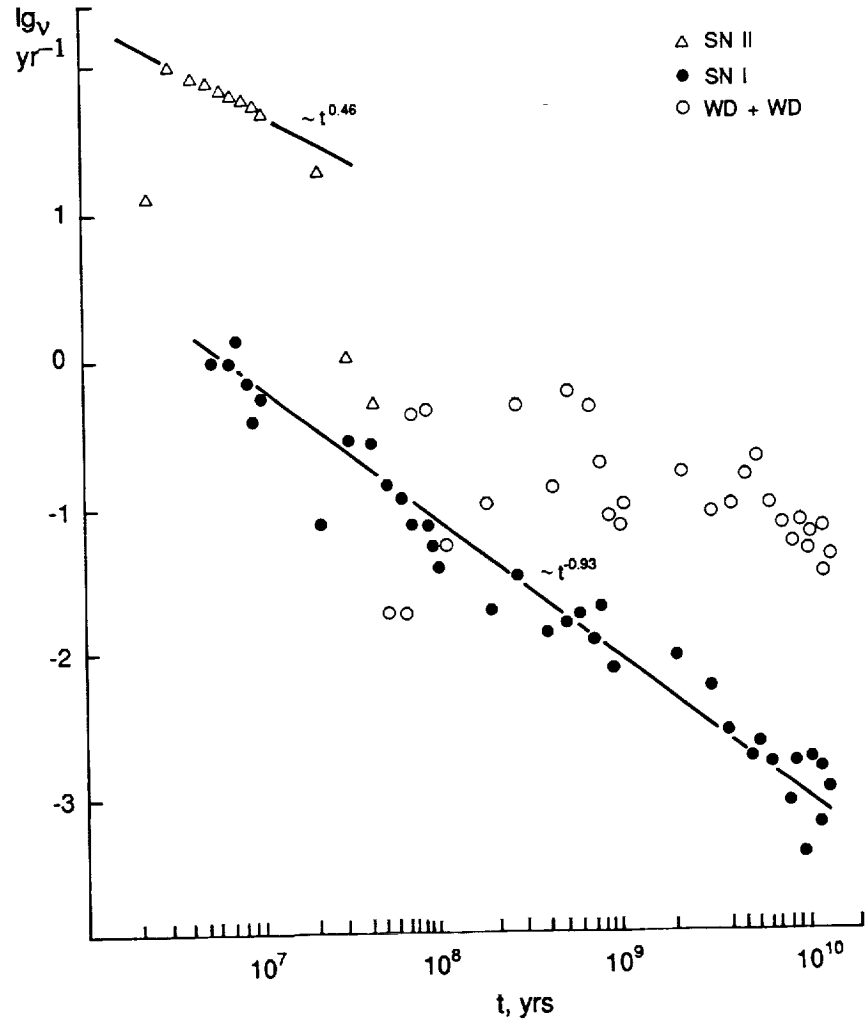


FIGURE 4 The rate of supernova explosions and of white dwarves coalescences in a galaxy with $\delta$-like star formation rate.

From all coalescing WDs we choose a group of binaries, whose total mass exceeds the Chandrasekhar limit. We consider such binaries as capable of producing the SNeI explosions. These events may be accompanied by supplementary GW pulses arising during a collapse into NS. The rate of SNeI between $6 \cdot 10^6$ and $1.5 \cdot 10^9$ years can be approximated as

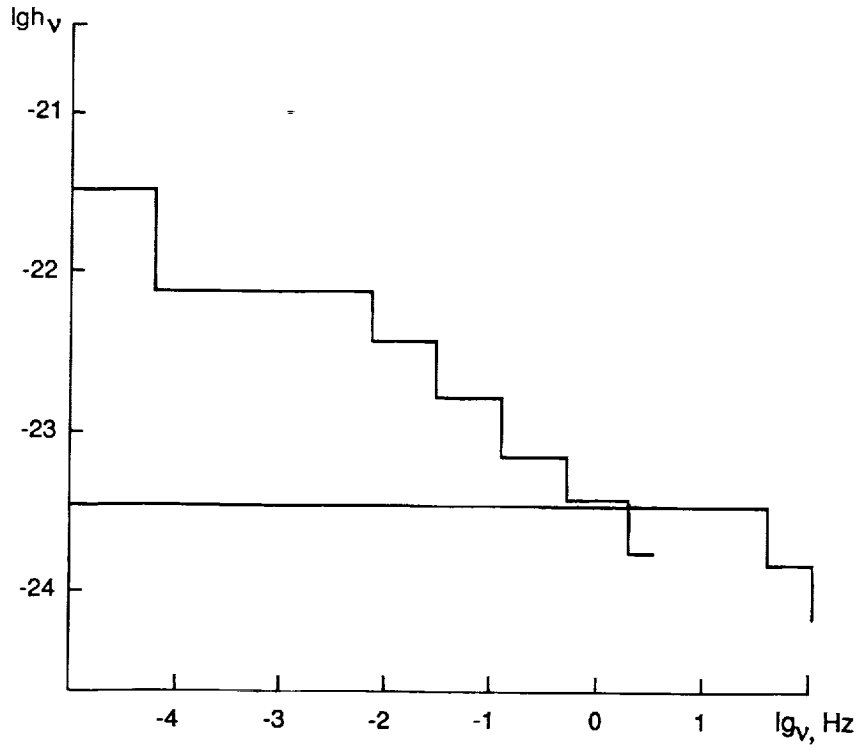


FIGURE 5 The dependence of the rate of GW pulses registration $\nu$ on a GW detector with the given sensitivity $h_\nu$.

$$f_{SNI}(t) = 1.8\frac{N}{10^{11}}\{\frac{t}{10^6 yr}\}^{-0.93}$$

Assuming the effectiveness of mass-energy conversion to be $\epsilon = 10\%$ of the total mass of a collapsing star we have estimated the dimensionless metric strain amplitude.

Integrating these expressions with the star formation rate functions for ellipticals and spirals and integrating over the whole space where the galaxies are thought to exist ($z \leq 3$) and using cosmological parameters described above, we have obtained the rate of arriving pulses with an amplitude not less than that given by the different kinds of SNe and of galaxies, i.e., the rate of the event's registration on a GW detector with the given sensitivity. This dependence is presented in Figure 5. The results for spirals were obtained analytically by Lipunov, Postnov *et al.* (1987).

## ACKNOWLEDGEMENTS

We would like to thank Dr. K.A. Postnov for useful discussions and comments.

## REFERENCES

Kornilov, V.G., and V.M. Lipunov. 1982. Sov. Astron. 27: 163.
Lipunov, V.M. 1987. Astrophys. Sp. Sci. 132: 1.
Lipunov, V.M., and K.A. Postnov. 1987. Sov. Astron. 31: 228.
Lipunov, V.M., and K.A. Postnov. 1987. Sov. Astron. 31: 288.
Lipunov, V.M., and K.A. Postnov. 1987. Sov Astoron. 31: 404.
Lipunov, V.M., and K.A. Postnov. 1988. Astrophys. Sp. Sci 145: 1.
Lipunov, V.M., K.A. Postnov, and M.E. Prokhorov. 1987. Astron. Astrophys. 176: L1.
Shapiro, S.L., and S.A. Teukolsky. 1983. Black Holes, White Dwarves, and Neutron Stars. Cornell University, Ithaca.
Thorne, K.S. 1987. In: Hawking, S.W., and W. Israel (eds.). 300 Years of Gravitation. Cambridge University Press, Cambridge. 330.
Zel'dovich, Ya.B., and I.D. Novikov. 1971. Relativistic Astrophysics. Chicago University Press. V. 1.

# Close Binary Stars in Globular Clusters

BRUCE MARGON
University of Washington

## ABSTRACT

Although close binary stars are thought theoretically to play a major role in globular cluster dynamics, virtually no non-degenerate close binaries are known in clusters. We review the status of observations in this area, and report on two new programs which are finally yielding candidate systems suitable for further study. One of the objects, a close eclipsing system in $\omega$ Cen, is also a blue straggler, thus finally providing firm evidence that globular cluster blue stragglers really are binary stars.

## INTRODUCTION

A growing body of theoretical work indicates that a small number of close binary stars dominate the dynamic evolution of globular star clusters (*e.g.*, Elson *et al.* 1987). For convenience, we here define a "close" binary as one with an orbital period of a few days or less. Such systems may have *binary* orbital velocities of several hundred km $s^{-1}$, compared with a typical single star *cluster* orbital velocity of just a few km $s^{-1}$. Therefore, literally just a handful of close binaries in a globular cluster can store as much kinetic energy of motion as possessed by the total of all $10^5$ single stars in the cluster! This energy may be liberated by three-body encounters of cluster single stars with the binaries, and this source term is likely to be the dominant counterbalance of kinetic energy sinks of stars escaping from the cluster. Cluster binaries may be primordial, or formed later through a variety of encounter processes, especially during the collapse of the cluster core due to the so-called "gravothermal catastrophe".

Elson *et al.* (1987) have pointed out the analogy of this energy source to thermonuclear fusion in stars: in this case, the cluster collapses, forms binaries, and then "burns" the orbital kinetic energy via encounters. A problem that observers may have with this elegant theoretical scenario is that virtually no close binary stars are known in globular clusters! Only one spectroscopic or eclipsing close binary, an object reported later in this paper, is known in any globular cluster. A small fraction of globular clusters are known to contain neutron star binary systems, evidencing themselves as either the X-ray bursters near the cluster centers, or as millisecond radio pulsars (although note that several of the latter systems are known to have binary periods of months rather than days, and thus store negligible kinetic energy). As only the very smallest fraction of globular cluster stars end their lives as neutron stars, however, one might expect binaries containing white dwarfs to be far more abundant in clusters (Verbunt and Meylan 1988), and systems with giant, subgiant, and main sequence components yet more common.

## SEARCHES FOR EVOLVED GLOBULAR CLUSTER BINARIES

White dwarf close binaries in globular clusters are probably most easily found if they are undergoing mass exchange. The analog of such a system in the field, outside of clusters, is the cataclysmic variable (CV). Of course, both novae and dwarf novae easily draw attention to themselves during their intense optical outbursts, but even in quiescence such systems can be located through a variety of techniques. The optical spectra of CVs in quiescence are highly distinctive (strong, broad emission lines), as are the colors (distinct ultraviolet excess). A decade of study has also revealed quiescent CVs to be prominent soft X-ray sources, with luminosities in the range $10^{30}$ through $10^{32}$ erg $s^{-1}$ (Córdova and Mason 1983, 1984).

Novae are relatively rare in the field, and so one might expect only a very small number in globular clusters. Indeed, only two such objects have ever been reported: one in NGC 6093 in the year 1860 (Pogson 1860; Luther 1860), and one in 1938 in M 14 (Hogg and Wehlau 1964; Shara *et al.* 1986), and cluster membership for the latter, although probable, is still uncertain. However, dwarf novae are more common in the field (Patterson 1984), and one might hope that the analog of these mass exchange red dwarf/white dwarf systems might be found in globular clusters. In fact, only two dwarf novae are known in globular clusters. These stars, both discovered long ago during outbursts, have been recently recovered in quiescence: V101 in M 5 (Margon *et al.* 1981), and V4 in M 30 (Margon and Downes 1983). These two objects are poorly studied to date; although at least V101 is known to still be undergoing outbursts (Shara *et al.* 1987), neither has ever been caught in outburst by a spectroscopist, and neither has been observed

for X-ray emission. Thus definite examples of white dwarf close binaries in globular clusters remain rare and poorly understood.

The suggestion by Hertz and Grindlay (1983*a*, *b*) that the low-luminosity X-ray sources observed outside of the cores of several globular clusters by the *Einstein* Observatory are mass-exchange close binary systems containing a white dwarf, analogous to the field cataclysmic variables (CVs), is therefore of great interest. These authors derive a luminosity function which implies that the galactic globular cluster system contains a total of $\sim 10^3$ such objects, a conclusion also reached by Krolik (1984) and Hertz and Wood (1985). *EXOSAT* observations have confirmed a few of these sources (Verbunt *et al.* 1986; Koch-Miramond and Aurière 1987; Aurière *et al.* 1989).

It is sometimes not amply enough stressed that all of the evidence which identifies these systems as white dwarf close binaries is quite indirect, based primarily on the fact that these sources have considerably lower X-ray luminosities than the highly luminous sources located within a few arcseconds of the cluster cores; the latter are now widely agreed to be neutron star binary systems (Lewin 1980; Lewin and Joss 1983; Grindlay *et al.* 1984). In particular, in spite of several sensitive attempts, there has never been an optical identification of a single one of these low-luminosity cluster X-ray sources.

Is there reason to suspect this evidence, and/or do reasonably plausible competing models exist? Verbunt *et al.* (1984) have pointed out the curious fact that all of these "low luminosity" sources, if in fact cluster members, have X-ray luminosities an order of magnitude larger than the classical U Gem systems in the field, despite their supposed physical similarity to those systems. Furthermore, if these systems share the most basic property of the known dwarf novae (*i.e.*, optical outbursts) it seems surprising that there could be a population of $10^3$ of them in the Galaxy, and not one has ever been reported in optical outburst, despite a century of intensive photographic study of globular clusters for variable stars. Crowding is not likely to totally suppress discovery of the outbursts, if the sources reported by Hertz and Grindlay (1983*b*) are indicative of the class; the majority of them are many core radii from the cluster centers, and inspection of catalogs of cluster variable stars (*e.g.*, Hogg 1973) show that there are numerous single variables cataloged equally close to the core, at magnitudes equivalent to that that would be reached by a globular cluster CV in outburst. The two known cluster CVs cited above were in fact initially found exactly this way, despite their location in relatively crowded regions of the cluster.

Verbunt *et al.* (1984) have suggested that the sources may instead be quiescent X-ray transients. Some of these sources may have an even simpler explanation: Hertz and Grindlay (1983*a*) calculate that ~3.3 of the 8 sources they discuss may be background QSO/AGN superpositions

or foreground stellar coronal sources. Furthermore, three clusters are reported to have spatially extended X-ray emission as well (Hartwick *et al.* 1982), raising the possibility that some of the reported point sources are confused or nonexistent. Margon and Bolte (1987) showed that if the X-ray sources reported by Hertz and Grindlay (1983*a*, *b*) in the cluster $\omega$ Centauri were indeed like the field dwarf novae, they might be optically identified due to their peculiar colors; yet these workers were unable to locate any such counterparts (see also Shara *et al.* 1988). We do know that the cluster CV M5 V101, with $(U - B) = -0.9$ in quiescence,[1] does show the distinctive color of the field CVs, so this negative result is significant. Thus, the nature of the low-luminosity cluster X-ray sources remains terribly uncertain, and it is far from obvious that all, or even many, are truly close binary stars.

Cluster binaries with red giant components at least have the virtue of being bright enough for easy spectroscopic observation. Gunn and Griffin (1979), working at a radial velocity precision of 1 km $s^{-1}$, failed to find even a single binary candidate amongst extensive observations of 111 giants in M3 spanning five years. However, a few successes are finally emerging. Pryor *et al.* (1988*a*) have shown that vZ 164 in M3 is probably a binary with a period of a few years, and Pryor *et al.* (1989) report a handful of further candidate binaries, all with periods of years. Although these systems are at least true cluster binaries in the classical sense, their very long periods of course imply that they store negligible orbital kinetic energy, and cannot contribute to the energy budget of cluster, the problem which introduces this paper.

The only other candidate for a short period globular cluster binary of which we are aware is V78 in the direction of $\omega$ Cen (Bailey 1902). This eclipsing Algol with a $1.2^d$ period appears frequently in the literature with comments of varying degrees of certitude that it is a cluster member (*e.g.*, Geyer 1967, 1971; Sistero 1968), but based on radial velocity it is now known definitely *not* to be a cluster member (Geyer and Vogt 1978).

The very limited success in finding cluster binaries with evolved companions, either degenerate stars or red giants, has led my colleagues and me to initiate a number of programs aimed at finding binaries with main sequence components. We believe we have met with success through two different approaches.

## AN ECLIPSING BLUE STRAGGLER IN A GLOBULAR CLUSTER

Blue stragglers, especially in globular clusters, have long rankled both

[1] Multicolor photometry for M5 V101 appears in Richer and Fahlman (1987), although the object is anonymous in that paper; it is the most extreme ultraviolet point in their Figure 11.

observers and theorists; their position on the color-magnitude diagram, with normal main sequence color and luminosity, but lying far hotter than the cluster turnoff, is simply inconsistent with stellar evolution. Explanations abound, but there are few hard facts to back up these theories. Specifically, for more than 20 years they have been said to be close binaries (McCrea 1964; Hoyle 1964), with their odd color/luminosity resulting from an extensive past episode of mass transfer, but there is no direct evidence for this: not a single globular cluster straggler is an eclipsing or spectroscopic binary. Alternative theories, involving long-lived single stars undergoing odd evolution, are also viable (Wheeler 1979). Some evidence that blue stragglers in NGC 5466 and NGC 5053 have a peculiarly concentrated spatial distribution, and thus a higher primordial mass than other evolved stars in the cluster, has been provided recently (Nemec and Harris 1987; Nemec and Cohen 1989). As has been previously stressed, however, this does not directly discriminate between binary mass exchange and mixing theories (Mathieu and Latham 1988).

Some hope of addressing the problem arose when the eclipsing system NJL 5 was identified in the field of $\omega$ Cen, and it was pointed out that the star lies near the blue straggler area of the cluster color-magnitude diagram (Niss *et al.* 1978). This object may be identified with entry no. 5876 in the Woolley catalogue (Woolley 1966), and star 5642 of Dickens *et al.* (1988). The period is $1.4^d$, and there is a deep (1.2 mag) primary eclipse. However, a strange twist of fate appears to have quenched interest in the system: based on early photometry and the shape of the light curve, it was concluded that NJL 5 is probably not a cluster member (Liller 1978). No spectra have ever been published for this object, although one unpublished spectrum has been cited as compatible with membership (Jensen and Jørgensen 1985). As it was obtained in the green and shows only two spectral lines (Jørgensen 1987), it must surely be regarded as inconclusive.

We obtained spectra of NJL 5 on five nights in 1988 at moderate (2 Å) spectral resolution, using the RGO spectrograph and IPCS detectors at the Anglo-Australian Telescope. The bright cluster horizontal branch star ROA 4153 (Cannon and Stobie 1973), of color similar to NJL 5, was used as a radial velocity standard. The average of the five velocities of NJL 5 at various phases throughout the $1.4^d$ photometric period is $8 \pm 7$ km s$^{-1}$ relative to the comparison star velocity, and thus, given the high velocity of $\omega$ Cen, 232 km s$^{-1}$ (Meylan and Mayor 1986), the object is most certainly a cluster member. Our individual absolute velocity determinations for both NJL 5 and ROA 4153, although less precise than the cross-correlation results, also clearly indicate that both stars are cluster members. NJL 5 is also almost certainly a blue straggler: the spectral type is near A5, and it is far below the cluster horizontal branch (DaCosta *et al.* 1986). The spectrum is quite ordinary: the dominant features are Balmer absorptions,

with both stellar and interstellar Ca K lines also visible. There is no sign of a secondary spectrum. We have also obtained one low resolution red ($\lambda\lambda$5500 – 10,000 Å) spectrum of NJL 5 with the Faint Object Red Spectrograph at the AAT, and again see no obvious sign of a secondary, although considerably more extensive phase coverage is desirable to strengthen this conclusion.

As a historical footnote, we point out that the $(B - V)$ color for the star listed in the Woolley (1966) catalogue differs from the normal color of the system by 1 mag, for reasons which are unclear. A correct color appears in more recent photometry (Jensen and Jørgensen 1985; Dickens *et al.* 1988).

NJL 5 now becomes very important: not only is it the first and only globular cluster blue straggler known to be a binary, but the very large eclipse depth shows the inclination is near 90°, and so the orbit is soluble and all system parameters may ultimately be obtained. Our existing moderate resolution spectroscopy is already tantalizing. Our five spectra have good phase coverage, and no radial velocity variations are convincingly detected; a conservative upper limit on the orbit $K$ velocity is 30 km $s^{-1}$. This already implies a very high mass ratio and an exotic, undermassive secondary (recall that the unseen companion has radius comparable to the A5 star to cause the deep primary eclipse). Thus it appears that the solution of the NJL 5 orbit may confirm the widely held but unproven scenario that blue stragglers result from a previous episode of very extensive mass transfer. There are several bright Algols in the field that have periods and light curves similar to NJL 5 and presage the probable parameters: RY Aqr (Helt 1987) and RT Per (Mancuso *et al.* 1977) both have $q \sim 0.2$, with K$\sim$ 30 and 60 km $s^{-1}$, respectively. The low amplitude we infer for the radial velocity variations is presumably responsible for the failure of many previous observers to detect the binarity of blue stragglers in old open clusters (Stryker and Hrivnak 1984). We have already obtained and are currently analyzing the necessary spectroscopy at much higher resolution to define the orbital parameters of NJL 5.

This work on NJL 5 was done collaboratively with Russell Cannon, and will be described more fully elsewhere (Margon and Cannon 1989).

## FAINT MAIN SEQUENCE BINARIES IN GLOBULAR CLUSTERS

What are the prospects for detection of main sequence binaries of later spectral type than blue stragglers, and thus at a less odd stage of evolution? A conceptually simple way of identifying such binaries in globular clusters has been known for many years (Steinlin 1956; Fernie and Rosenberg 1961): *if* a cluster color-magnitude (C-M) diagram can be obtained with very high photometric precision, and *if* nature cooperates with a metallicity spread

sufficiently small to cause the cluster main sequence to have negligible intrinsic width, then cluster binaries will be apparent by their location in the C-M diagram at a range of luminosity values slightly too high for their color, up to a cutoff luminosity of 0.75 magnitudes above the normal main sequence, corresponding to a binary with two equal mass components, and thus a luminosity enhancement of 2×. For the particularly simple case where the majority of binaries have equal mass components, a situation which is in fact thought by some to be dynamically favored (Hills 1975), then these binaries will form a distinct, second main sequence parallel to, but 0.75 mag above, the normal cluster sequence.

Until quite recently it has been impossible to test this simple concept, because very high precision photometry down to limiting magnitudes appropriate for the typical cluster main sequence was impossible, especially in the very crowded fields near the cluster core, where one expects binaries to sink in relaxed clusters, as they are the most massive stars. The advent of CCD detectors and several software systems suitable for precision photometry in crowded fields has changed the situation.

Some clusters prove to have broad main sequences, and this technique to search for binaries will clearly never be applied there. The foremost example is $\omega$ Cen, where spectroscopy of giants and subgiants has long indicated a range of metal abundances (*e.g.*, Norris 1980), thereby leading to the expectation that the main sequence would have similar metallicity dispersion, and thus a wide range of luminosities for a given color. Recent color-magnitude diagrams of $\omega$ Cen which reach the main sequence do indeed show this breadth (Walker 1986; Alcaino and Liller 1987; Shara *et al.* 1988), although perhaps one should be suspicious of too easily discovering what is expected! This cluster is of course at low galactic latitude, so foreground contamination of the color-magnitude diagram by non-members may be a problem; indeed, Bell *et al.* (1981) find that fully *half* of the subgiants for which they have spectra (admittedly in an outer field) are velocity non-members.

Regardless of the difficulties with $\omega$ Cen, recent precision photometry has uncovered a number of clusters with intrinsically very narrow main sequences, thus enabling a search for main sequence binaries. A good example is 47 Tuc (Hesser *et al.* 1987), where no binary sequence is evident. However, a candidate "parallel" main sequence has been noted in the sparse halo cluster E3 by Hesser *et al.* (1984). To our knowledge radial velocities are not yet available for these faint objects. Even if close binaries are ultimately found in E3, their applicability to the globular cluster dynamics paradox discussed above will be ambiguous, as E3 is such an extraordinarily sparse object, and indeed not even uniformly classified as globular.

We have recently been involved in a program of precision multicolor CCD photometry of four "traditional" globular clusters, and initial results

on the cluster ages, metallicities, chemical homogeneity, etc., have been published for NGC 362 (Bolte 1987*a*) and NGC 7099 (Bolte 1987*b*, 1989). The photometry, obtained with the CTIO 4m telescope, reaches far down onto the main sequence, and we do indeed find that its intrinsic width is unresolved at our level of precision, thereby enabling a search for the "parallel" main sequence due to putative binaries. For each of our four clusters, we have fields at three different core radii, potentially allowing a search for mass segregation as well. The quality of these data very substantially exceeds anything in the previous literature on these clusters, and a second main sequence separated by ~0.75 mag in luminosity would clearly stand out, greatly exceeding both the uncertainties in our photometry and the intrinsic (as yet unresolved) main sequence breadth. Sadly, no such sequence is apparent in any of the fields in any of our four clusters, with one exception: the most central field in NGC 288.

Perhaps with hindsight, NGC 288 is an ideal globular cluster for a search for main sequence binaries. It has a modest distance modulus, ~14.5 mag, permitting precise photometry far down on the main sequence. There is virtually no foreground contamination at this galactic latitude ($b = -89°$!). Most important of all, the object, although unquestionably a globular cluster by any definition, is sufficiently sparse to be virtually transparent almost all the way into the core. Thus, crowding is minimal in the innermost field, exactly where one expects the binaries to sink. In Figure 1 we show our C-M diagram of the central field in NGC 288. One sees immediately approximately one dozen stars displaced upward in luminosity from the otherwise cleanly defined main sequence. The displaced stars are spatially well separated by our reduction programs, so we have no particular reason to suspect that their distinguishing characteristic is merely poor quality photometry. As an interpretive aid, we show with the solid line where the fiducial main sequence would fall if displaced upward in luminosity by 0.75 mag, as expected for a sequence of equal mass binaries. The dozen outlying objects fall quite precisely on this sequence. This coincidence may be a conspiracy of nature, but if so it is particularly cruel that it occurs in the one field where we should have the best chance of seeing the binary sequence, namely the most central field we possess with precision photometry. We thus do not suggest that NGC 288 is in any way unique, but merely that if all clusters in fact possess a few of these objects, it is quite logical that we would see them in this cluster first.

One would be naïve to believe that the objects offset from the main sequence in Figure 1 are binaries strictly on the grounds of our photometry. Surely either eclipses or radial velocity variations must be required to convincingly argue that the first population of globular cluster main-sequence binaries has been discovered. Eclipses would be observationally straightforward to search for, but statistically unlikely to be observed. A negative

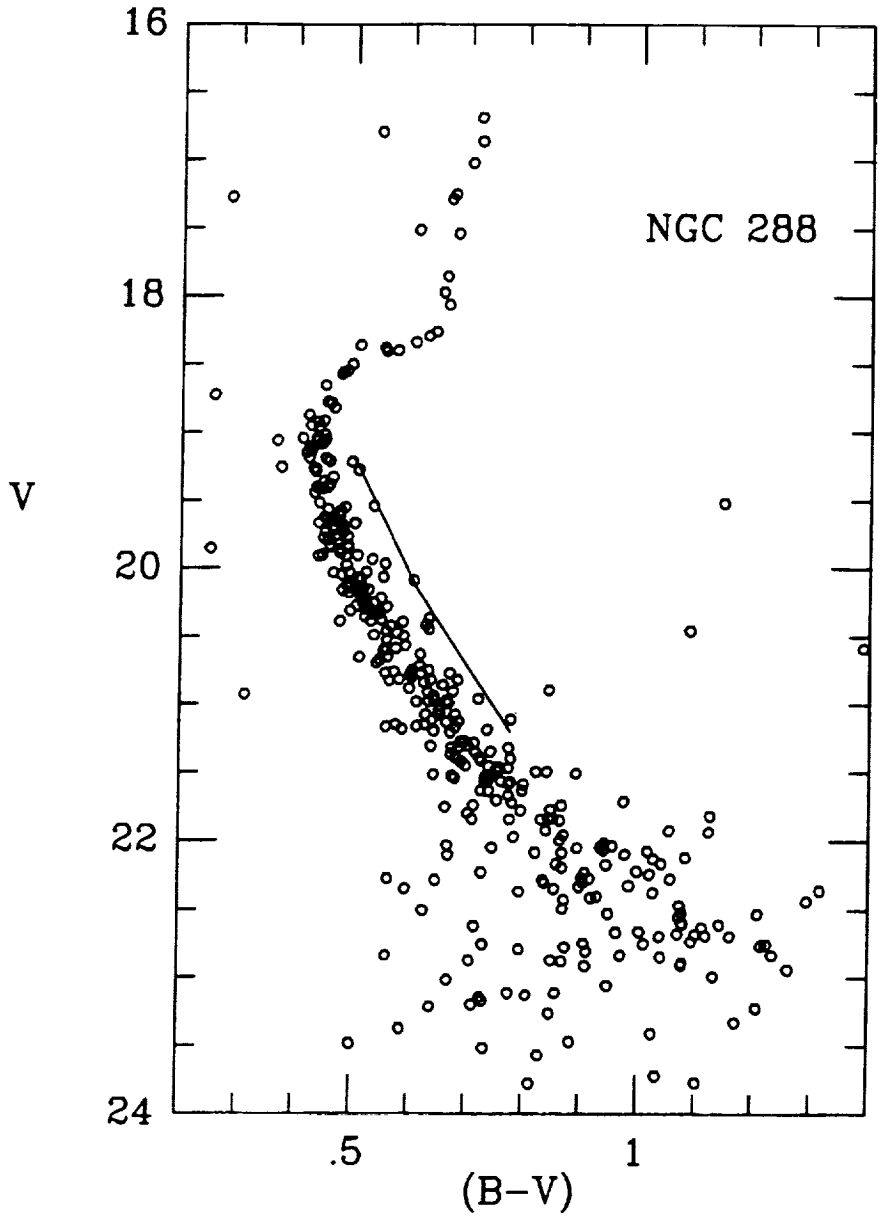


FIGURE 1 A color-magnitude diagram for NGC 288, derived from CCD photometry obtained at the prime focus of the 4m telescope of the Cerro Tololo Interamerican Observatory. The solid line is a locus offset by 0.75 mag from a fiducial main sequence. The dozen or so candidate main-sequence binaries, lying quite close to this line, are readily apparent.

result from an extensive series of eclipse observations would probably not be informative. Radial velocity variations, on the other hand, are certainly present if the objects are truly binaries, and, as always subject to the unknown inclination factors, will be substantial in the close binaries that we seek. Of course, with our dozen or so candidates, it is quite unlikely that all have unfavorable inclinations.

In collaboration with M. Bolte of the Dominion Astrophysical Observatory, we have begun a program to obtain repeated observations of radial velocities for the ten or so brightest, best separated objects on this parallel main-sequence in NGC 288. This is a difficult observational problem: we seek a large number of velocities of accuracy $\sim$10 km s$^{-1}$ on objects of $V \geq 19.5$. Until very recently, one would be hard pressed to find in the literature a spectrum of *any* cluster main sequence star, much less a program of repeated observations of many objects at reasonably high dispersion. The recent development in instrumentation that has made this program feasible is the introduction of multiple-object fiber-fed spectrographs at several of the world's 4m-class telescopes. This project is of course ideal for such an instrument, as all of the candidate stars are in immediate proximity, lying on the same $3' \times 5'$ CCD chip, and we desire all of the radial velocities simultaneously, not knowing which are true binaries, and which have favorable inclinations. Further, we can employ the many otherwise unused fibers to obtain spectra of brighter cluster members in the immediate proximity, which are not only of astrophysical interest, but provide a large number of local velocity standards,[2] as well as a variety of control objects so important to this precision work, *e.g.*, anonymous stars of comparable magnitude and crowding to our candidate binaries. The colors of the candidates indicate spectral types near solar, and so we may anticipate ample absorption lines for radial velocity determination.

We are conducting our observations using the fiber-optic coupled multi-object spectrograph (FOCAP) (Gray 1986; Parry and Gray 1986) at the 3.9m Anglo-Australian Telescope. This system uses approximately 60 fibers to feed as many star or sky spectra to the normal RGO spectrograph, using the Image Photon Counting System (IPCS) as a two-dimensional detector. We use a grating which yields $\sim$1000 Å of spectral coverage, with 2 Å resolution, centered near $\lambda$4200 to take advantage of the region of peak efficiency of the IPCS. We have thus far obtained observations at two epochs in 1987–88 which convince us that the project is (just!) feasible in excellent observing conditions; typical integration times to obtain $\sim$100 counts pixel$^{-1}$ above sky at this dispersion on these faint stars are 12,000 sec. In Figure 2, we show an example of one of the spectra so obtained of one of our main

[2] Several dozen giants and horizontal branch stars in NGC 288 already have velocities determined to an accuracy of $\sim$0.6 km s$^{-1}$ via radial velocity spectrometer observations (Pryor *et al.* 1988*b*).

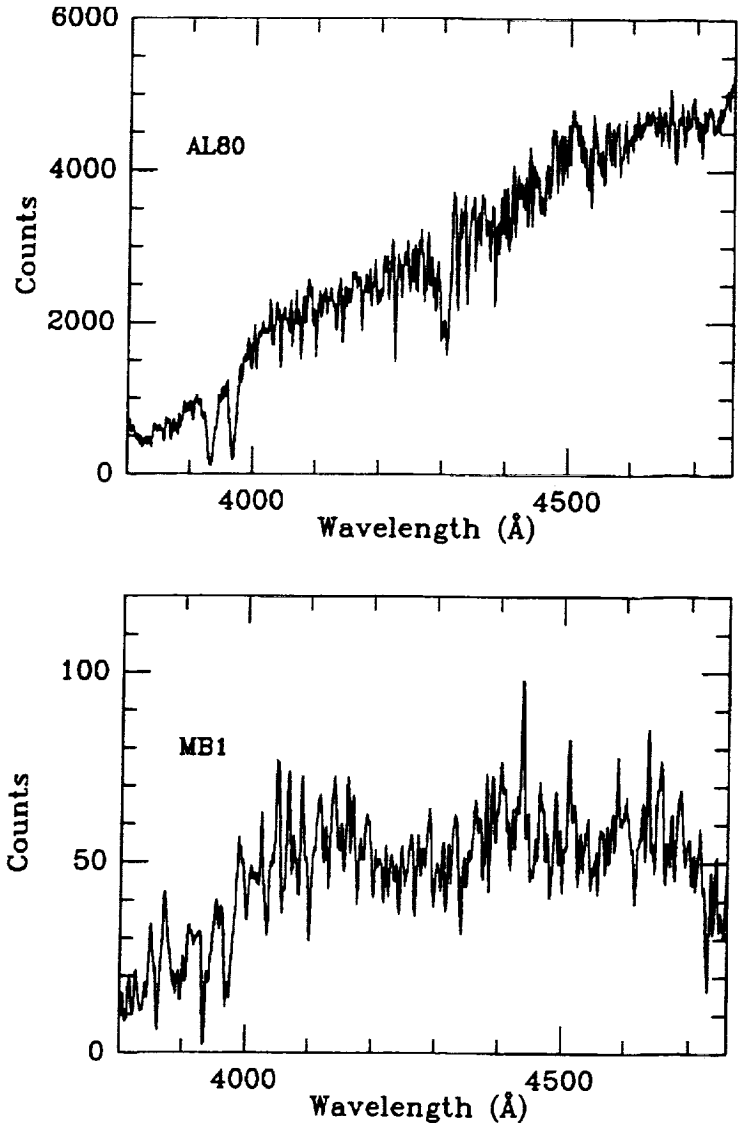


FIGURE 2 Two of the sixty spectra obtained simultaneously in the NGC 288 field at the Anglo-Australian Telescope in 1988 July, using the fiber-optic coupled multi-object spectrograph (FOCAP) and the Image Photon Counting System (IPCS) detector. Lower panel: One of the candidate main-sequence binaries, MB1, an object with $V = 19.2, (B-V) = 0.50$; despite the modest signal-to-noise ratio of the spectrum, one can clearly see $H\delta$, $H\gamma$, and Ca $H$ & $K$ absorption lines. Upper panel: one of the bright radial velocity standard stars in the cluster, AL80, a giant with $V = 13.89, (B-V) = 1.14$ (Alcaino and Liller 1980); a precise ($\pm 0.7$ km s$^{-1}$) velocity for this star has been obtained by Pryor *et al.* (1988*b*) with a radial velocity spectrometer. All of the features and structure in this spectrum are actual absorption lines in the object. At this dispersion, cross-correlation of the two stars can yield velocities of accuracy $\sim$6 km s$^{-1}$ if there is reasonable signal in the program objects.

sequence binary candidates, together with that of one of the bright giant radial velocity standards in the cluster. Cross-correlation analysis allows us to derive velocities for the binary candidates to an accuracy of $\sim$6 km $s^{-1}$. As the necessary multiple-epoch observations are still under way, these results must be viewed simply as a progress report at this time. However, for the candidates where we have sufficient signal, we can already say, based on their derived velocities, that these faint stars are indeed cluster members; their striking position on the C-M diagram cannot be explained merely by superposition of a non-member. Thus we are encouraged by the prospect that current instrumentation is indeed adequate to reveal radial velocity variations in main sequence binaries in this and similar clusters in the near future.

## CONCLUSION

In an interval of only a few years, we have progressed from knowing of literally *no* non-degenerate binary stars in globular clusters, to a short list of candidates of a variety of luminosities. Whether the very crowded inner cores of the clusters currently hide a population of close binaries that would otherwise be easily distinguished by their odd colors and luminosities will presumably become clear with even the first handful of multicolor images from the *Hubble Space Telescope.* Thus prospects are bright that in the next few years, observations will finally catch up to, and hopefully overtake, the theory of close binary stars in globular clusters.

## ACKNOWLEDGEMENTS

Most of what little I know about globular clusters and binaries therein has been taught to me by Michael Bolte, and I am indebted to him for his continued collaborative efforts in much of the work described here. I thank Russell Cannon and all of the staff of the Anglo-Australian Observatory for hosting me during the sabbatical year where much of this work was done; Warrick Couch was particularly essential in accomplishing many of these observations. I appreciate useful discussions with P. Hut, D. Popper, C. Pryor, and H. Richer. E. Wilcots has aided in the data reduction. I was a Visiting Astronomer at Cerro Tololo Interamerican Observatory, National Optical Astronomy Observatories, which is operated by AURA, Inc., under contract to the NSF. This work has been supported in part by NASA Contract NAS5-29293 and NASA Grant NGT-70050.

## REFERENCES

Alcaino, G., and W. Liller. 1980. The main sequence of the globular cluster NGC 288. Astronomical Journal 85: 1592–1603.

Alcaino, G., and W. Liller. 1987. BVRI CCD photometry of Omega Centauri. Astronomical Journal 94: 1585–1599.

Aurière, M., L. Koch-Miramond, and S. Ortolani. 1989. The X-ray source in the core of 47 Tucanae. Astronomy and Astrophysics 214: 113–122.

Bailey, S. I. 1902. A discussion of the variable stars in the cluster $\omega$ Centauri. Harvard Annals 38: 1–246.

Bell, R. A., G. L. H. Harris, J. E. Hesser, and R. D. Cannon. 1981. Spectroscopic evidence for a wide range in abundances among faint subgiant stars in the globular cluster Omega Centauri. Astrophysical Journal 249: 637–646.

Bolte, M. 1987*a*. Main sequence CCD photometry of the globular cluster NGC 362. Astrophysical Journal 315: 469–479.

Bolte, M. 1987*b*. Deep CCD photometry of the globular cluster NGC 7099. Astrophysical Journal 319: 760–771.

Bolte, M. 1989. Mass segregation in the globular cluster M30. Astrophysical Journal 341: 168–174.

Cannon, R. D., and R. S. Stobie. 1973. Photometry of southern globular clusters. I. Bright stars in $\omega$ Centauri. Monthly Notices of the Royal Astronomical Society 162: 207–225.

Córdova, F. A., and K. O. Mason. 1983. Accreting degenerate dwarfs in close binary systems. Pages 147–187 In: Lewin, W. H. G., and E. P. J. van den Heuvel (eds.). Accretion Driven Stellar X-ray Sources. Cambridge University Press, Cambridge.

Córdova, F. A., and K. O. Mason. 1984. X-ray observations of a large sample of cataclysmic variable stars using the Einstein Observatory. Monthly Notices of the Royal Astronomical Society 206: 879–897.

DaCosta, G. S., J. Norris, and J. V. Villumsen. 1986. The blue stragglers of Omega Centauri. Astrophysical Journal 308: 743–754.

Dickens, R. J., I. R. Brodie, E. A. Bingham, and S. P. Caldwell. 1988. A catalogue of magnitudes and colours in the globular cluster Omega Centauri. Rutherford Appleton Laboratory Publication RAL 88-004.

Elson, R., P. Hut, and S. Inagaki. 1987. Dynamical evolution of globular clusters. Annual Review of Astronomy and Astrophysics 25: 565–601.

Fernie, J. D., and W. J. Rosenberg. 1961. The effects of unresolved binaries in three-color photometry. Publications of the Astronomical Society of the Pacific 73: 259–263.

Geyer, E. H. 1967. Eine dreifarbenphotometrie von Omega Centauri (NGC 5139). Zeitschrift für Astrophysik 66: 16–32.

Geyer, E. H. 1971. A photoelectric investigation of the eclipsing binary V78 in Omega Centauri (NGC 5139). Pages 235–237 In: Proceedings of the IAU Colloquium 15, New Directions and New Frontiers in Variable Star Research, Veröffentlichungen der Remeis-Sternwarte Bamberg, IX, No. 100.

Geyer, E. H., and N. Vogt. 1978. On the membership of the RR$_s$ star V65 and the EA binary V78 in Omega Centauri (NGC 5139). Astronomy and Astrophysics 67: 297–299.

Gray, P. M. 1986. Anglo-Australian Observatory fibre system. Proceedings of the Society of Photo-Optical Instrumentation Engineers 627: 96–104.

Grindlay, J. E., P. Hertz, J. E. Steiner, S. S. Murray, and A. P. Lightman. 1984. Determination of the mass of globular cluster X-ray sources. Astrophysical Journal (Letters) 282: L13–16.

Gunn, J. E., and R. F. Griffin. 1979. Dynamical studies of globular clusters based on photoelectric radial velocities of individual stars. I. M3. Astronomical Journal 84: 752–773.

Hartwick, F., A. Cowley, and J. Grindlay. 1982. Evidence for extended X-ray emission from globular clusters. Astrophysical Journal (Letters) 254: L11–13.

Helt, B. E. 1987. Four-color photometry of eclipsing binaries. XXVI A. RY Aqr: a low-mass semidetached system with intrinsic variability. Astronomy and Astrophysics 172: 155–166.

Hertz, P., and J. E. Grindlay. 1983*a*. X-ray evidence for white dwarf binaries in globular clusters. Astrophysical Journal (Letters) 267: L83–87.

Hertz, P., and J. E. Grindlay. 1983*b*. An X-ray survey of globular clusters and their X-ray luminosity function. Astrophysical Journal 275: 105–119.

Hertz, P., and K. S. Wood. 1985. The nature of the low-luminosity globular cluster X-ray sources. Astrophysical Journal 290: 171–184.

Hesser, J. E., W. E. Harris, D. A. Vandenberg, J. W. B. Allwright, P. Shott, and P. B. Stetson. 1987. A CCD color-magnitude study of 47 Tucanae. Publications of the Astronomical Society of the Pacific 99: 739–808.

Hesser, J. E., R. D. McClure, T. G. Hawarden, R. D. Cannon, R. von Rudloff, B. Kruger, and D. Egles. 1984. A new color-magnitude diagram for the peculiar star cluster E3=C0921-770. Publications of the Astronomical Society of the Pacific 96: 406–418.

Hills, J. G. 1975. Encounters between binary and single stars and their effect on the dynamical evolution of stellar systems. Astronomical Journal 80: 809–825.

Hogg, H. S. 1973. A third catalogue of variable stars in globular clusters comprising 2119 entries. Publications of the David Dunlap Observatory 3, No. 6, 1–75.

Hogg, H. S., and A. Wehlau. 1964. A photographic nova in the globular cluster Messier 14. Journal of the Royal Astronomical Society of Canada 58: 163–166.

Hoyle, F. 1964. Clusters and stellar evolution. Royal Observatory Bulletin 82: 91.

Jensen, K. S., and H. E. Jørgensen. 1985. CCD based $B$ and $V$ lightcurves for the eclipsing binary NJL 5 in Omega Centauri. Astronomy and Astrophysics Supplement 60: 229–236.

Jørgensen, H. E. 1987. private communication.

Koch-Miramond, L., and M. Aurière. 1987. X-ray and UV observations of $\omega$ Centauri with EXOSAT. Astronomy and Astrophysics 183: 1–8.

Krolik, J. H. 1984. The appearance, number and history of highly compact binary systems in globular clusters. Astrophysical Journal 282: 452–465.

Lewin, W. H. G. 1980. X-ray burst sources in globular clusters and the galactic bulge. Pages 315–350 In: Hanes, D., and B. Madore (eds.). Globular Clusters. Cambridge University Press, Cambridge.

Lewin, W. H. G., and P. C. Joss. 1983. X-ray bursters and the X-ray sources of the galactic bulge. Pages 41–115 In: Lewin, W. H. G., and E. P. J. van den Heuvel (eds.). Accretion Driven Stellar X-ray Sources. Cambridge University Press, Cambridge.

Liller, M. H. 1978. An eclipsing binary in the field of $\omega$ Cen. Information Bulletin on Variable Stars 1527.

Luther, E. 1860. Beobachtung von veränderlichen sternen. Astronomische Nachrichten 53: 293.

Mancuso, S., L. Milano, and G. Russo. 1977. The semi-detached system RT Persei and its light curve. Astrophysics and Space Science 47: 277–298.

Margon, B., and M. Bolte. 1987. The low-luminosity X-ray sources in Omega Centauri. Astrophysical Journal (Letters) 321: L61–65.

Margon, B., and R. Cannon. 1989. An eclipsing blue straggler in $\omega$ Centauri. Observatory 109: 82–84.

Margon, B., and R. A. Downes. 1983. A second cataclysmic variable in a globular cluster. Astrophysical Journal (Letters) 274: L31–35.

Margon, B., R. A. Downes, and J. E. Gunn. 1981. M5 V101: a close binary system in a globular cluster. Astrophysical Journal (Letters) 247: L89–92.

Mathieu, R. D., and D. W. Latham. 1988. The spatial distribution of spectroscopic binaries and blue stragglers in M67. Pages 675–676 In: Grindlay, W. H. G., and A. G. Davis Philip (eds.). Proceedings of IAU Sympo sium 126, Globular Cluster Systems in Galaxies. Kluwer, Dordrecht.

McCrea, W. H. 1964. Extended main-sequence of some stellar clusters. Monthly Notices of the Royal Astronomical Society 128: 147–155.

Meylan, G., and M. Mayor. 1986. Studies of dynamical properties of globular clusters. II. The rotation, velocity dispersion and mass of $\omega$ Centauri and 47 Tucanae. Astronomy and Astrophysics 166: 122–142.

Nemec, J. M., and C. Harris. 1987. Blue straggler stars in the globular cluster NGC 5466. Astrophysical Journal 316: 172–188.

Nemec, J. M., and J. G. Cohen. 1989. Blue straggler stars in the globular cluster NGC 5053. Astrophysical Journal 336: 780–797.

Niss, B., H. E. Jørgensen, and S. Laustsen. 1978. A search for new variables in the globular cluster Omega Centauri. Astronomy and Astrophysics Supplement 32: 387–393.

Norris, J. 1980. The correlation of cyanogen, calcium, and the heavy elements on the giant branch of Omega Centauri. Pages 113–123 In: Hanes, D., and B. Madore (eds.). Globular Clusters. Cambridge University Press, Cambridge.

Parry, I. R., and P. M. Gray. 1986. An automated multiobject fibre optic coupler for the Anglo-Australian Telescope. Proceedings of the Society of Photo-Optical Instrumentation Engineers 627: 118–124.

Patterson, J. 1984. The evolution of cataclysmic and low-mass X-ray binaries. Astrophysical Journal Supplement 54: 443–493.

Pogson, N. 1860. Remarkable changes observed in the cluster 80 Messier. Monthly Notices of the Royal Astronomical Society 21: 32–33.

Pryor, C. P., D. W. Latham, and M. L. Hazen. 1988*a*. A search for spectroscopic binaries in the globular cluster M3. Astronomical Journal 96: 123–138.

Pryor, C., R. D. McClure, J. M. Fletcher, and J. E. Hesser. 1988*b*. A survey of globular cluster velocity dispersions. Pages 661–662 In: Grindlay, J. E., and A. G. Davis-Philip (eds.). Proceedings of IAU Symposium 126, Globular Cluster Systems in Galaxies. Kluwer, Dordrecht.

Pryor, C., R. D. McClure, J. E. Hesser, and J. M. Fletcher. 1989. The frequency of primordial binary stars in globular clusters. Pages 175–181 In: Merritt, D. (ed.). Dyanamics of Dense Stellar Systems. Cambridge University Press, Cambridge.

Richer, H. B., and G. G. Fahlman. 1987. Deep CCD photometry in globular clusters. V. M5. Astrophysical Journal 316: 189–205.

Shara, M. M., J. Kaluzny, M. Potter, and A. F. J. Moffat. 1988. A CCD search for faint variables in the field of an $\omega$ Centauri low-luminosity X-ray source, and in 47 Tucanae. Astrophysical Journal 328: 594–599.

Shara, M. M., A. F. J. Moffat, and M. Potter. 1987. Outburst and quiescence observations of the dwarf nova V101 in the globular cluster M5. Astronomical Journal 94: 357–359.

Shara, M. M., A. F. J. Moffat, M. Potter, H. S. Hogg, and A. Wehlau. 1986. First optical candidate for a recovered classical nova in a globular cluster: Nova 1938 in M14. Astrophysical Journal 311: 796–799.

Sistero, R. F. 1968. The eclipsing binary V78 in Omega Centauri. Information Bulletin on Variable Stars 316.

Steinlin, U. 1956. Zur Anwendung der dreifarbenphotometrie in der stellarstatistik. Zeitschrift für Astrophysik 39: 210–218.

Stryker, L. L., and B. J. Hrivnak. 1984. A search for radial velocity variations in the blue stragglers of NGC 7789. Astrophysical Journal 278: 215–219.

Verbunt, F., and G. Meylan. 1988. Mass segregation and formation of X-ray sources in globular clusters. Astronomy and Astrophysics 203: 297–305.

Verbunt, F., R. A. Shafer, F. Jansen, K. A. Arnaud, and J. van Paradijs. 1986. A soft X-ray observation of $\omega$ Centauri with EXOSAT. Astronomy and Astrophysics 168: 169–172.

Verbunt, F., J. van Paradijs, and R. Elson. 1984. X-ray sources in globular clusters. Monthly Notices of the Royal Astronomical Society 210: 899–914.

Walker, A. R. 1986. CCD photometry with small telescopes. Pages 33–46 In: Hearnshaw, J. B., and P. L. Cottrell (eds.). Proceedings of the IAU Symposium 118, Instrumentation and Research Programmes for Small Telescopes. Reidel, Dordrecht.

Wheeler, J. C. 1979. Blue stragglers as long-lived stars. Astrophysical Journal 234: 569–578.

Woolley, R. v. d. R. 1966. Studies of the globular cluster $\omega$ Centauri I. Catalogue of magnitudes and proper motions. Royal Observatory Annals 2: 1–128.

# The Large-Scale Surface Brightness Distribution of the X-Ray Background

RICHARD MUSHOTZKY
NASA/Goddard Space Flight Center

## INTRODUCTION

The X-ray background and the micro-wave background are the dominant "isotropic" radiation fields available for measurement. While there has been a convergence of opinion on the origin of the $\mu$-wave background and the measurement of its dipole variation and upper limits on higher order multipole terms (Klypin *et al.* 1987, Strukov *et al.* 1987) there has been no such agreement on the X-ray background. However, because of its relative uniformity (Schwartz and Gursky 1974; Schwartz 1979; Turner and Geller 1980) its seems fairly clear that the bulk of the $E > 2$ keV background is also of "cosmological" origin (e.g., due to objects or truly diffuse radiation originating at $z > 0.5$) and as such, is of great interest. At lower energies much of the observed flux is due to a galactic component. (For a recent extensive review on the cosmic X-ray background see Boldt 1987).

There has been extensive work on trying to determine the physical origin of the background. That is, whether it is due to a superposition of numerous faint "well-known" sources such as active galaxies (Giacconi *et al.* 1979), an early unidentified population of AGN at high redshift (Boldt and Leiter), a new population of objects, or to truly diffuse processes (Guilbert and Fabian 1986) or to a superposition of these. However while of great intrinsic interest these studies have not been aimed at using the XRB to provide the cosmological information that has been gleaned from the $\mu$-wave background. Our group has been attempting an alternate approach, to use the available information on the large, $> 5^{\circ}$, scale distribution of the sky flux to see if the XRB can provide such constraints.

As opposed to the $\mu$-wave background, much of the X-ray background is presumably due to sources at $z < 3$ (if it is due primarily to active galaxies) or $z < 10$ (as a very general limit). For the determination of large-scale motions the X-ray and $\mu$-wave backgrounds are thus complementary, both defining "distant" reference frames with respect to which one can measure motion. However, the X-ray background can provide information not contained in the $\mu$-wave background; the distribution of matter perturbations at intermediate ($0.1 < z < 3$) redshifts; (see the detailed discussion in Rees 1979 of how the optical galaxy counts, $\mu$-wave background measures and X-ray surface brightness measurements complement each other).[1] Warwick *et al.* (1979), and Rees (1979) have pointed out how measurements of the variation of the X-ray sky surface brightness on moderate angular scales can get the tightest constraints available on density perturbations in the universe on scales from 100-1,000 Mpc at redshifts $< 1$.

If the sources of the X-ray background are distributed roughly like matter, variations in the X-ray surface brightness are tracers of the matter distribution on large scales. Even if most of the sources responsible for the background are not distributed in such a fashion the best estimates are that $\sim$ 30-40% of the X-ray background comes from objects such as Seyfert galaxies, normal galaxies and clusters that are distributed like matter.[2] While, potentially, this information resides in the distribution of X-ray sources (in the way that the IRAS counts were used to examine the distribution of matter in the local universe), it is very difficult to obtain all of it from source counts alone because 1/2 of the sky surface brightness comes from sources dimmer than $3 \times 10^{-15}$ ergs/cm$^2$-sec or two orders of magnitude below the Rosat all-sky survey limit. Thus very deep surveys are required to "resolve out" the background (see below). Cataloging and identifying the $\sim 1 \times 10^6$ sources/sr, most of which will be quite faint optically ($M_v > 20$ mag), will be difficult.[3] In addition such surveys have

[1] Of course, the X-ray background does not contain the same information as the $\mu$-wave background on the spectrum and amplitude of primordial perturbations.

[2] In particular, Giacconi and Zamorani (1987) have estimated based on the optical-X-ray ratio of low redshift normal galaxies and the deep optical counts of Tyson (1988) that $\sim$ 13% of the X-ray background at 2 keV is due to normal galaxies. Persic *et al.* (1989b), based on the local luminosity function of Seyfert galaxies, have calculated that they contribute $\sim$ 25% of the background and various authors have calculated that clusters contribute $\sim$ 5-10% of the 2 keV X-ray background.

[3] The best such use of an all-sky catalog to obtain cosmological information has been from the IRAS all-sky survey. However, there are substantial differences between an X-ray and IR survey. The X-ray sources tend to be much more distant and have fainter optical counterparts. In addition, the X-ray source counts at high latitutde will be dominated by active galaxies rather than the star forming galaxies which dominate the IRAS counts. Perhaps the most fundamental difference is that the IR background is dominated by local, solar system, and galactic effects while the X-ray background is dominated by effects originating at $z > 0.5$.

strong selection effects due to source spectra and extent. However, it is clear that the Rosat all-sky data can be analyzed in a fashion similar to the IRAS data base to obtain another measure of our local velocity vector.

The simplest way to see the usefulness of measuring "lumps" in the X-ray surface brightness observation is to assume a Euclidian universe and that the sources of the X-ray background are distributed roughly like matter. Then (Rees 1979), the amplitude variation in the X-ray background $(\Delta I/I)_x$ due to perturbation in matter $(\Delta\rho/\rho)$ on a scale $\lambda$ compared to the Hubble scale, $\lambda_H$, is roughly $(\Delta I/I)_x = (\Delta\rho/\rho)\ (\lambda/\lambda_H)f$; where f is a parameter that describes cosmological effects and X-ray source evolution. Rees (1979) estimates that $f \sim 1/2$ (see Goicoechea and Martin-Mirones 1990 for a more detailed calculation). If we assume $(\Delta\rho/\rho) \sim 2$, as seems appropriate for the largest scale perturbation claimed to date (the Great Attractor) and similarly $(\lambda/\lambda_H) \sim 0.02$ ($\sim 100h^{-1}_{50}$ Mpc) then the predicted variations in the X-ray surface brightness on angular scales from 1/2 sterradian ($z \sim 0.01$) to 1-2 degrees ($z \sim 1$) should be of the order of 1-2% (see Shafer 1983 for a detailed discussion).

Similarly interesting results can be obtained by searching for a 24 effect in the distribution of the all-sky flux (Warwick and Fabian 1979) due to velocities induced by matter perturbations on scales $\lambda << \lambda_H$ (the Compton-Getting effect). The expected peak amplitude is $(\Delta I/I)_x \sim (3 + \alpha)V_{pec}/c \sim (\Delta\rho/\rho)(\lambda/\lambda_H)\Omega$; or more exactly (Peebles 1980) $(\Delta I/I)_x = (1 + \alpha/3)(\Delta\rho/\rho)(\lambda/\lambda_H)\Omega^{0.6}$, where $\alpha$, the effective energy index in the 2-20 keV X-ray band, is $\sim 0.4$ (Boldt 1987). Using the micro-wave dipole velocity of the sun as a scaling parameter we expect $(\Delta I/I)_x{}^{obs} \sim 0.4\%$. As opposed to the fluctuation amplitude, which is confined to a small region of the sky, the "dipole-like" term is an all sky effect and thus needs a large solid angle for its measurement. If the perturbations exist on larger scales $\lambda \sim \lambda_H$, (Warwick and Fabian 1979; Warwick *et al.* 1980) then one no longer has a dipole-like term but an oblate variation dominated by a 12-hour term. However the relative amplitude compared to the micro-wave dipole term is expected to be small, $< 0.6$, for reasonable ($\delta M < 10^{20}$ solar masses on scales $\Delta z \sim 1$), large-scale perturbations.

To summarize, the X-ray diffuse background should show a large-scale effect (spherical and harmonic) $(3 + \alpha)$ times larger in $(\Delta I/I)$ than the $\mu$-wave background and an effect due to the clumping of sources—which does not have a simple dipole-like shape, larger yet by a factor $(f/\Omega)$. The fact that the amplitude of any 24 hour-like variation in the X-ray background is smaller than 2% (see below; Boldt 1987; Shafer 1983; Warwick *et al.* 1980) gives a lower bound on the closure ratio and the relative contribution of sources (which are distributed like matter) to the XRB.

# RECENT RESULTS ON "STRUCTURES" IN THE X-RAY BACKGROUND

## HEAO-1 A-2 Capabilities

We have used HEAO-1 A-2 data, which is the only available all sky data base with sufficient sensitivity, to look for effects at $< 5\%$ level on angular scales $\geq 200$ square degrees. The limits on this data base are set by Poisson noise, sky fluctuations due to unresolved point sources and residual systematic errors. For the smallest field of view available from this detector ($3 \times 1.5$ degrees) the sky fluctuation variance is, using a point source estimator (Persic *et al.* 1989), $\sim 5.5 \times 10^{-12}$ ergs/cm$^2$sec in the 2-10 keV band and the error due to Poisson noise is $\sim 4 \times$ 10-12 for a total variance of $\sim 8\%$ of the sky flux in the beam. Using an estimator appropriate for the fluctuations (Shafer 1983) the variance due to fluctuations is $\sim 6.3 \times 10^{-12}$ for a total variance of $\sim 10\%$. In the absence of variance due to other causes (such as background variations) the absolute value of the noise due to the sky fluctuations scales as solid angle$^{1/2}$ as does the poisson error. Estimates of the variance in the internal background (Shafer 1983) are on the order of 2-3 $\times 10^{-12}$ergs/cm$^2$sec, which is not significant. Thus beam sizes of $> 75$ square degrees are necessary to examine surface brightness variations of $< 2\%$ with the HEAO-1 data.

## Galactic Component

Previous studies using this data base (Shafer 1983; Iwan *et al.* 1983) have shown that the strongest large-scale feature in the sky at galactic latitudes greater than 10 degrees is due to the galaxy. This component has an effective scale height of $< 15$ degrees (Figure 1 and Iwan *et al.*). This emission is not symmetric about the galactic plane or the galactic center and has a "softer" spectrum than the "extra-galactic" background. Because it is bright, roughly 7% of the diffuse X-ray background flux at b $\sim 10°$, l $\sim 45°$, it has been mapped by HEAO-1 A-2 with the full resolution of the detector. At lower latitudes this component has been studied in detail by Exosat (Warwick *et al.* 1985) and Ginga (Koyama 1988) and it is clear from the Tenma spectroscopy that most of the emission is due to thermal processes from plasmas of $T < 10$ keV but as of yet its physical origin has not been determined (Koyama 1988). It is the presence of this strong spatially complex Galactic component that makes determination of the X-ray surface brightness dipole moment in the direction of the micro-wave dipole difficult.

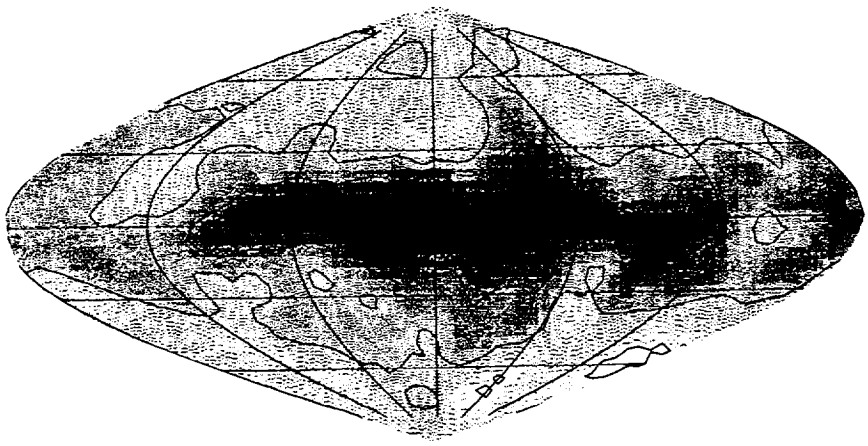

FIGURE 1 The 2-20 keV surface brightness of the sky in galactic coordinates boxcar smoothed by $10^{\circ}$. The contour levels represent -2.5%, 0, +2.5% and +5% of the mean high galactic latitude surface brightness.

## The Great Attractor Region

The next strongest feature in the high latitude sky is a "bright" spot at $b \sim 20^0$, $l \sim 330^0$ (Figure 1) which is located in the direction of the "Great Attractor" (GA) (Lynden-Bell *et al.* 1988) and the large concentration of clusters (Scaramella *et al.* 1989) located at $v \sim 14{,}000$ km/sec. This region has an enhancement of $\sim$ 4-5% of the average sky flux ($\Delta I_{GA} \sim 7.8 \times 10^{-13}$ ergs/cm$^2$sec/deg$^2$, Jahoda and Mushotzky 1989) and subtends a solid angle of $\sim$ 1,000 square degrees for a total flux of $\sim 10^{-9}$ ergs/cm$^2$-sec. If it were at the distance of the GA it would have a luminosity of $\sim 3 \times 10^{44}$ ergs/sec and if it were due to the superposition of objects at the distance of the large concentration of clusters $L_x \sim 3 \times 10^{45}$ ergs /cm$^2$-sec. We have visually compared our map of X-ray surface brightness with a smoothed map of the Abell cluster distribution (Figure 2), and this region appears to be the only place where an X-ray surface brightness enhancement at this level may be due to "superclusters" at $z < 0.1$. There is another region, a factor of 2 dimmer than may be associated with supercluster 12A in the list of Bahcall and Soneira (1984) at $l = 30$, $b = 70$ and $z \sim 0.07$. If this is a real association, and the lack of other "detections" places this in doubt, $L_X \sim 10^{44}$, roughly consistent with the Persic *et al.* upper limits. We may assign an upper limit to $(\Delta\rho/\rho)$ in the GA or similar region from the X-ray data of $(\Delta\rho/\rho) < (\Delta I/I)_x \Omega^{-0.6} (\lambda/\lambda_H)^{-1} f^{-1}$: using $(\Delta I/I)_x) < 0.05$ and $(\lambda/\lambda_H) \sim 0.02$ we find $(\Delta\rho/\rho)\Omega^{0.6} < 1.5 f^{-1}$, very similar to the values obtained

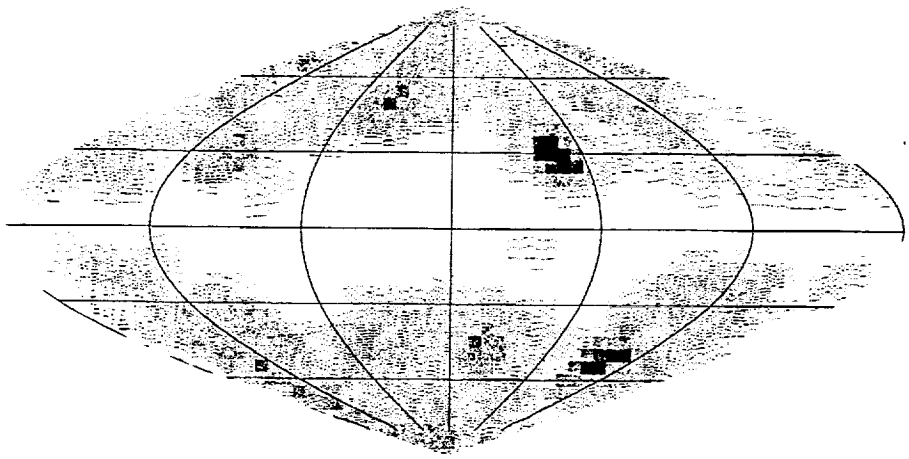

FIGURE 2 The surface density of D $\leq$ 4 Abell clusters smoothed by a 10° boxcar in Galactic coordinates on the same scale as Figure 1.

from model fitting the optical velocity data for the GA (Lynden-Bell *et al.* 1988) of $(\Delta\rho/\rho)\Omega^{0.6} \sim 0.4$.

Because the GA is located close to the galactic plane it is quite difficult to conduct an optical search for clusters of galaxies. It is thus not clear if, like other superclusters, the GA contains numerous rich Abell clusters. X-ray surveys at E > 2 keV are much less affected by reddening and sky confusion at | b| > 5° and thus are an efficient way of searching for X-ray luminous rich Abell clusters. We have searched for "pointlike" X-ray sources (clusters of galaxies and active galaxies) which could be associated with the GA (Jahoda and Mushotzky 1989) and have not found any down to a luminosity limit of $\sim 3 \times 10^{43}$ ergs/sec, which is considerably below the mean luminosity of Abell richness 0 clusters. We thus conclude that the GA if "real" it is not similar to other superclusters, which, by construction, are composed of rich Abell clusters. This raises the interesting question of whether other superclusters are similar to the GA in being composed primarily of "field" galaxies and poor groups and has important implications for studies of large-scale structures.

If the X-ray surface brightness enhancement detected in the region of the GA is due to hot gas located in the potential well of the supercluster we may estimate its core mass as:

$$M(gas) \leq 1.2 \times 10^{16} M_{\odot} (\Delta I_{GA})^{1/2} (T_{10})^{1/4} (D_{86}\Theta_{20})^{5/2};$$

where $\Theta_{20}$ is the radius of the GA in units of 20 degrees, D86 is the distance in units of 86 Mpc, and $T_{10}$ is the temperature in units of 10 keV.

## Superclusters

Persic *et al.* (1989b) have used the same data base to place tight upper limits on diffuse radiation from optically selected "pointlike" superclusters (e.g., they have assumed that the superclusters were of angular size $< 2°$). They find that for a sample of $< z > \sim .046$ an upper limit of $F_x < 5 \times 10^{-12}$ ergs/cm$^2$-sec. Using the HEAO-1 luminosity function of clusters of galaxies, they estimate that the Abell clusters in the superclusters would contribute an expectation value of $\sim 4 \times 10^{-12}$ ergs/cm$^2$-sec. They conclude that, on average, the X-ray luminosity of diffuse emission due to hot gas associated with superclusters is $< 4 \times 10^{43} h^2_{50}$ ergs/cm$^2$-sec, on the order of the detected diffuse emission in the direction of the GA. A uniform volume of hot gas of total mass $10^{16} M_{16}$ solar masses, temperature $T_{10}$ keV and linear size $10 h^{-1}_{50} R_{10}$ Mpc would have a luminosity of in the 2-10 keV band of $L_{gas} \sim 3 \times 10^{45} (M_{16})^2 (T_{10})^{1/2} (R_{10})^{-3} h_{50}$ ergs/sec.

The HEAO-1 data thus indicate that the non-cluster associated mass in hot gas associated with optically identified superclusters is $< 1.5 \times 10^{14}$ solar masses, on the order of the mass in hot gas associated with rich clusters. This limit already places tighter constraints (Persic *et al.* 1988) on the possible baryonic mass density than can be associated with superclusters or the fraction of supercluster mass that can be in hot gas.

The all-sky X-ray surface brightness data already indicate that enhancements of $(\Delta I/I)_x > 2\%$ on scales greater than 300 square degrees are rare. Then using the same formalism as for the GA and using a distance of 200 Mpc and an angular radius of $10^0$ (scaling from the GA) we can already place upper bounds of $M(gas) \leq 8 \times 10^{15} (D_{200} \Theta_{10})^{5/2}$ solar masses for any supercluster-like object of size $> 35$ Mpc whether or not it has been previously cataloged. If we assume superclusters to have a scale of 20 Mpc (Bahcall 1988) and properties similar to that of the GA ($(\Delta I/I) \sim 3\%$ of the X-ray background, $L \sim 10^{44}$ ergs/cm$^2$-sec, $(\Delta\rho/\rho) \sim 2$) then to detect such objects at $z < 0.5$ one needs a system capable of measuring the X-ray surface brightness at the level of 1-2% on scales of $> 1^\circ$. Thus an appropriately sensitive X-ray *surface brightness* survey might be the best way of searching for "non-Abell cluster" superclusters or any other virialized concentration of baryons which might make a significant contribution to the mass of the universe.

It is also of interest to determine whether the "voids" studied by Batuski and Burns (1985) (regions devoid of rich clusters of galaxies) have a systematically different X-ray surface brightness than the rest of the sky. If a considerable fraction of baryons in these regions did not form clusters and galaxies, the only place for this material to "hide" would be in the form of hot gas. Thus one might expect that the "voids" might be systematically brighter than the rest of the sky. Alternatively if the difference signal is

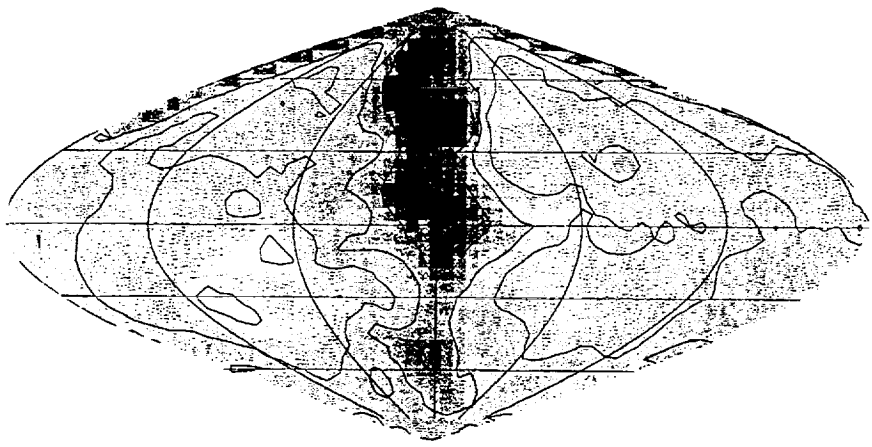

FIGURE 3 The 2-20 keV surface brightness of the sky in supergalactic coordinates smoothed by a 10° boxcar. The axis has been rotated so that the supergalactic l = 180 is at the center of the diagram.

dominated by the fluctuations due to unresolved sources such as clusters and active galaxies which tend to be missing from the voids one might expect a deficit of weak unresolved sources which will slightly lower the background intensity. A preliminary analysis of the HEAO-1 A-2 data is underway.

## OTHER STRUCTURES

It is apparent to the eye (Figure 1) that there are several "bright" and "dim" regions in the X-ray with relative differences of 1-2%. While visual inspection is always risky, comparison of the HEAO-1 data with the Uhuru data (Turner and Geller 1980) and the Ariel -V results (Warwick *et al.* 1979) shows fair overall agreement in both the location and amplitude of the surface brightness distribution. As indicated above, these are not associated with Abell clusters or "obvious" voids in their distributions. Projection of the HEAO-1 data in supergalactic coordinates (Figure 3) shows that most of the large-scale structure (other than in the GA region) is not directly assignable to the local supercluster. At the present time we do not know the physical origin of these "lumps," whether they are due to galactic or extragalactic effects or their possible relationship to other astrophysical objects.

We are in the process of correlating our data with galaxy catalogs (Lahav 1987) and are trying to determine the two-point correlation function

of our data on scales $> 10^0$. On smaller angular scales the HEAO-1 data have already placed tight bounds on the two-point correlation function (Persic *et al.* 1989a; deZotti *et al.* 1989) which constrain the two-point correlation function of clusters and active galaxies. The HEAO-1 fluctuation data already constrain models of the sponge-like or shell-like structure of the universe (Meszaros and Meszaros 1988).

Limits on the dipole in the X-ray background were obtained by Shafer (1983) from the HEAO-1 A-2 data using detectors with an effective beam size of $\sim 20$ square degrees. He found that the X-ray data were consistent with the same velocity and direction as the $\mu$-wave anisotropy. The major uncertainty was due to emission from the much larger galactic component, the small number of independent sky elements due to the dominance of sky fluctuation noise and the lack of information about structures like the GA. Boldt (1987) gives a nice graphic representation of the problem. We are trying to see if we can improve on his results using data with better angular resolution and different approaches to modeling the galactic contribution and the effects of the large-scale structures.

## FUTURE WORK

As indicated above, recent studies of the X-ray surface brightness distribution of the sky have been able to make interesting statements about our galaxy, the Great Attractor, the two-point correlation of clusters, the topology of the large-scale structure of the universe and nearby superclusters. In addition, a "new" unidentified component of the sky has been detected. The HEAO-1 A-2 data base is severely limited in angular resolution and sensitivity for future studies. The question is how to proceed further.

The Ginga satellite with a 2 square degree field of view and $\sim 6$ times the collecting area of the A-2 experiment can be a very powerful tool for the study of selected regions of the sky. There are already indications (Hayakawa *et al.* 1989) that it is capable of achieving sensitivity levels of $\sim$ 5% of the sky on angular scales of $\sim 2$ square degrees, e.g., 1/10 the beam size of the HEAO-1 experiment, and is only limited by the sky fluctuation signal. If there exist larger regions of the sky with surface brightness differences about this level Ginga can search for them. However, because Ginga is primarily a pointed satellite and the scanning mode is quite limited, the solid angle to be examined will only be a small fraction of the sky and thus it will have to search in "interesting" selected areas (such as optically selected superclusters) for such variations.

To obtain even better limits on even smaller solid angles will require an independent, simultaneous measurement of the weak sources responsible for the fluctuation signal in the 2-10 keV band. For a log N-log S slope of 1.5, most of the variance due to unresolved sources comes from objects of

flux $\sim$ 1/10 of the resolved source limit, while the sky flux is dominated by much weaker sources or truly diffuse emission. We show below that it is possible, with a combination of proportional counters and imaging optics, to obtain sensitive measures ($\sim$ 1%) of the sky brightness on angular scales of $\sim$ 1 square degree or less. The proposed scheme consists of collimated proportional counters of area $10^4$ A cm$^2$, and solid angle square degrees scanning the sky simultaneously with an imaging X-ray telescope sensitive in the 2-10 keV band and capable of detecting sources of flux $F_{2E-13} \sim 2 \times 10^{-13}$ ergs/cm$^2$-sec. In the limit of small (or extremely well known) internal background, the major variance in the proportional counter signal will be due to the sum of "real" variations in the "diffuse" sky signal and the fluctuation signal. The sky signal will be $\sim$ 17A cts/sec and thus will require exposures of $\sim 600(A)^{-1}$ seconds to obtain Poisson errors of 1%. The variance due to fluctuations will be 1.44 $(A)^{+1/2}$ cts/sec. However $\sim$ 75% of the variance ($\sim$ 1 cts/sec) is contributed by point sources brighter than $F_{2E-13}$ ergs/cm$^2$-sec. Thus detection and measurement of sources at this limit will allow determination of the "true" sky flux to an accuracy of $\sim$ 2%. For a Crab-like spectrum the BBXRT mirror+detector system (Serlemitsos 1988) with $\sim$ 1/2 square degree effective solid angle gets $6.6 \times 10^{-3} F_{2E-13}$ cts/sec per mirror in the 2-10 keV band. Thus such a system needs $\sim$ 1400 seconds to detect sources at the $F_{2E-13}$ flux level—a good match to the required proportional counter exposure. To obtain such data over the entire sky would require $\sim$ 4 years with one mirror system, well within the bounds of reason. With two X-ray mirrors the time would be halved to that required by the proportional counters. Thus the technical requirements to determine the absolute value of the flux of the sky on pixels of $\sim$ 1 square degree can easily be met by present technology. At the same time fluctuations in the X-ray background on this angular scale will constrain log N-log S down to flux levels of $\sim 5 \times 10^{-14}$ for direct comparison with imaging results from Astro-D, XMM, AXAF, and SODART.

To obtain similar accuracy on much smaller scales will require a very large imaging telescope, such as SODART or XMM, to obtain exposures of $\sim 10^4$ seconds per field or a required exposure time of $\sim$ 30 years to cover the entire sky. However, interesting selected regions of 100 square degrees can be easily observed and thus the surface brightness of the X-ray sky can be well measured with these imaging telescopes for many selected regions. Such data will allow a measurement of the covariance function of the diffuse flux for comparison with such data for clusters and active galaxies as a function of cosmological epoch, as well as constraints on the existence, flux, and temperature of Zel'dovich pancakes and any other large structures. Calculations of the expected properties of Zel'dovich pancakes (White *et al.* 1984) indicate that they are hot, $T \sim 10(1+z_s)(R_{25})^2$ keV

and large $\sim$ 50' at $z_s \sim 2$ ($R_{25}$ is the diameter of the pancake in units of 25 Mpc ). Their luminosity is uncertain, but if at least 1% of their total mass is in gas (as is necessary for them to collapse and form galaxies), $L(x) > 10^{45}$ ergs/sec. SODART and XMM with their great sensitivity to surface brightness should see these systems as large, > 20', ($H_0 = 50$, $q_0 = 1/2$) diffuse objects with a surface brightness of $\sim$ 1/10 of the diffuse X-ray background. Pancakes which have not collapsed or which have formed late might be visible as X-ray emitting larger objects at smaller redshifts.

## ACKNOWLEDGEMENTS

Most of all I would like to thank Keith Jahoda who has done all the really hard work and without whose efforts I would have had no results to present. I thank M. Persic for discussion of results before publication and E. Boldt for continuing and enlightening discussions. I also thank E. Boldt and the entire HEAO-1 A-2 team for their care and attention to detail 15 years ago that has made this data set available for analysis.

## REFERENCES

Bahcall, N. 1988. Ann. Rev. Astron. and Astrophys 26: 631.
Bahcall, N., and R. Soneira. 1984. Ap. J. 277: 27.
Batuski, D., and J. Burns. 1985. A. J. 90: 1413.
Boldt, E.A. 1987. Physics Reports 146: 216.
Boldt, E.A., and D. Leiter. 1987. Ap. J. Lett 322: L1.
De Zotti, G.F. *et al.* 1989. in preparation.
Giacconi, R. *et al.* 1979. Ap. J. Letters 234: L1.
Giacconi, R., and G. Zamorani. 1987. Ap. J. 313: 20.
Goicoechea, L.J., and J.M. Martin-Mirones. 1990. M.N.R.A.S. submitted.
Guilbert, P., and A. Fabian. 1986. M.N.R.A.S. 220: 439.
Hayakawa, S. *et al.* 1989. preprint.
Jahoda, K. 1989. B.A.A.S. 20: 1086.
Jahoda, K., and R. Mushotzky. 1989. Ap. J. 346 in press.
Klypin, A.A., M.V. Sazhin, I.A. Strukov, and D.P. Skulachev. 1987. Pos'ma Astron. Zh. 13: 259.
Koyama, K. 1988. In: Tanaka, Y. (ed.). Physics of Neutron Stars and Black Holes. Universal Academy Press, Tokyo, Japan.
Koyama, K. 1989. PAS J. 41: 679.
Lahav, O. 1987. M.N.R.A.S. 225: 213.
Lynden-Bell, D. *et al.* 1988. Ap. J. 326: 19.
Meszaros, A., and P. Meszaros. 1988. Ap. J. 325: 25.
Peebles, J. 1980. Physical Cosmology.
Persic, M., Y. Rephaeli, and E. Boldt. 1988. Ap. J. Letters 327: L1.
Persic, M. *et al.* 1989a. Ap. J. Letters 336: L47.
Persic, M. *et al.* 1989b. in preparation.
Rees, M. 1979. In: Giacconi, R., and Setti (eds.). X-ray Astronomy NATO Advance Study Institutes Series.
Scaramella *et al.* 1989. Nature 338: 562.
Schwartz, D. and H. Gursky. 1974. In: Giacconi, R., and H. Gursky (eds.). X-ray Astronomy.

Schwartz, D. 1979. In: Baity, and Peterson (eds.). X-ray Astronomy (COSPAR). Pergamon Press.
Serlemitsos, P. 1988. J. of Applied Optics. 27: 1447.
Shafer, R. 1983. Spatial Fluctuations in the Diffuse X-ray Background. Ph.D Thesis, University of Maryland.
Strukov, I.A., D.P. Skulacher, M.N. Boyarsky, and A.N. Kachev. 1987. Pis'ma Astron. Zh. 13: 163.
Turner, E., and M. Geller. 1980. Ap. J. 236: 1.
Tyson, J. 1988. A. J. 96: 1.
Warwick, R., and A. Fabian. 1979. Nature 280: 39.
Warwick, R., J. Pye, and A. Fabian. 1979. M.N.R.A.S. 190: 256.
White, S., M. Davis, and C. Frenk. 1984. M.N.R.A.S. 209: 27p.

# X-Ray Emission from Active Galactic Nuclei

RICHARD MUSHOTZKY
NASA/Goddard Space Flight Center

## INTRODUCTION

There have recently been a large number of good reviews in this subject (Mushotzky 1987; Elvis and Lawrence 1984; Urry 1988; Pounds and Turner 1989; McHardy 1989) which have extensively covered the X-ray spectral and temporal properties of Seyfert galaxies and quasars in the 0.1-20 kev band. Rather than reviewing this material again I would like to concentrate on several observation issues which have been raised recently and some theoretical consequences. I shall also stress what the next year will bring from Ginga, Rosat and BBXRT observations and re-analysis of Einstein data.

## THE FORM OF THE CONTINUUM

### E < 10 kev

Recently Elvis and co-workers (Elvis *et al.* 1986; Wilkes and Elvis 1988) have stressed that the form of the continuum in the 0.1-4 kev band as determined from Einstein imaging proportional counter (IPC) observations of quasars, differs markedly from that seen at higher energies in Seyfert I galaxies. When a powerlaw model is fit to the IPC data they find a correlation between X-ray spectral index and radio properties, with radio loud objects having an X-ray energy index $\alpha \sim 0.5$ and radio quiet objects have $\alpha \sim 1.0$. Their data also show a broad distribution in X-ray spectral indices. This is in contrast with the narrow distribution of spectral indices, strongly peaked around $\alpha \sim 0.7$, seen in the 2-20 kev data (Mushotzky

1982, 1984; Halpern 1982; Turner and Pounds 1989), independently of radio "loudness." Wilkes and Elvis also note that they find that their fits indicate a systematically low column density to many of their quasars which they feel is an indication of an additional extremely soft component which is only visible at very low energies, E < 0.25 kev. However, much of the comparison between the 0.1-4 kev and 2-20 kev data is between samples rather than objects. The objects in the Wilkes and Elvis IPC sample have considerably lower fluxes than the Seyfert galaxies observed by the Exosat and HEAO-1 proportional counters in the 2-20 kev band and thus comparison on an object by object basis (or even individual objects observed at different times) has been difficult. (but see below).

Recent analysis of the Einstein IPC Seyfert galaxy sample and the ability of the Japanese large area proportional counter experiment on the Ginga satellite to go to lower fluxes then previous experiments has allowed direct comparison of 2-20 kev and 0.1-4 kev data for the same objects. Kruper *et al.* (1989) have determined the 0.1-4 kev spectral properties of a large sample of Seyfert galaxies. The mean 0.2-4 kev spectral index of a well determined sub-sample is $< \alpha > = 0.81+/-0.03$ compared to $< \alpha > = 0.71+/-0.05$ in the 2-10 kev band (Turner and Pounds 1989). This small difference is caused, primarily, (Figure 1) by the few objects (in the overlapping sample) with very steep spectra. As shown in Figure 1 many of these objects have a soft excess over a simple power law fit in the Exosat data. It thus seems that a simple power law model is not an adequate fit to the spectrum of Seyfert galaxies in the 0.2-4.0 kev band and that both Exosat and the Einstein IPC frequently "agree" as to which objects are steep at low energies. At present the overlap between the published Exosat and Ginga quasar samples with the published IPC data are too small to have any definitive conclusions since there are only 4 objects in common (Exosat observations of IIIZW2 and 3C273, Ginga data on Mk205, 3C273,3C279)[1]

However, it is clear (Makino *et al.* 1988) that Ginga has sufficient sensitivity to determine the spectral indices of enough quasars and Seyfert galaxies to confirm or deny the IPC/Exosat result for Seyfert I's.

The importance of these "soft" X-ray spectral components for models of the origin of the X-ray continuum, the connection between the X-ray and UV spectral bands and the ionization of the broad line clouds have been discussed in the above review papers. Depending on the exact nature and luminosity of the "soft" components, there is a large number of likely physical sites for its production viz: 1) an extension to higher energy of

[1] Recent analysis of both Ginga (M. Turner 1989) and Exosat results (Mushotzky 1990) indicate that the 2-15 kev spectral indices of quasars are very similar to those of Seyfert I galaxies and do not show any trends with redshift. The overlap betwen the IPC and Exosat and Ginga samples is $\sim$ 12 objects and thus these results are similar to those for the IPC Seyfert sample.

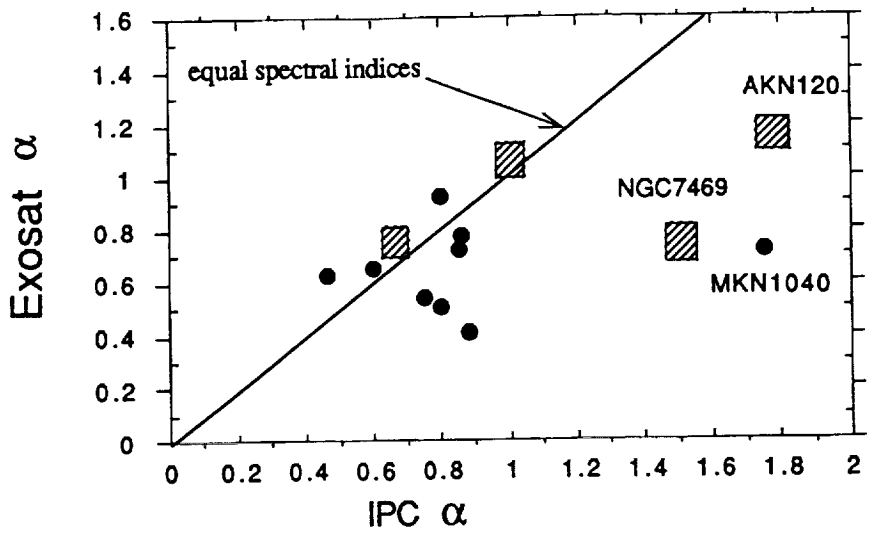


FIGURE 1 Comparison of the X-ray spectral indices of the overlapping sample of Seyfert I galaxies between the Einstein IPC and Exosat detectors. The objects indicated by a shaded box have soft components detected by Exosat (Turner 1988).

the radiation of an accretion disk (Czerny and Elvis 1987); 2) an extension of a "synchrotron" power law visible in the IR band; 3) a thermal photo-ionized plasma associated with the gas confining the broad line clouds; 4) an x-ray jet, associated with the radio jet frequently seen in so-called radio quiet objects (Haniff *et al.* 1989); 5) a very large number of x-ray binaries and SNR associated with a starbursts in these objects; 6) a "partial covering" of the emission line region by an absorbing cloud; 7) a galactic wind associated with either a starburst or nuclear phenomena; or 8) the signature of reprocessing of the nuclear radiation by a thermal accretion disk or "cold" accreting matter. It is, in fact, anticipated that all or most of these components have already been detected. However, it requires detailed spectroscopy, imaging and timing analysis to determine which or how many of these components are prominent in which objects. Many of these putative components can only be detected in the soft X-ray band. It is thus important to know the nature of the spectra of these soft components in detail. If possibility #1 is true in a fair number of objects it implies that a very significant fraction of the total energy in these objects is radiated in an accretion disk component (Sun and Malkan 1989).

It is possible to fit more complex models than single power laws to the combined simultaneous Einstein solid state spectrometer (SSS) and monitor proportional counter (MPC) data, or to the combined IPC and MPC data.

This extends the bandwidth for fitting the spectra to $\sim$ 0.1-15 kev for the IPC+MPC combination (with $E/\Delta E \sim 1$ for the IPC and $E/\Delta E \sim 3$ for the MPC) or to 0.6-15 kev for the SSS+MPC data (with however $E/\Delta E \sim 10$ for the SSS). These projects are underway at present. Preliminary results from the IPC+MPC fitting for 26 objects indicate that, for those objects for which the IPC data have been fit by single "steep" power laws that complex models are preferred systematically over single power laws. The indications are that an additional soft component is required for $\sim$ 2/3 of the observations and this component is very soft for only $\sim$ 1/3 of the these observations (e.g., $\sim$ 10% of the total sample). Most of the observations can be modeled by a flat power law of energy index $\sim$ 0.7 and a soft component which can be represented by a black body of $kT < 0.25$ kev or thermal bremsstrahlung of $kT < 1/2$ kev. However, it seems likely that the observed distribution of kTs is biased by the detailed form of the IPC transmission function and its poor energy resolution. For a few objects, these results are confirmed by a similar analysis of the Einstein SSS and MPC data and a re-analysis of the combined low energy (LE) and medium energy (ME) Exosat data. Use of these two component models eliminates the artifact of systematically low galactic column densities noted by Wilkes and Elvis and results in a good fit to the data. However neither the IPC nor SSS data can determine the form of the soft excess, in particular it is not clear if it a "pure" continuum or if spectral line radiation is important at $E < 1$ kev.

The Ginga and Exosat timing data indicate that there are several physical origins of the soft component. Sometimes the hard ($E > 2$ kev) flux varies faster than the "soft" (as in Mk335, Turner and Pounds 1988), while sometimes the soft component varies faster than the hard (NGC 4051 Kunieda *et al.* 1989) and sometimes the soft flux does not vary at all while the hard flux changes (NGC4151 Pounds *et al.* 1986 or NGC 7469, Barr 1986). However these data (mostly Exosat results) have suffered badly from a lack of spectral resolution at $E < 2$ kev and lack of sensitivity and bandwidth at $E > 10$ kev.

It is clear that what is needed to resolve this issue is a broad band telescope and sensitive spectrometer in the 0.2-12 kev band such as BBXRT (the Goddard Space Flight Center Broad Band X-ray Telescope Spectrometer) or SODART on Spectrum-X. We anticipate that the BBXRT spectra of $\sim$ 30 AGN will resolve the issue of the form of the continuum for this selected sample but will not be extensive enough to attack the issues of the dependence of the X-ray continuum form on optical and UV luminosity, redshift, IR or radio properties.[2] Concentrating on the low-energy data

[2] Results presented at the Bologna 1989 conference on active galaxies and the X-ray background indicate that there may be another continuum component which is becoming important at E >

alone, the spectral resolution ($E/\Delta E \sim 2.5$ at 1 kev) and sensitivity of the Rosat PSPC will be able to test whether complex spectral models in the 0.1-2 kev band are necessary for a large sample of objects and will allow direct comparison with the (non-simultaneous) Ginga results. However the lack of simultaneous $E > 2$ kev data will make the interpretation model dependent. I thus anticipate that in $\sim 2$ years from now that the form of the 0.1-10 kev continuum will be well determined for a reasonable sample of QSOs and Seyfert I galaxies.

With these data we will be able to start to understand the nature of spectral evolution and the statistical connections between the form of the X-ray continuum and the other properties of these objects (Mushotzky and Wandel 1989). The BBXRT data should be of high enough quality that the spectral nature of the soft component is clear and thus its connection (if any) to the UV bump and an "extension" of the IR "power law" or any of the other suggested models can be tested. BBXRT's great sensitivity to spectral lines will test whether any of the optically thin models for the formation of the soft component are "correct".

The frequent presence of "soft excess" in the spectra of active galaxies implies that if they are a major contributor to the cosmic X-ray background that the spectral form of the background should change at $E < 2$ kev (Boldt 1987). Thus comparison of the contribution of classes of object to the background must include an additional spectral uncertainty. If the temperature of this component is related to its luminosity or to cosmological epoch one might expect a strong change in the form of the continuum with redshift which has not been seen so far (Canizares and White 1989).

### The Continuum from 10-100 kev

By analogy with recent results on galactic black hole candidates perhaps the best clues to understanding the nature of the physical mechanisms responsible for the high-energy emission from AGN lies in the modeling of the $E > 10$ kev continuum. In particular the case for the effects of $e^+ - e^-$ pairs and reprocessing due to cold material cannot be strongly made until high quality spectral and temporal data are available in this energy range.

At these energies the data from HEAO-1 are still the best available for a "large" data set. While they are not of very high quality, the $E > 20$ kev data indicated that the form of the continuum was consistent with a single powerlaw being a good description of the continuum from 2-100 kev (Rothschild *et al.* 1983). In one object, NGC4151 (Baity *et al.*

15 kev. This component was hypothesized to be due to the reflection of the power law continuum off an accretion disk—see next section.

1984) there was evidence for a change (a steepening) in the slope of the high-energy continuum. Recent theoretical models (Lightman and White 1988; Ferland and Rees 1988; Guilbert and Rees 1988) indicate that if an accretion disk or other source of "cold material" exists close to the central engine, as is required in almost any accretion model of AGN, that significant reprocessing can take place which should distort the 10-200 kev spectrum in a particular fashion depending on whether reflectance or transmission dominates. There are indications from Ginga data (Matsuoka *et al.* 1989) that such an effect has been detected in > 3 objects.

The high-quality Ginga data that is available should serve to better define the continuum in the 10-37 kev band. However, the Ginga background in this energy band is relatively large (and variable) compared to the signal from most active galaxies and thus care must to taken in the analysis and interpretation of these data.

Progress in this field has been slow and it appears that the next improvements for weak sources may be a while in coming. It is quite possible that the mask technique used on Granat may make a major advance in this area. If this proves not to be true for unforeseen reasons, we must wait until the XTE and SAX missions which will provide chopping detectors of sufficient sensitivity to obtain samples of > 20 objects out to E > 50 kev.

As in the lower energy bands, the form of the AGN spectra appears to deviate from that of the X-ray background (XRB) radiation. In both the E < 2 kev band and the E > 2 kev domain the spectra of sources is steeper than the background (at E < 2 kev, $<\alpha>_{sources} \geq 1.0$ (Maccacaro *et al.* 1988; Canizares and White 1989), while $<\alpha>_{background}$ 0.8 (Fabian *et al.* 1989); at E>2 kev, $<\alpha>_{sources} \sim 0.7$ while $<\alpha>_{background} \sim 0.4$ (Boldt 1987).

As opposed to the 0.5-3 kev band where both luminosity and spectral evolution are needed for AGN to produce the background flux and spectrum in the E > 10 kev band only spectral evolution is needed. As many authors have pointed out (e.g., Rothschild *et al.* 1983), the flat AGN spectrum would predict too much sky flux at E > 50 kev if there is strong luminosity or density evolution at these energies. There is thus a strong requirement to measure the high-energy continuum of those objects thought to be responsible for the 0.5-3 kev background radiation. The spectral and density evolution of these objects must be very well tuned (Morisawa and Takahara 1989) in order to reproduce the high-quality XRB spectral data.

## X-RAY SPECTRAL FEATURES

As stressed by Elvis and Lawrence (1985) the energy resolution of most present day X-ray counters is sufficient to reveal only the very strongest

features. The only significant X-ray spectral feature seen in more than one object has been the "6.4 kev" line due to iron. Before the launch of Ginga this line had only been determined with $> 3\sigma$ significance in $\sim 6$ objects. However it was only for the two brightest AGN, NGC4151 and Cen-A, that the error bars were sufficiently small that detailed information could be gleaned.

As shown in detail by Makishima 1986, the iron line emission from Cen-A was consistent with fluorescence from a spherically uniform cold absorber with "solar" iron abundance which was also responsible for the low energy photoelectric absorption seen in this source. However, in the case of NGC 4151 the iron line was a factor of 3-6 times too strong for this to be the case. Part of this enhancement was most likely due to a greater than solar iron abundance (as is common in the central regions of spiral galaxies) but this could not reproduce the whole effect. The other explanations relied on either geometry or time variability. The geometrical explanations required that either the reprocessor or the radiation field be non-spherical. The time variability explanation relied on the fact that the region responsible for the iron line was most likely several light days from the nucleus and thus the observer, who sees the average over the whole iron emission line region, was seeing enhanced iron line radiation due to a brightening in the continuum that occurred prior to the observations lit up the Fe line producing region and had decayed away. However this explanation could not explain the systematically high iron line flux seen in this object (Warwick *et al.* 1989).

More recent observations (summarized by Warwick *et al.* 1989) show a very complex pattern with none of the expected behavior between source intensity, photoelectric absorption and iron line intensity. It is clear that the origin of the Fe line is not well understood, even for this the best observed AGN.

Pounds *et al.* (1989) have used Ginga data to study iron lines in three objects. In one of them, NGC5548 there is a weak $\sim 120$ ev equivalent width line (similar to Cen-A), but no evidence for absorption by cold material either at iron or at low energies (NGC5548, in fact, has a very strong, very soft "excess"). This is the second example of a fluorescent iron line without low energy absorption, Mk509 (Morini *et al.* 1987), being the other. This strongly suggests that geometrical effects can dominate the observed Fe line emission. Pounds *et al.* speculate that the iron line in NGC5548 is due to reprocessing in a "face-on" disk and that such re-processing is also associated with the presence of soft components.

As the observational situation has improved so the theoretical explanations for the origin of this line have increased in complexity. At present we have $> 6$ strong candidates for the physical origin of the iron line in AGN (some of which are directly connected to models of the low energy

continuum) viz: 1) fluorescence from the same clouds that produce the broad optical and UV lines; 2) fluorescence from the innermost regions of an accretion disk (Fabian *et al.* 1989); 3) recombination radiation from a cloud of "cold" electrons that are responsible for the "reflected" broad optical lines seen in Seyfert II galaxies (Krolik and Begelman 1988); 4) fluorescence from "cold" material being accreted by the central object (Ferland and Rees 1988); 5) recombination in a hot photo-ionized inter-cloud medium or in a galactic wind; or 6) in a jet (ala SS433). The situation is similar to the confusion that reigned ten years ago over the origin of the iron line in X-ray binaries.

High spectral resolution ($\Delta E/E \sim 30$) and signal to noise data are required to discriminate amongst these models. Fluorescence lines originating in an accretion disk should be broad and show velocity shifts which are easily resolved with detectors with 200 ev resolution. The energies and ratios of recombination lines originating in a photo-ionized plasma (Krolik and Begelman 1988) have characteristic energies and line ratios of a photo-ionized gas.

## TIME VARIABILITY

McHardy (1989) has recently reviewed the Exosat data on time variability in both the 2-10 kev and $E < 1$ kev bands. He concludes that while there may exist a variety of power density spectra (PDS) power law slopes, all the Exosat data are consistent with no cutoff in the high frequency spectrum and most sources exhibit power law slopes $\sim 1$ over a broad frequency range. He also concludes that the time series are stationary, e.g. that the form of the PDS is the same no matter what stretch of data is being analyzed.

A perhaps contrary observation is that of Urry *et al.* (1988) from analysis of the Einstein IPC data. For a large number of AGN observations of average length of a few thousand seconds with good signal to noise, only a very small number showed significant variability. We (Weaver *et al.* 1989) have recently analyzed a large number ($\sim 200$) of Einstein Solid State Spectrometer observations of AGN and have obtained similar results. Taken at face value this might indicate that, like low-mass X-ray binaries, sometimes AGN are in an active state and sometimes they are quiescent. Higher signal to noise and longer observations are necessary to test this hypothesis.

We (Awaki *et al.* 1989) have obtained long Ginga observations of two Seyfert I galaxies (NGC4593 and NGC6814) which were known to be variable from Exosat, HEAO-1 and Einstein data. Preliminary analysis of the NGC4593 data shows that during one of the two Ginga observations, on time scales less than 1000 seconds, the source showed *no* evidence for

variability at > 20% level. In strong contrast, the Ginga observation of NGC6814 showed extremely large amplitude variations ($\Delta I/I > 5$) on time scales < 500 seconds. It thus seems that there exists a wide variety of time variability behavior in AGN which is only beginning to be explored. There are indications from Ginga and Exosat data that some sources (such as Mk335; Turner and Pounds 1988 and NGC4051; Lawrence *et al.* 1987) show different time variability behaviors at low and high energies thus giving vital clues as to the origin of the continuum which may be connected to their spectral differences.

Ginga observations of Seyfert galaxies can explore the domain of fast ($\Delta t < 1000$ second) variability of AGN to examine the characteristic time scales expect with the innermost regions of an accretion disk around massive blackholes, $T \sim 50M_6$ sec. However the absence of low-energy X-ray detectors on Ginga (and XTE) will not allow follow-up of the exciting Exosat results. It will await the large collecting area and broad bandwidth of SODART and XMM to attack this area of research.

## REFERENCES


Baity, W. *et al.* 1984. Ap. J. 279: 555.
Barr, P. 1986. M.N.R.A.S. 223: 29.
Boldt, E.A. 1987. Physics Reports 146: 216.
Elvis, M. *et al.* 1987. Ap. J. 310: 291.
Canizares, C., and J. White. 1989. Ap. J. 339: 27.
Czerny, B., and M. Elvis. 1987. Ap. J. 321: 243.
Elvis, M., and A. Lawrence. 1985. Astrophysics of Active Galaxies and QSOs ed. J. Miller University Science Books.
Elvis, M. *et al.* 1987. Ap. J. 310: 291.
Fabian, A., C. Canizares, and X. Barcons. 1989. M.N.R.A.S. 234: 15.
Fabian, A., M. Rees, L. Stella, and N. White. 1989. M.N.R.A.S. 238: 729.
Ferland, G., and M. Rees. 1988. Ap. J. 332: 141.
Guilbert, P., and M. Rees. 1988. M.N.R.A.S. 233: 475.
Halpern, J. 1982. Harvard Ph.D. Thesis.
Haniff, C., A. Wilson, and M. Ward. 1988. Ap. J. 334: 104.
Krolik, J. and M. Begelman. 1988. Ap. J. 239: 702.
Kruper, J., C.M. Urry, and C. Canizares. 1989. Ap. J. in press.
Kunieda, H. 1990. private communication.
Lawrence, A., M. Watson, K. Pounds, and M. Elvis. 1987. Nature 325: 694.
Lightman, A., and T. White. 1988. Ap. J. 335: 57.
Maccacaro, T., I. Gioia, A. Wolter, G. Zamorani, and J. Stocke. 1988. Ap. J. 326: 680.
Makishima, K. 1986. In: Mason, K., M. Watson, and N. White (eds.). The Physics of Accretion on Compact Objects. Springer-Verlag, Berlin.
Makino, F. *et al.* 1988. In: Tanaka, Y. (ed.). Physics of Neutron Stars and Black Holes. Universal Academy Press.
Matsuoka, M., M. Yamauchi, L. Piro, and T. Murakami. 1989 preprint.
McHardy, I. 1989. Memorei della Societa Astronomica Italiana 59: 239.
Morini, M., M. Lipani, and D. Molteni. 1987. Ap. J. 317: 145.
Morisawa, K., and F. Takahara. 1989. P.A.S.J. 41: 873.
Mushotzky, R.F. 1982. Ap. J. 256: 92.
Mushotzky, R.F. 1984. In: Bignami, G., and R. Sunyaev (eds.). Adv. Space Res. 3: 157-165. Pergamon Press, New York.

Mushotzky, R.F. 1987. In: Miller, H.R., and P.J. Wiita (eds.). Active Galactic Nuclei. Springer-Verlag.
Mushotzky, R., and A. Wandel. 1989. Ap. J. 339: 674.
Pounds, K. *et al.* 1986. M.N.R.A.S. 218: 665.
Pounds, K., and T.J. Turner. 1989. Memorei della Societa Astronomica Italiana 59: 261.
Pounds, K., K. Nandra, G. Stewart, and K. Leighly, K. 1989. M.N.R.A.S. in press.
Rothschild, R. *et al.* 1983. Ap. J. 269: 423.
Sun, W-H., and M. Malkan. 1989. Ap. J in press.
Turner, M. 1989. Bologna Meeting on AGN and the X-ray Background N. White Editor.
Turner, T.J., and K. Pounds. 1987. M.N.R.A.S. 224: 443.
Turner, T.J. 1988. Ph.D Thesis University of Leicester.
Turner, T.J., and K. Pounds. 1988. M.N.R.A.S. 232: 463.
Turner, T.J., and K. Pounds. 1989. M.N.R.A.S. in press.
Urry, C.M. *et al.* 1986. In: Treves, A. (eds.). Proceedings of the Conference on Variability in Galactic and Extragalactic X-ray Sources (Milan Association for the Advancement of Astronomy).
Urry, C.M. 1989. In: Cordova, F. (ed.). Multiwavelength Astrophysics. Cambridge University Press.
Warwick, R. *et al.* 1989. P.A.S.J in press.
Wilkes, B., and M. Elvis. 1987. Ap. J. 323: 243.

# On the Observational Appearances of a Freely Precessing Neutron Star in Hercules X-1

K.A. POSTNOV, M.E. PROKHOROV, AND N.I. SHAKURA
Sternberg Astronomical Institute

## ABSTRACT

This paper is concerned with evidence for neutron star free precession, which is often presumed to be responsible for the observed 35-day cycle in Hercules X-1. The precise formula for the period derivative due to free precession is obtained under the assumption that the precession period is much longer than that of the neutron star rotation. The optical light curves to be seen from the binary, with freely precessing accreting neutron star are simulated numerically. This simulation takes into account the reflection effect on the surface of the secondary component and on the accretion disk itself for different diagrams of X-ray emission.

## INTRODUCTION

The eclipsing, pulsating binary X-ray source Hercules X-1 is known to be one of the most interesting accreting binary stars. Its properties are deduced from a wealth of X-ray and optical observations made during the past 17 years (see Ögelman and Truemper 1988, and references therein for a review of X-ray and Boynton 1978, for a review of optical data).

One of the most enigmatic X-ray features of Her X-1 is the 35-day intensity variation cycle. A number of explanations of this period has been proposed thus far. The major ones among them are: (1) a freely precessing neutron star (Brecher 1972; Shklovsky 1973; Novikov 1973; Truemper *et al.* 1986); (2) a precessing accretion disk (Katz 1973; Roberts 1974; Petterson (1975, 1976); (3) presence of a third body (Mazeh and Shaham 1977); non-linear oscillations excited on the outer part of the disk

(Meyer and Meyer-Hoffmeister 1984). None of the explanations suggested is commonly accepted. Although the model of the precessing disk which screens periodically the X-ray flux toward the Earth has managed to explain certain details in the optical and X-ray light curves of Her X-1 (Gerend and Boynton 1980; Howarth and Wilson 1983), its feasibilitiy remains unclear (Papaloizou and Pringle 1982; Kondo *et al.* 1983).

The recent extensive X-ray observations from EXOSAT show evidence for the free precession model underlying the 35-day cycle in Her X-1 (Ögelman and Truemper 1988). This model has been discussed in more detail by Shakura (1988). In this paper we investigate a precise formula for the timing of an X-ray pulsar due to the free precession of a neutron star. We show that the pulsar period variations with the precession phase has a special shape by measuring which one could check up the model. In the framework of this model we also simulate numerically optical light curves to be observed from such a binary, taking into account the reflection effect on the secondary star and on the disk itself, and investigate the impact of the X-ray emission diagram on the light curves.

## PERIOD DERIVATIVE OF THE PULSAR DUE TO FREE PRECESSION

Consider a freely precessing biaxial solid body rotating around axis OP (see Figure 1) with a frequency $\Omega = 2\pi/P$. Let the main inertial axis pierce the body at the point I, and the magnetic pole direction constitute the angle X with the axis OI and intersect the body's surface at point M. The body precesses slowly around axis OI with a frequency $\omega = 2\pi/P_{pr}$. Angle $\varphi$ between OP and OI keeps constant. As is well known, the precessional frequency in the case of a symmetrical rotator is $\omega = \Omega \cdot \cos\varphi \cdot (I_1 - I_3)/I_3$, where $I_1$ and $I_3$ denote moments of inertia, ($I_3$ being directed along the precessional axis OI). Let the X-ray emission originate at the magnetic pole M. Then the problem is to find the time interval $\Delta t$ between subsequent pulses registered by a distant observer.

There are different ways to solve this problem (see e.g. Bisnovatyi-Kogan *et al.* 1989, who independently have obtained the solution). Here we follow the way which seems to be the most simple and straightforward (Shakura 1988). In the stationary spherical frame with the origin in the center of the body, the position of the emitting spot on the surface can be described in terms of polar distance b and longitude $\lambda$, measured from the meridian plane composed by vector J and the line of sight.[1] The change in b results in the periodical (with the precessional period $P_{pr}$) disappearance

[1] We are working under the condition $\Omega/\omega \gg 1$, when the rotational axis of the body practically coincides with the angular momentum J. In a more general case one ought to introduce the latitude and longitude of the emitted area with respect to the vector of instant rotational velocity $\Omega$ which is not aligned with J and rotates with frequency $\Omega$ arount it (we thank Dr. R. Blandford for

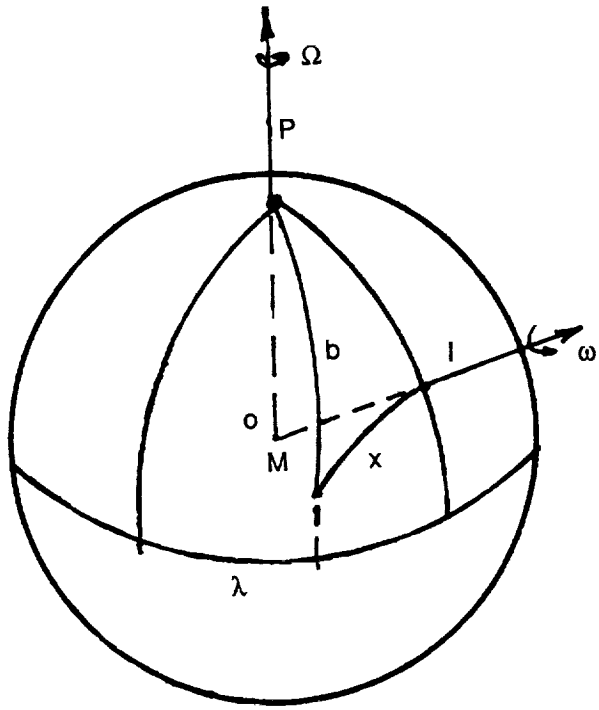


FIGURE 1 The schematic representation of the precessing neutron star geometry (see the text). The star rotates around vector OP with frequency $\Omega$ and slowly precesses around axis OI. the X-ray emission escapes from the magnetic pole M, whose coordinates ($\lambda$,b) are measured with respect to the pole P and meridian of the observer.

of the spot from the line of sight and *vice versa*. The change in $\lambda$ can lead to variations in the observing pulsar period (Sheffer 1987): $\Omega_{obs} = \Omega + d\lambda/dt = \text{const}$. If $d\lambda/dt = \text{const}$, $\Omega_{obs}$ is constant as well. But this is not the case for a precessing neutron star. Making use of familiar spherical trigonometric formulae one easily finds

$$d\lambda/dt = -\omega \frac{\sin\chi\cos\varphi - \sin\varphi\cos\chi\cos\omega t}{1 - (\cos\chi\cos\varphi + \sin\chi\sin\varphi\cos\omega t)^2} \qquad (1)$$

Obviously, $d\lambda/dt$ is related to the change in time of pulse arrival through the relation $\Delta P/P \cdot \Omega = d\lambda/dt$. The same expression can be obtained from differentiating directly moments of arrival for individual pulses, which is expressed by the equation

---

drawing our attention to this note). However, the approximation used is well suited for Hercules X-1.

$$\Omega t = 2\pi N - \arctan\left[\frac{\sin\chi\sin\omega t}{\sin\chi\cos\varphi\cos\omega t - \cos\chi\sin\varphi}\right], N = 1, 2, \ldots \quad (2)$$

Note that (1) is valid to the first order of $(\omega/\Omega)$, which is $\ll 1$ in our case (P = 1.24 s and $P_{pr}$ = 35 days).

The function $\Delta P/P(t)$ has a specific shape, by measuring which one could in principle check the predictions of the model. The precessing NS model implies that dP/dt should change its sign two times or four times per 35-day period depending on the geometry. To check this one needs simply to differentiate $d\lambda/dt$. The standard investigations show that this derivative vanishes at the following phases:

1. if $\chi < \varphi$ (i.e. the spot never crosses the pole) there are only two obvious roots defined by $\sin\omega t = 0$, which correspond to moments of crossing the meridian by the spot. In this case $d\lambda/dt = 0$ at the points $\cos\omega t = tg\chi/tg\varphi$.

2. if $\chi > \varphi$ (the spot can be behind the pole) $d\lambda/dt$ never vanishes; nevertheless two additional minima can arise as the solutions to the following equation:

$$\cos\omega t = \frac{tg\chi}{tg\varphi} - \frac{\sqrt{\sin^2\chi - \sin^2\varphi}}{\cos\chi\sin\chi\sin\varphi} \quad (3)$$

The necessary condition $|\cos\omega t| < 1$ put angles $\chi$ and $\varphi$ within the boundaries shown by the hatched area in Figure 2:

$$\forall\chi \text{ and } \omega \quad \text{if } \forall\chi + \omega > \pi/2;$$

$$\chi < 1/2\left[\arcsin(3\sin\varphi) - \varphi\right]$$

$$\chi > \pi/2 - 1/2\left[\arcsin(3\sin\varphi) - \varphi\right] \quad \text{if } \chi + \varphi < \pi/2 \quad (4)$$

Taking geometrical parameters of Her X-1 from Ögelman and Truemper (1988) to be $\varphi = 71°$, $\chi = 12°$, we find the $\Delta P/P$ curve of Her X-1 should pass through two additional extrema on the phases of the 35-day cycle to be found from (4). We conclude this section by stressing the necessity to make the precise X-ray pulsar timing in Her X-1 to check directly by this way the model of the free precession of the neutron star.

## OPTICAL LIGHT CURVES HZ HER IN THE MODEL OF A FREELY PRECESSING NEUTRON STAR

Synthesis of the light curves to be seen from binaries is a well-developed field of modern astrophysics (see e.g., Antokhina and Cherepashchuk 1987

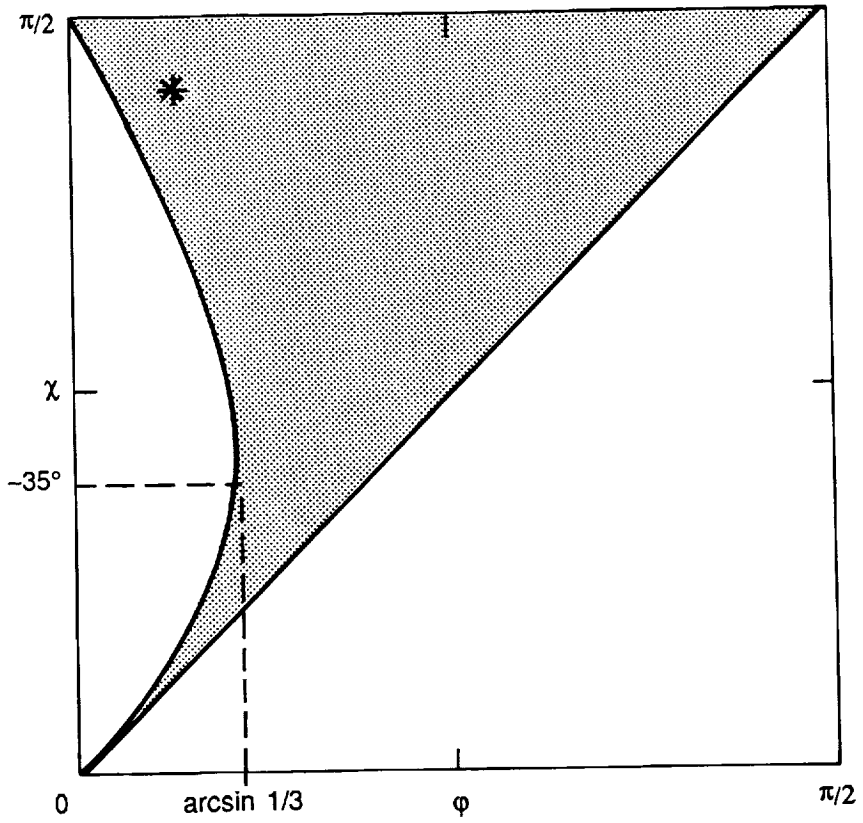


FIGURE 2 The $\varphi$ vs $\chi$ plane for magnetic pole location on the surface of the neutron star relative to pole P. The hatched area represents locus of $\Delta P/P(t)$ curve having four extrema. Asterisk marks the spot for Her X-1 geometry ($\varphi = 12°$, $\chi = 71°$) according to pulse deconvolution analysis (Ögelman and Truemper 1988).

for a review). Recently we have developed a computer code to calculate the light curve from any binary system (the description of the method used will be published elsewhere). Here we present some preliminary results showing synthetical optical light curves from Her X-1/HZ Her system in the framework of the precessing neutron star model. The parameters of the binary and of the neutron star have been chosen as follows.

The binary parameters:

Masses: $M_{HZ} = 2.2M_\odot$, $M_{ns} = 1.3M_\odot$; semimajor axis $a = 9.06R_\odot$; the binary inclination $i = 85°$.

The accretion disk parameters:

The accretion disk is supposed to be coplanar with the orbital plane. Its outer radius is $r_{out} = 3.2R_\odot$ (=0.8 of the neutron star's Roche lobe).

The inner disk radius is $r_{in} = 2 \cdot 10^8$cm. The disk is described in the terms of $\alpha$-theory and has thickness/radius dependence $H/r \propto r^{1/8}$ with $H(r_{out})/r_{out} = 0.1$.

The neutron star parameters:

The X-ray to optical luminosity $k_\chi = L_\chi/L_{opt} = 300$. The X-ray beam is taken to have a sine-like shape of width W and is inclined towards OP (spin axis) at the angle b. We assume that the spin axis of the neutron star can be directed arbitrarily relative to the orbital momentum L (at angle $\theta$) and to the line of sight at the phase zero of the binary period (at angle $\phi$).

The optical star parameters:

The optical star is assumed to fill its Roche lobe and has a polar temperature of 8000 K. The limb-darkening coefficient u = 0.4. The effectiveness of the X-ray conversion for reflection effect is $\kappa = 1$. The reflection effect from the optical star and the accretion disk itself have been accounted according to Khruzina *et al.* (1988).

The synthesized light curves are presented in Figures 3-4. In the case when the spin axis of the NS is normal to the orbital plane ($\theta = 0$) the light curves are symmetrical with respect to phase 0.5 for any precession phase. The curves, which look like those observed from HZ Her can be obtained only for an inclined neutron star. The figures also show the dependence of the curve shapes upon the X-ray beam width W = 45° and 90° for the neutron star orientations $\theta = 50°$, $\phi = 50°$.

## DISCUSSION

There are two general objections to the freely precessing neutron star model. First is that the difference of moments of inertia $\Delta I$ required to give rise to the precession frequency observed is $\Delta I/I \approx \omega/\Omega \approx 4 \cdot 10^{-7}$ which cannot be sustained by stresses in the neutron star crust (G.S. Bisnovatyi-Kogan). The second objection is that the crust of the precessing neutron star may break when relaxing to equilibrium shape caused by rotation (R. Blandford). Let's make use of simple estimations to show the feasibility of free precession in the case of Her X-1. The limiting crust deformation can be deduced from pulsar glitch observations to be $\Delta\epsilon \approx \Delta\Omega/\Omega \approx 2 \cdot 10^{-6}$ (for the Vela pulsar). Supposing the same crust properties for Her X-1, we can get $\Delta I/I \leq \Delta\epsilon$ which is enough to explain the observations. On the other hand, Her X-1 has a rotational oblateness $\approx\epsilon\ 10^{-7}$, which is less than the limiting deformation $\Delta\epsilon$. Then the precessional changing of the rotational axis in the body of the neutron star could not lead to the crust cracking.

In our opinion, the attractiveness of the model is dictated further by a possibility for an accreting magnetic neutron star to obtain a slight difference in its moments of inertia ($\Delta I$), which is enough to give rise to

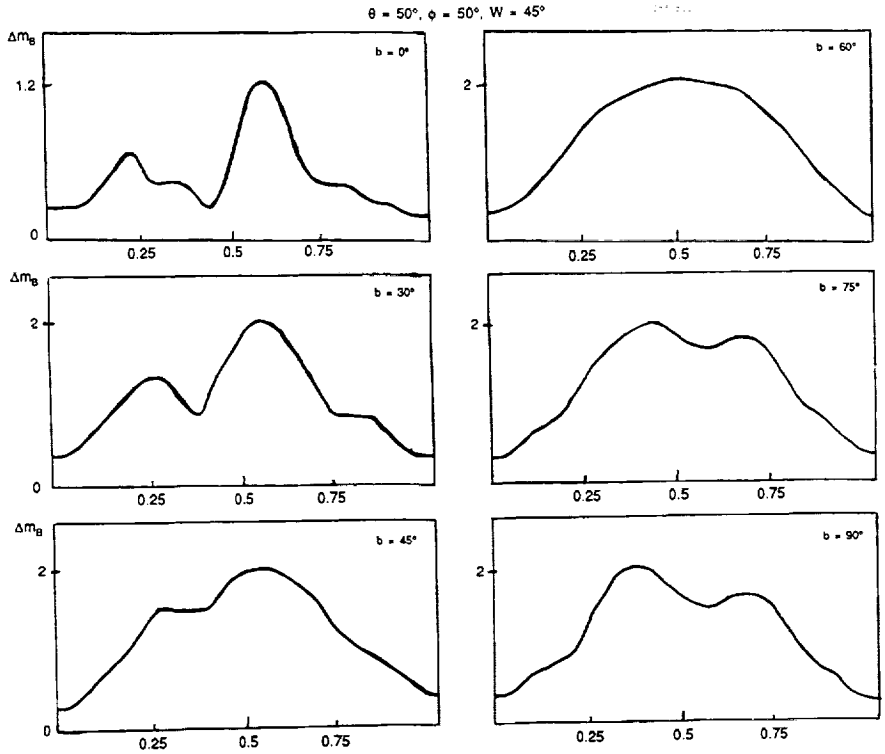


FIGURE 3 The synthesized B-light curves of Her X-1 in the model of a freely precessing neutron star with the parameters as described in the Section 3 for X-ray beam of width W = 45° shown at different latitudes b of the emitted area.

the free precession with the observed period in Her X-1 during the mass infall onto the star's surface throughout the magnetic poles (Novikov 1973). This idea nicely fits with the observational absence of free precession in radiopulsars.

The clock mechanism for the X-ray emission in Her X-1 then can be provided by change in the emitted area location on the stellar surface. The maximum of X-ray flux (so-called "main-on" state) is expected when the beam is in the upper position over the accretion disk plane. The "off"-state and "low-on"-state of Her X-1 might correspond to the situation when the magnetic poles are close to the plane of the disk and differ from each other by some azimuthal inhomogeneities on the disk caused by the X-ray heating. This does not seem to contradict the X-ray observations of low-massive X-ray binaries, which show modulations resulting from obscurarion by materials located in thick azimuthally structured accretion disks (Parmar and White 1988).

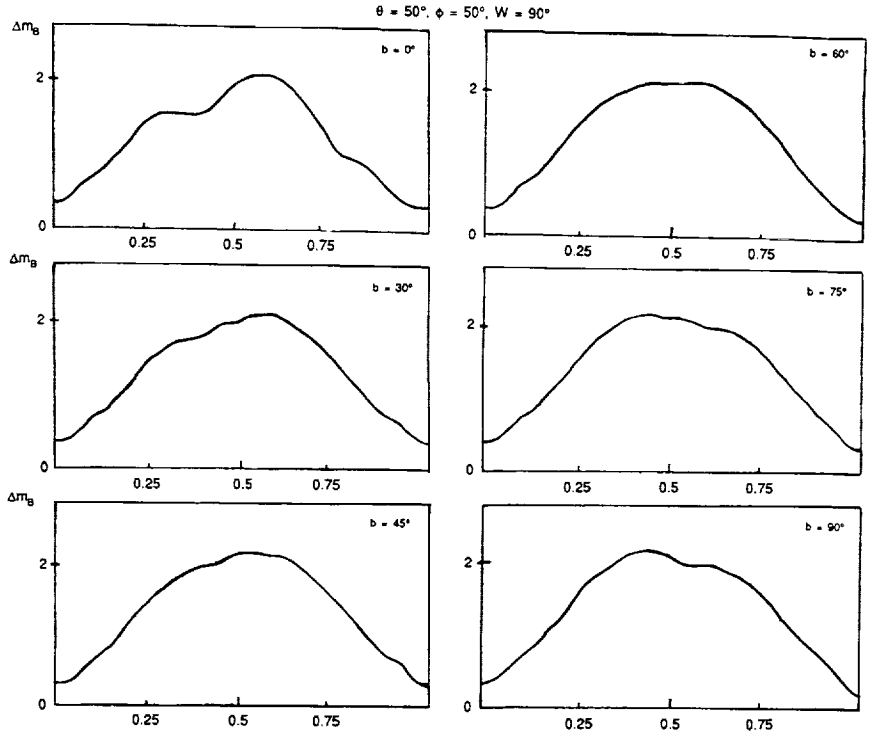


FIGURE 4 The same as Figure 3 for W = 90°.

In a stationary situation, the electrodynamical interaction of a rotating neutron star having a dipole magnetic field with a diamagnetic accretion disk, tends to make the dipole axis coplanar to the disk plane (Lipunov and Shakura 1980). We speculate that the precession of the neutron star might force the rotational axis to be non-parallel to the disk plane.

In general, the body of a neutron star could have a triaxial shape. As is well known, this would lead to a more complicated picture of the precessing motions (Landau and Lifshitz 1971). A situation is possible when the magnetic poles achieve their upper location above the disk twice during the precession period. Then the "low-on"-state can be interpreted in terms of the second upper position of the poles. Due to a large width of the beam both the poles could be visible as in fact is likely to be observed (Ögelman and Truemper 1988). The similar situation can take place in case of symmetrical rotator when the one magnetic pole crosses the disk plane and the second pole becomes visible as well.

## CONCLUSIONS

The model of freely the precessing neutron star underlying the famous 35-day cycle in Her X-1 has been considered. We have deduced a strict formula for the arrival times of X-ray pulses in the frame of this model. This expression can be used to check up the predictions of the model.

The preliminary results of the optical light curve synthesis from Her X-1/HZ Her show that the model of the precessing neutron star seems to be capable of describing the asymmetries and some features of the observed light curves. The neutron star, however, has to be inclined with respect to the orbital plane to make possible an anisotropic heating of the secondary. Observationally, this should manifest itself by a more pronounced mass outflow in the corresponding precessional phases. The more detailed calculation aiming to explain HZ Her optical light curves are now in progress and will be published later.

## ACKNOWLEDGEMENTS

We would like to thank Drs. G.S. Bisnovatyi-Kogan, R. Blandford, and E.K. Sheffer for discussions.

## REFERENCES

Antokhina, E.A., and A.M. Cherepashchuk. 1987. Astron. Zh. (in Russian) 64(3): 562.
Bisnovatyi-Kogan, G.S., G.A. Mersov, and E.K. Sheffer. 1989. Preprint IKI. 1532.
Boynton, P.E. 1978. In: Giacconi, R., and R. Ruffini (eds.). Physics and Astrophysics of Neutron Stars and Black Holes. Bologna. 121.
Brecher, K. 1972. Nature. 239: 325.
Gerend, D., and P.E. Boynton. 1980. Astrophys. J. 209: 562.
Howarth,??, and ??Wilson. 1983. Mon. Notic. Roy. Astron. Soc. 213.
Katz, J.I. 1973. Nature Phys. Scie. 246: 87.
Kondo, Y., T.C. van Flandren, and C.L. Wolf. 1983. 273: 716.
Khruzina, T.S., A.M. Cherepashchuk, N.I. Shakura, and R.A. Sunyaev. 1988. Adv. Space Res. 8:237.
Landau, L.D., and E.M. Lifshitz. 1971. Mechanics.
Lipunov, V.M., and N.I. Shakura. 1980. Pis'ma Astron. Zh. 6: 28.
Mazeh, T., and J. Shaham. 1977. Astrophys. J. 213: 117.
Meyer, F., and E. Meyer-Hoffmeister. 1984. Astron. Astrophys. 140: L35.
Novikov, I.D. 1973. Astron. Zh. 50: 459.
Ögelman, H., and J. Truemper. 1988. Mem. Soc. Astron. Ital. 59: 169.
Papaloizou, J. and J.E. Pringle. 1982. Mon. Notic. Roy. Astron. Soc. 200: 49.
Parmar, A.N., and N.E. White. 1988. Mem. Soc. Astron. Ital. 59. 147.
Petterson, J.A. 1975. Astrophys. J. 201: L61.
Petterson, J.A. 1977. Astrophys. J. 218: 783.
Roberts, J.M. 1974. Astrophys. J. 187: 575.
Shakura, N.I. 1988. In: Physics of Neutron Stars. Pulsars and Bursters. PTI. Leningrad. 34.
Sheffer, E.K. 1987. Pis'ma Astron. Zh. 13: 204.
Shklovsky, I.S. 1973. Astron. Zh. 50: 233.
Truemper, J., P. Kahabka, H. Ögelman, *et al.* 1985. Preprint MPI 41.

# The PSR 2127+12 as an Indicator of a Massive Black Hole in the Core of Globular Cluster M 15

K.A. POSTNOV, M.E. PROKHOROV, AND N.I. SHAKURA
Sternberg Astronomical Institute

## ABSTRACT

The 110-millicsecond pulsar PSR 2127+12 in the core of the globular cluster M15 is distinguished by having a negative period derivative $\dot{P} \approx -2 \cdot 10^{-17}$. This value cannot be provided by acceleration in the mean gravitational potential of the core. A flyby of a star $\approx$ 300 AU away could explain the $\dot{P}$ observed, but the probability of such an event is small ($\simeq 10^{-3}$). We suggest that the pulsar motion is governed by the presence of a moderately massive ($\simeq 2 \div 3 \cdot 10^4$ $M_\odot$) black hole in the cluster's center. The idea is further supported by an observed post-collapse morphology of the M15 core.

## INTRODUCTION

Two pulsars in globular clusters out of the seven known so far exhibit anomalous values of $\dot{P}$. The first one, the pulsar PSR 1821-24 in M28 with a period of 3 ms, has unusually large for millisecond pulsars dP/dt $= 1.6 \cdot 10^{-18}$ (Foster *et al.* 1988), and the second one, PSR 2127+12 in M15 with a period of 110 ms has negative period derivative dP/dt $\simeq$ -2 $10^{-17}$ (Wolszczan *et al.* 1989). The observed $\dot{P}$ in the PSR 1821-24 can be connected with the magnetic braking, while the arrival time analysis in the latter pulsar strongly evidences the Doppler shift due to a motion with acceleration toward the observer. In this note we concentrate on PSR 2127+12 and show that its acceleration can be due to the presence of a massive black hole in the core of the globular cluster M15. Other possible

reasons for acceleration of this pulsar fail in explaining the observational data or are very tentative.

## DYNAMICAL EFFECTS OF THE MEAN CORE POTENTIAL

Dynamical effects in the globular cluster should exert influence upon the pulsar timing because any change in pulsar radial velocity $v_r$ results in changing of the observed pulsar period according to the relation

$$\frac{dv_r/dt}{c} = \frac{dP/dt}{P} \tag{1}$$

with c as speed of light. This effect may mimic the proper pulsar dP/dt. The pulsar radial velocity can vary due to (i) the motion in the potential of the cluster's core and (ii) the motion in the potential of a nearby star. By measuring $\dot{P}$ one can discriminate between these two possibilities (Blandford *et al.* 1987).

The knowledge of the globular cluster parameters and the angular position of the pulsar in the cluster's core make it possible to estimate the maximal radial acceleration produced by the potential of the core which can evidently be both positive or negative. If the pulsar acceleration were produced solely by the core potential and not exceeded a maximal value, one could find in principle two possible spatial positions of the pulsar inside the core.

The maximal value of the acceleration in the framework of standard King model of M15 cluster structure (see Webbink 1985) is about $10^{-6}$ $cm^2/s$, whereas $g_r \approx 6 \cdot 10^{-6}$ $cm^2/s$ is required to explain properties of PSR 2127+12.

## ACCELERATION IN A NEARBY STAR POTENTIAL

Let's turn to the possibility of pulsar accelerating in the potential of a nearby star. For the potential required to be produced, the second star with a mass of 0.8 $M_\odot$ should be closer than $a \simeq 5 \cdot 10^{15}$ cm, which corresponds to a characteristic time of stellar encounter $\simeq$ 300 yrs. The probability of finding a star such as this in the dense core of a globular cluster is of the order of $(a/\langle a \rangle)^3 \simeq 10^{-3}$ (here $\langle a \rangle = n_*^{-1/3}$ denotes the mean distance between stars in the core) for a typical stellar density $10^5$ $pc^{-3}$. Note that whether or not this second star forms a binary system with the pulsar is of no importance. The existing data for PSR 2127+12 (Wolszczan *et al.* 1989) about the constancy of dP/dt during 9 months of observation rule out all binary periods less than 100 yrs.

A group of nearby stars may produce a fluctuation of the potential 6

times the mean core value, but the probability of such situation is extremely low.

## OTHER SOURCES OF ABNORMAL TIMING

### i) Gravitational Lensing

Gravitational lensing effect in the core of a globular cluster causes the brightness variations (see Sazhin 1987). The same effect should be seen in pulsar timing. The variations in pulsar period can be produced by a flyby of a star near the line of sight between the pulsar and the observer. Such a star will cause a delay in the time of arrival of radio pulses (so-called Shapiro delay). This results in a period derivative of order of

$$dP/dt_S \approx 2(r_g/c)(v/b)^2 P \qquad (2)$$

where $r_g$ is the star's gravitational radius, b is the impact parameter and v is the transversal velocity of the star. For a typical stellar mass 0.8 $M_\odot$ and velocity 10 km/s the impact parameter required to produce the observed in PSR 2127+12 $\dot{P}$ is $\simeq 3 \cdot 10^{11}$ cm. The probability of such event in the core is $(b/<b>)^2 \simeq 10^{-10}$ where $<b> \approx R_c/\sqrt{N} \approx 3 \cdot 10^{16}$ cm is the mean impact parameter, $R_c$ and N are the cluster core radius and the number of stars inside it. But the typical event duration is of the order of $\tau \simeq b/v \simeq 3 \cdot 10^5$ s and is too short. Note that the effect of the Shapiro delay produced by the core itself is estimated quite analogically by substituting $r_g$ for the core and v for the pulsar velocity, and is as large as the effect from the single star with the mean impact parameter <b>, i.e., is extremely small in amplitude although large enough in duration.

### ii) The Neutron Star Precession

Pulsar period variations could also be caused by some internal irregularities in the NS rotation. For example, neutron star free precession is known to change pulsar period as $\dot{P} \approx (P_{psr}/P_{pr})^2$. For $\dot{P} \simeq 10^{-17}$ and $P \simeq$ 0.1 s precession period required proves to be very small, about $3 \cdot 10^5$ s. So this possibility is ruled out by the observations. Geodetic precession of a NS in the cluster's core has, instead, a very large period $\approx T/(v/c)^2$ (where T denotes characteristic traveling time for a star with velocity v across the core; $T \cong 10^4$ yrs) and cannot produce any notable $\dot{P}$.

Another reason could be connected with the NS internal spinup/spindown like in the rotational pendulum. But it remains unclear why such universal effects are not seen in other pulsars.

## PULSAR MOTION IN THE POTENTIAL OF COLLAPSED CORE

Dynamical evolution of a globular cluster at the late stages can lead to a core collapse (see Spitzer 1985 for a review). As a result, a massive black hole can be formed. This observationally should be expressed by a cusp in the core stellar density and surface brightness. The globular cluster M15 is one of the clusters whose surface brightness can be interpreted as showing such a feature (Djorgovski and Penner 1985).

For an estimation of the acceleration produced by the collapsed core potential let's use again expression (1) in the form

$$g = \frac{GMy}{(x^2 + y^2)^{3/2}} \tag{3}$$

where x and y are cartesian coordinates as shown in Figure 1. The function has a maximum at $x = \sqrt{2}y$. x is observed to be 2", corresponding to $\simeq 0.1$ pc at a distance 10 kpc. Thus the central mass M capable of producing the acceleration required must be $\simeq 3\ 10^4\ M_\odot$, or $\approx 10\%$ of the total mass of the core. Such mass in the center of the cluster begins to significantly affect the cluster dynamics only in the innermost parts of the core. Two other millisecond pulsars recently discovered in M15 (Anderson *et al.* 1989) are situated 2' away from the center and thus should not be subjected to the central mass influence.

A black hole of similar mass will tidally disrupt the stars inside the loss cone at a rate (Hill 1975)

$$\dot{N}_{inf} = \sqrt{6\pi} n_* r_t r_h \sigma \simeq 710^{-7} m_\odot yr \tag{4}$$

(here $r_t$ and $r_h$ denote tidal disruption radius of the star and the black hole's capture radius, respectively, and $\sigma$ is the velocity dispersion). This rate agrees well with the simple estimate of the growing rate of the black hole during the Hubble time. So we conclude this hole could really be formed in the course of the cluster's evolution.

## CONCLUSIONS

The negative period derivative observed in the PSR 2127+12 must be due to an accelerated pulsar motion in the core of the globular cluster M15. The mean core potential under standard assumptions about the core structure can provide the acceleration an order of magnitude lower than the required $6 \cdot 10^{-6}$ cm$^2$/s, but a nearby star $\approx 300$ AU away from the pulsar would do. However the probability of this event is a rather small one, $\simeq 10^{-3}$. Measurements of $\dot{P}$ in the pulsar timing analysis would confirm or discard the latter possibility in the nearest future.

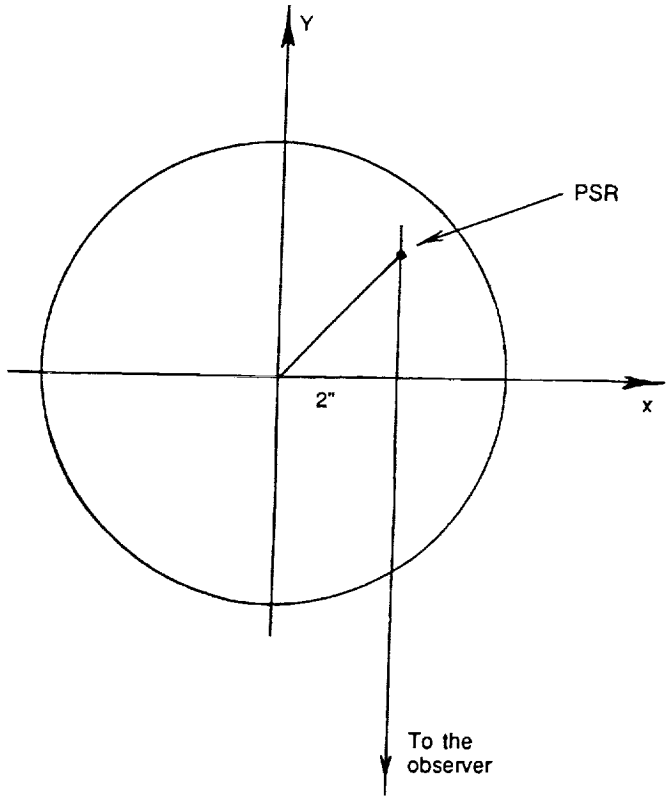


FIGURE 1 Geometry of pulsar position in the globular cluster core.

Other reasons for possible period changing, such as the neutron star precession or rotational pendulum-like motions seem inappropriate. The Shapiro delay in pulsar timing induced by a flyby of a field star across the line of sight fails as well.

We suggest that a black hole with a mass of $2 \div 3 \cdot 10^4\ M_\odot$ governs the pulsar motion. This black hole could be a remnant of the core collapse which occured in the course of the dynamical evolution of the cluster. Its mass would exert influence upon only the innermost regions of the core and would not contradict the cluster's age. This idea seems to be further supported by the observations of a steep brightness gradient in the core of M15—the phenomenon predicted by theories of the globular cluster cores having massive post-collapse remnants. The black hole in the cluster's center would also cause an anomalous ($\approx$ 30 km/s) velocity dispersion to be observed in the M15 core. So its measurements would be strongly desired.

Thus the pulsar timing analysis being a probe of the core gravitational potential can be an indicator of the core having a massive black hole in its center.

## ACKNOWLEDGEMENTS

We thank the staff of the relativistic astrophysics department for discussions.

## REFERENCES

Anderson, S., P. Gorham, S. Kulkarni, T. Prince, and A. Wolszczan. 1989. IAU Circ. 4762, 4772.

Blandford, R.D., R.W. Romani, and J.H. Applegate. 1987. Mon. Notic. Roy. Astron. Soc. 225: 51P.

Djorgovski, S., and H. Penner. 1985. In: Goodman, J., and P. Hut (eds.). Dynamics of star clusters. IAU Symp. 113: 73.

Foster, R.S., D.C. Backer, J.H. Taylor, and W.M. Goss. 1988. Astrophys. J. Lett. 326: L13.

Hills, J.C. 1975. Nature 254: 295.

Sazhin, M.V. 1987. In: 11th International Conference on General Relativity and Gravitation. Stokholm II: 519.

Spitzer, L., Jr. 1985. In: Goodman, J., and P. Hut (eds.). Dynamics of star clusters. IAU Symp 113: 109.

Webbink, R.F. 1985. In: Goodman, J., and P. Hut (eds.). Dynamics of star clusters. IAU Symp. 113: 541.

Wolszczan, A, S.R. Kulkarni, J. Middleditch, D.C. Backer, A.S. Fruchter, and R.J. Dewey. 1989. Nature 337: 531.

# The Formation and Evolution of Domain Walls

WILLIAM H. PRESS AND BARBARA S. RYDEN
Harvard-Smithsonian Center for Astrophysics
and
DAVID N. SPERGEL
Princeton University

## INTRODUCTION

Symmetry breakings in the early universe can produce stable topological defects: monopoles, cosmic strings and domain walls. While cosmic strings have attracted significant attention as possible seeds for galaxy formation (see Press and Spergel 1989 for review). Domain walls—sheet-like defects produced when the low energy vacuum has isolated degenerate minima—however, have been relegated to the list of cosmologically undesirable objects.

Domain walls were banished to the cosmological dog house by Zel'dovich *et al.* (1975), who noted that the energy density in domain walls falls much less fast, as the universe expands, than does the energy density in radiation or even matter. Thus, stable domain walls would quickly dominate the universe. Vilenkin (1985) reviews much of the early work on domain walls, which confirmed the dangers of an early-time domain wall producing phase transition. However, the failure of existing scenarios of galaxy formation have motivated a domain wall revival. Hill *et al.* (1989) suggested that a late-time (post-decoupling) phase transition could have produced cosmologically interesting "light" domain walls. They discussed a model proposed by Hill and Ross (1988a, b) in which a pseudo-Goldstone boson associated with the neutrino family of fermions undergoes a spontaneous symmetry breaking and acquires a mass on the order of $m_\nu{}^2/M_{GUT}$. Hill *et al.* speculate that the light, thick domain walls produced by these late-time phase transitions could account for much of the observed large-scale structure. Earlier, Wasserman (1986) had suggested that late-time phase transitions might explain the bubble-like topology seen in the CfA redshift

survey. Independently, Dimopolous and Starkman (1989) also proposed a family of models in which a technicolor axion acquires a mass at low temperature phase transition. These models also produce domain walls; however, they remain severely constrained by stellar evolution bounds on axion properties.

Unlike cosmic strings, whose dynamics have been studied in detail, little work has been done on domain wall dynamics. Many of the basic features of domain wall dynamics are not understood: How does the energy density in walls scale as the universe expands? Is most of the energy density in infinite walls or in closed domain wall "bags"? What is the lifetime of such bags? What is the typical wall velocity? Do most wall intersections lead to reconnection? How do wall oscillations damp? How does the characteristic wall size grow as the universe expands? Bill Press, Barbara Ryden and I have developed a computer simulation of domain wall evolution. This talk will describe our results (Press *et al.* 1989; Ryden *et al.* 1990) and discuss its implication for domain wall seeded large-scale structure.

Rather than following the motion of infinitely thin domain walls (e.g., Kawano 1989), our computer code follows the evolution of a scalar field, $\phi$, whose dynamics are determined by its Lagrangian density. The topology of the scalar field determines the evolution of the domain walls. This approach properly treats both wall dynamics and reconnection. We ran 10 separate 1024 x 1024 numerical simulations. A plot of the comoving wall area A times conformal time per comoving volume V, as a function of elapsed (conformal) time since the phase transition, is shown in Figure 1. One sees that, during the epoch when the conformal time (that is, light travel distance) $\eta$ is much greater than the wall thickness and much smaller than the length of an edge of the box, the wall area is well fitted by a power law

$$A/V \propto \eta^{\nu}.$$

with an exponent $\nu$ not very different from 1, the value that implies a scale-free evolution with, at all epochs, about one domain wall per horizon volume. The average wall velocity was mildly relativistic, 0.4 c.

We also ran 10 200 × 200 × 200 numerical simulations. The dynamics of walls in a three dimensional simulation is similar to that in a two dimensional simulation.

Figure 2 shows the domain wall structure in the 2 dimensional universe. Most of the walls are part of an infinite network that percolate across the simulation. Only a small fraction of the energy density is in small bubbles. This is a very different situation from that for cosmic strings, whose evolution and reconnection can leave behind a significant spectrum of smaller

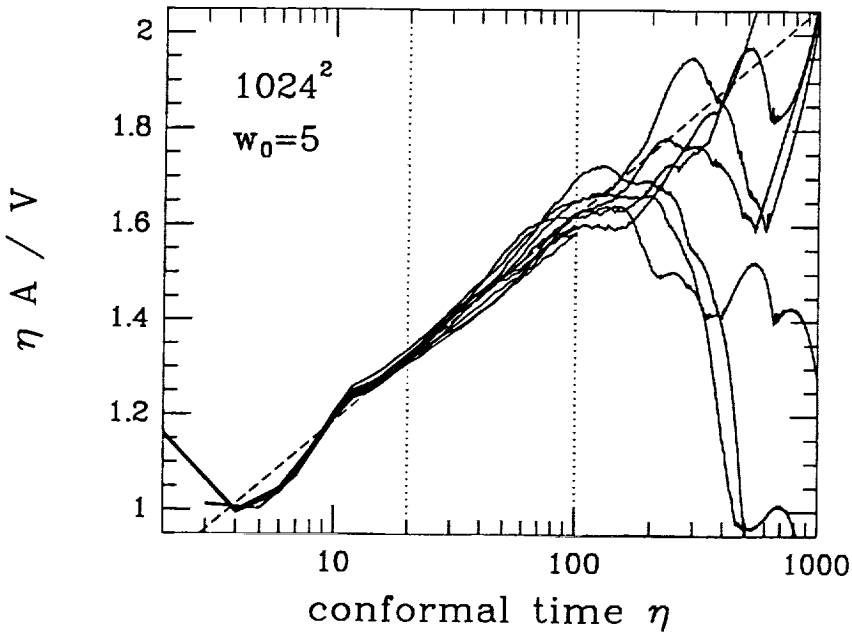


FIGURE 1 A linear-log plot of the comoving wall area per unit comoving volume of the two-dimensional simulations, multiplied by the conformal time $\eta$. Results are shown for ten 1024 × 1024 wall simulations. The dashed line is the best fitting relation of the form $\eta A/V = a + b \ln(\eta/\omega_0)$, fit in the interval $20 < \eta < 100$, marked by the dotted lines.

loops (Albrecht and Turok 1985; Bennett and Bouchet 1988; see Press and Spergel 1989, for additional references). The reason for the difference is: (i) Wall bubbles are formed, we find, relatively rarely (per horizon volume), and (ii) We find no instances of a wall bubble being formed in a configuration that is able to persist without immediately collapsing, self-intersecting, and radiating away its energy content as oscillatory excitations of the $\phi$ field (i.e., schizons). This difference from string loops is not unexpected, generically, simply as a consequence of the different dimensionality of a loop (one-dimensional) and a bubble (two-dimensional). Thin wall simulations confirm the behavior seen in these thick wall calculations (Kawano 1989). It is also supported by recent work of Widrow (1989a), who finds that spherical bubbles can "bounce" only a few times at most, and out to distances several times the wall *thickness*, before dissipating. Widrow (1989b) also finds that there is a tendency for nonspherical bubbles to become more spherical during the early stages of their collapse. This conclusion is supported by what we see in our evolutions.

An immediate consequence of these findings is that, as a consequence

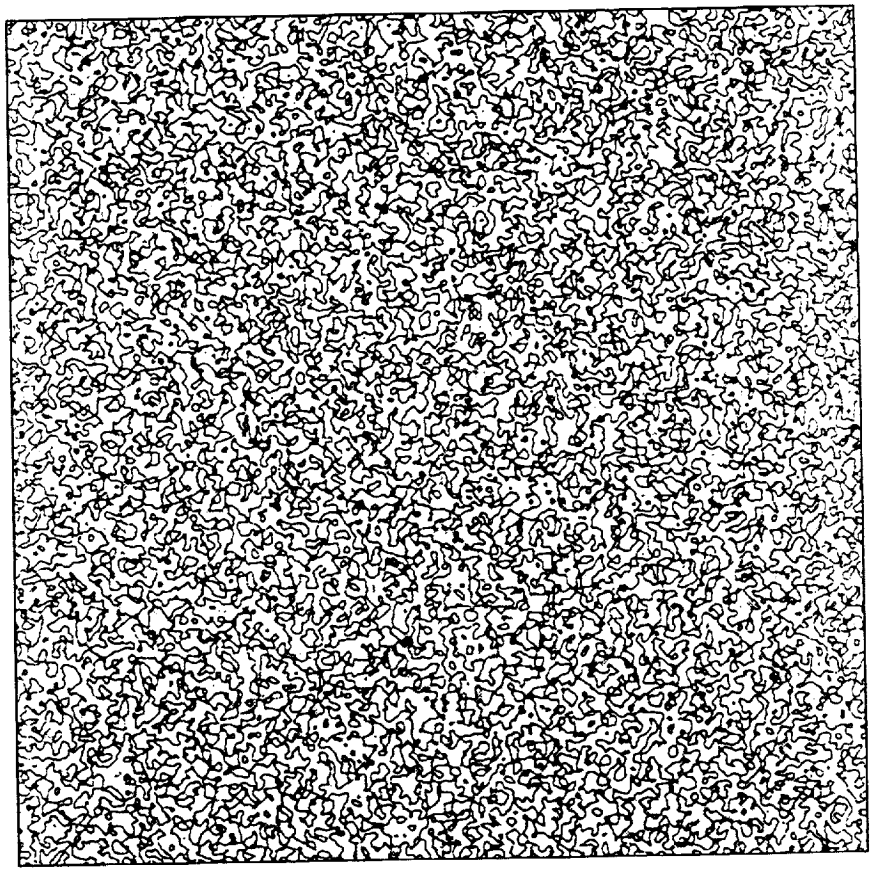

FIGURE 2 Pictures of the domain wall network in a 1024 × 1024 simulation with a wall thickness of $\omega_0 = 5$. Slab symmetry is here assumed in the third dimension (out of the page). Snapshots are taken at conformal times (a) $\eta = 9.6$, (b) $\eta = 32$, and (c) $\eta = 93$. (E.g., at $\eta = 93$ the horizon size is about 20 times the wall thickness and 1/10 times the size of the picture.) The gray scale map is chosen so that walls are gray on the side facing domains where $\phi$ is positive, black on the side facing domains where $\phi$ is negative.

of the observed lack of quadrupole microwave anisotropy, it is not possible to hide any significant amount of matter in walls at the present epoch. For the wall geometries that we see develop, one will always have $\delta T/T \sim \omega_{wall}\beta_{wall}$, so that $\omega_{wall}$ (the fraction of critical density in walls at the present epoch) must be $\lesssim 10^{-4}$.

This implies that walls cannot seed the formation of structure on smaller scales. Consider a comoving scale L. At a redshift of $(ct_0/L)^2$, when this scale was on order the horizon scale, the domain walls generated a

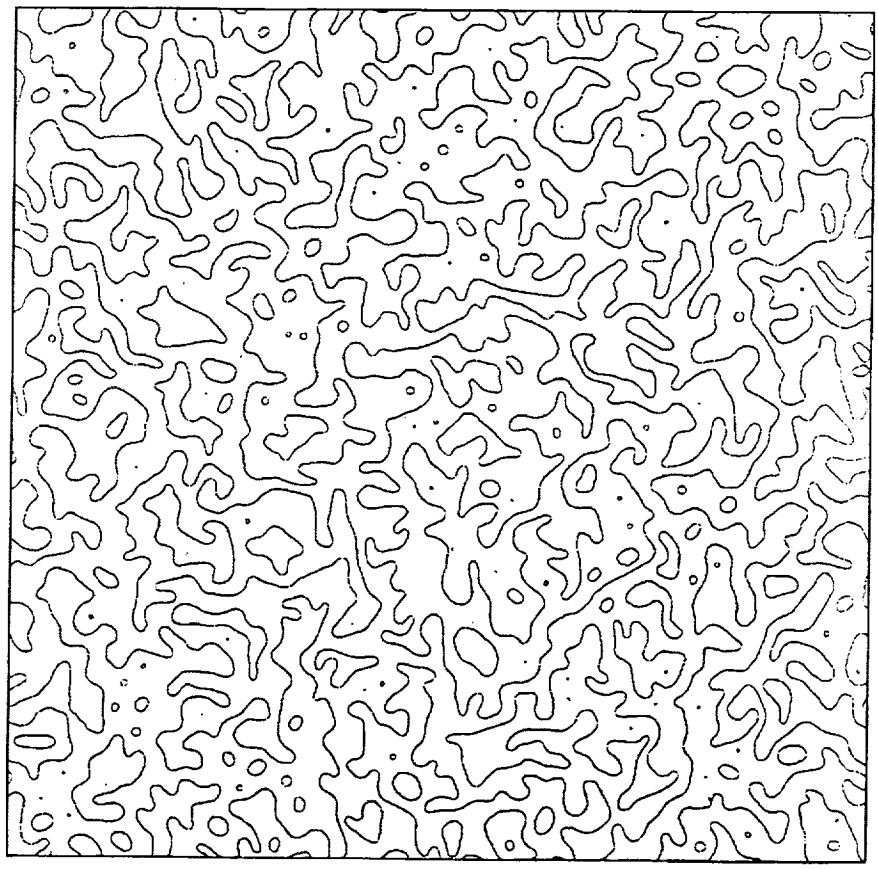

FIGURE 2b

perturbation $\omega_{wall}{}^{0}(ct0/L)^{3}$. This wall-induced perturbation grew linearly up to today and its current amplitude is $\omega^{0}{}_{wall}(ct_0/L)$ *The wall-induced perturbations with the highest amplitude are those near the size of the horizon*. The density perturbations on the horizon scale create a quadrupole anisotropy in the microwave background through the Sachs-Wolfe effect, with amplitude $\delta T/T \sim \delta\rho/\rho \sim \omega_{wall}$. Thus, if walls move freely in the manner computed in this paper, and if they survive to the present, then it is impossible for them both to generate large scale structure, and to be consistent with quadrupole microwave background anisotropy limits.

We investigated not only potentials that produce single domain walls, but also potentials that produce a network of walls and strings (Ryden *et al.* 1990). These networks arise in axion models where the U(1) Peccei-Quinn symmetry is broken into $Z_N$ discrete symmetries. If N = 1, the walls are

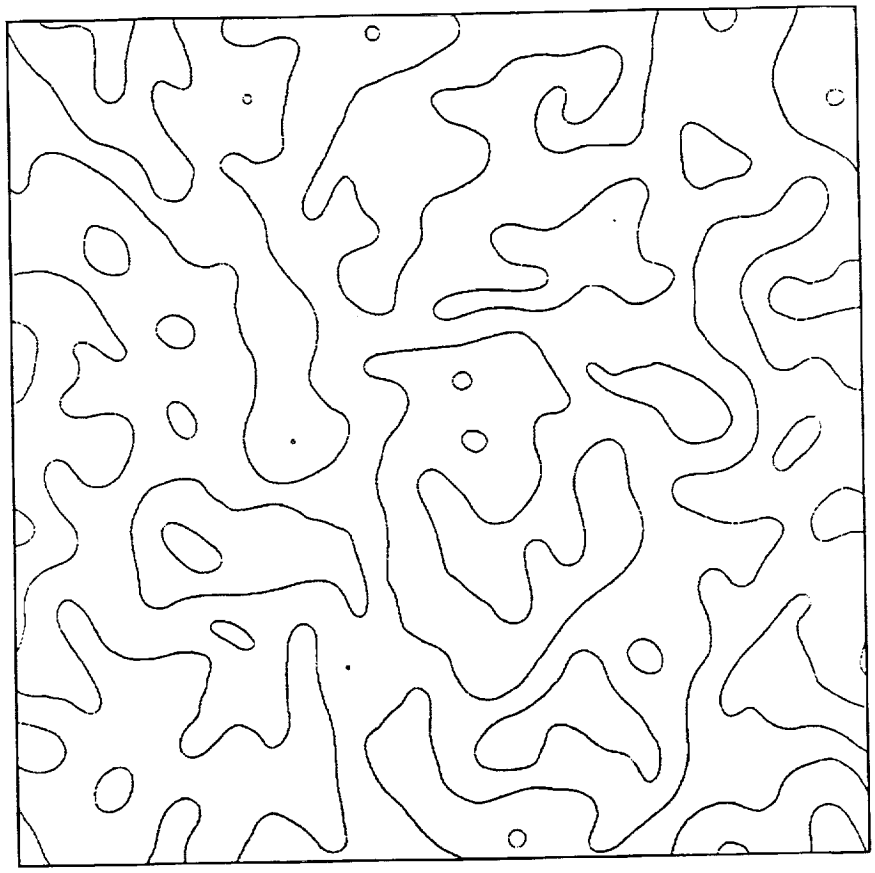

FIGURE 2c

bounded by strings and the network quickly disappears. For $N > 1$, the network of walls and strings behaved qualitatively just as the wall network shown in both figures. This both confirms our rather pessimistic view that domain walls can not play an important role in the formation of large scale structure and implies that axion models with multiple minimum can be cosmologically disastrous (see Everett and Vilenkin 1982; Vilenkin and Everett 1982; and Vachaspati and Vilenkin 1984).

## ACKNOWLEDGMENTS

We thank Larry Widrow, Terry Walker, Tod Lauer, David Nelson, Glenn Starkman, Curt Callan, Dave Schramm, Marcelo Gleiser, and Doug Eardley for helpful discussions. This work was supported in part by the

National Science Foundation: at Harvard University (PHY-86-04396), at Princeton University (NSF Presidential Young Investigator Award), and at the Institute for Theoretical Physics, Santa Barbara (PHY-82-17853), with supplementary support from the National Aeronautics and Space Administration. W.H.P. and D.N.S. thank the Institute for Theoretical Physics for hospitality during the early stages of this work. D.N.S. acknowledges support from the Alfred P. Sloan Foundation.

## REFERENCES

Albrecht, A., and P. Steinhardt. 1982. Phys. Rev. Lett. 48: 1220.
Albrecht, A., and N. Turok. 1985. Phys. Rev. Lett. 54: 1868.
Bennett, D., and F. Bouchet. 1988. Phys. Rev. Lett. 60: 257.
Bertschinger, E., and P.N. Watts. 1988. Ap. J., 316: 489.
Brandenberger, R., N. Kaiser, D.N. Schramm, and N. Turok. 1987. Phys. Rev. Lett. 59: 2371.
Dimopoulos, S., and G. Starkman. 1990. In preparation.
Everett, A.E., and A. Vilenkin. 1982. Nucl. Phys., B207: 43.
Frieman, J.A., G.B. Gelmini, M. Gleiser, and E.W. Kolb. 1988. Phys. Rev. Lett, 60: 2101.
Guth, A. 1981. Phys. Rev. D 23: 347.
Hill, C.T., and G.G. Ross. 1988a. Phys. Lett. B205: 125.
Hill, C.T., and G.G. Ross. 1988b. Nuclear Phys. B311: 253.
Hill, C.W., D.N. Schramm, and J.N. Fry. 1989. Comments on Nucl. Part. Phys. 19: 25.
Kawano, L. 1989. The Evolution of Domain Walls in the Early Universe. FERMILAB-Pub-89/208-a.
Linde, A. 1982a. Phys. Lett. 108B: 389.
Linde, A. 1982b. Phys. Lett. 114B: 431.
Press, W.H., B.P. Flannery, S.A. Teukolsky, and W.T. Vetterling. 1986. Numerical Recipes: The Art of Scientific Computing. Cambridge University Press, New York.
Press, W.H., and D. Spergel. 1989. Physics Today, 42(3): 29.
Press, W.H., B. Ryden, and D.N. Spergel. 1989. Astrophys. J. 347: 590.
Ryden, B.S., W.H. Press, and D.N. Spergel. 1990. Ap j. 357, 293.
Vachaspati, T., and A. Vilenkin. 1984. Phys. Rev. D 30: 2036.
Vilenkin, A. 1985. Phys. Reports 121: 263.
Vilenkin, A., and A.E. Everett. 1982. Phys. Rev. Lett. 48: 1867.
Wasserman, I. 1986. Phys. Rev. Lett. 57: 2234.
Widrow, L. 1989a. Phys. Rev. D 39, 5376.
Widrow, L. 1989b. Phys. Revd 40, 1002.
Zel'dovich, Ya.B., I.Yu. Kobzarev, and L.B. Okun. 1975. Sov. Phys. JETP 40: 1.

# A Statistical Analysis of Gamma-Ray Bursts Detected by the Konus Experiment on Venera 11 and 12

MAARTEN SCHMIDT
California Institute of Technology
and
J.C. HIGDON
Claremont Colleges

## ABSTRACT

We discuss the advantages of using the $V/V_{max}$ method to test well-defined samples of gamma-ray bursts for the spatial uniformity of their parent population. We have applied the $V/V_{max}$ test to gamma-ray bursts of duration longer than 1 second recorded by the Konus experiment aboard Venera 11 and 12. Based on a sample of 123 bursts, we find $< V/V_{max} > = 0.46 \pm 0.03$, consistent with a uniform distribution in space. We urge that experimenters give careful attention to the detection limit for each recorded gamma-ray burst, and that quantitative data for burst properties and detection limits be published.

## INTRODUCTION

As long as optical identifications of gamma-ray bursts are lacking (Hurley *et al.* 1986), our best hope for establishing their distances and luminosities is through the statistics of their observed properties. In particular, if evidence can be found for a departure from a uniform distribution in space, then the interpretation of this departure will provide a distance scale.

The space distribution of sources contains indirect information about their distances. The distribution of gamma-ray bursts on the sky appears to be isotropic (Mazets *et al.* 1981a; Atteia *et al.* 1987), allowing only distances that are either small on a galactic scale or large on a cosmological scale. In the radial direction, the space distribution is reflected in the observed distribution of burst intensities. Size-frequency distributions, i.e.,

the number of bursts detected per year greater than a given flux, have been much studied (e.g., Fishman 1979; Jennings and White 1980; Mazets and Golenetskii 1981, 1988; Jennings 1982, 1984, 1988; Higdon and Lingenfelter 1984, 1986). The observed flattening of the size-frequency distribution at low fluxes, below that of a $-1.5$ power law indicative of a spatially uniform distribution, has been interpreted as evidence for a source distribution confined to the galactic disk or halo (Fishman 1979; Jennings and White 1980; Mazets and Golenetskii 1981; Jennings 1982, 1984) or as evidence for cosmological distances (Paczynski 1986).

Burst detections are based on count rates rather than energy fluxes. The relation between the fluxes and the count rates is affected by the distribution of spectral shapes and of burst durations, both of which are poorly known. Higdon and Lingenfelter (1986) showed that the deviation of the Konus size-frequency distribution at low energy fluxes from a $-1.5$ power law is dominated by these effects. On the basis of similar arguments, Mazets (1986) suggested that the most appropriate form of data representation is the size-frequency distribution in terms of the peak count rates $N_{max}$ of the bursts.

Employing the complete Konus data bases (Venera 11 to 14) of sources with duration larger than 1 s, Mazets and Golenetskii (1988) found that the cumulative distribution of peak count rates "shows full agreement with a $-3/2$ law. Deviations in the region $N_{max} = 100$ to 400 can undoubtedly be attributed to the loss of weak events near the detection threshold." Since under a $-3/2$ law, 7/8 of all sources with $N_{max} > 100$ are in the range $N_{max} = 100$ to 400, the agreement with a $-3/2$ law appears to be based on only a small fraction of the observed bursts.

The effects discussed here are related to variations in the detection threshold caused by variations in the background. These will unavoidably lead to a flattening of the size-frequency distribution, even if the sources have a uniform space distribution. The $V/V_{max}$ test for uniformity of the space distribution takes into account the detection limit associated with each individual burst source. This test, which has several further advantages, is described below and then used on bursts recorded in the Konus experiment.

## THE $V/V_{MAX}$ TEST

The ratio $V/V_{max}$ characterizes for each individual burst in a survey its radial location within the volume of space in which it could have been observed above the detection limit. If the source population is spatially uniform, then the distribution of $V/V_{max}$ will be uniform between 0 and 1. The mean value of $V/V_{max}$ for such a sample, $< V/V_{max} >$, is 1/2, with an r.m.s. error of $(12n)^{-1/2}$, where n is the number of bursts in the sample. Values of $< V/V_{max} >$ smaller than 1/2 will result if the sources

are galactic and sampled to distances greater than the scale height of their parent population, or if sources at cosmological distances are evaluated using Euclidean geometry. $A < V/V_{max} >$ larger than 1/2 might indicate cosmological distances and evolutionary effects, such as have been found for quasars (Schmidt 1968).

The $V/V_{max}$ test can be applied to gamma-ray bursts as follows (Schmidt *et al.* 1988). Consider a burst with peak count $C_p$ over an integration time T. Let the limiting count that would trigger the detection of this burst be $C_{lim}$. In Euclidean space in which the count for a given source varies with distance as $r^{-2}$ and volume varies as $r^3$, the ratio of the volume V out to the source distance r, to the volume $V_{max}$ out to distance $r_{max}$ at which the source would produce a count $C_{lim}$ is

$$V/V_{max} = (C_p/C_{lim})^{-3/2} \tag{1}$$

Note that the distance r, which is unknown for gamma-ray bursts, does not appear in the expression for $V/V_{max}$. The limiting count $C_{lim}$ is usually set at a multiple of the noise associated with the background rate B.

In the Konus experiment, the noise is evaluated from a reference count that includes both background and some burst signal. In this case, the following more general formulation of the $V/V_{max}$ test should be applied. Based on the specific algorithm used to trigger burst detection, derive for each recorded gamma-ray burst a reduction factor $R_{min}$, defined such that if the amplitude of the burst is multiplied by $R_{min}$, it would just marginally be detected. In this case, it is easy to show that

$$V/V_{max} = R_{min}^{3/2} \tag{2}$$

There are several advantages associated with the $V/V_{max}$ test, all related to the fact that it treats sources in a sample individually, rather than as an ensemble as is done in the size-frequency distribution $N(>C_p)$. We mention three examples where the $V/V_{max}$ test accommodates the experimental situation accurately. None of these cases can be handled properly by the size-frequency distribution $N(>C_p)$.

1. Usually $C_{lim}$ is defined in terms of the noise associated with the background, so $C_{lim} = k(C_{bkgrd})^{1/2}$. Since the background shows considerable variations, $C_{lim}$ will be different for different bursts. $V/V_{max}$ takes this into account for each source.

2. If burst trigger detection requires that *two* detectors or experiments observe the burst, then each of the two observations produces a $V/V_{max}$ ratio. The requirement of two detections means that the smaller of the two $V_{max}$ volumes is relevant, therefore the *larger* of the two $V/V_{max}$ values should be used. This situation applies to the BATSE experiment aboard

GRO, where the burst recording trigger will demand detection by two or more detectors.

3. If burst detection requires that *either* of two detectors observe the burst and it is observed by both detectors, then the *smaller* of the two $V/V_{max}$ values should be used. This applies to the two time integration bins that are employed in parallel in the Konus experiment.

## DERIVATION OF $V/V_{MAX}$ FROM THE KONUS DATA

On Venera 11 and 12, each Konus detector system, covering the nominal energy band from 0.05 to 0.15 MeV, consists of six scintillator detectors aligned along the axes of a cartesian coordinate system (Mazets and Golenetskii 1981). These detectors operate in a triggered mode. In a paper discussing burst detection on the later Venera 13 and 14 flights, Mazets *et al.* (1983) indicated that the count rate of each detector is monitored through analog circuits with time constants of 0.25, 1.5, and 30 seconds. When the count rate of either the 0.25 or 1.5 s circuit exceeds the count rate of the 30 s circuit by $6\sigma$, a burst recording trigger pulse is generated. Mazets (1987) has confirmed that this strategy also applied to Venera 11 and 12. When this happens, the time and amplitude analyzers switch to the module most favorably oriented to view the gamma-ray burst and produce a digital record. These burst counts, plotted with 0.25 s resolution for 34 s and then with 1 s resolution for 32 s more, are displayed in the Konus catalog together with the mean background counts, measured before and after the burst (Mazets *et al.* 1981a, b, c). These times profiles were the source for our investigation of the Konus bursts.

The digital data cannot be used directly to perform the $V/V_{max}$ test, since the Konus burst detectors are analog devices which operate as resistor-capacitance circuits. These produce a voltage which, following a sharp pulse, decays exponentially with time constant T. If the digital burst count rate is D(t) and the analog output count is A(t,T), then

$$A(t,T) = \int_{-\infty}^{t} D(t')e^{\frac{-(t-t')}{T}}dt' \qquad (3)$$

For the present sample of bursts, the analog trigger criterion affects significantly the determination of $C_p$. The averages of the ratio of the peak A(t,T) to the digital peak are 0.64 and 0.82, for T = 0.25 and 1.5 s, respectively.

According to Mazets *et al.* (1981a), the detection of gamma-ray bursts is triggered when the count exceeds the background by $6\sigma$. In practice, the reference analog count (for T = 30 s) measures a pseudo background P(t) that includes both background (B is the background rate) and a contribution A(t,30) from the burst signal,

$$P(t) = 30B + A(t, 30) \tag{4}$$

The analog output S(t,T) for either of the time constants T = 0.25 s or T = 1.5 s contains the burst signal A(t,T) and background BT,

$$S(t, T) = A(t, T) + BT \tag{5}$$

The trigger mechanism checks for the excess E(t,T) of the signal S(t,T) over the pseudo background,

$$E(t, T) = S(t, T) - (T/30)P(t) \tag{6}$$

The r.m.s. uncertainty of E(t,T) is composed of the noise associated with each of the two terms in eq. (6). Since P(t) is derived over an effective integration time of as long as 30 s, its contribution to the statistical noise in E(t,T) is negligible compared to that of S(t,T). In evaluation the statistical noise in S(t,T), the experiment ignores the contribution of A(t,T) in eq. (5), and approximates the noise contribution of BT by that of (T/30) P(t). If the excess count E(t,T) exceeds the pseudo background by $k\sigma$, then

$$A(t, T) - (T/30)A(t, 30) > k\{BT + (T/30)A(t, 30)\}^{1/2} \tag{7}$$

In order to carry out the $V/V_{max}$ test, we now ask by what factor R(t) the burst amplitude should be multiplied to yield an excess of $6\sigma$ over the pseudo background, so

$$R(t)\{A(t, T) - (T/30)A(t, 30)\} = 6\{BT + R(t)(T/30)A(t, 30)\}^{1/2} \tag{8}$$

For each time bin t of the digital profiles, we derive A(t,T) and A(t,30) from eq. (3) and solve eq. (8) for R(t). The minimum value, $R_{min}$, of R(t) is then used to derive $V/V_{max}$ from eq. (2).

For each of the trigger integration times T = 0.25 and 1.5 s, we so derive the amplitude reduction factor $R_{min}$ that will just trigger burst detection $6\sigma$ of the background. Since triggering on either T = 0.25 or 1.5 s is sufficient for inclusion in the burst catalog, the smaller of the two $R_{min}$ values should be used to derive $V/V_{max}$ from eq. (2).

We have determined $V/V_{max}$ for the 123 Konus bursts with duration longer than 1 second observed aboard Venera 11 and 12. In 13 cases, both values of $R_{min}$ are larger than one, formally indicating that these bursts do not belong in the Konus catalog. We assume that they were actually detected above $6\sigma$, and suspect that the large $R_{min}$ values are caused by uncertainty about the prehistory, by errors made in reading the published digital profiles, or by an omission in the published time profile of a sharp

initial spike (several of the profiles show only the descending branch of a sharp initial spike). We have assigned a value of 0.9 to $V/V_{max}$ in each of these cases.

The average value of $V/V_{max}$ for the 123 bursts is $< V/V_{max} > = 0.46 \pm 0.03$. If we exclude the sources GB 790215, 790323, and 800127a and b which are suspected by Atteia *et al.* (1987) to be solar flares, $< V/V_{max} >$ is essentially unchanged at 0.46. The mean value $V/V_{max}$ is statistically indistinguishable from 0.50. We conclude that a uniform distribution in space of the parent population of gamma-ray bursts from which the Konus bursts are drawn is consistent with our statistical evaluation.

## CONCLUSION

We have employed the $V/V_{max}$ test on a set of gamma-ray bursts detected with the Konus experiment aboard Venera 11 and 12. Unlike size-frequency distributions, the $V/V_{max}$ test is insensitive to variations in detection limit and in instrumental sensitivity. Hence, every burst for which the detection limit is known can be used in the test. We find that the 123 bursts of duration greater than 1 second, detected at $6\sigma$ above background, have a $< V/V_{max} >$ compatible with a uniform distribution in Euclidean space. Therefore, the radial distribution of the Konus bursts gives us no clue to their distance scale.

The application of the $V/V_{max}$ test to gamma-ray bursts in this case is complex, because the Konus experiment produced digital time profiles, but triggered on exponential time-averaged counts produced by an analog circuit. Also, the reference count contained some burst signal. The $V/V_{max}$ test can handle this complex case. In contrast, size-frequency distributions of fluxes or peak counts would have been powerless in completely modeling this experiment.

It is obvious that the $V/V_{max}$ test can only be used to its full advantage, if the required data are available, including the detection limit. Therefore, we urge that for each observed gamma-ray burst not only the peak count $C_p$ be published, but also information about the detection limit, either in the form of the limiting count $C_{lim}$, or the minimum reduction factor $R_{min}$.

We would like to acknowledge discussions with G. Hueter, and a communication from E.P. Mazets which was most helpful in interpreting the published Konus data. This work was supported by a grant from the President's Fund of the California Institute of Technology.

## REFERENCES

Atteia, J.L., *et al.* 1987. A second catalog of gamma-ray bursts: 1978-1980 locations from the interplanetary network. Astrophysical Journal Supplement Series 64: 305-382.

Fishman, G.J. 1979. Galactic distribution models of gamma-ray burst sources. Astrophysical Journal 233: 851-856.

Higdon, J.C., and R.E. Lingenfelter. 1984. Size-frequency distributions of gamma-ray bursts from nuclear runaway on neutron stars accreting interstellar gas. Pages 568-577. In: Woosley, S.E. (ed.). High Energy Transients in Astrophysics. American Institute of Physics, New York.

Higdon, J.C., and R.E. Lingenfelter. 1986. Gamma-ray burst size-frequency distributions: Spectral and temporal selection effects. Astrophysical Journal 307: 197-204.

Hurley, K., T.L. Cline, and R. Epstein. 1986. Error boxes and spatial distribution. Pages 33-38. In: Liang, E.P., and V. Petrosian (eds.). Gamma-Ray Bursts. American Institute of Physics, New York.

Jennings, M.C. 1982. The Galaxy as the origin of gamma-ray bursts. II. The effect of an intrinsic burst luminosity distribution on log N(>S) versus log S. Astrophysical Journal 258: 110-120.

Jennings, M.C. 1984. The gamma-ray burst spatial distribution log N(>S) versus log S and N(>S,l,b) vs. S. Pages 412-421. In: Woosley, S.E. (ed.). High Energy Transients in Astrophysics. American Institute of Physics, New York.

Jennings, M.C. 1988. Intrinsic and artificial bias in the Konus cumulative number distribution. Astrophysical Journal 333: 700-718.

Jennings, M.C., and R.S. White. 1980. The Galaxy as the origin of gamma-ray bursts. Astrophysical Journal 238: 110-121.

Mazets, E.P. 1986. Observational properties of cosmic gamma-ray bursts. In: Proceedings 19th International Cosmic Ray Conference (La Jolla) 9: 415-430.

Mazets, E.P. 1987. Private Communication.

Mazets, E.P., and S.V. Golenetskii. 1981. Cosmic gamma-ray bursts. Astrophysics and Space Science Reviews 1: 205-266.

Mazets, E.P., and S.V. Golenetskii. 1988. Observations of cosmic gamma-ray bursts. Astrophysics and Space Physics Review 6: 281-311.

Mazets, E.P., *et al.* 1981a. Catalog of cosmic gamma-ray bursts from the Konus experiment data, Part I and II. Astrophysics and Space Science 80: 3-83.

Mazets, E.P., *et al.* 1981b. Catalog of cosmic gamma-ray bursts from the Konus experiment data, Part III. Astrophysics and Space Science 80: 85-117.

Mazets, E.P., *et al.* 1981c. Catalog of cosmic gamma-ray bursts from the Konus experiment data, Part IV. Astrophysics and Space Science 80: 110-143.

Mazets, E.P., *et al.* 1983. Energy spectra of the cosmic gamma-ray bursts. Pages 36-53. In: Burns, M.L., and A.K. Harding, and R. Ramaty (eds.). Positron-Electron Pairs in Astrophysics. American Institute of Physics, New York.

Paczynski, B. 1986. Gamma-ray bursters at cosmological distances. Astrophysical Journal (Letters) 308: L43-L46.

Schmidt, M. 1986. Space distribution and luminosity functions of quasi-stellar radio sources. Astrophysical Journal 151: 393-407.

Schmidt, M., J.C. Higdon, and G. Hueter. 1988. Applications of the $V/V_{max}$ test to gamma-ray bursts. Astrophysical Journal (Letters) 329: L85-L87.

# Extragalactic X-Ray Source Counts

MAARTEN SCHMIDT
California Institute of Technology

## ABSTRACT

Extragalactic x-ray source counts carry information about the luminosity function and cosmic evolution of galaxies, clusters of galaxies, BL Lac objects, Seyfert galaxies and quasars. We discuss two available x-ray source samples with complete optical identifications and redshifts. We find evidence for instrumental bias in the detection of clusters of galaxies for cosmic evolution of quasars, and of absorption effects in low-luminosity Seyfert galaxies. Modest spectral and density evolution of Seyfert galaxies would allow the soft x-ray background to be made up entirely of discrete sources. We present a source count prognosis for the AXAF energy range 0.5 – 10 keV.

## INTRODUCTION

Extragalactic x-ray sources are identified with galaxies, clusters of galaxies, BL Lac objects, Seyfert galaxies and quasars. Optical studies of these objects have shown strong cosmic evolution only for quasars. For galaxies, evolution is suspected but there is no well documented variation of the luminosity function. Clusters of galaxies are difficult to find optically at high redshift and no reliable counts are available. There is no well defined optical sample of BL Lac objects. Only one complete optical sample of Seyfert galaxies, based on the CfA redshift survey, is available.

Counts of extragalactic x-ray sources promise to play an important role in studying evolution. We discuss a non-parametric procedure for the derivation of luminosity function and source counts. We apply this

method to the two well defined x-ray samples that have complete optical identifications and redshifts. We find evidence for insturmental effects in the detection of clusters of galxies, for evolution of quasars, and for absorption effects in low-luminosity Seyfert galaxies. On the basis of the luminosity functions developed, we present an x-ray source count prognosis for the AXAF energy range 0.5 – 10 keV.

## DERIVATION OF LUMINOSITY FUNCTION

Consider an x-ray sample that is complete over a given area of sky to a limiting flux $S_{lim}$ in a given energy band. Since the luminosity function that is derived from such a sample is a linear combination of the contributions from the sample sources, we start by considering one single source.

Hypothetically, we move this source radially away from us, maintaining all its absolute properties. As the redshift z increases, the flux S declines: let S(z) be the flux-redshift relation for this source. We can invert this and derive z(S), which is the redshift at which the given source would have an observed flux S. Now let V (<z) be the co-moving observable volume out to redshift z, for a given cosmological model. Substitution of z(S) in V(<z) produces V(>S), which is the volume over which the source will be observed to have a flux of S or greater.

Since our sample was complete to flux $S_{lim}$, $V(>S_{lim})$ is the volume over which the given source will be included in the sample. Since the luminosity function is the space density of sources, as a function of their luminosity, the one source provides a contribution of $1/V(>S_{lim})$ to the luminosity function at the source's luminosity L. The total luminosity function is the sum of the contribution of the n sources that comprise the complete sample,

$$\Phi(L) = \sum_{i=1}^{n} \frac{\delta(L - L_i)}{V_i(> S_{lim})}$$

## DERIVATION OF SOURCE COUNTS

We now derive the source counts corresponding to the luminosity function just determined. Let us return to the one source in the original complete sample, which yielded a space density of $1/V(>S_{lim})$. At a flux larger than S, this source can be seen over a volume V(>S) and therefore we should observe $V(>S)/V(>S_{lim})$ of such sources brighter than S. The total source counts are again the sum of the n individual contributions,

$$N(> S) = \sum_{i=1}^{n} \frac{N_i(> S)}{V_i(> S_{lim})}$$

We illustrate this procedure by considering the counts produced by just one source in the HEAO1 A-2 survey (Piccinotti *et al.* 1982). We assume that it has a power law spectrum with energy spectral index $-0.7$. We employ a cosmological model with Hubble constant $H_o = 50$ km $s^{-1}M_{pc}{}^{-1}$, and $q_o = 0.5$. We also assume that there is a redshift cutoff at $z_{max} = 2$. Figure 1 shows the counts generated by the source, depending on its x-ray luminosity HX = $L_x$(2-10 keV), in erg/sec.

At the lowest luminosity illustrated, log HX = 41, the counts follow the $-3/2$ law expected in Euclidean space for fluxes larger than log S(2-10 keV) $\approx$ -13. For sources of higher luminosity, the slope at a given flux becomes progressively smaller. Clearly, for most extragalactic x-ray sources, the -3/2 law is a very poor approximation.

The striking differences in the predicted source counts for different luminosities are also reflected in the contribution to the x-ray background. In our example, the source counts corresponding to a single source of luminosity log HX = 41 contribute 13% to the observed background at 2 keV. For log HX = 43 the contribution is 1% and for log HX = 45 it is only 0.1%.

The non-parametric procedure for the derivation of luminosity function and source counts, described above, takes into account cosmology, in terms of S(z) and V(<z), as well as the shape of the spectral energy distribution, through S(z). No assumptions are needed about the shape of the luminosity function. If there is a need to account for luminosity or density evolution, then the luminosity or number density can be varied as a function of redshift for each of the n sources contributing to the luminosity function. The r.m.s. error of the predicted source counts (due to the sampling error in the sample used to generate the source counts) can be estimated by assigning an r.m.s. error of $\pm 100\%$ to each of the n contributions. For further details about the non-parametric derivation of the luminosity function, the reader is referred to Schmidt and Green (1986).

## TWO COMPLETE X-RAY SAMPLES

There are two x-ray samples for which optical idenitifications and redshifts are essentially complete. These are the HEAO1 A-2 survey (Piccinotti *et al.* 1982) and the Einstein Medium Sensitivity Survey (MSS) (Maccacaro *et al.* 1982; Gioia *et al.* 1983; Stocke *et al.* 1984). Sky coverage, energy bands, flux limits and numbers detected in the two surveys are given in Table 1. The MSS has a distribution of flux limits versus sky coverage. The flux limit given in Table 1 is an effective limit; this limit would produce the observed number of sources if it applied uniformly to the entire area of the survey.

Since the two surveys differ in flux limit by a factor of around 100, a

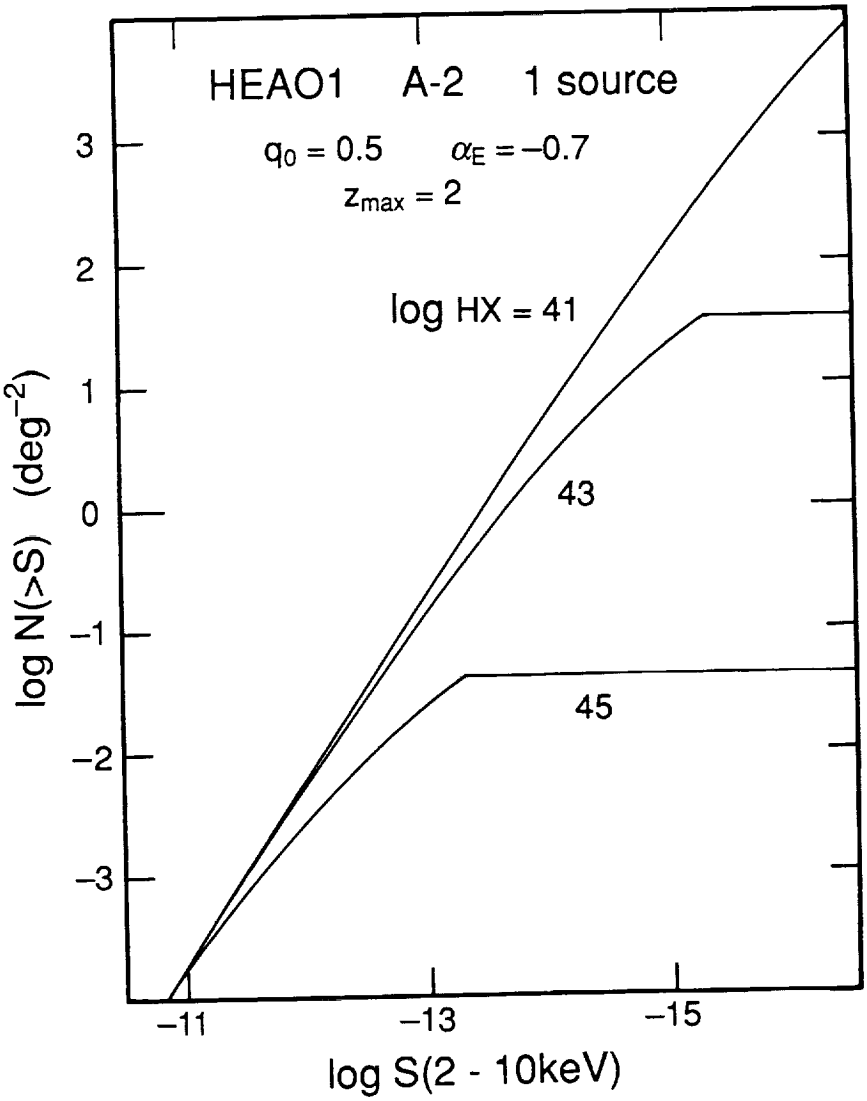


FIGURE 1 Source counts based on one single source of luminosity HX, hypothetically observed in the HEAO1 A-2 survey.

detailed comparison of their content is of interest. In making the comparison, we generally use the sample with the larger number of objects of a given class to predict the expected number in the other sample, following the procedure described in the preceding sections.

TABLE 1

X-RAY SURVEYS WITH COMPLETE IDENTIFICATIONS

| | *HEAO1* A-2 | *EINSTEIN* MSS |
|---|---|---|
| Area | 27,000 $deg^{-2}$ | 89.1 $deg^{-2}$ |
| Energy | 2–10 keV | 0.3–3.5 keV |
| Limit | $3 \times 10^{-11}$ cgs | $3 \times 10^{-13}$ cgs |
| BL Lacs | 4 | 4 |
| Galaxies | 1 | 3 |
| Clusters | 30 | 20 |
| Quasars | 1 | 23 |
| AGNs | 20 | 32 |

*BL Lacs*: The two samples, both very small, are consistent with each other for a uniform space distribution.

*Galaxies*: Based on the three galaxies in the MSS, we expect one galaxy in the HEAO1 A-2 for a uniform space distribution. Numbers are very small so there is large uncertainty.

*Quasars*: We define as quasars those active galactic nuclei with optical absolute magnitude $M_B < -23$. Besides the one quasar (3C 273) in the A-2 sample, there is the BQX sample, a small subsample of the Bright Quasar Survey (cf. Schmidt and Green 1986). Both of these samples contain fewer objects than are predicted from the 23 quasars in the MSS for a uniform space distribution. This constitutes pure x-ray evidence for the evolution of quasars, independent of optical evidence. We invoke luminosity-dependent density evolution to fit both the x-ray counts, as well as the total surface density of quasars with $z < 2$ of around 70 $deg^{-2}$. This evolution is somewhat different from that used by Schmidt and Green (1986).

*Clusters of galaxies*: Schmidt and Green (1986) found that there was a large difference between the luminosity distributions of clusters in the two samples. Further study shows that there is only a discrepancy at the bright end: based on the A-2 sample, we expect 25 clusters with log HX > 44.4 in the MSS, but none are observed. Part of the explanation is probably that

the MSS detection efficiency for clusters is low. If part of the discrepancy is due to cluster evolution, it would have to be very steep. For clusters of lower luminosity log HX < 44.4, the two samples are consistent with a uniform space distribution.

*AGNs*: We define as AGNs (or Seyfert galaxies) those active galactic nuclei with $M_B > -23$. Both samples contain substantial numbers of AGNs. There is a discrepancy opposite in sign from that found for clusters: based on the A-2 sample, we expect 25 AGNs with log HX > 43.5 in the MSS, but only 9 are observed. Following Reichert *et al.* (1985), we explain this as a consequence of absorption by clouds of $6x10^{22}$ H at $cm^{-2}$ with a coverage of 70%.

## SOURCE COUNT PROGNOSIS

We have derived a source count prognosis for the AXAF energy range 0.5-10 keV, based on the evaluation of the HEAO1 A-2 and Enstein MSS samples, discussed in the preceding section. The x-ray counts for the different classes of objects are shown in Figure 2. It is essential to keep in mind the uncertainty associated with this prognosis. As we saw in the preceding section, the reconciliation of the contents of the HEAO1 A-2 sample and the Einstein MSS sample require invoking evolution (for quasars), instrumental effects (for clusters), and absorption (for AGNs of lower x-ray luminosity). There is considerable uncertainty associated with each of these interpretations. In addition, we have assumed a uniform space distribution for galaxies, BL Lacs, clusters of galaxies and AGNs. Each of these objects probably exhibits some cosmological evolution.

The predicted number of x-ray sources with log S(0.5-2.0 keV) > -15 is 800 $deg^{-2}$, of which AGNs contribute 500 $deg^{-2}$. At this flux, total counts vary approximately as $S^{-0.9}$. The total x-ray background produced by descrete sources in this prognosis is 52% of the observed background at 2 keV, and 30% at 10 keV.

We also consider an alternative scenario, in which the entire background is accounted for by discrete sources. We postulate that the AGNs evolve in number and spectrum such that the background at 2 keV and at 10 keV is entirely due to discrete sources. This is achieved if the AGNs show density evolution $e^{2.15\tau}$ and have an energy spectral index of $-0.7 + 0.6\tau$, where $\tau$ is the light-travel time in terms of the age of the universe. In this scenario, the number of AGNs with log S (0.5- 2.0 keV) > -15 increases to 2500 $deg.^{-2}$. The median redshift of these AGNs would be around 1.0. While there is no physical basis for this AGN evolution scenario, it does illustrate, that AXAF may provide important clues to the composition and the nature of the x-ray background.

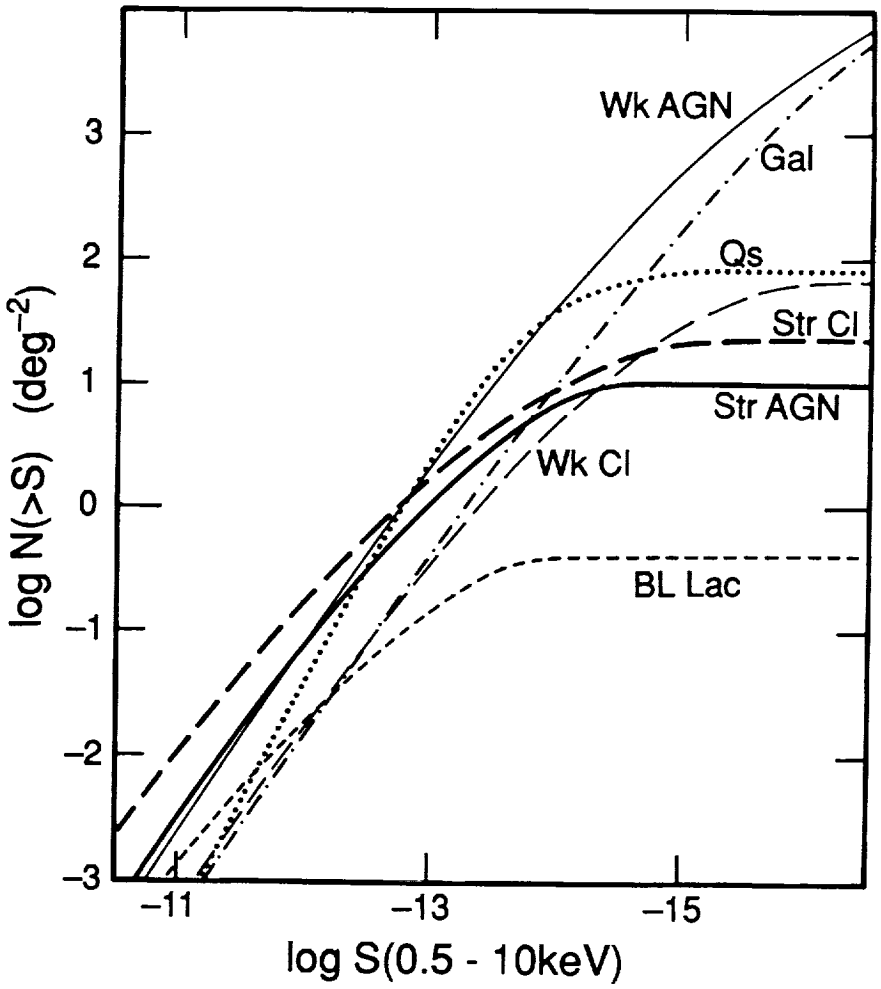


FIGURE 2 Source count prognosis for the AXAF energy band 0.5-10 keV. See text for a discussion of the uncertainties associated with this prognosis.

## DISCUSSION

The study of the evolution of extragalactic x-ray sources is clearly in its infancy, with only two samples available that have complete optical identifications and redshifts. Complications arise as a consequence of the reduced detection efficiency for clusters of galaxies and the internal absorption in low-luminosity Seyfert galaxies. These effects can be incorporated in the non-parametric derivation of the luminosity function and associated source counts described above.

Only for quasars can the effect of evolution be seen clearly in the available samples. We may hope that evolution of other x-ray sources such as clusters of galaxies and Seyfert galaxies may be derived from surveys to be carried out with ROSAT, AXAF and other missions. This would be of great interest, since no other—in particular, optical—evidence for the evolution of these objects exists at the present time.

## REFERENCES

Gioia, I.M., T. Maccacaro, R.E. Schild, J.T. Stocke, J.W. Liebert, I.J. Danziger, D. Kunth, and J. Lub. 1983. The medium sensitivity survey: A new sample of x-ray sources with optical identificiations and the revised extragalactic log N - log S. Astrophysical Journal 283: 495-511.

Maccacaro, T., E.D. Feigelson, M. Fener, R. Giacconi, I.M. Gioia, R.E. Griffiths, S.S. Murray, G. Zamorani, J. Stocke, and J. Liebert. 1982. A medium sensitivity x-ray survey using the Einstein Observatory: The log N —log S relation for extragalactic x-ray sources. Astrophysical Journal 253: 504-511.

Piccinotti, G., R.F. Mushotzky, E.A. Boldt, S.S. Holt, F.E. Marshall, P.J. Serlemitsos, and R.A. Shafer. 1982. A complete x-ray sample of the high-latitude ($|\ b\ | > 20^{\circ}$) sky from HEAO1 A-2: Log N—log S and luminosity functions. Astrophysical Journal 253: 485-503.

Reichert, G.A., R.F. Mushotzky, R. Petre, and S.S. Holt. 1985. Soft x-ray spectral observations of low-luminosity active galaxies. Astrophysical Journal 296: 69-89.

Schmidt, M., and R.F. Green. 1986. Counts, evolution, and background contribution of x-ray quasars and other extragalactic x-ray sources. Astrophysical Journal 305: 68-82.

Stocke, J.T., J. Liebert, I.M. Gioia, R.E. Griffiths, T. Maccacaro, I.J. Danziger, D. Kunth, and J. Lub. 1983. The Einstein Observatory medium sensitivity survey: Optical identifications for a complete sample of x-ray sources. Astrophysical Journal 273: 458-477.

# Ultraluminous Infrared Galaxies

B.T. SOIFER
California Institute of Technology

## ABSTRACT

The IRAS all-sky survey has provided astronomers with a first deep view of the sky in the "thermal infrared", i.e., from 10 microns to 100 microns. One of the major discoveries of this survey has been a population of sources having the bolometric luminosities of quasars, but where more than 90% of the luminosity emerges in the infrared. These objects, more numerous than quasars, are found exclusively in interacting/merging galaxies that are extremely rich in interstellar gas. We have accumulated evidence that suggests that these systems are indeed quasars obscured by many tens of magnitudes of extinction.

We have suggested that these Ultraluminous Infrared Galaxies are the formation stage of quasars, and that colliding galaxies, ultraluminous infrared galaxies, and quasars might all be linked through an evolutionary sequence where the infrared bright phase is one in which the quasar is formed in the nucleus of a merger system, and is enshrouded in gas and dust, while the UV excess quasars are the end state of quasar evolution where most of the enveloping dust cloud has been dissipated, and the quasar is visible directly.

## INTRODUCTION

Viewing the universe through a new portion of the electromagnetic spectrum has always lead astronomers to major discoveries. Quasars and neutron stars are just two examples of discoveries made as a result of the Radio and X-ray sky surveys of the 1950's, 1960's, and 1970's. In 1983 the

Infrared Astronomical Satellite (IRAS) performed the latest of these all sky surveys that has lead to major discoveries.

Before IRAS, our view of the infrared universe was limited to sky surveys at 2.2 microns (Neugebauer and Leighton 1969) and 4-30 microns (Price and Walker 1976) as well as studying objects found by other means. The infrared sky surveys vastly increased our understanding of the Galaxy and its constituents, but lacked the sensitivity to go significantly beyond the Galaxy. The Caltech 2 micron sky survey contained one external galaxy, M31, while the AFGL sky survey contained a handful of extragalactic objects.

The IRAS sky survey, with its 3 orders of magnitude improvement in sensitivity over previous surveys, and extension to 60 microns and 100 microns, drastically increased the numbers of galaxies detected purely by their infrared emission, finding $\sim$ 0.5 galaxies/square degree, and altered our understanding of the extragalactic sky, permitting an unbiased view of the local universe in the infrared.

## THE IRAS SKY SURVEY

The IRAS all sky survey was performed at 12 microns, 25 microns, 60 microns, and 100 microns using a 57 cm telescope and focal plane entirely cooled to 2.7K with superfluid helium. The telescope was contained in the toroidal shaped, 700 liter capacity helium cryostat. The satellite was launched on January 25, 1983, and collected data for the 300 days that the superfluid helium lasted. The primary scientific goal of the IRAS mission was to perform the all sky survey, and approximately 60% of the satellite's time was devoted to this purpose. To produce a highly reliable census of the inertially fixed sources in the presence of many "local" contaminants such as cosmic ray hits on the detectors, dust particles crossing the field of view of the telescope, asteroids and comets, the telescope scanned the sky 6 times over the 300 day mission. The multiple sightings of particular sources were used to filter and separate the inertially fixed sources from the "moving sources" such as asteroids and comets, and the transient events local to the telescope environment. These data were combined to produce the first IRAS Point Source Catalog which covered 96% of the sky. At high galactic latitude the IRAS Point Source Catalog was complete to 0.4, 0.5, 0.6, and 1.5 Jy at 12 microns, 25 microns, 60 microns, and 100 microns respectively with reliability $>$ 99.8%. Recently the same data have been reprocessed to produce a catalog at high galactic latitudes (the IRAS Faint Source Catalog) that is a factor of $\sim$ 2.5 more sensitive at all wavelengths, at the cost of reduced reliability ($>$ 98%).

The IRAS survey has a fairly modest sensivity compared to modern optical surveys. In flux per octave, i.e., $\nu S_\nu$, the IRAS Point Source Catalog

reached $3 \times 10^{-14}$ W/m$^2$ at 60 microns, equal to the flux per octave of a 15.0 mag object at B. In terms of detectable luminosity, extragalactic sources seen by IRAS are comparatively local. Sources with the infrared luminosity of the Milky Way are detected to a redshift $z \sim 0.03$, while sources with the bolometric luminosity of a quasar, where this energy emerges in the infrared, are detected to redshifts of $z \sim 0.3$ (in this paper, we adopt $H_o = 75$ Km/s/Mpc and $Q_o = 0$). Thus the IRAS survey is indeed a survey of the local universe. The combination of the sensitivity of the IRAS survey, and the wavelength at which the infrared luminosity emerges from galaxies results in the vast majority of the $\sim$ 20,000 extragalactic objects discovered in the IRAS Point Source Catalog being found at 60 microns.

Since the IRAS survey was done at wavelengths substantially longward of the peak in stellar photospheres, those sources seen in the infrared radiate via mechanisms substantially different from those found to be bright in optical surveys. The predominant mechanism responsible for the infrared flux from galaxies is thermal emission from dust; the dust absorbs and reradiates energy originally emitted at shorter wavelengths. Infrared bright galaxies are quite dusty and therefore have either been missed, or appeared innocuously in visible surveys.

## THE LOCAL UNIVERSE IN THE INFRARED

With an unbiased view of the infrared sky available for the first time, several groups have investigated the local luminosity function of infrared bright galaxies using IRAS data (Rieke and Lebofsky 1986; Soifer *et al.* 1986, 1987; Lawrence *et al.* 1987; Smith *et al.* 1987). All these analyses agree remarkably well, and have demonstrated that the space density of infrared bright galaxies does not vary significantly over a factor 3 in distance (from a median redshift of $< cz > \sim$ 2,200 Km/s in Soifer, *et al.* 1987; to $< cz > \sim$ 7,000 Km/s in Lawrence *et al.* 1987).

To understand the importance of such infrared bright galaxies requires placing this class of objects in the context of other known classes of extragalactic objects. We have done this by comparing the bolometric luminosity functions of the major classes of extragalactic objects (Soifer *et al.* 1987). Since most luminosity functions for extragalactic objects are derived at B (4400 A), it was necessary to apply bolometric corrections to most such luminosity functions, to place them in the same units. This comparison is shown in Figure 1.

The luminosity functions of these sources immediately shows that infrared bright galaxies are an important, but not dominant source of luminosity in the local universe. For $L_{bol} \lesssim 2 \times 10^{10}$ $L_\odot$, the infrared bright galaxies have a density about 20% of that for galaxies found in the visible. For $L_{bol} > 2 \times 10^{10}$ $L_\odot$, infrared bright galaxies become increasingly

C-5

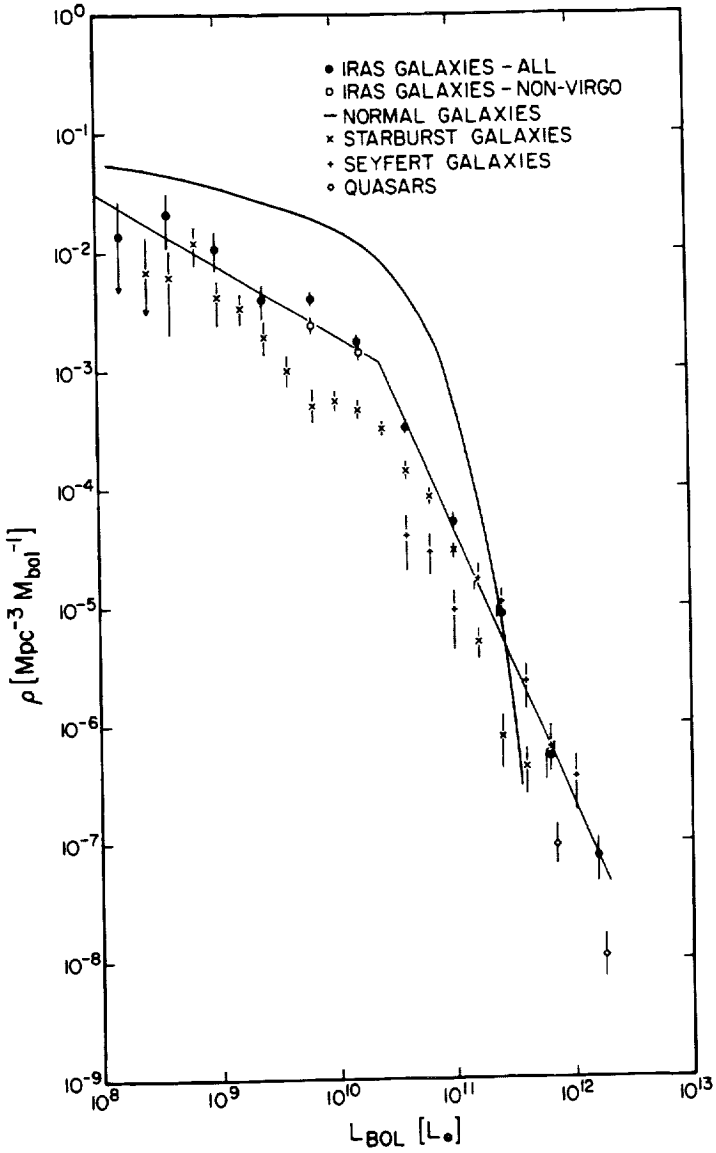


FIGURE 1 The bolometric luminosity functions of the major classes of extragalactic emitters (taken from Soifer *et al.* 1987). Separate bolometric corrections have been applied for each class of object. The infrared galaxies become the dominant extragalactic population at $L_{bol} > 3 \times 10^{11} L_{\odot}$.

important in the local universe, since the space density of normal galaxies drops exponentially with luminosity, while the infrared bright galaxies appear to decrease as $\sim L^{-2}$. At $L_{bol} > 3 \times 10^{11} L_{\odot}$, the infrared bright galaxies become the dominant population in the local universe, exceeding in space density the quasars. Overall the infrared luminosity of galaxies represents $\sim$ 25% of that emerging in stellar photospheres, and 60-80% of this infrared luminosity is due to young, massive stars (Soifer *et al.* 1987).

## ULTRALUMINOUS INFRARED GALAXIES

We have studied the $\sim$ 300 brightest extragalactic sources at 60 microns in 14,500 square degrees at high galactic latitude. This IRAS Bright Galaxy Sample has been most amenable to study at other wavelengths, since it represents the brightest of the infrared luminous galaxies. Of these IRAS Bright Galaxies 10 have bolometric luminosities equivalent to those of quasars. We have studied these 10 objects in great detail (Sanders *et al.* 1988a), and have found them to possess remarkable properties. The observed properties of these objects are summarized in Table 1.

Four of these Ultraluminous Infrared Galaxies were previously cataloged in other surveys. Two of them, Mk 231 and Mk 273, were found in the Markarian survey of UV excess galaxies, and were known to be peculiar objects. Markarian 231 has been known for nearly two decades as an extraordinarily luminous infrared galaxy (Rieke and Low 1972; Young *et al.* 1972). Arp 220 (IC4553) has also been identified as a galaxy with very peculiar properties. As can be seen immediately from Table 1, all of the Ultraluminous Infrared Galaxies are rather faint optical galaxies. The ratio of infrared to visible luminosity is quite large for the ultraluminous galaxies, ranging from 50-150, as compared to 0.3 for "typical" spirals or 1-5 for "typical" infrared selected galaxies (Soifer *et al.* 1987).

In the infrared these Ultraluminous Infrared Galaxies are unresolved at the IRAS angular resolution of $\sim$ 1 '. At optical wavelengths, CCD images show ALL these systems to be galaxies undergoing strong interactions/mergers. Contour plots of CCD images of these galaxies (Sanders *et al.* 1988a) are shown in Figure 2. All of these objects show evidence for recent or ongoing mergers, i.e., multiple nuclei, tidal tails, strongly distorted disks, etc.

Optical spectroscopy shows that all of these galaxies have strong emission lines. Three of the systems, MK 231, UGC 5101, and IRAS 0518-25, have H$\alpha$ line widths > 2,000 Km/s (FWZI). Mk 231 is a well known Seyfert 1 system, while U5101 and IRAS 0518-25 would be classified as intermediate Seyfert nuclei based on their optical spectra. Of the remaining 7 Ultraluminous systems, 6 show line widths > 1,000 Km/s, and line ratios ([OIII]/H$\beta$, [SII]/H$\alpha$, [NII]/H$\alpha$, [OI]/H$\alpha$) characteristic of AGN spectra:

TABLE 1.

PROPERTIES OF ULTRALUMINOUS IRAS GALAXIES

| IRAS Object | Other Name | CZ [Km/s] | Log $L_{ir}$ [$L_\odot$] | $B_{tot}$ mag | Log (IR/B) | Log $M_{H2}$ [$M_\odot$] | $L_{IR}/M_{H2}$ [$L_\odot/M_\odot$] |
|---|---|---|---|---|---|---|---|
| 0518-25 | | 12816 | 12.10 | 15.3 | 1.83 | 10.37 | 35 |
| 0857+39 | | 17480 | 12.09 | 14.8 | 1.38 | 9.84 | 25 |
| 0932+61 | U5101 | 12000 | 12.01 | 14.9 | 1.80 | 10.40 | 40 |
| 1211+03 | | 21788 | 12.29 | 16.9 | 2.08 | 10.62 | 38 |
| 1254+57 | Mk231 | 12660 | 12.52 | 12.9 | 1.72 | 10.19 | 144 |
| 1352+56 | Mk273 | 11132 | 12.14 | 14.9 | 1.77 | 10.24 | 62 |
| 1434-14 | | 24732 | 12.29 | 16.7 | 1.90 | 10.78 | 26 |
| 1525+36 | | 16000 | 12.00 | 16.2 | 1.78 | | |
| 1532+24 | Arp220 | 5450 | 12.19 | 14.0 | 2.19 | 10.28 | 70 |
| 2249-18 | | 23170 | 12.13 | 16.5 | 1.72 | 10.43 | 39 |

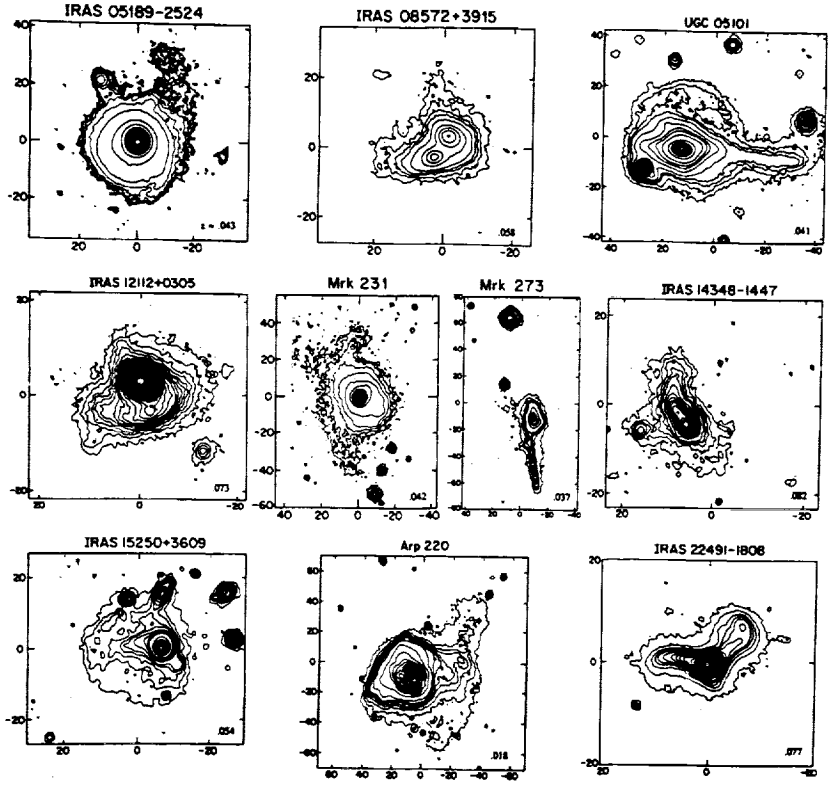


FIGURE 2 Contour maps of optical images of the 10 Ultraluminous Infrared Galaxies found in the IRAS Bright Galaxy Sample (from Sanders *et al.* 1988a). Note the irregular shapes, tidal tails and double nuclei; this is clear evidence of mergers in all these systems.

only IRAS 2249-18 is classified as an HII region spectrum based on the above line ratio.

Photometry of the nuclear regions of these galaxies reveals that the near infrared colors of these galaxies show a very large spread, spanning the entire range of colors from slightly reddened spiral galaxies to highly reddened quasars. As will be discussed later there is enough dust ($A_v \gtrsim 100$ mag) obscuring the underlying energy source that it is unclear whether these observations are a meaningful probe of the nuclear regions.

The overall energy distributions of these objects are shown in Figure 3. All of the objects plotted here have very large ratios of infrared to visible luminosity, immediately demonstrating why they are found in 60 micron selected samples. All of these systems have similar ratios of infrared to radio continuum emission, with log $[f_{ir}/\nu S_\nu$ (1.49Ghz)] $\sim$ 6.5, so these are indeed

"radio quiet" sources. The energy distributions are ordered by increasing $S_\nu$(60 microns)/$S_\nu$(100 microns) ratio. Two systematic trends emerge from this plot. The fraction of energy emerging at shorter infrared wavelengths increases with increasing $S_\nu$(60 microns)/$S_\nu$(100 microns) ratio, while the separation between cold dust and near infrared components becomes less obvious in the "warmer" objects.

The enormous infrared luminosities, coupled with the fact that the emission is clearly thermal emission by dust, implies that these are gas-rich systems. The amount of dust required to produce the observed infrared luminosity is $M_{dust} > 10^8 M_\odot$, so we would expect $> 10^{10} M_\odot$ of gas to accompany this dust. Surprisingly, the vast majority of this gas is in molecular form, with 9 of the Ultraluminous Galaxies having been detected in the 2.6mm J = 1-0 line of CO (table 1). Even more surprising has been the finding that a large fraction, as much as 70-80% of this gas is confined to the central few Kpc of the galaxy (Scoville *et al.* 1986; Scoville *et al.* 1989).

## COLLIDING GALAXIES FORMING QUASARS?

Based on the observations of the Ultraluminous Infrared galaxies found in the IRAS Bright Galaxy sample described above, we have suggested (Sanders *et al.* 1988a) that these systems are heavily dust enshrouded quasars. The evidence for this comes from the luminosities, emission lines, near infrared colors, and luminosity to gas mass ratios. We believe that a quasar is powering the vast luminosity emerging from these objects, however the quasar is so heavily enshrouded in dust that we view the quasar primarily through its bolometric luminosity. An alternate view of these Ultraluminous Infrared Galaxies, as systems undergoing "mega starbursts", has been presented by several groups (e.g., Rieke *et al.* 1985).

The fact that all of these systems are found in merging, gas-rich systems has lead us to suggest that the merger of two gas-rich galaxies is fundamental to the process of quasar formation. We believe that when two gas-rich galaxies interact in a near direct collision, the nuclei merge rapidly (Toomre and Toomre 1972), so disrupting the angular momentum and gravitational field of the system that the gas is funneled rapidly into the nuclear region of the merged system. This rapid accumulation of gas in the central environment of the galaxy will lead inevitably to an enormous "starburst." Enough gas accumulates in the central Kiloparsec of the system that the gas becomes self-gravitating, triggering further collapse of the gas. If a massive black hole exists in the center of the galaxy, as suggested by much current observational data (e.g., Filippenko and Sargent 1985; Dressler and Richstone 1988), this rapid funneling of interstellar gas into the central environment of the galaxy is exactly the source needed to trigger

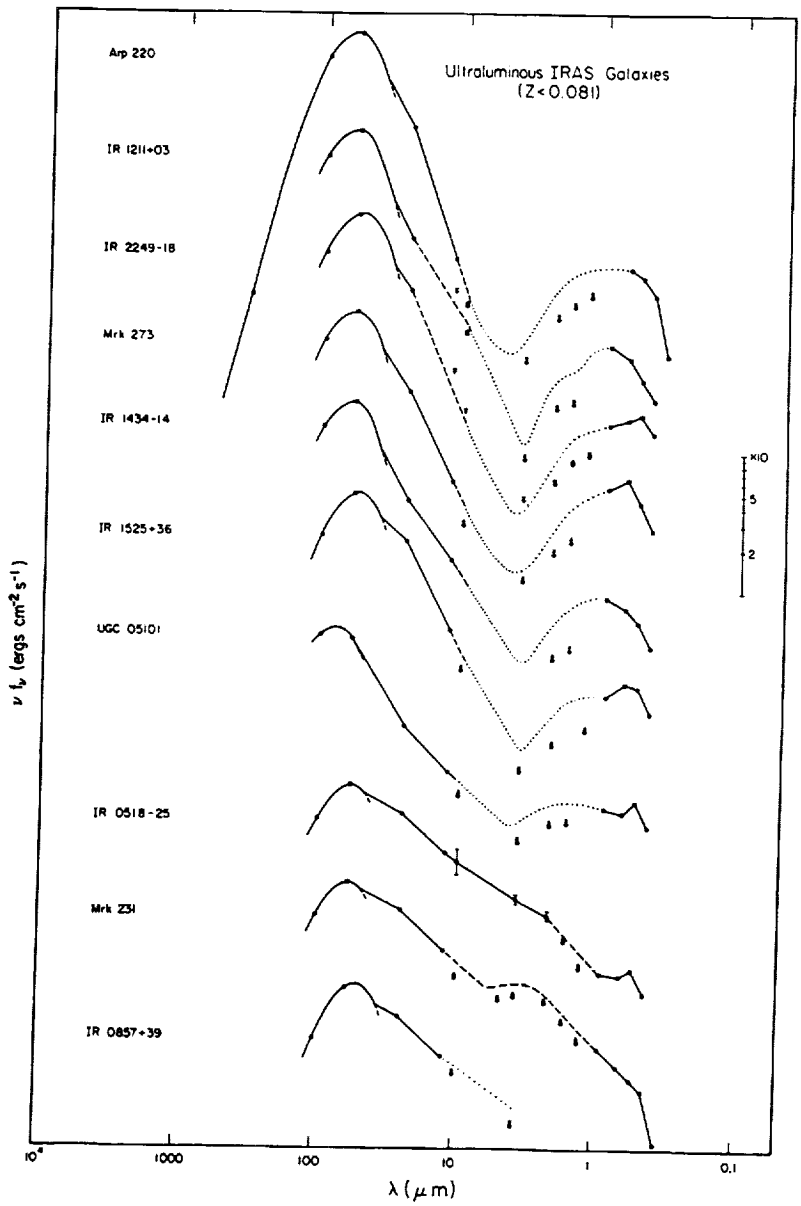


FIGURE 3 The energy distributions form 0.44 microns to 350 microns for the Ultraluminous Infrared Galaxies (from Sanders *et al.* 1988a). The energy distributions are ordered from lowest 60 microns/100 microns color temperature (top) to highest 60 microns/100 microns color temperature (bottom).

formation of the quasar that is powered by gravitational energy released as the gas falls onto the black hole.

We expect that the formation of a quasar embedded in $10^{10}M_{\odot}$ of gas and dust in the center of a galaxy is an enormously disruptive event, one that will ultimately result in a visible quasar. Qualitatively, we expect that as the energy release of the quasar begins to disrupt the surrounding gas and dust, the quasar will take on more and more of the properties of a "normal" quasar, i.e. revealing a strong nuclear optical/UV/near infrared continuum, very broad emission lines, etc. We have found evidence (Sanders *et al.* 1988b) for such an evolutionary sequence in the "warm" Ultraluminous galaxies found in the IRAS database as extragalactic objects with luminosities of quasars, but with infrared properties intermediate between those of the Ultraluminous Infrared Galaxies and the "normal" quasars. These systems, again selected by purely infrared flux density and color criteria, show equal numbers of Seyfert 1 and Seyfert 2 nuclei. Of these Warm Ultraluminous Infrared Galaxies, 9/12 are in strongly interacting/merging systems, and 3 are indeed classified as "normal" quasars by the criteria of Schmidt and Green (1983) and Veron-Cetty and Veron (1985).

As we propose this evolutionary scenario, ultimately the disruption of the surrounding medium is complete and the quasar emerges from its cocoon as a UV excess quasar. The residual dust and gas in the environment still produces a significant, but not dominant, fraction of infrared luminosity. Recently, we have studied in detail the energy distributions of the brightest UV excess quasars (Sanders *et al.* 1989), and found that they indeed emit approximately 20% of their bolometric luminosity in the infrared, consistent with this picture, while the infrared selected quasars studied by Low *et al.* (1989) might represent a slightly earlier phase in this sequence.

The ideas for the formation of quasars that we have suggested as a result of our study of the Ultraluminous Infrared Galaxies are not new, but rather bring new data to support rather old ideas. Alar and Juri Toomre (1972), in a seminal work, outlined most of these ideas for galaxy interaction triggering active nuclei, while modern, high dynamic range imaging and spectroscopy of quasars and their environments have lead many investigators to the conclusion that interactions play a significant role in quasars (Stockton and McKenty 1983; Hutchings *et al.* 1984). What we believe the IRAS data has provided is evidence for the formative stages of the quasar, where the gas and dust that converts the luminosity of the quasar into a bright infrared source effectively acts as a strong neutral density filter to allow us to study in detail the environment surrounding the quasar without the blinding effect of the exceedingly bright central source. Recent theoretical work (Norman 1989) suggests that the scenario we have described here is indeed a plausible outcome of a direct collision between two gas-rich galaxies.

The model we envision for quasar formation has the exceedingly attractive feature that it ties quasars, the most luminous and presumably violent objects in the universe to the rare occurrence of a direct merger of two gas-rich spiral galaxies. This model very nicely provides a physical process to explain the well known strong evolution of quasars, both in their rapid increase with redshift, and apparent cutoff at high redshift. The former is simply related to the higher rate of collisions of galaxies in the past, as a result of their closer proximity and their higher mean gas content, while the latter is a result of the fact that the galaxies must form and interact before a quasar can be formed. Clearly, for this model to work the ultraluminous infrared galaxies must follow the evolution found for the optically selected quasars (see e.g., Schmidt and Green 1983). This prediction is directly testable with the next generation of space infrared observatories, ISO and SIRTF.

## CONCLUSIONS

The new view of the universe provided by the IRAS survey has lead to the discovery of a new class of objects, the Ultraluminous Infrared Galaxies. We believe that these objects are the first formative stages of quasars in the nuclei of merging gas rich spiral galaxies. Such an explanation naturally ties the formation of quasars to a violent, but rare event in the evolution of spiral galaxies.

## ACKNOWLEDGEMENTS

Many colleagues have contributed in major ways to the development of the ideas presented here. Most notably these are Dave Sanders, Gerry Neugebauer, Jay Elias, and Nick Scoville. In addition, Keith Matthews, Dave Carrico, and James Graham have made major contributions to observations that have helped formulate these ideas. Finally, none of this work would have been done without the tremendously successful IRAS mission, and it is a great pleasure to acknowledge the many dedicated engineers, scientists, technicians, and managers who helped make this project the success it has been.

This research has been supported by NASA through the IRAS Extended Mission, and by the NSF.

## REFERENCES

Dressler, A., and D. Richstone. 1988. Ap. J. 324: 701.
Filippenko, A., and W.L.W. Sargent. 1985. Ap. J. Suppl. 57:503.
Hutchings, J.B., D. Crampton, and B. Campbell. 1984. Ap. J. 280: 41.
Lawrence, A., D. Walker, M. Rowan-Robinson, K.J. Leech, and

M.V. Penston. 1986. M.N.R.A.S. 219: 687.
Low, F.J., R.M. Cutri, S.G. Kleinmann, and J.P. Huchra. 1989. Ap. J. Letters 340: L1.
Neugebauer, G., and R.B. Leighton. 1969. Two Micron Sky Survey, A Preliminary Catalog, NASA Pub SP-3047.
Norman, C. 1989. Proceedings of Conference Windows on Galaxies, in preparation.
Price, S.D., and R.G. Walker. 1976. The AFGL Four Color Infrared Sky Survey: Catalog of Observations at 4.2, 11.0, 19.8, and 27 microns, AFGL Pub AFGL-TR-0208.
Rieke, G.H., R.M. Cutri, J.H. Black, W.F. Kailey, C.W. McAlay, M.J. Lebofsky, and R. Elston. 1985. Ap. J. 290: 116.
Rieke, G.H., and M. Lebofsky. 1986. Ap. J. 304: 326.
Rieke, G.H., and F.J. Low. 1972. Ap. J. Letters 176: L95.
Sanders, D.B., B.T. Soifer, J.H. Elias, B.F. Madore, K. Matthews, G. Neugebauer, and N.Z. Scoville. 1988a. Ap. J. 325: 74.
Sanders, D.B., B.T. Soifer, J.H. Elias, G. Neugebauer, and
K. Matthews. 1988b. Ap. J. Letters 328: L35.
Schmidt, M., and R.F. Green. 1983. Ap. J. 269: 352.
Scoville, N.Z., D.B. Sanders, A.I. Sargent, B.T. Soifer, S.L.
Scott, and K.Y. Lo. 1986. Ap. J. Letters 311: L47.
Scoville, N.Z., D.B. Sanders, A.I. Sargent, B.T. Soifer, and C.G. Tinney. 1989. Ap. J. Letters. submitted.
Smith, B.J., S.G. Kleinmann, J.P. Huchra, and Low, F.J. 1987. Ap. J.
Soifer, B.T, D.B. Sanders, G. Neugebauer, G.E. Danielson, C.J.
Lonsdale, B.F. Madore, and S.E. Persson. 1986. Ap. J. Letters 303: L41.
Soifer, B.T *et al.* 1987. Ap. J. 320: 238.
Stockton, A., and J.W. MacKenty. 1983. Nature 305: 678.
Toomre, A. and J. Toomre. 1972. Ap. J. 178: 623.
Veron-Cetti, M.-P., and P. Veron. 1985. Eso Sci. Rpt., No 4.
Young, E.T, R.F. Knacke, and R.R. Joyce. 1972. Nature 238: 263.

# The Peculiar Velocity Field Predicted from the Distribution of *IRAS* Galaxies

MICHAEL A. STRAUSS AND MARC DAVIS
University of California, Berkeley

## ABSTRACT

We present recent results from our full-sky redshift survey of IRAS galaxies. After briefly describing our sample selection and observations, we use the linear theory relation between acceleration and peculiar velocity to make predictions of the peculiar velocity field in the Local Universe. We compare our predictions with directly measured peculiar velocities from the Local Supercluster spiral galaxy sample of Aaronson *et al.* (1982) and the elliptical galaxy sample of Lynden-Bell *et al.* (1988). In a reference frame at rest with respect to the Cosmic Microwave Background, there is a systematic bulk flow in the residuals between observations and predictions. The Local Group itself takes part in this motion, so the bulk flow disappears in a frame at rest with respect to the Local Group. We show with the use of N-body techniques that this type of systematic effect is at least partly due to small-number statistics in the tracing of the density field. We conclude with a discussion of the challenges facing us in the future.

The N-body results show us that we have not yet achieved an optimum algorithm for translating from redshift space to real space; we briefly describe several alternative procedures. We compare the coherence of the observed and predicted peculiar velocity fields with predictions from several cosmogonical models.

## THE IRAS SAMPLE

Peebles (1976) describes the velocity field expected at late times in

linear theory; the dipole anisotropy of the galaxy distribution around a given galaxy is directly proportional to the peculiar velocity of that galaxy:

$$V = \frac{H_0 \Omega^{0.6}}{4\pi} \int \frac{\delta(x)\hat{x}}{x^3} d^3x, \quad (1)$$

where V is the peculiar velocity of the galaxy in question, $\Omega$ is the cosmological density parameter, and $\delta$(x) is the fractional density perturbation at position x. The following year, a dipole anisotropy was discovered in the Cosmic Microwave Background (CMB) (e.g., Lubin and Villela 1986), which was interpreted as due to a peculiar motion of the Local Group (LG) with respect to the rest frame of the CMB of 600 km $s^{-1}$. It was immediately realized that a measurement of the distribution of nearby galaxies could be used in concert with equation (1), and the measured LG peculiar velocity, to make an estimate of $\Omega$. This has been tried by many authors, usually with the simplifying assumption that the Virgo cluster is the only gravitating mass point (see, e.g., Davis and Peebles 1983; Huchra 1988). To do better requires galaxy samples that cover a large fraction of the sky. Pioneering work using optically selected samples of galaxies has been done by Lahav and collaborators (Lynden-Bell *et al.* 1989, and references therein). In this paper we describe a survey of galaxies observed by the Infrared Astronomical Satellite (IRAS). We have discussed our work before in two other conference proceedings (Strauss and Davis 1988a, 1988b; Yahil 1988), and in this paper will concentrate on new results obtained since the writing of those articles. A much more detailed account can be found in Strauss (1989), and in several papers in preparation.

The IRAS satellite surveyed the entire sky in four broad bands in the far-infrared, with a resolution of approximately 1' at 60$\mu$m. Because of the full-sky coverage and the lack of Galactic extinction in the far-infrared, the IRAS database offers a unique opportunity to study the large-scale distribution of galaxies. We have selected galaxy candidates from the IRAS Point Source Catalog (1985) using the following criteria:

1. $f_{60}/f_{12} > 3$, where $f_\lambda$ is the flux density at wavelength $\lambda$. This discriminates effectively between stars and galaxies.
2. $|b| > 5^\circ$, in a region not affected by confusion at 60$\mu$m. With these restrictions, our sample covers 87.6% of the sky.
3. $f_{60} > 1.936$ Jy.

We have obtained optical identifications and redshifts of the approximately 4,500 objects meeting these criteria, thus obtaining a sample of roughly 2,550 galaxies. The vast majority of the non-galaxies in the sample are associated with stars and infrared cirrus at $|b| < 10^\circ$ (see Yahil 1988 for a description of how optical identifications were made at these low latitudes). Below, we discuss some biases of the sample selection, and our

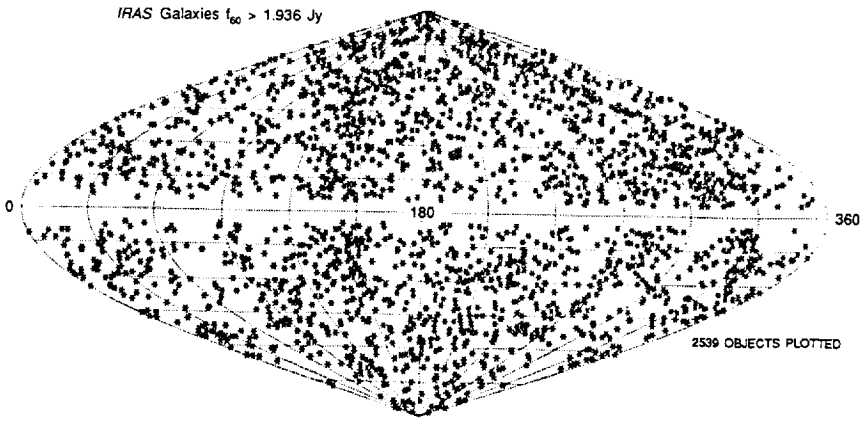


FIGURE 1 The distribution of galaxies in the survey, plotted in Galactic coordinates. The sample does not include galaxies at $|b| < 5^\circ$, and there are other regions at high Galactic latitudes which are not covered due to confusion or incompleteness of the IRAS survey.

attempts to correct for them. The distribution of all galaxies in the sample is shown in Galactic coordinates in Figure 1. Note the strong continuity of structures across the Galactic plane, in particular, the overdensities associated with Centaurus and the Pavo-Indus-Telescopium region ($l \approx 330^\circ$) appear to be physically associated. The Pisces-Perseus filament ($l \approx 135^\circ$) and the Hydra region ($l \approx 280^\circ$) also show continuity across the plane, as do the underdense regions centered at $l = 90^\circ$ and $l = 220^\circ$. Compare this figure with the corresponding Figure 1a in Yahil (1988); note how much stronger this sense of continuity is now that we have identified galaxies in the two strips $5 < |b| < 10^\circ$.

## THE PREDICTED PECULIAR VELOCITY FIELD

As described in detail in Strauss and Davis (1988b) and Yahil (1988), we have used equation (1) to predict the velocity flow field within 8,000 km $^{-1}$s of the Local Group. The procedure we follow is slightly modified from that of Yahil (1988). We first fill the missing Galactic plane strip with random "galaxies" with number density given by an interpolation of the density in strips with $5 < |b| < 20^\circ$, under the assumption that the continuity across the plane described in the last section is real. A selection function is derived using a maximum-likelihood estimator (Yahil 1988), which is used to weigh the galaxies to compensate for the magnitude limit of the sample. A value of $\Omega$ is derived by requiring that equation (1) reproduce the 600 km s$^{-1}$ peculiar velocity of the Local Group inferred from the CMB dipole.

For an adopted value of $\Omega = 0.7$, the predicted peculiar velocity of the Local Group is 650 km $s^{-1}$ towards $l = 250^\circ$, $b = +45^\circ$, some $22^\circ$ from the CMB dipole direction of $l = 270^\circ$, $b = +30^\circ$ (Lubin and Villela 1986). Strauss and Davis (1988b) show that the majority of this acceleration is due to material within 4,000 km $s^{-1}$ of the Local Group.[1]

We can go further by using equation (1) to make estimates of the peculiar velocity of every galaxy in the sample. We restrict ourselves to objects within 8,000 km $s^{-1}$ of the Local Group, because the sample becomes prohibitively sparse at greater distances. In practice, our estimate of the peculiar velocity of a galaxy at position x is given by:

$$V(x) = \frac{H_0 \Omega^{0.6}}{4\pi n_1} \sum_{galaxies\ i} \frac{S(|\, x - x_i\,|)(x - x_i)}{\phi(x_i)\,|\, x - x_i\,|^3} - H_0 \Omega^{0.6} x/3 + W(S). \quad (2)$$

Here $n_1$ is the measured galaxy density, $\phi(x_i)$ is the value of the selection function at distance $x_i$, and S is a smoothing on small scales, to be described further below. The second term corrects for the fact that the sum is not spherically symmetric for a point displaced from the origin, and W(S) is an additional correction applied when the source is within one smoothing length of the edge of the sample.

The measured redshift, cz, of a galaxy may be expressed as:

$$cz = \text{distance} + (V - V_{LG}) \cdot \hat{x}, \quad (3)$$

where V and $V_{LG}$ are the peculiar velocity vectors of the galaxy and the Local Group, respectively, and $\hat{x}$ is the unit vector pointing from the Local Group to the galaxy. We separate peculiar velocities and distances using an iterative procedure: galaxies are initially assumed to be at their redshift distances ($V \equiv 0$), and equation (2) is used to make a first estimate of the peculiar velocity field. Distances are then updated using equation (3) and the process is repeated until convergence. $\Omega$ is kept fixed throughout this procedure, and the value of $V_{LG}$ used is that *derived from the IRAS sample itself* on each iteration. A "buffer zone" between 8,000 km $s^{-1}$ and 10,000 km $s^{-1}$ prevents galaxies from being lost from the sample if their peculiar velocities take them beyond 8,000 km $s^{-1}$. The resulting peculiar velocity field converges with a standard deviation of residuals less than 10 km $s^{-1}$ after eight iterations.

There are several subtleties associated with this process. In regions that are virialized, or even overdense by a factor of several, equation (1) no longer holds, and this iterative procedure may cause chaos. Thus we

[1] We will express distances in terms of radial velocities, as we do here, in order to bypass the necessity of specifying the Hubble Constant.

will never be able to properly model the "Finger of God" effect seen in the cores of clusters. We have thus collapsed the galaxies in seven cluster cores (Virgo, Ursa Major, Fornax, Eridanus, Centaurus, Hydra, and Perseus) to a common redshift, and have suppressed the mutual gravitational attraction of galaxies within each cluster. Another related problem is that equation (2) diverges at small separations. Note that because the selection function drops sharply with distance, a pair of galaxies separated by a small amount at a large distance from us can give each other a tremendous kick. In order to suppress this, we adopt a smoothing law, $S(r) = (r/r_s)^3$ for $r < r_s$, where $r_s$, the smoothing length, is taken to be the mean interparticle spacing at that distance, or 500 km $s^{-1}$, whichever is larger.

The resulting velocity field is similar to that shown in Figure 10 of Yahil (1988), and will not be reproduced here. As those figures show, the predicted velocity field is dominated by two large mass concentrations in Hydra-Centaurus and Perseus-Pisces. We will compare these predictions with the observed velocity field in the next section.

## COMPARISON WITH THE OBSERVED PECULIAR VELOCITY DATA

Burstein (1989) reviews the current status of direct observations of the peculiar velocity flow field. In this paper, we will make comparisons of our predictions with two data sets: the subset of the Aaronson *et al.* (1982) Local Supercluster spiral galaxies with high-quality observations defined by Faber and Burstein (1988), and the independent peculiar velocities of individual galaxies, groups, and clusters of the Seven Samurai elliptical galaxy sample, listed in Table 4 of Faber *et al.* (1989). Figure 2 shows the distribution of peculiar velocities in a slice through the plane of the Local Supercluster, using the plotting technique introduced by Lynden-Bell *et al.* (1988). All galaxies in the two samples within 22.5° of the plane are plotted, and the length of the line attached to each point is equal to the radial peculiar velocity. Solid symbols are used for positive peculiar velocities, and open symbols are used for negative. In the first panel of this figure, we show the positions of the well-known clusters that fall in this projection; the symbols are indicated in the figure caption. In panel (b), the *observed* peculiar velocities are plotted, panel (c) shows the IRAS *predictions*, and panel (d) shows the difference of (b) and (c). It is indeed a remarkable fact that is able to reproduce the qualitative nature of the velocity flow field, perhaps the first *direct* indication that peculiar velocities are generated by gravity, and that galaxies at least approximately trace the mass distribution of the underlying dark matter. However, there are some systematic differences between observations and predictions. Note, for instance, that whereas the observed peculiar velocities (panel b) to the upper right of the Ursa Major region are large and negative, the predicted

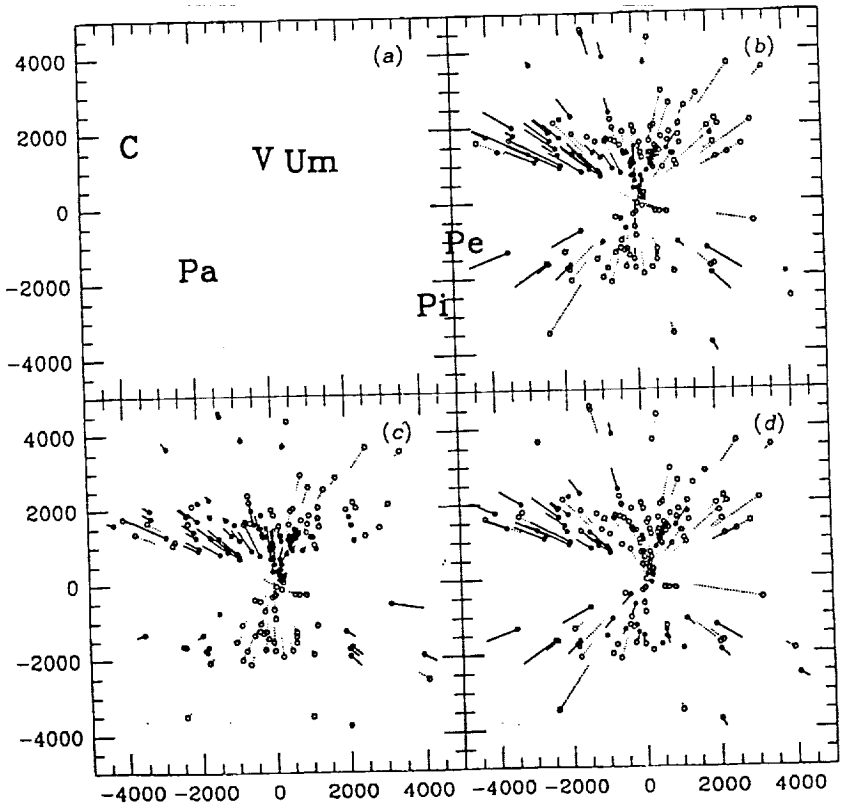


FIGURE 2 The velocity field of the Aaronson *et al.* and Faber *et al.* galaxy samples in a slice through the Local Supercluster plane, in the CMB frame. (a) The positions of the major clusters falling in the slice: V = Virgo, Um = Ursa Major, C = Centaurus, Pa = Pavo, Pe = Perseus, and Pi = Pisces. (b) The observed velocity field. (c) The IRAS predicted velocity field. (d) The difference between (b) and (c).

motions (panel c) are very quiet; predicts that the pulls of the Pisces-Perseus and Hydra-Centaurus superclusters approximately balance in this region. Note also the very large observed peculiar velocities towards Centaurus; IRAS predicts motion of the same sign, but of smaller amplitude. In panel (d), there is a systematic motion seen in the difference between predicted and observed peculiar velocities, as if there is a bulk flow component to the motion that IRAS does not see. We find consistent solutions for the bulk flow using the Aaronson *et al.* and Faber *et al.* galaxies separately as well as together: 250 km $s^{-1}$ pointing towards $l = 320^{\circ}$, $b = -35^{\circ}$.

In Figure 3, the same comparison of observed and predicted peculiar velocities is made, this time in a frame at rest with respect to the Local

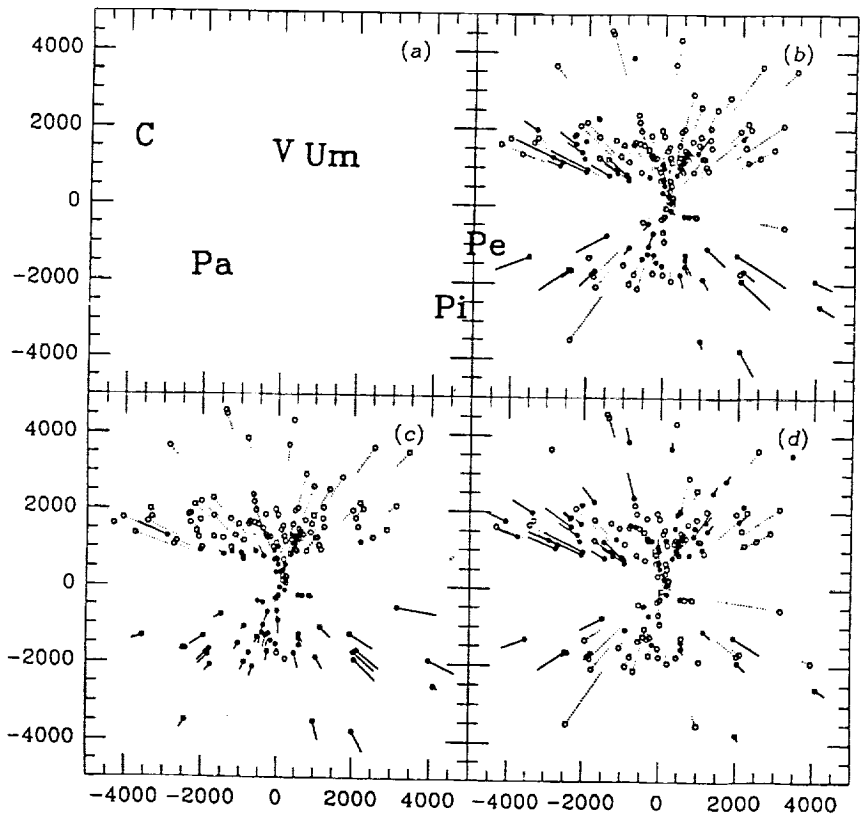


FIGURE 3 As in Figure 2, but plotted in the rest frame of the Local Group.

Group. This is not a trivial change, because in order to transform the IRAS predicted motions, we use the Local Group motion *as predicted by* IRAS, while the *observed* LG frame peculiar velocities are merely the difference between their redshift and observed distance. Note now in panel (d) that the sense of an overall bulk flow to the residuals between observed and predicted peculiar velocities has vanished, and we are left with mostly small-scale motions that we have not modelled correctly. Thus the Local Group itself takes part in the bulk flow seen in the residuals in Figure 2d. The only significant systematic effect remaining in the LG frame is a strong infall in the direction of Hydra-Centaurus that IRAS is unable to reproduce. This plot should be compared with Figure 7b, panel 2, of Faber and Burstein (1988), which shows residuals of observed peculiar velocities after subtracting away the predictions of their Great Attractor model.

This comparison shows that there is a bulk motion within a sphere of $\approx$ 4,000 km $s^{-1}$ radius, which IRAS is not properly modelling. Moreover,

the Local Group also takes part in this motion; most of the deviation of the IRAS calculated peculiar velocity for the Local Group from the value measured from the CMB dipole can be attributed to this motion. We show in the next section this may be explained as a purely statistical effect caused by dilute sampling of the density field.

## COMPARISON WITH N-BODY MODELS

Our iteration scheme can be tested with N-body models for which we know the true distances of every point. We used N-body models consisting of 262,144 particles in a box 360 Mpc on a side ($H_0$ = 50 km $s^{-1}$ $Mpc^{-1}$) in an $\Omega = 1$ universe, with an initial power spectrum of perturbations appropriate for universe dominated by Cold Dark Matter, and evolved until the *rms* density contrast in a sphere of radius 16 Mpc is $b^{-1} = 0.5$. The velocity field was smoothed with a Gaussian of width 100 km $s^{-1}$. Particles with peculiar velocities of 600 km $s^{-1}$, lying in regions of local overdensity $\delta$ with $-0.2 < \delta < 1.0$, and with smooth local velocity field, were chosen as Local Group candidates. "IRAS" flux-limited catalogues were constructed around these Local Group candidates by selecting objects according to the number density and selection function of the real data; no biasing was applied in the galaxy selection, so these objects do trace the mass of the simulation. For more details, see Gorski *et al.* (1989).

We then ran our iteration program on the N-body "IRAS" catalogue. That is, we gave the program only the information on the redshift of each particle as observed in the rest frame of the LG particle, and let it run to predict the true distances and the peculiar velocity field of the particles in the simulation. $\Omega$ was set equal to unity for these simulations. We emphasize that the motivation is not so much to test the Cold Dark Matter cosmogony, but rather to test our iteration scheme of peculiar velocities in the presence of non-linear effects and shot noise. A total of 18 realizations were run: nine with different "Local Groups," and nine more with a single "Local Group," but different random numbers selecting the galaxies in the survey. In Figure 4, we show the direction for the predicted peculiar velocity of the Local Group in each of these models. They all have been rotated so that the true direction of the Local Group particle in each case is $l = 270^\circ$, $b = +30^\circ$. Notice that the scatter is of the order of 15-20°, comparable to the difference between the true and predicted motions of the Local Group.

In one of these models, we selected a sample of points to match closely the distribution of galaxies with observed peculiar velocities in the samples used in the previous section. With this sample, we can make a direct comparison of true and predicted radial peculiar velocities, and see how these results compare with the real universe described in the

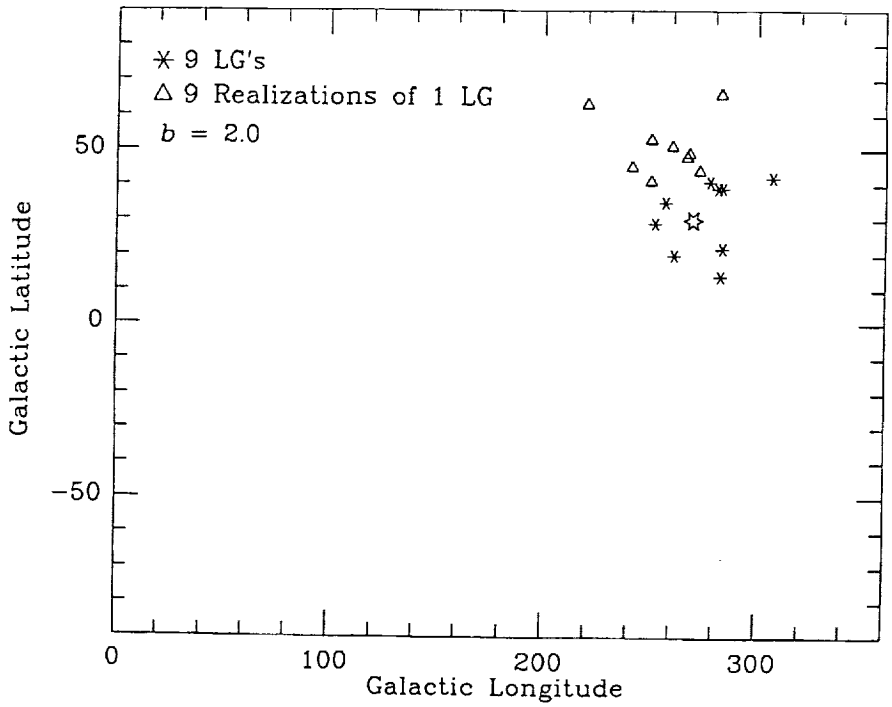


FIGURE 4 The distribution of predicted directions of the "Local Groups" in eighteen N-body realizations of the sample. The large star is placed at $l = 270^{\circ}$, $b = 30^{\circ}$.

previous section. The true peculiar velocities were perturbed by a gaussian "error" with a standard deviation of 15% of the true distance to mimic the observational situation. Unlike the real observations, we assume here that the distances are measured exactly. In Figure 5, we show the results. Panel (a) shows the distribution of true peculiar velocities in the CMB frame, in exact analogy with Figure 2b. Panel (b) is then the predicted peculiar velocity as given by the iteration procedure, and (c) is the difference between the two. Finally, (d) is the difference of "observed" and predicted, now in the LG frame. Note the very strong bulk flow seen in the residuals in panel (c), with an amplitude of $\approx 200$ km s$^{-1}$. Unlike the real universe, however, there is still a significant bulk flow in the LG frame residuals, with an amplitude of $\approx 100$ km s$^{-1}$ (panel d), which simply says that the deviation of the predicted LG motion from its true direction is at least partly due to small-scale effects in this model.

We have done the same experiment in which we have assigned 15% errors to the true distances of the galaxies to more closely simulate the

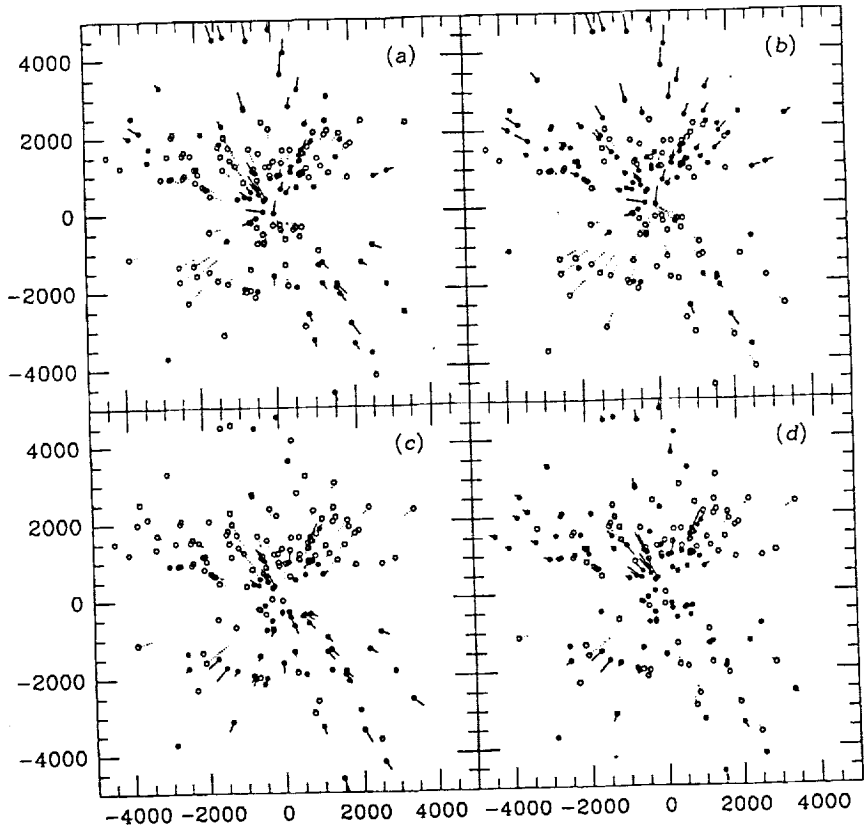


FIGURE 5 The results of an N-body experiment simulating the comparison between observed and predicted peculiar velocities. (a) The true peculiar velocity field in the CMB frame. (b) The predicted peculiar velocities for the same galaxies. (c) The difference between (a) and (b). (d) The difference between observed and predicted in the LG frame.

observations; we find that this seriously degrades the good agreement between "measured" and predicted peculiar velocity.

Why is it that there seems to be a missing component of gravity in the CDM model, where the points are explicitly chosen to trace the mass? In these models, there is very little power on scales larger than the sample (8,000 km $s^{-1}$) to cause the whole sample to translate (Juszkiewicz *et al.* 1989). Our interpretation is that this effect is caused by shot noise. Imagine a toy model in which the bulk of the motion of the region within 3,000 km $s^{-1}$ is caused by a large structure at 6,000 km $s^{-1}$. Because of the extremely dilute sampling of the catalogue, the overdensity of this structure may be traced by only a small number of points, and this number will be subject to Poisson statistics. Thus, the inferred gravity from this structure can be

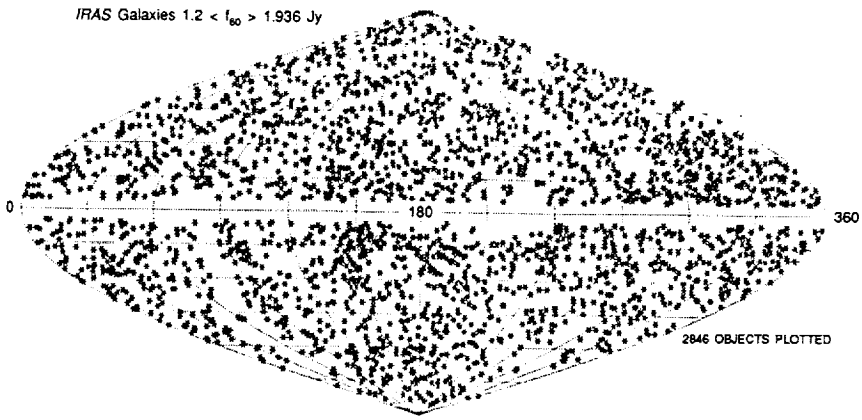


FIGURE 6 The distribution of galaxies in Galactic coordinates of objects in a deeper IRAS redshift survey, in preparation. Note the appreciable overdensities associated with the Perseus-Pisces ($l \approx 120 - 150^\circ$, $b \approx -30 - +30^\circ$) and Hydra-Centaurus ($l \approx 280 - 330^\circ$, $b \approx 0 - +45^\circ$) regions.

in error, affecting the predicted peculiar velocities in a systematic way. Detailed calculations of the noise in the acceleration of galaxies relative to the Local Group is consistent with the observed amplitude of the effect, which must be at least partly responsible for the missing bulk motions seen in the predicted velocity field of the real IRAS galaxies.

## UNRESOLVED ISSUES, AND THE WORK AHEAD

In the last section, we have identified shot noise as a stumbling block in the interpretation of the comparison of our predictions with observations. Thus we have started a deeper survey of IRAS galaxies, flux-limited to 1.2 Jy, to rectify this situation. When the survey is completed, hopefully in early 1991, we shall have redshifts for $\approx$ 5,500 IRAS galaxies selected uniformly over the sky. Figure 6 shows the distribution on the sky of the additional objects. Because this sample goes deeper, it emphasizes structures at distances of 3,000 - 5,000 km $s^{-1}$; note in particular the strong enhancements in the Perseus-Pisces region and the Hydra-Centaurus region.

We are in the process of using the IRAS predicted distances for the Aaronson *et al.* galaxies to construct Tully-Fisher diagrams. We hope to make a more robust estimate of $\Omega$ by finding that value that minimizes the scatter in the TF diagram. The recent work of Dekel and Bertschinger (1989) provides another powerful way of making comparison between IRAS predictions and observed peculiar velocities; we will soon be able to place

constraints on the relative overdensities of galaxies and dark matter in different regions of space.

## ACKNOWLEDGMENTS

We thank our collaborators in this project, Amos Yahil and John Huchra, for allowing us to use unpublished data, and for many helpful discussions. We are grateful to Dave Burstein for sending us machine-readable versions of the observed peculiar velocity data. MAS acknowledges the support of an NSF Graduate Fellowship.

## REFERENCES

Aaronson, M., J. Huchra, J.R. Mould, P.L. Schechter, and R.B. Tully. 1982. Ap. J. 258: 64.
Aaronson, M. *et al.* 1982. Ap. J. Suppl. 50: 241.
Bertschinger, E., and A. Dekel. (in press). In: Latham, D., and L. da Costa (eds.). Large Scale Structures and Peculiar Motions in the Universe. (ASP Conference Series).
Burstein, D. 1989. Rep. Prog. Phys. in press.
Davis, M., and P.J.E. Peebles. 1983. Ann. Rev. Astr. Ap. 21: 109.
Faber, S.M., and D. Burstein. 1988. In: Rubin, V.C., and G.V. Coyne, S.J. (eds.). Large Scale Motions in the Universe: A Vatican Study Week. Princeton University Press, Princeton. p. 116.
Faber, S.M., G. Wegner, D. Burstein, R.L. Davies, A. Dressler, D. Lynden-Bell, and R.J. Terlevich. 1989. Ap. J. Suppl. 69: 763.
G.orski, K., M. Davis, M.A. Strauss, S.D.M. White, and A. Yahil. 1989. Ap. J. in press.
Huchra, J.P. 1988. In: van den Bergh, S., and C.J. Pritchet (eds.). The Extragalactic Distance Scale, A.S.P. Conference Series Vol. 4. Astronomical Society of the Pacific, San Francisco. p. 257.
IRAS Catalogs and Atlases, Explanatory Supplement 1985. Beichman, C.A., G. Neugebauer, H.J. Habing, P.E. Clegg, and T.J. Chester (eds.). U.S. Government Printing Office, Washington, D.C.
IRAS Point Source Catalog 1985. Joint IRAS Science Working Group U.S. Government Printing Office, Washington, D.C. (PSC).
Juszkiewicz, R., N. Vittorio, and R.J. Wyse. 1989. Ap. J. in press.
Lubin, P.M., and T. Villela. 1986. In: Madore, B.F., and R.B. Tully (eds.). Galaxy Distances and Deviations from Universal Expansion. Reidel, Dordrecht. p. 169.
Lynden-Bell, D., S.M. Faber, D. Burstein, R.L. Davies, A. Dressler, R.J. Terlevich, and G. Wegner. 1988. Ap. J. 326: 19.
Lynden-Bell, D., O. Lahav, and D. Burstein. 1989. preprint.
Peebles, P.J.E. 1976. Astron. Astrophys. 53: 131.
Peebles, P.J.E. 1980. The Large Scale Structure of the Universe. Princeton University Press, Princeton.
Strauss, M.A. 1989. Ph.D. thesis. University of California, Berkeley.
Strauss, M.A., and M. Davis. 1988a. In: Audouze, J., M.-C. Pelletan, and A. Szalay (eds.). Proc. IAU Symp. No. 130, Large Scale Structures of the Universe. Reidel, Dordrecht. p. 191.
Strauss, M.A., and M. Davis. 1988b. In: Rubin, V.C., and G.V. Coyne, S.J. (eds.). Large Scale Motions in the Universe: A Vatican Study Week. Princeton University Press, Princeton. p. 256.
Yahil, A. 1988. In: Rubin, V.C., and G.V. Coyne, S.J. (eds.). Large Scale Motions in the Universe: A Vatican Study Week. Princeton University Press, Princeton. p. 219.

# X-Ray Radiation from Supernova 1987A The Results of the Kvant Module in 1987-1989

R.A. SUNYAEV, A.S. KANIOVSKY, V.V. EFREMOV, S.A. GREBENEV, A.V. KUZNETSOV, E. CHURASOV, M. GILFANOV, N. YAMBURENKO[1], J. ENGLHAUSER, S. DOEBEREINER, W. PIETSCH, C. REPPIN, J. TRUEMPER,[2] E. KENDZIORRA, M. MAISACK, B. MONY, R. STAUBERT,[3] G.K. SKINNER, T.G. PATTERSON, A.P. WILLMORE, O. AL-EMAM,[4] A.C. BRINKMAN, J. HEISE, J.J.M IN'T ZAND, R. JAGER[5]

## ABSTRACT

The results of two years SN1987A hard X-ray radiation observations by the HEXE instrument aboard the Kvant module are summarized. By May-June 1989, the hard X-ray flux had declined more than 8.5 times in comparison with the maximum of the X-ray light curve. The upper limit on the ratio of $^{57}Co/^{56}Co$ abundances at the level of ratio of $^{57}Fe/^{56}Fe$ abundances at the Earth by a factor of 1.5.

## INTRODUCTION

The Roentgen international X-ray observatory on the Kvant module of the Mir space station has been operating successfully since the beginning of June 1987. Four telescopes mounted onboard the Kvant module cover a wide energy range: Coded Mask Imaging Spectrometer TTM (2-30 keV), GSPC (2-100 keV); Phoswich type detectors HEXE (20-200 keV), and Phoswich type detectors Pulsar X-1 (50-1300 keV).

Many of the X-ray sources were observed in 1987-1989, and approximately 30% of the observations were devoted to SN1987A.

[1]Space Research Institute, Academy of Sciences, Moscow
[2]Max-Planck-Institut für Extraterrestrische Physik, Garching, FRG
[3]Astronomisches Institut der Universitat Tubingen, FRG
[4]Space Research Laboratory, Utrecht, The Netherlands
[5]Department of Space Research, University of Birmingham, UK

For the first time during two years of observing Supernova 1987A in June 1989, the Roentgen observatory aboard the Mir-Kvant module was not able to detect its hard X-ray radiation during the current series of observations. The radiation flux in energy band 45-105 keV decreased more than 8.5 times in comparison with the maximal flux detected in January 1988.

The results obtained during the two years of Supernova 1987A observations were given in papers (Sunyaev *et al.* 1987a,b, 1988, 1989). By the present time we have succeeded in calibrating the third and fourth detectors of the HEXE device using the results of the Crab Nebula observation. These detectors have a lower energy resolution in comparison with the first and the second ones. Therefore, we reprocessed all the obtained data about SN1987A hard X-rays using the results of all four detectors of the HEXE device, which increased data significance and decreased statistical errors.

In Figure 1a,b, the spectra of SN1987A hard X-ray radiation are presented. They were obtained in a series of seven intense observations carried out from the Roentgen observatory over two years. The spectra demonstrate an increase of the flux from August 1987 to January 1988. This increase is connected with a rapid decreasing of the envelope transparence. From January 1988 to June 1989 a continuous decline of the flux is observed which is mainly connected with a decreasing amount of $^{56}$Co in the envelope. Already in September 1988 a strong change of the spectral shape was detected. This is explained by a decreasing of the envelope optical thickness with respect to Thomson scattering. The number of successive scatterings experienced by the majority of photons became insufficent to decrease the energy of the $^{56}$Co decay gamma-photons due to a multiple recoil effect up to a value of $h\nu \leq 50$ keV.

Note that the sharp flux cutoff at the energies below 20 keV in August 1987 and January 1988 was connected with photoabsorption by heavy elements. At that time the photon diffusion in the envelope, accompanied by the recoil effect, moved the majority of photons in the band $h\nu \leq 20$ keV where the photoabsorption dominated.

In Figure 2 and 3, the light curves of the SN1987A emission in three energy bands: 15-45, 45-105, 105-200 keV (see also Table 1) are presented. Note here especially the point corresponding to observations on June 16, 1987, when the hard X-ray flux in the 45-105 keV spectral channel was detected at four standard deviation levels (it was first noticed by Englhauser *et al.* 1989).

The light curves (Figure 3) testified to a hard X-ray flux from the supernova, changed smoothly in accordance with predictions of the model of this radiation appearance due to radioactive cobalt decay in opaque envelope. For two years of observations we have not been able to observe

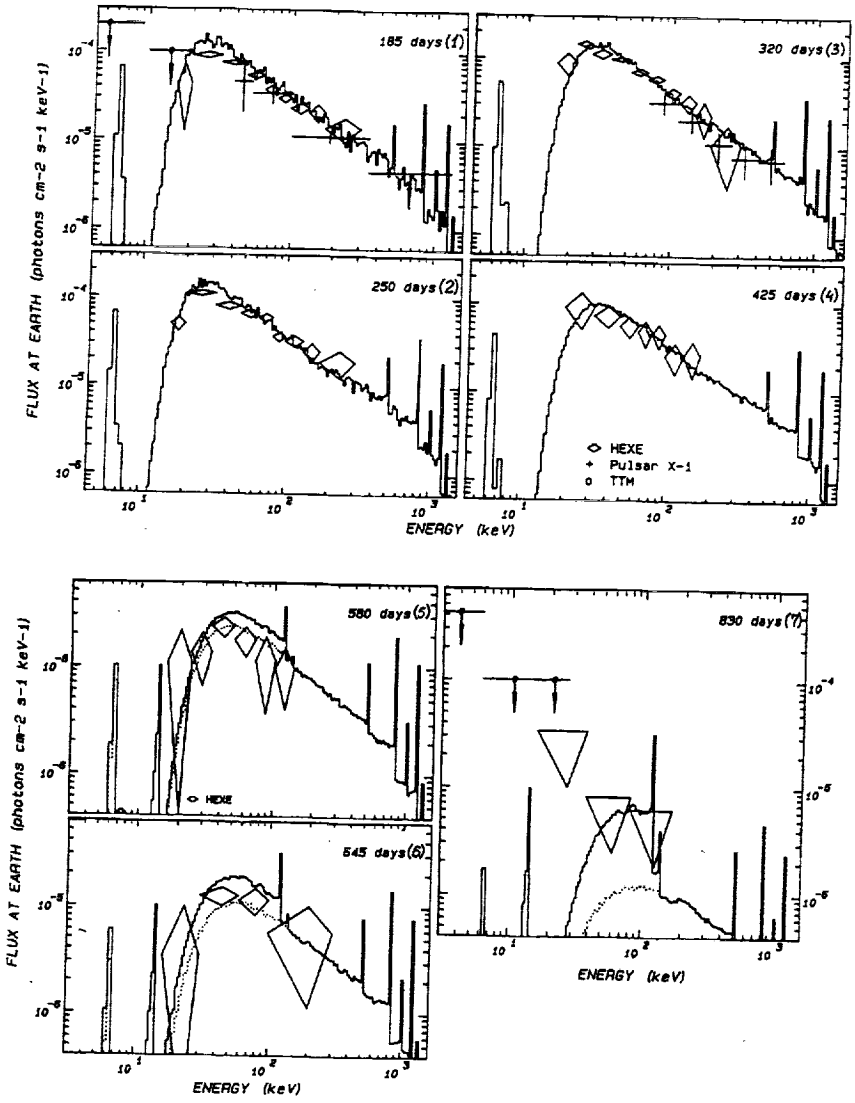


FIGURE 1 The SN1987A X-ray spectra obtained by the Roentgen observatory in August 1987 (1) and October - November 1987 (2), December 1987 - January 1988 (3), April 1988 (4), September - October 1988 (5) and November 1988 (6), May - June 1989 (7), (diamonds and crosses - the HEXE and Pulsar X-1 data respectively, crosses marked by circles - the TTM telescope upper limits). The errors correspond to one standard deviation, the upper limits - to three standard deviations (in the last graph the HEXE upper limits are shown by triangles). Results of the Monte-Carlo calculations carried out according to the envelope model accepted in the present paper are presented by solid lines (time after the outburst is shown near each curve). In graphs 5,6,7 a $^{56}$Co portion in the total $^{57}$Co emission is shown by dotted lines. The relative abundance of $^{56}$Co/$^{57}$Co is equal to two-abundance of $^{56}$Fe/$^{57}$Fe at the Earth.

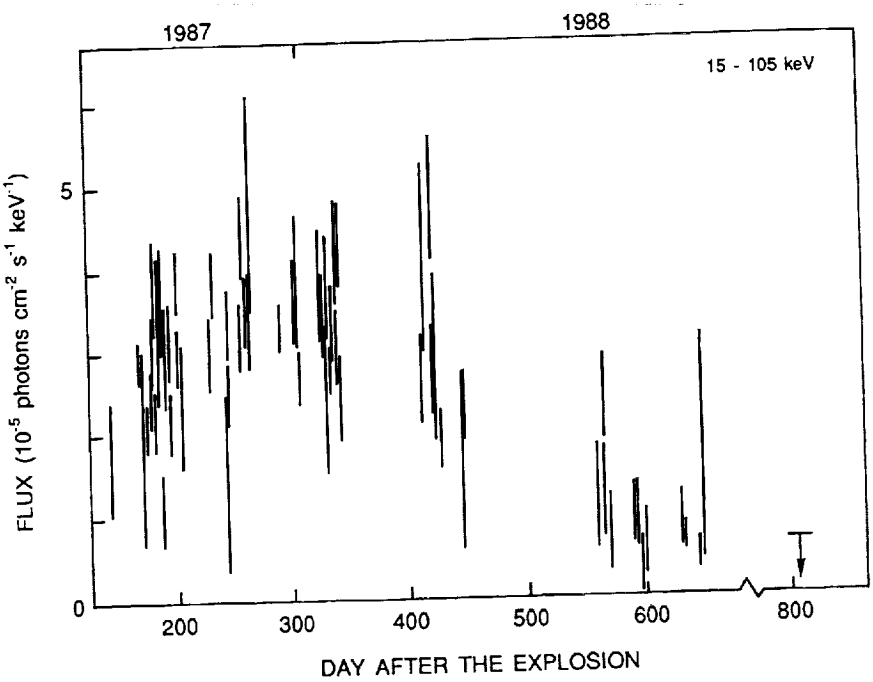


FIGURE 2 The SN1987A X-ray 15-105 keV flux as a function of time according to the HEXE observations. Each point corresponds to one observational day, the errors correspond to one standard deviation. Three sigma upper limit on the flux observed in May-June 1989 is presented.

the traces of a shock wave generated due to collision between the expanding envelope of the supernova and a stellar wind emitted by the presupernova on a red giant stage of the evolution. We were also unable to observe traces of X-ray radiation of the stellar remnant - a young pulsar or an accreting object or any manifestations of emission connected with cosmic rays.

## MIXING OF RADIOACTIVE ELEMENTS IN THE EXPANDING ENVELOPE

Early detection of the SN1987A hard X-ray radiation by the Ginga satellite and the Kvant module (Dotani *et al.* 1987; Sunyaev *et al.* 1987a,b) was the first evidence of a radioactive $^{56}$Co strong mixing over the envelope volume (Itoh *et al.* 1987; Ebisuzaki and Shibazaki 1988; Grebenev and Sunyaev 1988; Pinto and Woosley 1988). At present this conclusion is confirmed by direct observations of a velocity dispersion of infrared lines of the iron and cobalt ions (Ericson *et al.* 1988) and also by a broad

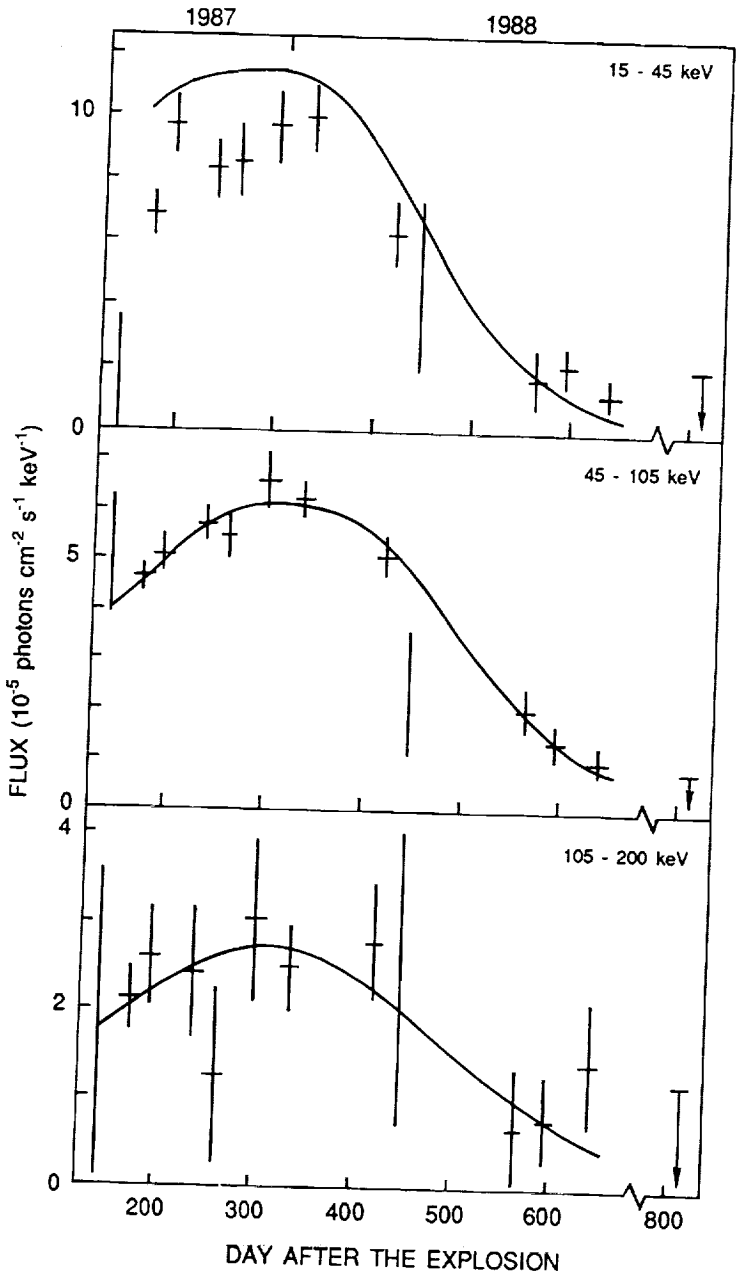


FIGURE 3 The SN1987A X-ray fluxes as functions of time according to the HEXE data in three colors 15-45, 45-105, and 105-200 keV. Each point presents data averaged over long period of observations. The errors correspond to one standard deviation. The results of Monte-Carlo simulations carried out for the envelope model accepted in the present paper are shown by solid lines.

TABLE 1 The SN1987A X-ray flux evolution in accordance with data of the HEXE device observations in 1987-1989

| Day since the outburst | Fluxes and 1σ errors [$10^{-6}$phot·cm$^{-2}$s$^{-1}$keV$^{-1}$] in the energy bands | | | | | |
|---|---|---|---|---|---|---|
| | 15 - 45 keV | | 45 - 105 keV | | 105 - 200 keV | |
| 143.9 - 144.1 | 2. | 34. | 51. | 12. | 18. | 17. |
| 169. - 182. | 68.2 | 5.7 | 46.7 | 2.1 | 21.3 | 3.3 |
| 186. - 204. | 96.7 | 8.5 | 50.9 | 3.5 | 26.0 | 5.2 |
| 231. - 247. | 83.1 | 8.3 | 57.4 | 3.3 | 24.3 | 7.2 |
| 258. - 266. | 85. | 10. | 55.2 | 4.4 | 12.8 | 9.7 |
| 291. - 309. | 97. | 11. | 66.1 | 5.6 | 30.4 | 8.9 |
| 328. - 343. | 100. | 10. | 62.6 | 3.5 | 25.1 | 4.8 |
| 413. - 426. | 63. | 9.5 | 51.1 | 3.8 | 27.9 | 6.1 |
| 444. - 446. | 46. | 27. | 24. | 12. | 24.0 | 16. |
| 559. - 569. | 17.2 | 9.6 | 20.5 | 4.1 | 7.2 | 6.5 |
| 590. - 599. | 21.4 | 6.1 | 14.5 | 3.0 | 8.2 | 4.7 |
| 630. - 648. | 12.2 | 4.1 | 10.6 | 2.6 | 14.5 | 7.0 |
| 820. - 840. | 8.2 | 7.0 | 3.8 | 2.9 | -2.8 | 4.2 |

spectral width of the $^{56}$Co direct escape gamma-lines (Matz *et al.* 1988; Rester *et al.* 1989). These direct observations testify to the presence of radioactive cobalt in the envelope layers having expansion velocities from 400 up to 3000 km/s. This would be impossible if the strongest mixing of envelope material due to generation of the Rayleigh-Taylor instability had not occurred (Hachisu *et al.* 1989; Arnett *et al.* 1989).

The supernova hard X-ray light curve provides an opportunity to estimate the distribution of radioactive cobalt over the envelope using the simplest assumptions. The $^{56}$Co distribution (mass-fraction) consistent with the observed light curve is shown in Figure 4 by crosses (the vertical line of a cross corresponds to an error at one standard deviation level). The problem of the reconstruction of cobalt distribution over the envelope is considerably simpler if cobalt radial distribution is searched as a superposition of two Gaussians: a narrow one localized near the envelope center and an extensive one with broader $^{56}$Co distribution over the envelope. The regions of $^{56}$Co distribution consistent with the observed light curve in this simple model are also presented in Figure 4.

It is obvious that two different approaches give quite close results. About 60% of cobalt is in the central region of the envelope having low

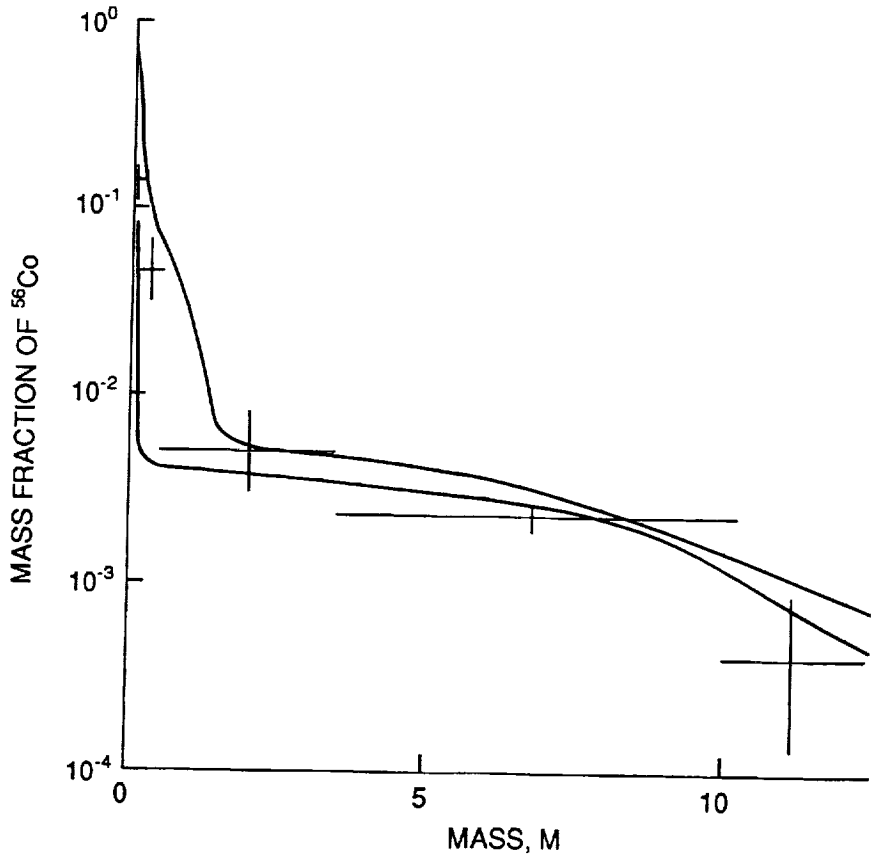


FIGURE 4 Region of the most probable $^{56}$Co distribution (mass-fraction) over the SN1987A envelope which gives a possibility to simulate the observed X-ray light curves of the source. The results of two independent approaches are presented. In the first approach it is assumed that cobalt is uniformly distributed over five spherical layers of the envelope (crosses, errors of the cobalt concentration in each layer are given at one sigma level). In the second approach the 67% confidence level region of the distribution described by superposition of two Gaussians is obtained. It is clear that both approaches give similar results.

velocities. And about 40% is mixed over all the envelope volume. Note that the data of only two hard energy bands 45-200 keV were used during the cobalt distribution reconstruction. The flux at lower energies strongly depends on photoabsorption in the envelope, but the photoabsorption efficiency strongly depends on the degree of the cobalt mixing.

All the calculations, the results of which were presented above and will be discussed below, were carried out on the basis of the velocity

and density distribution model resulted from hydrodynamics simulations by Arnett (1988).

In Figure 3 it is shown how the accepted model of cobalt distribution coincides with the observed X-ray light curve. Deviations are maximal at the beginning of the supernova X-ray observation in a soft 15-45 keV band. This points out a more strong photoabsorption in comparison with photoabsorption in the used model. It may be connected with the enhanced cobalt concentration in outer envelope layers. High X-ray and gamma-ray radiation from these layers appeared at early stages of the envelope expansion before the beginning of the Roentgen observatory systematical observations.

## ABUNDANCE OF $^{57}$Co

By the beginning of the second year after the explosion a $^{57}$Co isotope can become an important energy source in the supernova envelope since it decays 3.5 times more slowly than $^{56}$Co. The simulations of explosive nucleosynthesis (Woosley *et al.* 1986; Hashimoto *et al.* 1989) predicted a ratio of $^{57}$Fe/$^{56}$Fe abundances in the Earth. There are two ways to define the abundance of $^{57}$Co in the SN1987A envelope: the first, by direct determination of flux in the $^{57}$Co lines of 122 and 135 keV in the supernova spectrum and the second one, by the determination of a $^{57}$Co photon portion in the X-ray continuous spectrum in the 45-105 keV energy band. We mean the photons emitted in the $^{57}$Co lines 122 and 136 keV, but which undergo to multiple scattering in the envelope and decrease their energy due to the recoil effect. Because of relatively low energy resolution of Phoswich detectors, the HEXE device aboard the Mir-Kvant module gave considerably better results when the second method was used.

The results presented below depend on an accepted envelope model (the Arnett model [1988] is used) and on a cobalt distribution over the envelope (the distribution presented in Figure 4 is used). It is also supposed that $^{57}$Co is distributed similarly to $^{56}$Co.

For the whole period from September 1988 to June 1989 the Roentgen observatory has not detected a statistically significant enhancement of X-ray luminosity in the 45-105 keV energy band over the model predictions in which the whole observed flux is connected with the $^{56}$Co decay. The upper limits at three standard deviation levels for the ratio of $^{57}$Co/$^{56}$Co relative abundance in the supernova envelope to the Earth's $^{57}$Fe/$^{56}$Fe relative abundance were equal to 2.4 in September 1988, 3.3 in December 1988, and 1.8 in June 1989 at the accepted assumptions. Note that the ratio of $^{57}$Fe/$^{56}$Fe abundances at the Earth is 0.024 (Cameron 1986). All the data obtained from September 1988 to June 1989 allowed us to obtain a limit at three standard deviation levels for a portion of $^{57}$Co decay photons in the

light curve of the SN1987A hard X-ray radiation. This limit corresponds to the $^{57}Co/^{56}Co$ abundance in 1.5 times exceeding the Earth's $^{57}Fe/^{56}Fe$ relative abundance. The observations in May-June 1989 gave the upper limit on the cobalt 122 keV line flux $3.9 \cdot 10^{-4}$ photons $\cdot$ $cm^{-2}s^{-1}$ at $3\sigma$ level). This limit corresponds in frames of the model being discussed to the $^{57}Co/^{56}Co$ abundance six times exceeding the Earth's abundance of $^{57}Fe/^{56}Fe$.

The data obtained in May-June 1989 also provides a possibility to set up an upper limit on a fraction of the $^{22}Na$ and $^{44}Ti$ radioactive photons in the X-ray 45-105 keV flux from SN1987A in 830 days after the explosion. The corresponding upper limits at three standard deviation levels on mass of $^{22}Na$ and $^{44}Ti$ contained in the envelope at the moment of explosion are $1.3 \cdot 10^{-3}M_\odot$ and $9 \cdot 10^{-3}M_\odot$. These limits exceed the amount of $^{44}Ti$, $M_{44} \sim 1.2 \cdot 10^{-4}M_\odot$, and $^{22}Na$, $M_{22} \sim 3 \cdot 10^{-5}M_\odot$, predicted by Hashimoto *et al.* (1989) and Woosley *et al.* (1986) on the basis of the explosive nucleosynthesis calculations at one order of magnitude.

## LIMITS ON THE STELLAR REMNANT LUMINOSITY

The observations of the Roentgen observatory in May-June 1989 set up strong restrictions on X-ray luminosity of a stellar remnant produced during the explosion $L_x(1\text{-}6\ keV) \leq 3.6 \cdot 10^{36}$, $L_x(6\text{-}15\ keV) \leq 5.4 \cdot 10^{36}$ and $L_x(15\text{-}105\ keV) \leq 1.35 \cdot 10^{37}$ erg/s for the assumed distance 55 kpc (Sunyaev *et al.* 1990, Table 1). At that time a Thomson optical depth of the envelope yet exceeded 3-4, and an X-ray spectrum of the remnant was considerably distorted by photoabsorption and compton scattering. The absorbed energy went on the envelope heating and was reemitted in the infrared, submillimeter, and optical bands. The measurements by Bouchet *et al.* (1990) showed that emission of dust in the envelope had a black body spectrum with $T \simeq 160K$, and the supernova bolometric luminosity in 1030 days after the explosion was equal to $(2.0\text{-}0.1) \cdot 10^{38}$ erg/s. Using data from Monte Carlo calculations, the upper limit on the hard X-ray flux in the 15-105 keV band obtained by the HEXE device on the 830th day and the information on the envelope emission at low frequencies indicate that rather interesting restrictions on an intrinsic spectrum of the stellar remnant may be obtained. For example, assuming that the remnant (pulsar) has a power law spectrum in 1-1000 keV energy band, $I_\nu \sim \nu^{-\alpha}$ [photons $\cdot$ $cm^{-2}s^{-1}keV^{-1}$], and using the $3\sigma$ upper limit presented above for the X-ray 15-105 keV flux escaping the envelope on the 830th day, we obtain the $3\sigma$ upper limit on the pulsar luminosity in the 1-1000 keV energy band $L_B \leq 2.4 \cdot 10^{38}$ and $\leq 4.4 \cdot 10^{38}$ erg/s for two spectral indexes $\alpha = 1.5$ and 2.1. In neglecting the pulsar spindown and its luminosity changing we may find the upper limit on the energy absorbed in the envelope, that is,

its low frequency luminosity on the 1100th day $L_{IR} \leq 1.0 \cdot 10^{38}$ and $3.5 \cdot 10^{38}$ erg/s for $\alpha + 1.5$ and 2.1 correspondingly. It is clear that in the case when the spectral index is 1.5, such a spectrum is not able to give the observed low frequency luminosity of the envelope. It may be easily shown that any spectrum with $\alpha \leq 1.75$ does not coincide with the data obtained by Bouchet *et al.* (1990).

The presented example shows a possibility for using our data to obtain restrictions on parameters of a pulsar hidden inside the expanding envelope. In the case when an accreting object is situated in the envelope center our estimates are less definite. Nevertheless, such an analysis, using the HEXE data presented above, for the object with a spectrum similar to the spectrum of the well-known source Cygnus X-1 in a low state (Sunyaev and Truemper 1979), also demonstrates the impossibility of satisfying the low frequency data. If the infrared radiation is the result of dust, the reprocessing of a central object with hard emission from the X-ray spectrum of the stellar remnant should be soft enough.

Another way to explain the excess of infrared radiation detected by Bouchet *et al.* (1990) is that radioactive isotopes $^{57}$Co, $^{22}$Na and $^{44}$Ti are more abundant in the envelope than it was assumed. Their hard radioactive emission transforms in the opaque envelope into the low frequency emission which was observed. As the excess luminosity on the 1100th day after the explosion was equal to $2 \cdot 10^{38}$ erg/s it was necessary that about $4 \cdot 10^{-2} M_\odot$ of $^{57}$Co (that is the $^{57}$Co/$^{56}$Co ratio exceeded the Earth's $^{57}$Fe/$^{56}$Fe ratio about 22 times), or $9 \cdot 10^{-4} M_\odot$ of $^{22}$Na, or $9 \cdot 10^{-3} M_\odot$ of $^{44}$Ti were hidden inside the envelope. Comparing these values with the HEXE upper limits for $^{57}$Co, $^{22}$Na, and $^{44}$Ti abundances, $M_{57} \leq 2.8 \cdot 10^{-3} M_\odot$ and $M_{44} \leq 9 \cdot 10^{-3} M_\odot$, $M_{22} \leq 1.3\ 10^{-3}\ M_\odot$, we come to the conclusion that the assumption about the radioactive nature of excess has failed in the case of $^{57}$Co and is unlikely in the case of $^{44}$Ti and $^{22}$Na.

## TTM/COMIS UPPER LIMITS ON THE FLUX FROM SN1987A

The TTM/COMIS instrument on board the Kvant module is a coded mask-imaging spectrometer, sensitive in 2-30 keV energy, and with $7^\circ.5 \times 7^\circ.5$ FWHM field of view. We present below some results of the analysis of LMC field observations in November 1988-June 1989.

During this period about 130 sessions of LMC observations were performed. After the rejection of telemetric drop-outs and sessions with poorly defined pointing, the total exposure time for the observations analyzed here was $\sim$ 75,400 s.

A slice of TTM image ($7^\circ.8$ by $3^\circ.4$) in three energy bands is presented on Figure 5. This image was obtained by combining all the data of the period November 1988-June 1989. The sources LMC X-1, LMC X-2, LMC

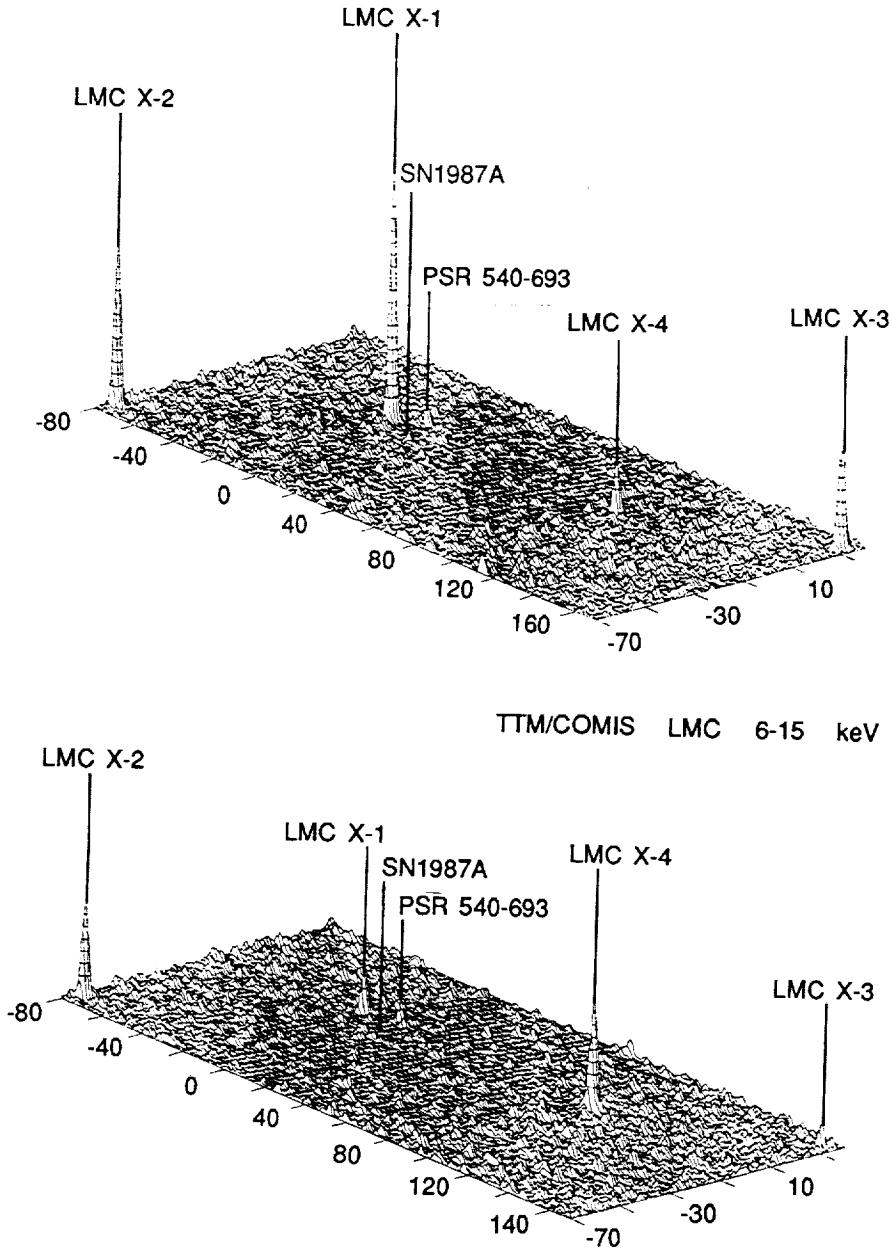


FIGURE 5 The 7°.8 by 3°.4 slices of LMC images in three different energy bands (2-6, 6-15, and 15-27 keV) obtained by TTM instrument during the observations of November 1988 - June 1989. The labels mark significantly detected LMC sources as well as the position of SN1987A. Coordinates shown correspond to TTM field of view. One pixel of TTM image has size of 1.86 arcmin.

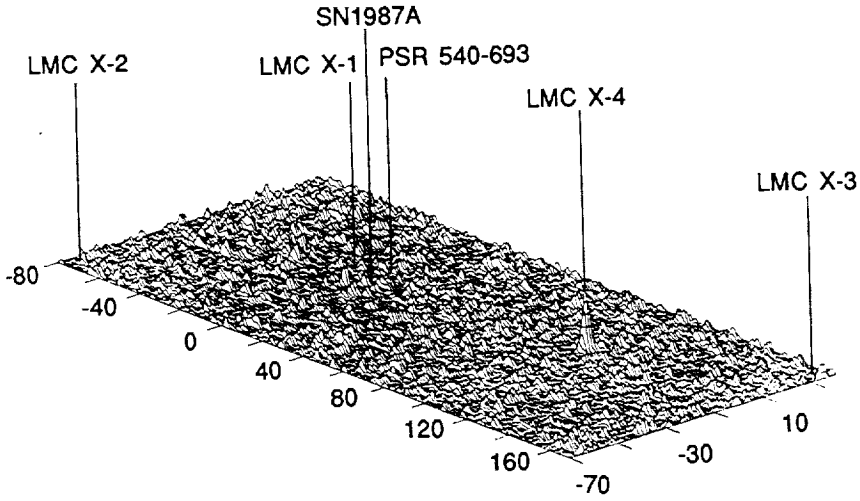


X-3, LMC X-4, and 50-millisecond pulsar PSRO540-693 are significantly detected. These sources are marked on Figure 5 by arrows as well as the position of SN1987A.

The TTM observations of SN1987A in June-August 1987 did not reveal any significant flux from the supernova in 2-30 keV energy band on the level 0.5 mCrab ($3\sigma$) (Sunyaev *et al.* 1987 a,b, 1988) when HEXE and Pulsar X-1 devices onboard Kvant detected strong hard X-ray radiation from the supernova. The further TTM observations of SN1987A were stimulated by the exciting Ginga discovery of the variable continuum of this source in 4-30 keV band (Dotani *et al.* 1987; Masai *et al.* 1987; Masai *et al.* 1988). During observations in November 1988 to June 1989 we again did not detect any significant flux from supernova in any part of 2-30 keV energy band (the efficiency of the TTM detector is highest at $\sim$ 8 keV, and diminishes towards higher and lower energies). The upper limit in the whole 2-27 keV energy band is equal to 0.6 mCrab for Crab-like spectrum. The upper limits obtained in three energy subbands are presented in Table 2.

In each particular session of observations ($\sim$ 1000 sec duration) we obtained an upper limit for the flux in the 2-27 keV band on the level of 5 mCrab. For each week's set of intense observations in November, December, or June, our $3\sigma$ upper limit in the 2-27 keV band is on the level of 1.2 mCrab. This upper limit is twice lower than the January 1988

TABLE 2 Upper limits (3 $\sigma$) of the flux from SN1987A obtained by TTM instrument during the observations in November, 1988 - June, 1989

| Energy (kev) | mCrab[1] | ph/sec/cm$^2$/keV [2] | ergs/sec/cm$^2$ [2] |
|---|---|---|---|
| 2 – 6 | 0.8 | $4 \cdot 10^{-4}$ | $1.0 \cdot 10^{-11}$ |
| 6 – 15 | 0.9 | $1 \cdot 10^{-4}$ | $1.5 \cdot 10^{-11}$ |
| 15 – 27 | 4.2 | $1 \cdot 10^{-4}$ | $4.0 \cdot 10^{-11}$ |

1) for Crab-like spectrum

2) for flat photons spectrum

outburst detected by Ginga in the same spectral band (Masai *et al.* 1988). Unfortunately, the TTM instrument did not operate when the source in the standard X-ray band, detected by Ginga, was the most bright. The data presented here corresponds to the time when the brightness of this source in hard X-rays decreased. Therefore we can only mention here that during periods of our observations, the standard X-ray band source in SN was in a relatively quiescent state with no outbursts of the January 1988 type.

All the HEXE upper limits for the September 1988 to June 1989 time span are below the TTM 3$\sigma$ upper limits for the 16-17 keV band for any power law extrapolation of detected HEXE flux towards lower energies with photon spectral index $\alpha > -4.5$.

The change in shape of the SN1987A spectrum, according to the HEXE data, in September 1988 undoubtedly shows that any flux at energies lower than 40 keV has an origin unrelated to the radioactive decay of both $^{56}$Co and $^{57}$Co. This fact makes a search for the flux from SN1987A in the standard X-ray band of enormous importance because it opens the way to discover X-ray emissions of a different, unknown nature, and therefore is more attractive for further investigation.

## CONCLUSION

All the data obtained by the four HEXE detectors in August 1987 to January 1988 confirm the identification of the hard X-ray source in the Large Magellanic Cloud having an unusual spectrum (see Figure 6) with SN1987A. The upper limits at 3$\sigma$ level obtained during this localization on the X-ray fluxes from LMC X-1 and 50-millisecond pulsar PSR 0540-693 are presented in Table 3.

In May-June 1989, the Kvant module did not detect a statistically

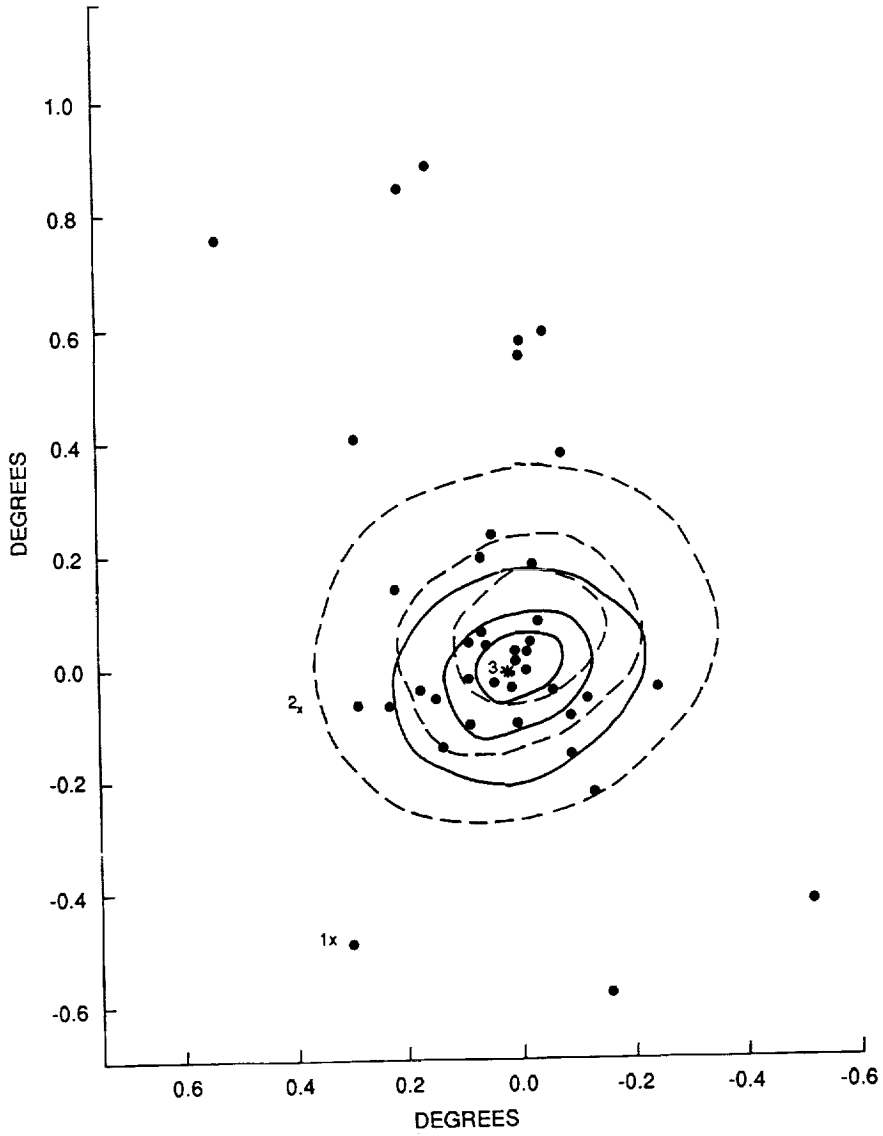


FIGURE 6 Localization of the hard X-ray source in the Large Magellanic Cloud according to the HEXE data obtained from August 1987 to January 1988. The contours of 67%, 99%, and 99.9% significance for the energy bands 15-45 (dotted lines) and 45-105 keV (solid lines) are presented. Positions of the sources LMC X-1 (1), PSR 0540-693 (2), SN1987A (3) are marked. Pointings of the HEXE device in different series of observations are shown by small crosses.

TABLE 3 The upper limits on the X-ray fluxes (in photons $\cdot cm^{-2}\ s^{-1}\ keV^{-1}$) from LMC X-1 and PSR 0540-693 at three standard deviation level in accordance with the HEXE data obtained in 1987 August - 1988 January. They were reconstructed during localization used a number of offset observations

| Source | 15-45 keV | 45-105 keV |
|---|---|---|
| LMC X-1 | $5.5 \cdot 10^{-5}$ | $8.0 \cdot 10^{-6}$ |
| PSR 0540-693 | $2.9 \cdot 10^{-5}$ | $6.8 \cdot 10^{-6}$ |

confident signal from the SN1987A region in spite of other X-ray sources LMC X-1 and PSR 0540-693 having been in the HEXE field of view. Taking into account the deviations between the direction of the telescope axis and directions on these X-ray sources, an efficiency of the flux detecting from different sources differed. The upper limits on the fluxes from SN1987A and other sources are presented in Figure 1 and 7 and also in Table 4.

The weakness of the hard X-ray flux from LMC X-1 in May-June 1989 (Sunyaev *et al.* 1989) and the closeness of the upper limit on the LMC X-1 hard emission obtained by the HEXE device to limits obtained during the HEAO A2 (Wait and Marshall 1984) and HEAO A4 (Matteson and Peterson 1987) experiments, testify to a small portion of the LMC X-1 flux to the flux detected by the Kvant module during August 1987 to April 1988. Note that the flux detected in January 1988 exceeds the upper limits obtained in May-June 1989 are about one order of magnitude.

Note in conclusion that the supernova light curve in 45-105 keV energy band did not show a single sharp statistically donfident burst similar to the burst observed by the Ginga satellite in January 1988 in the softer energy band. In hard X-rays the light curve was smooth as it was expected for the light curve of the source connected with radioactive decay.

## ACKNOWLEDGEMENTS

The authors are grateful to V.D. Blagov, V.M. Loznikov, V.G. Rodin, A.M. Prudkoglyd, the team headed by Yu.P. Semenov, and the cosmonauts working aboard the Mir space station for the observatory control.

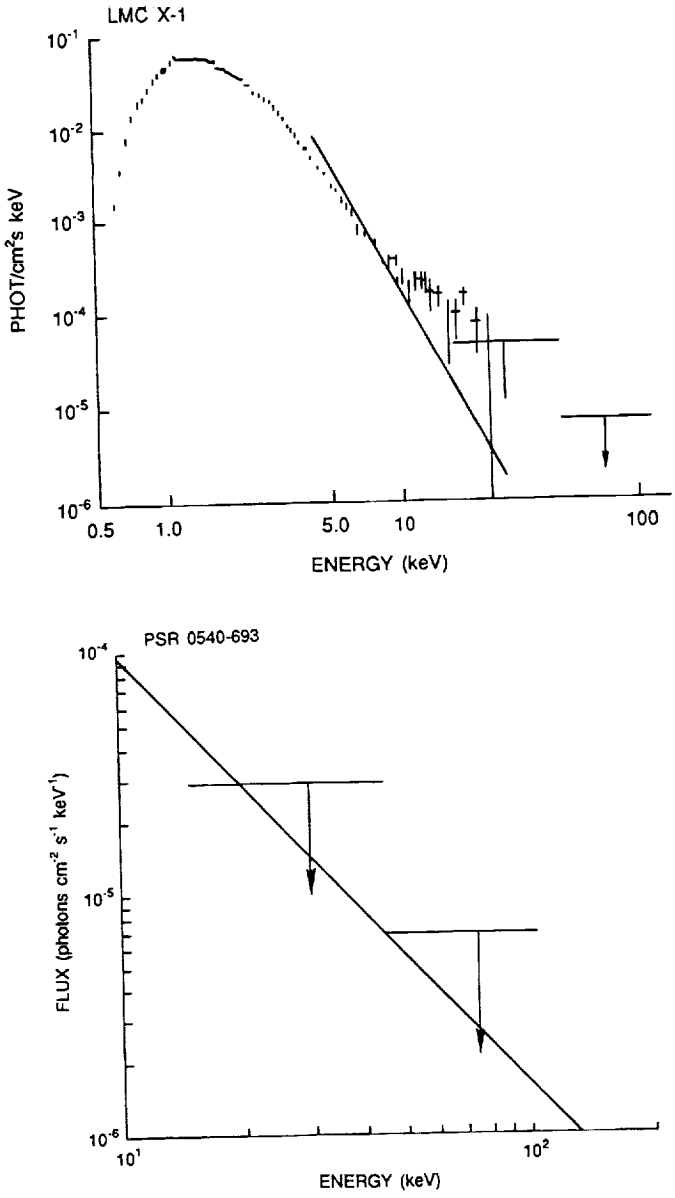


FIGURE 7 (a) Spectrum of LMC X-1 according to the HEAO A2 experiment (crosses) (Wait *et al.* 1984). The upper limits on the hard X-ray flux from this source according to the HEXE data. The analytical approximation of the TTM instrument data is shown by a solid line (Sunyaev *et al.* 1990). (b) Spectrum of PSR 0540-693 (a power law approximation) in accordance with the observatory Einstein (Clark *et al.* 1982; Seward *et al.* 1984) and the upper limits on the hard X-ray flux according to the HEXE data. The spectrum obtained by the TTM instrument (Sunyaev *et al.* 1990) coincides with the presented power law approximation within the limits of experimental data errors.

TABLE 4 The average efficiencies of the observatory Roentgen pointing and the corresponding upper limits at three standard deviation levels on the X-ray fluxes (in photons $\cdot cm^{-2} s^{-1} keV^{-1}$) from the LMC sources observed by the HEXE device in 1989 May-June.

| Source | Efficiency | 15-45 keV | 45-105 keV |
|---|---|---|---|
| SN1987A | 52 % | $2.1 \cdot 10^{-5}$ | $8.6 \cdot 10^{-6}$ |
| LMC X-1 | 32 % | $8.5 \cdot 10^{-5}$ | $1.2 \cdot 10^{-5}$ |
| PSR 0540-693 | 45 % | $3.4 \cdot 10^{-5}$ | $9.5 \cdot 10^{-6}$ |

## REFERENCES


Arnett, W.D. 1988. Astrophys. J. 331:377.
Arnett, W.D, B.A. Fryxell, and E. Muller. 1989. Astrophys. J. Letters 341:L63.
Bouchet, P., I.J. Danziger, and L.B. Lucy. 1990. IAU Circ. No. 4933.
Cameron, A.J.W. 1986. Page 33. In: Barnes, C.A., D.D. Clayton, and D.N. Schramm (eds.). Nuclear Astrophysics. Moscow: Mir.
Clark, D.H., I.R. Tuohy, K.S. Long, *et al.* 1982. Astrophys. J. 255:440.
Dotani, T, K. Hayashida, H. Inoue, *et al.* 1987. Nature 330:230.
Ebisuzaki, T, and N. Shibazaki. 1988. Astrophys. J. Letters 327:L5.
Englhauser, J., S. Doebereiner, E. Pietsch, *et al.* 1989. 23d ESLAB Symp. Proc.
Erickson, E.F., M.R. Haas, S.W.J. Colgan, *et al.* 1988. Astrophys. J. Letters 330:139.
Grebenev, S.A., and R.A. Sunyaev. 1988. Soviet Astron. Letters 14:675.
Hachisu, I., T Matsuda, K. Nomoto, and T Shigeyama. 1990. Astrophys. J. Letters. In press.
Hashimoto, M., K. Nomoto, and T Shigeyama. 1989. Astron. Astrophys. 20:L5.
Itoh, M., S. Kumagai, T Shigeyama, *et al.* 1987. Nature 330:233.
Masai, K., S. Hayakawa, H. Itoh, *et al.* 1987. Nature 330:235.
Masai, K., S. Hayakawa, H. Inoue, *et al.* 1988. Nature 335:804.
Matteson, J.L., and L.E. Peterson. 1987. Private communication.
Matz, S.M., G.H. Share, M.D. Leising, *et al.* 1988. Nature 331:416.
Pinto, P.a., and S.E. Woosley. 1988. Astrophys. J. 329:820.
Rester, A.S., R.L. Coldwell, F.E. Dunnam, *et al.* 1989. Astrophys. J. Letters 342:L71.
Seward, F.D., F.R. Harnden, and D.J. Helfand. 1984. Astrophys. J. Letters 287:L19.
Sunyaev, R.A., A.S. Kaniovsky, V.V. Efremov, *et al.* 1987a. Nature 330:227.
Sunyaev, R.A., A.S. Kaniovsky, V.V. Efremov, *et al.* 1987b. Soviet Astron. Letters 13:1027.
Sunyaev, R.A., V.V. Efremov, A.S. Kaniovksy, *et al.* 1988. Soviet Astron. Letters 14:579.
Sunyaev, R.A., A.S. Kaniovsky, V.V. Efremov, *et al.* 1989. Soviet Astron. Letters 15:291.
Sunyaev, R.A., M.R. Gilfanov, E.M. Churazov, *et al.* 1990. Soviet Astron. Letters. In press.
Sunyaev, R.A., and J. Truemper. 1979. Nature 279:506.
White, N.E., and F.E. Marshall. 1984. Astrophys. J. 281:354.
Woosley, S.E., and T.A. Weaver. 1986. Page 359. In: Barnes, C.A., D.D. Clayton, and D.N. Schramm (eds.). Nuclear Astrophysics. Moscow: Mir.

# Basic Physics and Cosmology from Pulsar Timing Data

J. H. TAYLOR
Princeton University

## ABSTRACT

Radio pulsars provide unparalleled opportunities for making measurements of astrophysically interesting phenomena. In this paper I concentrate on two particular applications of high precision timing observations of pulsars: tests of relativistic gravitation theory using the binary pulsar 1913+16, and tests of cosmological models using timing data from millisecond pulsars. New upper limits are presented for the energy density of a cosmic background of low frequency gravitational radiation.

## INTRODUCTION

Among the nearly 500 radio pulsars that have been discovered since 1967, some of the most rewarding to study have been the binary and millisecond pulsars. Like all radio pulsars, these spinning neutron stars are rotationally powered: that is, their energetics are dominated by their spindown luminosities, $\dot{E} = I\omega\dot{\omega}$. Their evolution has been modified, however, by spinup in a "recycling" process involving mass transfer from a companion star during its post-main-sequence evolution.

Recycled objects make up a small fraction of any sensitivity-limited pulsar sample. Fewer than 20 are presently known, and most of them are still members of gravitationally bound binary systems. Their typical rotation periods are substantially shorter than those of other pulsars, and detailed measurements of the arrival times of their pulses at Earth have provided observers with a wealth of information on a surprisingly diverse range of topics. In this paper I will summarize the present status of two particular

applications of timing observations of recycled pulsars: the detection and quantitative measurement of orbital decay caused by gravitational radiation from the binary pulsar 1913+16; and experimental limits on the cosmic gravitational wave background (GWB), based on timing observations of millisecond pulsars 1855+09 and 1937+21.

## TESTING RELATIVITY WITH PSR 1913+16

The first binary pulsar was found nearly 15 years ago, and its importance as a testbed for relativistic gravitation theories was recognized almost immediately (Hulse and Taylor 1975; see also Brumberg *et al.* 1975; Damour and Ruffini 1974; Esposito and Harrison 1975; Wagoner 1975). In the intervening years, much effort has been put into making increasingly accurate measurements of its pulse arrival times and comparing the results with parametrized models. Adequate models must include physics having to do with the pulsar's spin and orbit, the interstellar medium, and the motions of the Earth. Optionally, a model may also include phenomenological parameters designed to distinguish between different theories of gravitation. Diligent efforts on the part of both theorists and observers, aimed toward extracting the maximum possible information from the PSR 1913+16 system, have been well rewarded over the 15 years since its discovery. The latest results, which I summarize briefly here, have determined the orbital elements and masses of the pulsar and its companion star with unprecedented accuracy and established that the orbit is decaying at almost precisely the rate expected from gravitational radiation damping (Taylor and Weisberg 1989).

The PSR 1913+16 timing experiment is conceptually a simple one. Observations made over intervals of about five minutes, or 1% of the 8 hour orbital period, are used to accumulate samples of the periodic waveform received from the pulsar. The pulse profiles are recorded digitally, along with accurate timing information from a reference atomic clock. Subsequent analysis involves determining the equivalent topocentric time of arrival, or TOA, for a pulse near the midpoint of each integration. The complete set of TOAs is then analyzed in terms of a set of equations describing the pulsar's spin and orbital motions and the motions of the Earth. These equations are most naturally expressed in the coordinate system of an inertial reference frame, for which the solar system barycenter serves as an adequate approximation.

Necessary steps in the analysis include a relativistic transformation to convert topocentric TOAs to equivalent coordinate times at the solar system barycenter, and then to proper times at the pulsar. Through this procedure, the rotational phase of the spinning neutron star is computed for each of the measured arrival times. If reasonably accurate starting values

are available for the model parameters, the computed phases (expressed in cycles) will have integer parts corresponding to the number of pulse periods elapsed between observations, and fractional parts nearly equal to zero. Small systematic deviations of the fractional parts from zero are used to refine the model parameters, using standard linearized least squares techniques.

Blandford and Teukolsky (1976) derived the first useful formulae for analyzing TOAs from binary pulsars. They treated the orbit as a slowly precessing Keplerian ellipse; the effects of relativistic time dilation and gravitational redshift were grafted onto the non-relativistic model, and additional phenomenological parameters were added to allow measurement of the rate of periastron precession and testing the constancy of other orbital parameters. More elaborate models have been developed since 1976, and a thorough discussion of these is given by Taylor and Weisberg (1989). The most comprehensive treatment is that of Damour and Deruelle (1986), which uses a parametrization that cleanly separates several effects expected to differ in the strong-field limits of distinct gravitation theories.

As is the case for single-line spectroscopic binary stars, a Keplerian analysis of timing data from a binary pulsar determines the values of five orbital parameters. However, seven quantities are required to fully specify the dynamics of an orbiting system (up to uninteresting rotations about the line of sight). Therefore the measurement of $N$ "post-Keplerian" parameters in a binary pulsar system, in addition to the five readily measured Keplerian ones, provides the opportunity for $N - 2$ distinct tests of any particular theory of relativistic gravitation.

More than 4000 TOAs for PSR 1913+16 have been recorded at the Arecibo Observatory since 1974. Taylor and Weisberg (1989) have shown that the Keplerian parameters of the system are now determined with fractional accuracies of a few parts per million or better, and that as many as 5 post-Keplerian parameters are measurable with interesting accuracies. The two largest of these, which measure the rate of periastron advance and the combined magnitude of time dilation and gravitational redshift effects, are known with fractional accuracies of about $10^{-5}$ and $2 \times 10^{-3}$. Together, these seven quantities imply that the gravitational masses of the pulsar and its companion are $m_1 = 1.442 \pm 0.003$ and $m_2 = 1.386 \pm 0.003$ times the mass of the Sun, respectively. These masses, together with the orbital period and eccentricity, can be used to compute an explicit prediction for the energy losses caused by gravitational radiation within a particular theory of gravity.

Figure 1 presents a comparison of the observed orbital damping with that predicted by general relativity. Taylor and Weisberg (1989) show that the ratio of observed to expected effects is

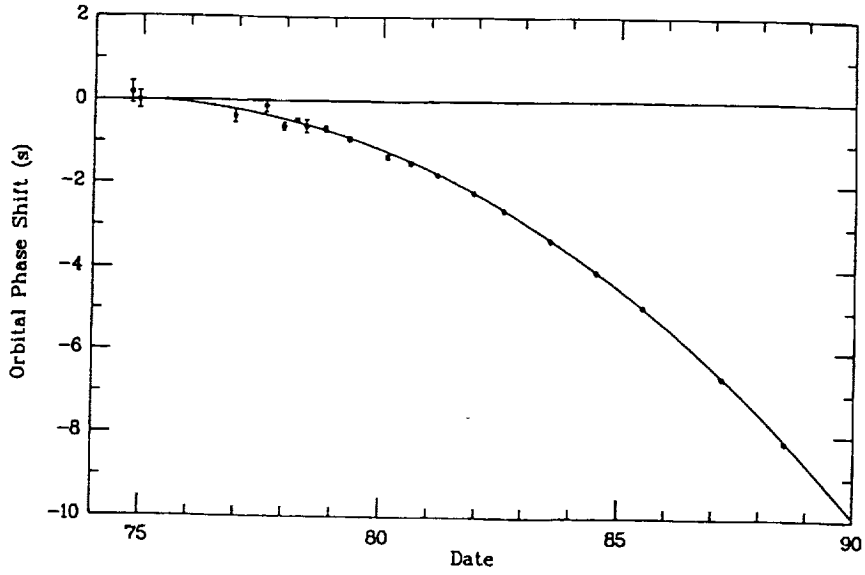


FIGURE 1 Filled circles represent the measured shifts of the times of PSR 1913+16's periastron passage relative to a non-dissipative model in which the orbital period remains fixed at its 1974.78 value. The smooth curve illustrates the prediction of general relativity. (After Taylor and Weisberg 1989.)

$$\frac{\dot{P}_b \text{ (Observed)}}{\dot{P}_b(\text{GR Theory}) = 1.010 \pm 0.011,}$$

where $\dot{P}_b$ is the rate of change of orbital period. This 1% agreement is an impressive confirmation of Einstein's theory, in a regime where gravitation theories have not previously been testable. The remaining post-Keplerian measurables have fractional accuracies of only ~ 10–50%, but it is notable that they, too, have been found to have values in accord with general relativity.

## THE COSMIC GRAVITATIONAL WAVE BACKGROUND

Millisecond pulsars, the most extreme examples of the recycled class, have periods as short as $P \approx 1.5$ ms and spindown rates as small as $\dot{P} \approx 10^{-20}$. According to conventional models, these parameters suggest unusually large ages and weak magnetic fields. Otherwise, however, the millisecond pulsars appear to be quite similar to their more slowly rotating cousins. Because pulsar timing accuracies tend to be a fixed fraction ($\sim 10^{-4}$ to $10^{-3}$) of a period, observations of millisecond pulsars

can provide results two to three orders of magnitude more precise than those from ordinary pulsars. For these reasons, millisecond pulsars make exquisite probes of any astrophysical phenomena that modulate the effective propagation time of pulsar signals as they travel toward Earth. One such phenomenon is a possible stochastic, isotropic background of gravitational radiation, such as might have been produced in the early universe through quantum gravity effects (Starobinsky 1979), a QCD phase transition from free quarks into nucleons (Witten 1984), or oscillating cosmic strings (Hogan and Rees 1984).

The use of pulsar timing data to detect or place limits on long wavelength gravitational radiation was suggested about 10 years ago (Sazhin 1978; Detweiler 1979) and put into practice a few years later (Romani and Taylor 1983; Hellings and Downs 1983). The basic idea is to treat the Earth and a pulsar as free masses, whose positions respond to changes in the instantaneous spacetime metric in their vicinities. Gravitational waves of sufficient amplitude will perturb the metric and thereby produce detectable fluctuations in the measured pulse arrival times. It is easy to show that the energy density in gravitational waves is proportional to the square of their contribution to the observed TOAs, and that the system has its most useful sensitivity to waves with frequencies $f \approx 1/\tau$, where $\tau$ is the time spanned by the data (see, for example, Witten 1984; Blandford *et al.* 1984).

Examples of the timing data for the millisecond pulsars 1937+21 and 1855+09 are presented in Figure 2. These graphs illustrate post-fit residuals, or differences between observed TOAs and those expected according to fitted models after all known instrumental corrections have been applied. Subsets of these data have been presented in earlier published works, and used to place limits on the energy density of the cosmic GWB (Davis *et al.* 1985; Rawley *et al.* 1987).

As shown by Romani and Taylor (1983), limits on the cosmic GWB from pulsar timing can be improved substantially by means of spectral analysis of the residuals. A distinct advantage of this approach is that spectral information can help to distinguish among various possible contributions to the total variance in the residuals. If the power spectrum of fluctuations is defined as $P(f)$ and modeled as a power law $P(f) = P_0 f^{-s}$, we expect that uncorrelated random measurement errors will exhibit a flat spectrum, with $s = 0$. In contrast, fluctuations caused by clock instabilities and errors in the solar system ephemeris will likely have $s \approx 2$; propagation through density irregularities in the interstellar medium will contribute noise with $s \approx 3$; and in most models the GWB is expected to have the steepest spectrum of all, with $s = 5$. Further details concerning expected spectral properties may be found in the paper by Blandford *et al.* (1984).

Transformation of the timing residuals to the spectral domain has a

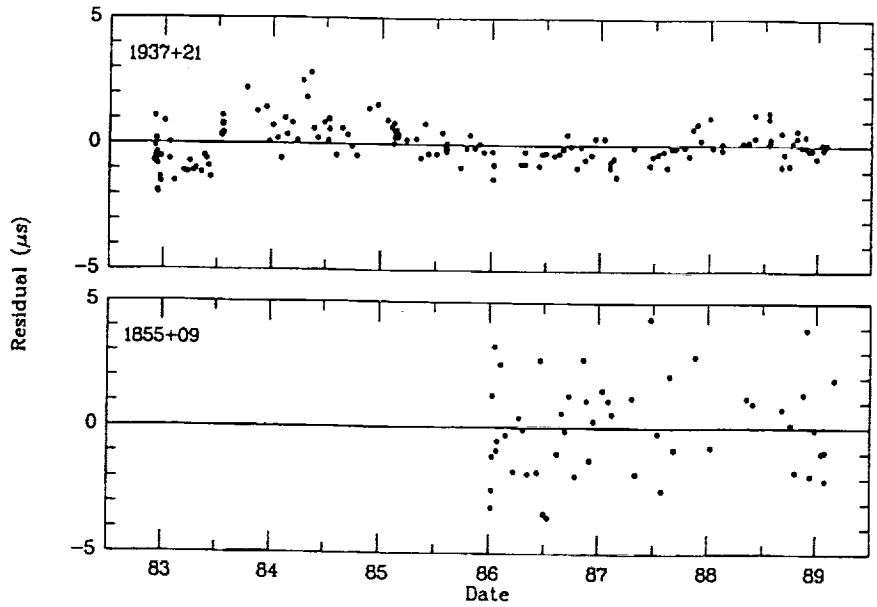


FIGURE 2 Timing residuals for PSRs 1937+21 and 1855+09 from observations made at Arecibo, Puerto Rico. Data quality has been uniform since the introduction of new equipment and procedures in October, 1984.

further important advantage: it facilitates making quantitative corrections for the complex instrumental response caused by irregular sampling and finite length of the data sets. Following Blandford *et al.* (1984), I define an instrumental response function $T(f)$ such that the observed spectrum of timing residuals is $S(f) = T(f)P(f)$: the product of the instrumental response and the intrinsic noise spectrum, $P(f)$. As illustrated in Figure 3, the most important features of $T(f)$ are a low frequency cutoff below $f \approx \tau^{-1}$ and a deep notch centered at $f = 1\ \mathrm{yr}^{-1}$, caused by the necessity to measure the celestial coordinates of the pulsar as part of the least-squares fitting process.

To make it easy to compare the observed fluctuation spectra with hypothetical intrinsic spectra, I have multiplied the computed $T(f)$ curves by power law spectra with $s = 0$, 2, 3, and 5. For convenience in plotting, the results were then normalized to the mean power level in the two lowest frequency channels of the observed spectra, $S(f)$. At the top of Figure 4, we see that the spectrum for PSR 1855+09 is reasonably well approximated by the spectrum labeled $s = 0$. In other words, there is no evidence for a significant contribution to these residuals beyond that of the random measurement errors. The equivalent mass density in a cosmic GWB corresponding to the dashed curve labeled $s = 5$ is $\rho = 2.2 \times 10^{-36}\ \mathrm{g\ cm^{-3}}$,

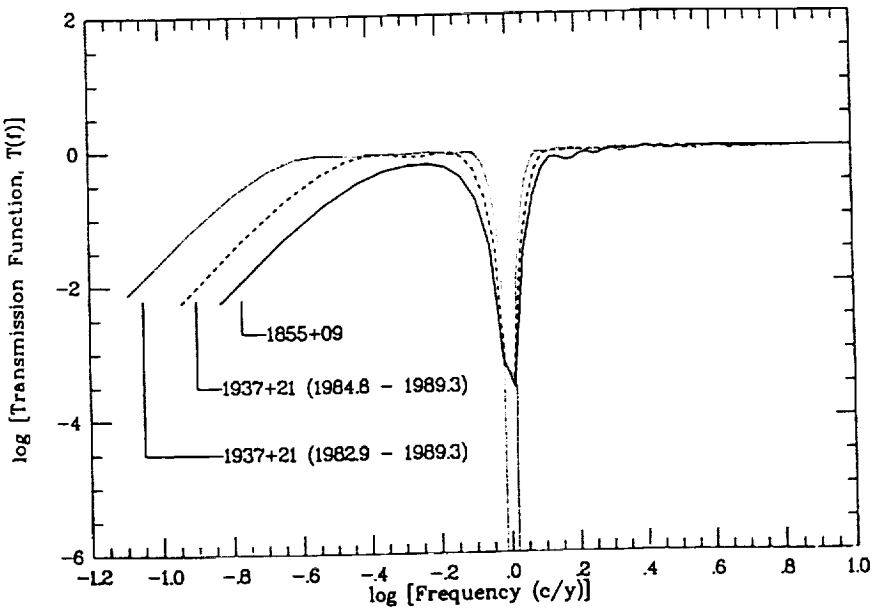


FIGURE 3 Instrumental transmission functions, T(f), corresponding to the data sets illustrated in Figure 2.

or $\Omega_g = 1.1 \times 10^{-7}$ for a Hubble constant $H_0 = 100$ km s$^{-1}$ Mpc$^{-1}$. The observed power in the lowest spectral channel is well below this curve, and yields the conservative upper limit for the GWB quoted in the first line of Table 1.

In the center and bottom portions of Figure 4 are similar plots showing the observed spectra for the data from PSR 1937+21, together with instrumentally-modified power laws. The spectrum at the center of the figure corresponds to the uniform, high-quality data obtained since October 1984, while the bottom plot corresponds to the entire 6.4 yr data span. In both of these spectra the frequencies $f \gtrsim 2$ yr$^{-1}$ are clearly dominated by white noise ($s = 0$), while lower frequencies show clear signs of contributions with $s > 0$. Although further analysis remains to be done, my colleagues and I believe that at frequencies $f < 1$ yr$^{-1}$ these spectra are dominated by a combination of clock errors, solar-system ephemeris errors, and unmodeled interstellar propagation effects. In any event, it is clear that if a cosmic GWB makes any significant contribution, it must be greatest in the lowest frequency channel of each spectrum. The dashed curves labeled $s = 5$ in the middle and bottom of Figure 4 correspond to fractional densities $\Omega_g = 3.8 \times 10^{-8}$ and $1.4 \times 10^{-8}$, respectively, and their positions

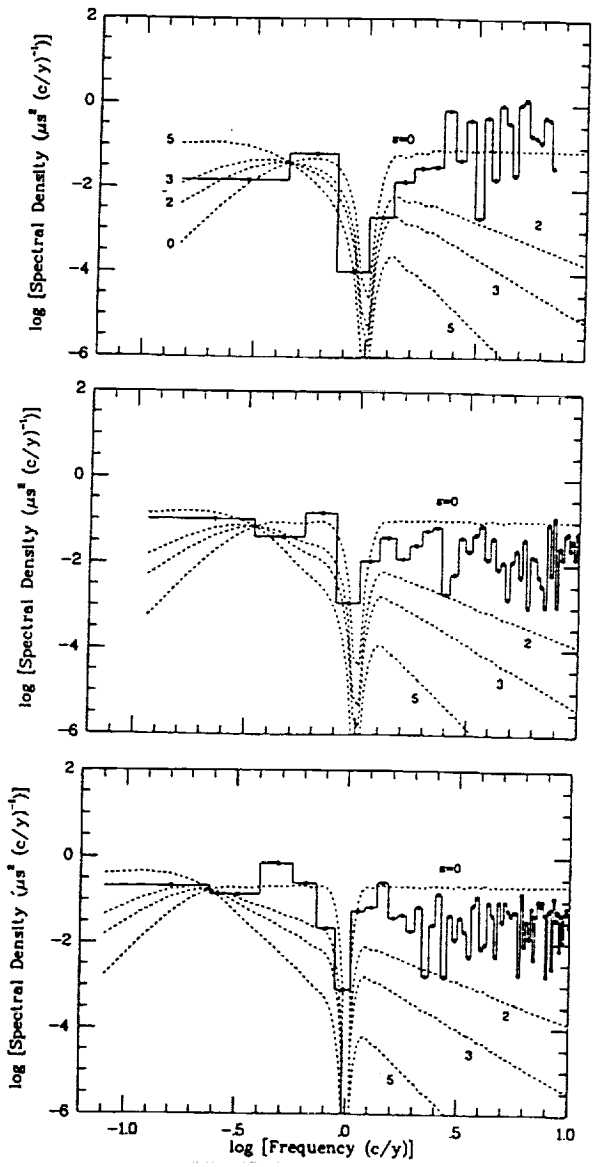


FIGURE 4 Solid lines and filled circles: observed residual spectra, S(f), corresponding to the data sets illustrated in Figure 2. Dashed curves: hypothetical power-law spectra modified by the instrumental response functions T(f), and arbitrarily normalized to the mean power level in the lowest two bins of S(f).

Table 1: Upper limits on the energy density of the cosmic GWB.

| Pulsar | Data span | $f, \Delta f$ ($\mathrm{yr}^{-1}$) | $\rho$ ($\mathrm{gm\ cm}^{-3}$) | $\Omega_g$ ($H_0 = 100$) |
|---|---|---|---|---|
| 1855+09 | 1984.8–1989.3 | 0.30 | $< 1.2 \times 10^{-36}$ | $< 6 \times 10^{-8}$ |
| 1937+21 | 1984.8–1989.3 | 0.22 | $< 1.6 \times 10^{-36}$ | $< 8 \times 10^{-8}$ |
| 1937+21 | 1982.9–1989.3 | 0.16 | $< 0.8 \times 10^{-36}$ | $< 4 \times 10^{-8}$ |

relative to the measured spectra lead to the remaining conservative upper limits quoted in Table 1.

The detailed implications of the numbers quoted in Table 1, particularly for model universes in which cosmic strings help to seed galaxy formation, are still somewhat controversial (Albrecht and Turok 1989; Bennett and Bouchet 1989). It is already clear, however, that the experimental limits are difficult to reconcile with the GWB energy density expected from cosmic string simulations, particularly when the strings retain sizes large enough to be useful in aiding galaxy formation.

## ACKNOWLEDGMENTS

Parts of this work were carried out in collaboration with L. A. Rawley, M. F. Ryba, D. R. Stinebring, and J. M. Weisberg. Our research is supported, in part, by the U.S. National Science Foundation.

## REFERENCES

Albrecht, A., and N. Turok. 1989. Phys. Rev. Lett., submitted.
Bennett, D.P., and F.R. Bouchet. 1989. Phys. Rev. Lett., submitted.
Blandford, R., R. Narayan, and R. Romani. 1984. J. Astrophys. Astr. 5: 369.
Blandford, R.D., and S.A. Teukolsky. 1976. Astrophys. J. 205: 580 (BT).
Brumberg, V.A., Ya.B. Zel'dovich, I.D. Novikov, and N.I. Shakura. 1975. Astr. Letters 1: 5.
Damour, T., and N. Deruelle. 1986. Ann. Inst. H. Poincaré (Physique Théorique) 44: 263 (DD).
Damour, T., and R. Ruffini. 1974. C. R. Acad. Sci. (Paris) 279: A971.
Davis, M.M., J.H. Taylor, J.M. Weisberg, and D.C. Backer. 1985. Nature 315: 547.
Detweiler, S. 1979. Astrophys. J. 234: 1100.
Esposito, L.W., and E.R. Harrison. 1975. Astrophys. J. (Letters) 196: L1.
Hellings, R.W., and G.S. Downs. 1983. Astrophys. J. (Letters) 265: L39.
Hogan, C.J., and M.J. Rees. 1984. Nature 311: 109.
Hulse, R.A., and J.H. Taylor. 1975. Astrophys. J. (Letters), 195: L51.
Rawley, L.A., J.H. Taylor, M.M. Davis, and D.W. Allan. 1987. Science 238: 761.
Romani, R.W., and J.H. Taylor. 1983. Astrophys. J. 265: L35.
Sazhin, M.V. 1978. Soviet Astronomy–AJ 22: 36.
Starobinsky, A.A. 1979. Soviet Physics–JETP Letters 30: 682.
Taylor, J.H., and J.M. Weisberg. 1989. Astrophys. J. In press.
Wagoner, R.V. 1975. Astrophys. J. (Letters) 196: L63.
Witten, E. 1984. Phys. Rev. D30: 272.

# Gas Flow and Generation of X-Ray Emission in WR + OB Binaries

V.V. Usov
Institute of Space Research

## ABSTRACT

The supersonic flow of the ionized gas in WR+OB binaries and X-ray generation are considered. X-ray emission is caused by gas heating up to temperatures of $10^7$-$10^8$ K behind the front of shock waves. These are formed in the collision of gas flowing out from the WR star with either the OB star's surface or the gas of the OB star's wind. The distribution of temperature and concentration behind the shock front are obtained. Using these distributions, the spectral power of bremsstrahlung X-ray emission of hot gas is calculated. Possible reasons that lead to considerable difference between the observed parameters of X-ray emission of the WR binary of the V 444 Cygni and the theoretically expected are discussed.

## INTRODUCTION

Wolf-Rayet stars (WR) possess a very intense stellar wind. The mass loss rate for WR stars, $\dot{M}_{WR}$, and the velocity of the matter outflow, $v_\infty^{(WR)}$, far from the star amount to $10^{-5}$ $M_\odot$/year and ~(1-3)·$10^8$ cm/s, respectively. No less than 40% of WR stars belong to rather close binaries. Young massive stars of the spectral type O and B are the second components of these systems. OB stars also possess the intense stellar ($\dot{M}_{OB} \sim 10^{-6} M_\odot$/year, $v_\infty^{OB}$ $10^8$ cm/s). More than a decade ago it was shown by Prilutskii and Usov (1975, 1976) that binary systems consisting of WR and OB stars should be rather strong X-ray sources (the X-ray luminosity can reach about $10^{33}$ to $10^{34}$ erg/s). According to Prilutskii and Usov (1975, 1976) the X-ray emission of such systems is due to heating the gas up to temperatures of

about $10^7$ to $10^8$ K behind the front of shock waves which are formed from the collision of the gas flowing out from a WR star either with the OB star surface or with the gas of the OB star stellar wind. To date, X-ray emission has been observed from more than twenty WR stars (Seward *et al.* 1979; Moffat *et al.* 1982; Caillout *et al.* 1985; Pollock 1987) and at least some of these stars possess X-ray emission of the nature described in Prilutskii and Usov (1975, 1976). Below we will discuss parameters of the X-ray emissions calculated for WR+OB binaries.

## CLASSIFICATION OF THE GAS FLOW IN WR+OB BINARIES

If the intensity of the stellar wind of WR and OB stars are comparable or if the distance D between the components of a binary is great enough (see below) the winds flowing out of WR and OB stars can collide. To estimate approximately the distances $r_{WR}$ and $r_{OB}$ from WR or OB stars, respectively, to the region where these winds meet, it is necessary to put dynamical gas pressures of both winds equal to each other:

$$\rho_{WR}(r_{WR}) \cdot [v_\infty^{(WR)}]^2 = \rho_{OB}(r_{OB}[v_\infty^{(OB)}]^2. \tag{1}$$

Thus we can get

$$\begin{aligned} r_{WR} &\approx \frac{[\dot{M}_{WR} v_\infty^{(WR)}]^{1/2}}{\dot{M}_{WR} v_\infty^{(WR)}]^{1/2} + [\dot{M}_{OB} v_\infty^{(OB)}]^{1/2}} D, \\ r_{OB} &\approx \frac{[\dot{M}_{OB} \bar{v}_\infty^{(OB)}]^{1/2}}{\dot{M}_{WR} v_\infty^{(WR)}]^{1/2} + [\dot{M}_{OB} v_\infty^{(OB)}]^{1/2}} D, \end{aligned} \tag{2}$$

here and below the index $\infty$ means that the given value should be taken at the great distance r from the star where this value is already independent of r.

The velocity of the matter outflow $v_{OB}(r)$ is varying from zero on the OB star surface to $v_\infty^{(OB)}$ for $r > r_*$ (Barlow 1982), where $r_*$ is approximately equal to (3-5)R, R is the OB star radius.

If $r_{OB} > r_*$ the stellar winds collide (see Figure 1). If $r_{OB} < r_*$ the stellar wind from an OB star may be suppressed from the side facing a WR star, and the gas of the WR stellar wind is colliding with the OB star surface. Below we will consider these cases.

## COLLISION OF WR STELLAR WIND WITH OB STAR SURFACE

First, let us discuss the flow of the completely ionized gas, flowing spherically-symmetrically out of a WR star, over an OB star. The effect of the OB star's gravitational field on the gas stream around this star will be

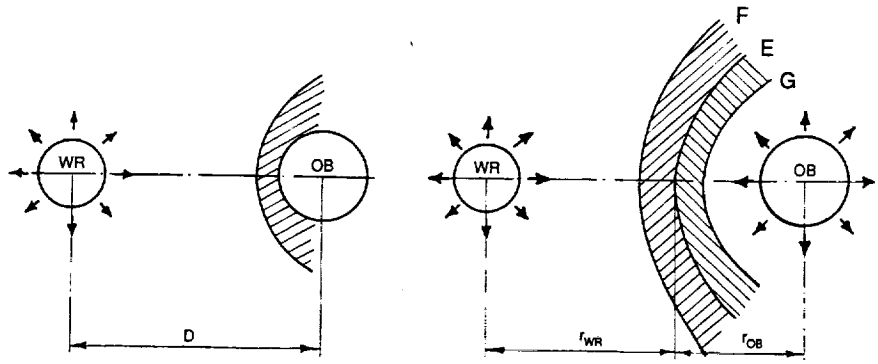


FIGURE 1 Formation of shock waves in WR+OB binaries: a) the flow over an OB star by the gas outflowing from a WR star; b) the collision of two stellar winds; F and G are shock waves; E is the contact surface. The region of hot gas is shaded.

negligible. In this case, since D >> R, the undisturbed gas stream in the vicinity of an OB star can be assumed plane-parallel.

For WR + OB binaries and with typical parameters of WR stars ($v_\infty = 10^8$ cm/s, $\dot{M} = 10^{-5}$ $M_\odot$/year, D = $10^{13}$cm, the stellar wind gas temperature T = $10^5$ K) the parameters of the gas ahead of the shock front in the OB star vicinity will be the following: the gas density $\rho_\infty = 10^{-14}$ g/cm$^3$, the sound speed $v_s = 10^6$ cm/s, the free-path length of particles 1 = $10^9$ cm, the Mach number $M = v_\infty/v_s = 10^2$, and the Reynolds number $Re = (R/1)(v_\infty/v_s) = 10^5$ (here R = 10 $R_\odot$ is the OB star radius). In this Section we will not write the index WR. With the above values of R/D, M, and Re, the gas flow in the shock layer around a star can be suggested to be supersonic, uniform, unviscous, and non-heat conductive.

The set of equations which describes the gas flow between the shock wave and the body will be the continuity equation:

$$div(\rho\vec{v}) = O \tag{3}$$

the momentum equation

$$(\rho\vec{v}\nabla)\vec{v} = -\nabla\rho \tag{4}$$

the energy equation:

$$\rho\vec{v}\nabla H = -Q, \tag{5}$$

where $H=H_o + |\vec{v}|^2/2$

Since the gas in the shock layer is almost totally ionized its pressure $p$ and its specific enthalpy $H_o$ can be expressed as

$$p = (N_+ + N_-)kT = \frac{\rho kT}{m_p \mu}, H_o = \frac{\gamma}{\gamma - 1}\frac{\rho}{\rho}, \tag{6}$$

here $N_+ = \rho/m_p A$ is the concentration of nuclei, $N_+ = N_+ Z$ is the concentration of electrons; A is the atomic weight; Z is their electrical charge; k is the Boltzmann's constant; $m_p$ is the proton mass; $\mu = A/(1+Z)$ is the mean molecular weight; $\gamma$ is the ratio of heat capacities with the constant pressure and the constant volume, equal to 5/3 for the rarefied totally ionized plasma.

Helium predominates in the gas of the WR stellar wind. In this case, $A = 4$; $Z = 2$; $\mu = 4/3$.

The ionized gas heated in the shock layer is emitted mainly due to free-free transitions of electrons in Coulomb fields of ions. Here the energy loss per unit gas volume by radiation is (Hayakawa 1973):

$$Q = \int Q_\nu d_\nu = C_1 N_+ N_- Z^2 T^{1/2} \quad \text{erg/s} \cdot \text{cm}^3 \tag{7}$$

where T is in degrees; $C_1 = 1.42_\odot\ 10^{-27}$ g(T); g(T) is the Gaunt factor which changes slightly with varying T (from 1.1 to 1.45),

$$Q_\nu \approx \frac{C_1 h}{kT^{1/2}} N_+ N_- Z^2 \exp\left[-\frac{h\nu}{kT}\right] erg/s \cdot cm^3 \cdot Hz \tag{8}$$

is spectral power of the bremsstrahlung at a frequency of $\nu$.

Let us now consider the boundary conditions for the set of equations (3) through (5). Gas parameters ahead of the shock front (index 1) and behind (index 2) are interrelated via the Rankine-Hugoniot relations

$$\begin{aligned} \rho_1 v_1^{(n)} &= \rho_2 v_2^{(n)}, \\ P_1 + \rho_1 [v_1^{(n)}]^2 &= \rho_2 + \rho_2 [v_2^{(n)}]^2, \\ v_1^{(\tau)} &= v_2^{(\tau)}, \quad H_1 = H_2. \end{aligned} \tag{9}$$

Indices n and $\tau$ denote the normal and tangential components of the vector $\vec{v}$. The condition $v^{(n)} = 0$ is met on the star surface.

The set (3) to (5) with the boundary conditions (9) can be solved by the method of expansion in terms of the small parameter $\epsilon$ which is the ratio of gas densities ahead and behind the shock front (Cherniy 1959). For our purposes, $M >> 1$, and the value $\epsilon$ is equal to $\gamma$-1)/($\gamma$+1) = 1/4. Using only the first elements of expansion in terms of $\epsilon$ one can get the following expressions for the pressure and temperature of the gas behind the shock front (Galeev *et al.* 1989):

$$p(\Theta, \Phi) = \rho_\infty v_\infty^2 (\cos^2\Theta - \frac{1}{3}\sin^2\Theta + \frac{1}{3}\frac{\sin^3\Phi}{\sin\Theta}), \tag{10}$$

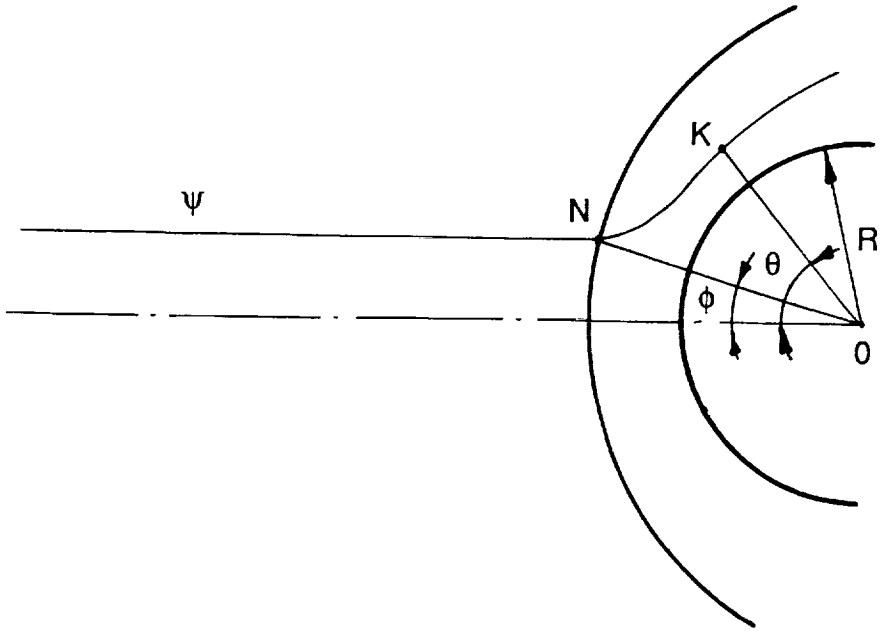


FIGURE 2 The flow over a star by the plane-parallel stream of the ionized gas. Here N is the point where the stream line with K-point on it intersects with the shock front.

$$T(\Theta,\Phi) = T_s(O)\left\{\cos^3\Phi - \frac{2}{3}\frac{\Gamma}{\sin\Phi}[\Theta - \Phi + \sin 2\Theta - \sin 2\Phi + \sin^3\Phi\right.$$

$$\left. = (\ln\frac{tg(\Theta/2)]}{tg(\Phi/2)}^{2/3}\right\}, \tag{11}$$

Where

$$T_s(O) = \varepsilon\mu m_p v_\infty^2 k^{-1} = 3\cdot 10^7 (v_\infty/10^8 \text{cm}\cdot\text{s}^{-1})^2 K, \tag{12}$$

$$\Gamma = \frac{4RC_1\rho_\infty v_\infty}{15k^2 T_s^{3/2}(O)}. \tag{13}$$

In the shock layer, the angles $\Theta$ and $\Phi$ are employed as coordinates of an arbitrary point K (see Figure 2).

With a distribution of $\rho$ and T known behind the shock front it is easy to find the spectral power of the bremsstrahlung of the gas heated in the shock

$$L_\nu = \int Q_\nu dV = \int_0^{\pi/2} \int_0^{\Theta} 2\Pi R^3 Q_\nu \frac{\rho\infty \cdot \cos\Phi}{\rho(\Theta,\Phi)} d\Phi d\Theta. \qquad (14)$$

Not to decrease essentially the accuracy of calculations of X-ray emission parameters, one can neglect the Busemann correction in the expressions for $P(\Theta,\Phi)$ and $T(\Theta,\Phi)$; (the Newton approximation). In this approximation for the case when the energy losses of the hot gas via radiation are small ($\Gamma << 1$) the value $L_\nu$ is determined by the expression (Galeev *et al.* 1989)

$$L_\nu = \frac{hL}{kT_s(O)}\left(\frac{\pi^2}{8}+\frac{1}{2}\right)\int_0^{\pi/2}\left[\frac{\pi}{2}-\Theta-\frac{1}{2}\sin 2\Theta\right]\exp\left[-\frac{h\nu}{kT_s(0)\cos^2\Theta}\right]d\Theta \qquad (15)$$

where

$$L = \pi\left(\frac{\pi^2}{8}+\frac{1}{2}\right)\frac{C_1 Z^3 \mu \rho_\infty^2 v_\infty^2 R^3}{m_p A^2 T_s(O)^{1/2} k} \approx$$
$$2\cdot 10^{33}\left(\frac{\dot{M}}{10^{-5}M_\odot/yr}\right)^2\left(\frac{R}{10^{12}cm}\right)^3 \qquad (16)$$
$$\left(\frac{D}{10^{13}cm}\right)^4\left(\frac{v_\infty}{10^8 cm/s}\right)^{-1}\text{erg/s}$$

is the total hot-gas bremsstrahlung power.

The bremsstrahlung spectrum of the gas heated in the shock wave during the supersonic flow over the star has an exponential drop at high frequencies ($h\nu >> kT_s(0)$) and a relatively complicated shape at the frequencies $h\nu \sim kT_s(0)$.

## COLLISION OF SUPERSONIC WINDS

Here we could discuss only parameters of the bremsstrahlung (X-ray) emission of rather wide binaries WR + OB ($r_{OB} > r_*$). The stellar wind of a WR star is much more powerful than that of an OB star ($M_{WR}\cdot v_\infty^{(WR)} >> M_{OB}\cdot v_\infty^{(OB)}$). In this case, one might assume that there is a collision of the stellar wind flowing out of an OB star with the plane-parallel gas flow whose density and velocity are $\rho_\infty = \dot{M}_{WR}/4D^2 r_\infty^{(WR)}$ and $v_\infty^{(WR)}$, respectively.

In a Newtonian approximation the contact surface equation will be:

$$r(\Theta) \approx r_{OB}\frac{\Theta}{\sin\Theta}. \qquad (17)$$

Using the method of expansion in terms of the small parameter $\epsilon$ to solve the problem where the plane-parallel gas flows over an axial-symmetric body with a surface described by equation (17), similar to the solution above for the case of the flow over the sphere we obtained the hot gas temperature and pressure distributions. With these values known we also got the total and spectral powers of the hot gas bremsstrahlung. This emission spectrum shape turned out to be close to that described by equation (15). The bremsstrahlung power increases significantly as compared with equation (16) and is equal to

$$L \approx 10^{36} \left(\frac{\dot{M}_{WR}}{10^{-5} M_\odot/yr}\right)^2 \left(\frac{D}{10^{13} cm}\right)^{-1} \left(\frac{v_\infty^{(WR)}}{10^8 cm/s}\right)^{-1} \left(\frac{\dot{M}_{OB} v_\infty^{(OB)}}{\dot{M}_{WR} v_\infty^{(WR)}}\right)^{3/2} \text{erg/s.} \quad (18)$$

This is due to increasing the size of an "obstacle" flowed over by the WR stellar wind gas.

## INTERPRETATION OF THE V 444 CYGNI X-RAY EMISSION

The system V 444 Cygni is one of the well-studied WR + OB binaries. It consists of the Wolf-Rayet star WN4 and the star of the O6 spectral type, and it has the following parameters (see Shore and Brown 1988): D = 40 $R_\odot$, $M_{WR}$= 10 $M_\odot$, $M_{O6}$= 25 $M_\odot$, $R_{WR}$ = 2.9 $R_\odot$, $R_{O6}$ = 10 $R_\odot$, $\dot{M}_{WR}$ = $10^{-5}$ $M_\odot$/year, $v_\infty(WR) = 2.5 \cdot 10^8$ cm/s. The stellar wind parameters: $\dot{M}_{O6} = 2 \cdot 10^{-6}$ $M_\odot$/year, $v_\infty^{(O6)} \approx v_\infty^{(WR)}$ seem to be most probable for the star of the O6 spectral type.

Using the model developed above for collisions of stationary stellar winds when gas velocities are equal to $v_\infty^{(O6)}$ and $v_\infty^{(WR)}$ ahead of shock fronts $L_x$ and kT value can be estimated from (12) and (18) as equal to $10^{35}$ erg/s and $\sim$ 10 keV respectively. Note that this $L_x$ value is only the theoretically expected lower limit since we do not take into account the emission of the gas outflowing from the O star and heated in the shock.

It was Moffat *et al.* (1982) who observed the X-ray emission of V 444 Cygni for the first time. The analysis of the variability in time and the energy spectrum of this emission evidences that the X-ray emission is generated in outer regions of the stellar wind (Moffat *et al.* 1982). The IUE satellite observations of the V 444 Cygni binary system emission in the ultraviolet range (Shore and Brown 1988) indicate also that there are collisions of stellar winds in this system. However, the V 444 Cygni X-ray parameters observed, $L_x \simeq 10^{33}$ erg/s and kT $\simeq$ 0.5 keV, are more than by

the order of magnitude lower than those expected from the simple theory for collisions of stationary winds (Prilutskii and Usov 1975, 1976). The accuracy of calculations of gas parameters behind the shock front and the gas emissions is of the order of $\epsilon$, i.e., several tens of percent. Thus, it is evident that the model for the gas flow in V 444 Cygni before its collision should be changed qualitatively.

A relatively low gas temperature behind the shock front ($kT \simeq O.5keV$) evaluated from the V 444 Cygni X-ray data shows that ahead of the shock front the stellar wind gas of the WR star has the velocity not higher than $10^8$ cm/s. At first sight, it seems to be unbelievable since at such a distance from the WR star ($r_{WR} \simeq 28\ R_\odot \simeq 10R_{WR}$) the gas flow velocity should be equal to $v_\infty^{(WR)}$. Note, however, that with V 444 Cygni parameters given above the distance from the contact surfact to the O star center is $r_{O6} \approx 1.2\ R_{O6}$ (see equation (2)), i.e. the wind collision occurs near the O star surface. In this case, the gas flowing out of the O star is accelerated due to the emission pressure only by a small fraction of $v_\infty^{(06)}$. In turn, the stellar wind gas of the WR star will be decelerated by the pressure of its emission while approaching the O star.

The law of how the velocity of the stellar wind gas of the WR star varies along the line connecting the centers of the WR and O stars can be written as:

$$v^{(WR)}{}_{(r)} = \left\{ \left[ v_\infty^{(WR)} \right]^2 + \left[ v^{(06)}(r) \right]^2 - \left[ v_\infty^{(06)} \right]^2 \right\}^{1/2}, \tag{19}$$

where $v^{(O6)}$ (r) is the O star's wind velocity at a distance of $r \geq R_{O6}$.

The distance $r_{O6}$ to the stagnation point of the contact surface from the O star center can be determined from the condition:

$$\frac{\dot{M}_{OB} v^{(06)}(r_{06})}{r_{06}^2} = \frac{\dot{M}_{WR} v^{WR}(r_{06})}{(D - r_{06})^2}. \tag{20}$$

From (19) and (20) we can get

$$\frac{\dot{M}_{06} v_\infty^{(06)}}{\dot{M}_{WR} v_\infty^{(WR)}} (D - r_{06})^2 v^{(06)}(r_{06}) = r_{06}^2 \sqrt{[v_\infty^{(WR)}]^2 + [v^{(06)}(r_{06})]^2 - [v_\infty^{06}]^2}. \tag{21}$$

In our case, $v^{(WR)}{}_\infty = v^{(06)}{}_\infty$ from Equation (21) it is evident that $r_{O6}$ coincides with (2) derived above, i.e., the allowance for the WR star wind deceleration does not change the position of the stagnation point of the contact surface. The velocity equality, $v^{(WR)}$ ($r_{O6}$) $\approx v^{(O6)}$ ($r_{O6}$), holds

true in this case. But the gas velocity ahead of the shock front can decrease drastically. Let us estimate the value $v^{(WR)}$ $(r_{O6})$.

So far the problem of how the velocity of the outflowing gas in the vicinity of the O star changes has been studied insufficiently (Barlow 1982). For example, assuming the linear law of the velocity change as $v^{(06)}$ (r) = $v_\infty{}^{(O6)}$ [(r/$R_{O6}$)-1] we can get $v^{(WR)}{}_{(rO6)} \approx 0.2\, v_\infty^{(WR)} \approx 0.5 \cdot 10^8$ cm/s. If the $v^{(06)}$(r) changes obeying the law $v^{(O6)}$ (r) = $v_\infty^{(06)}\sqrt{1-(R_{06}/r)}$ which seems to be more real, we can get $v^{(WR)}$ $(r_{O6}) \approx 10^8$ cm/s. Thus, the allowance for the deceleration of the gas of the WR star's stellar wind in the O star's vicinity can lead to gas velocities ahead of the shock front equal to about (0.5 to 1) $\cdot$ $10^8$ cm/s. This makes it possible to explain a low temperature in the X-ray spectrum of V 444 Cygni. The deceleration of the gas of the WR star's stellar wind and the X-ray absorption can result in lowering the X-ray luminosity of V 444 Cygni down to the observed value.

## REFERENCES


Barlow, M.J. 1982. Observations of mass loss from OB and Wolf-Rayet stars. Pages 149-172. In: Deloore, C.W.H, and A.J. Willis (eds.). Wolf-Rayet stars: Observations, Physics, Evolution. IAU Symp. No. 99. D. Reidel, Dordrecht.

Caillaut, J.P, G.A. Chanan, D.J. Helfand, J. Patterson, J.A. Nousek, L.P. Talako, G.D. Bothun, and R.H. Becker. 1985. The peculiar X-ray and radio star AS 431. Nature 313:376-378.

Chernyi, G.G. 1959. The Gas Flow with High Supersonic Velocity. Fizmatgiz, Moscow.

Galeev, A.A., N.N. Pilyugin, and V.V. Usov. 1989. Generation of X-ray and radio emission by binary Wolf-Rayet stars. Pages 125-129. In: Proc. Varenna-Abastumani International School and Workshop on Plasma Astrophysics, held in Varenna, Italy. Vol. 1.

Hayakawa, S. 1973. Origina of Cosmic Ray. Nagoya, Japan.

Moffat, A.F.J., C. Firmani, I.S. McLean, and W. Seggewiss. 1982. Time-dependent X-ray observations of Wolf-Rayet binaries with O-type and with suspected compact companions. Pages 577-581. In: de Loore, C.W.H., and A.J. Willis (eds.). Wolf-Rayet Stars: Observations, Physics, Evolution. IAU Symp. No. 99. Reidel: Dordrecht.

Pollock, A.M.T 1987. The EINSTEIN view of the Wolf-Rayet stars. Astrophys. J. 320:283.

Prilutskii, O.F., and V.V. Usov. 1975. On X-ray radiation of the close binaries with young massive stars. Astron. Circ. 854:1-2.

Prilutskii, O.F., and V.V. Usov. 1976. On X-radiation of double systems containing Wolf-Rayet-type stars. Soviet Astr. 20:2.

Seward, F.D., W. Forman, R. Giacconi, R. Griffiths, F.R. Harnden, Jr., C. Jones, and J. Pye. 1979. X-ray from Eta Carinae and the surrounding nebula. Ap. J. (Letters) 234:L55-L58.

Shore, S.N. and D.N. Brown. 1988. Colliding stellar winds in the eclipsing Wolf-Rayet binary V 444 Cygni. Ap. J. 334:1021-1037.

# Hydrodynamic Study of Supernova 1987A: The Phase of A Wave of Cooling and Recombination

V.P. UTROBIN
Institute of Theoretical and Experimental Physics

## ABSTRACT

A dependence of the bolometric light curve during the phase of a wave of cooling and recombination and the effective temperature on the density distribution within a progenitor and its chemical composition is investigated. We show that the outside layers of the blue supergiant Sk-69°202 just before the supernova 1987A outburst had the density distribution very close to that of the polytropic model with the index of n=3 and the chemical composition roughly close to that of the Sun. A mass of these layers is about $11M_{\odot}$.

The outburst of supernova 1987A in the Large Magellanic Cloud (LMC) allows very detailed observations to be made and gives an extremely rare chance to study this extraordinary event and the stellar evolution before it carefully. A supernova outburst and a stellar evolution before it are very complicated physical phenomena and, as a consequence, are investigated only in outline. For this reason, the hydrodynamic study of supernova outburst which does not account for the properties of the collapse and subsequent explosion and the results of evolutionary calculations is of great importance. A comparison of this study with observational data allows the general properties of an explosion mechanism and a stellar structure before the outburst to be specified.

The hydrodynamic models discussed below are based on the numerical integration of a set of spherically symmetrical hydrodynamic equations with radiation diffusion and self-gravitation taken into account. The radiation diffusion is treated with a flux-limited approximation. In this approximation, the radiation flux is defined by

$$F = \frac{f_D \cdot f_L}{(f_D + f_L)},$$

where $f_D$ is the flux given by theory of the equilibrium radiation diffusion and $f_L$ is a flux limiter. The latter is determined by

$$f_L = \frac{CU}{d},$$

where $\alpha$ is a coefficient, c is the velocity of light, and U is the radiation energy density. Note that the coefficient $\alpha$ is equal to $\sqrt{3}$ in optically thick regions and to 1 in a transparent medium. Shock waves are calculated by means of artificial viscosity. The set of equations is approximated by the difference equations in the implicit scheme. Initial conditions for hydrodynamic equations are the polytropic stellar model in hydrostatic equilibrium. The chemical composition of matter is taken as a mixture of hydrogen, helium, and some heavy element. The ionization equilibrium of this mixture is determined with an approximate method of calculation of the multi-stage ionization of heavy elements for each time step. The Rosseland mean opacity is calculated in the hydrogen-like approximation with regard for Thomson scattering on free electrons. An explosion of the star is simulated by a disturbance in the thermal energy near the stellar center at the initial time.

Now it is certain that the progenitor of supernova 1987A is the B31a type supergiant Sk-69°202 (Panagia *et al.* 1987; Sonnborn *et al.* 1987; Gilmozzi *et al.* 1987). According to Rousseau *et al.* (1978), this star had the following parameters: the apparent magnitude of V = $12^m.24$ and the color index of B - V = $+0^m.04$. At the LMC distance modulus of $18^m.6$ (Sandage and Tammann 1971), the interstellar extinction of $A_v$ = $0^m.6$ (Panagia *et al.* 1987), the effective temperature of $T_{ef}$ = 16300 K, and the bolometric correction of B.C. = $-1^m.15$ (Humphreys and McElroy 1984) these values correspond to the progenitor radius of about $47R_\odot$. We adopt the presupernova radius of $45R_\odot$. Other basic characteristics of the computed hydrodynamic models are the stellar mass of $16M_\odot$ and the explosion energy of $2\times10^{51}$ erg. To account for the exponential tail observed after the maximum of the bolometric light curve requires the amount of cobalt -56 of about $0.08M_\odot$. In calculating the hydrodynamic models, the energy of the radioactive decay of nickel -56 and cobalt - 56 is assumed to convert completely into thermal energy. The nickel is distributed uniformly over the central core mass of $0.1M_\odot$. The parameters under investigation are listed in the Table. The first column presents the number of the model; the second—the polytropic index n; the third—the mass fraction of hydrogen X with that of heavy elements of Z = 0,004; the

TABLE

The main characteristics of computed models

| Model | n | X | |
|---|---|---|---|
| 1 | 3 | 0.7 | $\sqrt{3}$ |
| 2 | 1.5 | 0.7 | $\sqrt{3}$ |
| 3 | 4.5 | 0.7 | $\sqrt{3}$ |
| 4 | 3 | 0.075 | $\sqrt{3}$ |
| 5 | 3 | 0.01 | $\sqrt{3}$ |
| 6 | 3 | 0.7 | 1 |

coefficient $\alpha$. In all the models, the chemical composition is homogeneous throughout the star.

The instantaneous energy release in the hydrodynamic model 1 leads to the formation of a strong shock wave which propagates towards the stellar surface. In propagating over the star, the shock wave heats the matter and accelerates it to the velocities increasing outward and exceeding the local escape velocity throughout. Approximately at the moment of 0.073 days, the shock wave arrives at the stellar surface and then heats its external layers: the effective temperature jumps to $2.3 \times 10^5$ K and the luminosity rises accordingly. After this the star begins to expand, its outside layers cool rapidly, and the luminosity decreases. A narrow luminosity peak forms as a result. The peak has a width of about 0.01 days and reaches the magnitude of $M_{bol} = -19^m.6$ at maximum. For the sake of clarity, it is omitted in the bolometric light curves shown below.

The further expansion of the envelope gradually creates the conditions favorable for the appearance of the specific cooling by radiation—a wave of cooling and recombination (WCR). Such a layered illumination of the ejected envelope is completed by about 10 days. From this time to about 40 days, the bolometric light curve plotted in Figure 1 is mainly determined by properties of the WCR. During this period, there is a good agreement between the calculated and observed bolometric light curves (Figure 1). After the WCR stage, the luminosity goes to increase in the following 43 days. This effect is caused by a radiation diffusion from the central region of the envelope involving the nickel. However, the internal energy of the envelope has been exhausted by some 80 days, and the expelled matter has become optically thin. As a result, the luminosity decreases abruptly to the instantaneous rate of energy input by the radioactive decay and then is

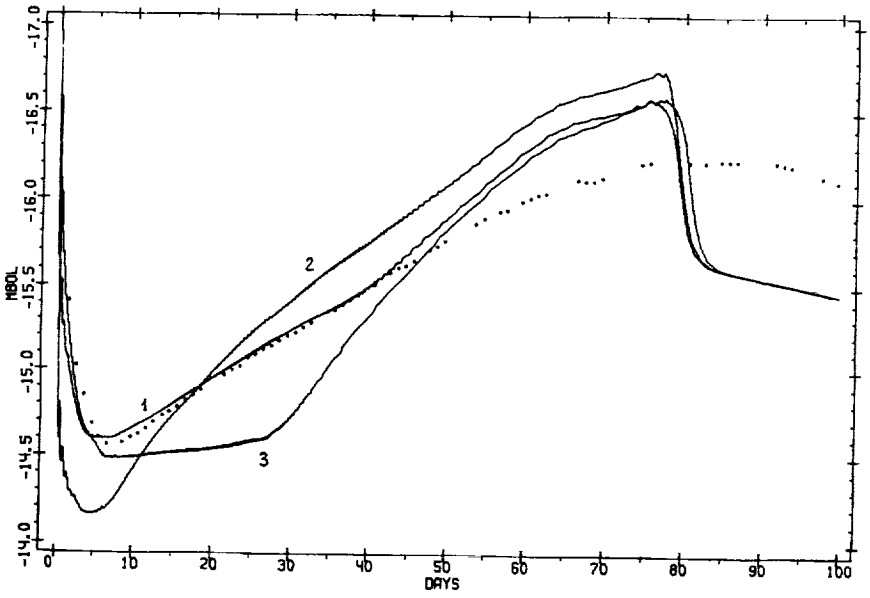


FIGURE 1 Bolometric light curves. Solid lines are the light curves for models 1, 2, and 3. Points are the observational data for the supernova 1987A (Catchpole *et al.* 1987) with time reckoned from the neutrino burst detected by Kamiokande II (Hirata *et al.* 1987) and IMB (Bionta *et al.* 1987) experiments.

completely determined by it. For this reason the calculated light curve is consistent with the observations after 120 days.

In the interval from 40 to 120 days the light curve of model 1 differs from the observed one first slightly and then increasingly (Figure 1). It requires a more adequate treatment of both the central region of the presupernova and the mechanism of the supernova explosion than discussed above, since during this period the flux is created by the most internal layers of the ejected envelope.

The phase of the WCR is a remarkable feature of the supernova 1987A outburst since it involves valuable information on the structure of the major portion of the progenitor. In the case of model 1, the WCR during the period from 10 to 40 days propagates through the mass of about $11M_{\odot}$ apparently comparable with the total mass of the progenitor. Note that the mass of the most external layers which are irradiating in the first 10 days is only about $0.1M_{\odot}$.

According to Grassberg and Nadyozhin (1976), the photometric characteristics of a supernova and the regularities of the propagation of the WCR in an expanding envelope depend basically on a density distribution of matter and its chemical composition. A radial distribution of density

$\rho$ in the ejected envelope is mainly determined by a structure of the progenitor. The smaller a polytropic index n, the greater an effective index $q = -\partial \ln \rho / \partial \ln r$ in the initial model and, as a consequence, in the ejected envelope. An increase of the effective index q at the level of the WCR propagating through the envelope of the homogeneous chemical composition leads to a rise in the luminosity rate. This is confirmed by the bolometric light curve calculated with the different polytropic index n (Figure 1). The slope of the light curve during the phase of the WCR increases with the decreased polytropic index n (models 3, 1, and 2). It weakly depends on the rest of the parameters of hydrodynamic models (Utrobin 1989). For the first 40 days, the light curve of model 1 fits the observed light curve well (Figure 1). We may draw a conclusion that the density distribution of the B31a type supergiant Sk-69°202 before the supernova 1987A outburst is very close to that of the polytropic model with the index of n = 3 over the outside layers of about $11M_{\odot}$.

Together with the bolometric light curve, the observations of the supernova 1987A have provided a time dependence of the effective temperature (Catchpole *et al.* 1987; Hamuy *et al.* 1988). The effective temperature during the phase of the WCR is determined by the chemical composition of matter. The smaller the mass fraction of hydrogen and the greater the mass fraction of helium the higher the effective temperature. This is verified by models 1, 4, and 5 with the mass fraction of hydrogen of X = 0.7, 0.075, and 0.01 respectively (Figure 2). Whereas the density distribution in the progenitor, its mass, radius, and the explosion energy do not affect the effective temperature (Utrobin 1989). This fact allows the mass fraction of hydrogen within the progenitor to be estimated by the effective temperature observed for the phase of the WCR.

In addition to the chemical composition, the effective temperature calculated with the flux-limited approximation depends on the coefficient $\alpha$. The transition from the limit of optically thick regions (model 1) to that of transparent medium (model 6) leads to rising in the effective temperature (Figure 3). It is to be noted that the value of $\alpha = 1$ is relevant, since an aim of the flux-limited approximation is to improve the equilibrium radiation diffusion in transparent regions. In this case, the time dependence of the effective temperature agrees well with that observed (Figure 3). Thus, the effective temperature of the supernova 1987A during the phase of the WCR shows that the outside layers of about $11M_{\odot}$ in the blue supergiant Sk-69°202 had the chemical composition roughly close to that of the Sun.

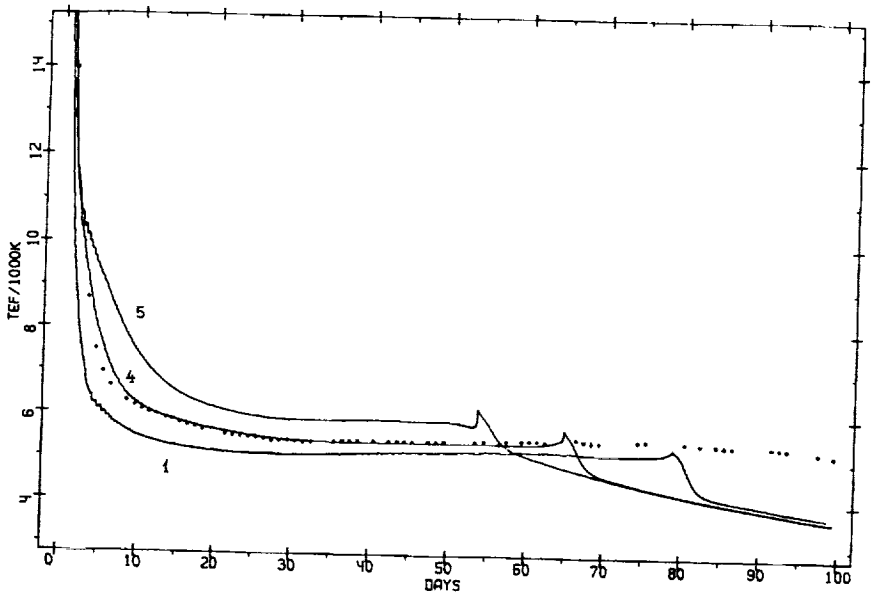


FIGURE 2 Time dependence of the effective temperature. Solid lines represent models 1, 4, and 5. Points show the observational data for the supernova 1987A (Catchpole *et al.* 1987).

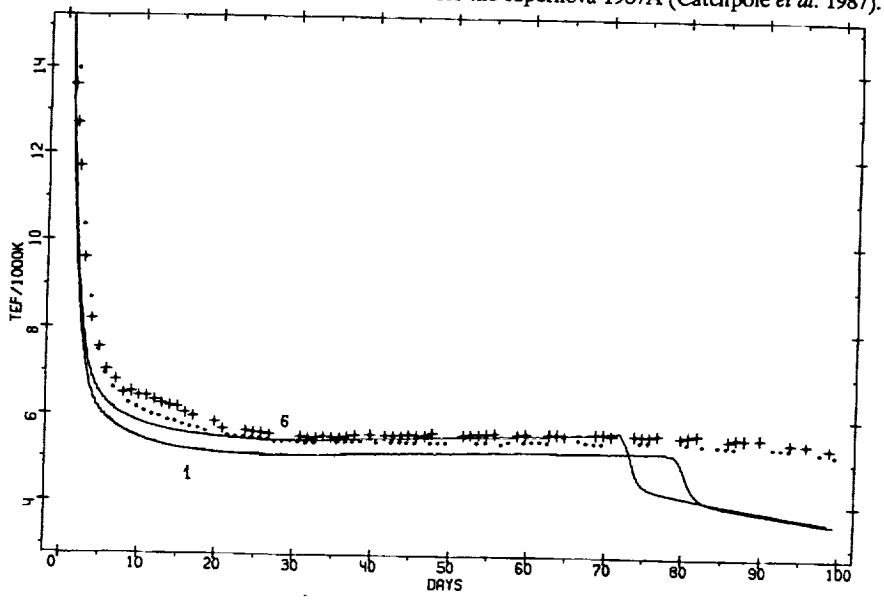


FIGURE 3 Time dependence of the effective temperature. Solid lines represent models 1 and 6. Points are the observational data of Catchpole *et al.* (1987) and crosses correspond to those of Hamuy *et al.* (1988).

## REFERENCES

Bionta, R.M., G. Blewitt, C.B. Bratton, *et al.* 1987. Phys. Rev. Letters. 58:1494.
Catchpole, R.M., J.M. Menzies, A.S. Monk, *et al.* 1987. Monthly Not. Roy. Astron. Soc. 229:15.
Gilmozzi, R., A. Cassatella, J. Clavel, *et al.* 1987. Nature. 328:318.
Grassberg, E.K., and D.K. Nadyozhin. 1976. Astrophys. and Space Sci. 44:429.
Hamuy, M., N.B. Suntzeff, R. Gonzalez, and G. Martin. 1988. Astron. J. 95:63.
Hirata, K., T. Kajita, M. Koshiba, *et al.* 1987. Phys. Rev. Letters. 58:1490.
Humphreys, R.M., and D.B. McElroy. 1984. Astrophys. J. 284: 565.
Menzies, J.M., R.M. Catchpole, G. van Vuuren, *et al.* 1987. Monthly Not. Roy. Astron. Soc. 227:39.
Panagia, N., R. Gilmozzi, J. Clavel, *et al.* 1987. Astron. and Astrophys. 117:L25.
Rousseau, J., N. Martin, L. Prevot, *et al.* 1978. Astron. and Astrophys. Suppl. Ser. 31:243.
Sandage, A., and G.A. Tammann. 1971. Astrophys. J. 167: 293.
Sonneborn, G., B. Altner, and R.P. Kirshner. 1987. Astrophys. J. (Letters) 323:L35.
Utrobin, V.P. 1989. Sov. Astron. Letters. 15:99.

# Appendix
# List of Workshop Presentations

*19 June 1990 Institute of Space Research, Moscow*

BARUCH T. SOIFER (California Institute of Technology) "Results from IRAS, the Infrared Satellite"
ROBERT T. KIRSHNER (Harvard-Smithsonian Center for Astrophysics) "Supernova 1987A"
MARGARET J. GELLER (Harvard-Smithsonian Center for Astrophysics) "Voids and the Large-Scale Structure of the Universe"

*20 June 1990 Presidium of Georgian SSR Academy of Sciences, Tbilisi*

RICCARDO GIACCONI (Space Telescope Science Institute) "Clusters of Galaxies"
GEORGE W. CLARK, NAS Chair (Massachusetts Institute of Technology) "X-Ray Eclipses and Cyclotron Spectral Features"
WALTER H.G. LEWIN, NAS Co-Chair (Massachusetts Institute of Technology) "Quasi-Periodic Oscillations in Low-Mass X-Ray Binaries"
BRUCE MARGON (University of Washington) "Main Sequence Binaries in Globular Clusters"
DAVID J. HELFAND (Columbia University) "The X-Ray Background"

*21 June 1990 Abastumani Astrophysical Observatory, Tbilisi*

YEVGENIY M. CHURASOV (Institute of Space Research) "Observations of X-Ray Pulsars and Galactic Bulge by Mir-Kvant"
G. CHIBISOV AND YU.V. SHTANOV (Lebedev Physical Institute) "Chaotic Inflationary Universes and the Anisotropy of the Large-Scale Structure"

M. KHLOPOV "Physical and Astrophysical Effects of the Broken Flavor Symmetry"
RICHARD F. MUSHOTZKY (NASA/Goddard Space Flight Center) "Active Galactic Nuclei"
S.A. SILICH (Kiev) "Asymmetric Remnants of Supernovae"
ROGER D. BLANDFORD (California Institute of Technology) "Active Galactic Nuclei"
S.A. GREBENEV (Institute of Space Research) "X-Ray Observations of Vulpecula"
V.V. USOV (Institute of Space Research) "Gas Flow and Generation of X-Ray Emmission in WR + OB Binaries"
S. FABRIKA (Six-Meter Telescope) "Photometry of SS 433 and Its Mass Functions"
A.M. CHEREPASHCHUK (Moscow State University) "Photometric Peculiarities of SS 433"
YU.YE. LUYBARSKY (Radioastronomical Institute) "The Structure of Pulsar Magnetospheres"
G.S. BISNOVATYE-KOGAN (IKI) "Free Precession of the Neutron Star in HER X-I"

*23 June 1990 Abastumani Astrophysical Observatory, Tbilisi*

V.S. BERESINSKY (Institute of Nuclear Research) "High-Energy Gamma-Radiation from Young Supernova Shells"
Yu.N. GNEDIN (Pulkovo Observatory) "Ultra-High Energy Gamma Rays from X-Ray Binaries"
R. DAGKESAMANSKY (Lebedev Physical Institute) "Radiotelescopes as the Detectors of Super-High Energy Neutrinos"
N.G. BOCHKAREV (Moscow State University) "Spectral Variability of AGNs. Six-Meter Telescope Data"
S. LEVSHAKOV (Ioffe Institute) "CO Abundance in a Galaxy with Redshift z = 2.3"
I.S. BESKIN (Lebedev Physical Institute) "Some Aspects of the Evolution of Radiopulsars"
A.F. ILLARIONOV, D.A. Upper Kompaneyets (Institute of Space Physics) "The Rotation Periods of Neutron Stars in X-Ray Binaries"
K.A. POSTNOV, M.E. PROKHOROV, N.I. SHAKURA (Moscow State University) "Free Precession in HER X-I"
KEVIN HURLEY (University of California, Berkeley) "Cosmic Gamma-Ray Bursts"
MAARTEN SCHMIDT (California Institute of Technology) "Statistics of Gamma-Ray Bursts"

ROGER BLANDFORD (California Institute of Techology) "The Physics of Cosmic Gamma-Ray Bursts"
I.G. MITROFANOV (Institute of Space Research) "Results from the Apex Gamma-Ray Burst Experiment on Phobos"
O.V. TEREKHOV (Institute of Space Research) "Results from the Lilas Gamma-Ray Burst Experiment on Phobos"
A. ILLARIONOV (Institute of Space Research) "Heavy Elements Absorption Lines in the Spectra of Gamma-Ray Bursts"
P. AMRUEL, O. GUSSEYROV (Baku) "Evolutionary Sequence of Low-Mass X-Ray Sources"

*25 June 1990 Abastumani Astrophysical Observatory*

MAARTEN SCHMIDT (California Institute of Technology) "The Faint End of Stellar Luminosity"
BRUCE MARGON (University of Washington) "A Low-Cost 3.5-Meter Optical Telescope at Apache Point"
G. KAHIDZE (Abastumani Astrophysical Observatory) "The Georgian Space Research Program"

*26 June 1990 Abastumani Astrophysical Observatory*

J.G. LOMINADZE (Town Laboratory of Abastumani Astrophysical Observatory) "Theoretical Activities at AAO"
G.D. CHAGELISHVILI, R.G. CHANISHVILI, J.G. LOMINADZE, S.A. SOKHADZE (Town Laboratory of Abastumani Astrophysical Observatory) "Large-Scale Magnetic Fields in Accretion Disks of Compact Objects and Their Manifestations"
A.Z. KAZBEGI, G.Z. MACHABELI, G.I. MELIKIDZE (Town Laboratory of Abastumani Astrophysical Observatory) and V.V. USOV (Institute of Space Research) "Theory of Pulsar Radio Emission: Possible Versions"
M.E. GEDALIN, J.G. LOMINADZE, E.G. TSIKARISHVILI (Town Laboratory of Abastumani Astrophysical Observatory) "Relativistic Plasma in the Crab Nebula"
T.J. TOROSHELIDZE (Abastumani Astrophysical Observatory) "A Search for a Precursor of Earthquakes in Airglow"
N.G. KOGOSHVILI, T.M. BORCHKHADZE (Abastumani Astrophysical Observatory) "The Merged Catalogue of Galaxies on Magnetic Tape and Some Results of Its Statistical Treatment"

*28 June 1990 Institute of Space Physics*

W. DAVID ARNETT (University of Arizona) "Supernovae"

D.K. NADYOZHIN (Institute of Theoretical and Experimental Physics) "Some Crucial Points in the Interpretation of SN 1987A Data"
S.V. BLINNIKOV (Institute of Theoretical and Experimental Physics) "Modeling of the Early SN87A Light Curve with Multi-Group Time-Dependent Radiative Transfer"
ROBERT P. KIRSHNER (Harvard-Smithsonian Center for Astrophysics) "Optical Data on Supernova 1987A"
V.P. UTROBIN (Institute of Theoretical and Experimental Physics) "The Internal Structure of the Progenitor of SN87A"
N.N. CHUGAY (Astronomical Council) "The Early Hard X-Ray and Gamma-Ray Luminosity of SN87A Derived from the Optical Spectra"
RASHID A. SUNYAEV, ASUSSR Chair (Institute of Space Physics) "Evolution of the Hard X-Ray Spectrum of SN87A"
JOSEPH H. TAYLOR, JR. (Princeton University) "Millisecond Pulsars"
DAVID J. HELFAND (Columbia University) "Supernova Remnant Population of the Galaxy"

*29 June 1990 Institute of Space Physics*

DAVID T. WILKINSON (Princeton University) "Anisotropy in $3^0$K Radiation"
I.A. STRUKOV (Institute of Space Physics) "Experimental Methods of Investigation of Large-Scale Anisotropy of MBR"
MARC DAVIS (University of California, Berkeley) "Cosmology Studies with the Infrared Satellite"
RICHARD F. MUSHOTZKY (NASA/Goddard Space Flight Center) "Large-Scale Structure of the Universe"
ALAN H. GUTH (Massachusetts Institute of Technology) "The Inflationary Universe"
ALEXEY A. STAROBINSKY (Landau Institute of Theoretical Physics) "Prospects for Proving the Existence of Inflation by Observations"
G.B. SHOLOMYTSKY (Institute of Space Physics) "Test for the Cosmological Constant"
MAARTEN SCHMIDT (California Institute of Technology) "Extragalactic X-Ray Source Statistics"
JOSEPH H. TAYLOR, JR. (Princeton University) "Millisecond Pulsars and the Background of Gravitational Waves"

*30 June 1990 (Institute of Space Physics)*

JACQUELINE N. HEWITT (Massachusetts Institute of Technology) "Gravitational Lenses"
DAVID N. SPERGEL (Princeton University) "Cosmic Walls"
ALAN H. GUTH (Massachusetts Institute of Technology) "Can a Man-Made Universe Be Achieved By Quantum Tunneling Without Initial Singularity?"
A. FRIEDMAN (Astronomical Council) "Observed Turbulence Spectra and Single Dipole Vortices"
E. KHACHIKYAN (Byurakan Observatory) "Double Galactic Nuclei"